CONTRACT REPORT NUMBER: 1SU81-00320

CONTRACTOR: University of Alberta

THE BEHAVIOUR AND DESIGN OF ROOFS SUPPORTED BY NON-TENSIONED RESIN BOLTS

(UP-A-261)

BY

B. STIMPSON

NOVEMBER, 1985

FINAL REPORT

480 pp.

Work on this project was conducted under the auspices of the Canada Centre for Mineral and Energy Technology, Energy, Mines and Resources, Canada.

D.S.S. File #: 01SU.23440-9055
D.S.S. Contract Serial #: OLST84-00-446
CANMET Scientific Authority: B.M. Das

APR 23 1988
MICROMEDIA

EXECUTIVE SUMMARY

Roof fixtures of various types play an important role in mine roof safety by reducing the incidence of roof falls. They may be classified into two general classes - active or passive depending upon whether they are pre-tensioned or not.

Resin grouted, non-tensioned bolts, the subject of this report, have several important advantages over conventional, point anchored bolts, the most important of these being improved pull-out strength and greater shear and axial stiffnesses. Poor installation procedures can seriously compromise these advantages.

While significant advances have been made in developing a range of rock fixture products, much remains to be learned about the design and behaviour of roofs supported by such devices. This report focuses on this problem with particular reference to resin bolting of horizontally bedded roofs with or without vertical cross joints.

The fundamental approach taken in this study is that in order to optimize the design of a resin rock bolt pattern it is necessary to understand (a) the mechanical behaviour of a single resin rock bolt unit, (b) the modes of displacement and failure that occur when a mine opening is excavated in horizontally bedded strata, and (c) the interaction between the rock fixture and the rock mass after the support has been installed and excavation continues.

Classical beam theory has been used in the past for the design of point-anchor, tensioned bolt layouts. It is here extended to the non-tensioned, resin bolt system. First, an analytical study was made of the effect of deformable abutments on beam behaviour, and includes the effect of a non-uniform "clamping" stress over the abutments such as might be expected where the abutments (pillars) are suffering peripheral failure. It is shown that under some circumstances reinforcement of the roof over the abutment will enhance roof stability.

Second, it is postulated that because of their high shear stiffness resin bolts should be most effective when installed at locations where differential slip between beds is greatest. Analytical studies for a variety of loading conditions were carried out and it was shown that the optimum shear stiffening effect of resin bolting should be obtained with bolts located over approximately the first third of the span in from the ribsides of an opening. This prediction was corroborated by model studies.

With a sufficient density of resin bolts this shear stiffening effect would cause separate roof layers to act as a single layer. A new analysis was developed which enables the engineer to determine the magnitude of reinforcement provided by a given resin bolt layout, or to determine the bolt spacing which will provide a given amount of reinforcement. The term "Degree of Reinforcement", used as a measure of bolt effectiveness, varies from 0 (no reinforcement), 1 (ideally reinforced), to greater than 1 (super-reinforcement).

The timing of installation, the axial stiffness of the rock fixture system, and the reaction of the strata to excavation determine the axial loads that develop in the supports. A new analysis was developed for conducting a complete ground convergence - support reaction curve type of analysis for bedded strata, taking into account the timing of istallation. This method provides a rational approach for determining bolt patterns. An example of its use for a multi-layer roof is provided.

Horizontally bedded strata commonly exhibit steeply inclined or vertical cross joints. In order to approach rock bolt pattern design rationally for this type of roof condition physical model studies were carried out to determine the mode of collapse. A new mode of failure, which the author has chosen to call the two-hinge collapse mechanism, was observed. A mathematical model was developed to study the influence of various geometrical and mechanical parameters. The analytical model demonstrates that this mode of failure is most likely for large spans in weak, thinly bedded strata. The classical Voussoir beam is shown to be a special case of two-hinge collapse.

During convergence of a rock bolt supported opening axial loads develop in the fixtures and thereby induce some confinement of the rock. This in turn increases the strength of the rock mass. An analysis was developed to examine the effectiveness of this mode of reinforcement. Using a Hoek-Brown failure criterion for the rock mass, it is shown that a significant increase in rock mass strength could only be developed by this mechanism with bolt spacings that would be impractically small.

A common mode of rock bolt support design is to assume the bolts will have to support a certain weight of rock. The determination of this zone of rock may be relatively simple where a zone of poor rock quality passes upward into a solid layer but this is not always the case. A new analysis was developed to deal with this latter case and is based on the concept of the formation of an elliptical zone of loosened ground above a rectangular opening. The size of this zone is dependent upon the height and span of the opening, the ratio of horizontal to vertical virgin principal stresses, and the rock quality as measured by the Bieniawski (CSIR) Rock Classification. Some case histories were examined in detail and it was found that predictions of the theory were in reasonable agreement with field measurements.

The application of some of the principles of design suggested by this research will require field testing for validation. From a rock mechanics viewpoint uniformly spaced, vertical bolts do not represent an optimum design. It is proposed that non-uniform spacing, inclined bolts, variable lengths, and even different types of bolt, depending upon location in the span, would enhance preformance. From a practical viewpoint some of these measures might be difficult to implement.

Finally, it is suggested that consideration be given to the development of graphics-supported microcomputer programs of the various design methods presented in this report.

RESUME DE DIRECTION

Dans la sécurité du toit des mines, le boulonnage de toit joue un rôle important, en réduisant l'effet de leur effondrement. On peut en distinguer deux grandes classes: les boulonnages actifs et les boulonnages passifs, selon qu'ils sont ou non prétendus.

Les boulons injectés à la résine, non prétendus, font l'objet de ce rapport. Ils ont plusieurs avantages importants par rapport aux boulons conventionnels, à ancrage ponctuel, les plus importants étant une meilleure résistance à l'arrachement et une plus grande raideur axiale et en cisaillement. Une mise en pauvre défectueuse peut compromettre sérieusement ces avantages.

On a fait de grands progrès dans le développement de produits variés de boulannage des roches, mais il reste beaucoup à apprendre sur le comportement et le dimensionnement des toits ainsi boulonnés. Ce rapport met l'accent sur ce probléme, en traitant plus particulièrement le cas des boulons à la resine supportant des toits à strates horizontales, avec ou sans fissuration verticale.

L'idée de base est de cette étude est que, pour optimiser un projet de boulonnage de roche à la résine, il est nécessaire de comprendre: (a) le comportement mécanique d'un seul boulon de ce type, (b) les modes de déformation et de rupture qui se produisent quand une excavation de mine est reallisée dans des couches à stratification horizontale, et (c) l'interaction entre le boulonnage et le massif rocheux, quand les boulons ont été mis en place et que l'excavation se poursuit.

On a utilisé dans le passé la théorie classique des poutres pour le dimensionnement des boulonnages à ancrage ponctuel et prétension. On l'étend ici au cas du boulonnage a la résine, sous prétension. Premiérement, on a analysé l'effect de culees deformables sur le comportement d'une poutre, en y inclucent l'effet de contraintes de blocage non uniformes au niveau des culées, ce qui est vraisemblable quand les culées (piliers) subissent

une rupture périphérique. On montre que sous certaines conditions, le boulonnage du toit au niveau des culées en amelioré la stabilité.

Deuxièmement, on postule qu à cause de leur grande raideur en cisaillement, les zones d'implantation à efficacité maximum sont, pour les boulons a la résine, calles où le glissement différential entre strates est le plus important. On a effectué des analyses pour des sollicitations diverses et on a montré que l'effet de raideur en cisaillement était le mieux mobilisé quand les boulons se trouvaient approximativement dans le tièrs de la portée, à compter des faces latérailes de l'excavation. Cette prédiction a été confirmée par des études sur modèles.

Avec une densité suffisante de boulons à la résine, cet effet de renforcement au cisaillement peut conduire des couches distinctes du toit à se comporter comme une seule couche. On a mis au point une nouvelle méthode de calcul, qui permet a l'ingénieur de déterminer le niveau de reinforcement correspondant à un boulonnage donné,ou bien de déterminer l'espacement des boulons nécessaire pour obtenir un niveau donné de reinforcement. Pour quantifier l'efficacité du boulonnage, on utilize le parametre "Degré de Renforcement", qui vaie de 0 (pas de renforcement) à 1 (renforcement idéal), et même au delà de 1 (super-renforcement).

Le délai de mise en place et la raideur axiale du système de boulonnage, ainsi que le comportement des strates à l'excavation, déterminent l'intensité des charges axiales qui se développent dans le boulons. On a mis a point une novelle méthode de calcul compléte pour des couches stratifiées, prenant en compte le delai de mise en place, methode du type convergence du sol - courbe de reaction du support. Cette méthode fournit une base rationnelle pour déterminer le plan de boulonnage. On montre un example d'application au cas d'un toit avec stratifications.

Les couches stratifiées horizontalment possèdent souvent des joints verticaux ou de forte inclinaison. Pour aborder rationnellement la détermination du plan de boulonnage

pour de tels toits, on a effectué des études sur modèles afin de déterminer le mode d'effondrement. On a observé un nouveau mode de rupture, que l'auteur a désigné sous le nom de mécanisme de rupture à deux articulations. On a développé un modele mathématique pour étudier l'influence des divers paramétres géométrique et mecanique. Ce modèle analytique montre que ce type de rupture est le plus probable dans le cas de grandes portées dans les couches peu résistantes, finement stratifiées. On montre que le mécanisme classique de la poutre à voussoirs est un cas particulier de la rupture à deux articulations.

La convergence d'une excavation supportée par boulonnage engendre des charges axiales dans les boulons, et par suite un serrage de la roche, ce qui, à son tour, accroit la résistance du massif rocheux. On a procidé a l'analyse de l'efficacité de ce renforcement. En utilisant le critére de rupture de Hoek-Brown pour le massif rocheux, on montre que ce mécanisme ne peut conduire à des augmentations significatives de la resistance du massif rocheux que pour des espacements entre boulons trop petits pour être réalisables.

Dans le dimensionnement des boulonnages, on fait souvent l'hypothese que les boulons ont à supporter un certain poids de roche. La détermination du volume à supporter peut être relativement simple dans le case où une zone de mauvaise qualité est surmontée par une zone de roche solide, mais ce n'est pas toujours le cas. On a mis au point une nouvelle méthode de calcul pour ces autre cas, reposant sur hypothèse d'une forms elliptique pour la zone de terrain decompactée située au desous d'un excavation rectangulaire. L'étendue de cette zone dépend de la hauteur et de la portée de l'excavation, du rapport de la contrainte horizontale principale vierge, à verticale, et de la qualité de la roche detérminée suivant la Classification des Roches des Bieniawski (CSIR). On a examiné en détail quelques dossiers de cas et on a trouvé que les prédictions de la théorie étaient en accord raisonnable avec les mesures sur site.

Certains principes de dimensionnement suggérés pour cette étude nécessitent d'ètre validés par des expériences sur site avant de passer dans la pratique. Du point de la mécanique des roches, des boulons verticaux, uniformement espacé ne représent pas un dimensionnement optimum. On indique que de meilleurs résultats pouraient étre obtenus avec des espacement variables, des boulons inclinés et de longueur variable, et même en changeant le type de boulon suivant sa position dans la voûte. D'un point de vue pratique, il pourrait étre difficile de realiser certaines de ces dispositions.

Enfin, on suggère d'envisager le développment de programmes graphiques pour micro-ordinateurs, correspondent aux diverses méthodes de calcul présentées dans ce rapport.

CONTENTS

CHAPTER 1 - INTRODUCTION

1.1 Safety and Roof Support

1.2 Types of Roof Support

1.3 Types of Internal Support

1.4 Full Contact, Passive or Bonded Dowel Systems

1.5 Design of Roof Support in Horizontally Bedded Strata With Full Contact, Passive, Rebar

CHAPTER 2 - THE FULL COLUMN RESIN BOLT SYSTEM

2.1 Installation and Practical Considerations

2.2 The Boltmeter

2.3 Bolt and Rock Properties and Mechanical Behaviour
  2.3.1 Resin Properties
  2.3.2 Bolt Materials
  2.3.3 Resin-Bolt and Resin-Rock Interface
  2.3.4 Annulus Size
  2.3.5 Creep Properties
  2.3.6 Axial and Bending Stiffnesses
  2.3.7 Shear Stiffness
  2.3.8 Load Transfer Along a Resin-Bolt Column
  2.3.9 Temperature

2.4 Measurement of the Behaviour of Full Column Grouted Untensioned Bolts in Mines

CHAPTER 3 - UNDERSTANDING THE MODE OF OPERATION OF FULL COLUMN UNTENSIONED RESIN BOLTS

3.1 Introduction

3.2 Localization of Shear and Tensile Loads

3.3 Tensile and Shear Stiffening

3.4 Increase in Strength of a Full Column Resin Bolted Joint

CHAPTER 4 - ANALYTICAL MODELLING OF THE BEHAVIOUR OF RESIN-BOLTED STRATA

4.1 Introduction

4.2 Approaches to the Numerical Modelling of Bolted Strata

4.3 Example of an Equivalent Materials Model of a Bolted Rock Mass

4.4 Examples of Discrete Models of Bolted Rock Masses

CHAPTER 5 - ON SITE OBSERVATIONS OF DEFORMATION AND FAILURE OF ROOFS IN HORIZONTALLY BEDDED STRATA

5.1 Introduction

5.2 Roof Failure Mechanisms

CHAPTER 6 - MECHANICS OF SUPPORT BY BOLTING OF HORIZONTALLY BEDDED STRATA

6.1 Introduction

6.2 Support Mechanisms
  6.2.1 Suspension Mode
  6.2.2 Reinforcement
    6.6.2.1 Beam Building
    6.2.2.2 Arch Formation
    6.2.2.3 Rock Mass Strength Increase

CHAPTER 7 - THE EFFECT OF ABUTMENT CONDITIONS ON BOLTING REQUIREMENTS

7.1 Introduction

7.2 Behaviour of Single Beams

7.3 Abutment Stresses

7.4 Theoretical Model

7.5 Analysis of Results
  7.5.1 Beam Over Opening
  7.5.2 Beam over Abutment

7.6 Conclusions

CHAPTER 8 - OPTIMIZING REINFORCEMENT USING SHEAR STIFFNESS OF UNTENSIONED, RESIN-GROUTED BOLTS

8.1 Introduction

8.2 Bedding Plane Slip During Roof Flexure - Theory

8.3 Bedding Plane Slip During Roof Flexure - Examples

8.4 Effect of Large Displacements and Layers of Different Flexural Rigidities

8.5 Experimental Confirmation of Optimization of Reinforcement

8.6 Reinforcement Using Multiple Bolts

8.7 Conclusions

Appendix: "Influence of rock bolt location on the reinforcement of horizontally bedded roofs by full column grouted bolts". Paper presented at the International Symposium on Rock Bolting, Abisko, Sweden, August/September 1983.

CHAPTER 9 - A LIMITING EQUILIBRIUM APPROACH TO ESTIMATING THE DEGREE OF REINFORCEMENT OF HORIZONTALLY BEDDED ROOFS BY NON-TENSIONED, RESIN-GROUTED BOLTS

9.1 Introduction

9.2 Theory and Concept of Degree of Reinforcement

9.3 Bolt spacings Required to Provide Degree of Reinforcement Equal to 1
    9.3.1 Discussion

9.4 Degree of Reinforcement Provided by a Given Rock Bolt Pattern

9.5 Spacing Design for a Specified Degree of Reinforcement

9.6 A Proposal for Modifying a Finite Difference Model of a Bolted, Multilayer Plate Resting on Elastic Pillars
    9.6.1 Introduction
    9.6.2 General Information
    9.6.3 Failure Criteria
    9.6.4 The Program
    9.6.5 Assumptions
    9.6.6 Model Responses
    9.6.7 The Solution Algorithm
    9.6.8 Input Data
    9.6.9 Governing Differential Equations
    9.6.10 Suggested Methodology or Incorporating Non-Tensioned, Resin-Grouted Bolts
    9.6.11 Recommendations

Appendix: "Analysis of Multilayer Plates on Elastic Pillars". Paper by Chugh, A.K., Gesund, H. and Wright, F.D. J. Struct. Div. ASEC (1975).

CHAPTER 10 - STABILITY AND SUPPORT OF CROSS-JOINTED HORIZONTALLY BEDDED STRATA

10.1 Introduction

10.2 Physical Modelling

10.3 Collapse Mechanism

10.4 Mathematical Modelling of 2-Hinge Collapse Mechanism
  10.4.1 Outline of Model
  10.4.2 Results
  10.4.3 Implications for Support Design

10.5 Roofs Most Subject to 2-Hinge Collapse Mechanism

10.6 Stable, Flat Arches
  10.6.1 Importance of Micro-Geology
  10.6.2 Predicting the Vertical Displacement of Stable, Flat Arches

10.7 Model Studies of Roofs with Rock Bolts

10.8 Significance of Cross-Joint Roughness
  10.8.1 Deflection of a Cross-Jointed Beam
  10.8.2 Experiments to Investigate Influence of Joint Roughness
  10.8.3 Conclusions

CHAPTER 11 - CONFINING STRESSES INDUCED BY BOLTING AND THE RESULTANT INCREASE IN ROOF STRENGTH

11.1 Introduction

11.2 Method

11.3 Rock Mass Failure Envelope

11.4 Estimating Rock Mass Strength Increase by Pattern Bolting

11.5 Results and Analysis

11.6 Conclusions

CHAPTER 12 - ROCK-BOLT INTERACTION ANALYSIS FOR BEDDED STRATA INCORPORATING TIMING OF INSTALLATION

12.1 Ground Convergence and Support Reaction

12.2 Timing of Installation

12.3 Ground Convergence Curve for the Roof Above a Rectangular Opening in Bedded Strata

12.4 Support Reaction Curve of a Pattern of Grouted, Untensioned Bolts
  12.4.1 Basic Formulae
  12.4.2 Sensitivity Study

12.5 Ungrouted, Point-Anchor Bolts vs. Grouted Bolts

12.6 Application to Design of Bedded Mine Roofs
  12.6.1 Design Problem
  12.6.2 Design Stages
  12.6.3 Design of Intersection

12.7 Effect of Roof Failure on Bolt Loadings

12.8 Conclusions

CHAPTER 13 - INCLINED BOLTS

13.1 Introduction

13.2 Experimental Data

13.3 Theoretical Models
  13.3.1 Ultimate Shear Resistance or Strength
  13.3.2 Shear Stiffness

13.4 Conclusions

CHAPTER 14 - ESTIMATING BOLT LOADINGS AND BOLT LENGTHS - A NEW TECHNIQUE

14.1 Introduction

14.2 Formation of a Stable Arch Above a Horizontal, Rectangular Opening

14.3 Corrections to Reduce Size of Zone Requiring Support

14.4 Discussion of Results

14.5 Shape of Volume of Rock to be Supported

14.6 Back Analysis

14.7 Rock Bolt Patterns

14.8 Conclusions

CHAPTER 15 - RECOMMENDATIONS FOR DESIGN AND OPTIMIZATION OF ROOF BOLTING IN LAYERED STRATA

15.1 Introduction
  15.2.1 Non-uniform Spacing
  15.2.2 Bolting Over Abutments
  15.2.3 Non-Uniform Bolt Lengths
  15.2.4 Replacement of Resin Grout
  15.2.5 Inclined Bolts
  15.2.6 Conceptual Design

15.3 Graphics Software for Microcomputers

15.4 In-Situ Determination of Roof bolting Spacing

15.4 Closure

TABLES

Table 1.1 Rock reinforcement nomenclature adopted by the Australian Mineral Industries Research Association (5)

Table 1.2 Use of different types of fixtures in National Coal Board Mines, 1969-1973 (6)

Table 2.1 Mechanical properties of filled polyester resins

Table 2.2 Selected data on creep rates of resin bonded bolts

Table 2.3 Selected data on axial stiffnesses of resin bonded steel bolts

Table 6.1 Depth into roof beyond which slip cannot be prevented

Table 10.1 Selected load points in two-element beam tests

Table 11.1 Predicted pattern rock bolt spacings

Table 12.1 Normalized pull-out strengths and system axial stiffnesses

Table 14.1 Cavern conditions (after Hibino, Motojima, and Kanagawa)

FIGURES

Figure 1.1 Classification of interior rock fixtures according to Scott (1)

Figure 1.2 Swedish PERFO system

Figure 1.3 Installation of most common type of rebar-resin passive fixture

Figure 1.4 Wooden dowels used to support poor roof ahead of long-wall coal face

Figure 1.5 Passive cable systems to support backs and hanging walls in large scale, underground, hard rock mining

Figure 2.1 Effect of temperature on a filled polyester resin

Figure 2.2 Typical in-situ rock bolt pull out test system

Figure 2.3 Borehole roughnesses used in assessing effect of roughness on bolt pull out strength

Figure 2.4 Load vs. Deflection from pull out tests on bolts installed in holes of different roughnesses (see Fig. 2.3)

Figure 2.5 Reduction in equivalent axial stiffness of full column resin bolts as a function of annulus thickness

Figure 2.6 Shearing of a full column resin grouted bolt along a natural joint

Figure 2.7 Beam on an elastic foundation model used to derive expression for shear stiffness of a full column resin grouted bolt

Figure 2.8 Reduction in shear stiffness of full column resin grouted bolt as a function of annulus thickness

Figure 2.9 Shear stress transmission into grout and rock from axial loading of a grouted bolt

Figure 2.10 Theoretical shear stress distributions along a grouted anchor

Figure 2.11 Finite element mesh used with ADINA code to model rock bolt subject to axial and shear loads

Figure 2.12 Effect of rock and bolt moduli on extent of shear stress transfer along rock/grout interface

Figure 2.13 Measured axial strains in resin-grouted bolt loaded to 20 kN in chalk, limestone and concrete

Figure 2.14 Measured bending strains in resin grouted bolt after 0.10 in. of shear displacement

Figure 2.15 Axial bolt force distributions measured in cement grouted, untensioned bolt in the Kiirunavaara Mine, Sweden

Figure 3.1 Development of bolt loads and interface stresses during joint shearing

Figure 3.2 Illustration of tension-stiffening effect

Figure 3.3 Shear resistance of a bolted joint as a function of angle of installation

Figure 3.4 Deformation of a dowel in shear

Figure 3.5 Free body diagram for a dowel in shear

Figure 3.6 Styles of failure assumed to occur in the grout or rock during shear of a bolted joint (expanding cylinder model in a elastic-brittle-plastic material)

Figure 3.7 Distribution of dowel forces after shear displacement

Figure 3.8 Distribution of tensile forces in bolt after shear displacement

Figure 3.9 Comparison of Dight's theory with experimental data

Figure 3.10 Comparison of Dight's theory with experimental data

Figure 3.11 Comparison of Dight's theory with experimental data

Figure 4.1 Two bolted rock masses analysed by Pande and Gerrard's equivalent materials model

Figure 4.2 Pande and Gerrard's rheological analogue of a bolted jointed rock mass

Figure 4.3 Results of sensitivity analysis of bolted pillar

Figure 4.4 Discrete element analysis of stability of tunnel in blocky ground

Figure 4.5 Detailed discontinuity mapping required for keyblock analysis

Figure 5.1 Roof fall resting on floor may not provide clear evidence of failure mechanics

Figure 5.2 Failure of roof block bounded by discrete geological discontinuities

Figure 5.3 Roof fall in region of "disturbed" geology - roll in roof seam, slickensiding and drawslates

Figure 5.4 Clay vein in slickensided roof

Figure 5.5 Sagging and failure in multiple layer roofs bounded by bedding planes

Figure 5.6 Sagging and failure of multiple layer, cross-jointed roofs bounded by bedding planes

Figure 5.7 Development of new fracture surfaces due to high lateral stresses and pillar punching into roof

Figure 6.1 Two major categories of roof: (a) layered strata without cross-joints, (b) layered strata with cross-joints

Figure 6.2 Effect of relative flexural stiffnesses and positions of layers on roof response. Flexural stiffness of beam A less than flexural stiffness of beam B.

Figure 6.3 Average normal stress required to eliminate interface slip for different roof spans and effective friction angles

Figure 6.4 Normal stress generated by bolt loads at different distances from point of load application

Figure 6.5 Panek's chart to estimating reinforcement effect

Figure 6.6 Simple arching structure

Figure 7.1 Bending moment diagrams for various beam configurations

Figure 7.2 Normal stress over abutment:(a) elastic, no yielding,(b) yielding of rib

Figure 7.3 Forces exerted on a small element of a beam

Figure 7.4 General model for vertical "clamping" stresses over abutments

Figure 7.5 Two simulated "clamping" stress distributions

Figure 7.6 Comparison of maximum flexural tensile stresses for beam over rigid and deformable abutments (Young's modulus of abutment = Young's modulus of beam = 2000 MPa, Poisson's ratio of abutment = Poisson's ratio of beam = 0.3, specific gravity of beam = 2.5, abutment thickness = 2 m, span = 5 m, beam thickness = 0.25 m)

Figure 7.7 Effect of Young's modulus of beam and abutment on flexural tensile stresses

Figure 7.8 Distribution of flexural tensile stress over yielded, deformable abutment - influence of variables K and L. (Young's modulus of beam = Young's modulus of abutment = 2000 MPa, Poisson's ratio of beam = Poisson's ratio of beam = 0.3, specific gravity of beam = 2.5, abutment thickness = 2 m, beam thickness = 0.2 m, w = 400)

Figure 7.9 Distribution of flexural tensile stress over yielded, deformable abutment - influence of ultimate vertical stress. (Young's modulus of beam = Young's modulus of abutment = 2000 MPa, Poisson's ratio of beam = Poisson's ratio of beam = 0.3, specific gravity of beam = 2.5, abutment thickness = 2 m, span = 5 m, beam thickness = 0.25 m, K = 75%, L = 5m)

Figure 7.10 Distribution of flexural tensile stress over yielded, deformable abutment - influence of span. (Young's modulus of beam = Young's modulus of abutment = 2000 MPa, Poisson's ratio of beam = Poisson's ratio of abutment = 0.3, specific gravity of beam = 2.5, abutment thickness = 2 m, beam thickness = 0.25 m, K = 75%, L = 5 m, w = 400)

Figure 7.11 Distribution of flexural tensile stress over yielded, deformable abutment - influence of abutment thickness. (Young's modulus of beam = Young's modulus of abutment = 2000 MPa, Poisson's ratio of beam = Poisson's ratio of abutment = 0.3, specific gravity of beam = 2.5, span = 5 m, beam thickness = 0.25 m, K = 75%, L = 5 m, w = 400)

Figure 7.12 Distribution of flexural tensile stress over yielded, deformable abutment - influence of Young's modulus of abutment. (Young's modulus of beam = 2000 MPa, Poisson's ratio of beam = Poisson's ratio of abutment = 0.3, beam span = 5 m, beam thickness = 0.25 m, abutment thickness = 2 m, specific gravity of beam = 2.5, K = 75%, L = 5 m, w = 400)

Figure 7.13 Distribution of flexural tensile stress over yielded, deformable abutment - influence of beam thickness. (Young's modulus of beam = Young's modulus of abutment = 2000 MPa, Poisson's ratio of beam = Poisson's ratio of abutment = 0.3, beam span = 5 m, abutment thickness = 2 m, K = 75%, L = 5 m, ultimate abutment stress equivalent to 100 m of overburden depth)

Figure 7.14 Distribution of flexural tensile stress over yielded, deformable abutment - influence of Young's modulus of beam. (Young's modulus of abutment = 2000 MPa, Poisson's ratio of beam = Poisson's ratio of abutment = 0.3, beam span = 5 m, abutment thickness = 2 m, beam thickness = 0.25 m, K = 75%, L = 5 m, w = 400)

Figure 7.15 Suggested reinforcement of roof beam above yielded, deformable abutment by non-tensioned, resin bolting

Figure 8.1 Roof displacement vs. bolt shear stiffness for a 4-layer roof, 6.1 m span, total thickness 40.6 cm. for zero shear stiffness of bedding planes (after (1))

Figure 8.2 Bedding plane slip - method 1

Figure 8.3 Slip between two beams of equal thickness and properties - method 2

Figure 8.4 Interlayer slip along different types of roof beam (span = 5 m, beam thickness = 0.25 m, thickness of abutment = 2 m, Young's modulus of beam and abutment = 2000 MPa, Poisson's ratio of beam and abutment = 0.3, specific gravity of rock = 2.5)

Figure 8.5 Effect of geometric and rock properties on distribution of interlayer slip for beams resting on deformable abutments

Figure 8.6 Variation of position of maximum interlayer slip with span for uniformly loaded beam resting on deformable abutments (beam thickness = 0.25 m, specific gravity of rock = 2.5, thickness of abutment = 2 m, Young's modulus of beam and abutment = 2000 MPa, Poisson's ratio of beam and abutment = 0.3)

Figure 8.7 Variation of position of maximum interlayer slip with abutment thickness for uniformly loaded beam resting on deformable abutments (beam thickness = 0.25 m, specific gravity of rock = 2.5, span = 5 m, Young's modulus of beam and abutment = 2000 MPa, Poisson's ratio of beam and abutment = 0.3)

Figure 8.8 Variation of position of maximum interlayer slip with Young's modulus of abutment for uniformly loaded beam resting on deformable abutments (beam thickness = 0.25 m, specific gravity of rock = 2.5, span = 5 m, Young's modulus of beam = 5000 MPa, Poisson's ratio of beam and abutment = 0.3)

Figure 8.9 Variation of position of maximum interlayer slip with Young's modulus of beam for uniformly loaded beam resting on deformable abutments (beam thickness = 0.25 m, specific gravity of rock = 2.5, span = 5 m, Young's modulus of abutment = 2000 MPa, Poisson's ratio of beam and abutment = 0.3)

Figure 8.10 Variation of position of maximum interlayer slip with beam thickness for uniformly loaded beam resting on deformable abutments (specific gravity of rock = 2.5, span = 5 m, Young's modulus of beam and abutment = 2000 MPa, Poisson's ratio of beam and abutment = 0.3)

Figure 8.11 Magnitudes of interlayer slip for different cases (span = 10 m, specific gravity of rock = 2.5, abutment thickness = 2 m, beam thickness = 0.25 m, Young's modulus of beam and abutment = 2000 MPa, Poisson's ratio of beam and abutment = 0.3)

Figure 8.12 Effect of span on maximum value of slip for a built-in beam under uniform loading (beam thickness = 0.25 m, Young's modulus = 2000 MPa, specific gravity of beam = 2.5)

Figure 8.13 Effect of Young's modulus on maximum value of slip for a built-in beam under uniform loading (beam thickness = 0.25 m, beam span = 5 m, specific gravity of beam = 2.5)

Figure 8.14 Effect of beam thickness on maximum value of slip for built-in beams (beam span = 5 m, Young's modulus = 2000 MPa, specific gravity of beam = 2.5)

Figure 8.15 Effect of load intensity at centre of parabolically loaded built-in beam on maximum value of slip (span = 5 m, beam thickness = 0.25 m, Young's modulus of beam = 2000MPa, specific gravity of beam = 2.5)

Figure 8.16 Two-beam model to test reinforcement hypothesis

Figure 8.17 Effect of bolt location on reinforcement

Figure 8.18 Various multiple bolt patterns tested in 2-beam model

Figure 8.19 Reduction in beam deflection for the various bolt patterns illustrated in Figure 8.17

Figure 8.20 Effect of number of bolts on beam deflection

Figure 9.1 Distribution of shear stress in a beam, depth d (A = upper surface, B = lower surface)

Figure 9.2 Two beams of equal thickness reinforced with non-tensioned, resin-grouted bolts

Figure 9.3 Multilayered beam with ubiquitous bedding planes reinforced with non-tensioned, resin-grouted bolts

Figure 9.4 Pattern of non-tensioned, resin-grouted bolts assumed for reinforcement analysis

Figure 9.5 Parabolically loaded beam

Figure 9.6 Bearing capacity failure beneath a resin-grouted bolt

Figure 9.7 Bearing capacity failure beneath a footing

Figure 9.8 Effect of yield stress of bolt material on required bolt spacing for a square pattern (for other parameters see text)

Figure 9.9 Effect of bolt diameter on required bolt spacing for a square pattern (for other parameters see text)

Figure 9.10 Effect of annulus thickness of required bolt spacing for a square pattern (for other parameters see text)

Figure 9.11 Effect of uniaxial compressive strength of rock on required bolt spacing for a square pattern (for other parameters see text)

Figure 9.12 Effect of uniaxial compressive strength of grout on required bolt spacing for a square pattern (for other parameters see text)

Figure 9.13 Effect of effective friction angle of rock on required bolt spacing for a square pattern (for other parameters see text)

Figure 9.14 Effect of effective friction angle of grout on required bolt spacing for a square pattern (for other parameters see text)

Figure 9.15 Effect of span on required bolt spacing for a square pattern (for other parameters see text)

Figure 9.16 Effect of rock density on required bolt spacing for a square pattern (for other parameters see text)

Figure 9.17 Effect of ratio of tensile force in bolt to yield strength of bolt on required rock bolt spacing for a square pattern (for other parameters see text)

Figure 9.18 Effect of non-uniform loading on required bolt spacing for a square pattern (for other parameters see text)

Figure 9.19 Required bolt spacing along row vs. bolt spacing along opening for two different spans (for other parameters see text)

Figure 9.20 Average bolt spacing in row vs. degree of reinforcement, RF, (spacing along opening = 1.75 m; 1 = bolt diameter, 1.9 cm; hole diameter = 2.54 cm; 2 = bolt diameter, 2.54cm; hole diameter, 3.18 cm; for other parameters see text)

Figure 9.21 Design options for (a) 3.18 cm. diameter and (b) 2.54 cm. diameter bolts

Figure 9.22 "Cohesion" of a bolted joint

Figure 10.1 Idealized cross-section of roof with vertical cross-joints

Figure 10.2 "Gyproc" beam in vice ready for fracturing

Figure 10.3 Rough tensile fracture formed in "Gyproc"

Figure 10.4 Frame for testing of cross-jointed roof beams

Figure 10.5 Sequence of photographs showing development of ultimate collapse in cross-jointed roof beams as span was increased

Figure 10.6 2-hinge collapse mechanism

Figure 10.7 Kinematics of 2-hinge collapse mechanism

Figure 10.8 Sequence of hinges examined in computer program

Figure 10.9 Relationship between initial Factor of Safety of roof beam and uniaxial compressive strength of intact roof beam rock (for variables assumed see Section 10.4.1) (0 max. Factor of Safety, 0 min. Factor of Safety)

Figure 10.10 Relationship between initial Factor of Safety of roof beam and uniaxial compressive strength of crushed rock (for variables assumed see Section 10.4.1) (0 max. Factor of Safety, 0 min. Factor of Safety)

Figure 10.11 Relationship between initial Factor of Safety of roof beam and roof beam thickness (for variables assumed see Section 10.4.1) (0 max. Factor of Safety, 0 min. Factor of Safety)

Figure 10.12 Relationship between initial Factor of Safety of roof beam and roof beam span (for variables assumed see Section 10.4.1) (0 max. Factor of Safety, 0 min. Factor of Safety)

Figure 10.13 Relationship between initial Factor of Safety of roof beam and force/weight multiplier (for variables assumed see Section 10.4.1) (0 max. Factor of Safety, 0 min. Factor of Safety)

Figure 10.14 Differential slip between beds in hinge element

Figure 10.15 Relative shear displacement vs. hinge rotation for beds of different thicknesses, b.

Figure 10.16 (a) Stable roof from development of flat arch,
(b) Unstable roof due to gravity collapse

Figure 10.17 Experimental principle for bolted, cross-jointed beam test

Figure 10.18 General experimental arrangement of two-layer, cross-jointed beam configuration

Figure 10.19 Individual block rotations of cross-jointed beam during "sagging" of roof

Figure 10.20 Interaction of asperities along contact between two rotating blocks

Figure 10.21 Two-element structure for investigating influence of joint roughness

Figure 10.22 Three types of joint roughness tested

Figure 10.23 Testing frame for investigating influence of joint roughness

Figure 10.24 Typical load vs. time curve for beam with central joint

Figure 10.25 Sequence of photographs from a single test of beam with central joint

Figure 11.1 Four basic types of support provided by pattern bolting

Figure 11.2 Distribution of normal stresses beneath bolt plate

Figure 11.3 Mohr circles of stress for element of rock mass before and after bolting

Figure 11.4 Predicted failure envelope for lithified argillaceous rocks for normal stresses less than 4 MPa

Figure 11.5 Predicted failure envelope for lithified argillaceous rocks for normal stresses less than (a) 200 kPa, (b) 10 kPa

Figure 11.6 Failure envelope constants m and s and their relationship to RMR and NGI rock mass classifications (after Hoek and Brown (3))

Figure 11.7 Scatter diagram of failure envelope constants m and s

Figure 11.8 Percentage increase in rock mass strength vs. rock bolt spacing for various RMR values

Figure 11.9 Percentage increase in rock mass strength vs. rock bolt spacing for various Q values

Figure 11.10 Percentage increase in rock mass strength vs. rock bolt spacing for various uniaxial compressive strength values

Figure 11.11 Percentage increase in rock mass strength vs. rock bolt spacing for various m values

Figure 11.12 Percentage increase in rock mass strength vs. rock bolt spacing for various bolt diameters

Figure 11.13 Tangential strength of rock in zone of uniform compression, MPa

Figure 11.14 Strength of rock mass/m length of bolt

Figure 12.1 Ground convergence and support reaction curves (a) Normal stress, p_o, at B prior to excavation, (b) Ground convergence curves for stable and unstable cases, (c) Support reaction curve and point of equilibrium with ground convergence curve

Figure 12.2 Effect of face on roof convergence

Figure 12.3 Effect of timing and support stiffness: (a) High stiffness support placed early, (b) Low stiffness support placed late (line 1 = unstable ground convergence curve, line 2 = stable ground convergence curve)

Figure 12.4 Ground convergence curve for a single, clamped, elastic beam, (a) p_o vs. u, (b) (p/p_o) vs. (u/u_{max})

Figure 12.5 Relationship between ground convergence, required support pressure, and distance from face

Figure 12.6 Relationship between ground convergence, required support pressure, and distance from face for failed and unfailed roof beams

Figure 12.7 Effect of rock bolt spacing on normalized support reaction curve

Figure 12.8 Effect of rock bolt diameter on normalized support reaction curve

Figure 12.9 Effect of Young's modulus of bolt material on normalized support reaction curve

Figure 12.10 Effect of Young's modulus of rock on normalized support reaction curve

Figure 12.11 Effect of roof span on normalized support reaction curve

Figure 12.12 Effect of roof beam thickness on normalized support reaction curve

Figure 12.13 Effect of anchorage length on normalized support reaction curve

Figure 12.14 Comparison of normalized support reaction curve of an ungrouted, point anchor system and a grouted bolt system

Figure 12.15 Roof strata conditions for design problem

Figure 12.16 Ground convergence-support reaction analysis of layer #1, lower bound on equivalent density

Figure 12.17 Ground convergence-support reaction analysis of layer #1, upper bound on equivalent density

Figure 12.18 Ground convergence-support reaction analysis of layer #5, lower bound on equivalent density

Figure 12.19 Ground convergence-support reaction analysis of layer #5, upper bound on equivalent density

Figure 12.20 Ground convergence-support reaction analysis of layer #1 at intersection, upper bound on equivalent density

Figure 12.21 Assumed pre-failure and post-failure state of roof layer

Figure 12.22 Ground convergence-support reaction analysis for a layer which fractures after bolt installation

Figure 13.1 Results from laboratory direct shear box tests on bolted joints (after (1))

Figure 13.2 Results from laboratory direct shear box tests on bolted joints (after (2))

Figure 13.3 Exploiting tensile behaviour of bolt by appropriate inclination of bolts in bedded mine roof

Figure 13.4 Development of tensile load in inclined bolt due to differential slip along bolted joint

Figure 13.5 Shear strength developed by components of tensile load in bolt

Figure 13.6 Dowel force, F, developed by bolt during differential slip along bolted joint

Figure 13.7 Component of dowel force along shear plane as a function of angle between joint and bolt

Figure 13.8 Laboratory testing arrangement used to examine influence of bolt inclination on roof beam reinforcement

Figure 14.1 (a) Bolts anchored into well-defined, massive bed
(b) Bolts anchoring well-defined wedge

Figure 14.2 Stresses and displacements around a rectangular opening in horizontally bedded strata. Upper diagram - Trajectories of principal stress ($_v$ ^{o} = initial vertical normal stress; v = induced vertical normal stress). Lower diagram - zones of disturbance above roof: I = Differential sag leading to bed separation, II = Layer sag without bed separation and reduced horizontal stress, III = Horizontal and vertical pressures build-up to their undisturbed values. (Modified from Fairhurst and Singh (18)).

Figure 14.3 Relationship between elliptical geometry and applied principal stresses.

Figure 14.4 Maximum roof volume requiring support.

Figure 14.5 Maximum and reduced roof volumes requiring support.

Figure 14.6 Relationship between maximum weight of roof requiring support and opening height (k = vertical/horizontal stress ratio = 2, span = 5 m, rock density = 2400 kg/cu.m.).

Figure 14.7 Relationship between maximum weight of roof requiring support and span (k = vertical/horizontal stress ratio = 2, opening height = 2.5 m, rock density = 2400 kg/cu.m.).

Figure 14.8 Relationship between maximum weight of roof requiring support and in-situ stress ratio (opening height = 2.5 m, span = 5 m, rock density = 2400 kg/cu.m.).

Figure 14.9 Relationship between weight of roof requiring support and CSIR Rock Mass Rating (k = vertical/horizontal stress ratio = 2, opening height = 2.5 m, span = 5 m, rock density = 2400 kg/cu.m.).

Figure 14.10 Variation of roof support volumes with opening height. (CSIR Rock Mass Rating = 50, rock density = 2400 kg/cu.m.).

Figure 14.11 Variation of roof support volumes with span (CSIR Rock Mass Rating = 50, rock density = 2400 kg/cu.m.).

Figure 14.12 Variation of roof support volumes with in-situ stress ratio (CSIR Rock Mass Rating = 50, rock density = 2400 kg/cu.m.).

Figure 14.13 Variation of roof support volumes with CSIR Rock Mass Rating (rock density = 2400 kg/cu.m.).

Figure 14.14 Ellipsoid of motion of granular particles above an open trap door (after Kvapil (17)).

Figure 14.15 Relationship between rock load height and span (____ equation (10), after Unal (2); _____ elliptical theory).

Figure 14.16 Relationship between maximum height of rock load arch and span/height ratio (____ span = 6 m; ____ span = 12 m; k = vertical/horizontal principal stress ratio, rock density = 2400 kg/cu.m., CSIR Rock Mass Rating = 50).

Figure 14.17 Relationship between maximum height of rock load arch and span/height ratio (____ span = 6 m; ____ span = 24 m; k = Horizontal/vertical principal stress ratio, rock density = 2400 kg/cu.m., CSIR Rock Mass Rating = 50).

Figure 14.18 Relationship between height of zone requiring support and span/height ratio for different CSIR Rock Mass Rating and spans of 5 m and 8 m (k = vertical/horizontal principal stress ratio = 2, opening height = 2.5 m, rock density = 2400 kg/cu.m.).

Figure 14.19 Relationship between height of zone requiring support and span/height ratio for different CSIR Rock Mass Rating (span = 5 m, k = vertical/horizontal principal stress ratio = 2, rock density = 2400 kg/cu.m.).

Figure 14.20 Effect of four-way intersection and rib failure on height of roof zone requiring support (k = vertical/horizontal principal stress ratio = 2, opening height = 2.5 m, CSIR Rock Mass Rating = 50, rock density = 2400 kg/cu.m.).

Figure 14.21 Effect of overstoping of rectangular opening on height of roof zone requiring support (k = vertical/horizontal principal stress ratio = 2, opening height = 2.5 m, span = 5 m, CSIR Rock Mass Rating = 50, rock density = 2400 kg/cu.m.).

Figure 14.22 Observed fracture orientations in failed stope back at Tsumeb Mine (after Stheeman (7)).

Figure 14.23 Relationship between height of void migration and span between coal pillars (o = arching in silty mudstones; o = arching in sandstones) (after Walton and Taylor (8)).

Figure 14.24 Vertical movements in roofs above large caverns (after Hibino, Motojama, and Kanagawa (13)).

Figure 14.25 Effect of rock bolt orientation on total length of bolts.

Figure 15.1 Example of non-uniform bolt lengths.

Figure 15.2 Conceptual design using various principles - non-uniform spacing, different lengths, inclined.

APPENDICES

APPENDIX A1 Estimating axial, bending and shear stiffness of a full column resin bolt

APPENDIX A2 Shear stiffness of a resin bolt incorporating rock and bolt properties, bolt inclination and bed separation

APPENDIX B Shear strength data from direct shear tests of resin bolted joints

APPENDIX C Beam equations for built-in beam with parabolic load distribution

APPENDIX D A new method for determining the degree of reinforcement of layered strata supported by non-tensioned, resin-grouted bolts

APPENDIX E Derivation of stability equations describing 2-hinge collapse mechanism in layered cross-jointed roofs

APPENDIX F Elliptical theory for determining rock bolt loadings and bolt lengths

APPENDIX G A laboratory rock bolt pull-out tester

APPENDIX H Suggested methods for estimating the reduced or effective Young's modulus of a cross-jointed roof and its application in layered roof stability analysis

APPENDIX I Ground convergence curve for a layer above a rectangular opening

APPENDIX J Axial stiffness of a grouted bolting pattern in laminated strata

APPENDIX FIGURES

Figure A1.1 Bolt subjected to direct shear

Figure A1.2 Cross section of bolt and assumed loading

Figure A2.1 Displacement of an inclined bolt subjected to direct shear along an open joint

Figure A2.2 Determination of foundation modulus of bolt

Figure A2.3 Effect of bolt inclination on shear stiffness for three joint openings (Young's modulus of rock = 20 GPa, Young's moduus of grout = 2 GPa,Young's modulus of bolt = 207 GPa, bolt diameter = 1.9 cm, hole diameter = 2.5 cm)

Figure A2.4 Effect of Young's modulus of rock on shear stiffness for three joint openings (Young's modulus of grout = 2 GPa, Young's modulus of bolt = 207 GPa, bolt diameter = 1.9 cm, hole diameter = 2.54 cm, bolt inclination = 90 deg.)

Figure A2.5 Effect of Young's modulus of bolt on shear stiffness for three joint openings (Young's modulus of rock = 20 GPa, Young's modulus of grout = 2 GPa, bolt diameter = 1.9 cm, hole diameter = 2.54 cm, bolt inclination = 90 deg.)

Figure A2.6 Effect of bolt diameter on shear stiffness for three joint openings (Young's modulus of rock = 20 GPa, Young's modulus of grout = 2 GPa, Young's modulus of bolt = 207 GPa, resin annulus thickness = 0.32 cm, bolt inclination = 90 deg.)

Figure A2.7 Effect of thickness of grout annulus on shear stiffness for three joint openings (Young's modulus of rock = 20 GPa, Young's modulus of grout = 2 GPa, Young's modulus of bolt = 207 GPa, bolt diameter = 1.9 cm, bolt inclination = 90 deg.)

Figure A2.8 Effect of Young's modulus of grout on shear stiffness for three joint openings (Young's modulus of rock = 20 GPa, Young's modulus of bolt = 207 GPa, bolt diameter = 1.9 cm, hole diameter = 2.54 cm, bolt inclination = 90 deg.)

Figure B1 Large shear box for testing rock bolted joints (after (1))

Figure B2 Shear behaviour of bolted joints in limestone and shale (5/8 in. conventional bolt, 7/8 in. grouted rebar in 1 and 3/8 in. holes) (after (2)).

Figure B3 Shear behaviour of bolted joints in limestone and shale (5/8 in. conventional bolt, 7/8 in. grouted rebar in 1 and 3/8 in. holes) (after (2))

Figure B4 Shear behaviour of bolted joints installed at various angles (after (5)).

Figure B5 Effect of installation angle on shear strength of bolted joints (after (6))

Figure C1 Two roof beam cases examined

Figure D1 Section of beam with moments acting

Figure D2 Assumed rock bolt pattern for reinforcement analysis

Figure E1 Schematic illustration of 2-hinge failure mechanism

Figure E2 Kinematics of one hinge

Figure E3 Geometry and forces acting on a single hinge

Figure E4 Assumed distribution of horizontal thrust

Figure E5 Method for estimating new value of x_{cc}

Figure F1 Rectangle bounded by ellipse when major principal stress horizontal - terminology

Figure F2 Deriving equation for roof volume - major principal stress horizontal

Figure F3 Rectangle bounded by an ellipse when major principal stress is vertical - terminology

Figure F4 Deriving equation for roof volume - major principal stress vertical

Figure H1 Jointed beam analysed by Olson (1)

Figure H2 Deflections of a fixed end beam for various joint set spacings at 60-120 deg. joint set angles

Figure H3 Relationship between (S_j/S_s) and (d/D)

Figure H4 Deflections of a fixed end beam for various joint set angles at 8 inch joint set spacing

Figure H5 Relationship between joint angle and maximum deflection

Figure H6 (E_j/E_i) vs. (d/D) relationship

Figure I1 Roof deflection and distance from face

Figure I2 Rectangular plate

Figure I3 Roof displacement vs. distance from face

Figure I4 Ground reaction curve for a beam

Figure I5 Ground reaction curve and timing of installation

Figure J1 Bolt spacing

Figure J2 Support reaction curve

CHAPTER 1

INTRODUCTION

1.1 SAFETY AND ROOF SUPPORT

The main cause of underground fatalities and disabling injuries continues to be roof falls. While the "cost" of these accidents to the victims and their families as measured by any criteria is the pre-eminent and overwhelming concern, the "cost" to the mining companies justifies a continuous effort to reduce the risk of injury from roof falls. "Costs" to the company include those of persons involved in investigations, hearings and in some cases, litigation proceedings, clean-up of roof fall(s), damage to equipment, loss of production, rescheduling of mining crews, and adverse publicity.

In many cases, the cost of clean-up alone could justify the salary of a rock mechanics specialist and instrumentation to provide improved quality control, design and monitoring of roof support systems. Estimates range from $140.00-$280.00 per cubic metre ($4.00-$8.00 per cubic foot). Thus, a roof fall measuring 5 m x 5 m x 2 m would penalize the company by $7,000.00-$14,000.00 on the basis of clean-up costs alone.

Following a roof fall, production in the affected section is immediately curtailed until normal working conditions can be re-established. What is perhaps less commonly realized is that production in the mine after the operation has been returned to "normality" may undergo a marked reduction from pre-fall values. In one case history (1) from the U.S.A. a section averaging 573 tons per shift, before a fatal roof fall, produced an average of only 392 tons per shift for a period greater than 30 days after the fall, i.e., a 32% reduction.

Equipment on which a roof fall has collapsed may be permanently damaged or, more likely, put out of production for days, or weeks, for repairs. If the only machinery available to move a fall of dense and strong roof rock was originally intended and designed to excavate coal, it may be damaged during the clean-up operation itself.

In the face area the development of temporary automated supports (2), which can be remotely operated by the miner from a safe, protected vantage point, will significantly reduce the exposure of miners to roof fall hazards. Similarly, improvements in remote sensing (3) to detect potential roof hazards ahead of mining will ensure additional protection. However, because mining is a dynamic process and because the physical properties of rock are subject to change with time, stress, and exposure, concern about roof stability does not cease after long-term supports are installed to replace the temporary support measures. Serious roof falls can occur many months after mining, particularly at drift or roadway intersections, and if they disrupt a travel road, or main ventilation road, the effects on mine production can be considerable. In the worst case the mine may have to shut down temporarily until improved and approved long-term support is installed, or until a modified or different mining method giving better ground control is implemented.

Because purchasing agents of companies tend to think in terms of the cost of the support only, e.g., steel beam, rockbolt, shotcrete, the true cost of roof control is probably completely known by only a few companies. Thus, while a 50-cent reduction in the unit cost of 25,000 support fixtures saves the company $12,500.00, the prevention of even one moderately sized roof fall through use of the most appropriate and high quality support can often justify the additional expense involved.

1.2 TYPES OF ROOF SUPPORT

The mining or geological engineer has two broad classes of roof support systems to choose from - external systems, such as steel sets, Moll arches, timber and hydraulic props, and internal systems, which include rock bolts and dowels. Some techniques, such as the roof truss (4), combine elements of both systems.

Internal support systems provide a number of operational advantages over external supports where the application of either would be possible and appropriate. Internal supports do not reduce the effective size of opening and cannot interfere with, or be demolished by, the manoevering of mining equipment. These, and other practical advantages, such as the relative ease of transportation in the mine and installation, have made the manufacture of internal roof supports a large industry. Billions are installed annually throughout the world at a cost of billions of dollars. In the U.S.A. the coal industry, for example, uses approximately 85 million per year, considerably more than the metal mining and construction industries (about 7 million).

A major drawback of internal support systems is that they do not generally provide early-warning signs of overloading, such as found so beneficial to the miner working under external supports, e.g., bending (steel beams), audible splitting (timber), and cracking (concrete). A practical means of instrumenting internal support systems on a routine basis has yet to be devised.

1.3 TYPES OF INTERNAL SUPPORT

The general term "bolting" is widely used when referring to any form of internal support which involves the anchoring of a bar, usually of steel, in a hole drilled into the rock mass. However, use of this term tends to obscure important differences between the mechanisms by which different types of internal support systems reinforce and support the rock mass. For this reason, it has been suggested (5) that there be a distinction made between "bolts" (sensu stricto) in which the member is anchored to the rock at distinct points and tensioned during installation, and "dowels" in which the member is anchored throughout its length and is not tensioned during installation. However, this nomenclature could also lead to some confusion, and so the author prefers the categorization suggested by Scott (1) between active and passive fixtures:

Active Fixture - one that loads the geologic mass in which it is placed immediately upon installation;

Passive fixture - one that is placed in the geologic mass and does not play a role in ground support until the mass moves and subsequently loads the fixture.

The term "fixture" used by Scott replaced the work "bolt", since, as he correctly notes, many roof support devices are not bolts in the sense commonly understood, i.e., a head and threaded shaft onto which a nut is mounted and tightened.

Further subdivision is possible on the basis of other features (e.g., point anchor vs. full contact, axial vs. radial loading), and can be used to develop a detailed classification such as Scott's (Fig. 1.1).

Another group that has seen the need to develop a standard nomenclature, which clearly distinguishes the different types of reinforcement and their modes of action, is the Australian Mineral Industries Research Association (AMIRA). The scheme shown in Table 1.1 has been adopted as a standard by AMIRA (5).

According to Scott's and AMIRA's nomenclature non-tensioned, fully resin grouted fixtures, which are the topic of this report, are classified as a full contact, passive, system, (Scott) or bonded dowels (AMIRA).

1.4 FULL CONTACT, PASSIVE OR BONDED DOWEL SYSTEM

Full contact, passive systems are an alternative to point anchor, active fixtures when the latter are unable to develop strong anchorage in the rock (the deficient anchorage would be revealed by pull-out tests), as, for example, in weathered rocks,

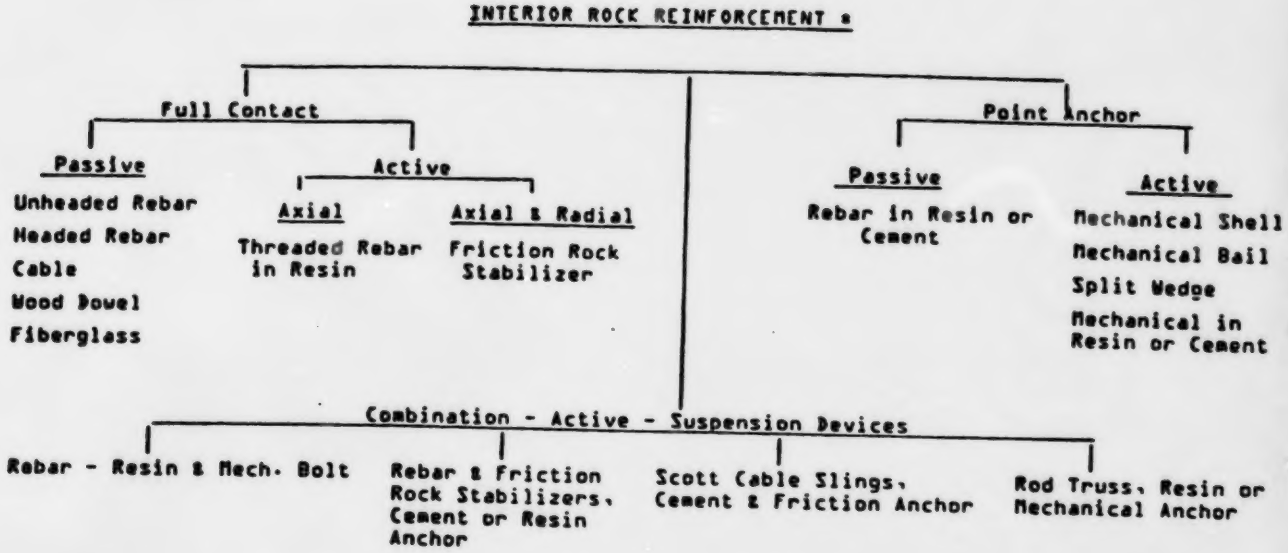
INTERIOR ROCK REINFORCEMENT *
Full Contact
Passive
Unheaded Rebar
Headed Rebar
Cable
Wood Dowel
Fiberglass
Active
Axial
Threaded Rebar in Resin
Axial & Radial
Friction Rock Stabilizer
Point Anchor
Passive
Rebar in Resin or Cement
Active
Mechanical Shell
Mechanical Bail
Split Wedge
Mechanical in Resin or Cement
Combination - Active - Suspension Devices
Rebar - Resin & Mech. Bolt
Rebar & Friction Rock Stabilizers, Cement or Resin Anchor
Scott Cable Slings, Cement & Friction Anchor
Rod Truss, Resin or Mechanical Anchor

Figure 1.1 Classification of interior rock fixtures according to Scott (1)

Item	Recommended Term	Comments/Definitions
1. Types of Reinforcement	Bolt	Initially fixed to the rock at distinct anchorage points and carrying an axial tensile load induced into the shank at installation
	Dowel	Bonded to the rock along its entire length but not tensioned at installation.
2. Types of Bolt	Conventional Rock Bolt	Fixed to the rock at distinct anchorage points, tensioned at installation. Applies an active load to the rock. Shank is a rigid bar.
	Cable Bolts	As above shank formed from one or more flexible wires or strands.
	Bonded Bolt	Bonded to the rock along its entire length after establishment of anchorage points and tensioning. Applies an active load to the rock and has a high passive resistance to movement.
3. Types of Bolt Anchorage	Slot & Wedge Anchorage	Bolt has slotted end. Driving bolt over wedge against hole end achieves anchorage. Only for rigid bolts. No good for cable bolts.
	Expansion Shell Anchorage	Bolt has threaded end. Plug moving down thread expands shell against wall of hole. Various types of shell include regular type, ball type, sliding wedge type. Only for rigid bolts. No good for cable bolts.
	Cone & Sleeve Anchorage	Bolt or cable has cone shaped wedge on end. Pulling through sleeve or expansion shell expands anchorage.

Table 1.1 Rock reinforcement nomenclature adopted by the Australian Mineral Industries Research Association (5)

Table 1.1 (cont)

Item	Recommended Term	Comments/Definitions
5. Types of Dowel	Cement Grouted Steel Dowel	Drill hole is filled with a viscous or thixotropic grout. A plain steel bar is hammered into the grout and wedged into position during hardening. A ribbed bar may be used to give better bonding.
	Grouted Cable Dowel	A cable is anchored in the drill hole by an expanding device. The hole mouth is blocked and the hole is grouted. The grout intake tube and the de-aeration tube are installed with the cable. More than one wire or strand may be used.
	Resin Bonded Dowel	Normally referred to as having full column resin anchorage. Either i) Premixed resin is injected into the drill hole, and a reinforcement bar is driven into it, or ii) A number of resin cartridges are inserted in the hole, and a reinforcement bar with a cusped end is rotated through them.
	Wooden Dowel	As above for resin bonded dowel, but plain wooden bar is used instead of re-bar. Useful where subsequent operations include cutting in reinforced zone, such as on a coal face.
	Perfo Bolt	Not a bolt. Perforated tube filled with cement grout or mortar is inserted in drill hole and a ribbed steel bar is hammered through it, extruding the mortar through the perforations.

Table 1.1 (cont)

Item	Recommended Term	Comments/Definitions
3. Types of Bolt Anchorage (cont.)	Single Point Resin Anchorage	Bolt has scrolled or paddled end. Rotating through unmixed resin cartridge produces high bond over short length of bar.
	Explosive Anchorage	Bolt has short tube containing an explosive charge welded onto its end. Never developed into regular usage.
4. Types of Bonded Bolt	Grouted Bolt	Normally refers to a bolt anchored by any of the methods under Item 3, which is surrounded by a cement grout after tensioning. Grout may be placed before tensioning as long as latter is carried out before grout sets.
	Grouted Cable Bolt	As above for grouted bolt. Shank formed from one or more flexible wires or strands instead of a rigid bar.
	Hollow Deformed Grouted Bolt	Normally an expansion shell anchor. Double purpose use of hollow deformed bar as bolt shank and breather tube allows elimination of latter as separate installation.
	Two Speed Resin Bonded Bolt	Fast setting resin cartridge produces single point anchorage. Tension then applied to bolt. Slow setting resin cartridges bond bar to rock along its entire length. All cartridges inserted before bolt which is rotated through all cartridges at the same time.

mudstones, siltstones and weak sandstones. They also provide better support where the roof is subjected to shear, and also have good corrosion and blast resistance.

An early full contact, passive system, which is still widely used in hard-rock excavations, is the PERFO bolt (Fig. 1.2), which uses cement grout. Improvements to the method of cement placement, illustrated in Figure 1.2, have been developed to increase the speed of installation.

In the late 1960's the resin grouted steel bolts were introduced and slowly displaced the steel tensioned bolt where their greater cost could be justified technically, economically, and practically. For example, Table 1.2 shows the increased use of this technique for strata reinforcement in the U.K.'s National Coal Board operations over the period 1969-1973. Scott (1) reports that fully grouted rebar fixtures have captured 30% of the coal mining roof market in the twelve to fifteen years since their introduction. Translated into numerical terms, this means 26 - 28 million units per year in the U.S.A.

In its most typical configuration the system comprises a headed rebar, which is spun into polyester resin cartridges (Fig. 1.3) inserted in the borehole. Activators mixed with the resin provide set times, ranging from as little as 20 seconds to greater than 8 minutes.

Owing to the high cost of resins, some manufacturers have developed capsules which produce a cement grout when spun in the borehole. For example, Cemicron 2000 is a British product in which the water is contained in micro-capsules which are ruptured during installation of the fixture. Other manufacturers offer capsules which must be pre-soaked in water prior to insertion in the borehole.

Unheaded rebar is used in a relatively inexpensive and easily installed pillar support system in the U.S.A.'s southeast Missouri Lead Belt (6) to protect pillars from external slabbing and fracturing. The rebar is inserted into horizontally, drilled

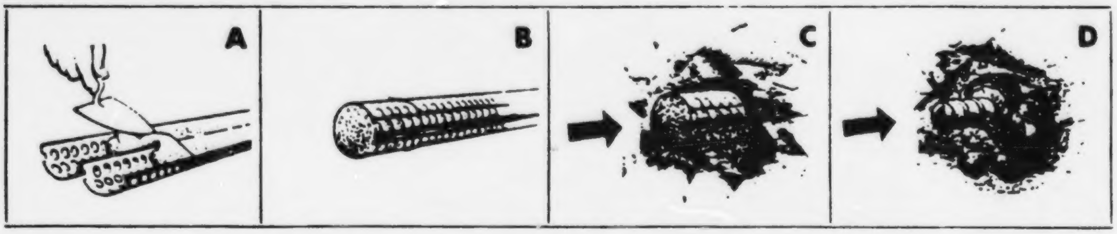

Figure 1.2 Swedish PERFO system

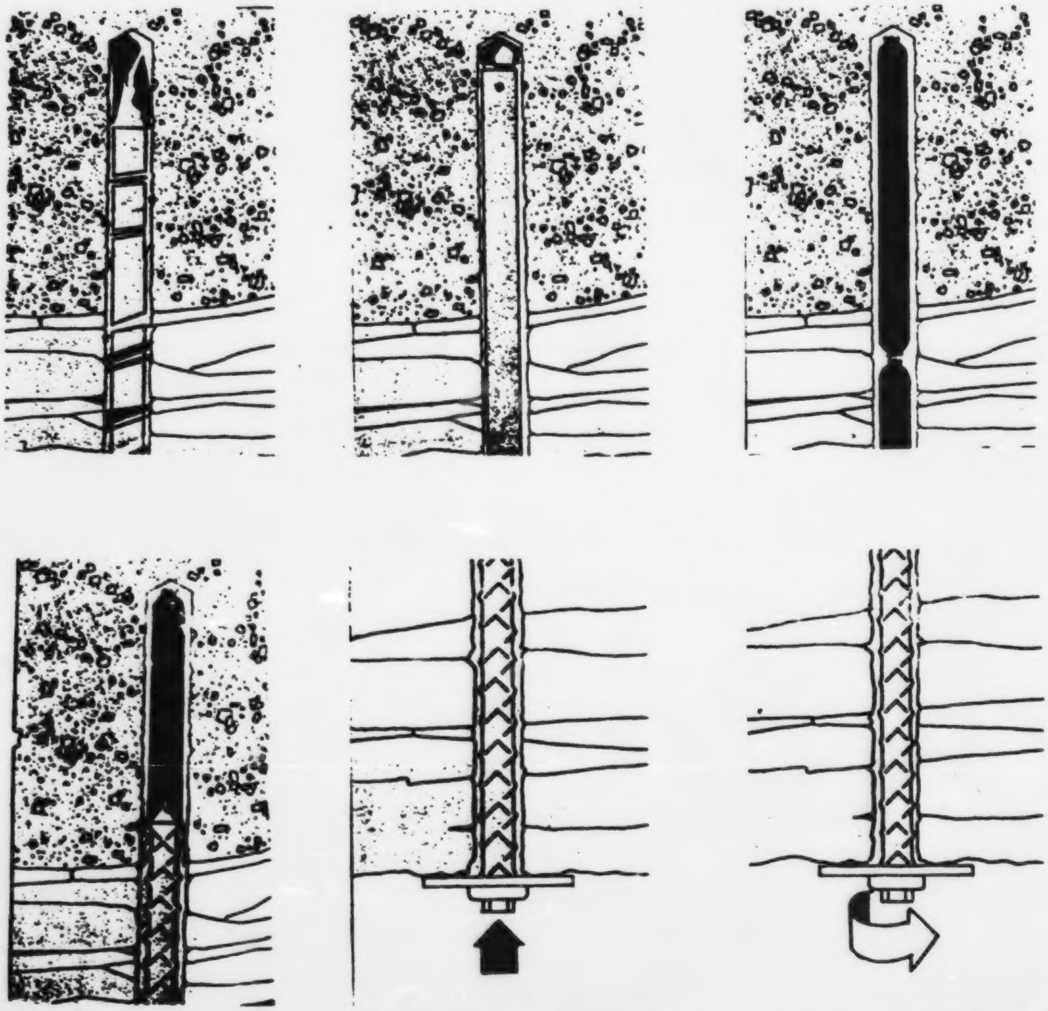

Figure 1.3 Installation of most common type of rebar-resin passive fixture

	Dowels		*Bolts*		*Wood Dowels used with Long Hole Resin Injection (6 ft lengths)*	*Yearly Totals*
Year	*Wood Resin*	*Steel Resin*	*Steel Resin*	*Steel Mechanical*		
1969	0	0	132 000	104 500	0	236 000
1970	292 000	5 120	159 000	101 000	0	557 120
1971	430 000	11 690	112 779	85 531	0	640 000
1972	449 591	36 565	91 358	65 000	0	642 524
1973	491 500	68 796	109 327	60 303	156 875	885 801

Table 1.2 **Use of different types of fixtures in National Coal Board Mines, 1969-1973 (6)**

holes which have been filled with a fluid cement-fly ash mixture.

Where ground conditions require substantial forepoling to support the strata ahead of the face and standard rebar would be inadequate, heavier steel sections may be cement-grouted into large diameter holes, e.g. 76 mm x 76 mm, 1.5 m long RSJ girders fishplated together and grouted into 114 mm diameter holes.

Cuttable forms of full contact passive systems have gained wide popularity in underground coal mining in Europe (8), where certain mining operations associated with the longwall mining method involve the cutting of reinforced strata, e.g., support of the coal face ahead of face operation (Fig. 1.4). 36 mm diameter hardwood dowels (see Table 1.2) used for such purposes in some of the U.K.'s coal mines can be purchased in 6-foot (1.83 m) or 8-foot (2.44 m) lengths and installed in tandem to provide reinforcement to depths up to 16 feet (4.88 m). Where greater shear strength is required, fibreglass dowels or hardwood dowels with a fibreglass core can be installed.

Wooden or fibreglass dowels have also found special application in helping to control wear of draw points and ore pass raises. Here their ability to wear away as the rock wears, yet to provide support to the rock along the remaining portion of the dowel, has been usefully exploited.

A closely related technology is that of injection dowelling (9) in which grout is injected under pressure around the steel or wooden/fibreglass dowel, so that not only is the dowel bonded into the hole, but any fractured strata around the borehole is infused with grout.

The development of full-contact, untensioned, passive cable support systems over the last decade represents a significant advance in strata control for large underground stoping and cut-and-fill operations (Fig. 1.5). For further information, the interested reader is referred to articles 10-12 in the Reference list.

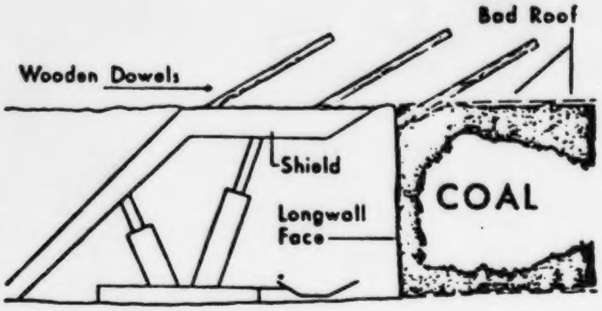
Bad Roof
Wooden Dowels
Shield
Longwall
Face
COAL

Bolting through the coal and into the roof. The longwall shearing machine can cut through the wooden dowels with ease

Figure 1.4 Wooden dowels used to support poor roof ahead of long-wall coal face

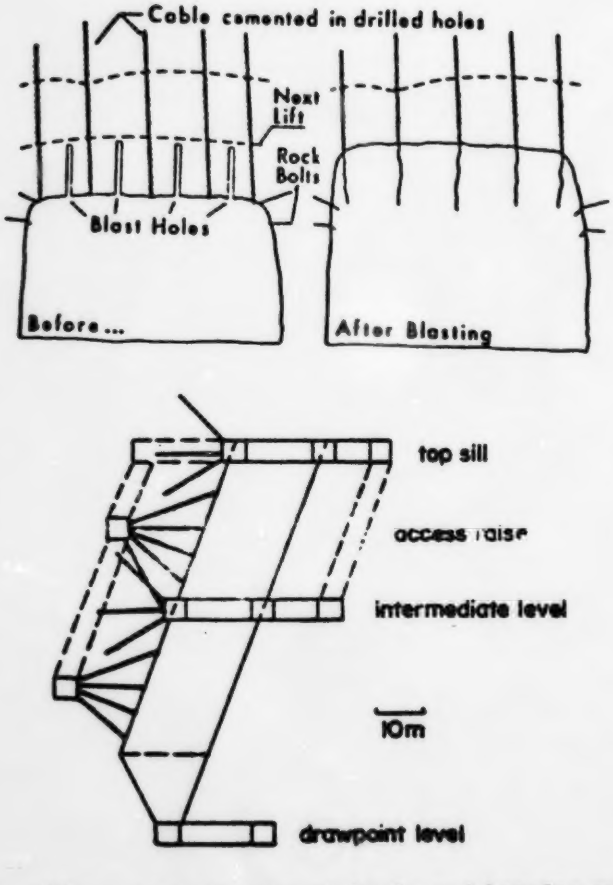
Cable cemented in drilled holes
Next
Lift
Rock
Bolts
Blast Holes
Before...
After Blasting
top sill
access raise
intermediate level
10m
drawpoint level

Figure 1.5 Passive cable systems to support backs and hanging walls in large scale, underground, hard rock mining

By far the greatest quantities of materials for full-contact, passive support systems are consumed for roof control, and the remainder of the report is therefore concerned with this major topic, with particular reference to steel-resin fixtures and horizontally bedded strata.

1.5 DESIGN OF ROOF SUPPORT IN HORIZONTALLY BEDDED STRATA WITH FULL CONTACT, PASSIVE, REBAR

The engineer responsible for developing a roof support plan in horizontally bedded strata must have one thought uppermost in his mind - safety. At the same time, he desires to design a safe system at minimum cost, where cost in this context must include a number of factors other than price of the fixtures alone, as discussed in Section 1.1. In order to do this he must have, or develop, an intimate knowledge of roof lithology, structure and failure mechanics. He must also be familiar in detail with the mechanical principles of support both as regards the properties of an individual support, i.e., a single bolt or dowel, and the behaviour of the complete system as it interacts with the rock.

In this report, the components of the design process are enunciated inasfar as current knowledge and our own research results can guide us at this time. The word "guide" is used here intentionally, for the variability of rock and the relative paucity of data about roof conditions ahead of the face requires that all calculations be tempered with experience and sound engineering judgement. It has been rightly said of the rock mechanics engineer (13), "The responsibility of the design engineer is not to compute accurately, but to judge soundly".

Finally, though the central topc in this report is the resin-rebar, passive system, several sections are applicable to the design of other types of internal roof support.

REFERENCES

1. Scott, J.J. Practical ground control as it relates to productivity, safety, and costs. Chapter 1, pp. 3-18, Proc. of the 1st. Inter. Conf. on Stability in Underground Mining, August, 1982, published by the Society of Mining Engineers of AIME, (1983).

2. Jansky, J.H. and Valane, R.F. Correlation of LANDSAT and air photo linears with roof control problems and geologic features. USBM Report of Investigations 8777, 22 pp. (1983).

3. Moy, D. The design and monitoring of rock bolt and dowel systems in underground excavations. Ph.D. Thesis, Imperial College, University of London, England. (1975).

4. Reed, J.J. Rock reinforcement and stabilization - Bolting alternatives. Mining Congress Journal, December. pp. 40-45. (1974).

5. Mines Safety and Health Commission. Paper on strata reinforcement by bolting, dowelling and injection techniques. Working Party on Strata Control (Roof Control). (1975).

6. Silvester, G.V. Strata reinforcement in the Barnsley area. Proc. of Strata Control Conference, Newcastle, England, published as Vol. 32, Developments in Geotechnical Engineering. (1983).

7. Bywater, S. and Fuller, P.G. Cable support of lead open stope hanging walls at Mount Isa Mines Limited. Proc. of Int. Symp. on Rock Bolting, Abisko, Sweden. (1983).

8. Lappalainen, P., Ulkkinen, J. and Kuparinen, J. Use of steel strands in cable bolting and rock bolting. Ibid. (1983).

9. Sellden, H. Cable bolting in Fabian ore body, Malberget. Ibid. (1983).

10. Hoek, E. and Londe, P. Surface workings in rock. Proceedings of the Third Congress of the International Society for Rock Mechanics, Vol. 1, Part A, pp. 613-654. (1974).

CHAPTER 2

THE FULL COLUMN, RESIN BOLT SYSTEM

2.1 INSTALLATION AND PRACTICAL CONSIDERATIONS

Modern practice in the installation of non-tensioned resin bolting systems relies upon pre-packaging of the resin cement in a twin-compartment capsule, which is designed to withstand the rigours of handling and installation (Fig. 1.3). The components are mixed in the bolt hole by penetration and rotation of the bolt through the capsule, resulting in the mechanical mixing of the resin and catalyst. The advantages of this system when it is operating well are ease and quickness of use, strong, consistent anchorages, no expansion stresses (cf. mechanical expansion anchors can induce tensile fracture of the rock in weak materials), good resistance to vibrations from blasting, able to be used in wet conditions, protection of bolt from corrosion and other forms of chemical attack, and grouting of fissures and fractures intersecting the hole (the extent of this "fissure invasion" will depend upon the viscosity of the resin mix selected).

Bolt holes should preferably be drilled to the specified depth with a rotary percussive drill with air or water flush. The hole should be cleaned and checked to ensure it is free of any blockages that could result in an irregular distribution of resin and difficulties in rotating the bolt. The capsule should be pushed carefully to the bottom of the hole with the bolt or a stemming rod. No more than one capsule should be inserted at a time in cases where more than one capsule is required to fill the annulus around the bolt. Following capsule insertion, it is the normal recommendation of manufacturers to insert the bolt to a point within 1 inch of the roof while slowly rotating. Very high speeds are not recommended. Typically, rotation speed is then increased to 200-450 rpm for 15-20 seconds to ensure complete mixing.

The bolt is held in position until the resin sets. The bolt must not be rotated once resin has started to gel. If some excess resin does not run out of the hole this may indicate the hole diameter is too big, the hole is too long, or there are fractures intersecting the hole and capturing resin.

Manufacturers offer the user a variety of resin types with different cure rates and viscosities to suit the prevailing temperatures and other practical considerations. For example, since set time decreases with increasing temperature, it would be wise to select a special "high viscosity" resin for a mine with high ambient temperatures. Time to initial set can be as little as 1/2 minute to 15 minutes. Where loads are to be applied to the bolt, an additional 20-60 minutes is commonly required (depending on resin type).

All resin capsules should be stored in a cool place. Shelf life is very dependent on the storage conditions.

To ensure a proper installation, holes must be sized correctly for the amount of resin to be placed. Over-sized holes may result in inadequate mixing of the resin components and reduced bond strength.

In highly fractured rocks, or when a particular fracture intersecting the bolt hole has a wide aperture, resin will escape from the hole and reduce the pull-out strength of the bolt. Until recently, there was no method for evaluating the extent of resin loss (see below).

It is tempting in the production-oriented environment of a mine to spin the bolt an inadequate length of time. Setting of the resin will then be irregular and its strength will vary from point to point, with soft spots where little mixing has occurred.

Insufficient mixing or quantities of resin may leave voids, or soft areas in the annulus through which water can reach the bolt and cause local corrosion.

2.2 THE BOLTMETER

The "Boltmeter" is a recent development of the Swedish firm Geodynamik which permits non-destructive testing of grouted bolts (1). Its principle of operation is the transmission of compression and flexural elastic waves through the bolt head and thence along the length of the bolt. The transmitter/detector is a piezo-electric crystal. As the energy passes along the bolt, some of it is refracted into the grout (resin or cement) annulus between the bolt and borehole wall. This results in a reduction in the amplitude of the energy pulse. Further reduction occurs as the wave is reflected from the bottom of the bolt and travels back to the sensor. Thus, a fully grouted hole lacking any voids would exhibit a more highly damped received wave than one in which grout is absent along some portion of the hole. The estimated state of the grout is flashed to the user by one of four colored indicator lamps on the portable unit.

At this stage in its development the "Boltmeter" is not foolproof. Some experiences from the studies reported by Thurner include:

(a) "Overcoring of tested bolts with documented insufficient function showed (several times) grout was missing in more than 1/3 of the bore hole length."

(b) "Cement grout with high water/cement ratio sometimes had not hardened, resulting in very poor grout condition. Percussion drilled bore hole had a much greater diameter than expected (90 mm instead of 45 mm in some cases)."

(c) "In a particular project every bolt out of a total of hundreds of bolts (of different types) were continuously tested with the Boltmeter during installation. In spite of the fact that proper function of each bolt was very important and that the contractor not only knew but even could see that the bolts were being tested, 48% of the bolts showed insufficient

> function when tested with the Boltmeter. Not much attention was paid to these test results until one bolt - after the test with the Boltmeter documented (it) as in bad condition - could be pulled out by means of a hydraulic jack."

In my opinion, this device will require further refinement and proving out in field situations before it can become a routine tool for the testing of bolts. It also raises a conundrum for the engineer who must interpret the results. When is a bad bolt really a bad bolt? Our bolt pattern design methods are based on simplified models of the rock mass and sound engineering practice demands conservatism in design where safety and production are involved. Is 1 poor bolt in 10 sufficient to threaten stability or 1 in 5? Should the location of the bolt and its relationship to adjacent bolts also be considered in deciding whether to reject or accept a given bolt? Who is to pay for additional bolts? Furthermore, use of this device will result in increased costs if all bolts deemed defective are replaced. Safety must take precedence over costs, but where safety cannot be proven to be compromised significantly, who is prepared to pay for these extra costs? These arguments are not intended to downgrade the significance of this technological development, but simply to call attention to these issues. The problem is essentially how to interpret the data the device provides to the engineer. Further technical developments and experience with the instrument will, no doubt, increase our ability to discriminate between good and bad bolts, but the other questions will remain until advances in roof stability design and prognostication occur.

A novel approach for evaluating the completeness of resin grout around the bolt was investigated by Stateham and Sun (2). Since resins used in bolting are exothermic, the temperature rise at the head of the bolt should be a measure of the amount of resin in the annulus; temperature rise for a fully grouted bolt should be greater than that for a partially grouted bolt. Experimental work confirmed results derived analytically. However, it is clear that this technique is not practical on a routine basis for the testing of hundreds of bolts in a mine.

2.3 BOLT AND ROCK PROPERTIES AND MECHANICAL BEHAVIOUR

In the final analysis, the stability of a bolted roof involves a complex interaction between the installed support and the rock mass. The accurate determination of this stability is the ultimate goal of the design engineer and rock mechanics researcher. However, the first step is to examine the characteristics of the various materials used in the resin bolt system and the mechanics of a **single** bolt to various types of loading.

Axial loading occurs typically, as a result of differential convergence between the anchor plate mounted on the rock surface and the extremity of the bolt at the bottom of the hole. This type of loading is simulated in the rock bolt pull-out test which has become the standard for testing bolt strength. In highly stressed ground, or where large displacements are taking place along joints and faults in the rock mass, the behaviour of bolts to shear is also very important.

2.3.1 Resin Properties

Physical and mechanical properties are provided by the manufacturers in their commercial literature, but the precise formulations of each are generally kept secret.

Only thermosetting resins, which gel by an exothermic chemical reaction between a resin and a catalyst, can be used for bolting. Thermo-plastic resin are too weak and also require external heating to cure.

Polyester type resins are more widely used than the epoxy type because they cure more quickly and are less expensive.

One drawback of the polyester resins is shrinkage during solidification (8-17%).

This is overcome by adding mineral fillers (typically limestone or silica, up to 70%) which, as well as reducing shrinkage, reduce the amount of resin required. Filler, then, does lower net costs but, on the negative side, it also increases the brittleness of the hardened product (3,4); its brittleness approaches that of rock.

The specific gravities of commercial resins are somewhat less than typical rocks encountered in mining and fall in the range 1.8 to 2.2 (2).

As might be anticipated, the induced brittleness arising from the addition of fillers results in a product whose uniaxial tensile strength is one-third to one-seventh that of its uniaxial compressive strength. Some typical values of these strengths and moduli are tabulated in Table 2.1. It is also noteworthy that the modulus of elasticity in tension is considerably higher than that in compression. Therefore, tensile failure of resin will occur at much smaller strains than compression failure, and it is therefore preferable to maintain the resin in compression.

In mines with high ambient temperatures the sensitivity of resin strength to temperature may be a consideration in selection of an appropriate resin. Figure 2.1 illustrates the sensitivity of the strength of an I.C.I. product to temperature; the lower the temperature the greater the strength and vice versa.

2.3.2 Bolt Materials

There are many manufacturers of roof bolts. In general, bolts for resin-grouted supports are manufactured from steel. Manufacturers will guarantee a mininum yield strength (the stress at which the bolt axial tensile stress vs. axial strain curve shows a sudden increase in bolt longation), an ultimate tensile strength (axial tensile load at failure/original cross-sectional area), and a percent elongation at ultimate strength. Bolt yield strengths typically range from 30,000 psi to 75,000 psi and in North America are classified into regular (30,000-35,000 psi), high (50,000-55,000 psi), and very high (approximately 75,000 psi) strengths. Carbon is used to increase

Type	Tensile Strength, psi	Compressive Strength, psi	Shear Strength, psi	Modulus of Elasticity, psi	Poisson's Ratio	Elongation	Ref.
Celtite	2,500	16,000	7,500	----------	-------	--------	(5)
Selfix	2,500	17,300	-----	$.38 \times 10^6$ compression	.30	--------	(7)
Celtite	2,650	------	-----	1.4×10^6 tension	-------	.2%	
Altek (71-63)	4,400.- (flexure)	12,500	-----	$1.3-1.6 \times 10^6$ (flexure) 1.9×10^5- compression	0.30	---------	(3)
Cyanamid EPX-295-1	4,200-8,900 (flexure)	------	-----	----------	-------	--------	(6)
Cyanamid EPX-289-4	1,600-3,600	------	-----	$(.68-.9 \times 10^6)$ flexure	-------	--------	(3)

(after (34))

---indicates properties not available

Table 2.1 Mechanical properties of filled polyester resins

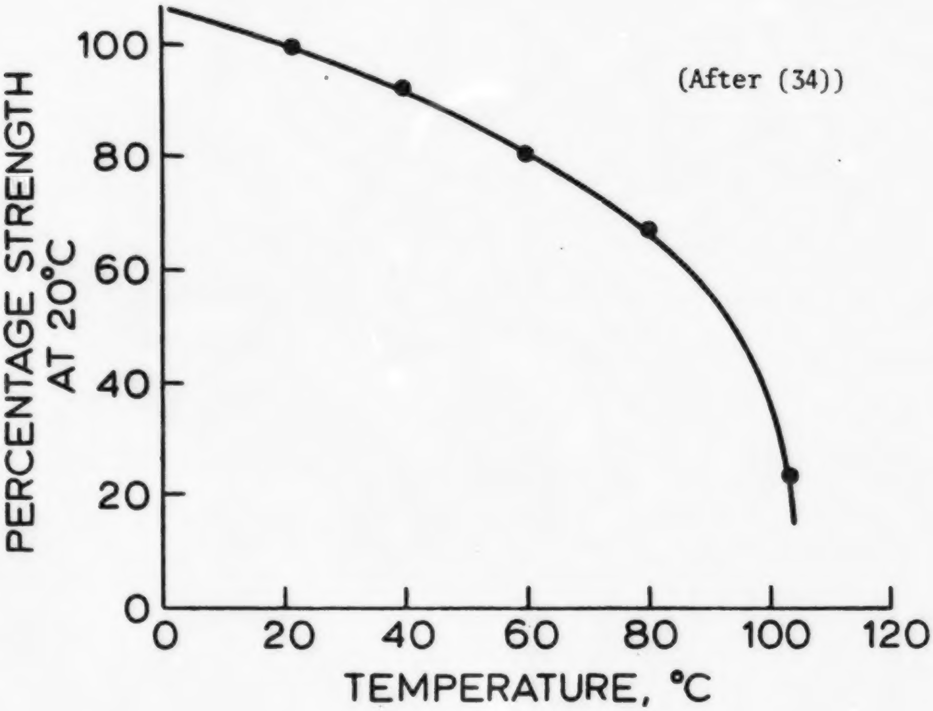

Figure 2.1 Effect of temperature on a filled polyester resin

yield strength, but at the expense of reduced ductility and increased brittleness.

Ductility is a particularly important, if not fully appreciated aspect of rock bolt support design. Barton and Bakhtar (9) suggest that the ultimate goal of the designer is to develop a reinforcement system in which the strength-deformation properties of the bolt and the rock mass are compatible. As they note, it makes little sense to have compressible slots in the shotcrete lining of the tunnel in squeezing ground and sliding joints in the steel ribs if the bolting system is much stiffer than these two components. It too should be capable of large deformations. If it is not, it will become highly loaded and likely fail. This scenario was, indeed, reported by Barton (10) in a major tunnel in which approximately 80% of the bolts failed because of incompatibility of stiffnesses among the support components; uncontrolled closure occured as a result.

With the growth in the magnitude of blasts underground through the introduction of new mining technologies, such as vertical crater retreat, bolts are being subjected to greater dynamic loads. Rock burst prone mines also are subjected to sudden loadings on supports. In these circumstances it may be preferable to use a very ductile bolt material that can absorb high stresses by deforming, rather than a high strength, yet brittle material, in an effort to resist the forces. In mining, large deformations are not necessarily unacceptable so long as production and safety are assured.

Finally, resin bolts are ribbed, serrated, or deformed, in order to improve mixing of the resin during bolt spinning and to increase anchor strength.

2.3.3 Resin-Bolt and Resin-Rock Interface

The bond strength of the resin-bolt and resin-rock interfaces is usually measured by a pull-out test (Fig. 2.2). It is generally accepted that this strength is mechanical in nature (friction plus roughness or interlock resulting from irregularities along

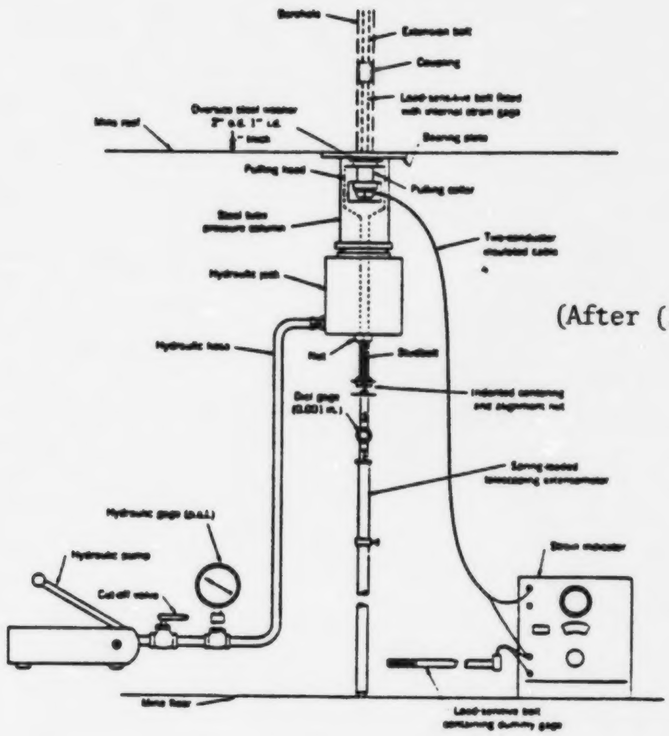
Borehole
Extension bolt
Coupling
Load-sensitive bolt fitted with internal strain gage
Oversize steel washer 2" o.d. 1" i.d.
1/4" thick
Mine roof
Bearing plate
Pulling head
Pulling collar
Steel tube pressure column
Two-conductor shielded cable
Hydraulic jack
Hydraulic hose
Nut
Studbolt
Indented centering and alignment rod
Dial gage (0.001 in.)
Spring-loaded telescoping extensometer
Hydraulic gage (p.s.i.)
Hydraulic pump
Cut-off valve
Strain indicator
Mine floor
Load-sensitive bolt containing dummy gage

(After (34))

Figure 2.2 Typical in-situ rock bolt pull out test system

the interface), but there has been some controversy over the existence of a chemical bond. There appears to be some evidence that this can occur in ideal laboratory conditions, but not in the wet mine environment (3,4). Some adhesion may also arise from Vander Vaal forces along the interface, but these will be removed after displacements of a microscopic scale.

It is important to determine whether one of these interfaces is the "weak leak" in the system or whether the bolt material could be taken to failure. There is no sure way to find this, other than by a pull-out test in the field.

Not surprisingly, tests show that bolt and borehole wall roughness improve pull-out strength. Thus, serrated rather than smooth bolts are employed.

Borehole wall roughness is dependent upon a number of factors, including rock type, natural jointing, drilling method, type of bit, and bit wear. Tests on resin bolts installed in holes in concrete and rock (11,12) all indicate a very significant effect of horehole roughness. In one set of experiments (12) three roughness states were formed in holes in cement with strength equivalent to soft rock (see Fig. 2.3) prior to inserting resin-grouted rock bolts with a 1/4 in annulus of resin in each case. For identical hole conditions, the 1 inch diameter hole would be expected to have the lowest strength, but in this case it exhibited the greatest strength, owing to the considerable wall roughness (Fig. 2.4). It is clear, then, that methods of increasing borehole wall roughness are desirable.

2.3.4 Annulus Size

Annulus size (difference between hole and bolt diameter) affects the axial and shear stiffness of the bolt (see Section 2.3.6). Dunham (14) also found that too large an annulus is deleterious in two ways. It inhibits complete mixing of resin during installation and results in low to very low pull-out strengths. He recommends that the hole diameter should be equal to the bolt diameter + 0.3 to 0.5 in (8-12 mm). Some manufacturers recommend an annulus as small as 0.25 in (6 mm).

(After (34))

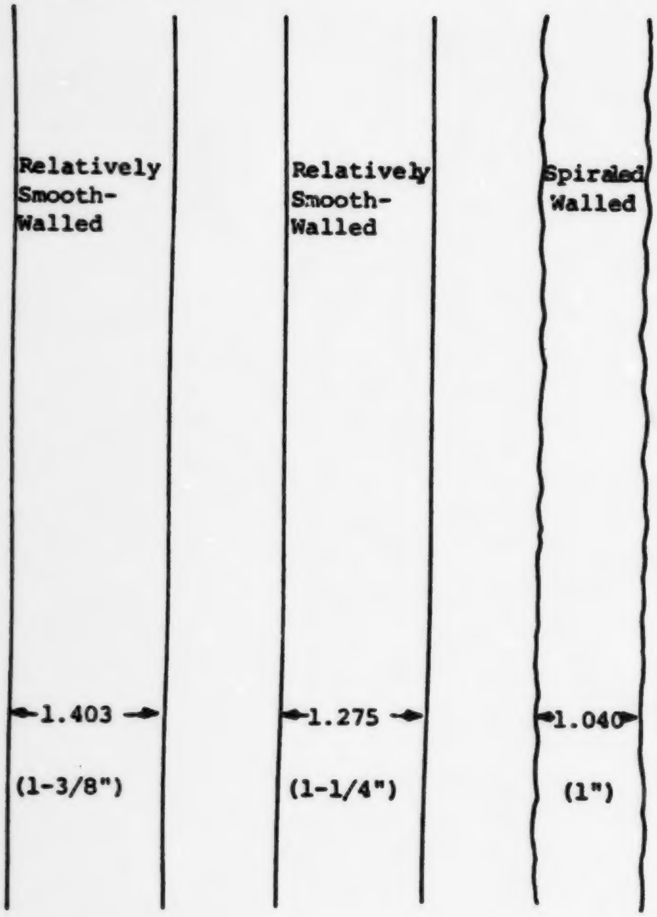
Relatively Smooth-Walled
Relatively Smooth-Walled
Spiraled Walled
1.403
1.275
1.040
(1-3/8")
(1-1/4")
(1")

Figure 2.3 Borehole roughnesses used in assessing effect of roughness on bolt pull out strength

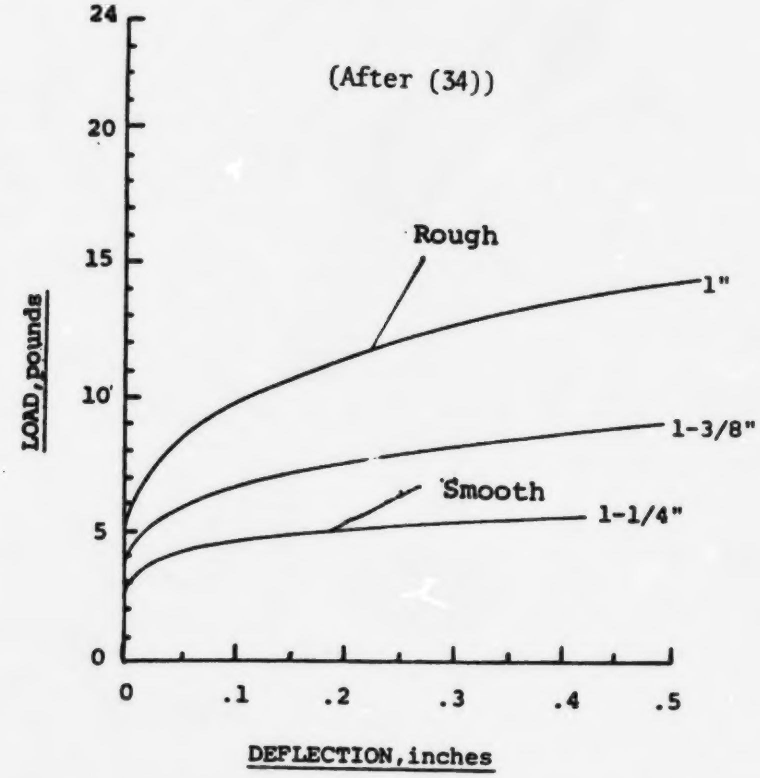

Figure 2.4 Load vs. Deflection from pull out tests on bolts installed in holes of different roughnesses (see Fig. 2.3)

2.3.5 Creep Properties

The creep properties of full-column resin-grouted bolts are generally superior to those of conventional expansion anchor bolts. The creep response is primarily dependent upon the creep behaviour of the resin-rock and/or resin-bolt interface, the resin properties, and the bond length (length of the bolt surrounded by resin).

A number of researchers have investigated creep of resin bolts in the laboratory (14-16) with broadly similar results (Table 2.2). For sandstone, Dunham (14) found that where the bond length was greater than 30 bolt diameters, the axial load on the bolt had to be increased to close to the pull-out strength of the bolt before significant creep was measured. Even for short bond lengths (approximately 15 bolt diameters), where failure was by bond rupture, the load had to be advanced to about 75% of pull-out strength before any appreciable creep could be generated.

2.3.6 Axial and Bending Stiffnesses

The axial stiffness of a resin-bonded bolt is an important design property, in addition to the axial pull-out strength, which is much more commonly measured. It has been demonstrated in numerous tests that resin bolts have axial stiffnesses 10 to 20 times larger than those of mechanical bolts. Where it is important to limit deformations, this high stiffness is desirable, providing the bolt strength can withstand the highr loads which result. The designer must try to achieve a suitable balance between the two end points of high loads and small deformations or low loads and larger deformations. Some axial stiffness data is tabulated in Table 2.3. Various studies, including our own, show that when a resin bolt is loaded in a conventional pull-out test (from which axial stiffnesses in Table 2.3 are obtained) only a small segment of the bolt is loaded, i.e., the axial stiffness is not dependent upon the total bolt length. This question of load transfer along a bolt is discussed in Section 2.3.8.

Diameter of Bolt, inch d_1	Diameter of Hole inch d_2	Rock Material	Load, lbs.	Creep Extension	Ref.
0.79	1.10	Scotswood Sandstone	16,400	0.016 in./10 days	(14)(b)
0.79	1.10	Dunhouse Sandstone	16,400	0.027 in./10 days	" (b)
0.875	1.375	Indiana Limestone	8,000	0.0007-.0029 in./30 days	(15)(c)
0.75	1.375	Indiana Limestone	8,000	0.012 in./30 days	" (c)
0.75	1.0	Indiana Limestone	8,000	0.014 in./30 days	" (c)
0.50	1.0	Indiana Limestone	3,540	0.020 in./30 days	" (c)
0.875	1.375	Indiana Limestone	16,000	0.004-0.016 in./30 days	" (c)
0.75	1.375	Indiana Limestone	16,000	0.007 in./30 days	" (c)
0.75	1.0	Indiana Limestone	16,000	0.034 in./30 days	" (c)
0.50	1.0	Indiana Limestone	5,890	0.090 in./30 days	" (c)

(a) See Figure 1.2

(b) Bonded length of 16 diameters

(c) Bonded length of 24 inches

(After (34))

Table 2.2 Selected data on creep rates of resin bonded bolts

(After (34))

Diameter of Bolt, inch d_1	Diameter of Hole, inch d_2	Rock Material	Axial Stiffness K, kip/inch	Ref.
1.0		Shale	360	(11)
1.0		Sandstone	280	(16)
0.625-1.0		"Sound firm strata"	250-1000	(17)
0.91	1.06**	Mudstone, Sandstone	400	(18)
0.75	1.0	Indiana Limestone	500	(15)
0.50	1.0	Indiana Limestone	290	(15)
0.75	1.375	Indiana Limestone	1390	(15)
0.875	1.375	Indiana Limestone	1130-3130	(15)
0.79	1.18	Sandstone and Diorite	450	(19)
0.87	1.18	Sandstone and Diorite	450	(19)
1.0	1.375	Sandstone and Diorite	250	(20)
1.375	1.75	Sandstone and Diorite	700	(20)

** Minimum

Table 2.3 Axial Stiffnesses (Force/Elongation) for Resin Bonded Steel Bolts

Axial stiffness is dependent upon the geometry and material properties of the resin and surrounding rock. Appendix A presents two theoretical models for estimating axial stiffness, which lead to the following equations:

Equivalent axial stiffness, R

$$= \frac{\pi}{4} d_1^2 E_B \left[1 + \frac{E_R}{E_B} \left(\frac{d_2^2 - d_1^2}{d_1^2} \right) \right] \quad \text{force/strain} \cdots\cdots \quad (2.1)$$

and

Axial spring constant, K_A

$$= \pi \left[\frac{G_R E_B}{2\left(\frac{d_2}{d_1} - 1\right)} \right]^{\frac{1}{2}} d_1 \quad \text{force/unit displacement} \cdots\cdots \quad (2.2)$$

where d_1 = bolt diameter

d_2 = hole diameter

E_B = modulus of elasticity of bolt steel

E_R = modulus of elasticity of resin

G_R = shear modulus of resin

Figure 2.5 summarizes the results of the first of these analyses (Eqn. 2.1). When the resin thickness is zero (i.e. the bolt fills the hole) the axial stiffness is identical to that of the steel bolt. As the resin thickness increases as a proportion of the hole diameter the axial stiffness decreases, first rapidly but at a steadily decelerating rate. The shaded area delineates the region in which commercial full column bolts lie. Although these simple models assume rigid rock, finite element analyses which simulate rock properties, show that for design needs the above formula are adequate.

A method for estimating bending stiffness is also presented in Appendix A. Figure 2.5 shows that bending stiffness is more drastically affected by the presence of the resin than axial stiffness.

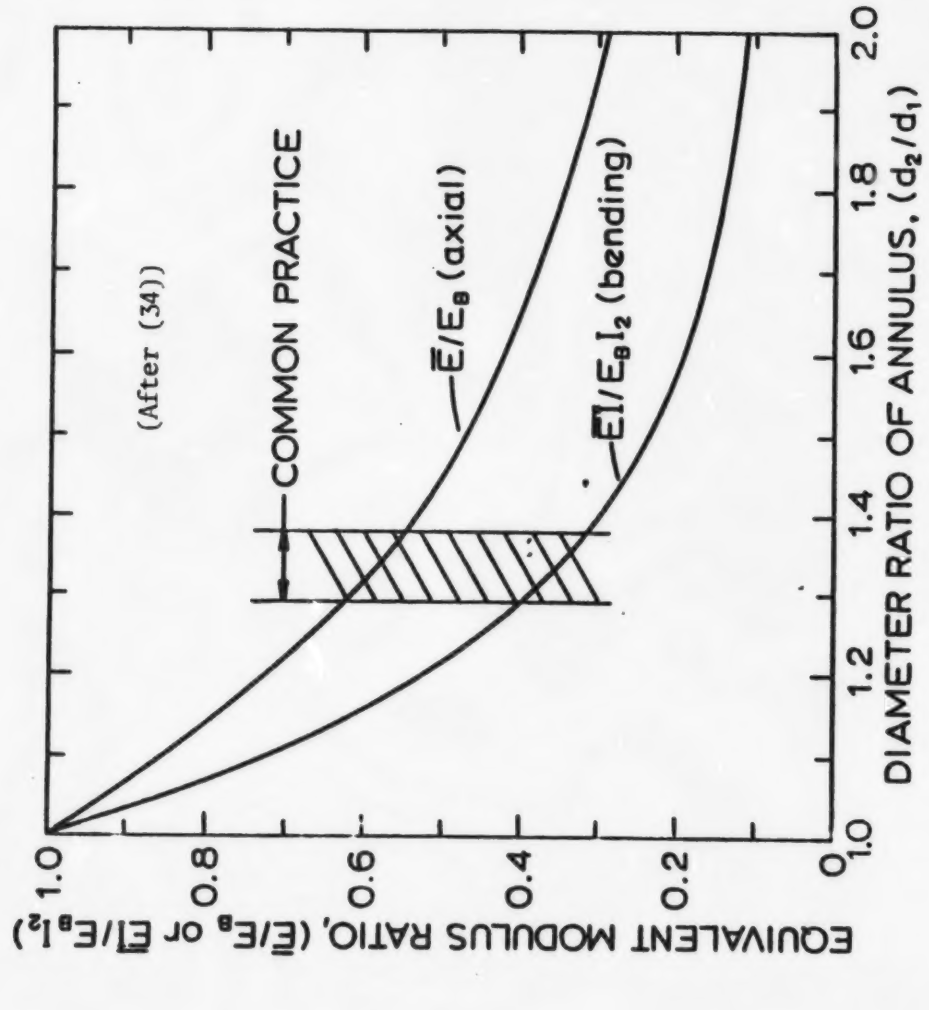

Figure 2.5 Reduction in equivalent axial stiffness of full column resin bolts as a function of annulus thickness

2.3.7 Shear Stiffness

One of the potential benefits commonly enlisted in favour of full column resin bolts is the resistance offered to shear movements in the rock mass along bedding planes, joints or other geological structures (Fig. 2.6). Direct shear tests of bolted joint blocks have, consequently, been undertaken to determine strengths and stiffnesses under these loading conditions (21,22); no in-situ methods analogous to the pull-out test for axial stiffness and strength are available. An example of shear testing data from these tests is provided in Appendix B. Shear stiffness can also be calculated from analytical models. Typically, these treat the bolt as a beam on an elastic foundation (Fig. 2.7). Two models are presented in Appendix A. The second of these models was developed in this project to include the effects of the rock and the width of joint opening. For typical rock properties and joint openings encountered in mine roofs (e.g., as a result of sagging and bed separation), the simple model which ignores these factors is adequate for design purposes and gives:

$$\text{Shear Stiffness} = EI\beta^3$$

$$\text{where } \beta = \sqrt[4]{\frac{k}{4EI}} \qquad \ldots\ldots\ldots\ldots\ldots \quad (2.3)$$

k = elastic foundation modulus of resin

I = second moment of area of the bolt

E = modulus of elasticity of steel.

In estimating shear stiffness by these methods it is assumed that only half the bolt is in contact with resin over half of its circumference (Fig. 2.6) and the half which is placed in tension is ignored. In effect, this is equivalent to assuming loss of the bond between the bolt and the resin. This seems a reasonable assumption given the relative weakness of this bond in tension. However, if full bonding is

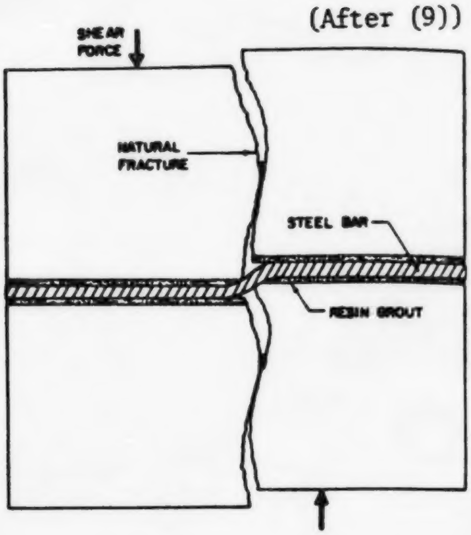
(After (9))

SHEAR FORCE
NATURAL FRACTURE
STEEL BAR
RESIN GROUT

Figure 2.6 Shearing of a full column resin grouted bolt along a natural joint

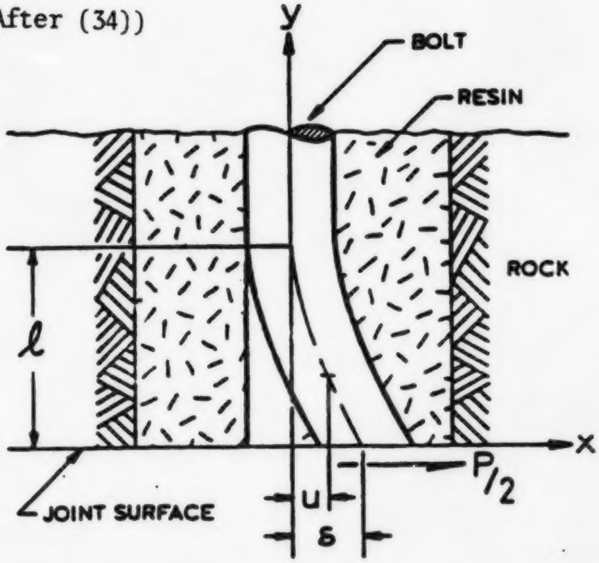
(After (34))

y
BOLT
RESIN
ROCK
ℓ
x
JOINT SURFACE
u
δ
P/2

Figure 2.7 Beam on an elastic foundation model used to derive expression for shear stiffness of a full column resin grouted bolt

included, the shear stiffness is approximately doubled, (Fig. 2.8). This is a considerable improvement and indicates potential for resin bolt system suppliers to research ways of improving resin-bolt interface strength in tension.

The predicted reduction in shear stiffness with increasing annulus thickness is similar in general form (Fig. 2.8) to that for axial and bending stiffness (Fig. 2.5). The introduction of even a thin annulus of resin considerably reduces the shear stiffness below that which would be acting were the hole completely filled with a steel bar perfectly bonded to the rock, but in the range of thicknesses used in practice (0.25-0.5 in. or 6-12 mm) the rate of reduction is less pronounced.

There is no question that both shear stiffness and shear strength of joints bolted with full column resin bolts will, in most cases, be superior to that provided by conventional tensioned anchor bolts. However, the question of the bolt density required to significantly reduce shear displacements in a mine roof in horizontally bedded strata has to be addressed. In the laboratory the area of bolt/unit area of joint is much larger than pertains to the typical mining roof support pattern. Hence, the relative improvement in shear load vs. shear displacement characteristics of the laboratory tested joint is greater than will be encountered in standard roof bolt practice. This problem is further addressed in Chapter 9 .

2.3.8 Load Transfer Along a Resin Bolt Column

It has already been noted in Section 2.3.6 that when a full column resin bolt is loaded axially in the standard pull-out test, only a small length of the bolt is sensibly stressed. This "load transfer" phenomenom will also apply to any other section of the bolt which is subjected to axial load and is commonly stated to be one of the particular advantages of grouted bolts. For example, if bed separation occurs in the roof, only a small length of bolt around the joint is loaded. Along this section shear stresses develop along the resin-rock and resin-bolt interfaces (Fig. 2.9). The response of the bolt to axial loading depends, then, on the distribution of shear stresses.

Theoretical and numerical studies of this problem have been supplemented with experimental data and are qualitatively in agreement. Closed form solutions have been published by several authors (23-26). The shear stress distribution and decay is typically modelled by an exponential relationship of the form:

$$\tau_x = \tau_o \, e^{-\frac{\alpha x}{d}} \qquad \text{...............} \quad (2.4)$$

where d = diameter of bolt

x = position along bolt

τ_x = shear stress at x

τ_o = shear stress at $x = 0$

α = constant

The decay length is controlled by the constant α . Figure 2.10 shows the theoretical distribution of shear stress as a function of α . Obviously, α can be fitted to match experimental results. The theories are therefore of a semi-empirical form.

Finite element analysis has also been brought to bear on the load transfer phenomena, in particular to examine the role of the moduli of elasticity of rock, bolt and resin. A typical finite element mesh developed for this study for running with the linear elastic option of the ADINA code at the University of Alberta is shown in Figure 2.11. Subsequently, our literature review brought to light finite element work on the same, or similar problems, by other authors (27-33) as reported by Gerdeen et al (34).

Finite element results show that rate of decay of shear stresses along the bolt is dependent upon the relative stiffness of the anchor system and the rock. The

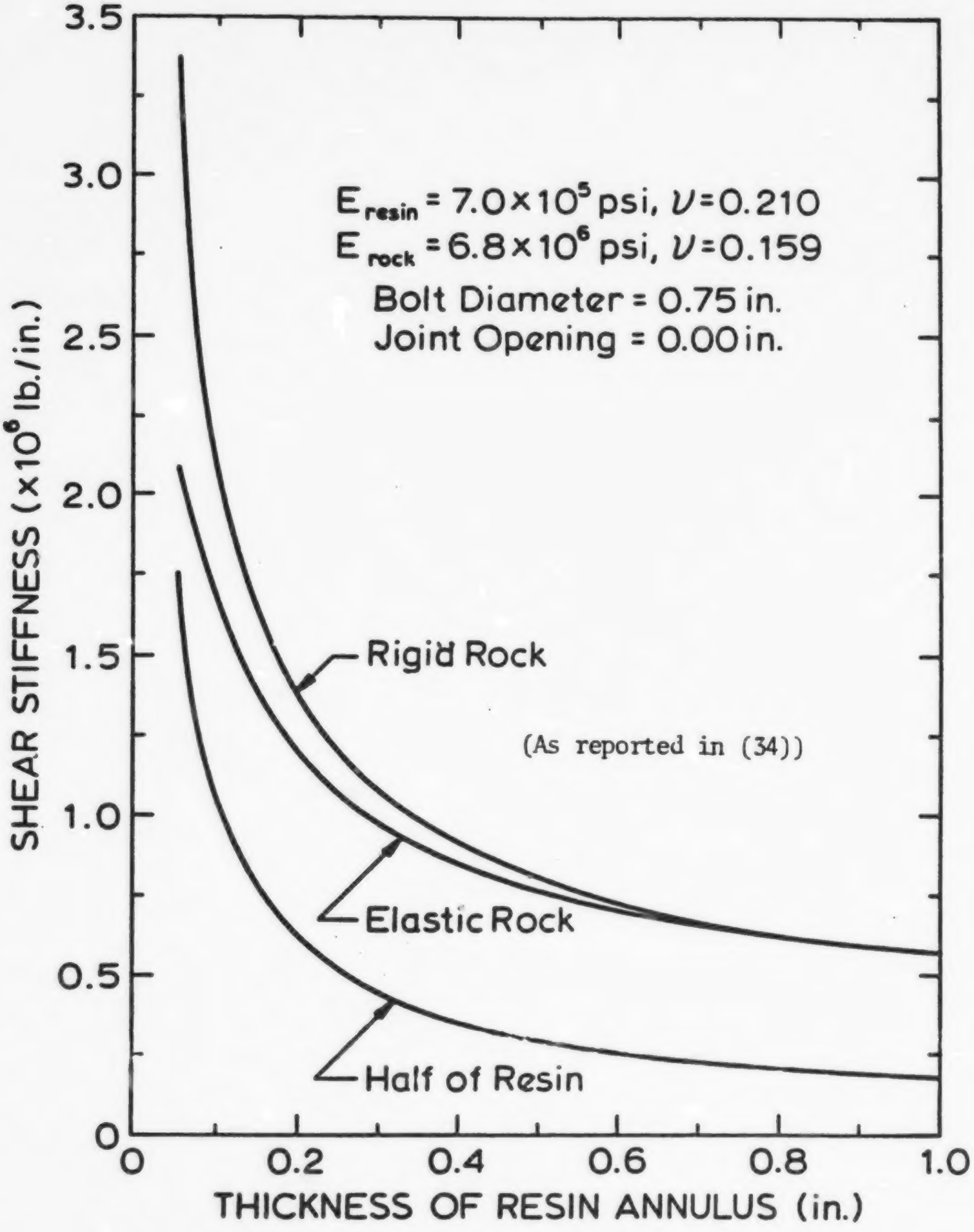

(As reported in (34))

Figure 2.8 **Reduction in shear stiffness of full column resin grouted bolt as a function of annulus thickness**

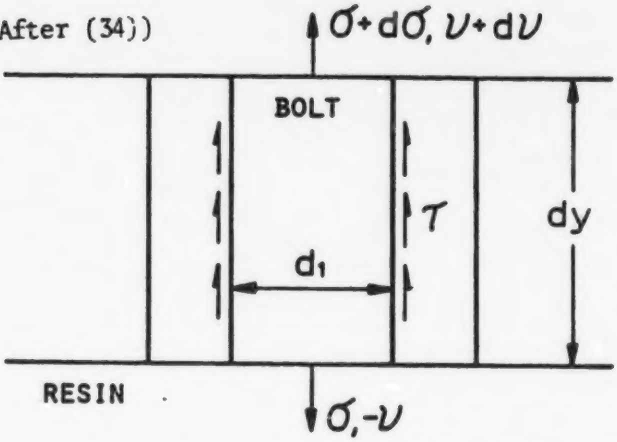
$\sigma + d\sigma$, $\nu + d\nu$
BOLT
τ
dy
d_1
RESIN
σ, $-\nu$

(After (34))

Figure 2.9 Shear stress transmission into grout and rock from axial loading of a grouted bolt

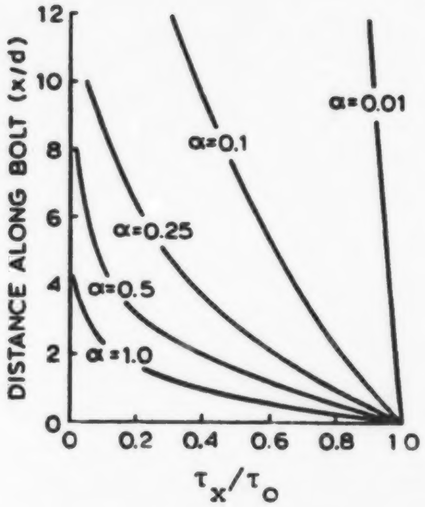

(As reported in (34))

Figure 2.10 Theoretical shear stress distributions along a grouted anchor

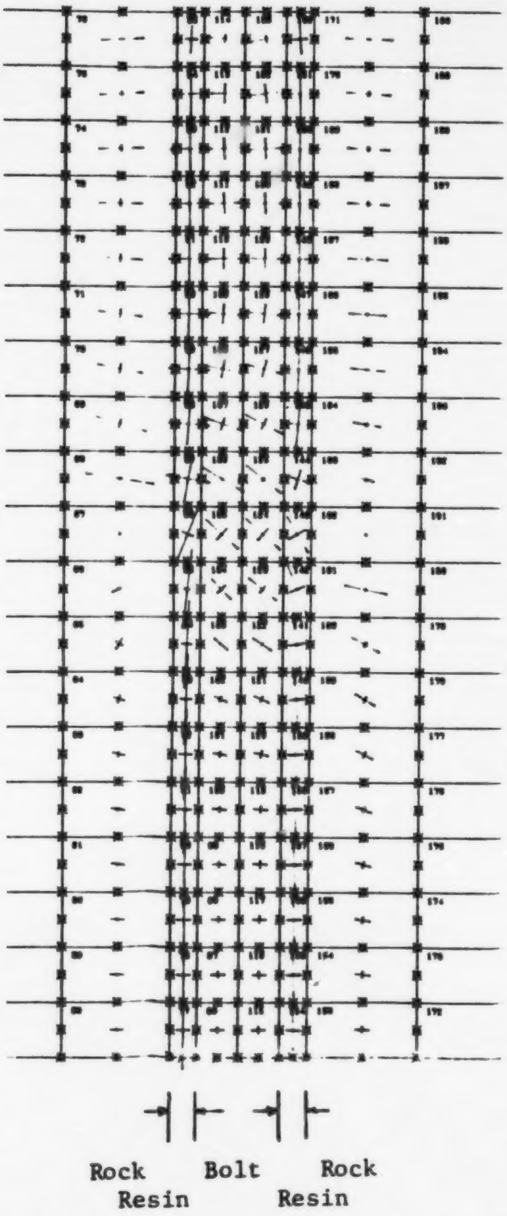
Rock
Resin
Bolt
Rock
Resin

Figure 2.11 Finite element mesh used with ADINA code to model rock bolt subject to axial and shear loads

softer the rock with respect to the anchor system the more slowly shear stresses decay with distance from the point of load application (Fig. 2.12). Poor mixing of resin can also lead to increased decay lengths.

Experimental data do not regularly concur with closed form or numerical solutions. The degree of agreement varies from study to study. In these experiments electrical resistance strain gauges are bonded to the bolt prior to insertion in the bolt hole and grouting. As an example, Figure 2.13 illustrates the results of laboratory tests by Farmer (23) in which 20 mm diameter steel bars were resin grouted into 28 mm holes. Discrepancies between theory and experiment probably arise from lack of homogeneity of the resin bond, creep, and progressive failure. The latter would be expected to lead to more linear stress distributions.

In all but the softest rocks the assumption that load transfer is sensibly complete by a distance from the loading point of at least 30 x bolt diameters would appear to cover most cases. For hard rock, the distance may be as small as 5-10 x bolt diameter.

From the design and performance viewpoint, it is obviously preferable to keep the decay length as small as possible. The writer suggests that in comparing resin rock bolt systems by in-situ pull-out tests the bolts should be instrumented to measure the transfer of load; decay length could then be used as a criterion for selection of bolts.

Load transfer also takes place during bending. Limited experimental data indicates that until large displacements occur load transfer is confined to short distances from the plane of the joint (Fig. 2.14).

2.3.9 Temperature

Installation of resin bolts at sub-freezing temperatures can jeopardize the anchorage strength. Dunham (14) found that anchorage pull-out strength at -1°C

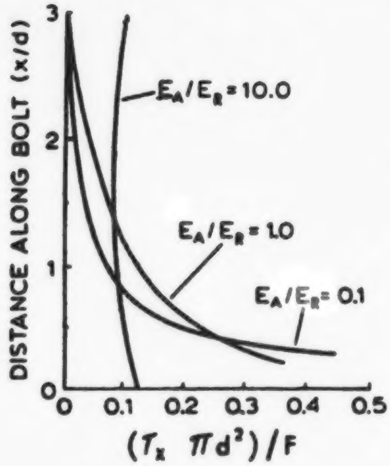

E_A = Modulus of Elasticity of anchor.

E_R = Modulus of Elasticity of rock

(As reported in (34))

Figure 2.12 Effect of rock and bolt moduli on extent of shear stress transfer along rock/grout interface

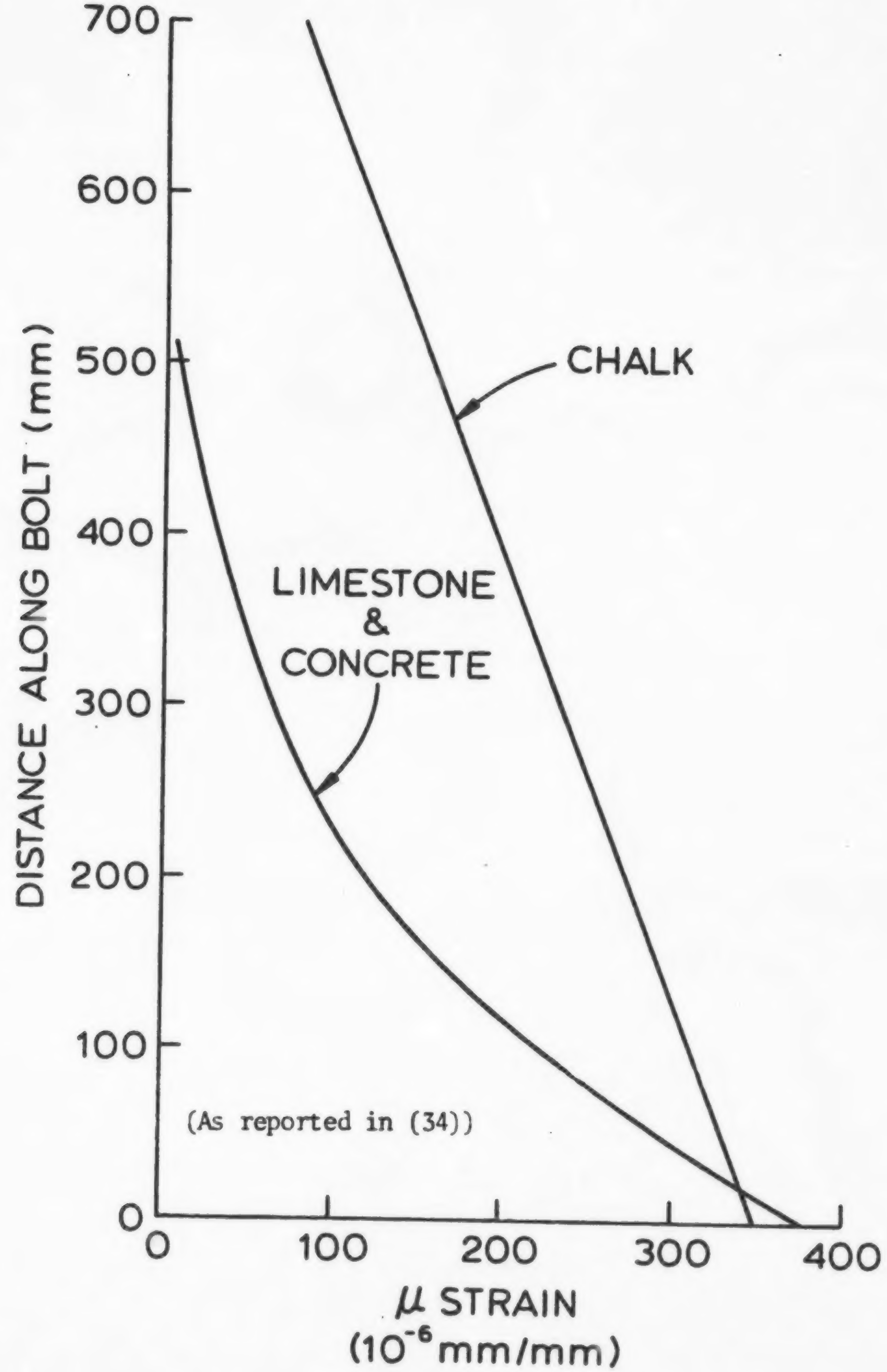

Figure 2.13 Measured axial strains in resin-grouted bolt loaded to 20 kN in chalk, limestsone and concrete

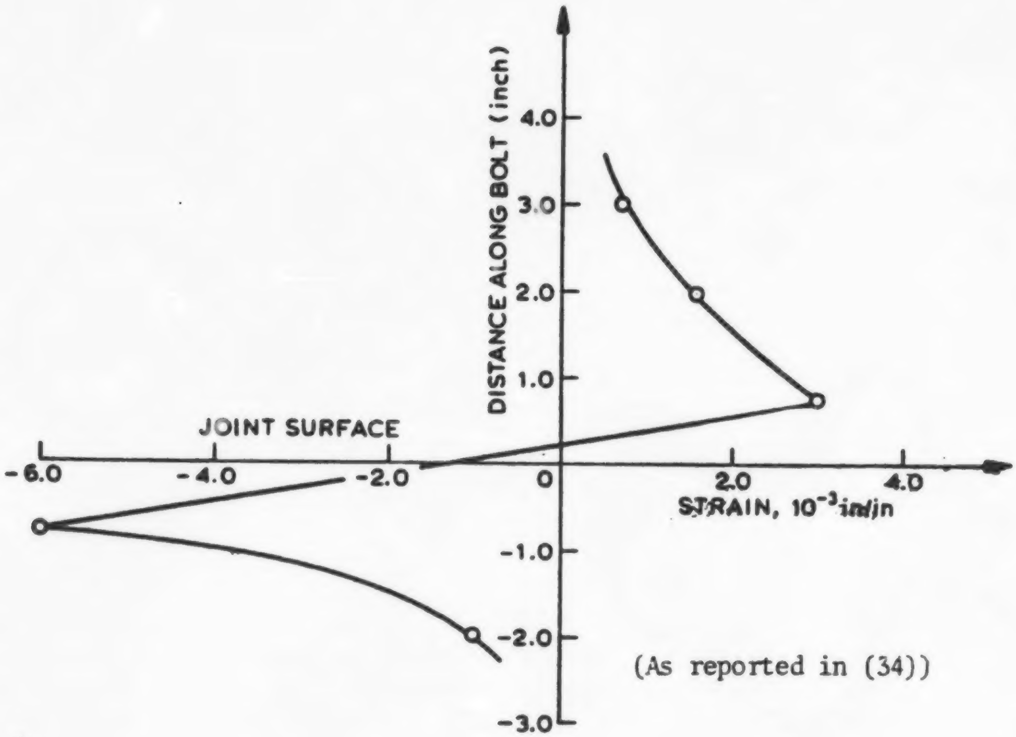

(As reported in (34))

Figure 2.14 Measured bending strains in resin grouted bolt after 0.10 in. of shear displacement

was little affected, but at -7°C there was a major reduction. It is attributed to incomplete curing of the resin because of excessive heat loss from the exothermic reaction.

2.4 MEASUREMENT OF THE BEHAVIOUR OF FULL COLUMN GROUTED UNTENSIONED BOLTS IN MINES

When resin bolts were first introduced into North America in the 1960's mining companies and government research institutions undertook numerous trials at mine sites (36-42) to compare the new system with the older methods, which at that time were primarily mechanical, point-anchored, tensioned bolts. The latter were not always successful, particularly in soft rocks.

Typically, several stations were established (with similar geology) at which roof patterns using the old and new systems were installed. Comparisons of effectiveness were based on a few, or all of the following: pull-out strength tests, differential sag measurements in the roof, convergence between roof and floor, and occurrence of rock falls from the roof. Rarely, was the response of the rock bolt themselves measured to determine load distribution in them. It is understandable why this was not done (the measurements actually made are relatively simple to collect and can be directly interpreted in terms of better or worse performance in comparison with other installations, all other things being equal). However, improved knowledge about rock bolt-roof interaction can only come about as a result of measuring bolt as well as roof response.

Instrumentation of full column resin bolts has been undertaken in a few on-site experiments. In a series of tests in three coal mines in the Eastern States (42) the following observations were made from the measurements:

1) Axial stresses along the bolt varied considerably, and most noticeably when mining was taking place locally.

2) Compressive and tensile stresses were encountered along the bolt, indicating bending.

3) Very high tensile stresses, sometimes exceeding the elastic limit, were measured at points coinciding with strata separations.

Probably the most comprehensive monitoring program completed to date was reported in 1983 (43). A test drift in hard, jointed syenite porphyry, at the 514 m level of the Kiirunavaara Mine in Northern Sweden was selected for this major installation, comprising 20 strain gauged rock bolts (cement grouted, untensioned), 50 bolts each combined with a single anchor extensometer, 23 multiple borehole extension meters, 45 convergence measurement stations, precise levelling, and 14 stress change monitors to record tangential stress around the opening. The goal was to investigate interaction between a system of rock bolts and the rock mass under conditions of variable loading.

Figure 2.15 illustrates graphically the variability with time and location of bolt loads. Again, large loads were recorded where the bolt intersected major discontinuities. It was also noted that during the early stages of monitoring forces are concentrated in small areas where joint displacements can appear and that uniform load distribution tends to occur when the bolt forces are large. Though the authors do not comment on the significance of this latter point, it would seem likely that it indicates loss of bonding between the bolt and resin.

The Kielder experimental tunnel in Northern England was another well instrumented excavation. Freeman (44) reports on the development of stresses in grouted untensioned bolts as tunneling progressed. Convergence of the rock mass was shown to develop tensile stresses in the bolt up to a maximum distance from the surface, or so-called "neutral point". This distance was interpreted as the "pick-up" length and the remaining section of the bolt (about 2/3 rds. of its total

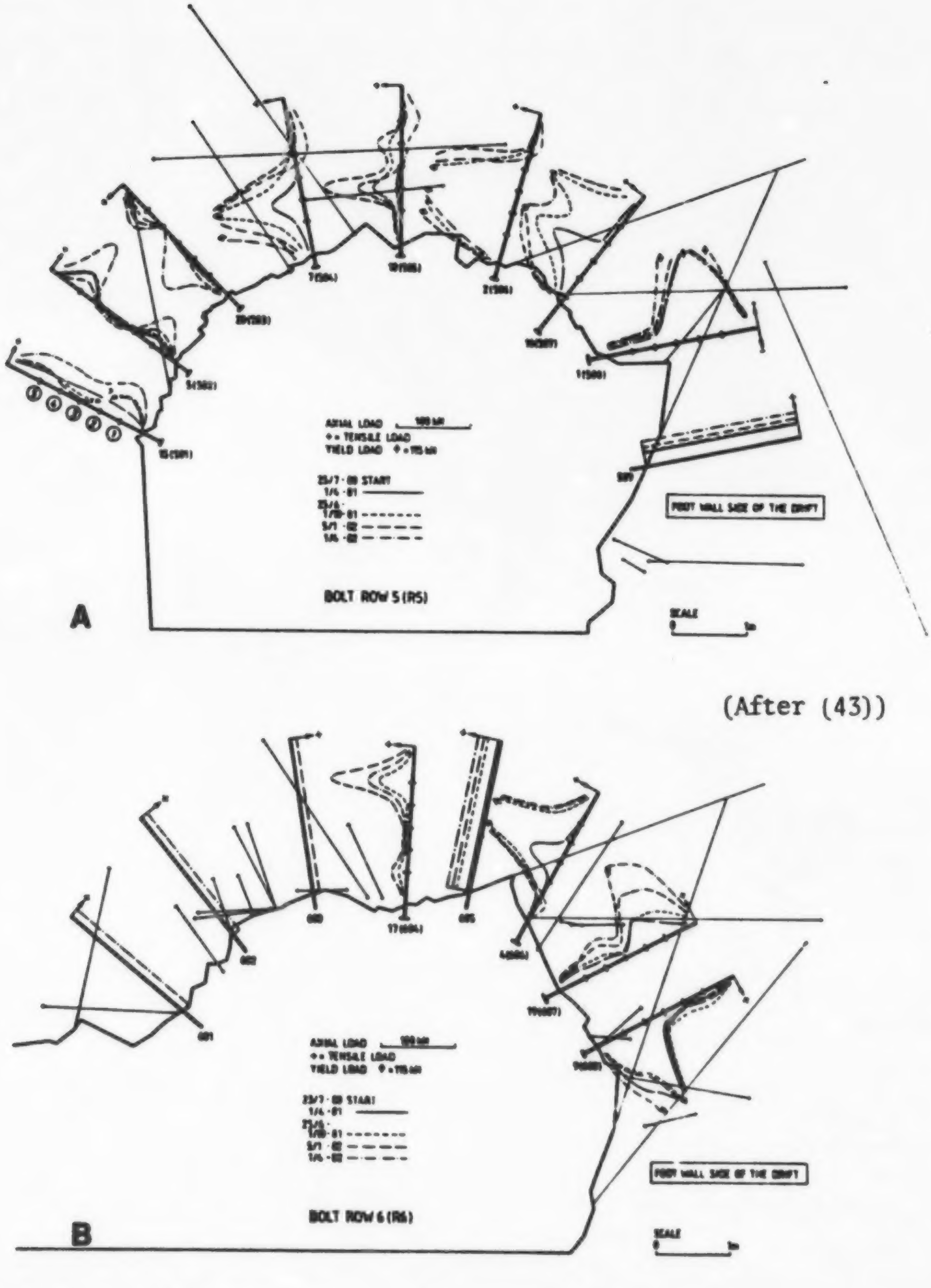
A
AXIAL LOAD 100 kN
◆ = TENSILE LOAD
YIELD LOAD ◆ = 115 kN
25/7-80 START
1/6-81
25/6-
1/10-81
5/1-82
1/6-82
BOLT ROW 5 (R5)
FOOT WALL SIDE OF THE DRIFT
SCALE
0 1m
B
BOLT ROW 6 (R6)

(After (43))

Figure 2.15 Axial bolt force distributions measured in cement grouted, untensioned bolt in the Kiirunavaara Mine, Sweden

length) was regarded as the anchor. Shear stresses between the grout and bolt were zero at the surface and at the "neutral point" and the signs of the shear stresses were opposite in the "pick-up" and "anchor" lengths of the bolts.

REFERENCES

1. Thurner, H.F. Detection of invisible faults on rockbolts in-situ. Proc. Int. Symp. on Rock Bolting, Abisko, Sweden, pp. 477-480. (1983).

2. Stateham,R.M. and Sun, M.C. Temperature investigations of resin-anchored bolts. DMRC, RI 8178. (1976).

3. Schwendeman, J.L., Sun, S.M. and Salyer, I.O. Plastic liners extended with sand and other fillers for use in coal mines. U.S. Bureau of Mines OFR-60-73. (1972).

4. Daugherty, R.A. Roof stabilization through chemical additions. SME Mining Engineering Handbook, Vol. 1, pp. 125-134. (1973).

5. "Resin Anchor Systems for the Mining and Construction Industries", Celtite, Inc. (1975).

6. Raff, R.A.V., Subramanian, R.V. and Austin, H.F. The application of polymers for rock bonding and reinforcement of coal mine structures. U.S. Bureau of Mines OFR-15-75. (1975).

7. "Selfix-Celtite System". Celtite, Inc. (1972).

8. Beveridge, R.L.W. The resin anchor in strata reinforcement. Finnish Society of Engineering Geology. (1974).

9. Barton, N. and Bakhtar, K. Bolt design based on shear strength. Proc. Int. Symp. on Rock Bolting, Abisko, Sweden, pp. 367-376. (1983).

10. Barton, N. Characterizing rock masses to improve excavation design. Panel Report, Theme II - Tunnelling and Excavation, 4th Congress IAEG, New Delhi.

11. Dunham, R.K. Field testing of resin anchored rock bolts. Colliery Guardian. (1974).

12. Karabin, G.J. Jr., and Debevec, W.J. Comparative evaluation of conventional and resin bolting systems. Preprint No. 76-F-32, SME-AIME Meeting, Las Vegas. (1976).

13. Barry, A.J. and McCormick, J.A. Evaluating anchorage testing methods for expansion-type mine roof bolts. BuMines RI 5649. (1960).

14. Dunham, R.K. Some aspects of resin anchored rock bolting. Rock Mechanics Research Laboratory, University of Newcastle, Tunnels and Tunnelling. (1973).

15. Haas, C.J., Keith, H.S., Nitzsche, R.N., Dave, J., Hoffmann, R.L., and Patrick, W.C. An investigation of the interaction of rock and types of rock bolts for selected loading conditions. 2nd. Annual Report, Rock Mechanics and Explosives Research Centre, Univerity of Missouri-Rolla, U.S. Bureau of Mines, Contract H0122110. (1975).

16. Stefanko, R. and Choi, D.S. Anchorage performance in rock bolting. Trans. Soc. Mining Engineers of AIME, Vol. 247, pp. 88-92. (1970).

17. Barnes, E.L.S. Rock bolting testing. Symposium on Rock Bolting, The Australian Institute of Mining and Metallurgy. (1971).

18. McCoy, A.E.R., Vnenk, L. and Hargraves, A.J. Symposium on Rock Bolting, The Australian Institute of Mining and Metallurgy. (1971).

19. Pells, P.J.N. The behaviour of fully bonded rockbolts. Advances in Rock Mechanics. Proc. of 3rd. ISRM Congress, Vol. 2, pp. 1212-1217. (1974).

20. Franklin, J.A. and Woodfield, P.F. Comparison of a polyester resin and a mechanical rockbolt anchor. Inst. Min. & Met., London, Trans., Vol. 80, pp. A91-A100. (1971).

21. Haas, C.J. Analysis of rock bolting to prevent shear movement in fractured ground. Mining Engineering, pp. 698-704. (1981).

22. Bjurstrom, S. Shear strength of hard rock joints reinforced by grouted untensioned bolts. Advances in Rock Mechanics. Proc. ISRM 3rd. Int. Congress on Rock Mechanics, Denver, Vol. 11B, pp. 1194-1199.

23. Farmer, I.W. Stress distribution along a resin grouted rock anchor. Int. J. Rock Mech. Min. Sci. & Geomech. Abst., Vol. 12, pp. 347-351. (1975).

24. Hawkes, J.M. and Evans, R.H. Bond stresses in reinforced concrete columns and beams. Structural Engineer, Vol. 29, No. 12, pp. 323-327. (1975).

25. Littlejohn, G.S. and Bruce, D.A. Rock anchors - Design and quality control, Part I: Design. Ground Engineering, pp. 25-32, 41-48. (1975).

26. Littlejohn, G.S. and Bruce, D.A. Rock anchors - design and quality control. Proc. 16th. Symp. Rock Mech., Minnesota. (1975).

27. Coates, D.F. and Yu, Y.S. Three dimensional stress distribution around a cylindrical hole and anchor. Proc. 2nd. Int. Conf. on Rock Mechanics, Belgrade, Vol. 2, 175-182. (1970).

28. Haas, C.J., Dean, K.H., Nitzsche, D.J., Janakkumar, D., Hoffman, R.L., and Patrick, W.C. An investigation of the interaction of rock and types of rock bolts for selected loading conditions. (1975).

29. Roegiers, J-C. and Nelson, C. The improved performance of rock bolts anchored with resin. Univesity of Minnesota Report. (1970).

30. Gerdeen, J.C., Viegelahn, G.L., Snyder, V.W., Schwab, P.M., Schuyten, H., Wick, C.J., and Collison, T.J. Finite element analysis applied to resin and mechanical roof bolting systems for strata bound deposits. U.S. Bureau of Mines Contract H0230014, Michigan Technological University, Houghton, Michigan. (1976).

31. Wade, L.V., and Stahl, P.A. Effects of specimen radius on the stress state near a roof bolt anchor. U.S. Bureau of Mines, RI 7748. (1977).

32. Kamal, S.A. Analysis of multi-axial anisotropic creep, roof resin bolts and bed separation in rock structures using the finite element method. Ph.D. Michigan Technological University. (1974).

33. Dejean, M. and Tournaire, A. Mathematical model study of the influence of certain factors on the action of roof bolts on the strata. Technical Report on Strata bolting No. 1, Laboratoire de Mecanique des Terrains, Ecole Des Mines de Nancy. (No year given).

34. Gerdeen, J.C., Snyder, V.W., Viegelahn, G.L., and Parker, J. Design criteria for roof bolting plans using fully resin-grouted nontensioned bolts to reinforce bedded mine roof. U.S. Bureau of Mines, Final Report on Contract No. J0366004, Michigan Technological University. (1977).

35. Kwitowski, A.J. and Wade, L. Laboratory data on shear and bending of resin bolts. U.S. Bureau of Mines, Bruceton, unpublished data, September. (1975).

36. Anderson, R.B. Use of resin-anchored roof bolts in adverse conditions. Min. Cong. Jnl., Vol. 60, pp. 37-40. (1974).

37. Anon. Clay mine switches rather than fight. Eng. Min. Jnl., Vol. 173, pp. 128-129. (1972).

38. Bennett, G., Herrick, J. and Conway, J. Resin bolting cost reductions at the White Pine Mine. Rapid Excavation Conf., San Francisco. (1974).

39. Caverson, B. and Parker, J. Roof bolts hold best with resin. Mining Engineering, Vol. 23, pp. 54-57. (1971).

40. Maher, J. and Bennet, G. Resin bolting developments at the White Pine Mine. Skillings' Mining Review, Vol. 64, No. 30, pp. 6-9. (1975).

41. McCormick, J.A. Experience with roof bolts anchored with a resin cartridge. Proc. Coal Mining Inst. America, Pittsburgh, pp. 120-126. (1965).

42. Sawyer, S.G. and Karabin, G.J. Jr. The development of instrumentation for the in-situ measurement of axial loads in a fully resin-grouted roof bolt. 1st. Symp. on Underground Mining, Vol. II, NCA/BCR, Coal Conference and Expo II, Louisville. (1975).

43. Bjornfot, F. and Stephansson, O. Interaction of grouted rock bolts and hard rock masses at variable loading in a test drift of the Kiirunavaara Mine. Proc. Int. Symp. on Rock Bolting, pp. 377-395. (1983).

44. Freeman, T.J. The behaviour of fully-bonded rock bolts in the Kielder experimental tunnel. Tunnels and Tunnelling, Vd. 10, No. 5, pp. 37-40. (1978).

CHAPTER 3

UNDERSTANDING THE MODE OF OPERATION OF FULL COLUMN UNTENSIONED RESIN BOLTS

3.1 INTRODUCTION

In 1983, a group of people from various parts of the world with a common interest in rock bolting (researchers, mining, civil and geological engineers, and rock bolt manufacturers) met together in the first international conference devoted to this subject (1). It was clear at the close of this specialized conference that while, over the last decade, new types of support have been developed and the engineer therefore has a greater choice of support measures available to him, there are still many controversial questions and uncertainties concerning the correct rock bolting design methods to use and the mode of operation of bolts. For example, arguments about beam building vs. arch formation and the merits and demerits of tensioning vs. non-tensioning of bolts were still very much in evidence.

3.2 LOCALIZATION OF SHEAR AND TENSILE LOADS

Though study of the mechanics of untensioned grouted bolts remains an area of active research, some general principles have begun to emerge. It is generally agreed on the basis of theoretical considerations and experimental investigations (see Chapter 2) that tensile and shear loads concentrate around points where natural discontinuities in the rock, or developing fractures intersect the bolt hole. This localized interaction must be taken into account in any model that seeks to explain the bolting mechanism. It is advanced as one argument in favour of grouted bolts over ungrouted bolts. For example, Fairhurst and Singh (2) in their study of bolting of layered strata, suggested that support is provided independently to each layer so that local bolt failure at one horizon does not necessarily harm the support capacity of other sections of the bolt.

From reviewing the most recent experimental work on bolted joints and pull-out tests, Gerrard (3) suggests that the patterns of stresses developed at bolt/joint intersections are of the form illustrated in Figure 3.1. Axial bolt tension is a maximum at the joint and decreases away from it as load is transferred by shear into the grout and rock mass. At a critical value of shear stress, τ_i, the bolt/grout bond fails and the interface becomes a frictional surface only with slippage between the bolt and grout. It is postulated that failure takes place when:

$$(|\tau_i| - \sigma_n \tan\delta - a) = 0 \quad \ldots\ldots\ldots\ldots\ldots \quad (3.1)$$

where a and δ are the adhesion and angle of friction of the interface and σ_n is the normal stress across it.

Actual behaviour is undoubtedly more complicated than this. Strain hardening followed by strain softening behaviour is indicated from pull-out tests by several researchers (4-6). In addition, Gerrard (3) notes the possible influence of contraction of the bolt diameter under tensile load. This may reduce the normal stress across the bolt/grout interface. For example, if the bolt tension increases by $\Delta\sigma_b$ and the far field compression in the rock mass increases by Δp, then the net increment in the normal stress across the bolt/grout interface will be negative if:

$$\Delta\sigma_b > \frac{2E_b}{\nu_b\ E_r} \cdot \Delta p \quad \ldots\ldots\ldots\ldots\ldots \quad (3.2)$$

Plane stress

or

$$\Delta\sigma_b > \frac{2(1-\nu_r^2)E_B}{\nu_b\ E_r} \cdot \Delta p \quad \ldots\ldots\ldots\ldots\ldots \quad (3.3)$$

Plane strain

where E_r, E_b, ν_r, ν_b, are the Young's moduli and Poisson's ratio of the rock mass and bolt, respectively.

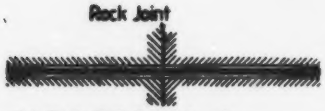

(a) Rock Bolt,Grout Annulus

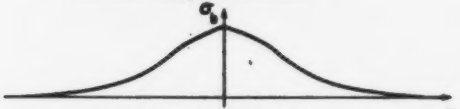

(b) Tensile Stress in bolt

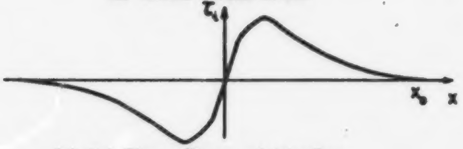

(c) Net Shear Stress at interface

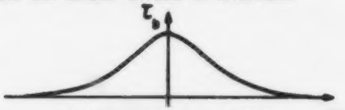

(d) Shear Stress in bolt

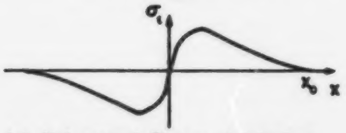

(e) Net normal Stress at interface

(After (3))

Figure 3.1 Development of bolt loads and interface stresses during joint shearing

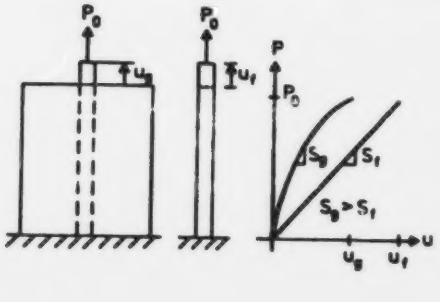
P_0
u_g
P_0
u_f
P
P_0
S_g
S_f
$S_g > S_f$
u
u_g
u_f

(After (9))

Figure 3.2 Illustration of tension-stiffening effect

If the bolt tension is generated by opening or pulling apart of the joint by tensile loads normal to its plane, the increment in far field stress Δp is probably zero. However, where the joint opens due to shearing of a rough joint (dilatancy effect) the field stress increment, Δp, may be expected to increase where there are conditions of lateral restraint. Hence the distribution of normal stress along the bolt/grout interface is complex, particularly in situations of combined shear and axial displacement.

Figure 3.1 (d,e,) also illustrates the development of shear stress in the bolt as a result of shear loading from movement along a joint. Gerrard (3) suggests that the "persistence" of this shear stress is more localized than in axial loading, in part due to the development of a net normal stress, σ_l, acting between the grout and the sides of the bolt (Fig. 3.1(e)).

With shear loading, the bolt may either fail in shear or by compressive failure of the bolt/grout interfact. Compressive failure of the rock mass may also be involved (see Section 3.4).

3.3 TENSILE AND SHEAR STIFFENING

The localization of stresses and deformation in the manner described in Section 3.2 leads to the phenomena of tensile and shear stiffening by which the axial and shear stiffnesses of the combined resin/bolt unit are greater than those of the free bolt without grout. This effect is illustrated in Figure 3.2 for axial loading where S_g and S_f are the axial stiffness of the grouted and ungrouted bolts, respectively.

As noted in Section 3.2 this localized support function is seen as a benefit of this particular type of support. It may also be a disadvantage, since the increased stiffness means that stresses may locally reach the yield point of the bolt after only relatively small movements of the rock mass. Solutions to this problem have been suggested by several authors. Gerrard (3) advocates using bolts of extremely high ductility and/or the inducement of bond failure by ensuring that the ratio of critical embedment length to joint spacing is sufficiently high. Here Gerrard is referring to the occurrence of a critical length of bolt beyond which a pull-out test will fail the bolt material and below which the bolt/grout bond will fail and interface slip will occur. If the critical embedment length to joint spacing is sufficiently high, bond failure and slippage will occur, rather than bolt failure.

Ortlepp's test results (7) showed that with bond failure and slippage, residual bolt loadings of 50-100% of peak strength could be sustained over bolt elongations up to 40 cm. On the contrary, with tensile failure of the bolt, maximum elongations were limited to 1.5 cm.

3.4 INCREASE IN STRENGTH OF A FULL COLUMN RESIN BOLTED JOINT

The strength of a natural joint or bedding plane bolted with a full column resin bolt is attributable to several factors (Fig. 3.3):

i) Shear strength of the joint under normal stresses existing prior to bolt installation.

ii) An increment in joint shear strength due to the component of axial bolt stress normal to the joint plane. This increment will be positive if the joint dilates during shear and the bolt is installed at an angle which will result in tensile bolt stresses as shear takes place (Fig. 3.3).

iii) A resisting force provided by the resolved bolt force parallel to the joint plane.

iv) Dowel action induced by the shear and bending deformation of the bolt.

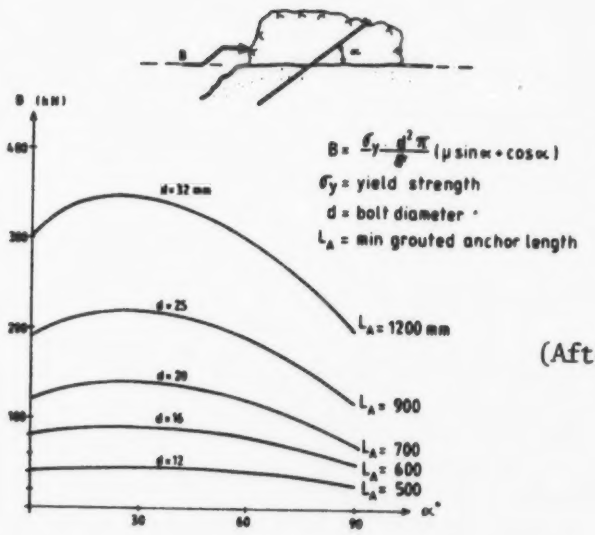

(After (10))

Figure 3.3 Shear resistance of a bolted joint as a function of angle of installation

Dowel action is very difficult to estimate because it depends on several parameters, including bolt size, thickness of grout annulus, strengths and moduli of bolt, resin and rock mass, rock damage around the bolt, and joint dilatancy.

This problem is very similar to that of reinforcing bars in concrete and rock mechanics researchers have made use of concepts and ideas from this field (e.g. (8)).

Larsson and Olofsson (9) report on the results of measurements of maximum dowel forces made by Bjurstrom (10) in a series of experiments on bolted joints in a large shear box. From these tests it was possible to estimate the maximum dowel force, but only by determining empirical constants for the equations. This necessarily limits their use to the specific conditions of the test and rock samples used.

The simplest approach is to assume that bolt yielding occurs when sliding of the joint plane begins at which time the maximum dowel force, F_d, is mobilized. That is to say, during the elastic part of joint shear dowel action is absent. From the standpoint of this model, the dowel forces can be treated as equivalent to an increase in joint cohesion. The total joint cohesion, c_T, is composed of the joint cohesion, c_j, and the effective cohesion from dowelling action, c_d:

.... (3.4)

c_d is calculated from:

.... (3.5)

where A = tributary area of the joint surface per bolt, (e.g. for a square bolt pattern with spacing, D, tributary area is D^2),

α = is the angle between the bolt and joint plane (Fig. 3.3).

The maximum dowel force, F_{max}, may be estimated by adopting a suitable failure criterion. For example, Larsson and Oloffson (9) determined F_m from the Von Mises yield criterion and by assuming pure shear:

$$F_{max} = \tau_{max} \ A = \frac{\sigma_y \ \pi r^2}{\sqrt{3}} = 1.81 r^2 \sigma_y \ .... \qquad (3.6)$$

where r = bolt radius,

and σ_y = yield stress of bolt.

From Bjurstrom's work mentioned earlier (10), the dowel force, F_d, was found to be approximately proportional to the angle between the bolt and shear plane (Fig. 3.3):

$$F_d = \begin{cases} F_{max} \frac{\alpha}{90} & \text{if } \alpha \leq 90° \\ F_{max} \frac{(180-\alpha)}{90} & \text{if } \alpha > 90° \end{cases} \ .... \qquad (3.7)$$

The actual dowel force developed in a given installation may be less than, or greater than, that given by equations 3.6 or 3.7. Much will depend upon the strength of the resin and rock and joint dilatancy. Probably the most rigorous attempt to date to develop a theoretical model for the shear behaviour of grouted, untensioned bolts into the plastic range and which includes failure of the grout and rock is that of Dight (11). The goal of his 1983 Ph.D. thesis entitled, "Improvements to the Stability of Rock Slopes in Open-Pit Mines", was to establish the technical feasibility of steepening open pit slopes through the systematic installation of this type of support in bench faces, i.e., increase overall slope angle by steepening all bench faces.

His experimental work indicated the need to develop a theory which would correctly model the response of the bolt to shearing, the point of flexure of the bolt (plastic hinge), and the bearing capacity of the rock/grout as a function of shear displacement (Fig. 3.4). The interested reader should refer to the thesis for the full development of this interesting model. In summary, the following steps are taken:

i) Assume a free body diagram for the dowel (Fig. 3.5);

ii) Following Dulacska (8) (plastic theory, Tresca material), find the location of the plastic hinge, 1, and the dowel or shear force, F (Fig. 3.5):

$$F = Dp_u\{ -\frac{t}{2} \pm \sqrt{\frac{t^2}{4} + \frac{1.7}{16}\frac{\sigma_y}{p_u} \cdot \frac{\pi D_b^3}{D}(1-(T/T_y)^2)}\} \quad \ldots \qquad (3.8)$$

$$1 = -\frac{t}{2} \pm \sqrt{\frac{t^2}{4} + \frac{1.7}{16}\frac{\sigma_y}{p_u}\frac{\pi D_b^3}{D} \cdot (1-(T/T_y)^2)}\} \quad \ldots \qquad (3.9)$$

where t = the infill thickness along the joint or depth of cracking occurring in the grout and/or rock during shearing;

D = D_b , the diameter of the bolt when the grout is weaker than the rock;

D = D_h , the diameter of the grout when the grout is stronger than the rock;

P_u = bearing capacity of the rock or grout,

σ_y = yield strength of bolt;

T = tensile force in bolt (which influences the moment distribution and hence the position of the plastic hinge);

T_y = tensile force at bolt yield.

When the infill thickness, $t = 0$:

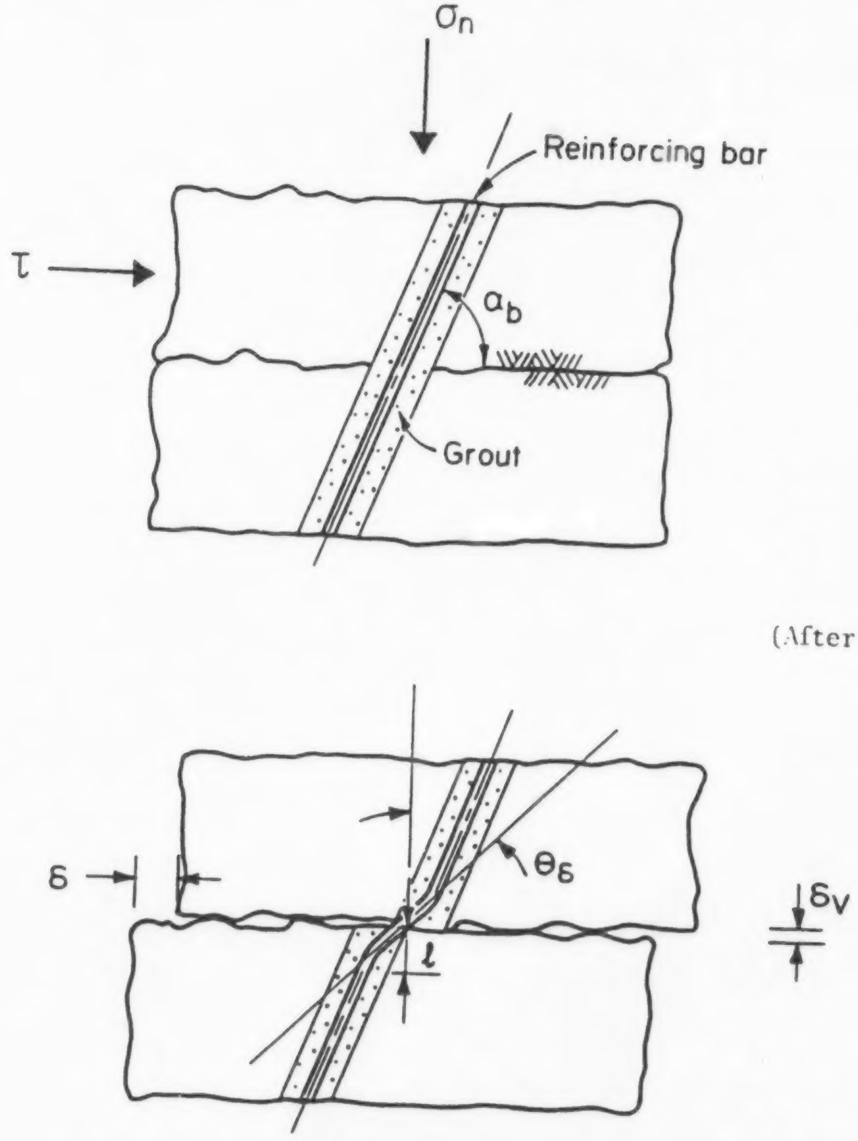
σn
Reinforcing bar
τ
ab
Grout
δ
θδ
δv
l

(After (11))

$$\text{Angle of Dilation} = \text{ATAN}\left(\frac{\delta_v}{\delta}\right) = i$$

Figure 3.4 Deformation of a dowel in shear

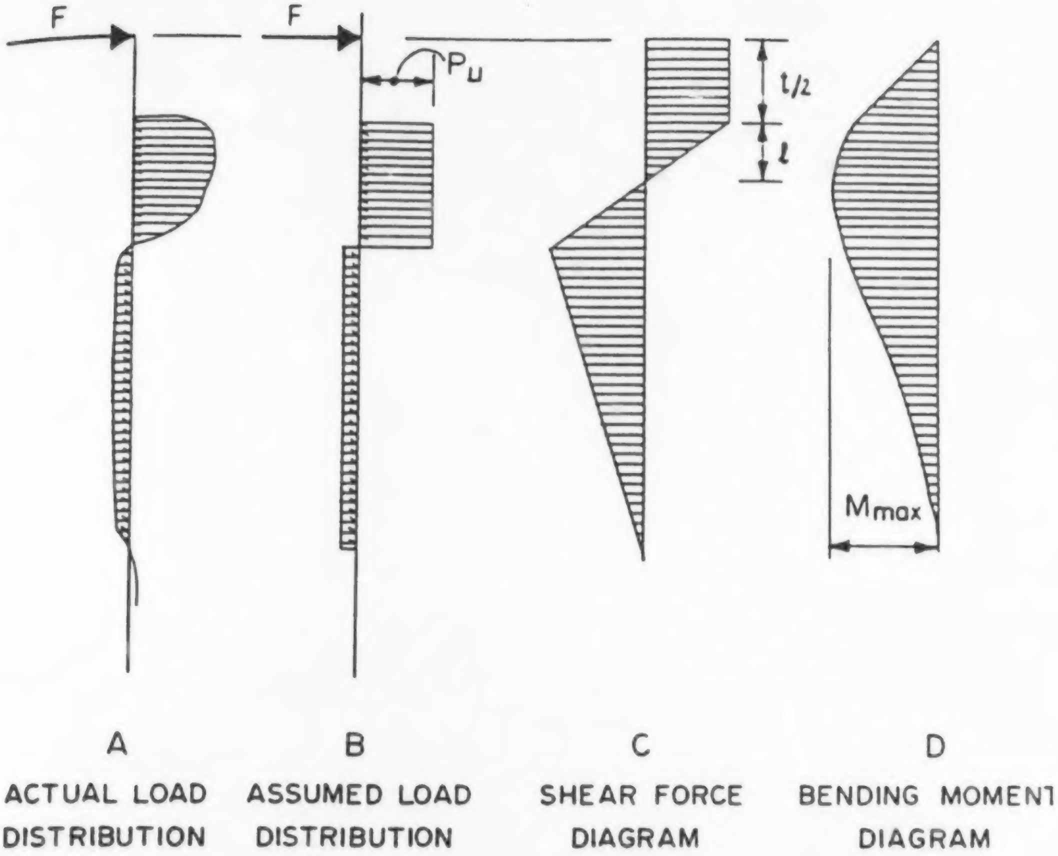
F
F
P_u
$t/2$
l
M_{max}
A
ACTUAL LOAD DISTRIBUTION
B
ASSUMED LOAD DISTRIBUTION
C
SHEAR FORCE DIAGRAM
D
BENDING MOMENT DIAGRAM

$\frac{t}{2} = \frac{1}{2}$ joint thickness (in case of joint infill)

$(\frac{t}{2} + l)$ = distance to maximum moment from shear plane

(After (11))

F = shear force perpendicular to dowel

Figure 3.5 Free body diagram for a dowel in shear

$$F = \frac{D_b}{4}\sqrt{1.7 \cdot \sigma_y \cdot P_u \, \pi D_b \cdot D(1-(T/T_y)^2)} \quad \cdots\cdots\cdots\cdots \quad (3.10)$$

$$\ell = \frac{D_b}{4}\sqrt{1.7 \cdot \frac{\sigma_y}{P_u} \cdot \pi \, \frac{D_b}{D}\,(1-(T/T_y)^2)} \quad \cdots\cdots\cdots\cdots \quad (3.11)$$

when crushing occurs in the rock, and,

$$F = \frac{D_b^2}{4}\sqrt{1.7 \, \sigma_y \cdot P_u \, \pi(1-(T/T_y)^2)} \quad \cdots\cdots\cdots\cdots \quad (3.12)$$

$$\ell = \frac{D_b}{4}\sqrt{1.7 \, \frac{\sigma_y}{P_u} \cdot \pi(1-(T/T_y)^2)} \quad \cdots\cdots\cdots\cdots \quad (3.13)$$

when crushing occurs in the grout.

iii) Calculate the bearing capacity, P_u, as a function of shear displacement using Ladanyi's elastic-brittle-plastic, expanding cavity theory (12,13) (Fig. 3.6).

iv) Since the bolt rotates (assuming rigid body movements) (Fig. 3.4), calculate dowel force in direction of shearing, F_s, (Fig. 3.7):

$$F = \frac{F}{\cos\theta_\delta} \quad \cdots\cdots\cdots\cdots \quad (3.14)$$

where the angle, θ_δ, is determined from the hinge length, l, and the shear displacement at that stage.

v) Find the components of the tensile force developed in the bolt parallel and perpendicular to the direction of shearing (Fig. 3.8) and determine the shearing resistance of the joint, T_b :

$$T_b = T_y(\sin\theta_\delta + \tan(\phi_b + i)\cos\theta_\delta) \quad \cdots\cdots\cdots \quad (3.15)$$

where ϕ_b = base friction angle of joint

i = roughness or dilation angle of joint.

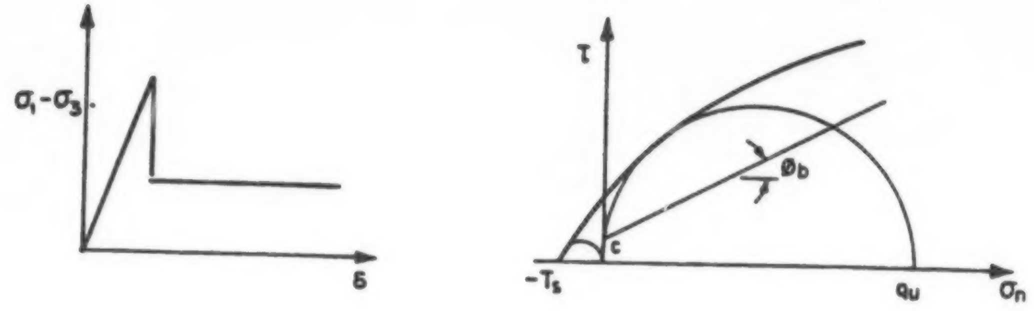
$\sigma_1 - \sigma_3$
δ
τ
$\emptyset_b$
c
$-T_s$
q_u
σ_n

a) Constitutive behaviour of an ELASTIC-BRITTLE-PLASTIC MATERIAL

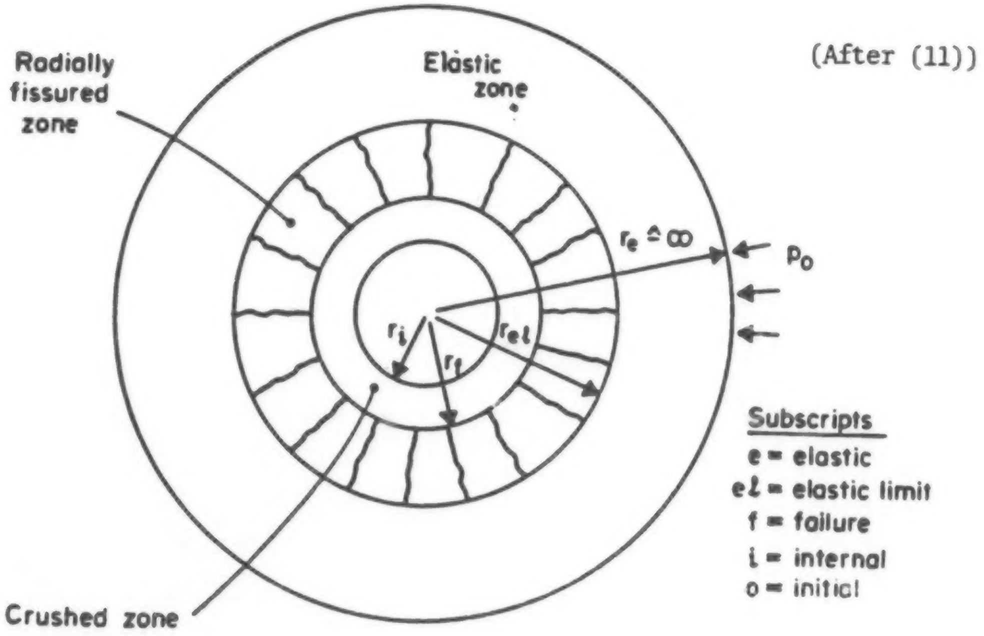
Radially fissured zone
Elastic zone
$r_e \triangleq \infty$
p_0
r_i
r_f
r_{el}
Crushed zone
Subscripts
e = elastic
el = elastic limit
f = failure
i = internal
o = initial

(After (11))

b) Plan view of an EXPANDING CYLINDER IN AN ELASTIC-BRITTLE-PLASTIC MATERIAL

Figure 3.6 Styles of failure assumed to occur in the grout or rock during shear of a bolted joint (expanding cylinder model in a elastic-brittle-plastic material)

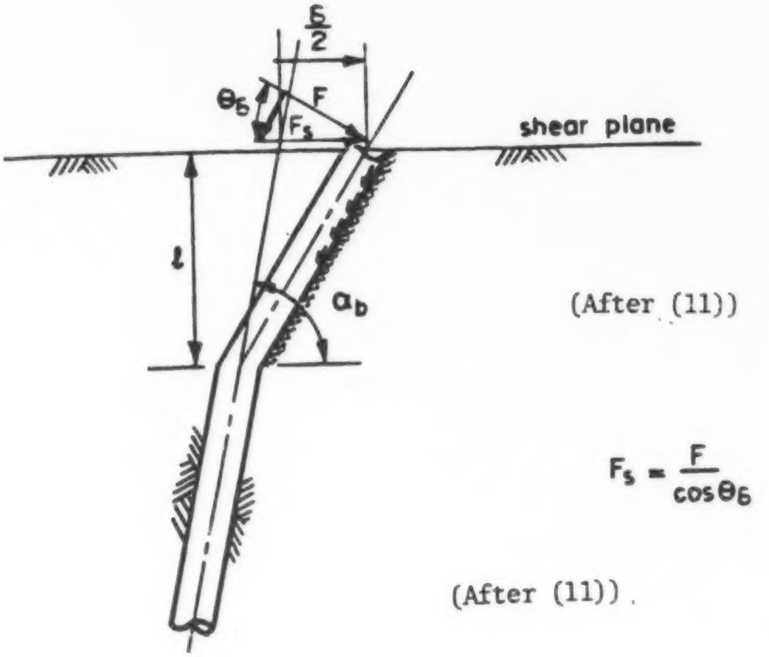

δ/2
θδ
F
Fs
shear plane
l
αb

(After (11))

$$F_s = \frac{F}{\cos\theta_\delta}$$

(After (11)).

Figure 3.7 Distribution of dowel forces after shear displacement

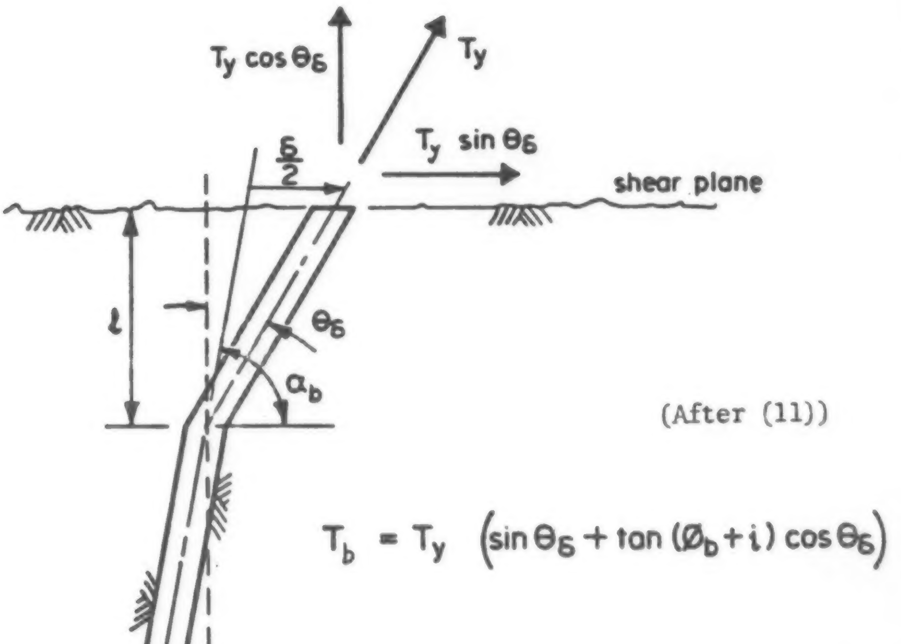

Ty cos θδ
Ty
Ty sin θδ
δ/2
shear plane
l
θδ
αb

(After (11))

$$T_b = T_y \left(\sin\theta_\delta + \tan(\emptyset_b + i)\cos\theta_\delta\right)$$

Figure 3.8 Distribution of tensile forces in bolt after shear displacement

The shear strength of the bolt at this point is:

$$0.5\ T_y/\cos\ \theta_\delta$$

$$= 1.57\ r^2\ \sigma_y/\cos\ \theta_\delta \quad \text{(cf. Equation 3.6))}$$

where r = bolt radius,

and σ_y = yield stress of bolt.

Four series of tests were conducted to evaluate the theory and involved the shearing of model dowels, rebar and destressing strand in plaster, basalt and steel. Joints of various dilation or roughness angles were used and dowels were installed at various angles. In general, the theory was found to be a good predictor of measured response. Figures 3.9 - 3.11 are three examples of shear displacement vs. shear force from experiments and the predicted curves.

Dight's theoretical model is a major step in our ability to predict bolt behaviour. The theory does involve some significant approximations, yet for design purposes the predictions are sufficiently close to actual response.

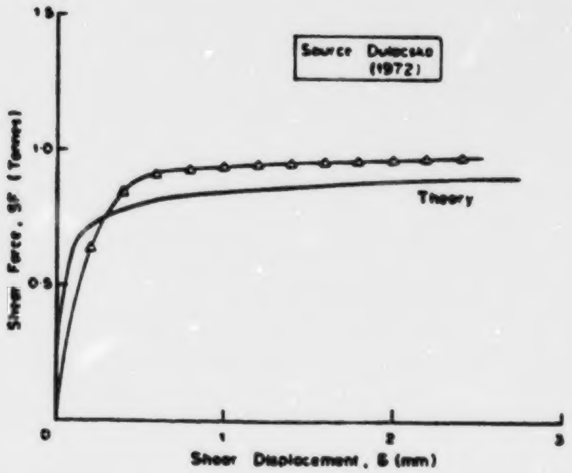

(After (11))

Figure 3.9 Comparison of Dight's theory with experimental data

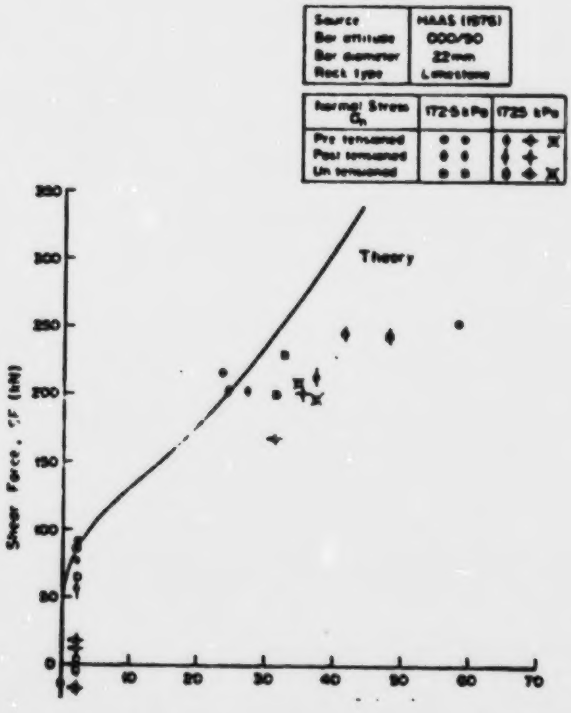

(After (11))

Figure 3.10 Comparison of Dight's theory with experimental data

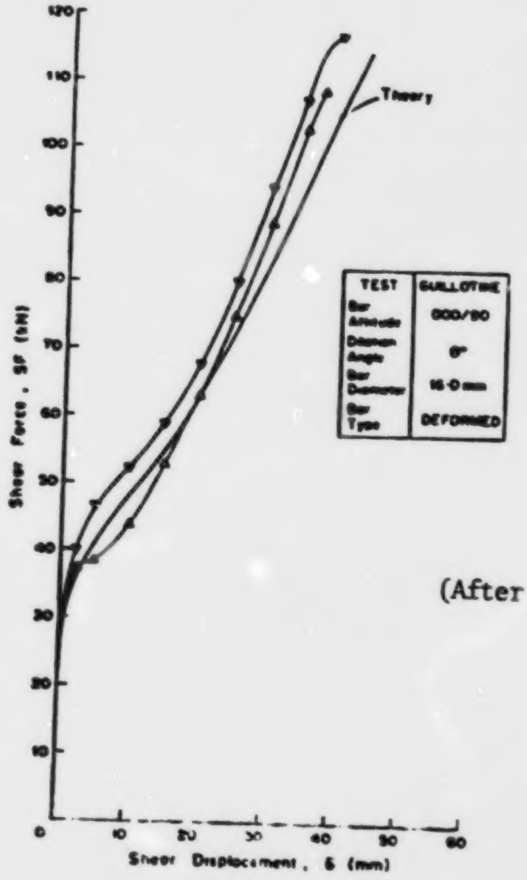

(After (11))

Figure 3.11 Comparison of Dight's theory with experimental data

REFERENCES

1. International Symposium on Rock Bolting. Abisko, Sweden, August - September 1983. Proceedings edited by Ove Stephansson and published by A.A. Balkema/Rotterdam/Boston. (1984).

2. Fairhurst, C. and Singh, B. Roof bolting in horizontally laminated rock. Engineering and Mining Journal, February, pp. 80-90. (1974).

3. Gerrard, C. Rock bolting in theory: a keynote lecture. Proc. Int. Symp. on Rock Bolting, Sweden, pp. 3-32. (1983).

4. Pells, P.J.N. The behaviour of fully grouted rock bolts. Proc. 3rd. Congr. Int. Soc. for Rock Mech., Denver, Vol. 2, Part B, pp. 1212-1217. (1974).

5. Fuller, P.G. and Cox, R.H.T. Mechanics of load transfer from steel tendons to cement based grout. 5th Australian Conf. Mech. of Structures and Materials, Melbourne, pp. 189-203. (1975).

6. Natau, O.P. and Wullschager, D.H. Theoretical and experimental studies in bearing behaviour and corrosion protection of rock anchors up to a load limit of about 4900 kN. Proc. 5th. Cong. Int. Soc. for Rock Mech., Melbourne, pp. A59-A64.

7. Ortlepp, W.D. Considerations in the design of support for deep hard-rock tunnels. Proc. 5th. Cong. Int. Soc. for Rock Mech., Melbourne, pp. D179-D187. (1983).

8. Dulacska, H. Dowel action of reinforcement crossing cracks in concrete. J. Am. Concrete Inst., Vol. 69, No. 12, pp. 754-757. (1972).

9. Larsson, H. and Olofsson, T. Bolt action in jointed rock. Proc. Int. Symp. on Rock Bolting, Abisko, Sweden, pp. 33-46. (1983).

10. Bjurstrom, S. Bergbultforband i sprucket berg. Fortifikationsforvaltningen, Forskningsbyran, Rapport nr. 121:3, Stockholm. (1973).

11. Dight, P.M. Improvements to the stability of rock slopes in open-pit mines. Ph.D. Thesis, Monash University, Australia. (1983).

12. Ladanyi, B. Failure mechanism of rock under a plate load. Proc. 1st. Cong. Int. Soc. Rock Mech., Lisbon Vol. 1, pp. 415-420. (1966).

13. Ladanyi, B. Expansion of cavities in brittle media. Int. J. Rock Mech. Min. Sci., pp. 301-328. (1967).

CHAPTER 4

ANALYTICAL MODELLING OF THE BEHAVIOUR OF RESIN-BOLTED STRATA

4.1 INTRODUCTION

The modern development of digital computers has given us the necessary tool to exploit analytical methods of stress analysis. Numerical methods, in particular, have become widely used for simulating the behaviour of rock masses. Empirical and simple analytical models are still generally used for practical rock bolt pattern design, but development of improved numerical models and the expanding memory capacity and speed of computers will in time make these computer-based techniques suitable for practical application on an increasing scale.

Numerical methods are not without their problems and should only be used when the assumptions and limitations of the program are well understood. Also, and particularly for the more complex programs, the input parameters are known only with limited accuracy, if at all. Thus, the major value at this time of numerical methods in the study of bolted strata is in improving our understanding of the interaction between the support and the rock mass under conditions of varying loads, excavation geometries, and in various types of rock mass. This improved understanding should lead to better ground control strategies and procedures.

4.2 APPROACHES TO THE NUMERICAL MODELLING OF BOLTED STRATA

In general, if linear elastic models of rock behaviour are assumed there is little interaction between the support and the rock mass. Realistic simulations require that larger displacements are modelled, for it is precisely in these situations that rock support is mandatory. This constraint means that, ideally, the various non-linear and time-dependent features of rock masses should be modelled and this necessarily means programs are complex and costly.

Rock Mechanics numerical analysts are divided into two schools as regards the basic approach to use in simulating a resin bolted rock mass. One school seeks to formulate the jointed and bolted rock mass as an "equivalent" continuous material. The other school believes it is necessary to model all of the rock discontinuities and bolts separately. There is also a "hybrid" position.

The advantages of the "equivalent" materials method are economy, simplification of analysis and the ability to use well established principles of continuum mechanics. Where the rock mass behaviour is clearly controlled by prominent discontinuities, such as in horizontally bedded coal mine roof with discrete separation (bedding) planes, this method is not applicable. It is more permissible when joint and bolt spacings are close and regularly spaced and are smaller than the critical dimension of the opening (e.g. span).

4.3 EXAMPLE OF AN EQUIVALENT MATERIALS MODEL OF A BOLTED ROCK MASS

A number of researchers at the 1983 International Symposium on Rock Bolting in Abisko, Sweden, presented results of their latest work using the equivalent materials approach (1-3). For example, Gerrard and Pande's (1) simulations of a bolted rock pillar subject to compression and a bolted set of joints subjected to shear (Fig. 4.1) are examples of state-of-the art development. They used an elasto-visco-plastic rheological unit (Fig. 4.2) (4) in which springs, sliders and dashpots are combined to model elastic response and time-dependent yielding in either tension or shear. The mechanical properties of the rock, each joint set, and each set of reinforcements, are described by separate rheological units. By connecting the unit for the rock

(After (1));

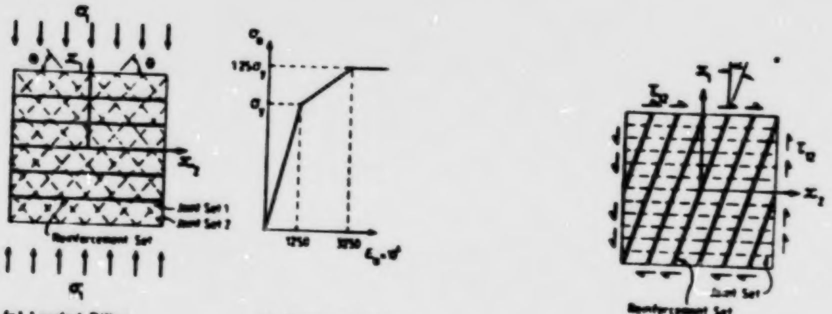
σ_1
τ_1
x_2
Joint Set 1
Joint Set 2
Reinforcement Set
σ_1
σ_b
$1.25\sigma_y$
σ_y
1250
3250
$\epsilon_b \cdot 10^6$
x_1
τ_{12}
x_2
Joint Set
Reinforcement Set

(a) Loaded Pillar

(b) Strain Hardening Curve

(a) Bolted Joint Set Undergoing Shear

Figure 4.1 Two bolted rock masses analysed by Pande and Gerrard's equivalent materials model

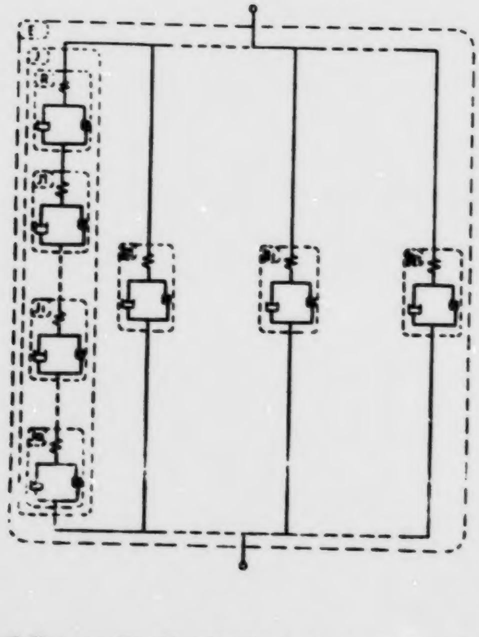

(After (4))

Figure 4.2 Pande and Gerrard's rheological analogue of a bolted jointed rock mass

material in series with that for the rock joints a representation of the jointed rock mass is achieved. The effect of reinforcement by bolting is then obtained by tying the jointed rock unit in parallel with each of the units representing the various reinforcements all experience the same global strain and share the global stress, in accordance with the assumption of perfect bonding between bolt and rock.

The pillar (Fig. 4.1) simulation assumes the mechanical properties of the joints sets are defined by a cohesion, c, an angle of friction, ϕ, an angle of dilation, ψ , and an elastic compliance, $\underset{\sim}{S}$. The intact rock is isotropic and elastic with a Young's modulus of 70 GPa and Poisson's ratio of 0.3. The steel reinforcement comprises a proportion, p , of the total volume of the pillar and has a Young's modulus of 200 GPa, a Poisson's ratio of 0.3, and a uniaxial yield stress, σ_y, od 250 MPa. It was assumed in some cases to have a strain hardening behaviour (Fig. 4.1). A standard case was established with the following set of properties

ϕ = 40 deg.

ψ = 10 deg.

c = 50 kPa

θ = 45 deg. (inclination of one joint set to x_2 axis (see Fig. 4.1))

p = 0.1 %

No prestressing ($\sigma_0 / \sigma_y = 0$)

No strain hardening of steel bolt

S^{s}_{11} = 0.1 GPa^{-1}

S^{s}_{22} = 0.2 GPa^{-1}

$S^{s}_{12} = S^{s}_{21}$ = 0 GPa^{-1}

A sensitivity study was then conducted by varying each constant in turn while keeping all other constants with their standard case values. In Figure 4.3 the axial pillar stress, σ_1, and lateral strain, ε_2, are plotted against the axial strain, ε_1.

Clearly, behaviour is extremely sensitive to a number of these properties. Gerrard and Pande summarize the results as follows:

i) There was a marked variation in strength (i.e. maximum load attained) with both ϕ and θ, with sharp rises accompanying either a small increase in ϕ or a small decrease in θ;

ii) There appears to be linear relations between increases in c or p and the resultant increases in strength;

iii) The form of strain hardening assumed, as shown in Figure 4.1, is reflected in the 25% increase in strength attained after very high levels of strain.

iv) The strength produced with a reinforcement proportion of $p = 0.2\%$ is about 10 times greater than for the non-reinforced case.

v) The axial strain, ε_1, for a given applied load increased with increases in θ and $\underset{\sim}{S}$, and decreases in ϕ, c, p, ϕ and σ_0/σ_g.

vi) The strength remained coonstant when ϕ, σ_0/σ_y, and $\underset{\sim}{S}$ were varied.

vii) The lateral strain, ε_2, for a given applied load behaves ina similar fashion to ε_1, with the exception that it shows insignificant variations with ϕ and $\underset{\sim}{S}$.

viii) The axial strain, ε_1, at which strength is attained is minimal when σ_0/σ_y is high or $\underset{\sim}{S}$ is low and maximal for the case of strain hardening.

ix) A condition can be reached where the steel yields before the rock joints. This occurs for very high values of either σ_0/σ_y or $\underset{\sim}{S}$. On the assumption of ductile reinforcement, the rock joints will continue to resist increased load elastically until their yield conditionis reached, after which failure ensues.

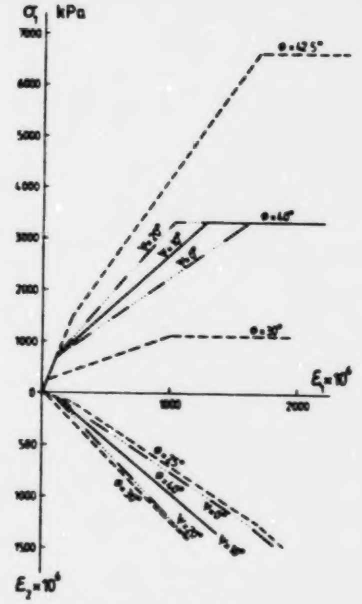

(a) Effects of φ, ψ

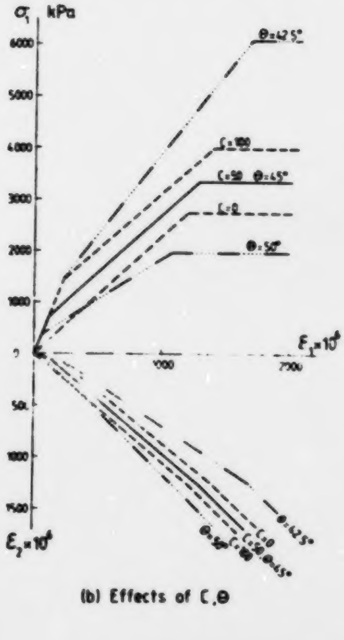

(b) Effects of C, θ

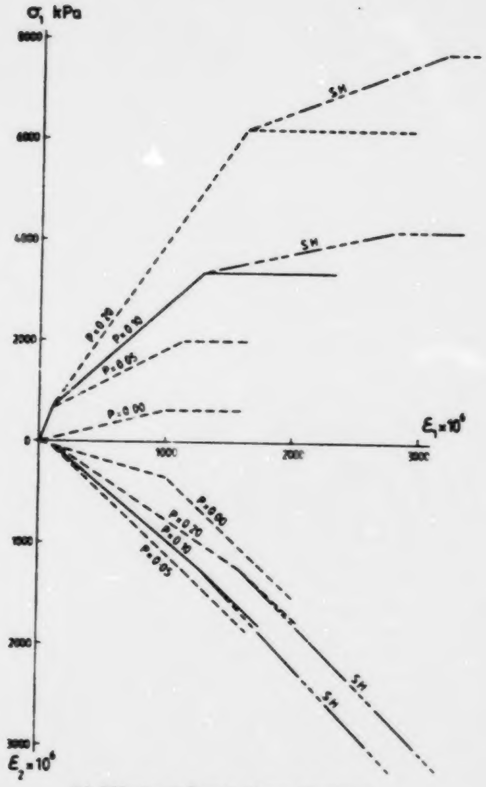

(c) Effects of P and Strain Hardening

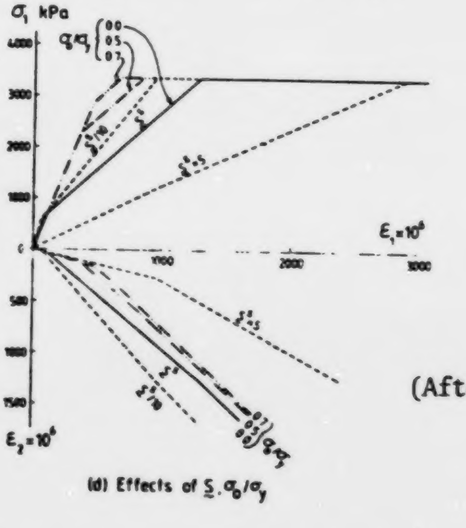

(d) Effects of S, σ0/σy

(After (1))

Figure 4.3 Results of sensitivity analysis of bolted pillar

Sensitivity studies, based on models such as this, give assistance to the practicing engineer by indicating the critical parameters on which efforts to obtain quantitative values should be concentrated if a reliable design is to be arrived at.

4.4 EXAMPLES OF DISCRETE MODELS OF BOLTED ROCK MASSES

Cundall's discrete element method (5) treats the rock mass as a discontinuum and through successive application of Newton's Second Law and the force-displacement law at each joint contact is able to simulate large total displacement in small time steps. A most interesting demonstration of the importance of local geological detail in controlling roof stability was described in (6). In a tunnel modelled in blocky rock (Fig. 4.4) it was shown that a slight change in the orientation of one joint would change the opening from stable (no support needed) to unstable (needing support). The latter case was analysed by Asai et al (7) using a numerical model of rigid blocks separated by special joint elements and was shown to be capable of support by three bolts.

The "key block" method of design developed by Shi and Goodman (8) is a most innovative approach. Using topological theory, it identifies the size and shape of key blocks which should be supported and the amount of support needed. These key blocks "tie" in the rest of the rock mass. This technique is particularly applicable to hard rock masses with discontinuous and rather irregularly spaced and oriented rock joints and other discontinuities. It does, however, require a detailed mapping of discontinuities (Fig. 4.5).

Several finite element programs have been developed for modelling bolted and jointed rock masses. Various approaches have been taken to model the bolt. Either a special element is incorporated, or it is assumed the bolt increases the stiffness and strength of the joint. The joint stiffness and strength is then modified to reflect the presence of the joint (9-11).

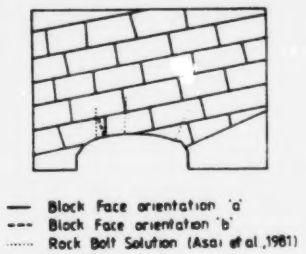
Block Face orientation 'a'
Block Face orientation 'b'
Rock Bolt Solution (Asai et al ,1981)

(a) Tunnel in Blocky Rock

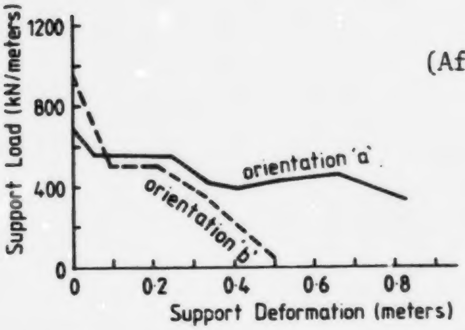

(After (6))

(b) Ground Support Interaction Curves

Figure 4.4 Discrete element analysis of stability of tunnel in blocky ground

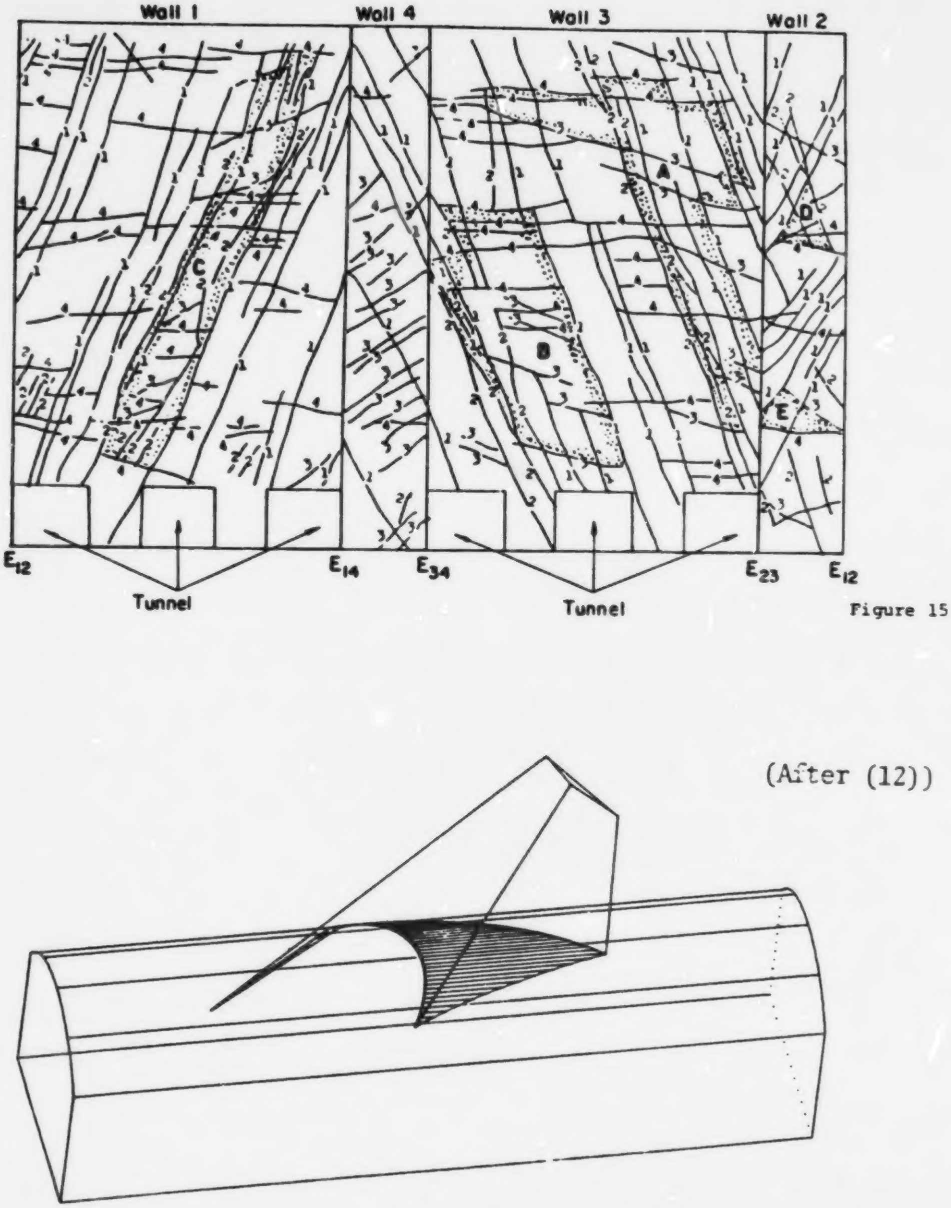
Wall 1
Wall 4
Wall 3
Wall 2
A
B
C
D
E
E$_{12}$
E$_{14}$
E$_{34}$
E$_{23}$
E$_{12}$
Tunnel
Tunnel

Figure 15

(After (12))

Figure 4.5 Detailed discontinuity mapping required for keyblock analysis

4.5 CONCLUSION

The development of analytical models is proceeding at a rapid pace. There is a need for the results of this work to be presented in useful format for the practicing engineer to assist him in achieving improved support designs and strategies.

REFERENCES

1. Gerrard, C. and Pande, G. Predicted responses of two cases of reinforced rock. Proc. Int. Symp. on Rock Bolting, Abisko, Sweden, pp. 47-54. (1983).
2. Larsson, H. and Olofsson, T. Bolt action in jointed rock. Ibid, pp. 33-46.
3. Wullschlager, D. and Natau, O. Studies of the composite system of rock mass and non-prestressed grouted rock bolts.
4. Pande, G.N. and Gerrard, C.M. The behaviour of reinforced jointed rock masses under various simple loading states. Proc. 5th Cong. Int. Soc. for Rock Mech., Melbourne, pp. F217-F223. (1983).
5. Cundall, P.A., Marti, J., Beresford, P., Lasti, N. and Asgian, M. Computer modelling of jointed rock masses. Tech. Report N-78-4, U.S. Army Corps of Engineers, Waterways Experiment Station, Vicksburg, Miss. (1978).
6. Voegele, M., Fairhurst, C. and Cundall, P. Analysis of tunnel support load using a large displacement, distinct block model. Rockstore 77, 1st. Symp. on Large Caverns, Stockholm, pp. 247-252. (1977).
7. Asai, T., Nishimura, M. and Saito, T. A numerical modelling technique for analyzing the behaviour of discontinuous rock masses. Proc. Int. Symp. on Weak Rock, Tokyo, pp. 737-742. (1981).
8. Goodman, R.E. and Shi, G. Block theory and its application to rock engineering. Prentice-Hall, Inc. (1985).
9. Kamal, S.A. Analysis of multi-axial anisotropic creep, roof resin bolts and bed separation in rock structures using the finite element method. Ph.D. Dissertation, Michigan Technological University. (1974).
10. Gerdeen, J.C., Viegelahn, G.L., Snyder, V.W., Schwab, P.M., Schuyten, H., Wick, C.J., and Collison, T.J. Finite element analysis applied to resin and mechanical roof bolting systems for strata bound deposits. Final report, U.S. Bureau of Mines, Contract H0230014, Michigan Technological University. (1976).
11. Heuze, F.E. and Goodman, R.D. Finite element and physical model studies of tunnel reinforcement in rock. Proc. 15th. U.S. Rock Mechanics Symp. (1974).
12. Shi, LG. and Goodman, R.E. Keyblock bolting. Proc. Int. Symp. on Rock Bolting, Abisko, Sweden, pp. 143--168. (1983).

CHAPTER 5

ON-SITE OBSERVATIONS OF DEFORMATION AND FAILURE OF ROOFS IN HORIZONTALLY BEDDED STRATA

5.1 INTRODUCTION

On-site observations of deformation and failures in mine roofs are an important source of information for design. Where a new mine is under development in a region with existing operations, experience gained in the latter will be used as a primary guide for ground control engineering in the new mine.

Roof instruments and studies of roof failures in mines are routinely used to monitor stability and to improve support procedures. Reasons for failure are looked for and solutions researched and applied.

A collapsed mass of rock on the mine floor is the ultimate stage of a progressive process. In general, it would be necessary to have a complete record of stress changes and displacements in the roof and bolting system and the roof's lithologies and geological structures, in order to obtain a thorough description and understanding of the failure process. Because all this data is rarely collected it is not always possible to determine the precise mechanisms which have led to failure (Fig. 5.1).

Finally, the root cause for a collapse may not be related to natural causes at all, but to poor installation of the support, e.g., incomplete breakage and mixing of resin capsule because the bolt hole was drilled too deep, or the resin was powdered because the capsule was spun too long, etc.

5.2 ROOF FAILURE MECHANISMS

Though many categories of roof failure in horizontally bedded strata have been described, they fall into only a few broad categories:

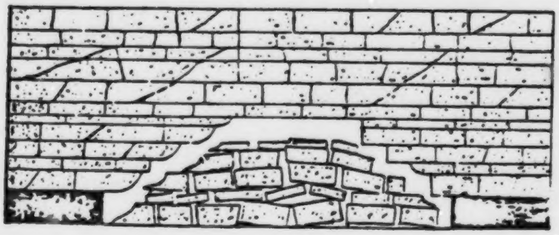

Figure 5.1 Roof fall resting on floor may not provide clear evidence of failure mechanics

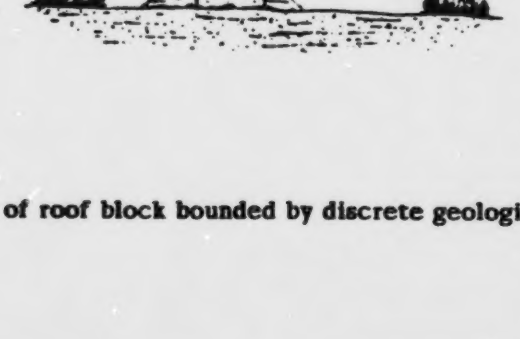

Figure 5.2 Failure of roof block bounded by discrete geological discontinuities

i) Gravity collapse of discrete blocks (Fig. 5.2) defined by geological structures.

ii) Gravity collapse of disrupted and disturbed strata from faulting, slickensiding, clay veins, coal rolls, etc. (Fig. 5.3).

iii) Sagging and failure of multiple layers bound by bedding planes (Fig. 5.4).

iv) Sagging and failure of multiple, cross-jointed layers bound by bedding planes (Fig. 5.5).

v) Development of new fractures and crushing due to high horizontal stresses or pillar punching (Fig. 5.6).

vi) Weakening and shrinkage/swelling of strata due to cyclical humidity changes, ventilation, and blasting.

The kinematics, mechanics and support of block failures (category (i)) are covered by Hoek and Brown (1) and by Goodman and Shi (2) in their textbooks.

Reliable stability analysis of highly disturbed ground (category (ii)) is difficult and in most cases instabilities are treated on an operational and pragmatic basis in the mine.

Failure mechanics and roof support design in situations of high lateral stress in bedded strata (category (v)) are dependent on stress levels. The latter may vary from layer to layer and even from one section of a mine to another, or from one part of a geological structure to another. Also, stiffer strata such as sandstones tend to have higher lateral stresses than softer materials, such as shales. No analytical methods are capable of predicting the virgin state of stress with any assurance and in-situ measurements, which are costly, are the only recourse if absolute stress values are required.

Special instability problems can arise from slake-prone shales, which shrink and swell and ultimately fail under the action of seasonal changes in humidity, or of the introduction of ventilation and its drying effect. Sealing of the shale by surface spraying of special sealants, or the protection of the shale by leaving a thin layer of coal in the roof, for example, are special techniques which may be called upon in these situations. Likewise, damage from heavy blasting can be avoided by judicious design of blast patterns, delays, choice of explosives, charge loads per delay, and sequencing. In many mines in horizontally bedded strata excavation is performed by continuous miners so that blasting is not, then, a problem.

The remainder of this report will be concerned primarily with the behaviour and support of roofs in categories (iii) and (iv), though some of the material is applicable to category (i) also.

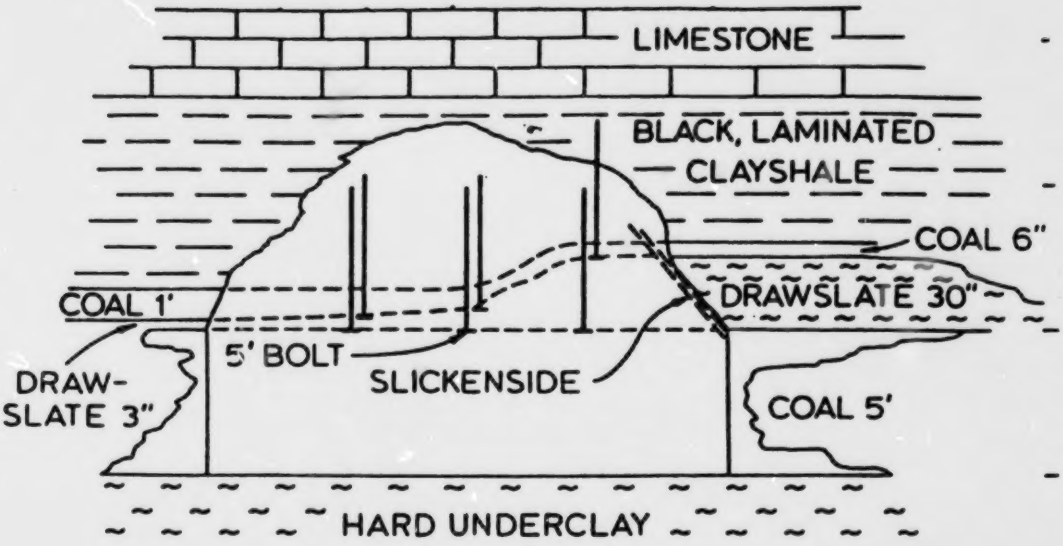
LIMESTONE
BLACK, LAMINATED
CLAYSHALE
COAL 6"
DRAWSLATE 30"
COAL 1'
5' BOLT
SLICKENSIDE
DRAW-
SLATE 3"
COAL 5'
HARD UNDERCLAY

Figure 5.3 Roof fall in region of "disturbed" geology - roll in roof seam, slickensiding and drawslates

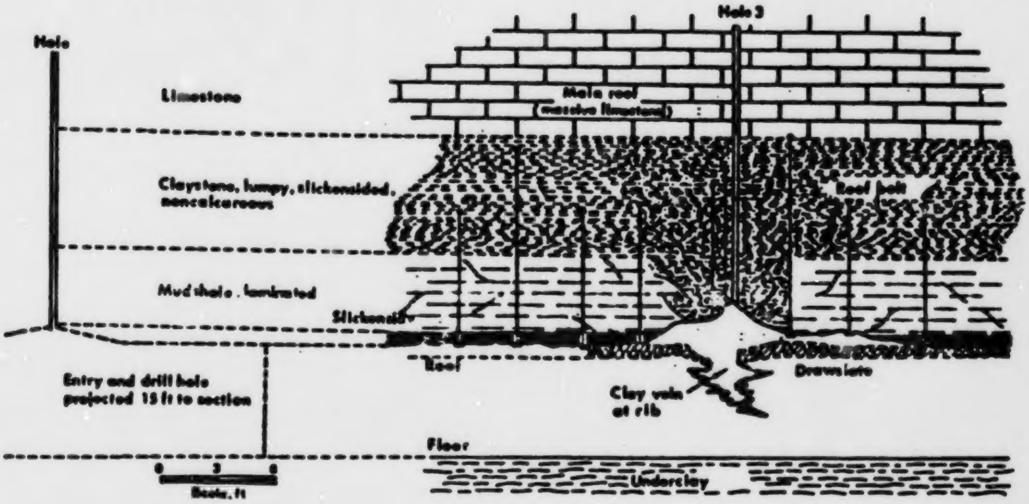
Hole 3
Hole
Limestone
Main roof
(massive limestone)
Claystone, lumpy, slickensided, noncalcareous
Roof bolt
Mudshale, laminated
Slickenside
Roof
Drawslate
Entry and drill hole projected 15 ft to section
Clay vein
at rib
Floor
0
3
6
Scale, ft
Underclay

Figure 5.4 Clay vein in slickensided roof

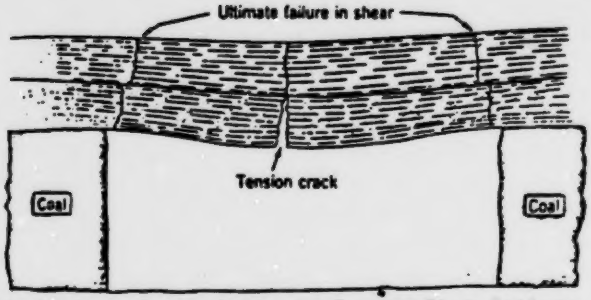
Ultimate failure in shear
Tension crack
Coal
Coal

(a) Action of immediate roof preceding failure.

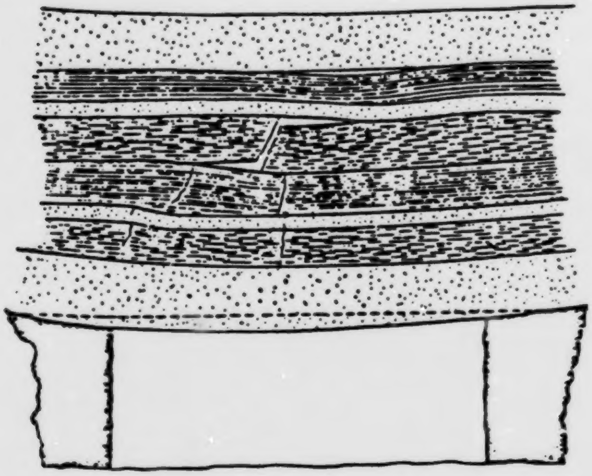

(After (5))

(b) Possible development of 'cutters'.

Figure 5.5 **Sagging and failure in multiple layer roofs bounded by bedding planes**

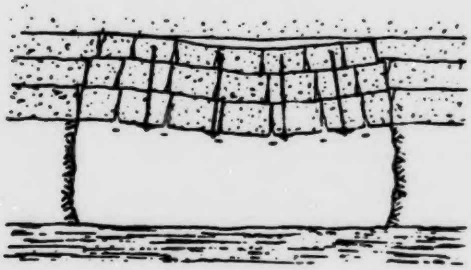

(After (4))

Figure 5.6 **Sagging and failure of multiple layer, cross-jointed roofs bounded by bedding planes**

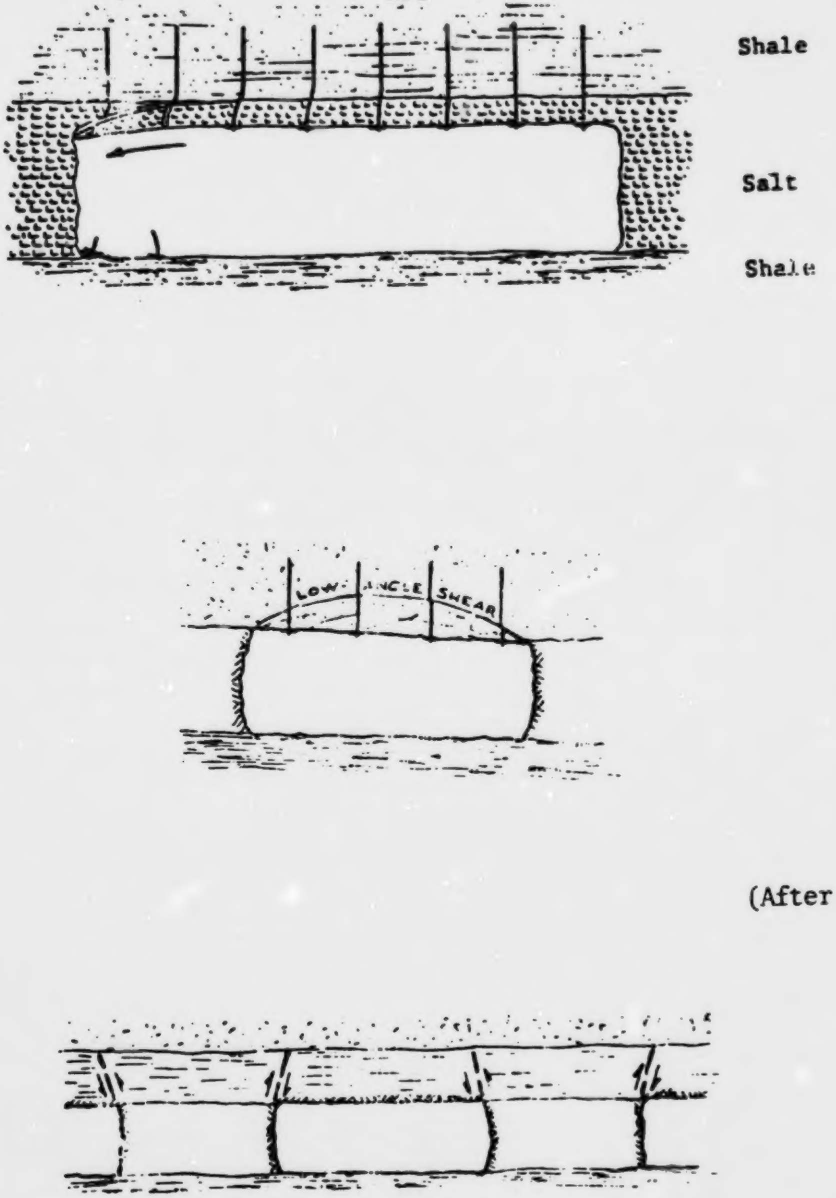
Shale
Salt
Shale
LOW ANGLE SHEAR

(After (4))

Figure 5.7 Development of new fracture surfaces due to high lateral stresses and pillar punching into roof

REFERENCES

1. Hoek, E. and Brown, E.T. Underground excavations in rock. Inst. of Mining and Metallurgy, London. (1980).

2. Goodman, R.E. and Shi, G. Block theory and its application to rock engineering. Prentice-Hall, Inc. (1985).

3. Moebs, N.N. Unpublished internal memo, Pittsburgh Mining and Safety Centre, USBM as reported in Final Report on: Design criteria for roof bolting plans using resin-grouted, nontensioned bolts to reinforce bedded mine roof. Contract No. J0366004, U.S.B.M. (1977).

4. Peng, S.S. Coal mine ground control. John Wiley & Sons. (1978).

5. Thomas, E. Roof bolting. CIM Bulletin, May. (1950).

CHAPTER 6

MECHANICS OF SUPPORT BY BOLTING OF HORIZONTALLY BEDDED STRATA

6.1 INTRODUCTION

Chapter 5 closed with the statement that the remainder of this report will deal with roof categories (iii) and (iv). These comprise mine roofs which may be treated as a series of vertically stacked layers, each layer separated by horizontal planes (typically weak bedding surfaces) and either intact (solid beam) or traversed by vertical cross-joints (Fig. 6.1). They represent the two most general cases, which can be examined by various analytical and physical modelling techniques to determine some general support principles and strategies. The other categories must be treated more on a case by case basis.

6.2 SUPPORT MECHANISMS

Support mechanisms may be usefully divided into two broad categories as follows:

i) Suspension
ii) Reinforcement

In the suspension mode, the dead load of that portion of the bolted roof which is sagging, is assumed to be transferred to the bolts. Bed separation is reduced; long-term support is ultimately determined by bolt length and long-term pull-out strength.

In the reinforcement mode the bolts improve (reinforce) the rock mass by increasing strength and stiffness and its self-supporting capacity. A number of separate mechanisms operate in reinforcement and will be discussed individually in Section 6.2.2 below.

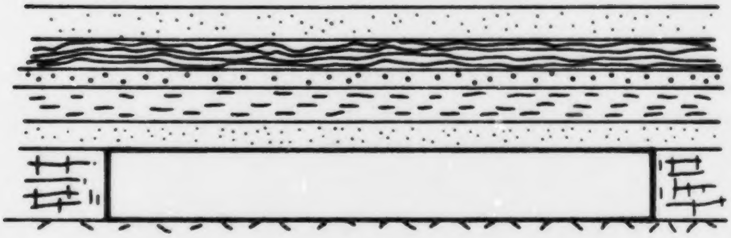

(a)

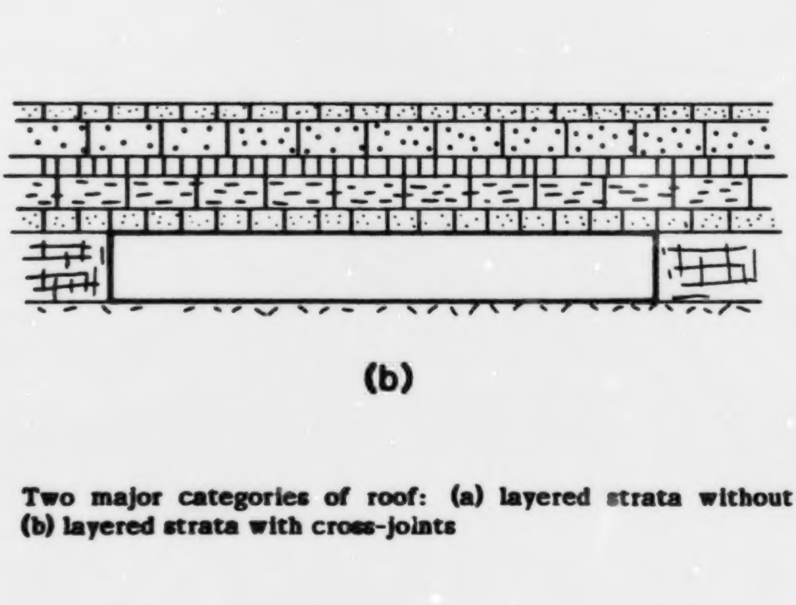

(b)

Figure 6.1 Two major categories of roof: (a) layered strata without cross-joints, (b) layered strata with cross-joints

6.2.1 Suspension Mode

In using the suspension mode for design, it is usually assumed that the full load of the volume of rock, which could collapse, is to be supported by the bolts, i.e., no contribution to support by the abutments or the rock mass itself. Calculations are then quite sraightforward. For example, if there are n, bolts in each row and n_2 rows, the load per bolt, P, is:

$$\frac{\gamma LBd}{(n_1 + 1)(n_2 + 1)} \quad \ldots\ldots\ldots\ldots\ldots \quad (6.1)$$

where γ = unit weight of roof strata,

L = length of roof along axis of heading,

B = roof span,

d = thickness of strata to support.

Suspension effects also describe the situation where tensioned bolts are employed to support a group of layers with different flexural stiffnesses. For example, if a layer of lower flexural stiffness underlies a layer of greater flexural stiffness, an installed bolt will come under load as the lower layer tries to separate. To eliminate this separation, each bolt must apply a force per unit area, Δf. The total force per unit area of each beam is then

$$(\gamma_1 d_1 + \Delta f) \text{ , for the lower beam} \quad \ldots\ldots\ldots\ldots\ldots \quad (6.2)$$

$$(\gamma_2 d_2 - \Delta f) \text{ , for the upper beam} \quad \ldots\ldots\ldots\ldots\ldots \quad (6.3)$$

where d_1 and d_2 are the thicknesses of the lower and upper beams, respectively, and γ_1 and γ_2 are the unit weights of the lower and upper beams, respectively.

Viewed another way, these equations may be interpreted as showing a reduction in the unit weight of the lower beam and an increase in the unit weight of the upper beam.

If it is assumed that both layers behave like a clamped elastic beam, then the maximum deflection, u , of each beam is given by:

$$u^{max}_{lower} \ , \ u^{max}_{upper} = \frac{\gamma B^4}{32Ed^2} \qquad \ldots\ldots\ldots\ldots\ldots \qquad (6.4)$$

where γ = effective unit weight of layer (from eqns. 6.2 and 6.3),

B = roof span,

E = Young's modulus of layer,

d = thickness of layer.

But, because of bolting, it may be assumed that the deflections are equal. Therefore, by equating the two deflections from equation 6.4, it is found that:

$$\Delta f = \frac{\gamma_2 d_2 E_1 d_1^3 - \gamma_1 d_1 E_2 d_2^3}{E_1 d_1^3 + E_2 d_2^3} \qquad \ldots\ldots\ldots\ldots \qquad (6.5)$$

This type of suspension will also redistribute stresses in the two layers. For example, for the same assumption of a linear elastic clamped beam, the maximum tensile fibre stress, in each layer is:

$$\sigma^{max}_{upper} = \frac{(\gamma d + \Delta f)B^2}{2d^2} \qquad \ldots\ldots\ldots\ldots\ldots \qquad (6.6)$$

and,

$$\sigma^{max}_{lower} = \frac{(\gamma d - \Delta f)B^2}{2d^2} \qquad \ldots\ldots\ldots\ldots\ldots \qquad (6.7)$$

where γ = unit weight of layer.

The suspension mode remains the primary mode of design for roof support. A new method for estimating roof loadings for design is developed in Chapter 14.

6.2.2 Reinforcement

Several modes of reinforcement have been postulated, but may all be reduced to three general categories:

i) Beam building
ii) Arch formation
iii) Rock mass strength increase.

6.2.2.1 Beam Building

Beam building constitutes any procedure by which the stack of layers of different flexural stiffnesses is constrained to behave like a single, thick beam. Since, for an end-clamped elastic beam, the maximum bending strain is inversely proportional to thickness, the thicker the beam the smaller the induced strains and the greater the Factor of Safety against fracture.

In the general case, layers either separate or remain in contact and undergo relative shear displacement along the contact as sagging of the roof develops. Which of these responses occurs depends upon the flexural stiffnesses and relative positions of the layers (Fig. 6.2).

Bed separation is reduced, or prevented, by the installation of bolts with high axial stiffness (untensioned resin bolts), or by using tensioned, point anchored bolts. These mechanisms are essentially the "suspension" effect discussed earlier.

True beam building is developed by reducing (and ideally) eliminating relative shear displacement between the layers. This can be achieved by increasing the shear stiffness and strength of the interface. With non-tensioned resin bolting the shear stiffness, shear strength of the bolt (see Chapter 2) and bedding plane friction contribute to beam building. With tensioned, ungrouted bolts, only frictional effects are developed. In this case, loss of bolt tension involves loss of any beam building

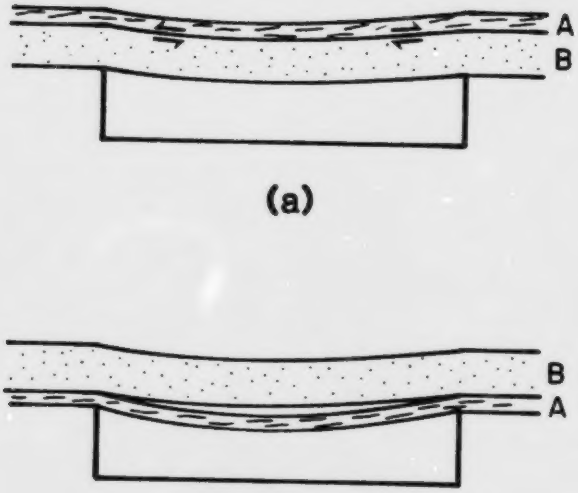

(a)

(b)

Figure 6.2 Effect of relative flexural stiffnesses and positions of layers on roof response. Flexural stiffness of beam A less than flexural stiffness of beam B.

effects.

Some concept of the magnitude of bolt tension required to prevent bedding plane slip can be estimated by appealing to linear elastic, clamped beam theory used earlier in this Chapter. For this case, the maximum shear stress at any point distant x from one end of the beam, selected as origin, is:

$$\tau^{max} = \frac{3\gamma}{2}\left(\frac{B}{2} - x\right) \qquad \text{..............} \quad (6.8)$$

The average frictional resistance developed by an average normal bolt stress, σ_b, is $\sigma_b \tan \phi_b$, where ϕ_b is the effective angle of friction of the bedding plane. At limiting equilibrium frictional stress will be equal to the applied shear stress (eqn. (6.8)):

$$\sigma_b \tan\phi_b = \frac{3\gamma}{2}\left(\frac{B}{2} - x\right) \qquad \text{..............} \quad (6.9)$$

or

$$\sigma_b = \frac{3\gamma}{2 \tan\phi_b}\left(\frac{B}{2} - x\right) \qquad \text{..............} \quad (6.10)$$

Shear stresses are highest at the ends of the beam (x = 0). Therefore, to eliminate all slip:

$$\sigma_b \geq \frac{3\gamma B}{4 \tan\phi_b} \qquad \text{..............} \quad (6.11)$$

Figure 6.3 is a graphical representation of eqn. (6.11) for a range of spans and demonstrates that the bolt normal stress required to prevent slip is very sensitive to roof span and frictional properties of the interface. The normal stress developed by bolts at typical spacings is relatively small, except close to the bolt. If a very high strength bolt (yield strength 517 MPa and diameter = 2.54 cms) is torqued to 50 percent of its yield strength, and the normal stresses are distributed into the rock mass in a 45 degree cone (Fig. 6.4), the normal stresses developed at different distances into the roof can be estimated (Fig. 6.4). From Figures 6.3 and 6.4 the depth into

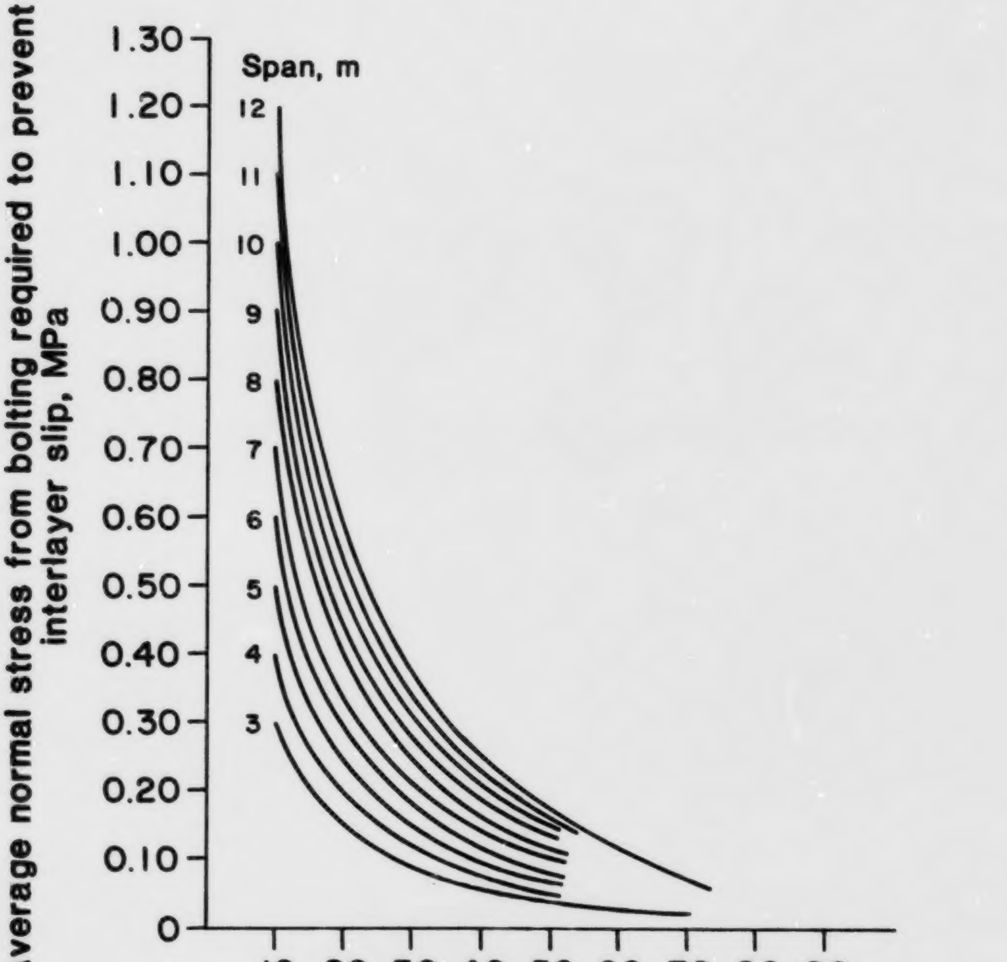

Figure 6.3 Normal stress generated by bolt loads at different distances from point of load application

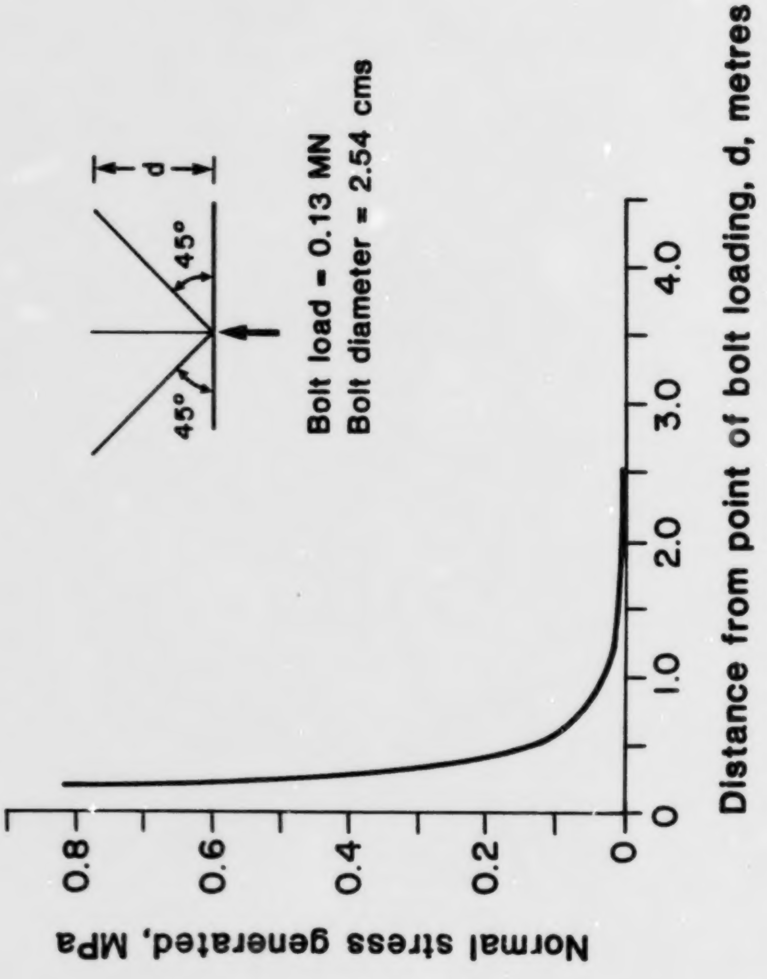

Figure 6.4 Average normal stress required to eliminate slip between for different roof spans and effective friction angles

the roof beyond which slip will not be prevented for different interface friction angles and spans can be estimated (Table 6.1).

TABLE 6.1

DEPTH INTO ROOF BEYOND WHICH SLIP CANNOT BE PREVENTED

Friction Angle, degree	Limited Depth, m
Span = 12 m	
10	0.12
20	0.25
30	0.32
40	0.38
50	0.45
60	0.53
70	0.70
Span = 3 m	
10	0.35
20	0.48
30	0.60
40	0.72
50	0.88
60	1.02
70	1.20

The depths listed in this Table suggest that the so-called "friction" effect is limited to the immediate "skin" of rock in the first 0.7 m of thickness of roof at best. It should be remembered that the bolt load used to develop the Tables is high (0.13 MN) and that in practice it can be only one quarter this value; anchor slip may prevent bolt loads from being increased to 50 percent of yield strengh.

Some superposition of adjacent "cones of stress" will occur, but for typical bolt spacings it is readily demonstrated that this will occur at depths at which the normal stresses generated from each bolt are already very small.

The reinforcement effect was investigated in considerable depth by Panek (1) in a classic series of model tests using a centrifuge to simulate gravitational loading.

As a measure of reinforcement for comparative purposes he defined the reinforcement factor, RF, for layers of equal thickness:

$$RF = \frac{1}{1 + (\epsilon_f/\epsilon_{fu}} \quad \ldots\ldots\ldots\ldots\ldots \quad (6.13)$$

where ϵ_f, ϵ_{fu} are the maximum strains in the bolted and unbolted roof.

A chart (Fig. 6.5) was developed for evaluating the friction effect. A close examination of it shows that the friction effect decreases with roof span, but improves with increasing bolt spacing, bolt tension, and number of bolted layers.

With non-tensioned resin bolts friction effects will generally be negligible because the bolts are a passive system. Furthermore, since installation occurs some distance from the face of the heading, bed separation has already taken place.

Further developments of the beam model undertaken in this investigation are covered in subsequent chapters. In Chapter 7 the influence of abutment stiffness and loading conditions are examined. In Chapter 8 the question of bolt spacing is tackled and it is suggested that non-uniform bolt spacing should be used to maximize reinforcement effects.

6.2.2.2 Arch Formation

Arching is the mechanism by which structures formed of discrete blocks (brickwork), masonary, drywall, and jointed rock masses) distribute loads laterally across a span and permit the structure to support vertical loading from self-weight or external loads (Fig. 6.6). It is a well known principle that has been used for centuries in construction, but much remains to be learned about its application to rock engineering practice and how to use bolting to enhance natural arching.

In Chapter 9 the development of flat arches in horizontally bedded strata is demonstrated and the implications for bolting design considered.

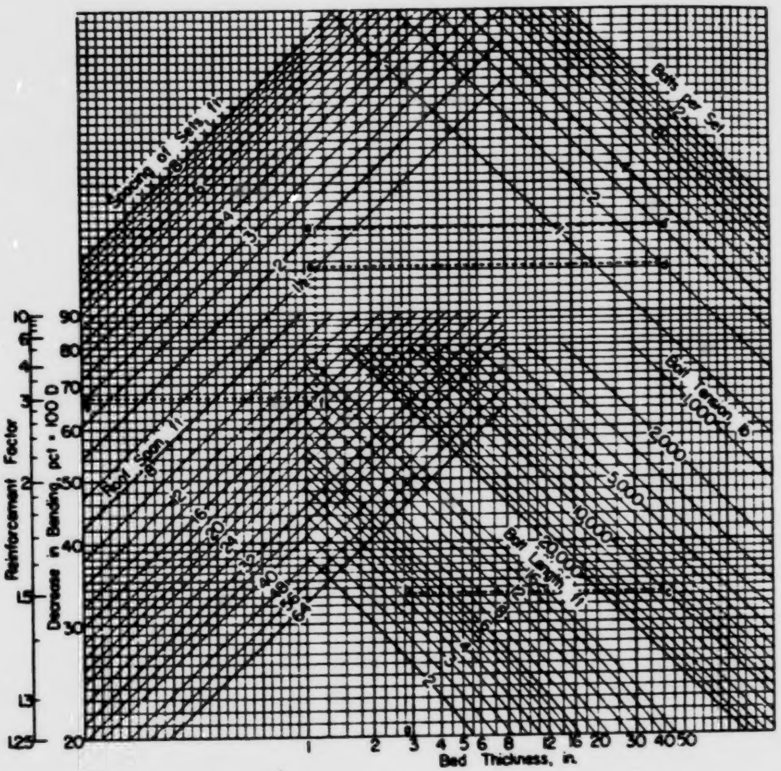

(After (1))

Figure 6.5 Panek's chart to estimating reinforcement effect

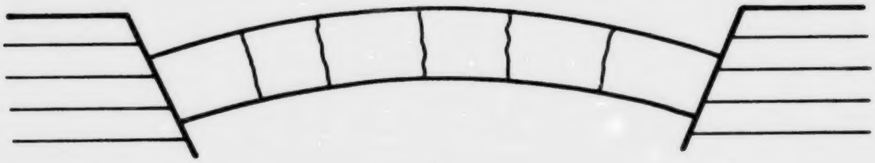

Figure 6.6 Simple arching structure

6.2.2.3 Rock Mass Strength Increase

Either as a result of bolt tensioning or of bolt loads generated by rock movements, confining stresses develop in the bolted rock mass. This is the general case of the "friction effect" where the strength increase of the rock mass as a whole is examined, rather than individual bedding planes (see Section 6.2.2.1).

In Chapter 10 a theory is developed to examine this mode of reinforcement and to determine its effectiveness under conditions of typical rock bolt spacings and rock mass shear strength properties.

REFERENCES

1. Panek, L.A. Principles of reinforcing bedded mine roof with bolts, U.S.B.M., RI 5156. (1956).

CHAPTER 7

THE EFFECT OF ABUTMENT CONDITIONS ON BOLTING REQUIREMENTS

7.1 INTRODUCTION

Underground openings in horizontally bedded sedimentary strata are normally rectangular in shape and the roof is formed by layers of rock of different thicknesses and mechanical properties. The stability of the first layer is of special importance because its failure may permit the collapse of higher beds. The exact sequence of events that would take place upon collapse of the first layer is dependent on many variables, and conditions can be envisaged ranging from complete stability following failure of the first layer to complete unravelling and caving to a height of 5-10 m or greater above the opening.

The objective of this Chapter is to present a mathematical solution for the bending moments (and by extension, the vertical displacements and normal stresses) in a single elastic layer resting on compressible abutments, and to comment on the implications of predicted behaviour for bolting design.

7.2 BEHAVIOUR OF SINGLE BEAMS

Three different cases of increasing complexity have been derived by earlier investigators and these include the two classic problems met in simple beam theory of a gravity-loaded beam resting freely on supported ends and a gravity-loaded beam with built-in ends resting on rigid abutments. The bending moment distributions for these two cases are illustrated for a particular geometry and mechanical properties in Figure 7.1. Stephansson (1) examined the more complex case of a gravity loaded beam resting on elastic abutments and an example of the bending moment distribution predicted by his solution is shown in Figure 7.1 for the same conditions as for the freely supported and built-in beams.

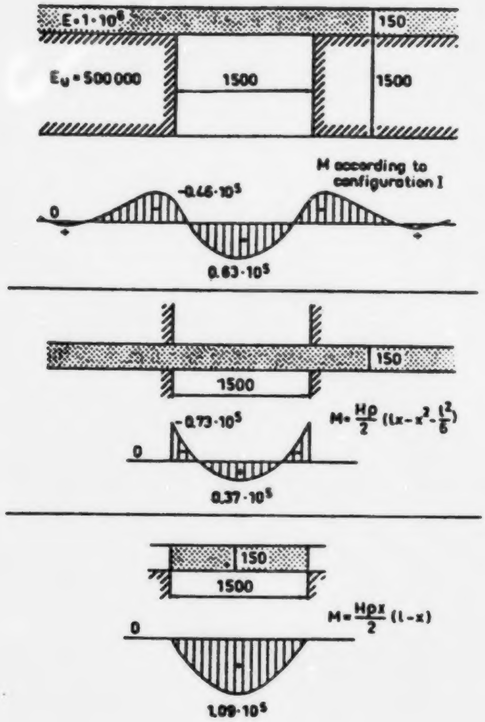
E = 1 · 10⁶
150
Eᵤ = 500 000
1500
1500
M according to configuration I
0
−0.46 · 10⁵
0.83 · 10⁵
150
1500
−0.73 · 10⁵
M = Hp/2 (lx − x² − l²/6)
0
0.37 · 10⁵
150
1500
M = Hpx/2 (l − x)
0
1.09 · 10⁵

(After (1))

Case 1

Case 2

Case 3

Figure 7.1 Bending moment diagrams for various beam configurations

It is instructive to consider the implications of the three cases shown in Figure 7.1 for failure and roof support.

In Case 1 (freely supported beam) the maximum bending moment, and therefore the maximum tensile stress in the layer is at the mid-point of the span. This case approximates the situation in which prominent, natural vertical joints are present at the ribside, or edge of the opening. In Case 2 the maximum bending moment and tensile stresses are immediately above the edge of the opening, but are smaller in magnitude than the mid-span moment in Case 1. This case corresponds to an unjointed beam and suggests that the most critical location for support and reinforcement is at the immediate ribside in the roof. Should the tensile stresses at this point exceed the tensile strength of the roof rock, a vertical tensile crack could propagate down through the layer and change the configuration of the roof to Case 1. Thus, the presence of vertical, open cracks at mid-span (Case 1) may, in some cases, represent a later stage of movement in a roof where the initial tensile failure occurred above the ribside.

Another important difference between Case 1 and Case 2 is the change in sign of the bending moments in Case 2. Interpreting this change in terms of induced tensile stress in the beam, it may be seen that the locus of tension passes from the lower surface of the beam where the bending moment is positive to the upper surface of the beam where the moment is negative. Therefore, theoretically, tensile cracking above the ribside would occur initially on the upper surface of the beam where it would, generally, not be visible.

Also note that in both Cases 1 and 2 the predicted moments above the abutments in the solid are zero. This is not true of Case 3 where the influence of the compressible abutment is evident by the extension of a zone of finite bending moments well into the abutments. For the particular geometry and mechanical properties selected to derive Figure 7.1 the maximum bending moment is at mid-span, but moments of smaller though roughly comparable magnitude (but opposite in sign) are apparent above the abutment. Thus, tensile cracking could take place along the upper surface of the roof beam at distances well into the solid above the abutment. This result has some bearing on the question of the location and orientation of rock bolts, and also suggests that during widening of the span, as for example in pillar recovery, the newly exposed roof may be disturbed and fractured by reason of the stresses induced in it during the development of the first span.

Case 3 approaches the real situation of an unjointed roof beam more closely than Case 1 or Case 2, but is approximate in that the section of the beam above the abutments is assumed to be loaded only by self-weight. In reality, these sections of the roof beam are clamped in by vertical stresses induced around the opening.

7.3 ABUTMENT STRESSES

In linear elastic rock which has not reached failure, the abutment stresses can be predicted from either closed form or numerical solutions which are published in standard rock mechanics texts. For the rectangular opening, the vertical normal stresses at mid-height of the ribside are greatest at the surface and decline to the virgin stress value away from the opening (Fig. 7.2 (a)). However, when yielding of the abutments occurs the distribution of vertical stresses over the abutments is greatly altered (Fig. 7.2 (b)). Stresses close to the face are reduced. This failure process is of importance to roof support because the span of the opening is, in some degree, effectively increased. In the remainder of this chapter a theoretical model is developed to model this situation and its implications for roof support are examined.

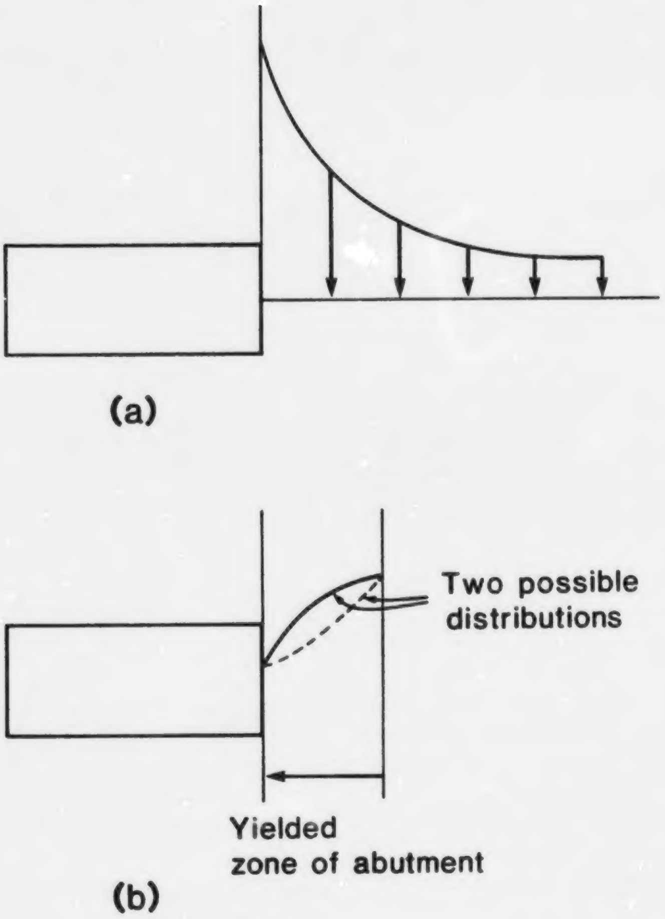
(a)
Two possible distributions
Yielded zone of abutment
(b)

Figure 7.2 Normal stress over abutment:(a) elastic, no yielding,(b) yielding of rib

7.4 THEORETICAL MODEL

In order to derive the basic equation describing the bending moments and deflections for this case the usual assumptions for simple beam theory are made:

1. The length, L, of the beam is long compared to its thickness, t, ($L/t > 5$).
2. The material of the beam is homogeneous, isotropic and linearly elastic.
3. Loads are applied in a direction normal to the longitudinal axis of the beam and in the plane of symmetry.
4. The beam is of uniform cross-section with a longitudinal plane of symmetry.
5. Plane sections in the unloaded beam remain plane during bending.
6. The abutments have identical linear, elastic properties and rest on rigid bases.
7. Deflections of the beam are small in comparison to the beam thickness, t.
8. The contact between the beam and the abutments is frictionless.

Following Stephansson's (1) nomenclature, the general equation of equilibrium for a small element of the beam of length, dx , is given by (Fig. 7.3):

$$T - (T + dT) + cydx - pdx = 0 \quad \ldots\ldots\ldots\ldots\ldots \quad (7.1)$$

where T = side shearing forces on the element

y = the vertical deflection of the beam

c = the modulus of the foundation or abutment such that the vertical reaction force of the abutment, $q = cy$.

p = the normal stress from self-weight and other external stresses, such as water pressure acting on the beam.

$$\text{Hence } \frac{dT}{dx} = cy - p \quad \ldots\ldots\ldots\ldots\ldots \quad (7.2)$$

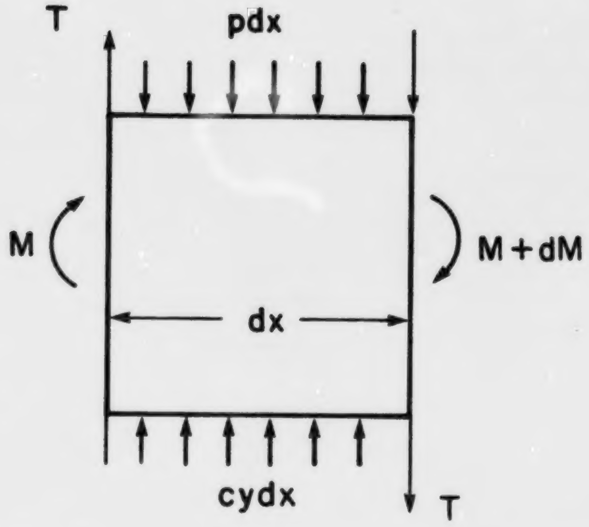
T
pdx
M
M + dM
dx
cydx
T

Figure 7.3 Forces exerted on a small element of a beam

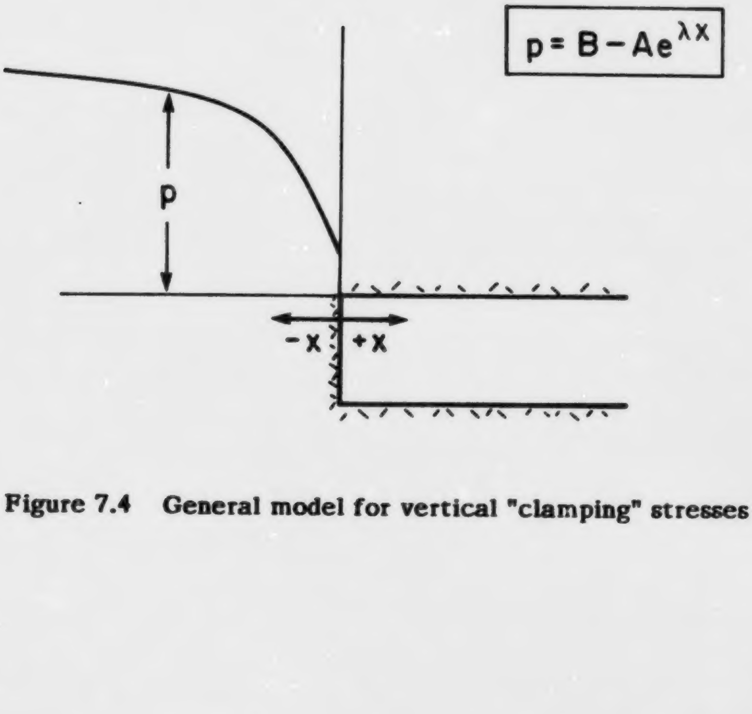

Figure 7.4 General model for vertical "clamping" stresses over abutments

But, since $T = \frac{dM}{dy}$, (M = bending moment)

$$\frac{dT}{dx} = \frac{d^2M}{dx^2} = cy - p \qquad \text{.............. (7.3)}$$

Now, for a beam in bending it can be shown that:

$$EI \frac{d^4y_4}{dx^4} = -\frac{d^2M}{dx^2}$$

$$= p - cy \text{ from (3)} \qquad \text{.............. (7.4)}$$

where I = the moment of inertia.

Equation (7.4) is the basic equation which must be solved to obtain the displacements, y , of the beam. Having solved for y the bending moments can be obtained from:

$$EI \frac{d^2y}{dx^2} = -M$$

The normal 'clamping stress' applied to the beam at the abutments is assumed to have the general form shown in Figure 7.4 and models the stresses in the yield zone only (Fig. 7.2(b)) where the "clamping" forces are most critical for roof support. The shape of this distribution may be described by a general equation of the form:

$$p = B - Ae^{\lambda x} \; (-\infty \le x \le 0) \qquad \text{.............. (7.5)}$$

where A, B and λ are constants, which can be determined when boundary conditions are specified. These are:

$$\text{at } x = 0 \text{ , } p = p_1 \qquad \text{.............. (7.6)}$$

$$\text{at } x = -\infty, \; p = p_2 \qquad \text{.............. (7.7)}$$

$$\text{at } x = -L,\ p = kp_2 \qquad \ldots\ldots\ldots\ldots\ldots \quad (7.8)$$

where K is a constant $(0 \le k \le 1)$.

The third boundary condition is particularly important as it controls how rapidly the normal stress, p , rises from the boundary of the opening (x = 0) to x = - L. Two cases are shown in Figure 7.5. For line (a) the value of k is 0.9 and L = 1 m, and for line (b) k is 0.9, but L = 10 m. In the first case, the normal stress is permitted to rise to 90% of the maximum value, p_2, within a horizontal distance of 1 m from the edge of the abutment (x = 0),whereas in the second case this distance is increased to 10 m. The form of the equation allows variety of 'clamping force' distributions to be simulated.

Inserting the boundary conditions of equations (7.6) - (7.8) in (7.5) the equation for the normal clamping stresses becomes:

$$p = p_2 - (p_2 - p_1)e^{[\ln \frac{p_2 - p_1}{p_2(1-k)} /L]x} \qquad \ldots\ldots\ldots\ldots \quad (7.9)$$

i.e., the constants of equation (7.5) are therefore:

$$A = p_2 - p_1 \qquad \ldots\ldots\ldots\ldots\ldots \quad (7.10)$$

$$B = p_2 \qquad \ldots\ldots\ldots\ldots\ldots \quad (7.11)$$

$$\lambda = \ln\left(\frac{p_2 - p_1}{p_2(1-k)}\right)/L \qquad \ldots\ldots\ldots\ldots\ldots \quad (7.12)$$

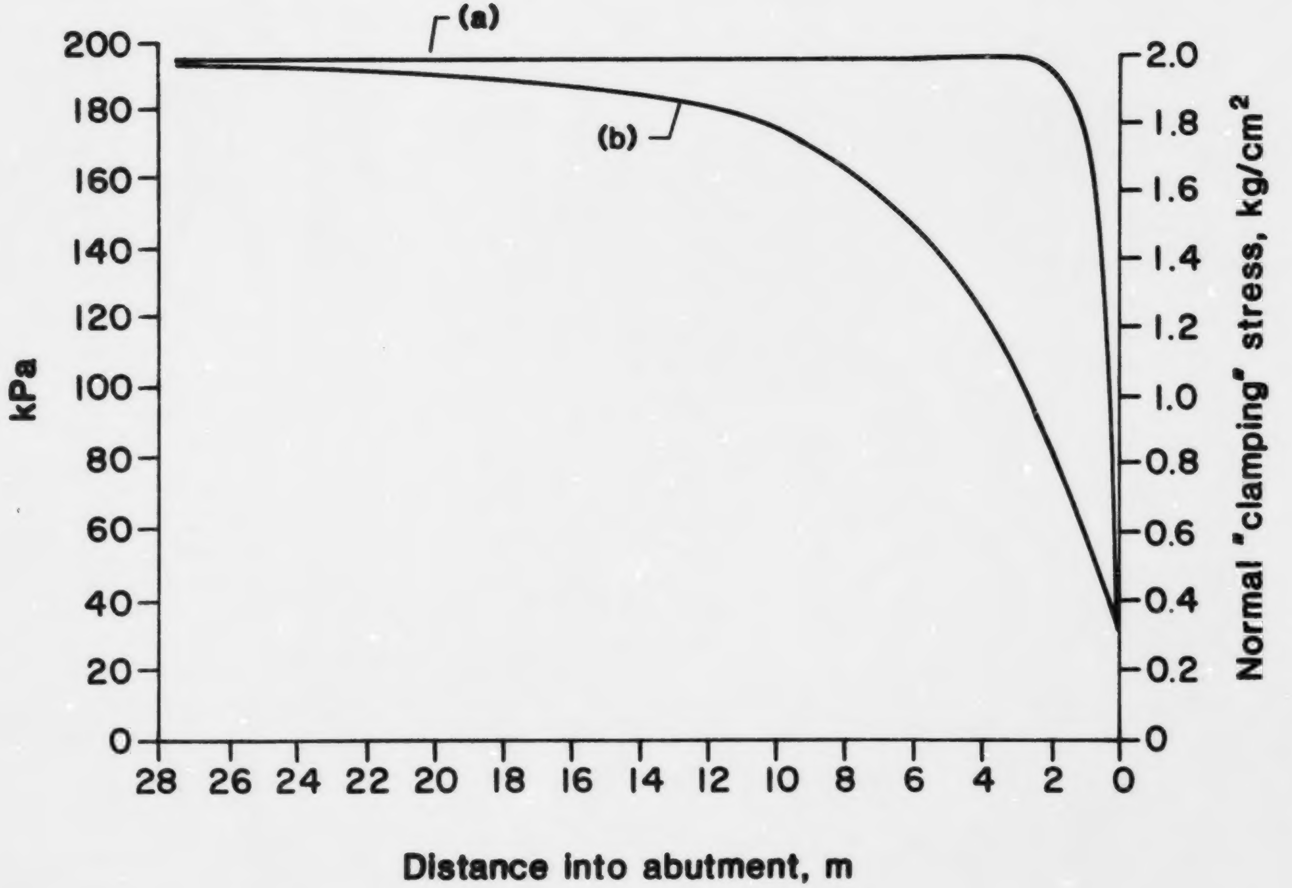

Figure 7.5 Two simulated "clamping" stress distributions

For the purposes of the remainder of this analysis, it is assumed that p , the vertical stress at $x = 0$, is produced only by the self-weight of the beam of thickness, H .

Solution ($1 \le x \le 0$)

Hofer and Menzel (2) showed that for homogeneous, elastic abutments with thickness, h , modulus of elasticity, E_u, and Poisson's ratio, ν_u, the modulus of the foundation, $c = c_u$, is given by:

$$c_u = \frac{E_u}{h(1-\nu_u^2)} \quad \ldots\ldots\ldots\ldots\ldots \quad (7.13)$$

For a thin plate of thickness H whose length is much greater than its span, the theory of thin plates gives the differential equation describing the vertical deflections, y , of the plate as:

$$\begin{aligned} K \frac{d^4y}{dx^4} &= - cy + p \\ &= - c_u y + p \end{aligned} \quad \ldots\ldots\ldots\ldots\ldots \quad (7.14)$$

where $K = \dfrac{EI}{1-\nu_1^2}$

wherein E is the modulus of elasticity of the plate

I is the moment of inertia $= H^3/12$ for a rectangular cross section

ν_c is the Poisson's ratio of the plate.

Substituting (7.5) in (7.14)

or, since from (11) $B = p_2$,

$$K \frac{d^4y}{dx^4} = - c_u y + B - Ae^{\lambda x} \quad \ldots\ldots\ldots\ldots\ldots \quad (7.15)$$

The general solution of equation (7.15) is comprised of the complementary function, which is a general solution of the equation:

$$K \frac{d^4y}{dx^4} = - c_u \, y$$

or

$$K \frac{d^4y}{dx^4} + c_u \, y = 0 \qquad \ldots\ldots\ldots\ldots\ldots \quad (7.16)$$

and a particular integral for equation (7.15).

Complementary Function

Using the concept of characteristic equations the general solution of this second order, linear equation (eqn. (7.16)) can be shown to be of the form

$$y = (A_1 \sin \alpha x + B_1 \cos \alpha x)e^{\alpha x} + (C_1 \sin \alpha x + D_1 \cos\alpha \, x)e^{-\alpha x}$$

$$\text{where} \quad \alpha = \left(\frac{c_u}{4K}\right)^{\frac{1}{4}} \qquad \ldots \quad (7.17)$$

Particular Integral

It can be demonstrated that

$$y_p = b + ae^{\lambda x}$$

will satisfy equation (7.15) providing that for all x

$$a = \frac{-A}{K\lambda^4 + c_u}$$

and $$b = \frac{P_2}{c_u}$$

or $$y_p = \frac{P_2}{c_u} + ae^{\lambda x} \qquad \ldots\ldots\ldots\ldots\ldots \quad (7.18)$$

General Solution

From equations (7.17) and (7.18) the general solution of equation (7.15) is:

$$y = (A_1 \sin\alpha x + B_1 \cos\alpha x)e^{\alpha x} + (C_1 \sin\alpha x + D_1 \cos\alpha x)e^{-\alpha x} + \frac{P_2}{c_u} + ae^{\lambda x} \quad (7.19)$$

However, at large distances from the opening ($x \rightarrow -\infty$), the deflection, y, of the beam should equal the deformation of the abutment, i.e., $y \rightarrow \frac{P_2}{c_u}$ as $x \rightarrow -\infty$. Equation (7.19) can only satisfy this condition if C_1 and D_1 are both equal to zero. Therefore, the equation reduces to

$$y = (A_1 \sin\alpha x + B_1 \cos\alpha x)e^{\alpha x} + \frac{P_2}{c_u} + ae^{\lambda x} \quad \ldots\ldots\ldots \quad (7.20)$$

TO FIND A_1 AND B_1

Let $y = y_I$ at $x = 0$ and $\frac{dy}{dx} = \tan\phi_I$ (slope) at $x = 0$

Now, differentiating equation (7.20) with respect to x

$$\frac{dy}{dx} = \alpha(A_1 \sin\alpha x + B_1 \cos\alpha x)e^{\alpha x} + (\alpha A_1 \cos\alpha x - \alpha B_1 \sin\alpha x)e^{\alpha x} + a\lambda e^{\lambda x} \quad . \quad (7.21)$$

But, since $\frac{dy}{dx} = \tan\phi_I$ at $x = 0$, from equation (7.21)

$$\tan\phi_I = \alpha B_1 + \alpha A_1 + a\lambda \quad \ldots\ldots\ldots\ldots\ldots \quad (7.22)$$

Also, since $y = y_I$ at $x = 0$, from equation (7.20)

$$y_I = B_1 + \frac{P_2}{c_u} + a$$

and therefore

$$B_1 = y_I - \frac{P_2}{c_u} - a \quad \ldots\ldots\ldots\ldots\ldots \quad (7.23)$$

General Solution

From equations (7.17) and (7.18) the general solution of equation (7.15) is:

$$y = (A_1 \sin\alpha\ x + B_1 \cos\alpha\ x)e^{\alpha} + (C_1 \sin\alpha\ x + D_1 \cos\alpha\ x)e^{-\alpha x} + \frac{P_2}{c_u} + ae^{\lambda x} \quad (7.19)$$

However, at large distances from the opening ($x \to -\infty$), the deflection, y, of the beam should equal the deformation of the abutment, i.e., $y \to \frac{P_2}{c_u}$ as $x \to -\infty$. Equation (7.19) can only satisfy this condition if C_1 and D_1 are both equal to zero. Therefore, the equation reduces to

$$y = (A_1 \sin\alpha\ x + B_1 \cos\alpha\ x)e^{\alpha x} + \frac{P_2}{c_u} + ae^{\lambda x} \ \ldots\ldots\ldots\ldots \quad (7.20)$$

TO FIND A_1 AND B_1

Let $y = y_I$ at $x = 0$ and $\frac{dy}{dx} = \tan\phi_I$ (slope) at $x = 0$

Now, differentiating equation (7.20) with respect to x

$$\frac{dy}{dx} = \alpha(A_1 \sin\alpha\ x + B_1 \cos\alpha\ x)e^{\alpha x} + (\alpha A_1 \cos\alpha\ x - \alpha B_1 \sin\alpha\ x)e^{\alpha x} + a\lambda e^{\lambda x} \ \ldots \quad (7.21)$$

But, since $\frac{dy}{dx} = \tan\phi_I$ at $x = 0$, from equation (7.21)

$$\tan\phi_I = \alpha B_1 + \alpha A_1 + a\lambda \ \ldots\ldots\ldots\ldots\ldots \quad (7.22)$$

Also, since $y = y_I$ at $x = 0$, from equation (7.20)

$$y_I = B_1 + \frac{P_2}{c_u} + a$$

and therefore

$$B_1 = y_I - \frac{P_2}{c_u} - a \ \ldots\ldots\ldots\ldots\ldots \quad (7.23)$$

Substituting equation (7.23) in equation (7.22) and by algebraic rearrangement

$$A_1 = \frac{1}{\alpha} [\tan\phi_I - \alpha(y_I - \frac{P_2}{c_u}) + a(\alpha-\lambda)] \ldots\ldots\ldots\ldots \quad (7.24)$$

Stephansson's analysis (1) for the deflection of the section of the beam of span, L, which is loaded by its own weight over the opening, gives for y_I and tan ϕ_I as follows:

$$y_I = \frac{P_2}{c_u} (\ell\alpha^3\beta + 1) \qquad \ldots\ldots\ldots\ldots\ldots \quad (7.25)$$

and

$$\tan\phi_I = \frac{P_1 \; l\alpha^2}{c_u} (2\alpha^2\beta-1) \qquad \ldots\ldots\ldots\ldots\ldots \quad (7.26)$$

$$\text{where } \beta = \frac{\frac{\ell^2}{6} + \frac{\ell}{\alpha} + \frac{1}{\alpha^2}}{(\alpha l + 2)}$$

These approximated values of y_I and tan ϕ_I can be substituted in equations (7.23) and (7.24) to find values for A_1 and B_1 .

SUMMARY OF EQUATIONS;

The deflection, y , of the beam over the abutment can be described by

$$y = (A_1 \sin\alpha\, x + B_1 \cos\alpha\, x)e^{\alpha x} + \frac{p_2}{c_u} + ae^{\lambda x} \quad \ldots\ldots \quad (7.27)$$

where:

$$A_I = \frac{1}{\alpha}\left[\tan\phi_I - \alpha\left(y_I - \frac{p_2}{c_u}\right) + a(\alpha - \lambda)\right] \quad \ldots\ldots \quad (7.28)$$

$$B_1 = y_I - \frac{p_2}{c_u} - a \quad \ldots\ldots \quad (7.29)$$

$$a = \left(\frac{c_u}{4K}\right)^{1/4} \quad \ldots\ldots \quad (7.30)$$

$$\tan\phi_I = \frac{p_1 \; 1\alpha^2}{c_u}(2\alpha^2\beta - 1) \quad \ldots\ldots \quad (7.31)$$

$$y_I = \frac{p_1}{c_u}(1\alpha^2\beta + 1) \quad \ldots\ldots \quad (7.32)$$

$$a = -\frac{A}{K\lambda^4 + c_u} \quad \ldots\ldots \quad (7.33)$$

$$\lambda = \ell n\left(\frac{p_2 - p_1}{p_2(1-k)}\right)/L \quad \ldots\ldots \quad (7.34)$$

The deflection, y , of the beam over the opening is given by the following expressions derived by Stephansson (1):

$$= \frac{p_1}{c_u} [1 + e^{\alpha x}\ l\alpha\{\alpha^2\beta(\sin\alpha\ x + \cos\alpha\ x) - \sin\alpha\ x\}] \cdots\cdots\cdots \quad (7.36)$$

Bending Moments (1 ≤ x ≤ 0)

The bending moments in the portion of the beam resting on the abutment can be readily obtained since:

$$K \frac{d^2y}{dx^2} = - M \text{ from beam theory} \quad \ldots\ldots\ldots\ldots\ldots \quad (7.37)$$

Differentiating (27) twice with respect to x and rearranging terms, it may be shown that:

$$M = 2K\alpha^2\ e^{\alpha x}\ (A_1 \cos\alpha\ x - B_1 \sin\alpha\ x) - K a\lambda^2\ e^{\lambda x} \ldots\ldots\ldots\ldots \quad (7.38)$$

The bending moments, M , in the beam over the opening are given by the following expressions derived by Stephansson:

$$M = -\frac{p_1\ x^2}{2} + \frac{pl}{2}\ (x + \frac{1}{\alpha} - \alpha\beta) \quad \ldots\ldots\ldots\ldots\ldots \quad (7.39)$$

Equations (7.36), (7.26), (7.38) and (7.39) may be used to predict the bending moments and deflections in a beam over the opening and above the abutments for various conditions of the thickness, modulus of elasticity, Poisson's ratio and span of the beam, for different values of the thickness, modulus of elasticity, and Poisson's ratio of the abutment, and for various assumed distributions of the vertical "clamping" stress in the peripheral yielded zone of the abutment.

7.5 ANALYSIS OF RESULTS

Because the uniaxial tensile strength of rock is only 1/5th to 1/30th of its uniaxial compressive strength, the development of tensile stresses in roof beams is of primary interest. The following analysis examines the influence of the variables used in the model on the distribution and magnitudes of flexural tensile stresses.

7.5.1 Beam Over Opening

The following trends in flexural stresses in the beam over the opening are predicted by the model (Figs. 7.6 and 7.7):

i) Flexural stresses lower than in the classic case of a linear elastic, clamped beam.

ii) Young's modulus of beam has no effect on flexural stresses in a linear elastic, clamped beam, but does have with this model. As Young's modulus of beam increases, flexural stress decreases.

iii) Flexural stresses increase with increasing stiffness of abutment.

iv) Poisson's ratio of beam has negligible effect.

v) Flexural stresses decrease with increase in thickness of abutment.

In summary, thick, very compressible abutments are conductive to stability of the roof beam over the opening as they reduce the magnitudes of tensile stresses in the layered strata.

7.5.2 Beam Over Abutment

As has been noted earlier, yielding of the ribs may be seen in an approximate manner as effectively increasing the span of the opening. Therefore, in analysing the model results the development of tensile stresses was used as the primary criterion for indicating potential for failure and therefore the need for reinforcement.

The effect of the rate at which the "clamping" stress increases is plotted in Figure 7.8. The maximum tensile stress occurs immediately over the edge of the rib and is greater than that predicted by classical clamped beam theory. The stresses decline with distance into the abutment, but persist perceptibly for 1-2 m and alternate from the lower to the upper surface. The worst case occurs where the abutment

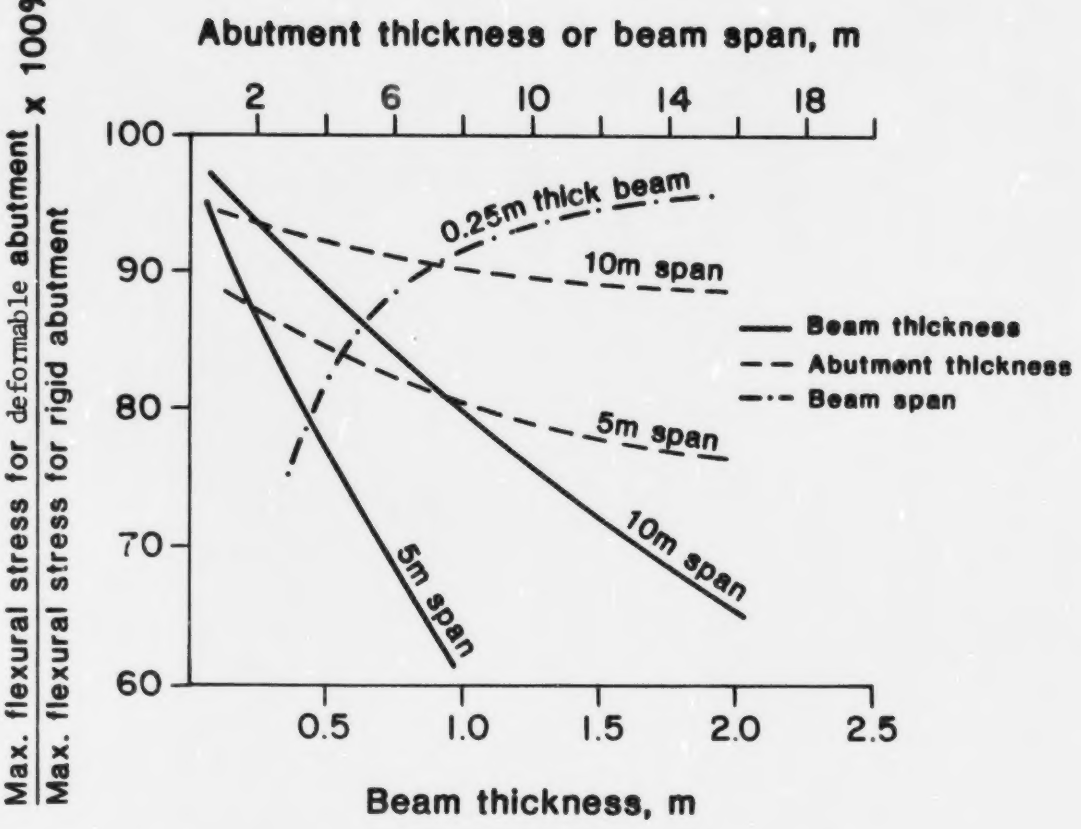

Figure 7.6 Comparison of maximum flexural tensile stresses for beam over rigid and deformable abutments (Young's modulus of abutment = Young's modulus of beam = 2000 MPa, Poisson's ratio of abutment = Poisson's ratio of beam = 0.3, specific gravity of beam = 2.5, abutment thickness = 2 m, span = 5 m, beam thickness = 0.25 m)

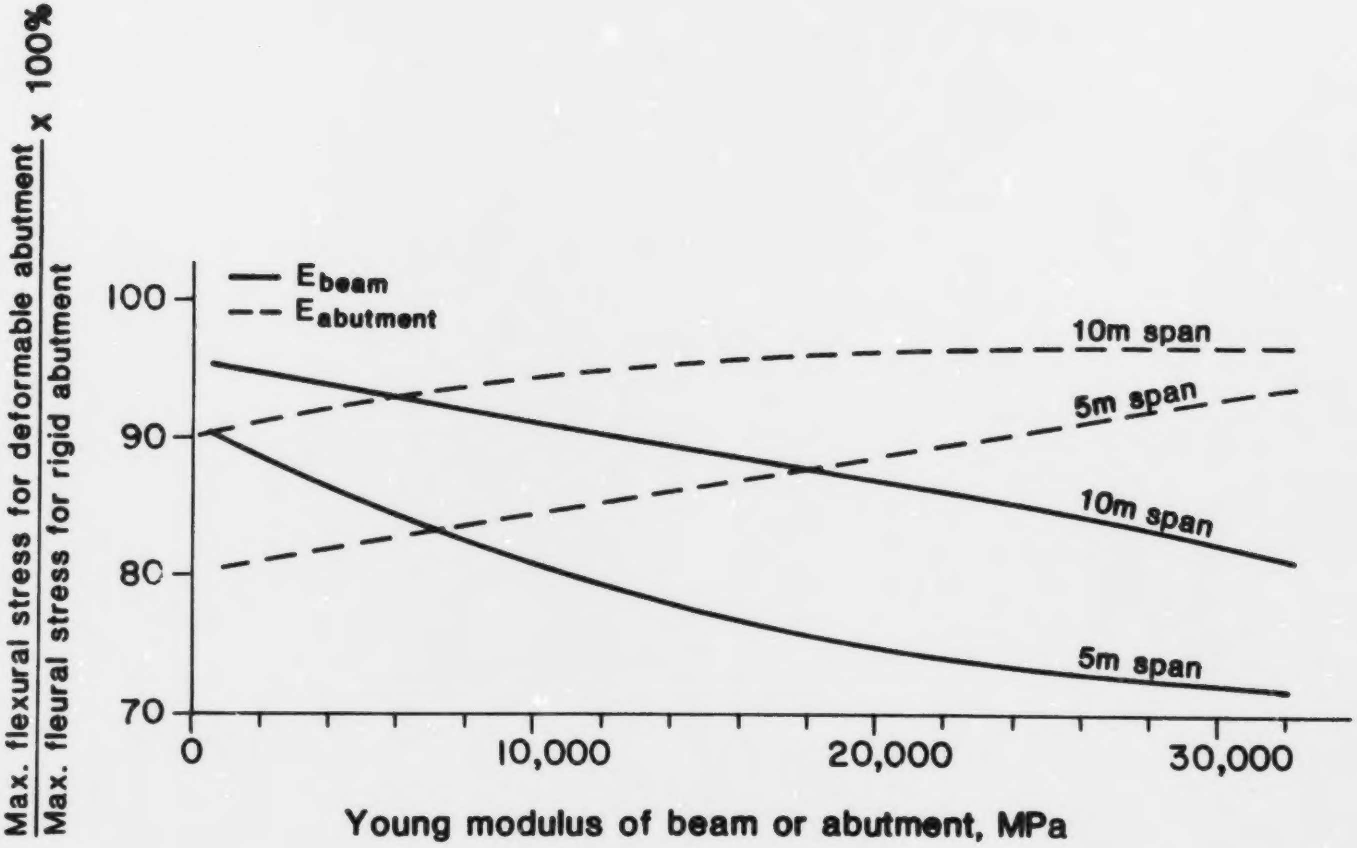

Figure 7.7 Effect of Young's modulus of beam and abutment on flexural tensile stresses

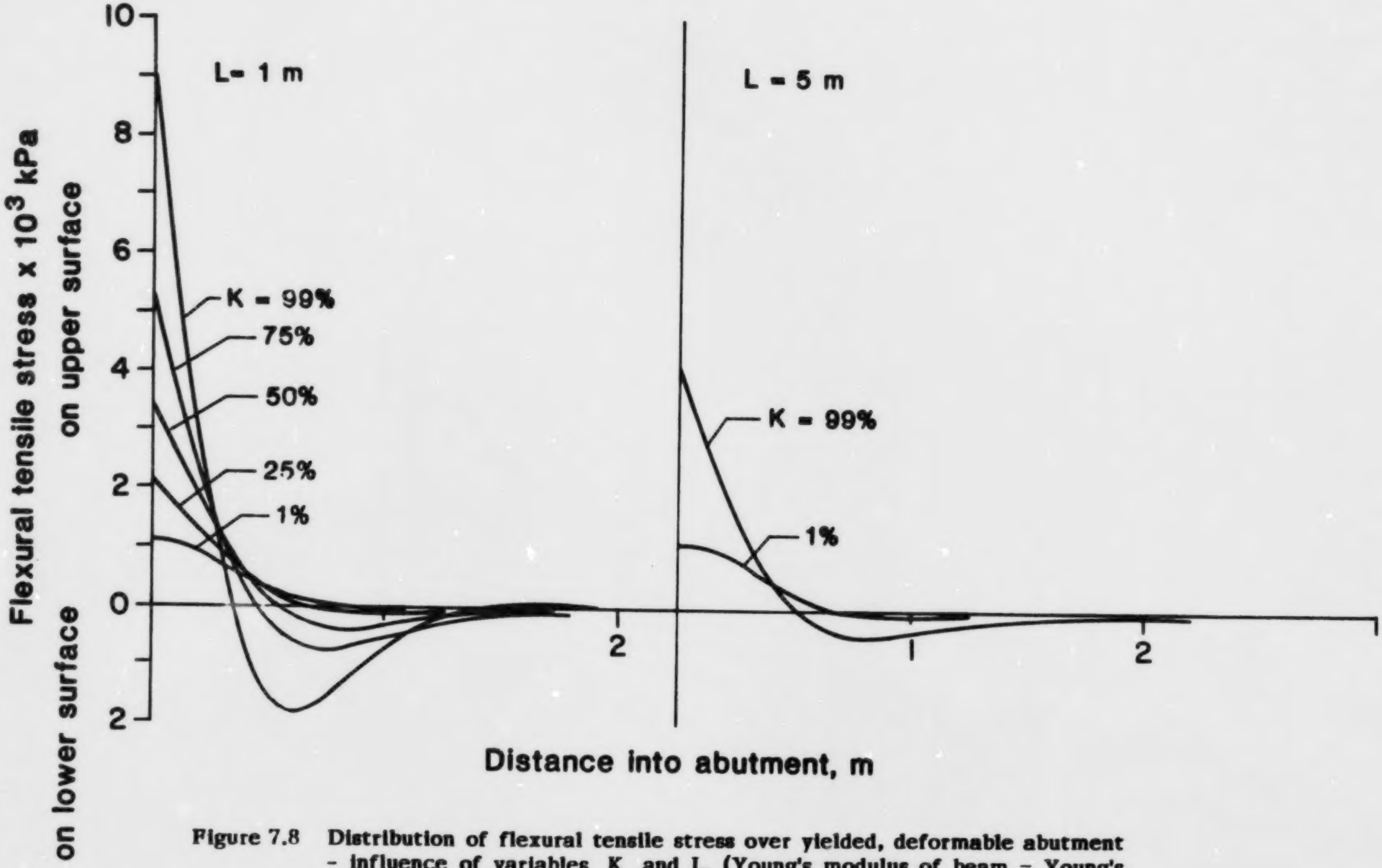

Figure 7.8 Distribution of flexural tensile stress over yielded, deformable abutment - influence of variables K and L. (Young's modulus of beam = Young's modulus of abutment = 2000 MPa, Poisson's ratio of beam = Poisson's ratio of beam = 0.3, specific gravity of beam = 2.5, abutment thickness = 2 m, beam thickness = 0.2 m, w = 400)

stress changes most rapidly, i.e., k = 99%, L = 1 m.

The graph showing the effect of ultimate abutment stress distant from the opening (Fig. 7.9) is similar in character to Figure 7.8 because it, in effect, also reflects different rates of increase of "clamping" stress.

The effect of span is illustrated in Figure 7.10. Tensile stresses over the abutment are greatest for the largest span, but in all cases decline to similar values within approximately the same distance (about 0.9 m for the particular variables used in this example).

The thickness of the abutment and its stiffness also have a significant influence on the development of flexural tensile stresses over the abutment (Figs. 7.11 and 7.12). As abutment thickness increases the tensile stresses increase and extend further into the abutment. The contrary correlation is seen with abutment stiffness. As it increases, the flexural tensile stresses decrease.

Finally, the effect of beam geometry and mechanical properties are illustrated in Figures 7.13 and 7.14. Increasing beam thickness decreases flexural tensile stresses, but increasing the Young's modulus of beam decreases them.

7.6 CONCLUSIONS

Yielding and compressible abutments have a potentially significant effect on roof stability. The most important variable is the size of the abutment yield zone since this largely determines the lateral extent of tensile stresses into the roof beam above the abutment. It also influences the magnitude of tensile stresses, but the latter are also dependent upon various geometric and mechanical properties of the roof beam and abutment. For a given size of yield zone, the highest tensile stresses will develop for a thin, high stiffness roof beam resting on a thick, low stiffness abutment. It is interesting to note that for the portion of the roof beam over the opening, the **LOWEST** tensile stresses will develop under the same conditions, i.e., there is a

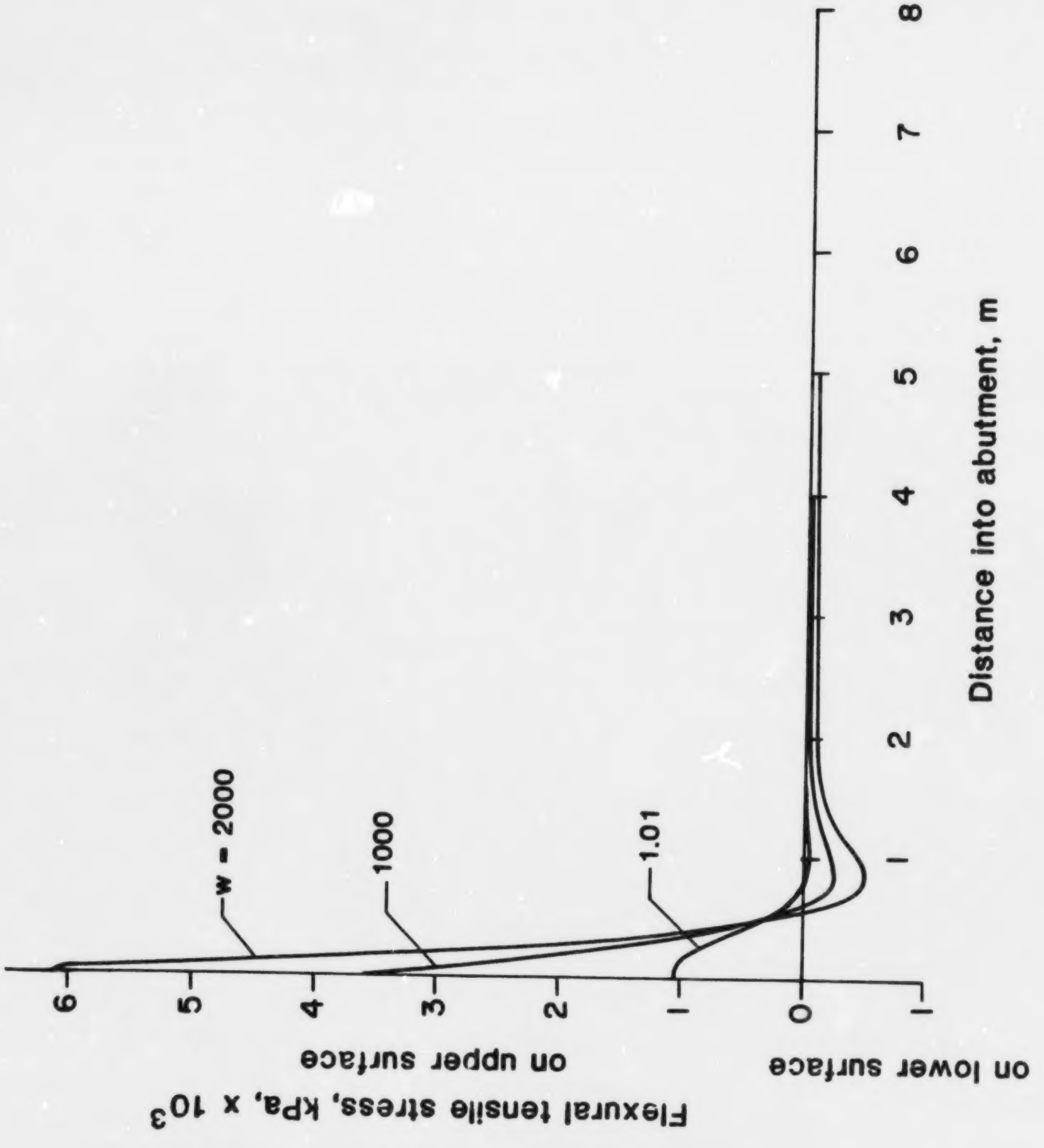

Figure 7.9 Distribution of flexural tensile stress over yielded, deformable abutment - influence of ultimate vertical stress. (Young's modulus of beam = Young's modulus of abutment = 2000 MPa, Poisson's ratio of beam = Poisson's ratio of beam = 0.3, specific gravity of beam = 2.5, abutment thickness = 2 m, span = 5 m, beam thickness = 0.25 m, K = 75%, L = 5m)

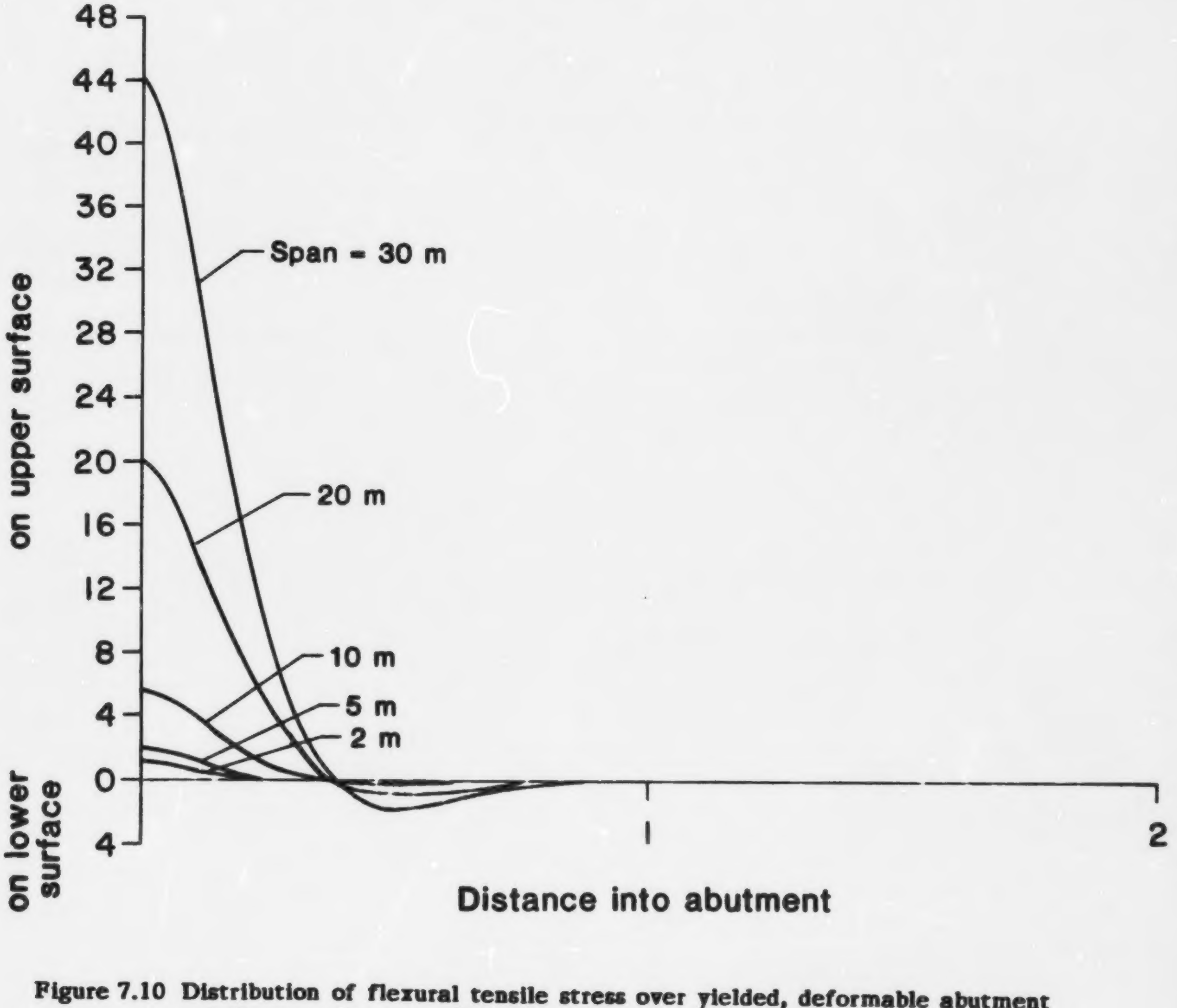

Figure 7.10 Distribution of flexural tensile stress over yielded, deformable abutment - influence of span. (Young's modulus of beam = Young's modulus of abutment = 2000 MPa, Poisson's ratio of beam = Poisson's ratio of abutment = 0.3, specific gravity of beam = 2.5, abutment thickness = 2 m, beam thickness = 0.25 m, K = 75%, L = 5 m, w = 400)

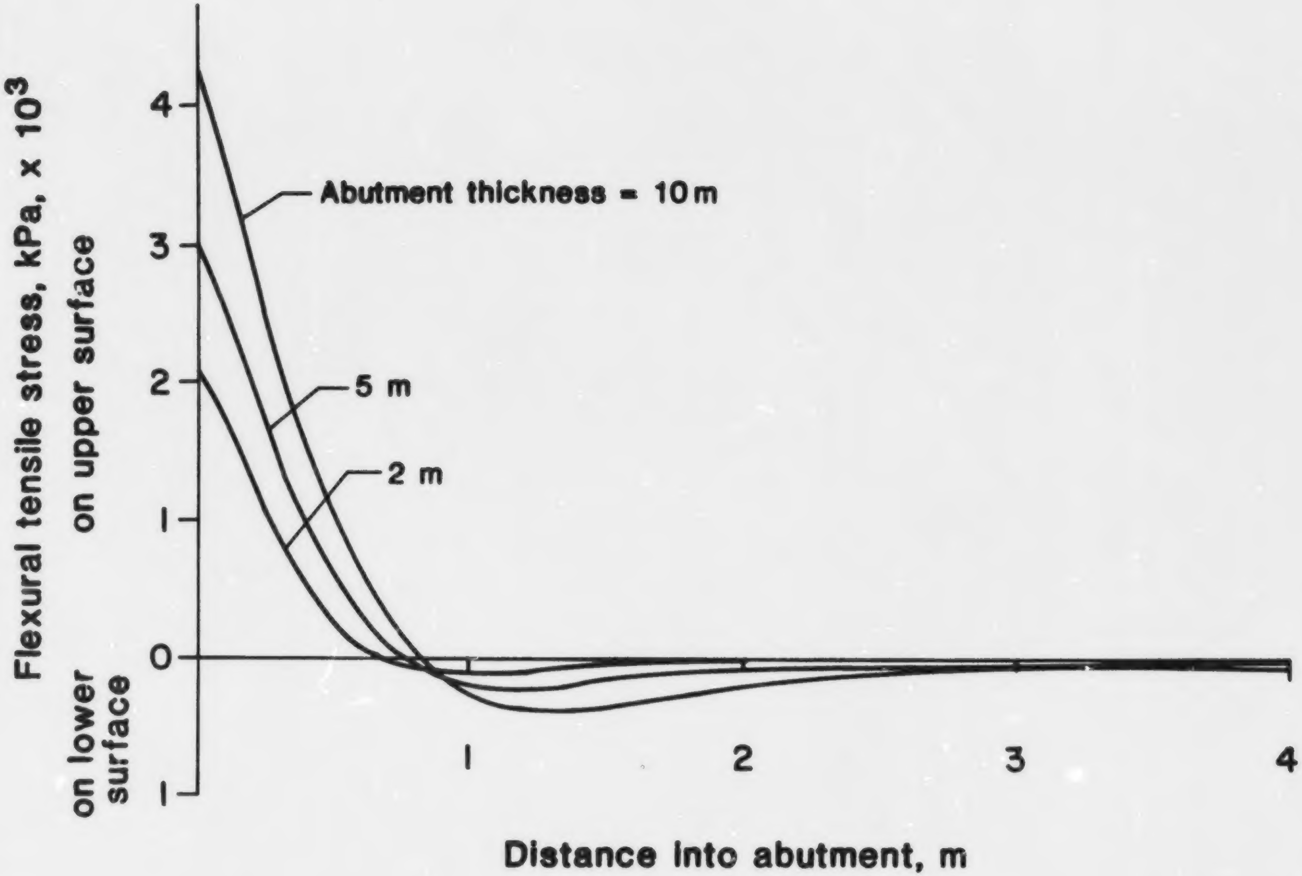

Figure 7.11 Distribution of flexural tensile stress over yielded, deformable abutment - influence of abutment thickness. (Young's modulus of beam = Young's modulus of abutment = 2000 MPa, Poisson's ratio of beam = Poisson's ratio of abutment = 0.3, specific gravity of beam = 2.5, span = 5 m, beam thickness = 0.25 m, K = 75%, L = 5 m, w = 400)

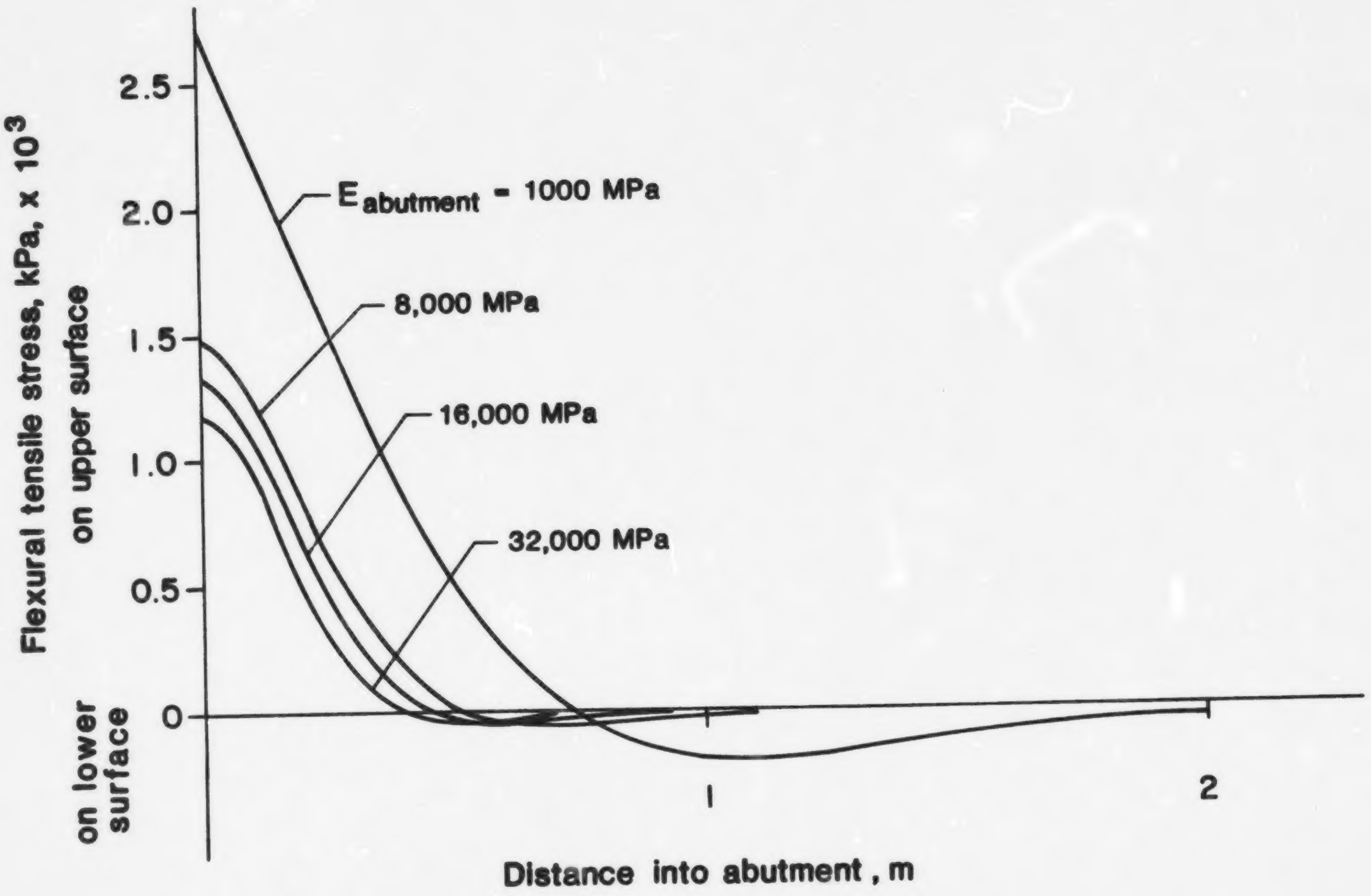

Figure 7.12 Distribution of flexural tensile stress over yielded, deformable abutment - influence of Young's modulus of abutment. (Young's modulus of beam = 2000 MPa, Poisson's ratio of beam = Poisson's ratio of abutment = 0.3, beam span = 5 m, beam thickness = 0.25 m, abutment thickness = 2 m, specific gravity of beam = 2.5, K = 75%, L = 5 m, w = 400)

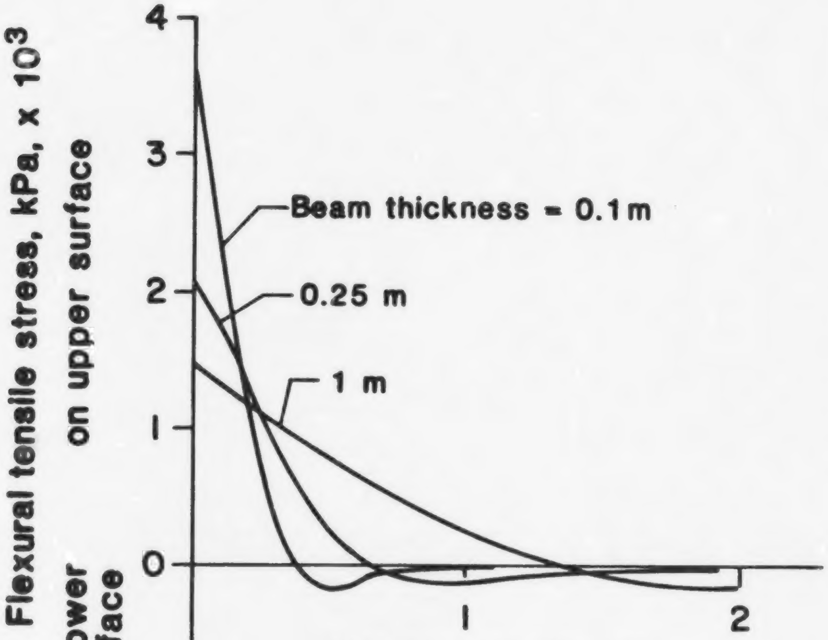

Figure 7.13 Distribution of flexural tensile stress over yielded, deformable abutment - influence of beam thickness. (Young's modulus of beam = Young's modulus of abutment = 2000 MPa, Poisson's ratio of beam = Poisson's ratio of abutment = 0.3, beam span = 5 m, abutment thickness = 2 m, K = 75%, L = 5 m, ultimate abutment stress equivalent to 100 m of overburden depth)

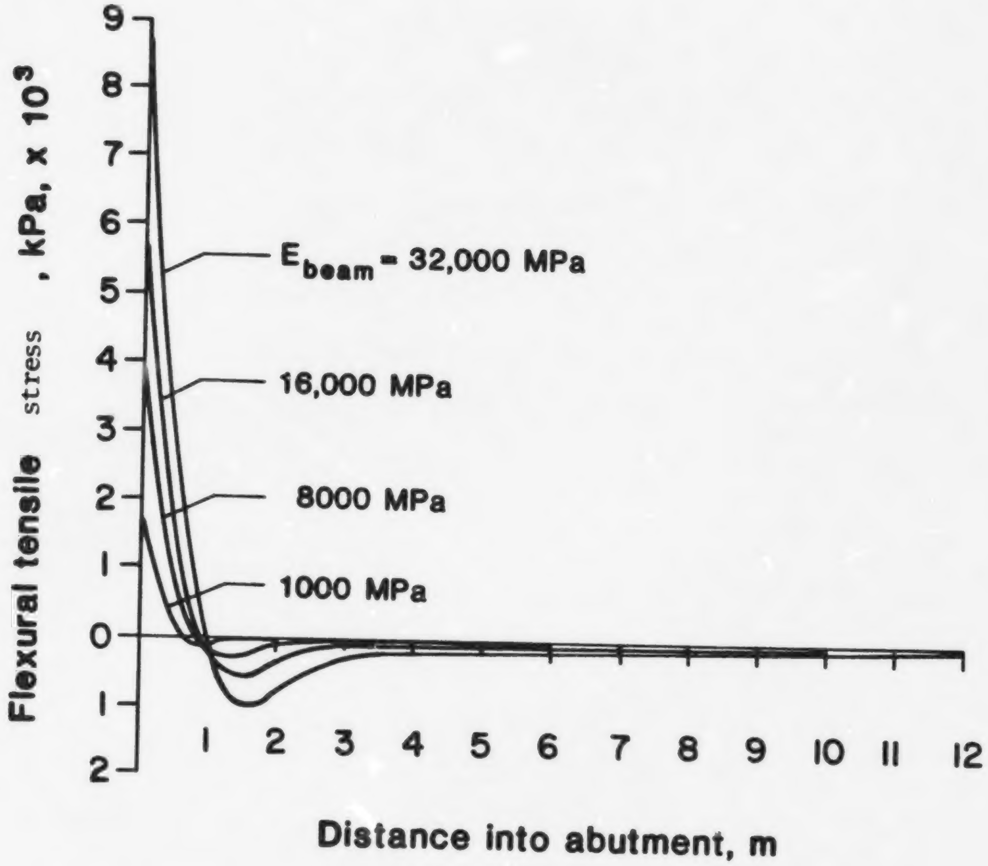

Figure 7.14 Distribution of flexural tensile stress over yielded, deformable abutment - influence of Young's modulus of beam. (Young's modulus of abutment = 2000 MPa, Poisson's ratio of beam = Poisson's ratio of abutment = 0.3, beam span = 5 m, abutment thickness = 2 m, beam thickness = 0.25 m, K = 75%, L = 5 m, w = 400)

redistribution of beam stresses from the section of the beam over the opening to the section of the beam over the abutment.

It is clear, then, that under some circumstances significant tensile stresses can develop over the abutment. This zone is a region of rapidly changing stresses and under certain combinations of parameters may be where roof failure actually begins. Once tensile failure has occurred in this region the beam approximates a simply supported beam resting on deformable abutments (see Fig. 7.1) and roof failure may then be instigated through tensile fracturing at mid-span.

Reinforcement of this region by inclined untensioned resin bolts is suggested (Fig. 7.15).

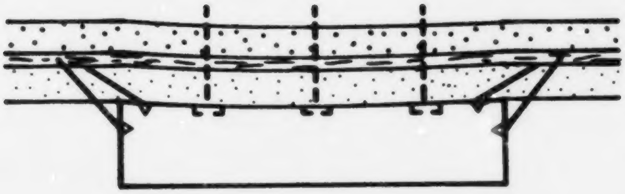

Figure 7.15 Suggested reinforcement of roof beam above yielded, deformable abutment by non-tensioned, resin bolting

REFERENCES

1. Stephansson, O. Stability of single openings in horizontally bedded rock. Eng. Geology, 5, pp. 5-71. (1971).

2. Hofer, K.H. and Menzel, W. Comparative study of pillar loads in potash mines established by calculation and by measurements below ground. Int. J. Rock Mech. Mining Sci., 1, pp. 181-198. (1964).

CHAPTER 8

OPTIMIZING REINFORCEMENT OF ROOFS USING SHEAR STIFFNESS OF UNTENSIONED, RESIN-GROUTED BOLTS

8.1 INTRODUCTION

Chapters 2 and 3 described the significant mechanical properties and in-situ behaviour of non-tensioned resin bolts, and it was noted that among the most significant of these is the shear stiffness. When installed into bedded strata, the bolts serve as shear stiffeners. Also, as noted in Chapter 4, the bolts may be seen as adding cohesion to the bedding planes.

A properly installed resin bolt is much stiffer than a point anchored, tensioned, ungrouted bolt. Indeed, the shear stiffness of the latter is ineffective in controlling roof displacements (Fig. 8.1). In this diagram, which is based on work by Fairhurst and Singh (1), the shape of the curve is derived for a specific set of conditions - number of roof layers, roof span, bolt spacing, elastic properties of the rock, and normal and shear stiffnesses of the bedding planes. Bearing in mind the specific nature of the conditions used to derive this curve, it is worth noting that the effectiveness of increasing the bolt shear stiffness declines markedly at high stiffnesses. Roof deflection is little affected by increasing bolt shear stiffness beyond about 10 N/cm.

Conventional rock bolt design is based largely on suspension principles, and the simple models used to estimate roof loads typically result in regular spacing patterns across the span and along the axis of the tunnel or entry, i.e., square or rectangular patterns. In suspension design rock displacements are of no concern, but in considering reinforcement by shear stiffening, the distribution of shear displacements along bedding planes as the roof beams sag is critical. Optimum reinforcement would be obtained by ensuring that resin bolts were installed in those regions where shear displacement

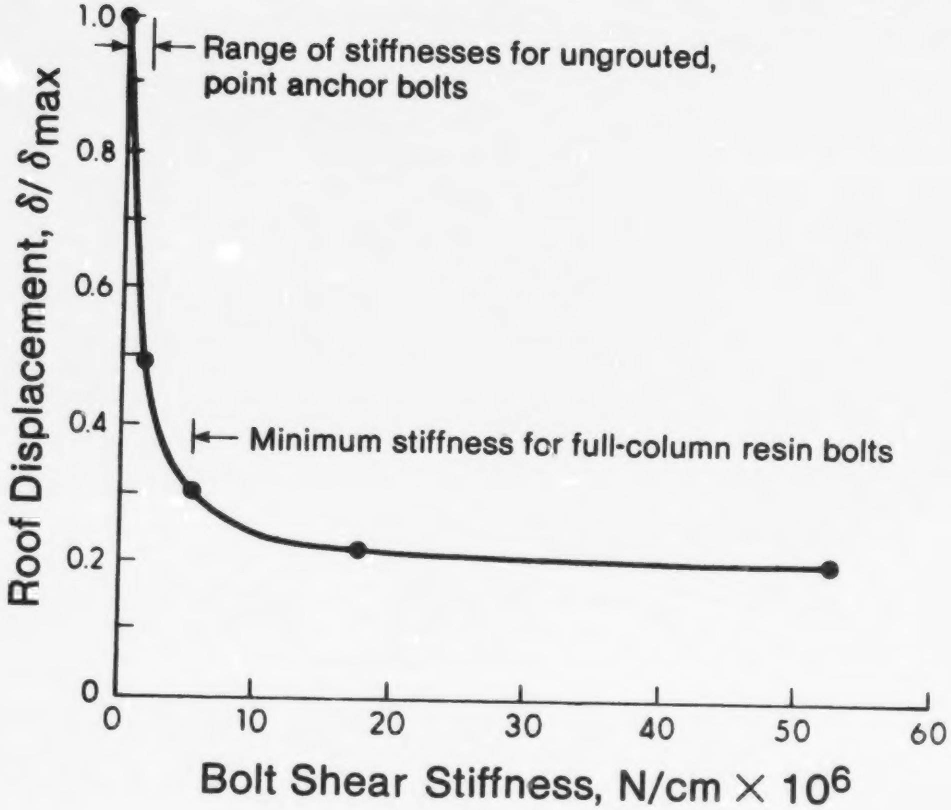

Figure 8.1 Roof displacement vs. bolt shear stiffness for a 4-layer roof, 6.1 m span, total thickness 40.6 cm. for zero shear stiffness of bedding planes (after (1))

in the unbolted roof is greatest. Conversely, where shear displacements along bedding planes are zero, untensioned, resin-bolts will not act as shear stiffeners and, therefore, it may be beneficial to consider cheaper grouting materials for bolts in these zones.

In the remainder of this Chapter the results of investigations to optimize resin bolt patterns for shear stiffening effect are presented. Some of the work reported here was presented to the International Symposium on Rock Bolting, Abisko, Sweden, September 1983. The paper is included as an Appendix to this Chapter.

8.2 BEDDING PLANE SLIP DURING ROOF FLEXURE - THEORY

Method I:

A small section of a sagging roof beam is illustrated in Figure 8.2 to an exaggerated scale.

Suppose the section shown can be approximated by two circular arcs with radii of curvature and included angle l_1 , ϕ_1 , and l_2 , ϕ_2 , respectively.

The bedding plane slip, EF,

$$= DF - CJ$$

$$= \phi_1 \ H \ (\phi_1 \text{ in radians}) \qquad \ldots\ldots\ldots\ldots\ldots \quad (8.1)$$

where H = layer thickness. Likewise, the bedding plane slip, GH,

$$= DH - CI$$

$$= (\phi_1 + \phi_2)H \qquad \ldots\ldots\ldots\ldots\ldots \quad (8.2)$$

The shearing strain, γ ,

$$\gamma = \tan\theta$$

$$= \alpha_b \text{ , for small angles}$$

where α_b = angle of bedding plane to the horizontal in radians

$$= \frac{dy}{dx} \ (\text{radians}) \qquad \ldots\ldots\ldots\ldots\ldots \quad (8.3)$$

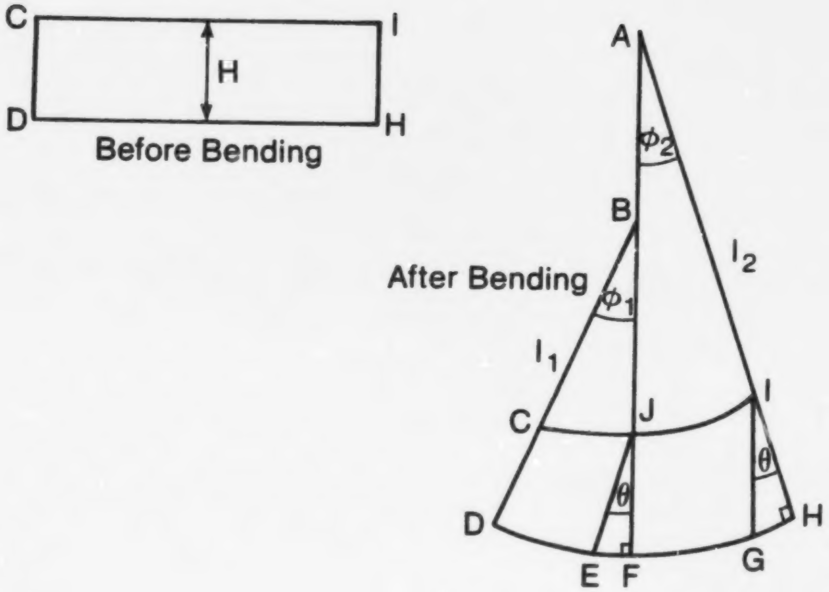
C
I
H
D
H
Before Bending
A
ϕ_2
B
l_2
After Bending
ϕ_1
l_1
I
C
J
θ
θ
D
H
E
F
G

Figure 8.2 Bedding plane slip - method 1

where y is the vertical deflection of the deflected layer.

Shearing strain

$$\gamma = \frac{dy}{dx} \quad . \qquad \ldots\ldots\ldots\ldots\ldots \quad (8.4)$$

The shearing strain will reach a maximum value where $d^2y/dx^2 = 0$. Also, from classical beam flexure theory, the bending moment in a beam is given by $M = EI\ d^2y/dx^2$. Hence, the shearing strain reaches a maximum value where the bending moment is zero.

Method 2:

Two elastic beams of equal thickness and elastic properties laid one over the other will deflect equally under load. For small deflections, the shear displacement along the interface is given by (Fig. 8.3):

$$\frac{v}{2} = d\ \frac{dy}{dx} \qquad \ldots\ldots\ldots\ldots\ldots \quad (8.5)$$

where y = vertical displacement.

The total relative slip between the bedding planes is twice the amount given by Equation 8.5,

$$v_t = 2d\ \frac{dy}{dx} \qquad \ldots\ldots\ldots\ldots\ldots \quad (8.6)$$

The maximum relative slip will occur where $dv_t/dx = 2d\ d^2y/dx^2 = 0$. But, the bending moment along the beam is given by $M = EI\ d^2\ y/dx^2$. Therefore, the maximum relative slip takes place at positions where the bending moment is zero.

8.3 DISTRIBUTIONS OF INTERFACE SLIP FOR DIFFERENT ROOF CONDITIONS

Distributions of interface slip were examined for four different cases as follows:

i) Built-in beam with uniform loading.

ii) Simply supported beam with uniform loading.

iii) Beam resting on deformable abutments and uniformly loaded.

iv) Built-in beam with parabolic load distribution, maximum load at centre.

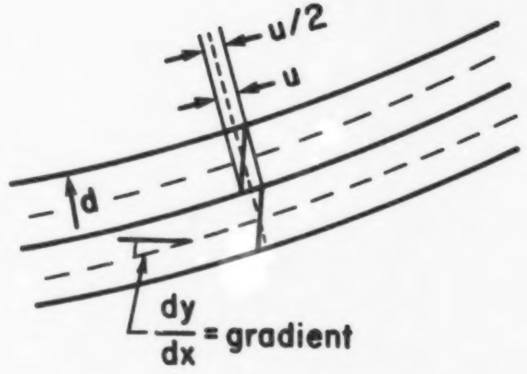
u/2
u
d
$\frac{dy}{dx}$ = gradient

Figure 8.3 Slip between two beams of equal thickness and properties - method 2

The theory for the last case (iv) is developed in Appendix C. It is well known that the zone of loosening above a roof is arch shaped. It was therefore of interest to determine the behaviour of a beam in the immediate roof under conditions of non-uniform loading from the strata above.

Figure 8.4 illustrates the distribution of interlayer slip with distance along the roof beams for these various cases. Theoretically, for the built-in beam with uniform loading the point of maximum slip is located 0.211 B from each end. There is little difference between this case and non-uniform loading, but for the other two cases the point of maximum slip is closer to the abutment.

For cases (i), (ii) and (iv) the positions of maximum slip are independent of material geometric properties and loadings; these only affect slip magnitudes. This is not so where the roof beams are resting on deformable abutments. Figure 8.5 shows the distribution of slip for three different sets of material and geometric properties. The stiffness and thickness of the abutment are most significant. As abutment stiffness decreases and/or thickness increases, the point of maximum slip moves towards the abutment. Likewise, as beam stiffness increases and beam thickness increases, the same trend is evident. Thus, case A (Fig. 8.5) approaches the conditions of a built-in beam with uniform loading and case B is close to that of a simply supported beam.

The influence of span, abutment thickness, Young's modulus of the abutment, Young's modulus of the beam, and beam thickness on the position of point of maximum slip, are further illustrated in Figures 8.6 - 8.10. These Figures show more clearly that the point of maximum slip moves towards the abutment as:

i) Span decreases,
ii) Abutment thickness increases,
iii) Young's modulus of abutment decreases,
iv) Young's modulus of beam increases, and
v) Beam thickness increases.

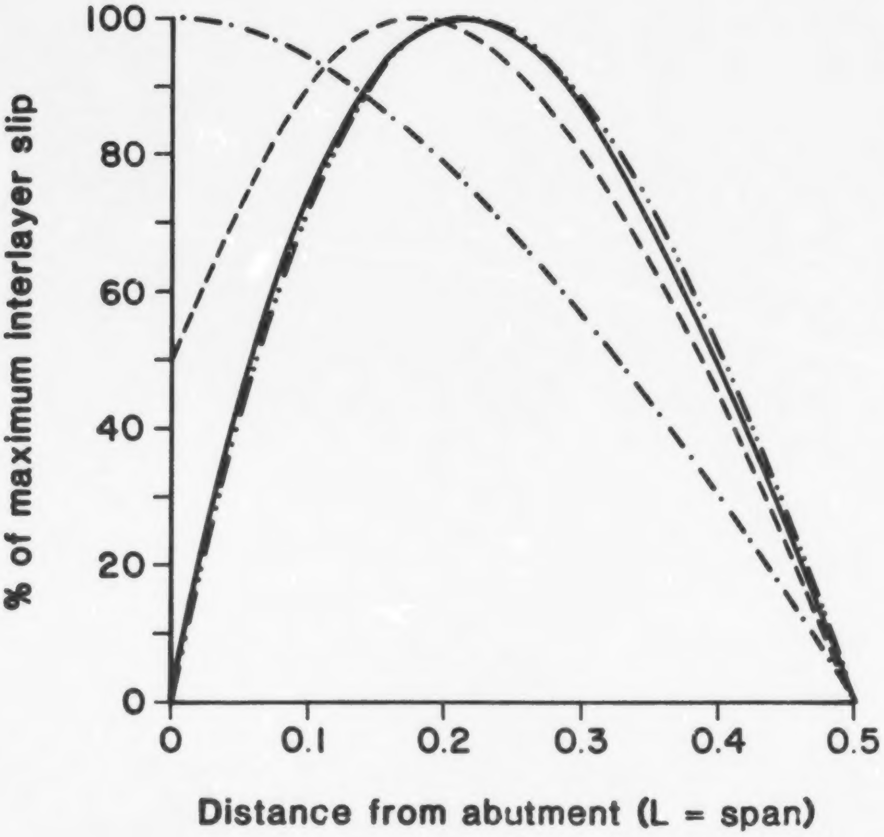

Figure 8.4 Interlayer slip along different types of roof beam (span = 5 m, beam thickness = 0.25 m, thickness of abutment = 2 m, Young's modulus of beam and abutment = 2000 MPa, Poisson's ratio of beam and abutment = 0.3, specific gravity of rock = 2.5)

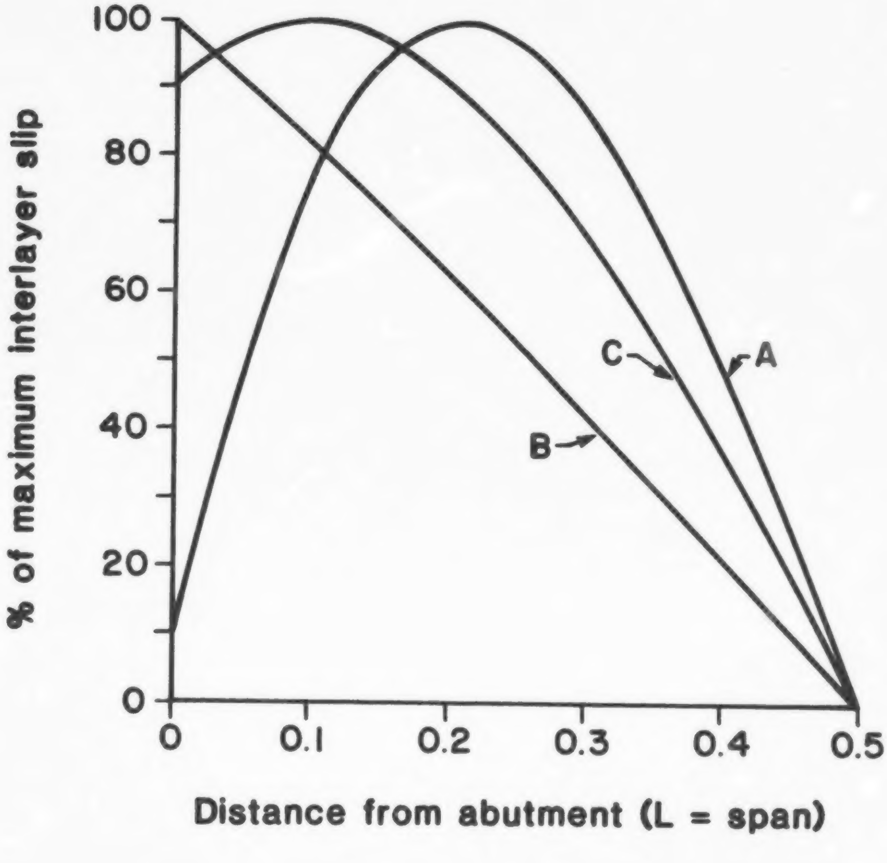

Figure 8.5 **Effect of geometric and rock properties on distribution of interlayer slip for beams resting on deformable abutments**

	A	B	C
Span, m	10	2	6
Beam thickness, m	0.1	2	1
E of abutment, MPa	32000	1000	16000
E of beam, MPa	1000	32000	16000
Abutment thickness, m	1.5	12	7
Poisson's ratio of beam	.3	.3	.3
Poisson's ratio of abutment	.3	.3	.3
Specific gravity of rock	2.5	2.5	2.5

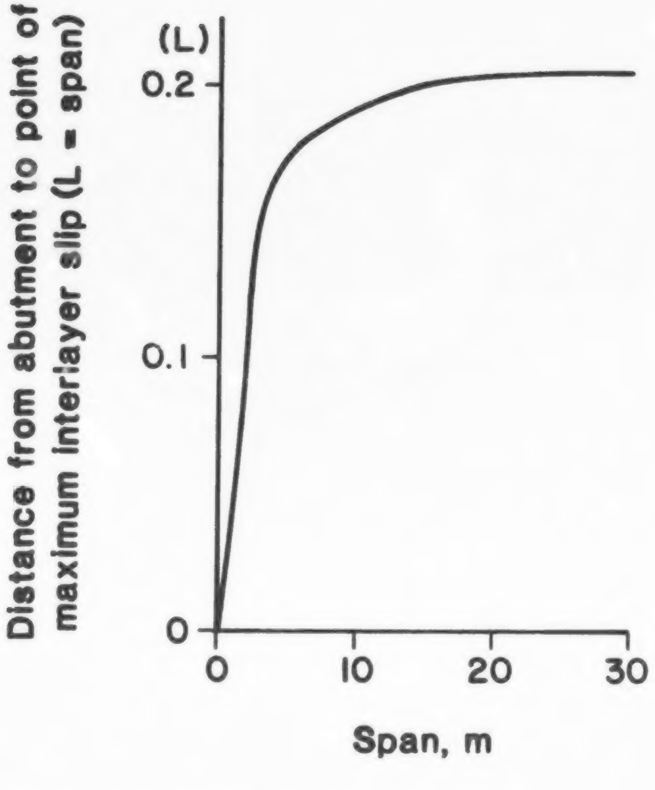

Figure 8.6 Variation of position of maximum interlayer slip with span for uniformly loaded beam resting on deformable abutments (beam thickness = 0.25 m, specific gravity of rock = 2.5, thickness of abutment = 2 m, Young's modulus of beam and abutment = 2000 MPa, Poisson's ratio of beam and abutment = 0.3)

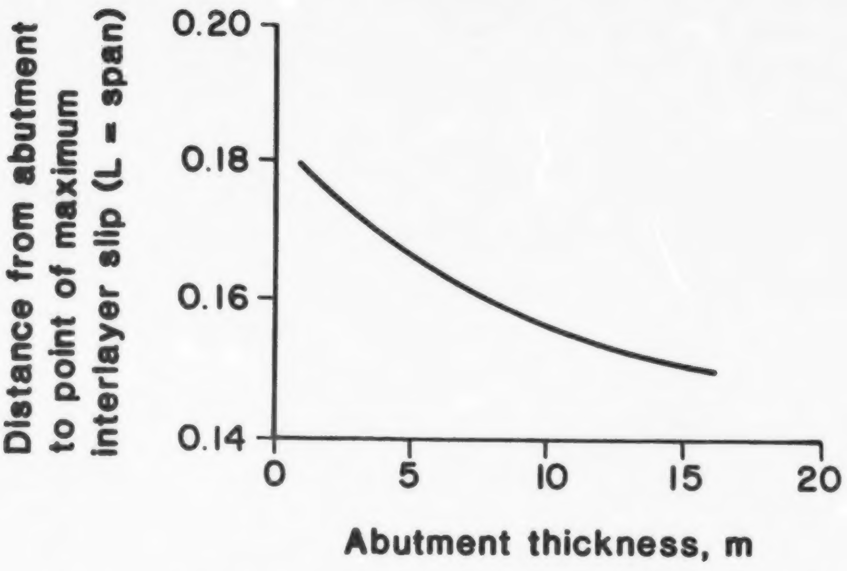

Figure 8.7 Variation of position of maximum interlayer slip with abutment thickness for uniformly loaded beam resting on deformable abutments (beam thickness = 0.25 m, specific gravity of rock = 2.5, span = 5 m, Young's modulus of beam and abutment = 2000 MPa, Poisson's ratio of beam and abutment = 0.3)

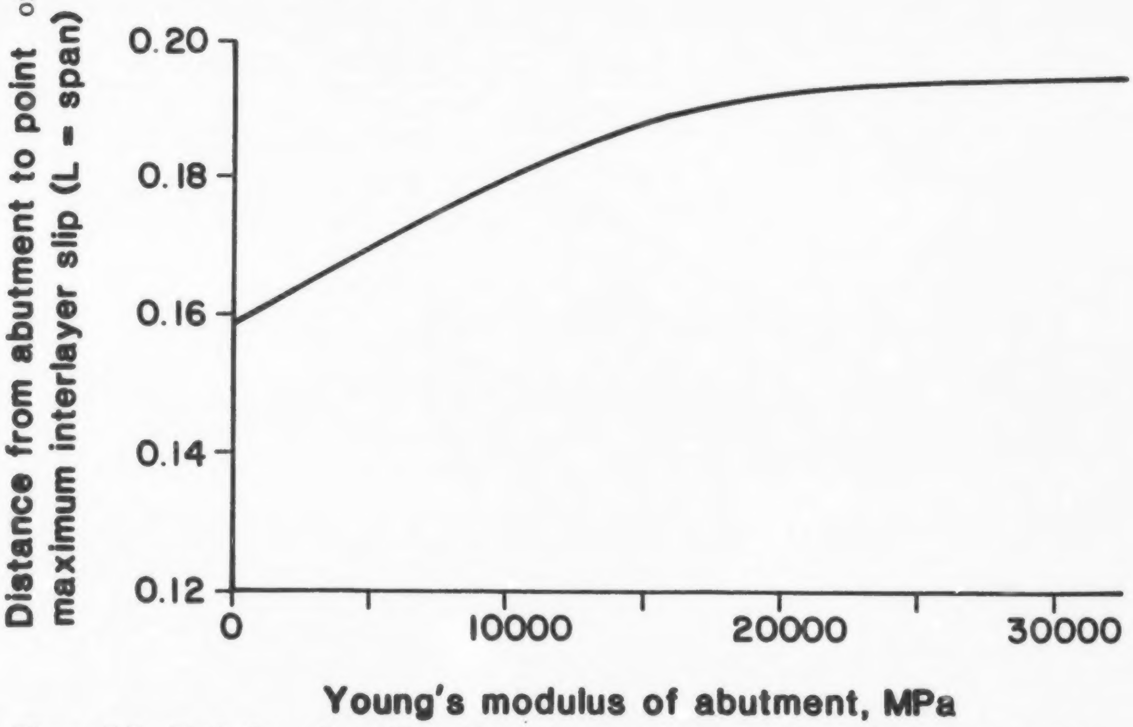

Figure 8.8 Variation of position of maximum interlayer slip with Young's modulus of abutment for uniformly loaded beam resting on deformable abutments (beam thickness = 0.25 m, specific gravity of rock = 2.5, span = 5 m, Young's modulus of beam = 5000 MPa, Poisson's ratio of beam and abutment = 0.3)

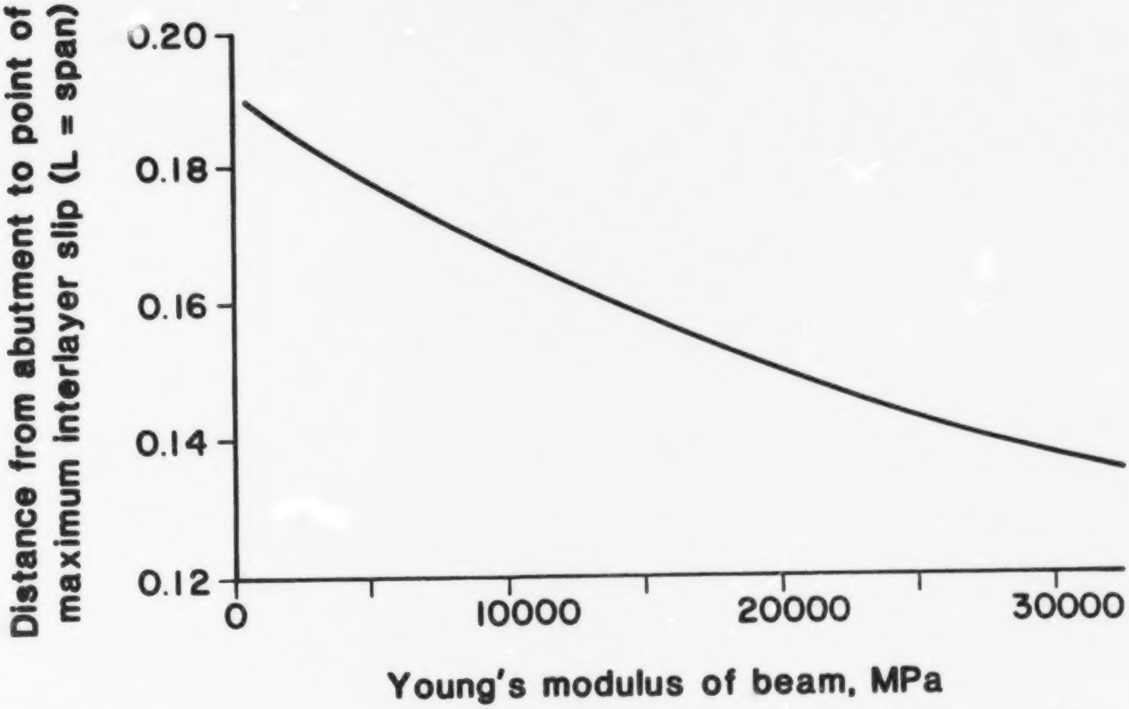

Figure 8.9 Variation of position of maximum interlayer slip with Young's modulus of beam for uniformly loaded beam resting on deformable abutments (beam thickness = 0.25 m, specific gravity of rock = 2.5, span = 5 m, Young's modulus of abutment = 2000 MPa, Poisson's ratio of beam and abutment = 0.3)

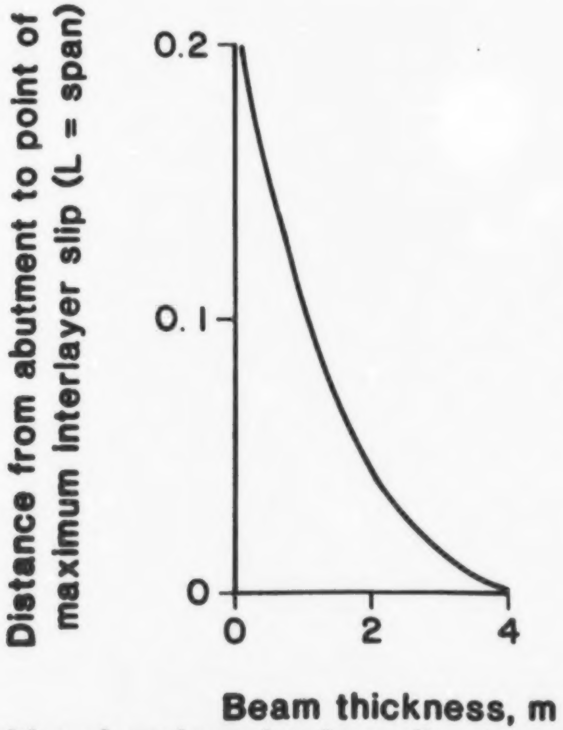

Figure 8.10 Variation of position of maximum interlayer slip with beam thickness for uniformly loaded beam resting on deformable abutments (specific gravity of rock = 2.5, span = 5 m, Young's modulus of beam and abutment = 2000 MPa, Poisson's ratio of beam and abutment = 0.3)

The magnitude of slip varies significantly between the four cases studied (Fig. 8.11). Clearly, the deformable abutments and non-uniform loading substantially increase shear displacement. The case of non-uniform loading **AND** deformable abutments was not studied, but would obviously lead to even greater displacements than shown in Figure 8.11.

For all cases, slip increases with increasing span and with decreasing beam thickness and Young's modulus of abutment. Note that for all three variables there is a rapid rate of increase in displacement above or below certain values (Figs. 8.12 -8.14). For example, thinly laminated roofs in low stiffness materials and with wide spans would exhibit considerable interlayer slip.

For the parabolically loaded beam there is a linear rate of increase in shear displacement with increasing load intensity at the centre of the span (Fig. 8.15).

8.4 EFFECT OF LARGE DISPLACEMENTS AND LAYERS OF DIFFERENT FLEXURAL RIGIDITIES

The theory developed above applies to cases of small displacements and layers of equal thickness and properties. If displacements are large and/or layers are not uniform, what differences will these conditions bring to the general conclusions reached above?

Beam bending theory for large displacements, involving complex elliptic integrals, could be used to extend these ideas to such cases. The distribution and magnitudes of slip will be different in detail. The point of maximum slip will shift towards the abutment; in other words, the small displacement case provides a bound, e.g., for a built-in beam under uniform loading the point of maximum slip will never be further from the abutment than 0.211 B (B = span).

As noted in an earlier Chapter, the response of a stack of layers of different

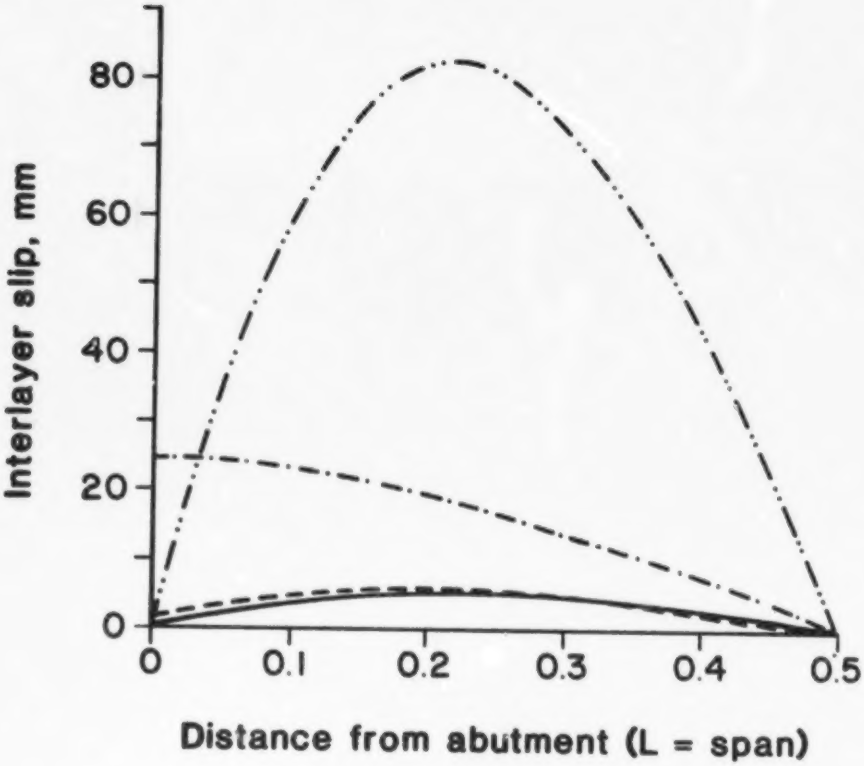

Figure 8.11 Magnitudes of interlayer slip for different cases (span = 10 m, specific gravity of rock = 2.5, abutment thickness = 2 m, beam thickness = 0.25 m, Young's modulus of beam and abutment = 2000 MPa, Poisson's ratio of beam and abutment = 0.3)

— Built-in beam with uniform loading

—·—Simply supported beam with uniform loading

- - -Beam resting on deformable abutments

—··—Built-in beam with parabolic loading (max. load at centre ≡ 20 x beam thickness)

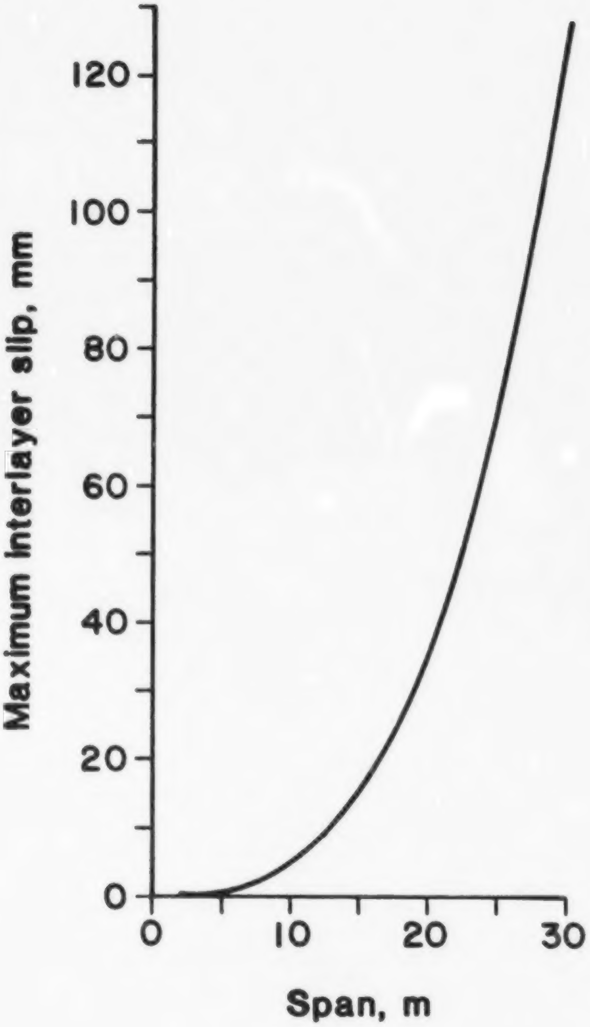

Figure 8.12 Effect of span on maximum value of slip for a built-in beam under uniform loading (beam thickness = 0.25 m, Young's modulus = 2000 MPa, specific gravity of beam = 2.5)

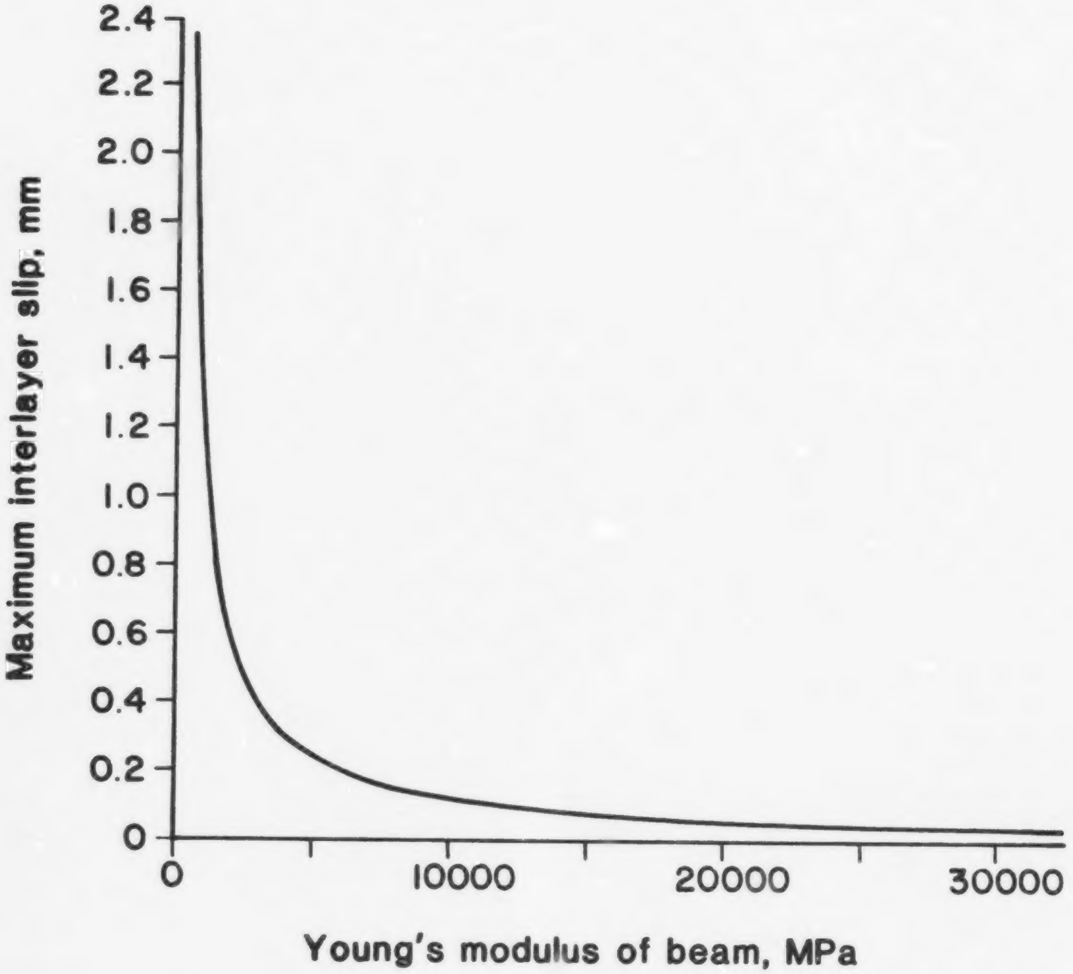

Figure 8.13 Effect of Young's modulus of maximum value of slip for a built-in beam under uniform loading (beam thickness = 0.25 m, beam span = 5 m, specific gravity of beam = 2.5)

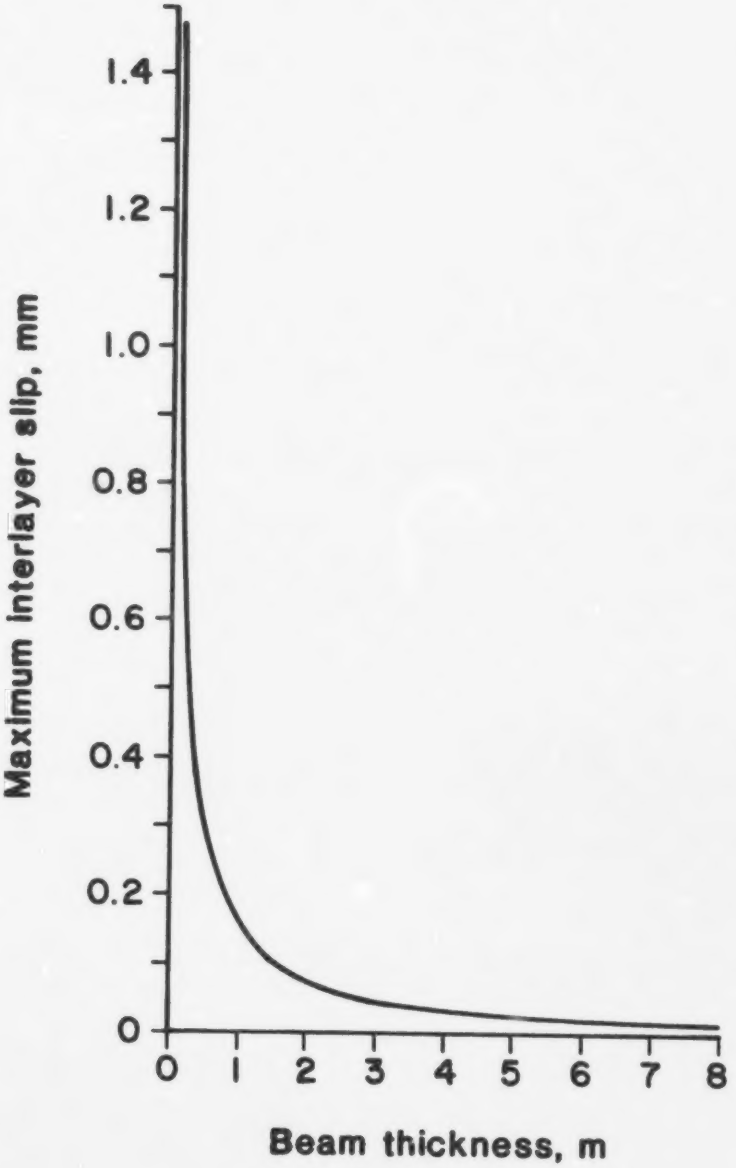

Figure 8.14 Effect of beam thickness on maximum value of slip for built-in beams (beam span = 5 m, Young's modulus = 2000 MPa, specific gravity of beam = 2.5)

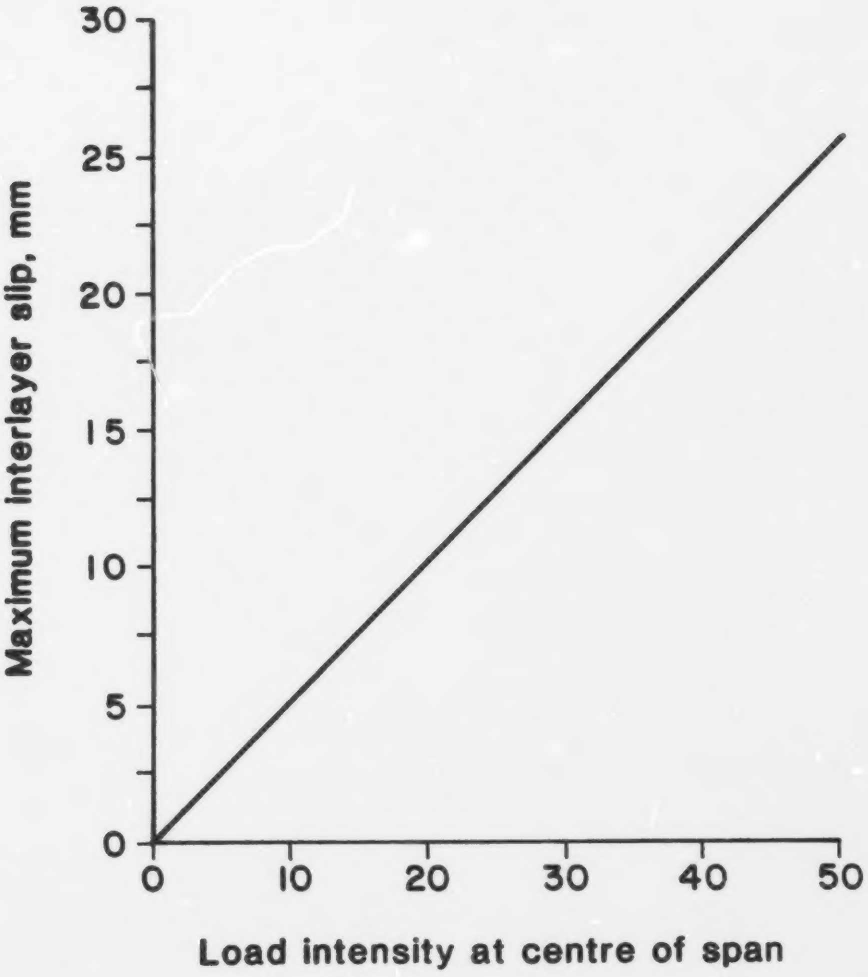

Figure 8.15 Effect of load intensity at centre of parabolically loaded built-in beam on maximum value of slip (span = 5 m, beam thickness = 0.25 m, Young's modulus of beam = 2000MPa, specific gravity of beam = 2.5)

flexural stiffnesses to gravitational load has an infinite number of permutations and combinations, depending on the relative stiffnesses and positions of the layers. Bed separation would occur at some interfaces, while at other points an upper bed would sag onto a lower bed. Also, for each beam the abutment conditions are changing since the beams below it constitute part of its abutment. Such a problem could only be solved by a numerical method, such as finite element analysis. However, it can be stated once again that the point of maximum slip for each interlayer will be located in the region between the abutment and 0.211 B. For some layers this point could be near the abutment and for others close to 0.211 B, depending on specific conditions.

8.5 EXPERIMENTAL CONFIRMATION OF OPTIMIZATION OF REINFORCEMENT

If a shear stiffener is installed at the point of maximum slip optimum reinforcement should occur. The vertical defletion of the beam provides a suitable measure of reinforcement.

To test this hypothesis, a two-layer model was constructed in the laboratory from K3 resin-bonded particle board. Measuring 1.6 cm x 10.2 cm x 121.9 cms, the two beams were clamped, one on top of the other, between specially built screw clamps (Fig. 8.16) to give an overall span of 111.8 cms. The aluminum end clamps provided stiff abutment conditions. To simulate soft abutments, 7.6 cms of cork in layers of 9.5 mm thick were inserted beneath the beams at the clamps.

Uniform loading was obtained by laying 5.1 cm diameter steel mill balls along the upper surface (Fig. 8.16). The total loading for the soft abutments was reduced from 224.6 N to 117.4 N to avoid excessive deflections.

Untensioned resin bolts were modelled by 4.8 mm diameter acrylic rods set in 7.9 mm holes drilled into the K3 board perpendicular to the layers. Sulfur set (a mixture of sulfur and clay (10:1) heated to 130 deg. C.) was poured into the bolt holes to simulate the resin.

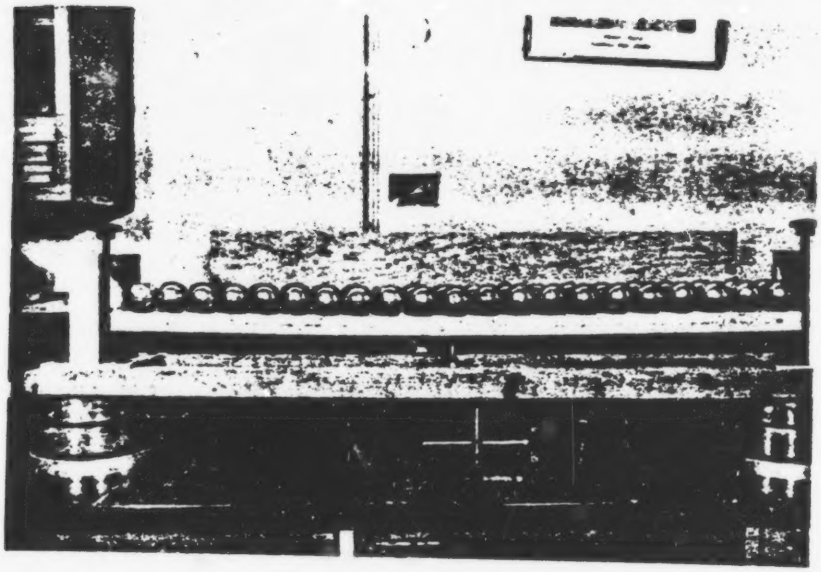

Figure 8.16 Two-beam model to test reinforcement hypothesis

Vertical deflections at the centre of the model were measured with a standard dial gauge to an accuracy of 0.01 mm.

A series of tests were conducted in which the uniform load was held constant, but the position of two bolts placed symmetrically about the centre was varied. Thus, for each test the beam was reinforced by two bolts placed at equal distances from the abutments. The results of the experiments are summarized in Figure 8.17, which clearly shows that there is an optimum point for reinforcement which agrees very well with the theoretical prediction of 0.211 B (B = span).

There is no discernible difference between the positions of optimum reinforcement for stiff and soft abutments. This is also in agreement with predictions of the theory for a beam resting on a deformable abutment. The laboratory model simulates a wide span of stiff, thin roof beams, resting on a relatively thin (compared to span) but soft abutment. Referring to Figures 8.6 - 8.10, it may be seen that this case of deformable abutments will respond in a manner approaching that of a built-in beam. In particular, the thickness to span ratio is a controlling factor.

Scatter of data points is evident in Figure 8.17. Some of this is, no doubt, due to random error, but, in addition, clamping conditions were not precisely reproducable from test to test, and the K3 board was found to deflect in a time-dependent manner. The effect of the latter was minimized by recording deflections at the same time after loading for every test, but hysteresis effects probably occurred, since the same beams were used for all tests (i.e. effect of successive loadings and unloadings of a creep-prone material).

8.6 REINFORCEMENT USING MULTIPLE BOLTS

Although the position of optimum reinforcement has been determined and shown to result in minimizing deflections as compared to other bolt locations, additional

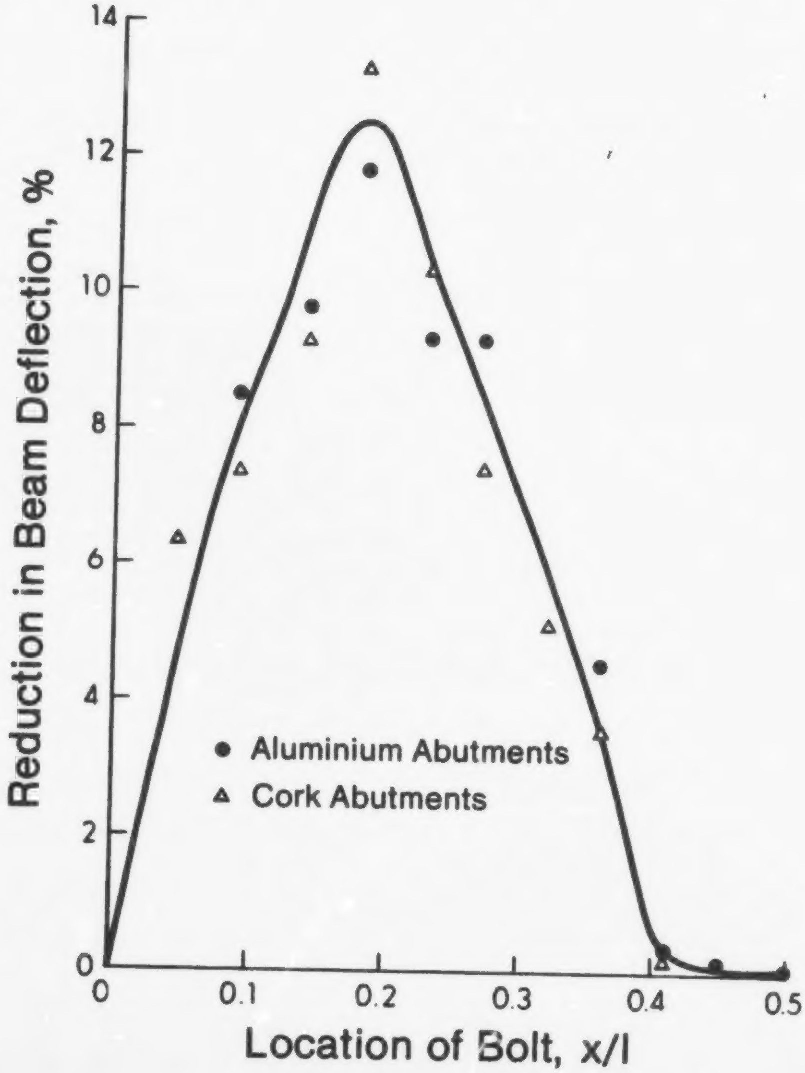

Figure 8.17 Effect of bolt location on reinforcement

bolts should be installed to increase total shear stiffness further. Where should these be placed? A series of model tests were carried out with the 2-beam configuration used above to examine the degree of reinforcement obtained by different multiple bolt patterns. The various patterns used are shown in Figure 8.18 and results summarized in Figures 8.19 and 8.20. Case #1 is close to the position of optimum reinforcement for two bolts. Though the other patterns included as many as 10 bolts, the additional increase in reinforcement is not large (Fig. 8.19). It is, therefore, concluded that:

i) The two bolts at the optimum locations contribute most reinforcement. Additional bolts, while further decreasing roof beam deflections, are not as effective.

ii) For the 2-layer model the inclusion of more than four bolts across the span results in negligible additional reductions in roof beam deflection.

8.7 CONCLUSIONS

It has been demonstrated in this Chapter, on the basis of theoretical and experimental approaches, that the most critical zone for reinforcement lies between the abutments and about 1/5 of the span in from each ribside. In particular, when the abutments are thick and of low stiffness relative to roof strata, or have yielded, or where roof fracturing is developing over or near the abutments (cf. Chapter 7), interlayer slip is highest in this region (see Figs. 8.4 and 8.5). These results suggest a closer spacing of bolts in this region, in order to concentrate reinforcement where it is most needed and can be of greatest benefit. Further discussion of the implications for rock bolt layout are left to Chapter 15.

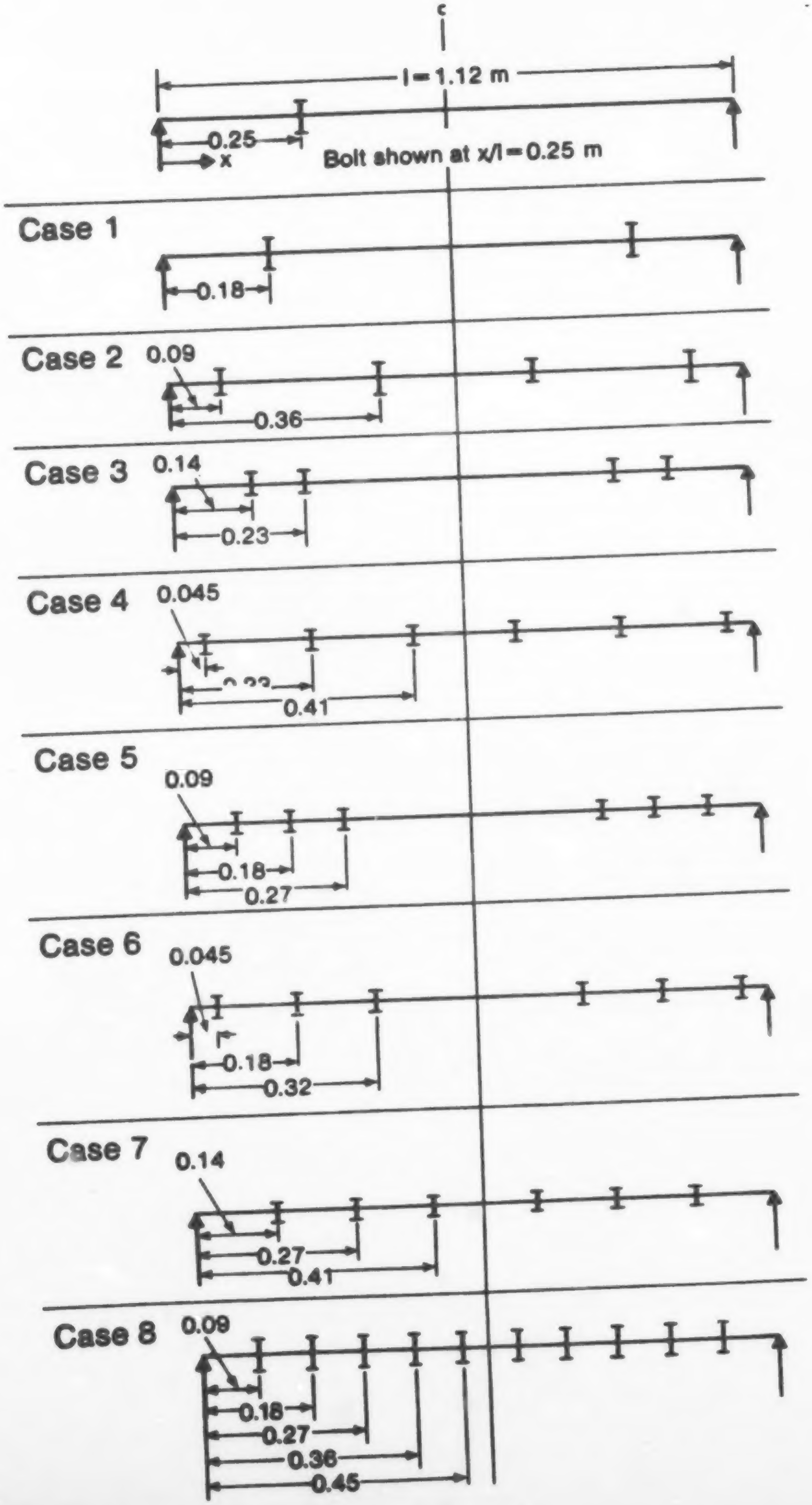
c
l = 1.12 m
0.25
x
Bolt shown at x/l = 0.25 m
Case 1
0.18
Case 2
0.09
0.36
Case 3
0.14
0.23
Case 4
0.045
0.23
0.41
Case 5
0.09
0.18
0.27
Case 6
0.045
0.18
0.32
Case 7
0.14
0.27
0.41
Case 8
0.09
0.18
0.27
0.36
0.45

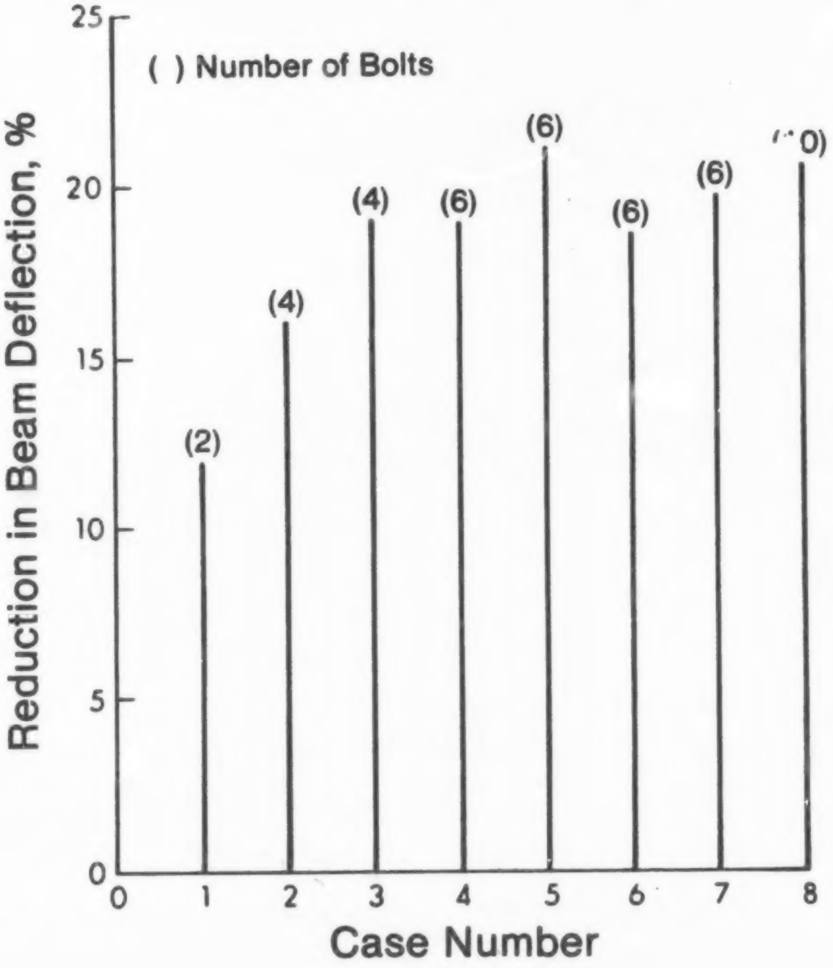

Figure 8.19 Reduction in beam deflection for the various bolt patterns illustrated in Fig. 8.18

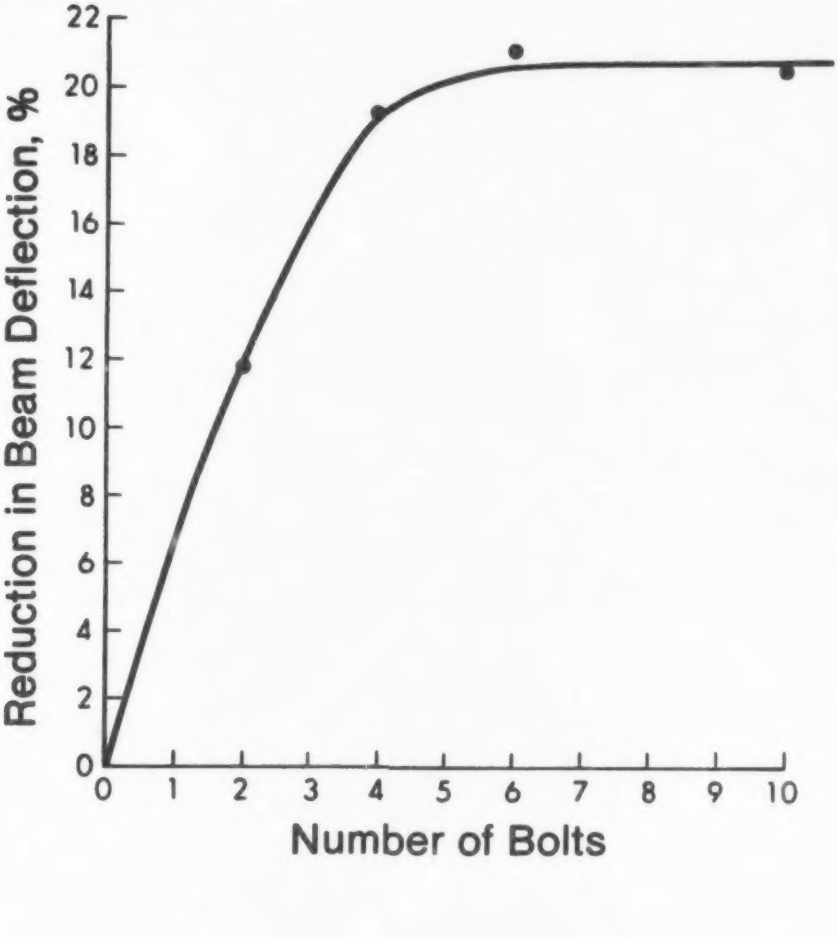

Figure 8.20 Effect of number of bolts on beam deflection

REFERENCES

1. Fairhurst, C. and Singh, B. Roof bolting in horizontally laminated rock. Engineering and Mining Journal, 175, pp. 80-88, 90. (1974).

Appendix

Copy of paper, " The influence of rock bolt location on the
reinforcement of horizontally bedded roofs
by full column grouted bolts."

Presented at the First International Symposium on Rock Bolting, Abisko, Sweden, Aug/Sept. 1983.

Rock Bolting, Abisko, Sweden, Aug/Sept. 1983.

The influence of rock bolt location on the reinforcement of horizontally bedded roofs by full column grouted bolts

B.Stimpson
Department of Mineral Engineering, Edmonton, Alberta, Canada

ABSTRACT: Results of mathematical analysis and laboratory experiments indicate that for resin bolting of roofs in horizontally bedded strata there is an optimum location of bolts for maximum reinforcement under both uniform and non-uniform loads. Rigid and non-rigid abutments are modelled and it is shown that the effect of non-rigid abutments is to move the zone of maximum bedding plane slip towards the abutment. It is suggested that for maximum reinforcement there be a non-uniformity of bolt spacing with a smaller spacing towards the abutment or rib-side.

1 INTRODUCTION

Excavation in horizontally bedded strata typically produces rectangular shaped openings with flat backs. Model studies (Hobbs 1969) and experience indicate that this shape is not the most stable geometry for these geological conditions and some form of internal or external support is frequently required unless the span is small.

The widespread use of point anchor, ungrouted, tensioned bolts, which were the first form of rock bolt support widely used in bedded deposits, has since been challenged by a variety of bolts operating on different principles. Of these the full column, grouted, non-tensioned bolts in which the annular space between the bolt and the drill hole wall is filled with a stiff grout of resin or inorganic filler such as cement, have become popular, more notably in Europe.

In this paper the research work to be described was directed to the full column, grouted bolt system, but several of the principles emerging from this study may also be applicable to point anchor, tensioned, bolt layouts.

2 THEORY OF BOLTING IN HORIZONTALLY BEDDED STRATA

In horizontally bedded strata the two principle modes of action of rock bolts - suspension and reinforcement - may be operating in any given excavation. Separation of the two modes as to their relative importance is difficult and is dependent on site conditions and the layout and design of the roof bolt support system.

In the suspension mode the bolts are considered to support the dead weight of rock in the roof which may otherwise collapse. The anchorages must be located in self-supporting beds overlying the strata requiring support; the identification of suitable horizons for anchorage and the estimation of loads require a detailed knowledge of the geology of the roof, especially bed thicknesses, strengths, deformabilities and jointing.

In the reinforcement mode bolting acts to increase the resistance of the strata to applied loads. Specifically, in horizontally bedded strata bolting of the immediate roof layers increases the resistance to shear along bedding planes. If slip is entirely prevented the roof layers in the bolted assemblage will behave as a single beam of thickness equal to the sum of their individual thicknesses. The effect of this ideal situation on roof deflection and bending stresses is readily demonstrated using classical beam bending theory. For a clamped beam the maximum bending stress in tension, $(\sigma_x)_{max}$ is generated on the upper surface immediately above the clamped edge and is given by:

$$(\sigma_x)_{max} = wl^2/2H$$

The influence of rock bolt location on the reinforcement of horizontally bedded roofs by full column grouted bolts.
B. STIMPSON [illegible]

where w = unit weight of rock, l = span, H = beam thickness. Similarly, the maximum deflection, δ_{max}, of the beam at the centre is given by:

$$\delta_{max} = \rho l^4/32EH^2$$

when E - modulus of elasticity of beam.

Therefore, if five layers of equal thickness can be bolted together in such a manner as to prevent all bedding plane slip then the maximum bending stress will be reduced to 1/5 and the roof deflection to 1/25 of their magnitudes in the unbolted beam.

This paper is concerned only with the reinforcement mode of roof bolt support.

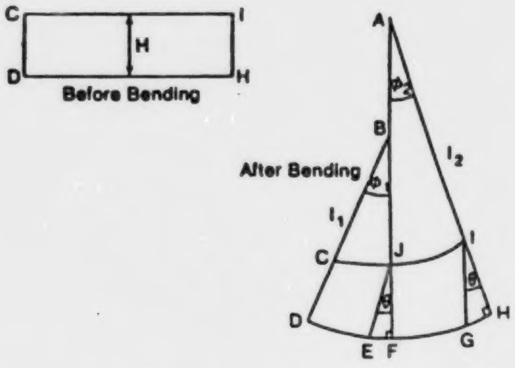

Figure A1. Bedding Plane Slip

3 FULL COLUMN GROUTED BOLTING

Full column grouted bolts reinforce bedded strata by resisting slip along bedding planes. A useful measure of the 'rate' at which a rock bolt can provide resistance to shear is its shear stiffness or the increase in shear resistance with unit shear displacement. In this respect a properly installed resin-bolt in which there are no voids or gaps with missing grout is much stiffer than a point anchor, ungrouted, tensioned bolt. This is illustrated in Fig. 1 which is derived from the publication of Fairhurst and Singh (Fairhurst and Singh 1974) and describes the relationship between bolt shear stiffness and roof deflection for a specific set of conditions of number of roof layers, roof span, bolt spacing, elastic properties of the rock, and normal and shear stiffnesses of the bedding planes. Therefore, while the precise shape and location of the curve is determined by these selected parameters, the trends illustrated in the Figure are of general application. It appears, for example, that the incremental effectiveness of increasing the bolt shear stiffness declines markedly as higher stiffnesses are considered. In this particular case (Fig. 1) roof deflection is little affected by increasing bolt shear stiffness beyond about 10^7 N/cm. The minimum stiffness of full-column resin bolts is considerably greater than the stiffness of ungrouted, point anchor bolts. From the viewpoint of reinforcement by preventing or reducing bedding plane slip, the latter type of bolt is essentially ineffective (Fig. 1).

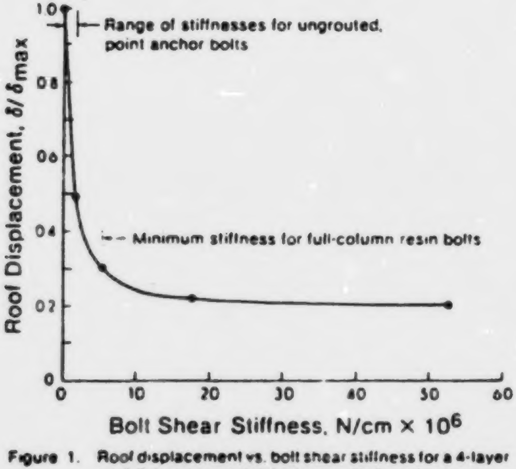

Figure 1. Roof displacement vs. bolt shear stiffness for a 4-layer roof, 6.1 m span, total thickness 40.6 cm for zero shear stiffness of bedding planes (derived from Fairhurst and Singh, 1974)

3.1 Bolt location for maximum effectiveness in providing reinforcement to resist bedding plane slip-theory

If the deflection of a laminated roof beam can be controlled by the installation of full column, grouted bolts which act as shear stiffeners, then the question may be asked as to the optimum location for installing bolts, i.e. the location that would result in the greatest decrease in roof deflection. At the Department of Mineral Engineering, University of Alberta, research is being undertaken to answer this question for two types of horizontally bedded roof which represent idealized models of reality. The first model treats the roof as comprised of an assemblage of unjointed beds separated by bedding planes, Fig. 2.

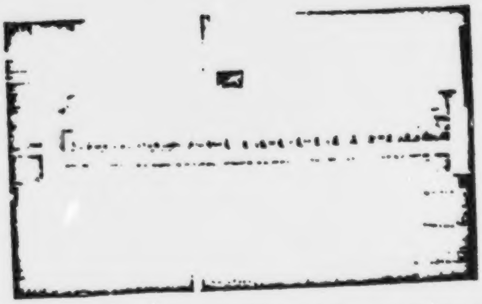

Figure 2. Physical Model of Two Unjointed Roof Layers

while the second model introduces the additional complexity of rough, vertical cross joints in each of the roof layers Fig. 3. The objective of this paper is to report on the results of our study of the first model.

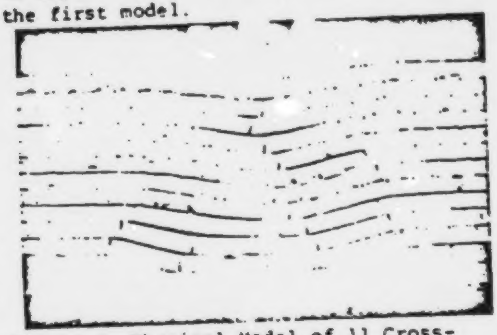

Figure 3. Physical Model of 11 Cross-Jointed Roof Layers

The flexural slip which takes place along bedding planes when an assemblage of roof beams deflects is not constant in magnitude from the abutment to the centre of the span. Its magnitude and distribution are dependent upon the elastic properties of the layers, their thicknesses, the load distribution on the layers and the boundary conditions at the abutments. In Appendix II it is shown that the slip, δ, at any point along a bedding plane in the roof strata is given by:

$$s = \alpha_b H \tag{1}$$

where α_b = angle of bedding to horizontal in radians and H = thickness of bed, and the shearing strain, γ, is expressed by:

$$\gamma = \alpha_b \tag{2}$$

Equations (1) and (2) can be used to calculate the distribution of slip between roof layers and hence to locate the points of maximum slip. It is at these points that at least two of the roof bolts should be located symmetrically about either side of the centre line of the tunnel. It is further shown in Appendix II that the location of maximum slip corresponds to those points in the beam at which the bending moment, M, is zero.

Case A - Clamped beam with non-uniform loading, rigid abutments (Fig. 4)

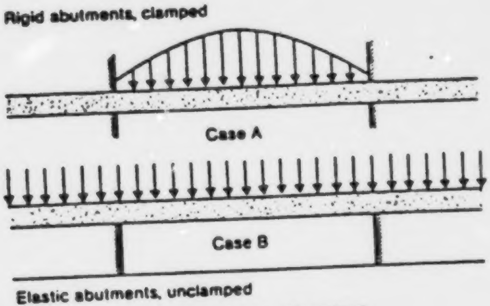

Figure 4. Two Roof Beam Cases Examined.

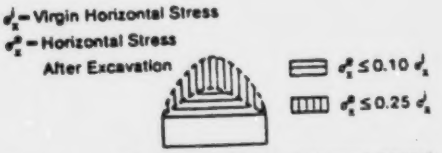
σ_x^i – Virgin Horizontal Stress
σ_x^e – Horizontal Stress After Excavation
$\sigma_x^e \leq 0.10\, \sigma_x^i$
$\sigma_x^e \leq 0.25\, \sigma_x^i$

Figure 5. Zones of reduced horizontal stress around rectangular opening in horizontally bedded rock (after Singh, 1972)

In the roof of an excavation in horizontally bedded strata the lower bolted beds may be called upon to resist non-uniform loading owing to the manner in which the upper beds deform. Fig. 5 illustrates the zones of reduced horizontal stress above an opening in thinly bedded rock. An approximately parabolic - shaped zone of 'loosened' rock is formed and it is conceivable that under the worst conditions the weight of rock in this volume could provide a non-uniform, external load to the roof beams immediately above the opening (Fig. 4). For purposes of analysis this load distribution is assumed to be described by the following relationship:

$$q = q_o + bx(l-x) \tag{3}$$

where q = load density at x

q_o = load density at $x=0$

l = roof span

b = constant

x = horizontal distance from abutment

With this loading distribution the shear strain, γ, along the beam is given by (see Appendix III for derivation):

$$\gamma = \frac{1}{EI}\left[\frac{q_o x^3}{6} - \frac{\alpha x^5}{60} + \frac{\alpha x^4 l}{24} + \frac{Ax^2}{2} + Bx\right] \quad (4)$$

where E = modulus of elasticity

I = moment of inertia

A,B = constants

In Fig. 6 the normalized bedding plane slip (S/S_{max}) is plotted against location in the beam for a specific roof geometry and elastic properties and for a variety of values of b in equation (3) ranging from zero (uniform load) to a value which represents a high degree of non-uniformity of load (load density at centre of span equal to 20 x load density at abutment). The curves of normalized shear strain or slip vs. location along the span are, for all practical purposes, coincident and therefore a single, universal curve has been drawn. The maximum amount of slip takes place at a distance of approximately 0.21 x span from the abutments. This would be the optimum location for installation of full column, grouted bolts.

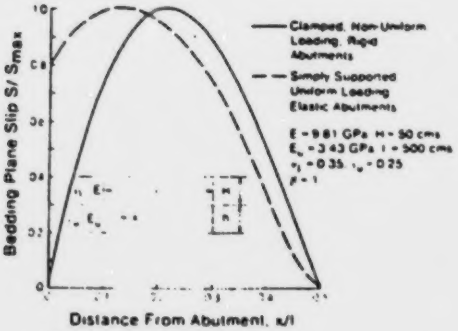

Figure 6 Bedding Plane Slip vs. Distance from Abutment

Though the shape of the curve and the point of maximum slip is not affected by the degree of non-uniformity of loading the magnitude of slip is. As the load density in the centre of the beam increases the bedding plane slip at the point of maximum slip, $x = 0.21 \times$ span, increases. In Fig. 7, for a specific roof geometry and properties, the maximum slip is 18 times greater than that for a uniform load when the loading density at the centre of the span is 20 times larger than the loading density at the abutment.

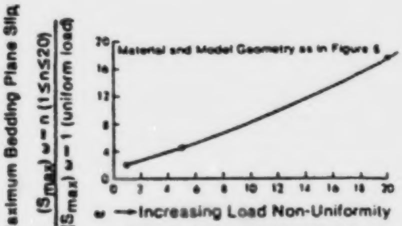

Figure 7. Maximum Bedding Plane Slip vs. Non-uniformity of Load

Case B - Simply supported beam, uniform loading, elastic abutments

In Case A the abutments were rigid. In practice, roof beams rest on abutments or pillars which are deformable. For the purposes of this study and because an analytical solution was available, elastic abutments were assumed for Case B.

It is well known in coal mining that at sufficient depth the edges of abutments and pillars suffer failure and the normal stress is considerably reduced (Fig. 8). The roof beam may not, therefore, be clamped by a high load over the immediate abutment. For purposes of simplication, it is assumed that the load density over the abutment continues unchanged from the uniform loading over the span. This model (Fig. 4) has been analysed by Stephansson (Stephansson 1971). The shear strain along the beam

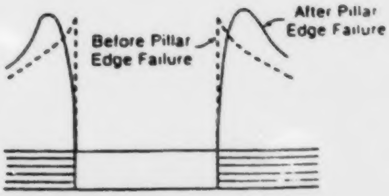

Figure 8 Vertical Stress Distribution Over Abutments (After Fairhurst and Singh, 1974)

may be derived from Stephansson's equation for roof deflection (see Appendix IV) and is given by:

$$Y = \frac{p}{c_u}\left[\alpha^4 \left(\frac{2x^3}{3} - x^2 l - \frac{2lx}{\alpha} - \frac{1}{\alpha^2} + 2l\beta + 2l\alpha\beta x\right)\right] \qquad (5)$$

where p = uniform load density

c_u = foundation modulus,

l = roof span

α, β = constants

Again, the normalized bedding plane slip is plotted against location along the beam in Fig. 6. The significant effect of the deformable abutments is the shifting of the point of maximum slip towards each abutment to x = 0.13 x span and the concentration of bedding plan slip within the initial quarter span distance from the abutment. These results from theory indicate that for maximum reinforcement full-column, grouted bolts should be installed close to the rib and a greater density of bolts provided in this region, i.e. non-uniform bolt spacing.

It was noted earlier that the points of maximum slip correspond to the locations where the bending moment, M, is zero. For the Case B model the bending moment, M, is given by (Stephansson 1971):

$$M = -\frac{px^2}{2} + \frac{p}{2}\left(x + \frac{l}{\alpha} - \alpha\beta\right) \qquad (6)$$

Therefore, M = 0, where

$$x = x_{op} = \frac{l}{2} \pm \sqrt{\frac{l^2}{4} + l\alpha\left(\frac{l}{\alpha^2} - \beta\right)} \qquad (7)$$

The constants in equation (7) involve the elastic constants and geometry of the opening. It is therefore useful to investigate the sensitivity of the location of maximum slip, x_{op}, to these various parameters. Results from this sensitivity analysis are displayed in Figs. 9-12 and may be summarized as follows:

1. x_{op} moves away from the abutment as
   - a) roof span increases
   - b) modulus of elasticity of abutment increases
   - c) Poisson's ratio of abutment increases
2. x_{op} moves towards the abutment as
   - a) modulus of elasticity of roof beam increases
   - b) Poisson's ratio of roof beam increases
3. As the thickness of the roof beam increases x_{op} at first moves away from the abutment but then moves towards the abutment (Fig. 9)
4. x_{op} is unaffected by the density of the roof beam (Fig. 12)
5. x_{op} may become negative, (i.e. point of maximum slip is over abutment) as abutment thickness increases.
6. For x_{op} to be close to the abutment the excavation should have the following properties:
   - a) thick abutment or pillar
   - b) small roof span
   - c) low Poisson's ratio of abutment
   - d) stiff roof beam, i.e. high modulus of elasticity
   - e) high Poisson's ratio of roof beam
   - f) thick roof beam
   - g) soft abutment or pillar, i.e. low modulus of elasticity

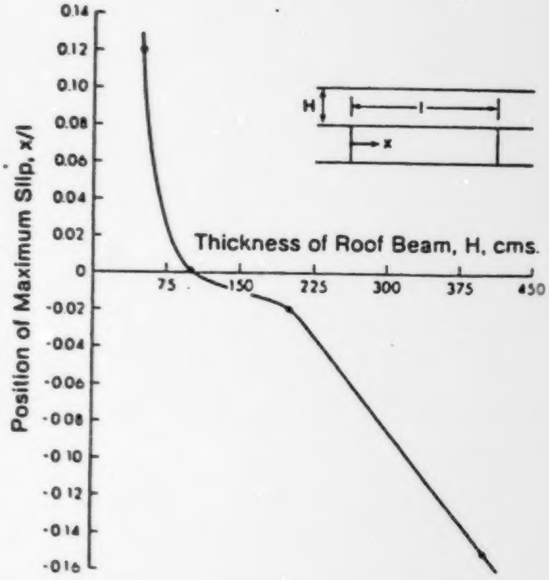

Figure 9. Position of Maximum Slip vs Thickness of Roof Beam

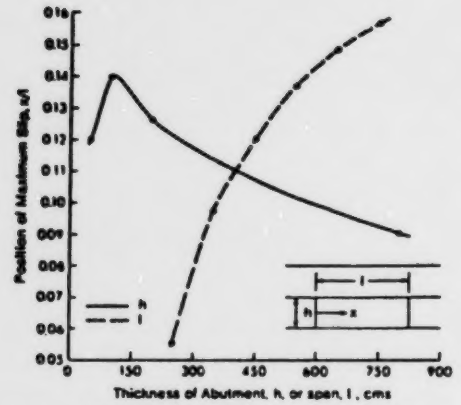

Figure 10. Position of Maximum Slip vs. Thickness of Abutment, h, and Span, l.

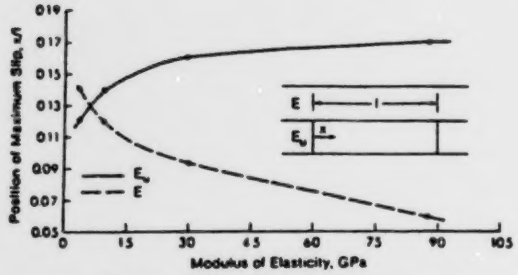

Figure 11. Position of Maximum Slip vs. Modulus of Elasticity of Abutment, E_u, and Roof, E.

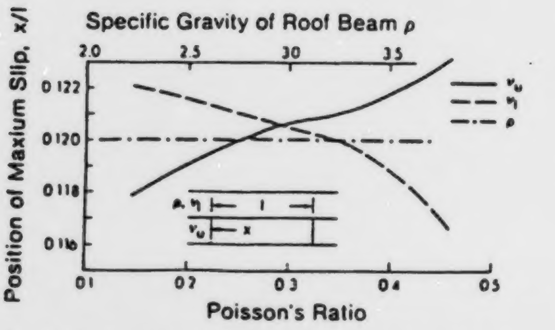

Figure 12 Position of Maximum Slip vs Poisson's Ratio of Abutment, ν_u, and Roof Beam, ν_l, and Specific Gravity of Roof Beam, ρ

3.2 Bolt location for maximum effectiveness in providing reinforcement to resist bedding plane slip - experiment

Experiments were conducted in the laboratory on a 2-layer physical model consisting of two lengths of K3 particle board measuring 1.6 cm x 10.2 cm x 121.9 cm. The two beams were laid on top of one another and clamped in a specially built screw clamp constructed from aluminium (Fig. 2). The final span of the 2-layer beam was 111.8 cm. A uniform load was applied to the upper surface with 5.1 cm diameter steel mill balls. The aluminum clamp provided a relatively stiff abutment condition; a soft abutment was simulated by inserting 7.6 cms. of cork in layers 9.5 mm thick. With the stiff abutment a total load of 224.6 N was applied across the span but the load was reduced to 117.4 N for the soft abutments to avoid excessive deflections.

Full column, grouted rock bolts were modelled using 4.8 mm diameter acrylic rod set in 7.9 mm diameter drilled holes with sulfur set (a mixture of sulfur-clay (10:1 heated to 130°C))poured into the bolt holes.

A dial gauge was positioned under the apparatus to measure the vertical deflections of the span to the nearest 0.01 mm (Fig. 2).

To investigate the effect of bolt location on this model two bolts were placed symmetrically about the centre line at various distances from the abutment and the vertical deflection (convergence) under the same uniform load recorded and used as a measure of the degree of reinforcement.

The results of this experimental work are summarized in Fig. 13. The scatter of points is, the author believes, primarily attributable to variability of the mechanical properties of K3 board and a time dependent response to load. However, the significant feature of an optimum location of a rock bolt is clearly demonstrated. For both cork and aluminium abutments the value of x_{op} is approximately 0.18 x span, compared to 0.21 x span and 0.13 x span for the theoretical Cases A and B respectively. The results, as is to be expected from the model configuration and boundary conditions, agree more closely with Case A than Case B, i.e. the perfectly clamped beam. Some theoretical work has been completed in which the normal stress distribution over the abutment is modelled (Fig. 8) and it is intended to publish this at a later date.

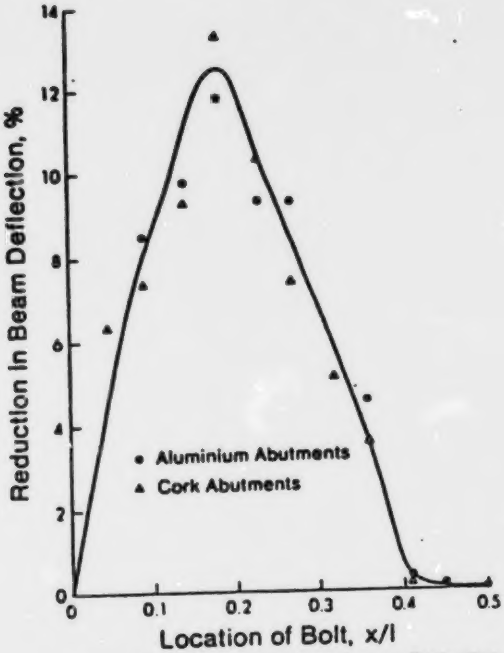

Figure 13. Effect of Bolt Location on Reduction in Beam Deflection.

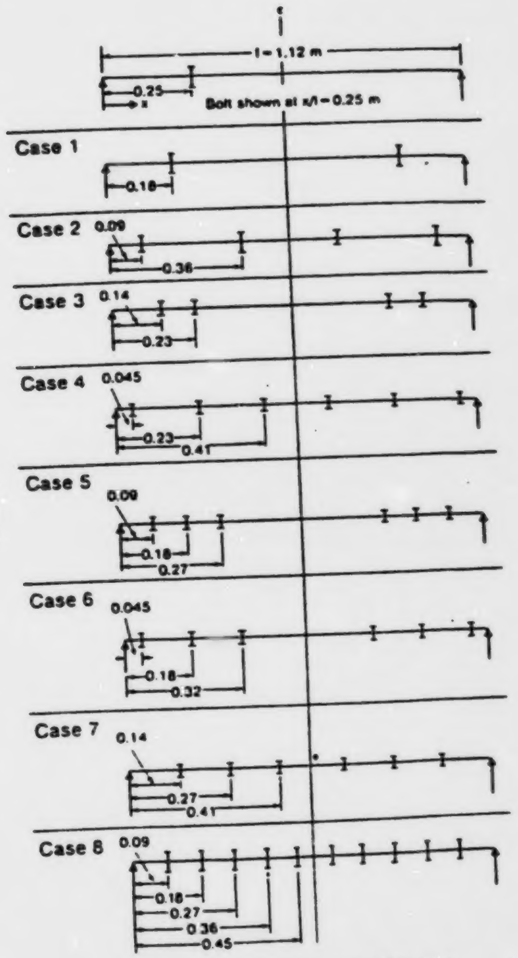
℄
l = 1.12 m
0.25
x
Bolt shown at x/l = 0.25 m
Case 1
0.18
Case 2
0.09
0.36
Case 3
0.14
0.23
Case 4
0.045
0.23
0.41
Case 5
0.09
0.18
0.27
Case 6
0.045
0.18
0.32
Case 7
0.14
0.27
0.41
Case 8
0.09
0.18
0.27
0.36
0.45

Figure 14. Rock Bolt Patterns used in Beam Tests

3.3 Multiple bolts

Both the theoretical and experimental work support the concept of an optimum location for full column, grouted rock bolts. If only two bolts were to be installed across each span then these should be placed about 1/5 th of the span in from the rib side (Case 1, Fig. 14).

A series of experiments were performed with the 2-layer model to investigate the degree of reinforcement obtained from a number of different multiple bolt layouts involving more than two bolts. The various configurations used are shown in Fig. 14 and the results summarized in Figs. 15 and 16. The following major conclusions have been reached on the basis of this experimental work:

1. The two bolts at the optimum locations contribute most to reinforcement. The insertion of other bolts provides additional, secondary reinforcement.
2. For the 2-layer model the inclusion of more than four bolts across the span provides negligible further reinforcement (Fig. 16).

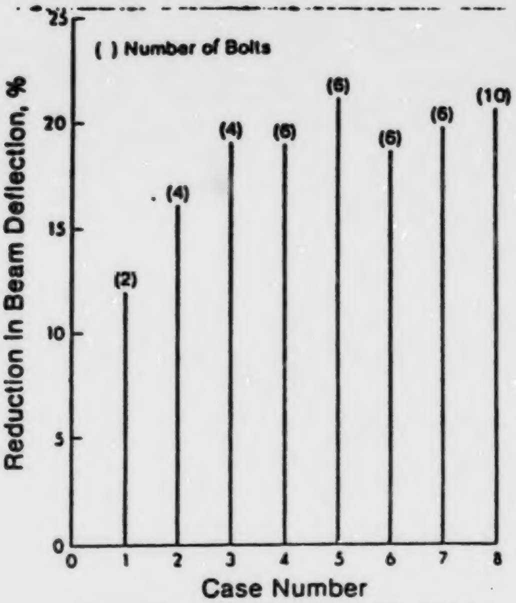

Figure 15. Reduction in Beam Deflection for Various Bolt Patterns (See Fig. 14.)

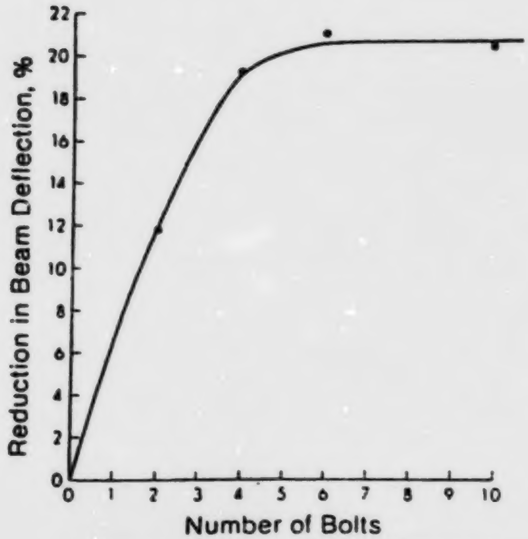

Figure 16. Reduction in Beam Deflection vs Number of Bolts

3.4 Conclusions

It has been shown that for the reinforcement mode full-column, grouted bolts should be placed in a pattern centered about the optimum point, S_{opt}, and that bolt spacing should be closer towards the rib than towards the span centre (see Case 5, Fig. 14).

It is, perhaps, necessary to repeat that this study only examined the reinforcement mode. In the suspension mode the design rules are based on different considerations. Also the role of inclined full column, grouted bolts needs to be examined. For optimum overall support a combination of bolt spacings, lengths, inclinations and types may be necessary.

ACKNOWLEDGEMENTS

The work described in this paper is part of the investigations into resin bolting being carried out with the financial support of CANMET under Contract #ISU81-00320. The experimental work was conducted by Mr. D. Booth and appreciation for his participation and assistance is hereby acknowledged.

REFERENCES

Fairhurst, C. & Singh, B. 1974. Roof bolting in horizontally laminated rock. Engineering and Mining Journal. 175: 80-88, 90.

Hobbs, D.W. 1969. Scale model studies of strata movement around mine roadways: V. Roadway shape and size. Int. J. Rock Mech. Min. Sci., 6: 365-404.

Singh, B. 1973. Continuum characterization of jointed rock masses Part II: Significance of low shear modulus. Int. J. Rock Mech. Min. Sci. 10: 337-350.

Stephansson, O. 1971. Stability of single openings in horizontally bedded rock. Eng. Geology, 5: 5-71.

APPENDIX I

List of Symbols

b = constant

c_u = foundation modulus

E = modulus of elasticity of roof layer

E_u = modulus of elasticity of abutment

h = thickness of abutment

H = thickness of roof beam

I = moment of inertia

l = roof span

M = bending moment

p = vertical load per unit area or load density

q = load density on roof beam

q_o = load density on roof beam at abutment

s = bedding plane slip

s_{max} = maximum value of s

w = unit weight of rock

x = horizontal distance from abutment

x_{op} = value of x at which bedding plane slip maximum

y = vertical deflection of roof beam

y_{max} = maximum value of y

α_b = angle of bedding plane to horizontal, radians

w_1 = non-uniform loading coefficient (centre of roof)

γ = shearing strain

ρ = specific gravity of rock

σ_x^e = horizontal normal stress after excavation

σ_e^i = virgin horizontal normal stress

δ = vertical roof displacement

δ_{max} = maximum value of δ

ν_1 = Poisson's ratio of roof layer

ν_u = Poisson's ratio of abutment

S_1 = non-uniform loading coefficient (abutment)

APPENDIX II

Bedding plane slip during flexure

A small section of a sagging roof beam is illustrated in Fig. A1 to an exaggerated scale. (For Fig. see main text, second page)

Suppose the section shown can be approximated by two circular arcs with radii of curvature and included angle l_1, ϕ_2, and l_2, ϕ_2 respectively.

The bedding plane slip, EF, = DF - CJ

$$= \phi_1 H \text{ } (\phi_1 \text{ in radians})$$

where H = layer thickness.

Likewise, the bedding plane slip, GH,

$$= DH - CI$$

$$= (\phi_1 + \phi_2)H \tag{A1}$$

The shearing strain, γ, = tan θ

$$= \alpha_b \text{, for small angles}$$

$$\alpha_b = \text{angle of bedding plane to the horizontal, in radians}$$

$$= \frac{dy}{dx} \text{ (radians)}$$

where y is the vertical deflection of the deflected layer.

$$\text{Shearing strain, } \gamma = \frac{dy}{dx} \tag{A2}$$

The shearing strain will reach a maximum value where $\frac{d^2y}{dx^2} = 0$.

However, from classical beam flexure theory the bending moment in a beam is given by $M = EI \frac{d^2y}{dx^2}$.

Hence the shearing strain reaches a maximum value where the bending moment is equal to zero.

APPENDIX III

Clamped beam with non-uniform loading, rigid abutments (Fig. 4)

The load density across the beam is assumed to have the following distribution:

$$q = q_o + \alpha x \text{ } (l-x) \tag{A3}$$

Suppose that at the abutment

$$q_{(x=0)} = q_o = \beta_1 H\rho \tag{A4}$$

and at the centre of the span

$$q_{(x=l/2)} = w_1 H\rho \tag{A5}$$

Substituting (A4) and (A5) into (A3) it can be shown that

$$\alpha = \frac{H\rho(w_1 - \beta_1)}{0.25 \quad l^2} \qquad \text{(A6)}$$

Now, from classical beam flexure theory

$$EI\,\frac{d^4y}{dx^4} = q$$

$$= q_o + \alpha x(l - x) \qquad \text{(A7)}$$

Integrating (A7) four times

$$EIy = \frac{q_o x^4}{24} - \frac{\alpha x^6}{360} + \frac{\alpha x^5 l}{120}$$

$$+ \frac{Ax^3}{6} + \frac{Bx^2}{2} + Cx + D \qquad \text{(A8)}$$

where A, B, C, and D are constants.

The following boundary conditions enable values for these constants to be obtained:

$x = l, \quad y = 0$

$x = 0, \quad y = 0$

$x = l, \quad dy/dx = 0$

$x = 0, \quad dy/dx = 0$

.˙. it is found that

$$A = -l\left(\frac{q_o}{2} + \frac{\alpha l^2}{12}\right) \qquad \text{(A9)}$$

$$B = l^2\left(\frac{q_o}{12} + \frac{\alpha l^2}{60}\right) \qquad \text{(A10)}$$

$$C = 0 \qquad \text{(A11)}$$

and $D = 0$ (A12)

.˙. from (A9 - A12), the beam deflection y is given by

$$y = \frac{1}{EI}\left(\frac{q_o x^4}{24} - \frac{\alpha x^6}{360} + \frac{\alpha x^5 l}{120}\right.$$

$$\left. + \frac{Ax^3}{6} + \frac{Bx^2}{2}\right) \qquad \text{(A13)}$$

Differentiating (A13) once to find the shear strain,

$$\gamma = \frac{dy}{dx} = \frac{1}{EI}\left(\frac{q_o x^3}{6} - \frac{\alpha x^5}{60}\right.$$

$$\left. + \frac{\alpha x^4 l}{24} + \frac{Ax^2}{2} + Bx\right) \qquad \text{(A14)}$$

APPENDIX IV

Simply supported beam, uniform loading, elastic abutments (Fig. 4)

Equation (10) of Stephansson (Stephansson 1971) gives the beam deflection, y, over the unsupported span as

$$y = \frac{P}{c_u}\left[\alpha^4 x\left(\frac{x^3}{6} - \frac{x^2 l}{3} - \frac{lx}{\alpha}\right.\right.$$

$$\left.\left. - \frac{1}{\alpha^2}\right) + l\,\alpha^3\,\beta\,(1 + \alpha x)^2 + l\right] \qquad \text{(A15)}$$

.˙. where α, β are constants given by:

$$\alpha = \left(\frac{c_u\,(1 - \nu_1^{\,2})}{4\,EI}\right)^{1/4}$$

$$\text{and} \quad \beta = \frac{\frac{l^2}{6} + \frac{l}{\alpha} + \frac{1}{\alpha^2}}{(\alpha l + 2)}$$

Differentiating (A15) once to find the shear strain,

$$\gamma = \frac{dy}{dx} = \frac{P}{C_u}\left[\alpha^4\left(\frac{2x^3}{3} - x^2 l\right.\right.$$

$$\left.\left. - 2\,x\,l - \frac{1}{\alpha^2} + 2\,\beta + 2\,\alpha\beta x\right)\right] \qquad \text{(A16)}$$

CHAPTER 9

A LIMITING EQUILIBRIUM APPROACH TO ESTIMATING THE DEGREE OF REINFORCEMENT OF HORIZONTALLY BEDDED ROOFS STRENGTHENED BY NON-TENSIONED, RESIN BOLTS

9.1 INTRODUCTION

Shear displacements along bedding planes (and therefore roof sag) can be reduced by appropriate placement of non-tensioned resin bolts, as discussed in the previous Chapter. Ultimately, if sufficient bolts were installed, there would be no difference in behaviour between the bolted layers and a single layer of the same total thickness.

In this Chapter, a new approach is developed for determining bolt spacings required to reach this ideal, and for estimating the degree to which any given roof bolt pattern attains such "perfect" reinforcement.

9.2 THEORY AND CONCEPT OF DEGREE OF REINFORCEMENT

The theory developed below is essentially an application of limiting equilibrium analysis to the roof beam problem.

From classical beam theory and assuming equal moduli in tension and compression, it can be shown that the shear stresses across a beam are distributed parabolically with a maximum value at the neutral axis (Fig. 9.1).

Let us imagine two beams of equal thickness, d , and material properties (Fig. 9.2). By installing resin-grouted bolts across the two beams the shear strength of the interface is increased. Ultimately, as the number of bolts increases, the shear strength, s_b , would reach a value, $s_{b(crit)}$, equal to the maximum shear force, s_{max} , that would be induced in a beam of thickness 2d. Therefore:

$$\frac{s_{b(crit)}}{s_{max}} = 1.0 \qquad \ldots\ldots\ldots\ldots\ldots \quad (9.1)$$

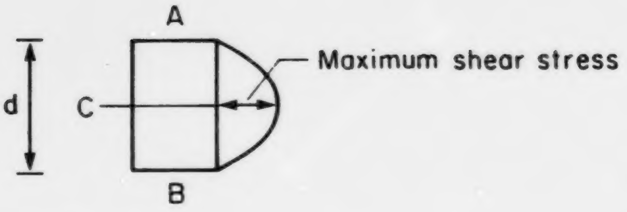
A
Maximum shear stress
d
C
B

Figure 9.1 Distribution of shear stress in a beam, depth d (A = upper surface, B = lower surface)

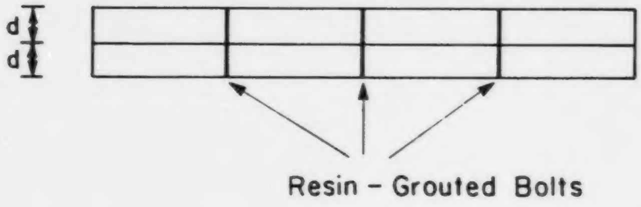
d
d
Resin - Grouted Bolts

Figure 9.2 Two beams of equal thickness reinforced with non-tensioned, resin-grouted bolts

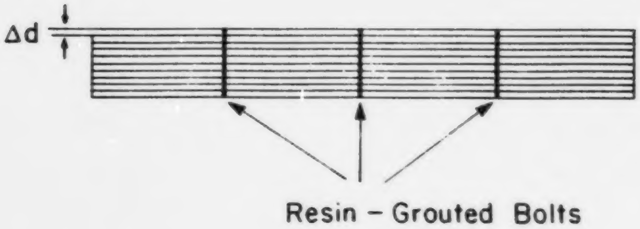
Δd
Resin - Grouted Bolts

Figure 9.3 Multilayered beam with ubiquitous bedding planes reinforced with non-tensioned, resin-grouted bolts

For the general case, where $s_b \neq s_{max}$, the ratio s_b/s_{max} may be greater or less than one. If greater than 1, the amount of reinforcement is more than required for the theoretical equilibrium and if less than 1 is smaller than required. In the latter case, the two beams will respond to some degree as separate structures, the extent depending on the difference between the actual s_b/s_{max} value and the ideal of 1. It is useful to define s_b/s_{max} as the degree of reinforcement. Thus:

$$RF = \frac{s_b}{s_{max}} \quad \ldots\ldots\ldots\ldots\ldots \quad (9.2)$$

where RF <1.0 = sub-optimum reinforcement, RF = 1.0 = optimum reinforcement, RF> 1.0 = super-optimum reinforcement.

Let us now assume that instead of two beams there is a ubiquitous system of bedding planes at very close, equal intervals, such that for any given total thickness one plane will lie along the neutral axis (Fig. 9.3). Since the optimum shear force is mobilized along this plane all the other planes will be super-optimally reinforced <RF> 1.0 if the central plane is optimally reinforced (RF= 1.0).

For a real mine roof there is no ubiquitous system of bedding planes, but the same principle will apply, ie., if optimum reinforcement is designed for the plane along the neutral axis (in this case there may or may not be a real bedding plane coincident with this position) all other planes will be super-optimally reinforced.

9.3 BOLT SPACING REQUIRED TO PROVIDE DEGREE REINFORCEMENT EQUAL TO 1

The derivations of the equations used in this Section and Section 9.4 are given in Appendix D.

Since no differential slip occurs at the centre of a span no shear stiffening or shear strength would be mobilized by installing a bolt at that location. It is therefore assumed that the bolts are placed symmetrically about the centre with an average spacing, b , along rows and spacing, d , along the opening. The specific row geometry envisaged is shown in Figure 9.4. Two bolts are placed 0.5 x average spacing from the rib to provide additional reinforcement in that region where shear stresses are highest and differential bedding plane slip is often most pronounced. In practice, a central bolt to act primarily in the suspension mode may be installed, but since the analysis to be developed here is for shear reinforcement only, this bolt is not included.

For clamped beams with parabolic loading (Fig. 9.5), a Degree of Reinforcement of 1.0 will be obtained when:

$$b = \frac{LF}{0.375\ K\gamma d + F} \qquad \ldots\ldots\ldots\ldots\ldots \qquad (9.3)$$

where L = span

$$K = (\beta L^2 + 0.833\,(\omega - \beta)\,(L^2)) \qquad \ldots\ldots\ldots\ldots\ldots \qquad (9.4)$$

where β = load multiplier at abutment

ω = load multiplier at centre (see Fig. 9.5 and Appendix C)

= density of rock

F = maximum shear resistance of a single bolt.

The value of F is derived from Dight's (1) theoretical model:

$$F = \frac{D_b}{4}\,(1.7\sigma_y\ P_u\ \pi D_b\ D(1 - (T/T_y)^2)^{\frac{1}{2}} \ \ldots\ldots\ldots\ldots \qquad (9.5)$$

for failure in rock (see Fig. 9.6),

or

$$F = \frac{D_b^2}{4}\,(1.7\sigma_y\ \pi P_u(1 - (T/T_y)^2)^{\frac{1}{2}} \ \ldots\ldots\ldots\ldots\ldots \qquad (9.6)$$

for failure in grout (see Fig. 9.6),

where D_b = diameter of bolt

D = diameter of bolt hole

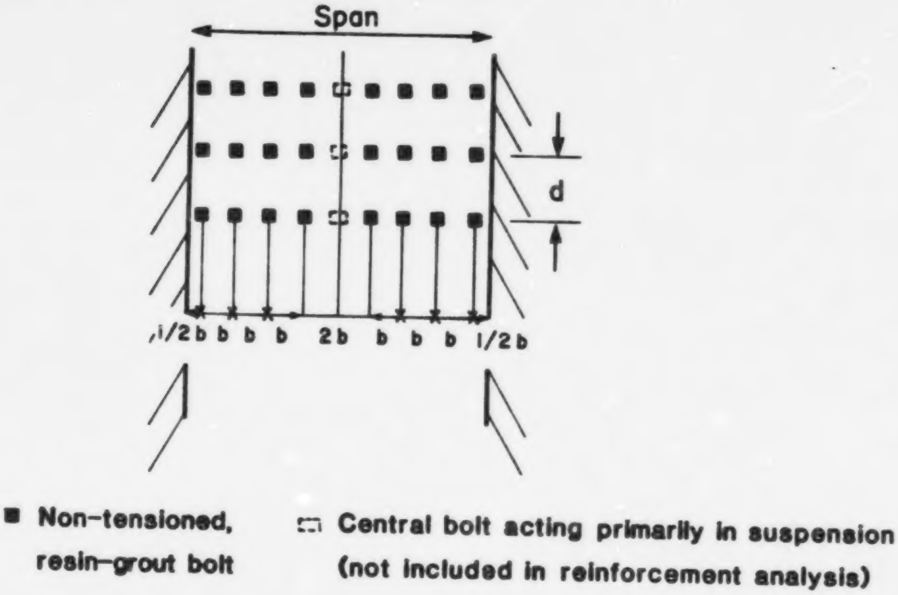
Span
d
1/2b b b b 2b b b b 1/2b
■ Non-tensioned, resin-grout bolt
▭ Central bolt acting primarily in suspension (not included in reinforcement analysis)

Figure 9.4 Pattern of non-tensioned, resin-grouted bolts assumed for reinforcement analysis

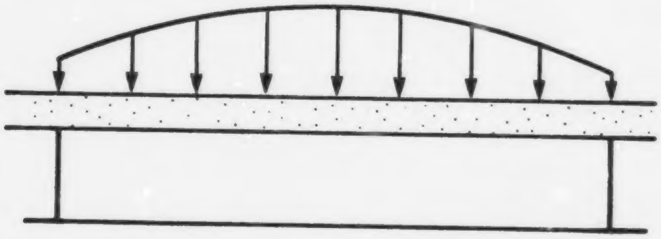

Figure 9.5 Parabolically loaded beam

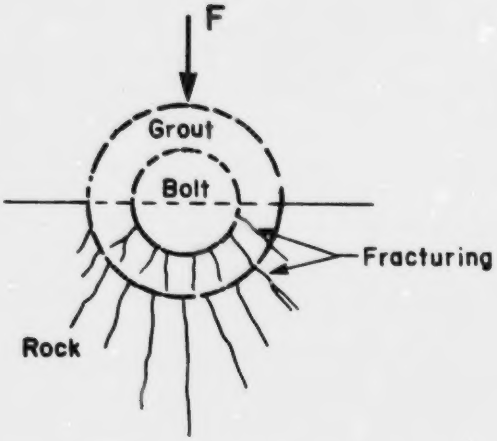
F
Grout
Bolt
Fracturing
Rock

Figure 9.6 Bearing capacity failure beneath a resin-grouted bolt

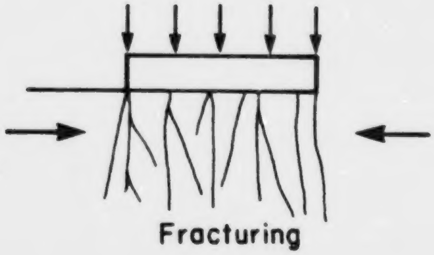
Fracturing

Figure 9.7 Bearing capacity failure beneath a footing

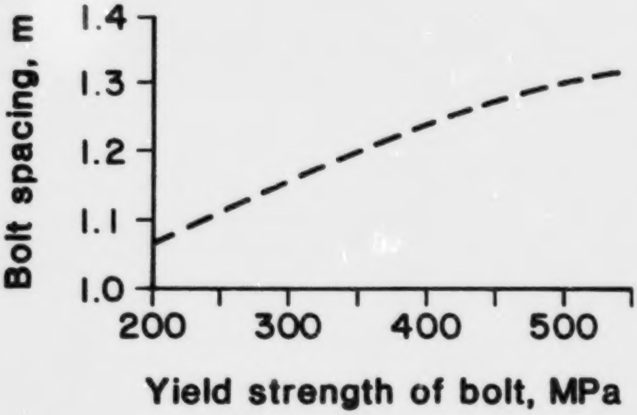

Figure 9.8 Effect of yield stress of bolt material on required bolt spacing for a square pattern (for other parameters see text)

σ_y = yield strength of bolt material

p_u = bearing capacity of rock or grout

T_y = yield strength of bolt

T = tension in the bar at plastic moment.

For estimating bearing capacity, it is assumed that the bolt acts similarly to a strip footing. Fracturing takes place beneath the bolt (Fig. 9.7), and the highest confining pressure that can be mobilized to support the fractured material is the unconfined compressive strength of the intact rock, σ_c. Assuming a Mohr Coulomb material, it can be shown (2) that:

$$p_u = \sigma_c(N_\phi + 1) \qquad \text{..............} \quad (9.7)$$

where $N_\phi = \tan^2(45 + \phi/2)$

where ϕ = effective angle of friction of intact rock or grout.

For uniform loading, $\beta = \omega$, equation (9.3) simplifies to:

$$b = \frac{LF}{0.375\beta\gamma\ L^2 d + F} \qquad \text{..............} \quad (9.8)$$

Note that to find the average spacing along rows from (9.3) or (9.8) a value for the spacing along the opening, d , must be assumed.

For the special case when average spacing in rows and spacing along the opening are equal (b = d):

$$b = \frac{-F + (F^2 + 1.5\gamma\ KLF)^{\frac{1}{2}}}{0.75\gamma K} \qquad \text{..............} \quad (9.9)$$

Again, for uniform loading (9.9) reduces to:

$$b = \frac{-F + (F^2 + 1.5\gamma\ L^3 F)^{\frac{1}{2}}}{0.75\beta\gamma\ L^2} \qquad \text{..............} \quad (9.10)$$

Sensitivity analyses were carried out using equation (9.10) for uniform loading. A base case was assumed and each variable was varied in turn while keeping all other values constant. For a base case:

Yield strength of bolt material = 360 MPa
Diameter of bolt = 1.9 cms
Diameter of bolt hole = 2.54 cms
Unconfined compressive strength of rock = 70 MPa
Unconfined compressive strength of grout = 100 MPa
Rock density = 2800 kg/cu.m.
Roof span = 5 m
Effective angle of friction of rock = 45 deg.
Effective angle of friction of grout = 45 deg.
Ratio of bolt tensile load/bolt strength, (T/T_y) = 0

The results of the sensitivity studies are illustrated in Figures 9.8 - 9.17.

Required bolt spacing is reduced by increasing the yield strength of bolt material and bolt diameter (Figs. 9.8 and 9.9). Of the two, bolt diameter is more significant.

As the annulus of resin increases in thickness the required bolt spacing also increases (Fig. 9.10). Initially, for the parameters selected, the bearing capacity of the rock is exceeded before the bearing capacity of the grout for small annulus thicknesses. Above a certain critical thickness this state reverses and the grout's bearing capacity is exceeded first.

Bolt spacing is dependent upon the uniaxial compressive strength of grout and rock (Figs. 9.11 and 9.12). Sensitivity of spacing to strength is greatest at low strength values.

For typical friction angles in the range 30-50 deg. for rock and grout the changes in required spacing are small, (Figs. 9.13 and 9.14).

The required bolt spacing is inversely related to span (Fig. 9.15) and rock density

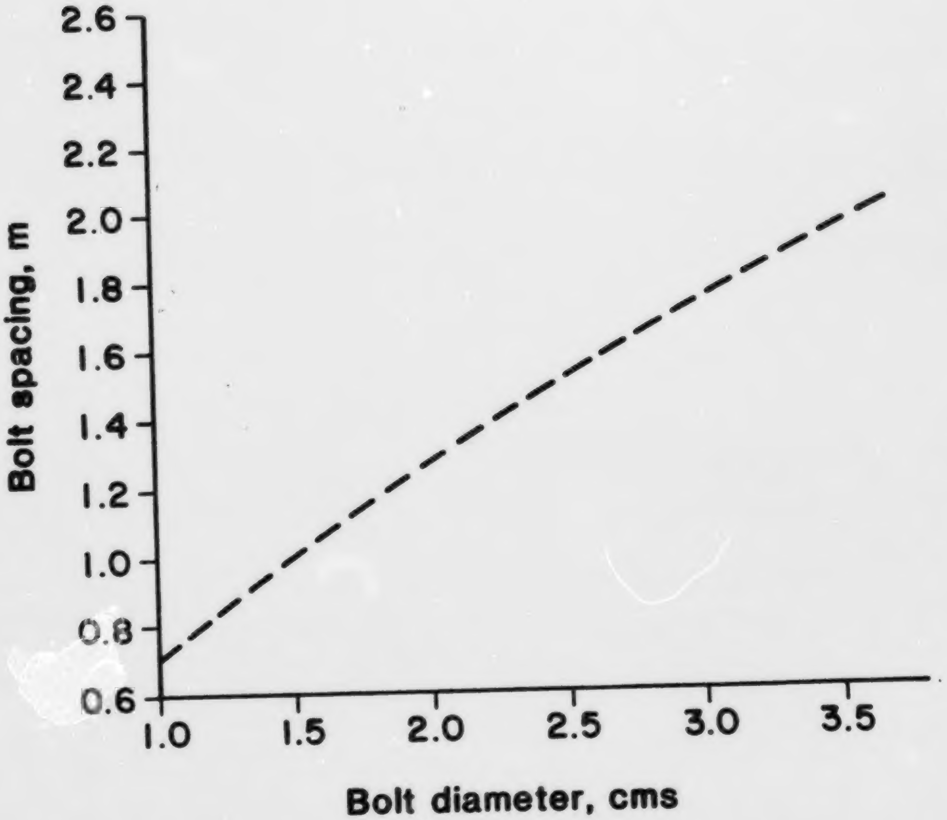

Figure 9.9 Effect of bolt diameter on required bolt spacing for a square pattern (for other parameters see text)

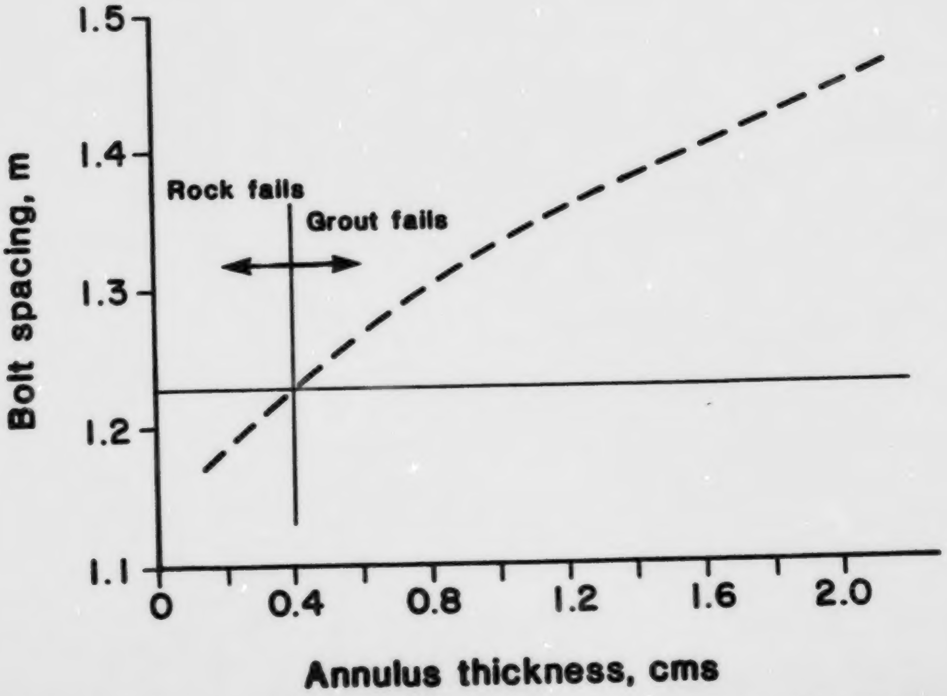

Figure 9.10 Effect of annulus thickness on required bolt spacing for a square pattern (for other parameters see text)

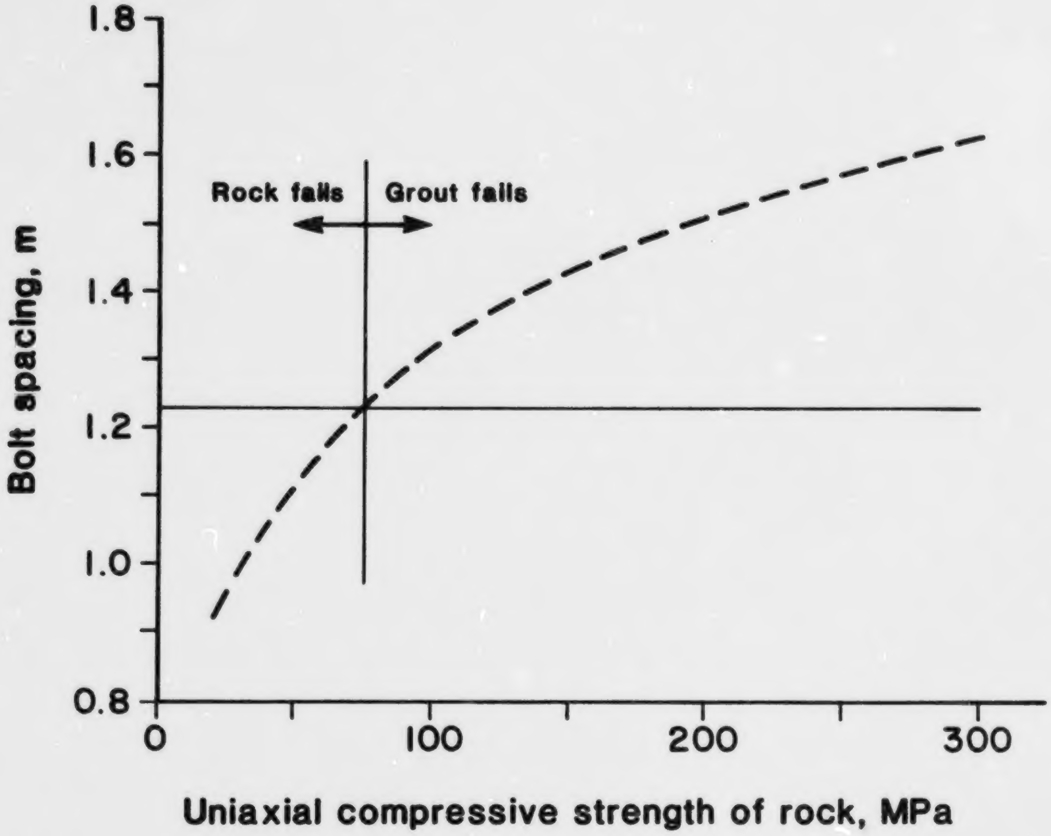

Figure 9.11 Effect of uniaxial compressive strength of rock on required bolt spacing for a square pattern (for other parameters see text)

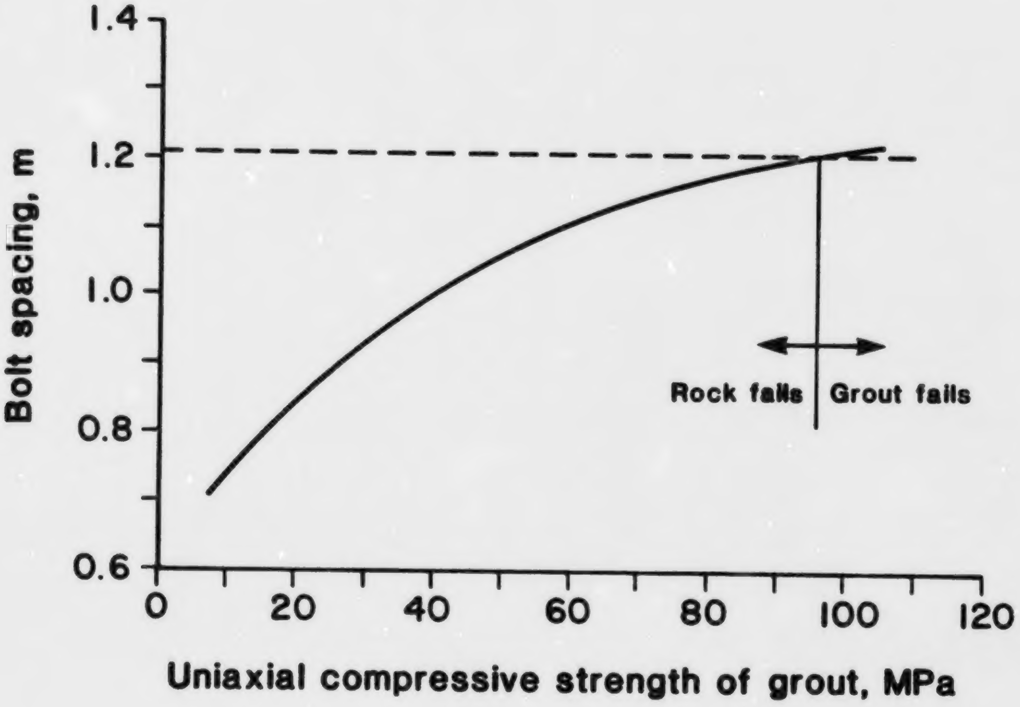

Figure 9.12 Effect of uniaxial compressive strength of grout on required bolt spacing for a square pattern (for other parameters see text)

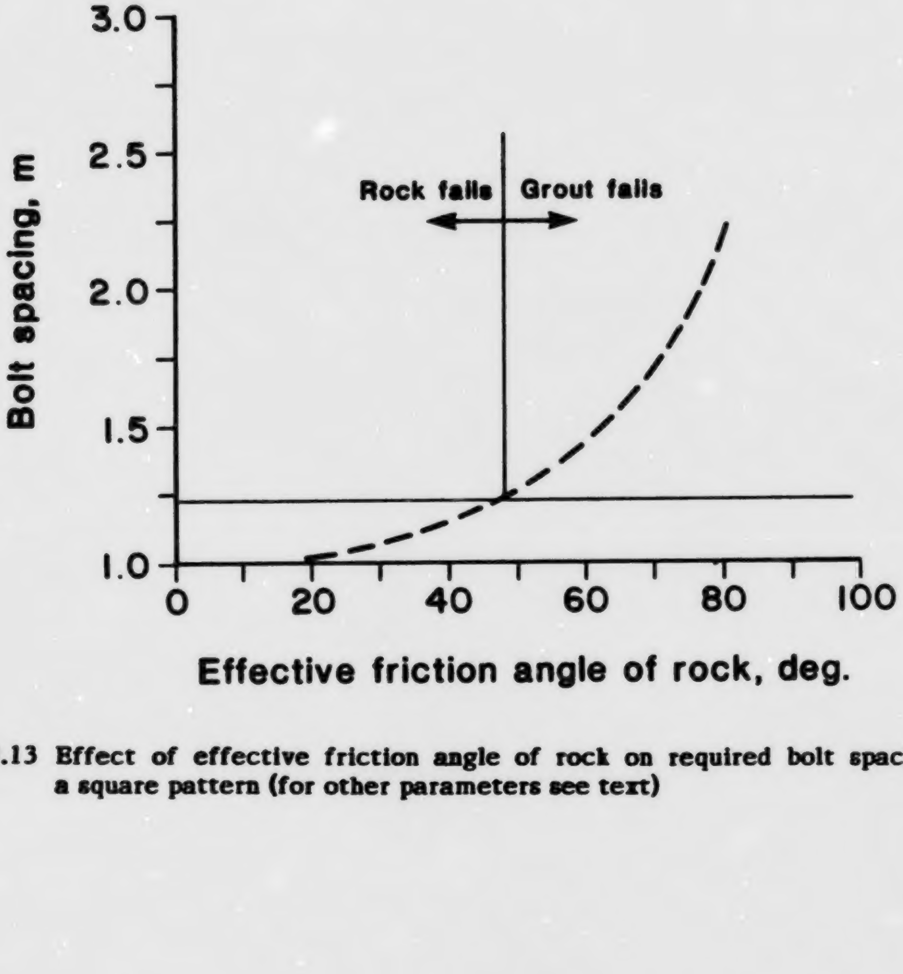

Figure 9.13 Effect of effective friction angle of rock on required bolt spacing for a square pattern (for other parameters see text)

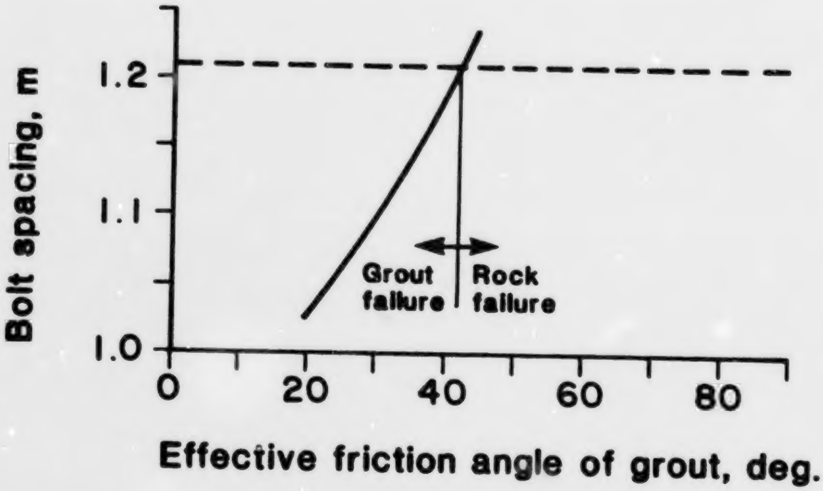

Figure 9.14 Effect of effective friction angle of grout on required holt spacing for a square pattern (for other parameters see text)

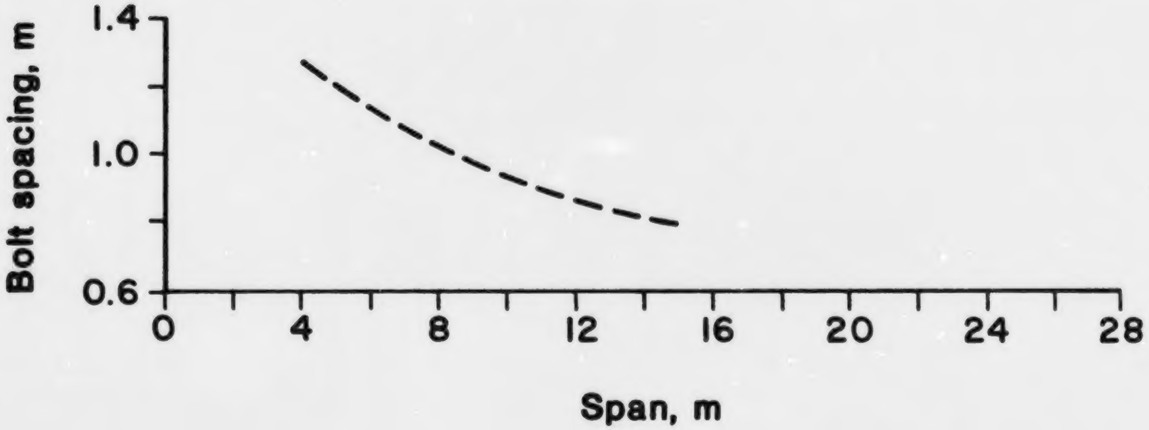

Figure 9.15 Effect of span on required bolt spacing for a square pattern (for other parameters see text)

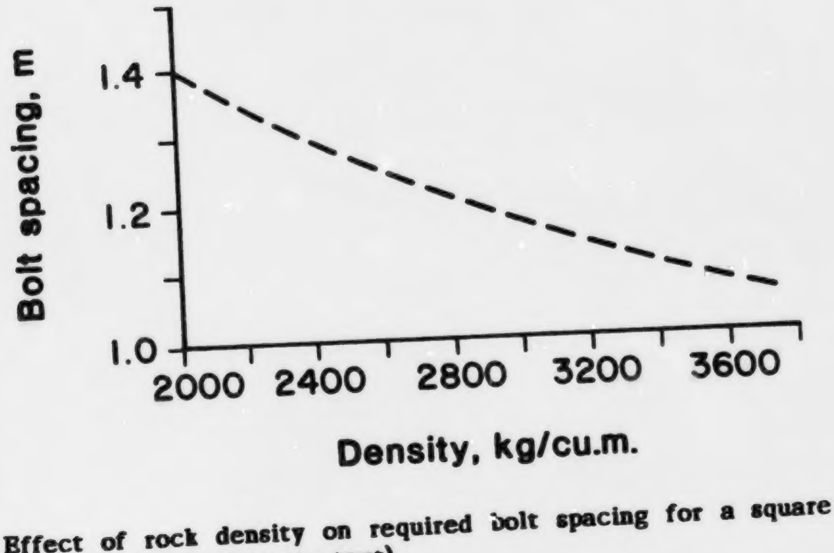

Figure 9.16 Effect of rock density on required bolt spacing for a square pattern (for other parameters see text)

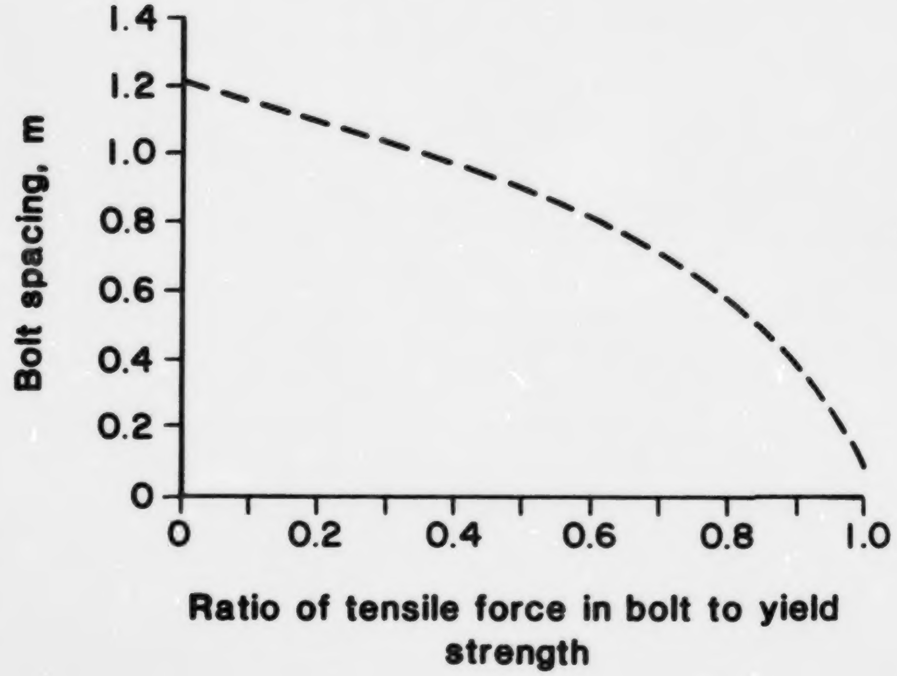

Figure 9.17 Effect of ratio of tensile force in bolt to yield strength of bolt on required rock bolt spacing for a square pattern (for other parameters see text)

(Fig. 9.16).

The state of tensile stress generated in the bolt by shear displacements reduces the resisting force, F , mobilized in the bolt. The effect on required bolt spacing becomes particularly marked when the ratio of tensile load to yield load of the bolt is greater than about 0.6 (Fig. 9.17).

Non-uniform loading of the roof with higher vertical loads in the central area of the roof increases shear stresses and hence bolt spacing must decrease. The scale of this effect for parabolic loading is illustrated in Figure 9.18. Relatively modest changes from uniform to non-uniform loading result in significant changes in bolting requirements.

Rectangular patterns of bolting, in which spacing along the opening is different from spacing along rows, is often used. In Figure 9.19 the required spacing along rows for various spacings along the opening is plotted for two roof spans. Clearly, increased spacing along the opening necessitates an increased bolting density along rows.

9.3.1 Discussion

The bolt spacings predicted in the sensitivity studies are generally smaller than those used in practice. This indicates that in practice bolting patterns are sub-optimal. However, this does not necessarily mean that roof collapse is imminent. Much will depend on the other mechanisms of support (suspension, friction), which may also be in operation.

Frictional resistance of bedding planes has also been ignored in this analysis. In some circumstances, an upper bed will sag onto and load a lower bed and frictional resistance will then be mobilized. On the other hand, bed separation results in zero frictional resistance. For this latter reason, the assumption of no frictional resistance can be justified for design purposes, especially where it is known that bed separation does occur.

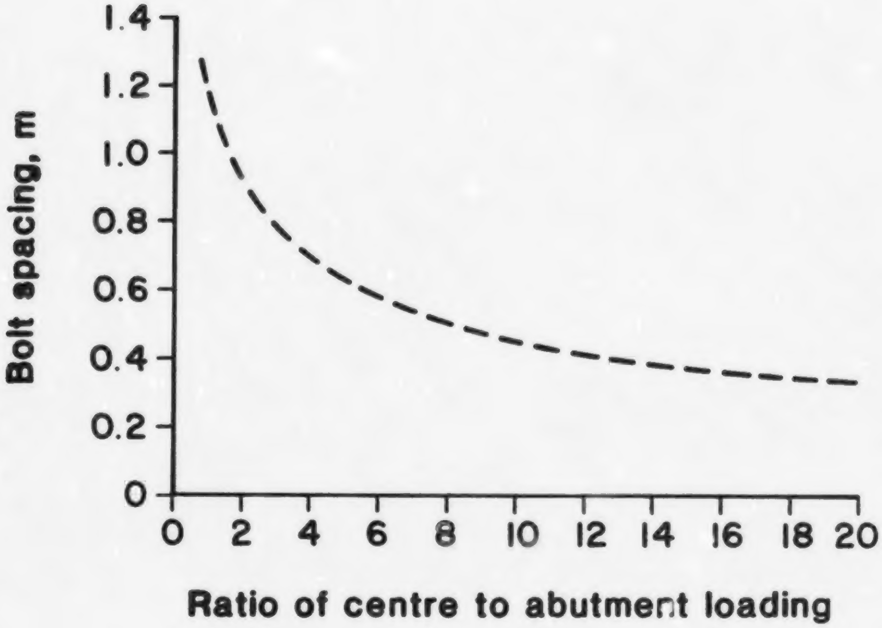

Figure 9.18 Effect of non-uniform loading on required bolt spacing for a square pattern (for other parameters see text)

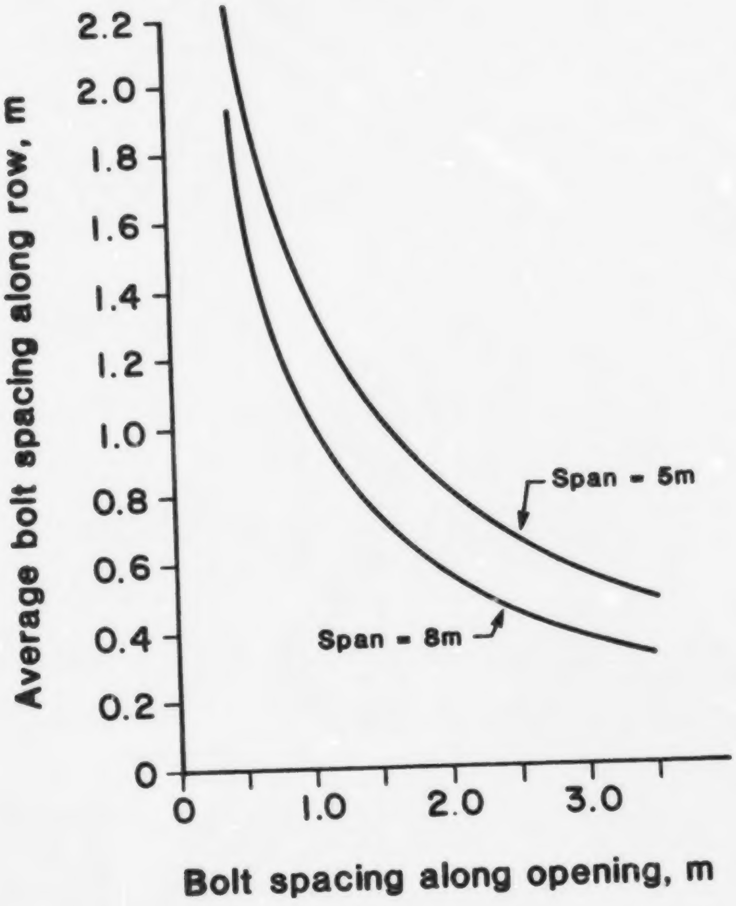

Figure 9.19 Required bolt spacing along row vs. bolt spacing along opening for two different spans (for other parameters see text)

The three most critical parameters are roof loading, induced tension in the bolt at points of shear and bolt diameter; the first two factors are practically difficult to determine.

Additional discussion of this analysis and its application to a general roof bolting design method may be found in Chapter 15.

9.4 DEGREE OF REINFORCEMENT PROVIDED BY A GIVEN ROCK BOLT PATTERN

The RF value for a rock bolting pattern already installed may be obtained from this analytical method through the following equation:

$$RF = \frac{nF}{0.375\gamma Kd} \qquad \ldots\ldots\ldots\ldots\ldots \quad (9.11)$$

where n = number of bolts in a row

d = spacing along opening

K = constant (see equation (9.4))

F = maximum shear resistance of a single bolt (see equations 9.5 and 9.6)

γ = rock density.

Two values of RF are obtained, one for the Degree of Reinforcement with respect to grout strength and the other with respect to rock strength. For example, an operating mine has the following general layout and material properties for its 5 m span headings:

Yield stress of bolt	= 360 MPa
Diameter of bolt	= 1.9 cms
Diameter of bolt hole	= 2.54 cms
Unconfined compressive strength of rock	= 70 MPa
Unconfined compressive strength of grout	= 100 MPa

Rock density = 2800 kg/cu.m.

Uniform loading

Number of bolts in row = 4

Spacing of bolts along opening = 1.9m

Effective friction angle of rock = 45 deg.

Effective friction angle of grout = 45 deg.

Ratio of tensile bolt load to yield strength of bolt, (T/T_y) = 0

For these values:

Degree of Reinforcement = 0.818 with respect to rock strength.

Degree of Reinforcement = 0.845 with respect to grout strength.

In this case the roof is not completely reinforced in shear, but the RF values are high and indicate a high degree of reinforcement both with respect to rock and grout strengths.

9.5 SPACING DESIGN FOR A SPECIFIED DEGREE OF REINFORCEMENT

A back analysis of a stable roof by the method outlined in Section 9.4 provides an estimate of the RF value. If this RF value is deemed to provide satisfactory support, it may be used as the basis for subsequent design where one or more parameters are to change, e.g., span, bolt diameter, bolt strength, loading, rock strength, etc. Obviously, judgement will have to be used where rock conditions might change sufficiently to require a different RF value.

Let the required RF value = RF_{des} . Then the average spacing, b , along rows can be estimated from

$$b = \frac{FL}{0.375\ R_{des}\ \gamma K d + F} \qquad \text{..............} \qquad (9.12)$$

where L = span

K = constant (see eqn. 9.4)

d = bolt spacing along opening

F = maximum shear strength of bolt (see eqns. 9.4 and 9.5)

γ = rock density.

In order to solve for b from (9.12), the spacing along the opening, d, must be assumed. A typical design chart is shown in Figure 9.20. The only change in parameters between the two pairs of curves is bolt and hole diameter; the annulus thickness is the same in both cases (0.32 cm). For the lower pair of curves the bolt diameter and bolt hole diameter are 1.9 cm and 2.54 cm., respectively. For the upper two curves the corresponding values are 2.54 cm and 3.18 cm. The bolt spacing along the opening is constant at 1.75 m and loading is assumed uniform. Other conditions assumed were:

Unconfined compressive strength of rock	=	70 MPa
Unconfined compressive strength of grout	=	100 MPa
Span	=	5 m
Effective friction angle of rock	=	45 deg.
Effective friction angle of grout	=	45 deg.
Ratio of tensile load in bolt to bolt yield strength, (T/T_y)	=	0
Rock density	=	2800 kg/cu.m.

The application of a design curve like that shown in Figure 9.20 is not completely straightforward because the required bolt spacing for a given RF value may not give an integral number of bolts per row. Furthermore, for the pattern assumed (Fig. 9.4) only even numbers of resin bolts can be used, with the option of an additional central bolt primarily to act in the suspension mode.

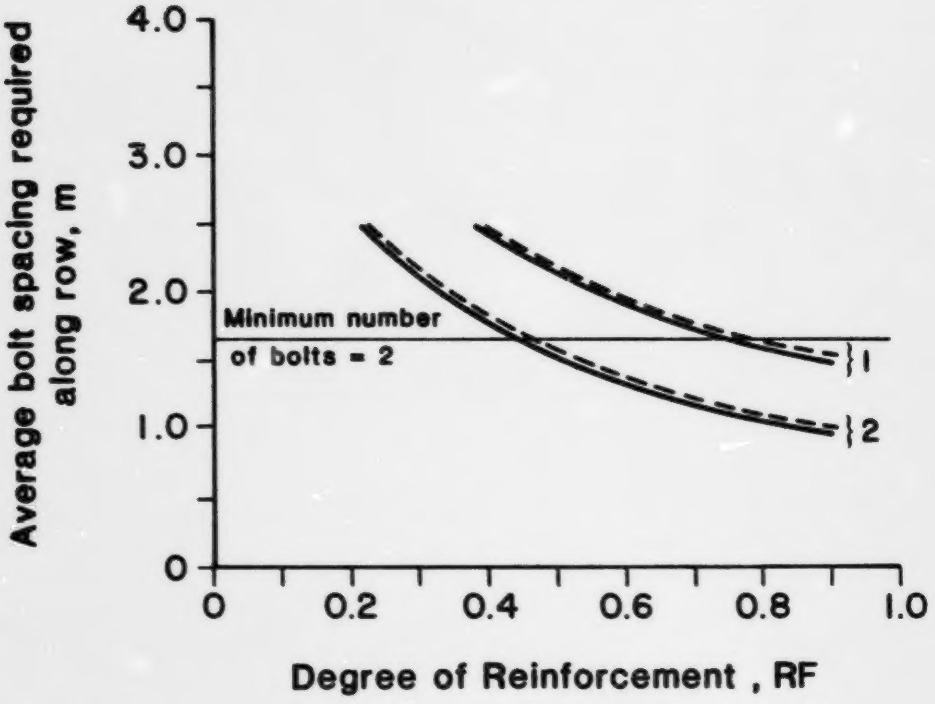

Figure 9.20 Average bolt spacing in row vs. degree of reinforcement, RF, (spacing along opening = 1.75 m; 1 = bolt diameter, 1.9 cm; hole diameter = 2.54 cm; 2 = bolt diameter, 2.54cm; hole diameter, 3.18 cm; for other parameters see text)

Example:

An RF value of about 0.7 is required. Design a row of bolts to meet this condition.

From Figure 9.20 the average bolt spacings along a row for an RF of 0.7 are 1.75 m and 1.2 m for the larger and smaller diameter bolts, respectively. On the basis of the general bolt pattern of Figure 9.4, lay out a row of bolts with these average spacings, starting from the centre of the opening (Fig. 9.21). Note that in neither case is the spacing from the rib to the first bolt equal to half the average bolt spacing, as required by the ideal pattern of Figure 9.4. For the smaller diameter bolts, this distance is only 0.1 m; for practical reasons these bolts would be offset a greater distance from the ribside.

The actual average spacing of bolts in these two cases is 1.67 m for the 2-bolt layout and 1 m for the 4-bolt layout. For these conditions the RF values are as follows:

2-bolt layout (3.18 cm bolts)	4-bolt layout (2.54 cm bolts)
RF (rock) = 0.77	RF (rock) = 0.89
RF (grout) = 0.82	RF (grout) = 0.92

The smaller diameter bolts give a greater RF value, but the number of bolts has been doubled. The next step would be to increase the spacing along the opening (Fig. 9.20 is for a spacing along the opening of 1.75 m) to reduce the RF value to 0.7 for the smaller diameter bolts. After achieving an acceptable pattern, the economics of the various layouts would have to be examined and the optimum solution found.

9.6 A PROPOSAL FOR MODIFYING A FINITE DIFFERENCE MODEL OF A BOLTED, MULTILAYER PLATE RESTING ON ELASTIC PILLARS

9.6.1 Introduction

The analysis of reinforcement described above does not take into account specific discontinuities or the precise location of bolts. To this end, a finite difference program

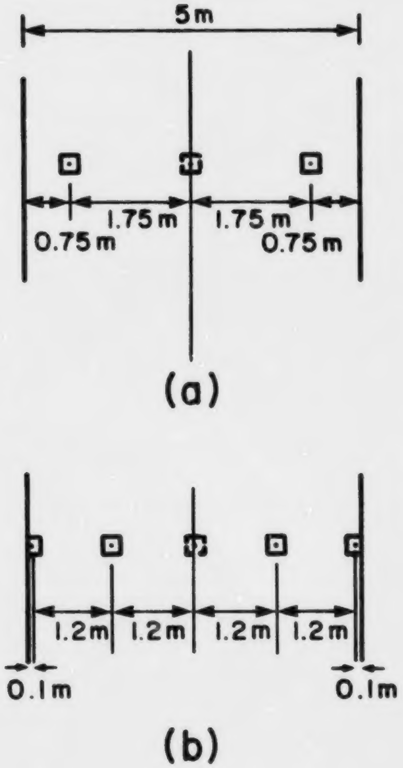
5m
1.75m
1.75m
0.75m
0.75m
(a)
1.2m
1.2m
1.2m
1.2m
0.1m
0.1m
(b)

Figure 9.21 Design options for (a) 3.18 cm. diameter and (b) 2.54 cm. diameter bolts

developed for tensioned, ungrouted rock bolts by Chugh, Gesund and Wright (3) was examined to determine its suitability for modification to meet the conditions for non-tensioned, resin-grouted bolts.

A published account of the method is provided in an Appendix to this Chapter.

9.6.2 General Information

The computer program was developed in 1973 at the College of Engineering, University of Kentucky, Lexington, Kentucky. It is written in FORTRAN IV for an IBM 360 computer to run under the FORTG compiler.

The program, as written, is for the study of roof failures in a bedded deposit with deformable support pillars. In utilizing the program, the total load support characteristics of the roof can be determined for a single load, (e.g. the self-load) or the maximum load bearing capacity of the roof may be determined.

The input data is extremely involved, which means that the user has great control over the many different parameters affecting the roof characteristics. This also means however, that a great deal of time is spent in preparing and entering the data. Some of the built-in flexibilities are: allowance for rigid or deformable pillars, multiple or single roof layers, pre-fractured layers or areas, and different sizes and patterns of roof bolts.

Many of these options are allowed for by specifying different material characteristics at different locations in the roof. For example, if an area of one layer is fractured this can be specified by changing the strengths, frictional constants, Young's modulus and Poisson's ratio at that location.

9.6.3 Failure Criteria:

Four types of failure criteria are considered.

Local Slip: - only resultant shear stresses can cause local slip failures at the interfaces;

- resultant shear stress vectors are calculated from total shear stress components which exist in the slab

Local Flexural Failure:

- caused by principal normal flexural stress vectors based on the total flexural stress components that exist within the slab;

Slip Failures:

- when these failures occur they occur at only one point on one interface;
- for additional loading the slab stiffness at that point is taken as the sum of the individual layer stiffnesses at that point.
- a slip is a localized phenomena and spreads over the interface as loading increases.

Flexural Failures:

- implies that a crack or crushing has occurred in a layer;
- this results in decreased stiffness of the slab and requires a redistribution of the stresses;
- this will affect the response of the total load and may initiate a series of slips or additional flexural failures without an increase in the load.

9.6.4 The Program

The problem as envisioned by the authors was essentially that of the analysis of plate bending with arbitrary conditions and geometrical configurations. Two methods commonly used in the analysis of plate bending are the finite element and finite difference techniques. In finite element analysis, the plate is discretized into a set of finite elements connected at nodes and the equations describing their relationship to each other solved. Finite difference analysis transforms the governing differential equations into a series of linear algebraic equations through the use of special operators.

The researchers decided that equally valid results could be obtained through the use of either method and elected to use the finite difference solution, based on the standard differential equations for a transversly loaded thin plate.

9.6.5 Assumptions:

The following assumptions and/or conditions were imposed on the model:

- material is brittle (high compressive, low tensile strength);
- slab consists of many layers, each with different properties;
- interlayer slip will occur when an interlayer frictional strength is exceeded (less than the material shear strength);
- critical shear stress may be different at every point of every layer interface;
- external horizontal forces will cause the same in-plane stress in each layer;
- material is linearly elastic, homogeneous and isotropic up to failure;
- out-of plane deflections are independent of the z coordinate and are small compared to the layer thickness;
- interaction between in-plane, external loads and out-of-plane deflections can be ignored;
- supports may undergo elastic deflections.

9.6.6 Model Responses

Based on the above assumptions, the following mechanisms are assumed for the roof model:

1) Before the first slip occurs it behaves as a one layer slab.

2) The first slip results in two-layer action.
3) Additional slips will cause additional layers to form.
4) It is assumed that new units formed are not allowed to separate (i.e. bed separation) and therefore each will support a portion of the load proportional to the stiffness of the layer.
5) Eventually with increasing load a local flexural failure will occur.
6) This will cause a local change in slab stiffness which results in the redistribution of the stresses in the structure.
7) Once a crack has occurred, the slab may not be able to support the load, or the next load increment may not be supported.

9.6.7 The Solution Algorithm

1) The composite properties of the layered slab are computed.
2) The nodal indices at each node are computed.
3) The coefficient matrix is constructed using the standard biharmonic operator.
4) The coefficient matrix is factored into an upper and lower triangular matrix.
5) The matrix is solved for the deflections at each note.
6) All moments and shears are computed at each node.
7) The flexural stresses at each surface and interfacial shear stresses are computed.
8) The principal normal flexural stresses are computed from the component flexural stresses.
9) Resultant shear stresses are computed.
10) A test is applied to determine whether or not the applied load has caused one or more failures or slips by comparing the calculated stresses to input strengths.
11) If a failure has occurred the load is reduced and the process repeated.

12) The procedure terminates when the bottom layer and a predetermined number of other layers has failed in flexure.

9.6.8 Input Data

A) Finite Difference Variables

i) Number of rows in the grid;

ii) Number of columns in the grid;

iii) Number of nodes to be used - differs for different geometries;

iv) Number of nodes with freedom to deflect in the 'z' direction;

v) Number of the node where the pillar begins;

vi) Control values for the nodes which are free to deflect and those which are not.

B) Material Variables

i) Number of layers;

ii) Thickness of each layer;

iii) Grid size in feet;

iv) Young's modulus of each layer;

v) Poisson's ratio for each layer;

vi) Density of each layer;

vii) External in-plane thrusts and shears;

viii) Compressive strength of each layer;

ix) Tensile strength of each layer;

x) Compressive strength of the pillar;

xi) Tensile strength of the pillar;

xii) Friction strength at each node of each interface.

9.6.9 Governing Differential Equations

The governing differential equations are based on the following equations:

1) Moment equilibria for a flat plate subject to a transverse distributed load, elastically supported with the support reaction normal to the plate.
2) Deformation equations of an elastic, homogeneous and isotropic plate with small deflections and linear strain distribution.
3) The shear forces per unit length.

9.6.10 Suggested Methodology for Incorporation Non-Tensioned, Resin Grouted Bolts

A copy of the program was obrained on magnetic tape. Difficulties, which proved time-consuming to attempt to solve, were experienced in understanding the documentation, output data, and complexity of input data. Some "bugs" were also encountered in the program and there were also differences between the program on the tape provided and that used to develop the documentation. As a result, the program has not run satisfactorily.

The methodology suggested for adapting this program to non-tensioned, resin-bolts is as follows:

As developed, the program allows for the modelling of tensioned, ungrouted rock bolts by using an appropriate angle of friction for each nodal point on the interface between layers. For untensioned, resin-grouted bolts, their presence may be considered to add cohesive resistance to the potential slip surface. At 0 (Fig. 9.22), the shear resistance is:

$$\tau = \sigma_n \tan\phi_{eff} = c + \sigma_n \tan\phi \quad \ldots\ldots\ldots\ldots\ldots \quad (9.13)$$

Therefore,

$$\phi_{eff} = \tan\left(\frac{c}{\sigma_n} + \tan\phi\right) \quad \ldots\ldots\ldots\ldots\ldots \quad (9.14)$$

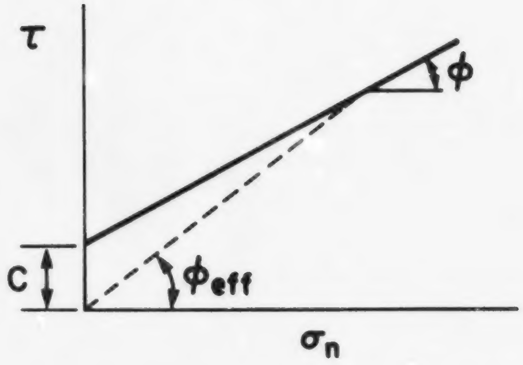

Figure 9.22 "Cohesion" of a bolted joint

where σ_n = normal stress acting across the interface

ϕ = effective angle of friction of interface

c = "cohesion" of interface due to bolting

ϕ_{eff} = modified effective angle of friction of interface due to bolting.

Cohesion, c , may be obtained by calculating the maximum shearing resistance of a single bolt, F , from equations (9.5) and (9.6) and substituting in:

$$c = \frac{F}{bd} \qquad \text{.............. (9.15)}$$

where b and d are bolts spacing along and between rows, respectively.

If this cohesion is added to every nodal point along layer interfaces the effect of bolt location on roof behaviour will be lost. It is suggested that an increased value of cohesion, c_i , be applied to nodal points at and adjacent to each bolt, such that:

$$c_i = \frac{cbd}{A} \qquad \text{.............. (9.16)}$$

where A is the area encompassing all nodel points where c_i is assumed to act. In order to concentrate the strengthening effect of c locally, A should be small.

The value of ϕ_{eff} (eqn. 9.14 e) is dependent upon the normal stress across the interface. It is therefore proposed that in the first few iterations the interfaces would be assumed to have no cohesion. Values of normal stress, σ_n , across each interface generated from these computations could then be used to derive values of cohesion from equation (9.15).

9.6.11 Recommendations

Numerical results of running the program in its current mode were not satisfactory. However, the program has potential for adaptation and further work is recommended.

11738 NOVEMBER 1975 ST11

JOURNAL OF THE
STRUCTURAL DIVISION

ANALYSIS OF MULTILAYER PLATES ON ELASTIC PILLARS

By Ashok K. Chugh,[1] A. M. ASCE, Hans Gesund,[2] F. ASCE,
and Fred D. Wright[3]

INTRODUCTION

The problem to be treated herein is the analysis of a transversely loaded plate, composed of an arbitrary number of layers, and supported on elastic pillars. Each layer may have a different thickness and different material properties from all other layers, though the thickness of each layer must be constant and the materials isotropic. Material properties can, however, vary from point to point within each layer. The interfaces between layers are assumed to have certain friction properties which must be equal in all directions, but may be different for each interface, and for each location within each interface.

An incremental load method of analysis is used to follow the local responses, such as interface slip and local fracture, singly or in combination, of the extremely redundant structure until a permanent decrease in load carrying capacity is encountered. The structural problem that gave rise to the study was the need to predict and enhance the strength of the roof at tunnel intersections in mines and other underground structures.

The roofs of such intersections are frequently found to be slabs composed of several layers of rock, lying above one another, with some mechanical (frictional) bond at the interfaces. This frictional bond may be enhanced by the use of rock bolts. Figs. 1 and 2 show layouts of two tunnel intersection configurations to which the method of analysis to be described herein has been applied. The similarity to a plate supported on relatively large columns is apparent.

The load acting on a mine roof may actually be resisted by a combination of plate action and arch action. The arch action depends upon the rigidity of the end abutments. In the room and pillar method of mining, the end abutments are pillars whose rigidity may be questionable due to creep in both the pillar

---

Note.—Discussion open until April 1, 1976. To extend the closing date one month, a written request must be filed with the Editor of Technical Publications, ASCE. This paper is part of the copyrighted Journal of the Structural Division, Proceedings of the American Society of Civil Engineers, Vol. 101, No. ST11, November, 1975. Manuscript was submitted for review for possible publication on February 2, 1975.

[1] Research Assoc., Univ. of Kentucky, Lexington, Ky.

[2] Prof. of Struct. Engrg., Univ. of Kentucky, Lexington, Ky.

[3] Prof. of Mining Engrg., Univ. of Kentucky, Lexington, Ky.

and the roof material. The arching action may thus be partially or completely lost with the passage of time, leaving only the slab action of the immediate roof to resist the load. Even if arch action can be maintained, the analysis based on slab action will still give a lower bound on the load carrying capacity of a mine roof. The possible transitory arching action can then be considered to provide an additional safety factor.

Little has previously been published on this problem. Lekhnitskii (9) has given expressions for equivalent moduli and for flexural and shearing stresses in plates composed of an odd number of symmetric layers under distributed transverse load. Ambartsumyan (1) and Ashton and Whitney (2) have considered the theoretical analysis of multilayer orthotropic plates. No consideration, however, was given in any of this work to possible local sliding between layers when interlayer friction is overcome, or to possible local rupture of the individual layer materials when their strengths are exceeded.

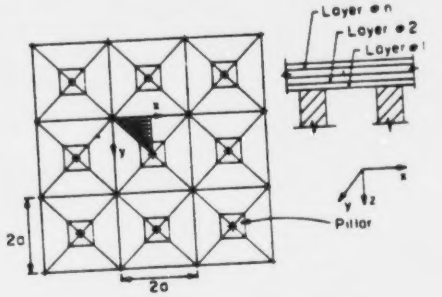

FIG. 1.—Regular Pillar Pattern

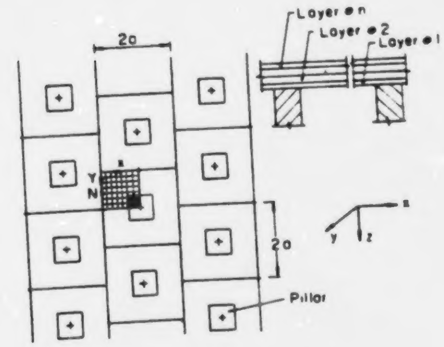

FIG. 2.—Staggered Pillar Pattern

One way in which the step-by-step analysis of a multilayer plate can be carried out is to consider the multilayer medium initially as a composite body, with perfect shear transfer capabilities. This requires that the layered body be transformed into an "equivalent" homogeneous body that lends itself more readily to mathematical analysis. The results of this analysis may then be translated back to the layered medium by use of a reverse transformation procedure. Refs. 3 and 11 summarize the historical developments in the determination of elastic constants of equivalent homogeneous bodies under various loading

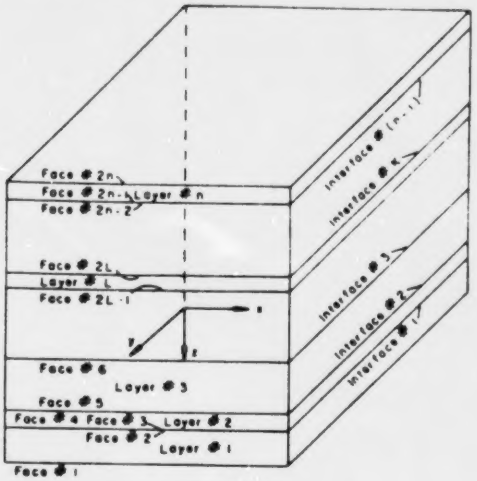
Face # 2n
Face # 2n-1
Layer # n
Face # 2n-2
Face # 2L
Layer # L
Face # 2L-1
x
y
z
Face # 6
Layer # 3
Face # 5
Face # 4
Face # 3
Layer # 2
Face # 2
Layer # 1
Face # 1
Interface # (n-1)
Interface # K
Interface # 3
Interface # 2
Interface # 1

FIG. 3.—Element of Multilayer Slab Showing Layer Numbering Convention

$$\Delta\Delta = \frac{1}{h^4}\left[\begin{array}{ccccc} & & 1 & & \\ & 2 & -8 & 2 & \\ 1 & -8 & 20 & -8 & 1 \\ & 2 & -8 & 2 & \\ & & 1 & & \end{array}\right]$$

FIG. 4.—Biharmonic Operator

configurations. This approach will be used herein. Fig. 3 shows the meaning of many of the terms to be used hereafter.

ASSUMPTIONS

The following assumptions will be made.

1. The material of each layer of the multilayer slab is linearly elastic, homogeneous, and isotropic until fracture or crushing occurs. The material is

brittle, with relative high compressive but low tensile strength. The material strengths and elastic properties may, however, be different for each layer and may also differ at various locations within each layer.

2. Out-of-plane deflections of the slab are independent of the z-coordinate and remain relatively small compared to thickness of layers.

3. The layers will slip relative to one another when some predetermined interlayer friction strength is exceeded. The interlayer friction strength is assumed to be less than the shear strength of the adjacent layer materials, to be equal before and during sliding, and may be different for each interface and for every point within each interface. It is also always assumed to be equal in all directions.

4. No perpendicular separation ever occurs between layers, even at slipped interfaces.

5. Flexural cracking or crushing in a layer at a point reduces the flexural stiffness of that layer to 0 at that location.

6. Possible external horizontal pressures causing in-plane stresses in the slab will cause the same stress in each layer. Furthermore, the effects of interaction between the external in-plane loads and the out-of-plane deflections of the slab are sufficiently small to be safely ignored.

7. The failure of a multilayer slab may be progressive, i.e., one or more layers may crack or crush at some point or points, and slip may occur at several locations between various layers without causing collapse of the slab. Both phenomena will, however, cause redistribution of loads and stresses. Due to these redistributions, it is quite likely that the maximum load carrying capacity will be reached only after several local slip or flexural failures, or both, have occurred.

In the work reported herein, the loads were symmetrically applied and the supports symmetrically placed with respect to a rectangular grid. This implies that the slab is continuous and can be divided into an infinite number of rectangular panels, each with identical conditions of elastic equilibrium, so that only one panel need be analyzed. In addition, the supports were assumed to be elastic. These conditions frequently correspond to reality. The assumption of equal static and sliding friction resistance between the layers appears reasonable in view of the fact that possible interlocking protrusions will not all break simultaneously.

RESPONSE TO PROGRESSIVE TRANSVERSE LOADING

Considering the foregoing assumptions, there are three possible modes of progressive failure for a multilayer slab under increasing transverse loading:

Local Shear Failure.—When the resultant interlayer shear stress at some point $i, j\,(x = j,\ y = i)$ on interface K, due to some distributed transverse load $q_1(x, y)$, reaches the available friction resistance on that interface at that point, a slip will occur at that point and interface without, however, reducing the friction stresses acting there. Mathematically, therefore, for a slip to occur

$$\tau_{ij,K,r} = \sqrt{(\tau^2_{zx,ij,K} + \tau^2_{zy,ij,K})} = S_{ij,K} \quad \ldots\ldots\ldots\ldots\ldots\ldots \quad (1)$$

See Appendix III for the meanings of the symbols. For all additional loading, stiffness of the total slab at that point may accurately enough be taken as the sum of the stiffnesses of the layered units thus formed. Since no perpendicular separation is permitted between the layers at the slipped interface, the units of layers formed will share the additional transverse load in proportion to their stiffnesses. Thus for U units ($U \leq n$) formed at point i,j, the additional load, q', carried by each unit is

$$\left.\begin{array}{l} q_1(i,j): q_2(i,j): q_3(i,j): \ldots : q_U(i,j) :: D_1(i,j): D_2(i,j): D_3(i,j): \ldots : D_U(i,j) \\ \text{in which} \quad q_1(i,j) + q_2(i,j) + q_3(i,j) + \ldots + q_U(i,j) = q'(i,j) \end{array}\right\} \quad (2)$$

Further load may cause additional slips at other locations on the same interface, another interface at the same location, or other interfaces at other locations, or all three. It may also cause flexural failures. Thus a slip is a localized phenomenon in the initial stages of loading and spreads over an interface as the loading is increased, reducing overall strength and stiffness against the additional loads.

Flexural Failure.—When the principal tension or compression stress at some point i,j of a layer L, face $F(F = 2L - 1$ or $F = 2L)$, caused by some external load $q_2(x,y)$, equals the corresponding material strength (tension or compression), a flexural crack or a crushing failure of the layer will occur at that point only. Mathematically, therefore for a tension crack

$$\sigma_{ij.LF.T} = \frac{1}{2}\left[\sigma_{xx.ij.LF} + \sigma_{yy.ij.LF} + \sqrt{(\sigma_{xx.ij.LF} - \sigma_{yy.ij.LF})^2 + 4\tau^2_{xy.ij.LF}}\right] = T_L \quad \ldots \quad (3)$$

and for a compression failure

$$\sigma_{ij.LF.C} = \frac{1}{2}\left[\sigma_{xx.ij.LF} + \sigma_{yy.ij.LF} - \sqrt{(\sigma_{xx.ij.LF} - \sigma_{yy.ij.LF})^2 + 4\tau^2_{xy.ij.LF}}\right] = C_L \quad \ldots \quad (4)$$

Such damage to a layer will obviously reduce the total stiffness of the slab at point i,j requiring a redistribution of stresses throughout the slab. Unlike the case of slip in which only response to additional load was affected, a local flexural failure will affect response to the total load. The slab may or may not be able to carry the load that just caused the local flexural failure, depending on whether the redistributed stresses can be resisted everywhere. If not, they may produce a combination failure as described in the next section.

Combination Failure.—In any given slab with given load, physical constants, and boundary conditions, the response to increasing load is likely to consist of a combination of slips, cracks, and crushing failures. The sequence of these will depend entirely on relative strengths and the pattern of stress redistributions. A localized flexural failure may well initiate a whole series of slips and perhaps additional flexural failures even without additional load. A local slip, on the other hand, can only lead to additional slips or flexural failures if the load is increased.

FORMULATION OF PLATE EQUATIONS

Within the assumptions previously enumerated, and before any local failure

TABLE 1.—Comparison of Theoretical and Experimental Maximum Load Carrying Capacity

Model (1)	Maximum Load, $w_l + w_m$, in pounds per square foot	
	Measured[a] (2)	Predicted (3)
1	230	258
2	288	287
3	201	122

[a] The laboratory models did not immediately collapse at these loads, probably due to "arching" effect. All models showed rather extensive cracking on the top and bottom surfaces at the indicated loads, and two of them also exhibited marked deflections underneath the slab. Collapse occurred after several hours when the indicated loads were left on the structures.

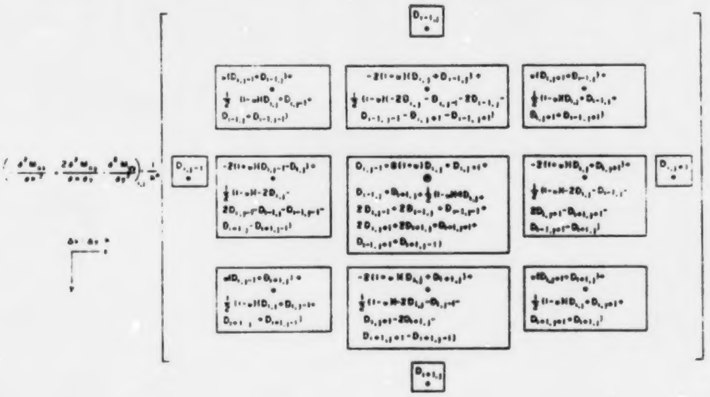

FIG. 5.—Dot Diagram for $[(-\partial^2 M_{xx}/\partial x^2) + 2(\partial^2 M_{xy}/\partial x \partial y) - (\partial^2 M_{yy}/\partial y^2)]_{i,j}$ Expressed in Terms of $\omega(x, y)$

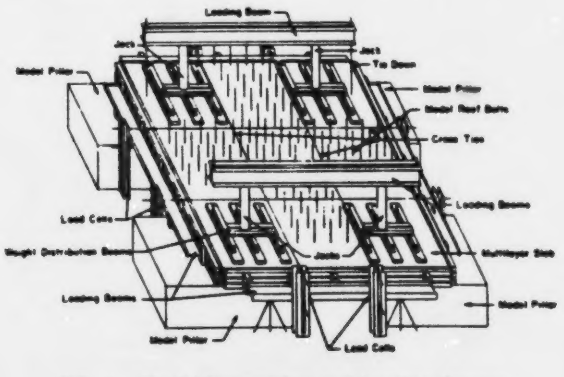
Loading Beam
Jack
Jack
Tie Down
Model Pillar
Model Pillar
Model Roof Beams
Cross Ties
Loading Beams
Load Cells
Multilayer Slab
Weight Distribution Beams
Jacks
Loading Beams
Model Pillar
Model Pillar
Load Cells

FIG. 6.—Model Intersection and Loading System

occurs, a multilayer slab behaves essentially as a one-layer slab of an equivalent homogeneous, isotropic, and linearly elastic material. In this stage of analysis, the slab stiffness, D, is constant and the classic (10) plate equation

$$D\Delta\Delta\omega(x,y) = q(x,y) \quad \ldots\ldots\ldots\ldots\ldots\ldots\ldots\ldots\ldots (5)$$

is directly applicable. A procedure for calculating an approximate but reasonably accurate value of D for the equivalent single layer slab is given in Appendix I.

After the first occurrence of a local slip or fracture, the slab stiffness is no longer constant but instead becomes a function of the in-plane coordinates (x,y). While Timoshenko (10) has given the differential equation for the bending of thin plates of nonuniform (variable) thickness subjected to distributed transverse load, neither it nor even Eq. 5 can be solved explicitly for many practical slab boundary conditions. Acceptable numerical solutions of Eq. 5 have long been obtained by the use of the method of finite differences. The central finite difference operator most frequently used for this purpose is shown in dot diagram in Fig. 4 (10). More recently the symmetrical central difference operator shown in Fig. 5 was developed to deal with plates of varying stiffness (5). As can be seen, it simplifies to the standard operator when D is constant. The finite difference method was used rather than the finite element method, because the finite difference formulation is inherently computationally more efficient and economical (4,8). The final failure of a multilayer slab is invariably preceded by a multitude of local failures, requiring many repetitions of the basic calculations, which would make the use of the finite element method for a problem of this scope and complexity prohibitively expensive, if not impossible.

STEP-BY-STEP SOLUTION ALGORITHM

The logic behind a step-by-step procedure for following the progressive failure of a multilayer slab under distributed load can be outlined as follows.

Step 1.—A finite difference grid is superimposed on the slab, and all calculations are carried out in finite difference form. The operator in Fig. 5 is used.

Step 2.—Initially, there is no sliding between the layers. The given multilayer slab is regarded as a single-layer slab made of an equivalent material which is homogeneous, isotropic, and linearly elastic. The elastic constants and the plate stiffness, D, for the equivalent material may be calculated by the method of Appendix I at every node of the finite difference mesh. At first, a transverse load, w_m, equal to the self-weight of the slab is applied, and shear and flexural stresses are calculated in the equivalent one-layer slab on the basis of ordinary slab theory, which disregards shear deformations. Straight line flexural strain distribution and parabolic shear stress distribution are assumed over the depth of the slab. The flexural stress components are then multiplied by E_i/E to obtain the real stresses in the multilayer medium. Stress components due to possible externally applied in-plane pressure loads are added algebraically to the computed flexural stresses due to w_m.

Step 3.—Resultant shear stresses at all layer interfaces are compared with the interlayer friction strength to check for possible interlayer slips.

Step 4.—Principal in-plane tension and compression stresses in the top and bottom faces of every layer in the multilayer slab at all nodes are compared with the material strengths to check for possible local material failures.

Step 5.—The transverse load, w_m, is reduced, if necessary, sufficiently so that the stresses in Steps 3 and 4 are less than the corresponding specified strength values. Let w'_m denote the intensity of this reduced transverse load.

Step 6.—An additional unit superimposed transverse load, w_l, is applied to the multilayer slab and new flexural and shear stresses calculated at all nodes.

Step 7.—The magnitude of w_l is then multiplied by a proportionality factor of such magnitude that the resulting flexural and shear stresses in combination with the stress state obtained in Step 5 will cause either the principal in-plane tension or compression stress at some node to equal the material strength, or the resultant shear stress to equal the interlayer friction strength. The proportionality factors α, β, and γ, for local slip, tension, and compression failure, respectively, at location *i,j* are

$$\alpha = \frac{-(\tau_{zx,l}\tau_{zx,m} + \tau_{zy,l}\tau_{zy,m})}{\tau^2_{zx,l} + \tau^2_{zy,l}} \pm \frac{\sqrt{S^2(\tau^2_{zx,l} + \tau^2_{zy,l}) - (\tau_{zx,l}\tau_{zy,m} - \tau_{zx,m}\tau_{zy,l})^2}}{\tau^2_{zx,l} + \tau^2_{zy,l}} \quad \dots\dots\dots\dots\dots (6)$$

$$\beta = \frac{[\sigma_{xx,l}\sigma_{yy,m} + \sigma_{yy,l}\sigma_{xx,m} - 2\tau_{xy,l}\tau_{xy,m} - T(\sigma_{xx,l} + \sigma_{yy,l})]}{2(\tau^2_{xy,l} - \sigma_{xx,l}\sigma_{yy,l})}$$
$$\pm \frac{\{T^2[(\sigma_{xx,l} - \sigma_{yy,l})^2 + 4\tau^2_{xy,l}] + 2T[2\tau_{xy,l}\tau_{xy,m}(\sigma_{xx,l} + \sigma_{yy,l}) - 2\tau^2_{xy,l}(\sigma_{xx,m} + \sigma_{yy,m}) + (\sigma_{xx,l} - \sigma_{yy,l})(\sigma_{yy,l}\sigma_{xx,m} - \sigma_{xx,l}\sigma_{yy,m})] + [(\sigma_{xx,l}\sigma_{yy,m} - \sigma_{yy,l}\sigma_{xx,m})^2 + 4(\tau_{xy,m}\sigma_{yy,l} - \tau_{xy,l}\sigma_{yy,m})(\sigma_{xx,l}\tau_{xy,m} - \tau_{xy,l}\sigma_{xx,m})]\}^{1/2}}{2(\tau^2_{xy,l} - \sigma_{xx,l}\sigma_{yy,l})} \quad (7)$$

$$\gamma = \frac{[\sigma_{xx,l}\sigma_{yy,m} + \sigma_{yy,l}\sigma_{xx,m} - 2\tau_{xy,l}\tau_{xy,m} - C(\sigma_{xx,l} + \sigma_{yy,l})]}{2(\tau^2_{xy,l} - \sigma_{xx,l}\sigma_{yy,l})}$$
$$\pm \frac{\{C^2[(\sigma_{xx,l} - \sigma_{yy,l})^2 + 4\tau^2_{xy,l}] + 2C[2\tau_{xy,l}\tau_{xy,m}(\sigma_{xx,l} + \sigma_{yy,l}) - 2\tau^2_{xy,l}(\sigma_{xx,m} + \sigma_{yy,m}) + (\sigma_{xx,l} - \sigma_{yy,l})(\sigma_{yy,l}\sigma_{xx,m} - \sigma_{xx,l}\sigma_{yy,m})] + [(\sigma_{xx,l}\sigma_{yy,m} - \sigma_{yy,l}\sigma_{xx,m})^2 + 4(\tau_{xy,m}\sigma_{yy,l} - \tau_{xy,l}\sigma_{yy,m})(\tau_{xy,m}\sigma_{xx,l} - \tau_{xy,l}\sigma_{xx,m})]\}^{1/2}}{2(\tau^2_{xy,l} - \sigma_{xx,l}\sigma_{yy,l})} \quad \dots\dots (8)$$

in which $(\tau_{zx,l}, \tau_{zy,l})$ and $(\tau_{zx,m}, \tau_{zy,m})$ are the shear stress components at some location *i,j* on interface *K* due to transverse load w_l and w_m, respectively; S = the corresponding friction strength at that location; $(\sigma_{xx,l}, \sigma_{yy,l}, \tau_{xy,l})$ and $(\sigma_{xx,m}, \sigma_{yy,m}, \tau_{xy,m})$ are the flexural stress components at some location *i,j* in layer *L*, face *F*, due to transverse load w_l and w'_m, respectively; and *T* and *C* are the corresponding material strengths in tension and compression.

The sign in front of the radical in Eqs. 6, 7, and 8 will be determined by the fact that α, β, and γ must be positive. The smallest of these proportionality factors will determine the load which, in combination with the stress state obtained in Step 5, will cause just one failure. In case this failure takes the form of a local slip, an increment in the transverse load will be required to cause the next response and the procedure must therefore go to Step 8.

If the failure takes the form of a local in-plane material failure, a redistribution of stresses must occur in the slab. Due to the brittle nature of the material, it is assumed that the failure reduces the strength and flexural stiffness of the entire layer thickness to 0 instantaneously. In this case, the procedure goes to Step 9.

Step 8.—Once a local sliding failure has taken place, free sliding is assumed to occur on the slipped interface at the affected node for all higher loads applied in this cycle of calculations. This requires that new values of D and ν be calculated at that point. The method of Appendix I may be used. The total stiffness at the slipped location is assumed to be equal to the sum of the stiffnesses of the unslipped units. Thus, the slab stiffness, D, no longer remains constant over the slab and the use of the difference operator in Fig. 5 becomes mandatory for further incremental load analyses.

A unit incremental transverse load is again applied and flexural and shear stresses are obtained everywhere in the multilayer slab. Note that Eq. 2 applies at the slipped location. The incremental load is proportioned by use of Eqs. 6, 7, and 8 so that the incremental stress state in combination with the stress state in the slab before the application of incremental load just causes the next local failure response.

If this response is a slip, the proportional incremental stress components are added to the stress state existing before the application of the incremental load, creating a new state of stress in the slab, and procedure returns to the start of Step 8. Note that previously slipped interface locations are considered to remain slipped.

Step 9.—Local in-plane flexural failure response will cause a redistribution of stresses throughout the slab and will require readjustments at slipped locations. Thus, previously (prior to the local failure response) slipped locations may offer a renewed (though perhaps reduced) friction resistance to reversed movements in a locally fractured slab seeking a new equilibrium state. To follow this search for the new state of equilibrium mathematically would require many small iteration steps which, considering the size of the program and the number of times such a local failure can occur, would be computationally prohibitive.

To overcome this problem, the following shortcut approximation was devised. The slab stiffness, D, is recomputed without reflecting the latest local flexural failure and as if the slab had not undergone any prior local slips. The slab is then unloaded with a load equal in magnitude to the one that caused the flexural failure. The externally applied in-plane pressure loads are also reversed in direction The stresses calculated for this reversed loading condition, when added to the state of stress in the slab prior to unloading, give a set of residual stresses in the slab for 0 load. These stresses reflect the effect of local slips, if any, which precede the occurrence of the flexural failure. The elastic constants of the failed layer and therefore its stiffness are reduced to 0 at the affected node and the procedure goes back to Step 2.

COMMENTS

The preceding algorithm produces one local failure for each increment of transverse load. The procedure can be made to accelerate by specifying an acceptable tolerance on the material strengths such that the corresponding local failure response would be assumed to have occurred at every node at which the computed stresses for some transverse load fall within the acceptable strength band. This will produce multiple local failure responses for each increment of transverse load. A tolerance factor of ±5%-±10% has given acceptable results with a marked improvement in the computational efficiency.

The entire procedure is independent of the particular boundary or support conditions to be used for any multilayer slab and also is not affected by the friction and material characteristics and their distributions. Maximum use should be made of symmetry in all cases. In many circumstances, it will also be advantageous to use a finite difference formulation of elastic pillar supports even when the boundaries are quite rigid. Additional equations may be introduced thereby, but avoiding the complexities of some boundary conditions may well be worth the extra computational effort.

The computer program is designed to do most of the aforementioned work automatically. It computes the loads that will cause a failure, keeps track of the past failure records, and does the unloading and reloading analysis in a continuous fashion.

A "User Information Manual" gives the source listing of the computer program and lists instructions for its use. The necessary documentation can be obtained from the writers. The computer program can handle intersection configurations of the types shown in the figures. The data preparation is simple. The program generates the coefficient matrix automatically using the procedure of Ref. 6. It can accommodate initially cracked layers or initially slipped interfaces, or both. It can analyze a given multilayer slab with a defined bolting pattern and pillar spacing. The present form of the computer program can handle a multilayer slab with up to 12 layers and up to 66 independent nodes. These limitations on problem size are strictly dictated by the IBM 360/65 computer available at the University of Kentucky. A simple change in the dimension statement of the main program will expand the program capabilities to take advantage of larger machines. All subroutines are designed to become automatically dimensionally compatible with the main program. A variety of output options are available. In brief, the program gives the load at which a local failure response will occur in a multilayer slab, incorporates the response, and automatically computes the load at which the next response will occur. The execution of the program can be stopped by limiting the number of computational cycles. (A computational cycle is defined as the complete analysis for the response to the application of one load increment.) The program execution can be accelerated by using a large value for the tolerance parameter without changing the mesh size. A 12-layer slab using 66 independent finite difference nodes and run for 50 computational cycles cost approximately $25.00 on the IBM 360/65 computer.

THEORETICAL AND EXPERIMENTAL VERIFICATION

Due to the lack of theoretical and experimental work on the subject in the technical literature, it was necessary to construct three quarter scale laboratory models of minee intersections. The results of the mathematical analysis were compared with those observed in the laboratory. A plan view of the models is shown in Fig. 6. The slabs in two of the models consisted of 12 1-in. thick layers of a weak mortar, and the third slab consisted of four layers of unequal thickness of the same material. Variations of friction were assured through use of bolts passing through the layers at discrete points, and uniform loading was applied with bags of lead shot. Details of these tests may be found in Ref. 12. The predicted and observed maximum loads carried by these models are shown in Table 1.

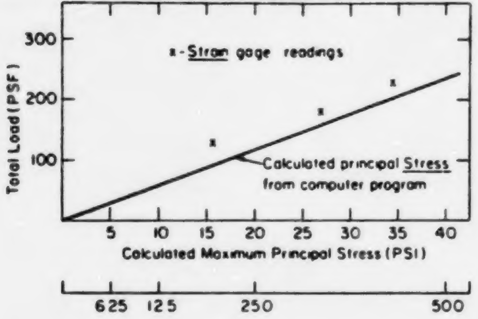

FIG. 7.—Laboratory Model Number 1, Node 46, Face Number 24

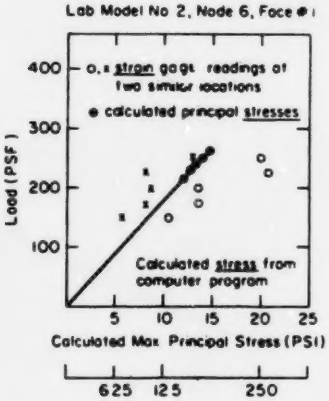

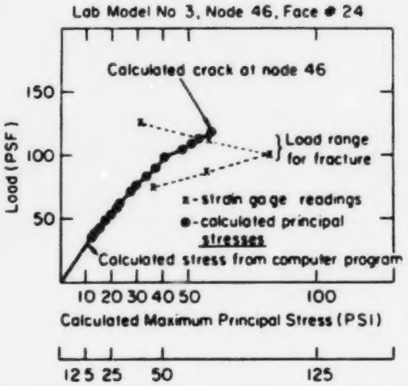

FIG. 8.—Laboratory Model Number 2, Node 6, Face Number 1

FIG. 9.—Laboratory Model Number 3, Node 46, Face Number 24

Figs. 7-9 show graphs of calculated principal stresses from the program plotted against load for some locations on the slab models. On the same figures are shown measured principal strains for the same points. The stress and strain scales in these graphs are related through a parameter reflecting both the measured Young's modulus of the material and the Poisson's ratio.

The end of the plotted line in Fig. 9 indicates the load at which the slab was predicted to crack at the location in question. The points on the graph at which the measured strains started decreasing with increasing load indicate the loads at which cracks must have formed near the ends of the strain gages. As can be seen, the correspondence between predicted and observed cracking is quite good. The calculations predicted formation of these first cracks after several slips had taken place.

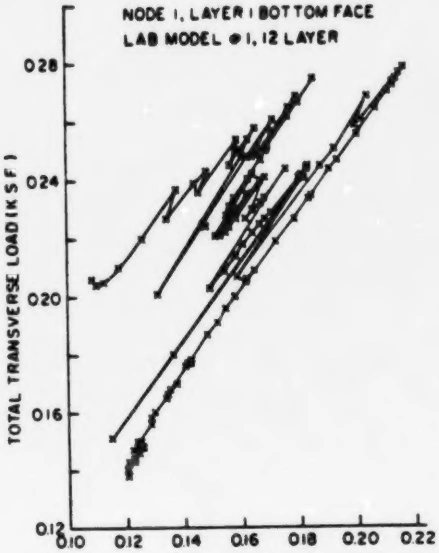

FIG. 10.—Node 1, Layer 1 Bottom Face, Laboratory Model Number 1; 12-Layer Slab

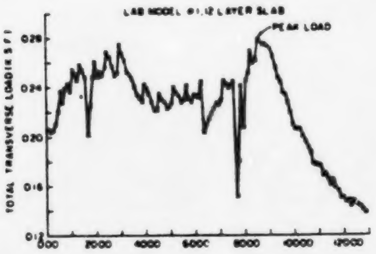

FIG. 11.—Laboratory Model Number 1; 12-Layer Slab

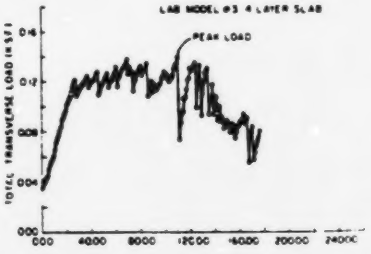

FIG. 12.—Laboratory Model Number 3; Four-Layer Slab

As a matter of interest, maximum principal stress is plotted versus total applied load for model No. 1 in Fig. 10. Cumulative local failures are plotted versus the total load applied in Figs. 11 and 12 for laboratory models No. 1 and No. 3. It is a characteristic of some calculations of this type that the apparent load resistance decreases for some steps before increasing again. Therefore, decreasing load capacity should not be taken as a cause for termination of the calculations until it has been repeated for a number of cycles (see Fig. 11). The predicted and observed crack patterns for laboratory model No. 3 are shown in Figs. 13 and 14.

For additional verification, computed values of moments and shears were checked for some multilayer slabs along a number of sections and found to satisfy the equations of static equilibrium very closely.

Convergence (obtaining increased accuracy with decreasing finite difference mesh size) of the finite difference procedure was studied by testing: (1) The approximate stability of the equations produced by use of the finite difference operator of Fig. 5; (2) the effect of varying mesh size on the load carrying capacity of a multilayer slab; and (3) the effect of varying mesh size on the condition number of the coefficient matrix of the finite difference equations.

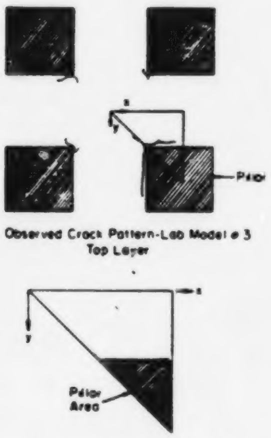

FIG. 13.—Crack Patterns—Top Layer

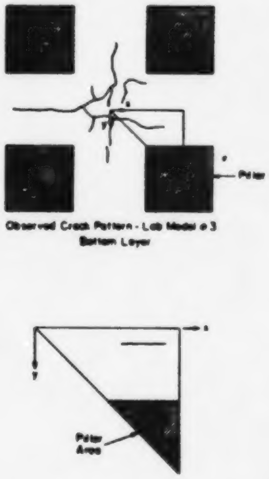

FIG. 14.—Crack Patterns—Bottom Layer

It was found (5) that the operator of Fig. 5 produces a very stable set of equations, that it converges well with decreasing mesh size, and that the condition number, calculated using the infinity norm on a row scaled matrix increases with decreasing mesh size and tends to level off for mesh size smaller than $a/16$.

The algorithm and the computer program based on it (7) were designed to enable the engineer to answer such problems as:

1. What is the structural strength of an immediate mine roof slab for a given pillar size and spacing?
2. Can the structural strength be enhanced by use of rock bolts and if so, by how much? In other words, what is the optimum bolting pattern?
3. For a given roof span (and bolting pattern), what is the optimum pillar spacing?

The formulation is general enough to handle any "thin" flat slab, multilayer or not, subjected to transverse load. The optimization can be done through trial. There remains the problem of arching effect in the underground roof slab due to the presence of in-situ field stresses and of the precise definition of the immediate roof slab in terms of its geometry and gross thickness.

The analysis presented in this paper makes use of simplified but reasonably acceptable assumptions to make the real problem mathematically tractable. Even though the present formulation makes a formal assumption that each layer of the roof slab extends over the full span of the intersection, it is not a prerequisite for the validity of the proposed procedure. When the immediate roof of a tunnel opening detaches itself from the adjacent and overlying continuum, the separation may occur along a curved surface which in case of an intersection takes the form of a dome. The shape of the dome will define the geometry of the immediate roof slab but its precise determination is not considered in this paper. Some naturally occurring layered media have material discontinuities (such as vertical jointing in mine roofs) that reduce the structural strength of the assumed continuum. It is recommended that the material discontinuities be represented by use of small material strength or small material elastic constants, or both, at the location of joints. It is also conceivable that the interface surfaces of naturally occurring layered media may have protrusions. These material protrusions at the layer interfaces can be easily accommodated by specifying larger friction strengths. No specific recommendations are made on the thickness of the roof slab but it probably should not exceed the pillar spacing.

CONCLUSIONS

The general response of a "thin" multilayer slab to incremental transverse load can be calculated. An algorithm for calculating the load carrying capacity of multilayer slabs subjected to uniformly distributed load is described. The cracking loads and the maximum load carrying capacities predicted by the mathematical analysis are shown to be in good agreement with those observed in laboratory tests. A computer program has been developed to implement the algorithm.

As part of the analysis, a method is presented for obtaining good approximate values of the elastic constants, E and ν, of a single layer slab which will be equivalent to a multilayer slab with different E and ν in the various layers.

ACKNOWLEDGMENTS

The analysis presented herein was carried out as a part of a project sponsored by the U.S. Bureau of Mines under Grant No. G0111803. The friendly guidance and help of Lewis V. Wade and financial assistance provided by the Bureau are gratefully acknowledged.

APPENDIX I.—DERIVATION OF ELASTIC CONSTANTS OF AN EQUIVALENT ONE-LAYER SLAB

Let there be n layers in a multilayer slab, with Young's modulus of the ith layer being E_i and its Poisson's ratio ν_i. Consider a section of unit width through this multilayer slab, as shown in Fig. 15. Initially, a perfect shear transfer capability is assumed at each interface of the multilayer slab. Thus the cross section of Fig. 15 can be viewed as a composite body and the section can be standardized to one common E, e.g., E_s, by varying the widths of the various layers as shown in Fig. 16. The new width of the ith layer will then be $1/m_i$ where $m_i = E_s/E_i$. The distance to the horizontal centroidal axis of the section shown in Fig. 16, measured from the bottom face of layer No. 1, can be found from

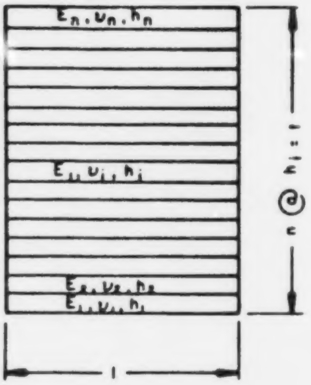

FIG. 15.—Cross Section of Multilayer Slab

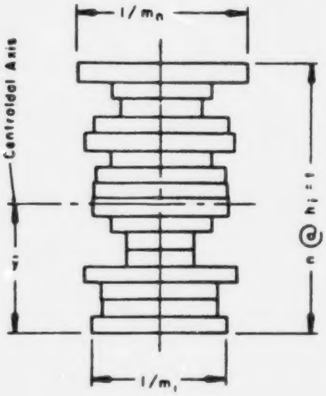

FIG. 16.—Standardized Cross Section of Multilayer Slab to Common E

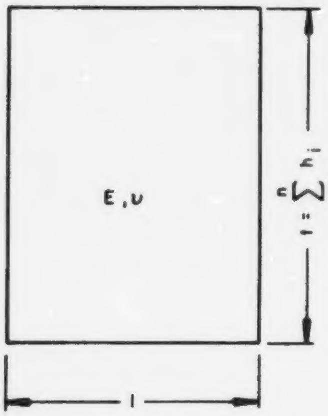

FIG. 17.—Cross Section of Equivalent Slab

$$\sum_{i=1}^{n}\frac{h_i}{m_i}\left[\left(\sum_{k=1}^{i} h_k\right)-\frac{1}{2}h_i\right]=\bar{y}\sum_{i=1}^{n}\frac{h_i}{m_i} \qquad (9)$$

which gives $$\bar{y} = \frac{\displaystyle\sum_{i=1}^{n} \frac{h_i}{m_i}\left[\left(\sum_{k=1}^{i} h_k\right) - \frac{1}{2} h_i\right]}{\displaystyle\sum_{i=1}^{n} \frac{h_i}{m_i}} \quad \text{. . . . . (10)}$$

The moment of inertia, I_t, of the composite section about its horizontal centroidal axis can be written as

$$I_t = \sum_{i=1}^{n} \left[\frac{h_i^3}{12 m_i} + \frac{h_i}{m_i}\left(\bar{y} - \frac{1}{2} h_i - \sum_{k=1}^{i} h_k\right)^2\right] \quad \text{. . . . . (11)}$$

Letting the modulus of elasticity of the equivalent one layer slab be E, one can consider a section of constant (unit) width of this equivalent slab, as shown in Fig. 17. The moment of inertia, I_e, of the unit width section about the horizontal centroidal axis of the composite section is

$$I_e = \frac{1}{12}\left(\sum_{i=1}^{n} h_i\right)^3 + \left(\bar{y} - \frac{1}{2}\sum_{i=1}^{n} h_i\right)^2 \left(\sum_{i=1}^{n} h_i\right) \quad \text{. . . . . (12)}$$

If the bending stiffness of this unit width slab is to be equal to that of the composite slab, it is necessary that

$$E_1 I_t = E I_e \quad \text{. . . . . (13)}$$

so that $$E = \frac{E_1 I_t}{I_e} \quad \text{. . . . . (14)}$$

Substitution of the expressions for I_t and I_e from Eqs. 11 and 12 into Eq. 14, one obtains the transformed modulus of elasticity

$$E = \frac{E_1 \displaystyle\sum_{i=1}^{n} \left[\frac{h_i^3}{12 m_i} + \frac{h_i}{m_i}\left(\bar{y} - \frac{1}{2} h_i - \sum_{k=1}^{i} h_k\right)^2\right]}{\displaystyle\frac{1}{12}\left(\sum_{i=1}^{n} h_i\right)^3 + \left(\bar{y} - \frac{1}{2}\sum_{i=1}^{n} h_i\right)^2 \left(\sum_{i=1}^{n} h_i\right)} \quad \text{. . . . . (15)}$$

The second elastic constant, ν, of the equivalent slab can be taken as a modified average of the Poisson's ratios of the individual layers in the multilayered slab. Consequently

$$\nu = \frac{\displaystyle\sum_{i=1}^{n} (E_i \nu_i)}{\displaystyle\sum_{i=1}^{n} E_i} \quad \text{. . . . . (16)}$$

The plate stiffness, D, then becomes $D = E I_e/(1 - \nu^2)$. Lekhnitskii gives expressions for the equivalent plate constants, D and ν, for a plate composed of an odd number of symmetric layers. The numerical values of these two slab constants, calculated from Eqs. 15 and 16 for extreme values of individual elastic properties, were compared with those obtained for the same conditions using the expressions in Ref. 9. The values of flexural rigidity were within less than ±1% of each other while Poisson's ratios varied up to ±10%. However, computer analyses of several multilayer slab problems with extreme values of Poisson's ratio, all else being equal, showed variations in maximum load carrying capacity of less than ±2%. It is obvious, therefore, that the maximum error introduced by the simplified method of calculating Poisson's ratio will be very small.

APPENDIX II.—REFERENCES

1. Ambartsumyan, S. A., *Theory of Anisotropic Plates*, Vol. 2 Translated from the first Russian Edition, Technomic Publishing Company, Stamford, Conn., 1970.
2. Ashton, J. E., and Whitney, J. M., *Theory of Laminated Plates*, 1st. ed., Vol. IV, Technomic Publishing Company, Stamford, Conn., 1970.
3. Chou, P. C., Carleone, J., and Hsu, C. M., "Elastic Constants of Layered Media," *Journal of Composite Materials*, Vol. 6, Jan., 1972, pp. 80-93.
4. Chugh, A. K., "Stress Analysis of Multilayer Plates Considering Local Material Failures and Interlayer Slips," thesis presented to the University of Kentucky, at Lexington, Ky., in 1973, in partial fulfillment of the requirements for the degree of Doctor of Philosophy.
5. Chugh, A. K., and Gesund, H., "Difference Operator for Variable Stiffness Plate," *International Journal for Numerical Methods in Engineering*, Vol. 9, No. 3, 1975, pp. 701-709.
6. Chugh, A. K., and Gesund, H., "Automatic Generation of the Coefficient Matrix of Finite Difference Equations," *International Journal for Numerical Methods in Engineering*, Vol. 8, No. 3, 1974, pp. 662-670.
7. Chugh, A. K., Wright, F. D., and Gesund, H., "User Information Manual for Multilayer Slab Analysis Program," Department of Civl Engineering, University of Kentucky, Lexington, Ky., May, 1973.
8. Ghali, A., and Neville, A. M., *Structural Analysis*, 1st. ed., Intext Educational Publishers, Scranton, Pa., 1972.
9. Lekhnitskii, S. G., *Anisotropic Plates*, Translated from the Second Russian Edition, Gordon and Breach Science Publishers, New York, N.Y., 1968.
10. Timoshenko, S., and Woinowsky-Krieger, S., *Theory of Plates and Shells*, 2nd ed., McGraw-Hill Book Company, Inc., New York, N.Y., 1969.
11. Wardle, L. J., and Gerrard, C. M., "The 'Equivalent' Anisotropic Properties of Layered Rock and Soil Masses," *Journal of the International Society of Rock Mechanics*, Vol. 4, No. 3, Nov., 1972, pp. 155-175.
12. Wright, F. D., et al., "Stresses and Safe Bolting Patterns in Coal Mine Roof Rocks at Intersections—Experimental Report," Department of Civil Engineering, University of Kentucky, Lexington, Ky., 1975.

APPENDIX III.—NOTATION

The following symbols are used in this paper:

a = finite difference grid size;
C_L = compression strength of material in layer L;
D = slab stiffness per unit width;
$D_K(i,j)$ = slab stiffness per unit width of Kth group of unslipped layers at location i,j;
E = modulus of elasticity of material of equivalent one-layer slab;
E_i = modulus of elasticity of material of ith layer of actual multilayer slab;
E_s = modulus of elasticity of composite slab (see Appendix I);

F = face $F = 2L - 1$ or $2L$;
h_i = thickness of ith layer;
I_e = planar moment of inertia of unit width segment of equivalent one-layer slab (see Appendix I);
i,j = location of point ($x = j$, $y = i$);
K = interface number;
L = layer number;
m_i = E_1/E_i;
n = total number of layers in multilayer slab under consideration;
$q(x,y)$ = transverse distributed load per unit area;
$q_U(i,j)$ = transverse load per unit area supported by Uth group of unslipped layers at location i,j;
$q'(x,y)$ = additional transverse distributed load per unit area;
$S_{ij,K}$ = available friction per unit area on interface K at location i,j;
T_L = tension strength of material in layer L;
U = number of units of slab at point i,j created by interlayer slip at that location;
w_l = external applied transverse distributed load per unit area;
w_m = self-weight of multilayer slab per unit area;
w'_m = reduced self-weight of multilayer slab per unit area;
α, β, γ = proportionality factors for local slip, tension, and compression failure, respectively;
$\Delta\Delta$ = biharmonic operator;
ν = Poisson's ratio of equivalent one-layer slab;
ν_i = Poisson's ration of ith layer;
$\sigma_{ij,LF,C}$ = smallest principal in-plane stress acting in layer L, at surface F, at location i,j;
$\sigma_{ij,LF,T}$ = largest principal in-plane stress acting in layer L, at surface F, at location i,j;
$\sigma_{xx,ij,LF}$ = normal flexural stress acting on x-face, in x direction in layer L, at surface F, at location i,j;
$\sigma_{yy,ij,LF}$ = normal flexural stress acting on y-face, in y direction in layer L, at surface F, at location i,j;
$\tau_{ij,K,r}$ = resultant shear stress acting on interface K, at location i,j;
$\tau_{xy,ij,LF}$ = shear stress acting on x-face, in y direction, on surface F of layer L at location i,j;
$\tau_{zx,ij,K}$ = shear stress acting on interface K, in x direction at location i,j;
$\tau_{zy,ij,K}$ = shear stress acting on interface K, in y direction at location i,j; and
$\omega(x,y)$ = displacement in z direction.

REFERENCES

1. Dight, P.M. Improvements to the stability of rock slopes in open pit mines. Ph.D. Thesis, Monash University, Australia (1983).

2. Goodman, R.E. Introduction to Rock Mechanics. John Wiley & Sons (1983).

3. Chugh, A.K., Gesund, H. and Wright, F.D. Analysis of multi-layer plates on elastic pillars. J. Structural Division, ST11, Am. Soc. Civ. Engrs., pp. 2405-2422 (1975).

CHAPTER 10

STABILITY AND SUPPORT OF CROSS-JOINTED, HORIZONTALLY BEDDED STRATA

10.1 INTRODUCTION

Sedimentary strata are commonly dissected by cross-joints which intersect the bedding planes at large angles. Such cross-joints are probably of tensile origin (1) and are often characterized by a rough and irregular geomtry. Two sets are usually found approximately at right angles, although one set may be better developed than the other. These joints typically are confined within each bed, i.e., the joints are discontinuous and limited in length to the thickness of the bed, and are usually more closely spaced in thin beds than in thick beds.

In view of the common occurrence of this geological structure it seems important to extend the rock bolting studies to this type of roof condition and to attempt to understand the mechanics of displacement and failure of such a roof and, subsequently, examine the implications for rock bolting layouts.

For simplification, it was assumed that a jointed roof may be modelled as a series of stacked horizontal beams, each beam intersected by a series of equally spaced, vertical joints (Fig. 10.1).

10.2 PHYSICAL MODELLING

The most direct method of approach to this problem seemed to be through physical modelling. Though this experimental method appears to have suffered some demise and criticism with the advent of the digital computer and numerical methods, it is still a very useful and practical tool. In its most highly developed form where conditions of exact similitude are satisfied, the model is actually an analogue computer, though it is rarely understood in these terms.

Stimpson (2) has made a thorough evaluation of modelling materials for use in

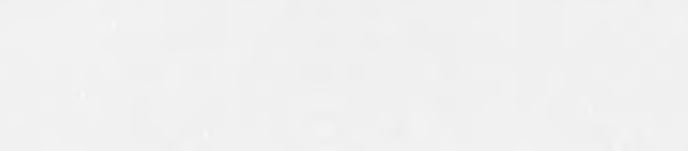

Figure 10.1 Idealized cross-section of roof with vertical cross-joints

rock mechanics. The most common material in use is plaster, as it is brittle and has practical advantages of cheapness and availability. The major disadvantage is that the ratio of uniaxial compressive strength to uniaxial tensile strength (which should be the same as that of rock for exact similitude) is smaller than that of rock. However, for the conditions to be simulated in this study, complete failure in tension seemed unlikely and therefore this deficiency of plaster was not considered a hindrance.

From previous experience with physical modelling, the writer wished to avoid, if possible, the preparation of a suitable model material from basic ingredients; the work required is tedious and time consuming. It was also necessary to find a material in which rough cross-joints could be formed. For these reasons, various manufactured products, which come in board form and can be readily cut, were investigated. Some were subjected to bending tests to determine their strengths and deformation properties and from this group two materials were selected for further study, namely K3 board, a compressed, resin-bonded chipboard, and "Gyproc", a plaster board sandwiched between paper. The K3 board was subsequently used for the physical model studies reported in Chapter 8.

Further investigations of "Gyproc" were directed at evaluating various methods of reducing its strength to better meet the similitude conditions required. These comprised weakening by dehydration of the gypsum in an oven at 90°C for several days and wetting of the plaster in various agents, including water. In all cases, weakening was so great that the material could not be handled without creating fresh fractures. It was therefore decided to use the untreated material and to investigate ways of introducing rough tensile fractures into it. The "Gyproc" material so chosen was purchased in sheets measuring 2.44 m x 1.22 m and a thickness of 12.7 mm.

A very simple procedure was used for creating rough, tensile fractures to simulate cross-joints. Model beams of the required length and width were first cut from the large sheet with a jig or band saw. Then lines marking the required location of each joint were marked on each beam and a cut very carefully made with a band saw along each line. The depth of this cut was such as to penetrate the thin paper covering the plaster and to make a shallow groove or notch in the plaster itself. Next, each beam was inserted in a vice and one by one each groove was aligned so as to just appear above the plane of the top of the vice (Fig. 10.2). A rotational motion of the hand was found to result in the formation of a rough tensile fracture, the sides of which interlocked perfectly (Fig. 10.3). Only one side needed to be grooved with the band saw. After the fracture was formed the thin layer of paper on the ungrooved side was carefully stripped off. To make reconstruction of the beam from its constituent pieces easier each piece was numbered. This was found to be especially useful in rebuilding models after a roof collapse had been simulated in a test.

Suitable materials and methods for simulating a resin bolted rock bolt to a small scale were investigated. Number 35 test nylon fishing line of about 150 N tensile strength grouted with Lepage's paper paste in small diameter holes drilled into the "Gyproc" and allowed to cure for 1.5 hours, provided a simple and inexpensive simulation.

A frame (Fig. 10.4) was constructed for the testing of model beams. It was designed to accommodate a series of stacked layers with cross joints between two flat end pieces and to permit vertical loading of the beam by a uniformly distributed or a central load.

The initial experimental work was designed to examine the mode of failure of unsupported roof beams, since a rational rock bolt design cannot be attempted without this understanding.

10.3 COLLAPSE MECHANISM

Several roof models comprising eleven layers of equal thickness and cross-joints spaced at intervals of about 13 mm were built and tested as follows. The roof layers were constructed layer by layer on top of a wooden base which itself was cut into 13

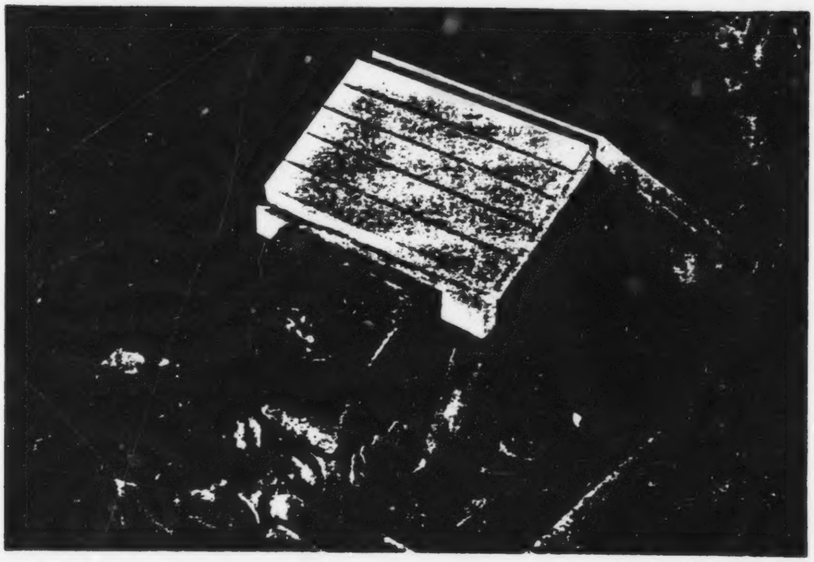

Figure 10.2 "Gyproc" beam in vice ready for fracturing

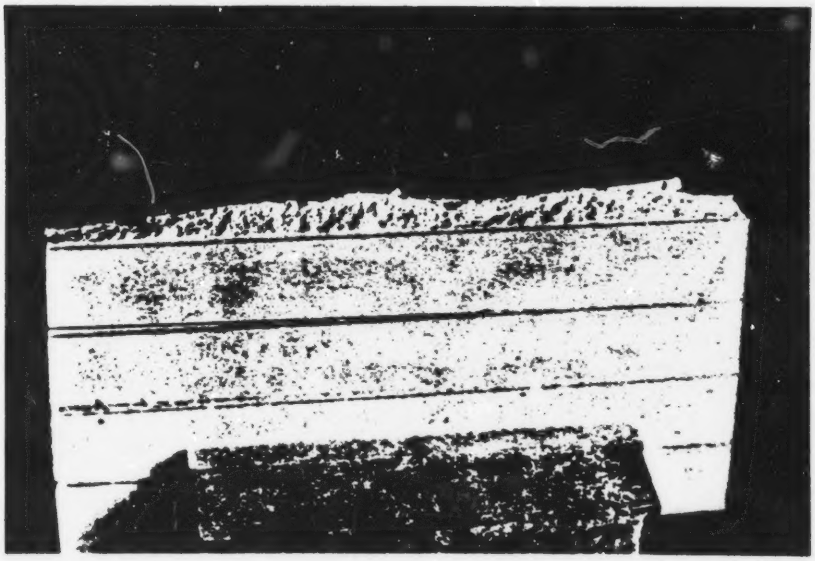

Figure 10.3 Rough tensile fracture formed in "Gyproc"

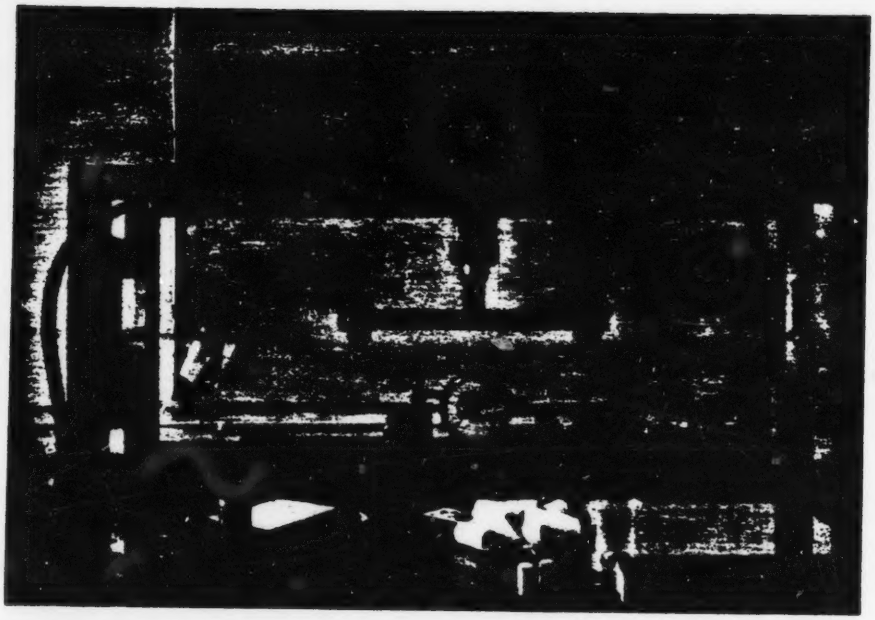

Figure 10.4 Frame for resting of cross-jointed roof beams

mm slices. This base layer represented the material to be excavated, e.g., coal seam. Failure in the 11-layer roof was induced by carefully removing these slices, one at a time, starting at the centre of the span. In this way the mining span was gradually increased. Loading in these models was by self-weight only. Photographs of one such test are illustrated in Figure 10.5.

Several important features are evident from these model tests:

1) Initial sagging of the roof progresses from the lowest layer into the roof as the span increases.
2) Significant movements in the roof are restricted to an arch-shaped zone so that disturbance extends to a greater height above the centre of the span than at the abutments. (The concept of an elliptically shaped arch is developed in Chapter 14 as a design tool for estimating bolt lengths and loadings).
3) Ultimate collapse of the roof takes place catastrophically, i.e., a small increase in span will precipitate sudden collapse.
4) For the particular geometry of the model roofs the ultimate collapse was by a mechanism which the writer has chosen to call "2-hinge failure", in which a central portion of the roof displaces vertically by pivoting about 2-hinge zones (Fig. 10.6).
5) Lateral stresses applied to the model significantly affected the span at which ultimate collapse occurred. Zero lateral stress led to the smallest stable spans.

The reality of this mode of failure was established by conducting several more tests. Mathematical modelling of the mechanism was then undertaken to better understand its characteristics and the range of conditions in which it can occur.

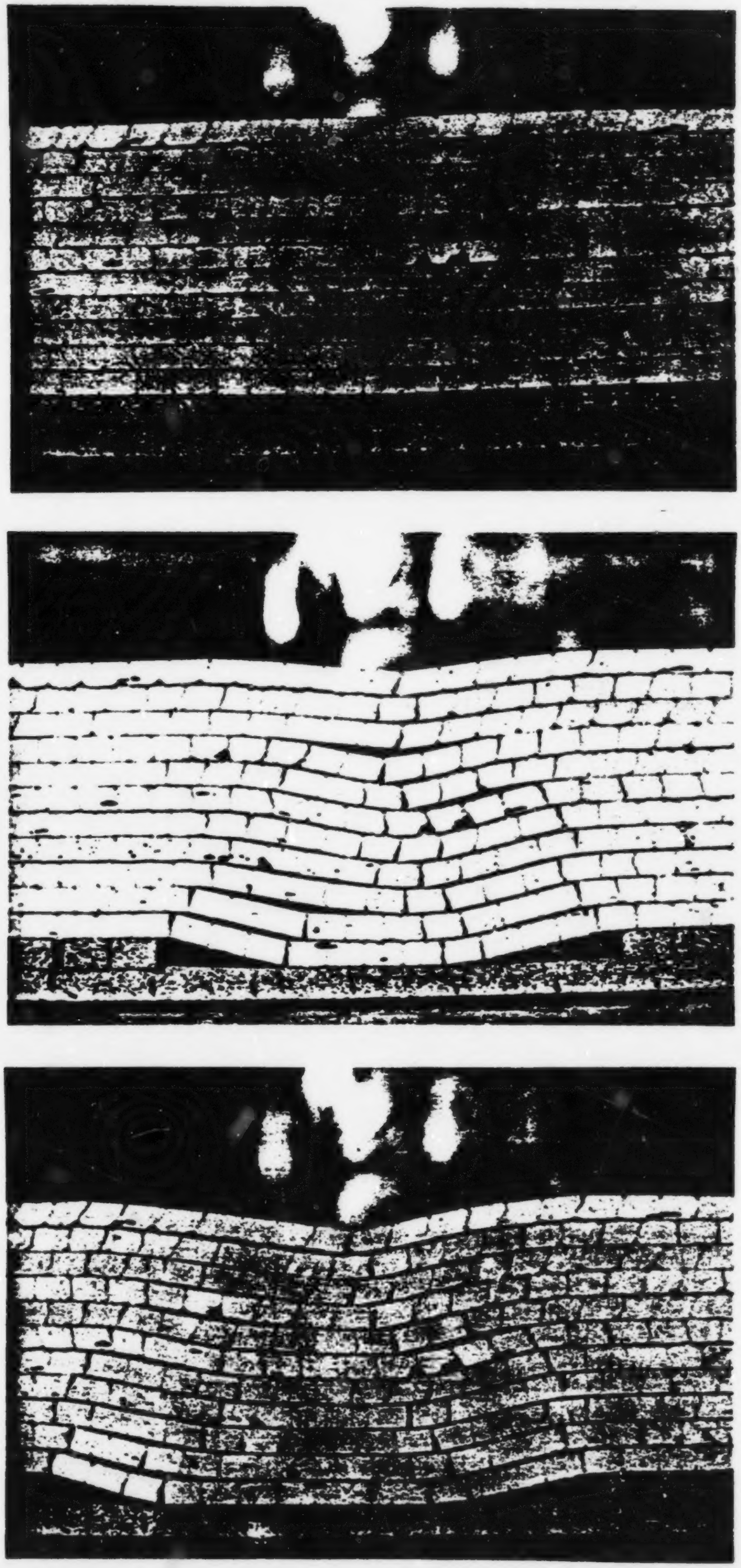

Figure 10.5 Sequence of photographs showing development of ultinate collapse in cross-jointed roof beams as span was increased

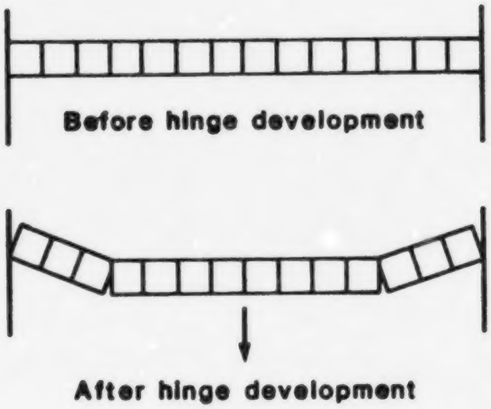
Before hinge development
After hinge development

Figure 10.6 2 hinge collapse mechanism

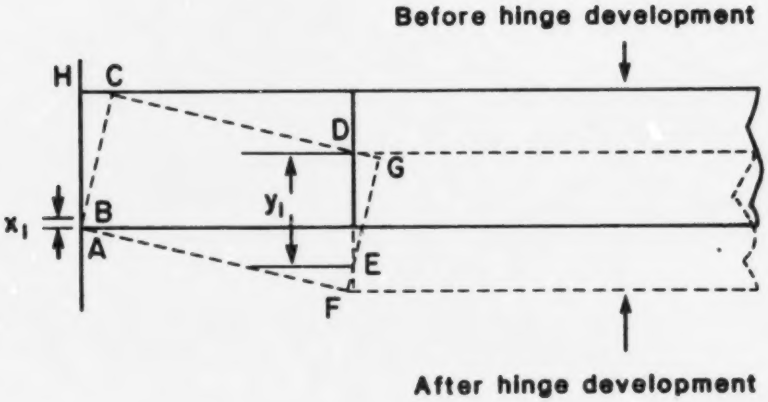
Before hinge development
H
C
D
G
x_1
B
y_1
A
E
F
After hinge development

Figure 10.7 Kinematics of two-hinge collapse mechanism

10.4 MATHEMATICAL MODELLING OF 2-HINGE COLLAPSE MECHANISM

10.4.1 Outline of Model

Details of a mathematical model are provided in Appendix E. The essential features of the model are summarised below.

The 2-hinge collapse mechanism develops by progressive crushing about two pivot points on each hinge block (Figs. 10.6 and 10.7) as the central roof block lowers. Therefore, it was necessary to simulate progressive crushing by an iterative approach which required solution on a micro-computer. In the absence of any contrary evidence, it was assumed that crushing occurs at these pivot points when the uniaxial compressive strength of the material is reached. Such failure occurs initially at the top of the beam (Fig. 10.7) and then progresses vertically downwards as horizontal thrusts are redistributed. Sudden collapse is assured when the sense of rotation of the moments generated by the horizontal thrusts reverses, i.e., stabilizing moments become destabilizing moments. The vertical displacement of the central roof beam at ultimate collapse is calculated.

The computer program also checks to determine if blocks can simply slide out of the roof due to insufficient frictional resistance along their boundaries.

In the most simple case the roof beam is loaded by its own weight, but in some circumstances the roof beam may be loaded by superincumbent strata. This situation can be simulated in the numerical model.

Zero horizontal stresses assumed in the model as this is the least conservative case.

The following data are required for input into the program:

1) Uniaxial compressive strength of rock.
2) Uniaxial compressive strength of crushed rock.
3) Thickness of roof beam.

4) Spacing between cross-joint spacing.
5) Density of roof beam.
6) Force/weight multiplier (this increases loading on roof beam for cases where overlying strata have sagged or collapsed and are adding additional load).
7) Effective angle of friction of cross-joints.

The program generates the following output:

1) Initial Factor of Safety and subsequent Factors of Safety as the hinge rotate and the roof lowers. Factor of Safety is defined as the ratio of the maximum horizontal stress generated at the hinge pivot zones and the uniaxial compressive strength of the rock. If this value is less than one, local failure occurs.
2) Reason for ultimate failure.
3) Vertical displacement of roof at ultimate collapse.

All possible hinge geometries are examined in the analysis in a sequence beginning from the centre of the span (Fig. 10.8). The iterative analysis of each hinge is continued until ultimate collapse or stability is predicted. The program is then directed to the next hinge and the analytical procedure is repeated.

10.4.2 Results

Sensitivity studies were carried out to determine the significance of the various modelling parameters. For a base case the following conditions were assumed:

- Uniaxial compressive strength rock = 30 MPa
- Uniaxial compressive strength of crushed rock = 0 MPa
- Thickness of roof beam = 0.15 m
- Spacing of cross-joints = 0.25 m
- Beam span = 7 m
- Density of roof beam = 2800 kg/cu.m.
- Force/weight multiplier = 5 (i.e. roof beam loaded by a weight equivalent

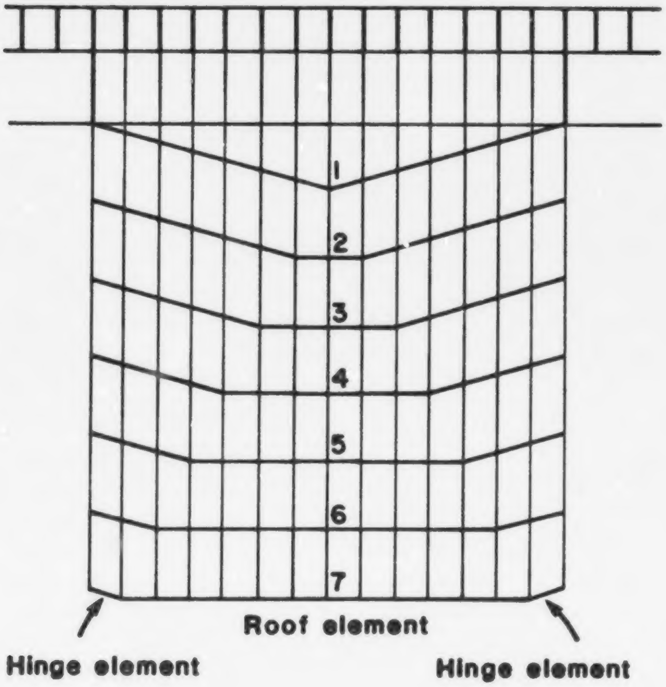
1
2
3
4
5
6
7
Roof element
Hinge element
Hinge element

Figure 10.8 Sequence of hinges examined in computer program

to 5 times its own thickness, in addition to its self-weight)

- Effective friction angle of cross-joints = 45 degrees.

Results of all computer runs with this mathematical model corroborate the type of failure mechanism observed in the physical model tests. They also show that if the initial Factor of Safety is less than 1.0 the hinge mechanism will progress to ultimate collapse, i.e., a position of new equilibrium is not reached, rather the stability of the roof continues to decrease and collapse is lifely to be sudden.

Figures 10.9-10.13 graphically illustrate the results of the sensitivity studies. In these figures the upper curve represents the Factor of Safety of the roof beam where the hinge element is smallest, i.e., 0.25 m in length or equivalent to condition #7 in Figure 10.8. The lower curve is for the largest hinge length, i.e., 3.5 m in length or equivalent to condition #1 in Figure 10.8. Other hinge configurations between the extreme conditions #1 and #7 are also possible and are analysed in the computer program, but are not included in Figures 10.8-10.13 for clarity. The numbers in brackets ( ) in these figures show the shortest hinge element which has an initial Factor of Safety less than 1.0. For example, in Figure 10.8, for a uniaxial compressive strength of 20 MPa, hinges of lengths less than 2.0 m in length will have initial Factors of Safety less than 1.0 and those of 2.0 m in length or greater, larger than or equal to 1.0.

There is a linear relationship between the initial Factor of Safety and the uniaxial compressive strength of the intact rock (Fig. 10.8). The uniaxial compressive strength of the crushed rock, which is produced at the hinge pivot areas, has no influence on the initial Factor of Safety (Fig. 10.9). However, it has a significant influence on the vertical displacement, which occurs before ultimate collapse occurs. For example, if the rock strength reduces to zero after crushing, ultimate collapse is predicted to occur after 1.28 cm of vertical displacement of the centre of the roof, but if the strength only reduces by 1/3 of its intact value the vertical displacement before ultimate collapse increases to 10.0 cms.

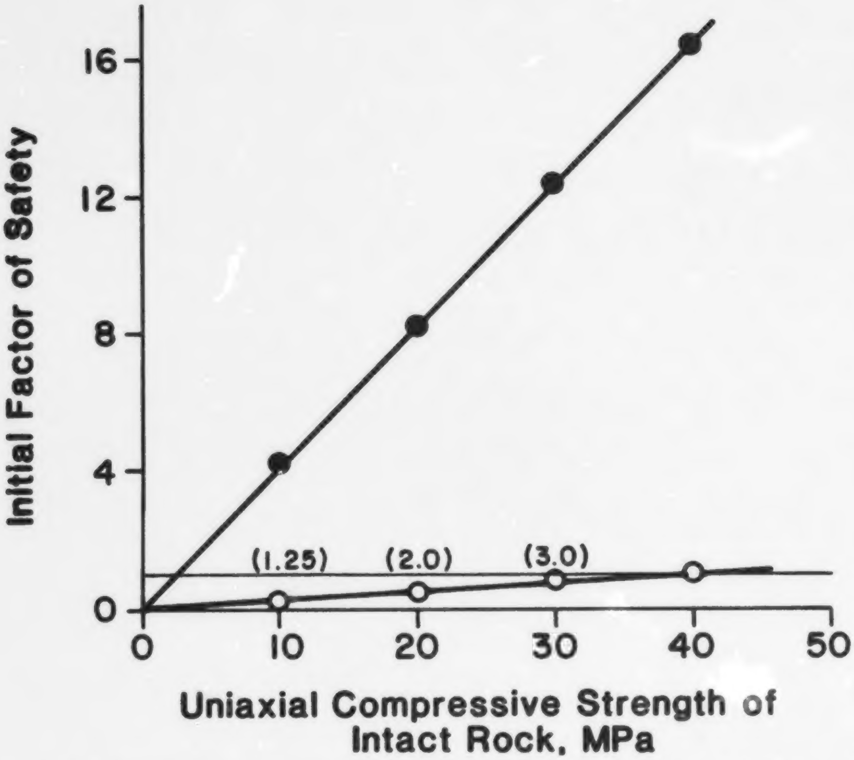

Figure 10.9 Relationship between initial Factor of Safety of roof beam and uniaxial compressive strength of intact roof beam rock (for variables assumed see Section 10.4.1) (● max. Factor of Safety, ○ min. Factor of Safety)

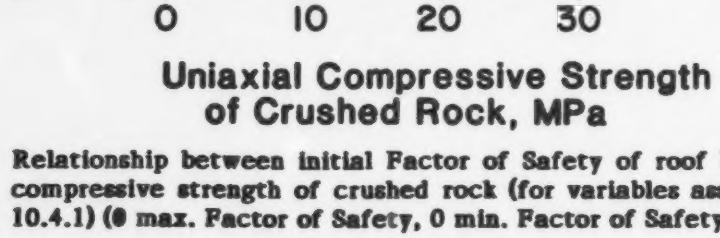

Figure 10.10 Relationship between initial Factor of Safety of roof beam and uniaxial compressive strength of crushed rock (for variables assumed see Section 10.4.1) (● max. Factor of Safety, ○ min. Factor of Safety)

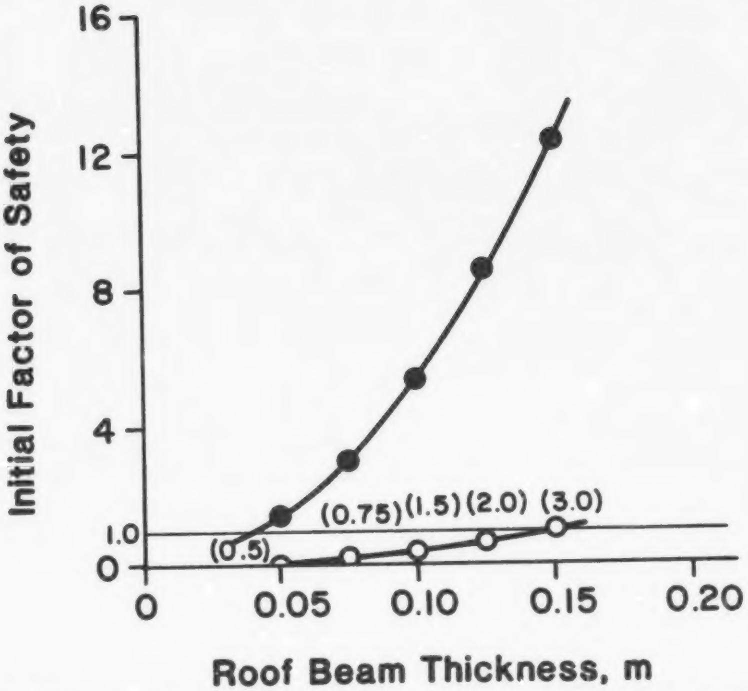

Figure 10.11 Relationship between initial Factor of Safety of roof beam and roof beam thickness (for variables assumed see Section 10.4.1) (● max. Factor of Safety, 0 min. Factor of Safety)

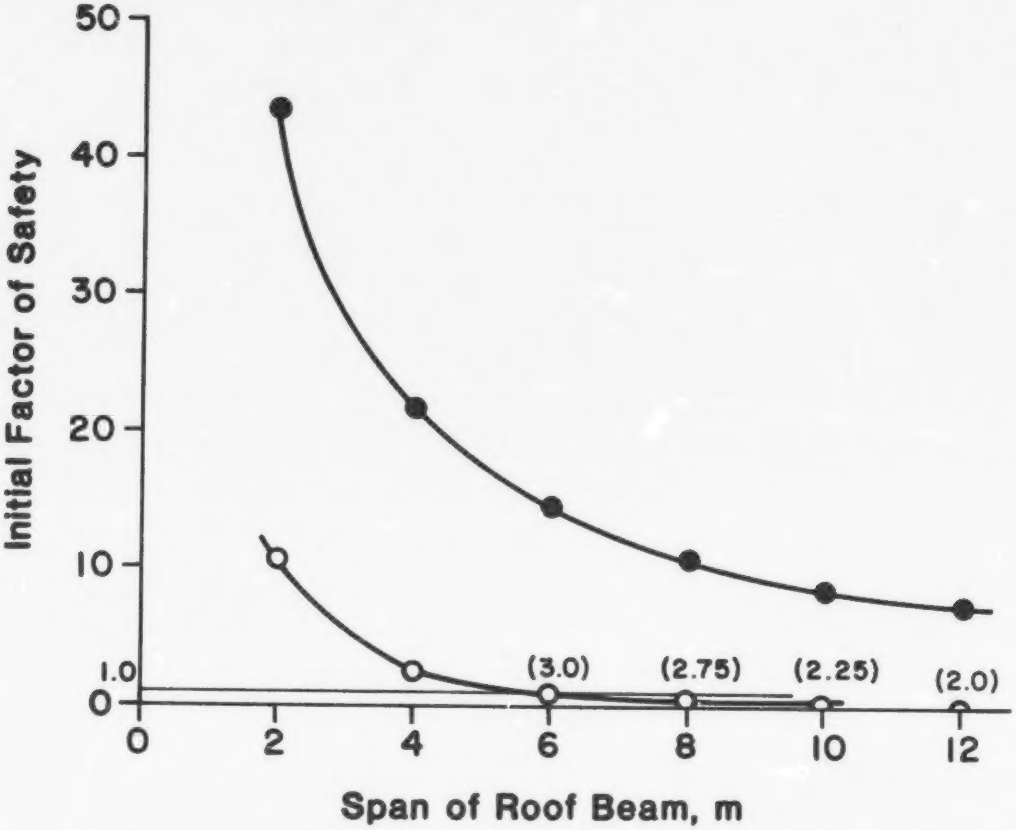

Figure 10.12 Relationship between initial Factor of Safety of roof beam and roof beam span (for variables assumed see Section 10.4.1) (● max. Factor of Safety, 0 min. Factor of Safety)

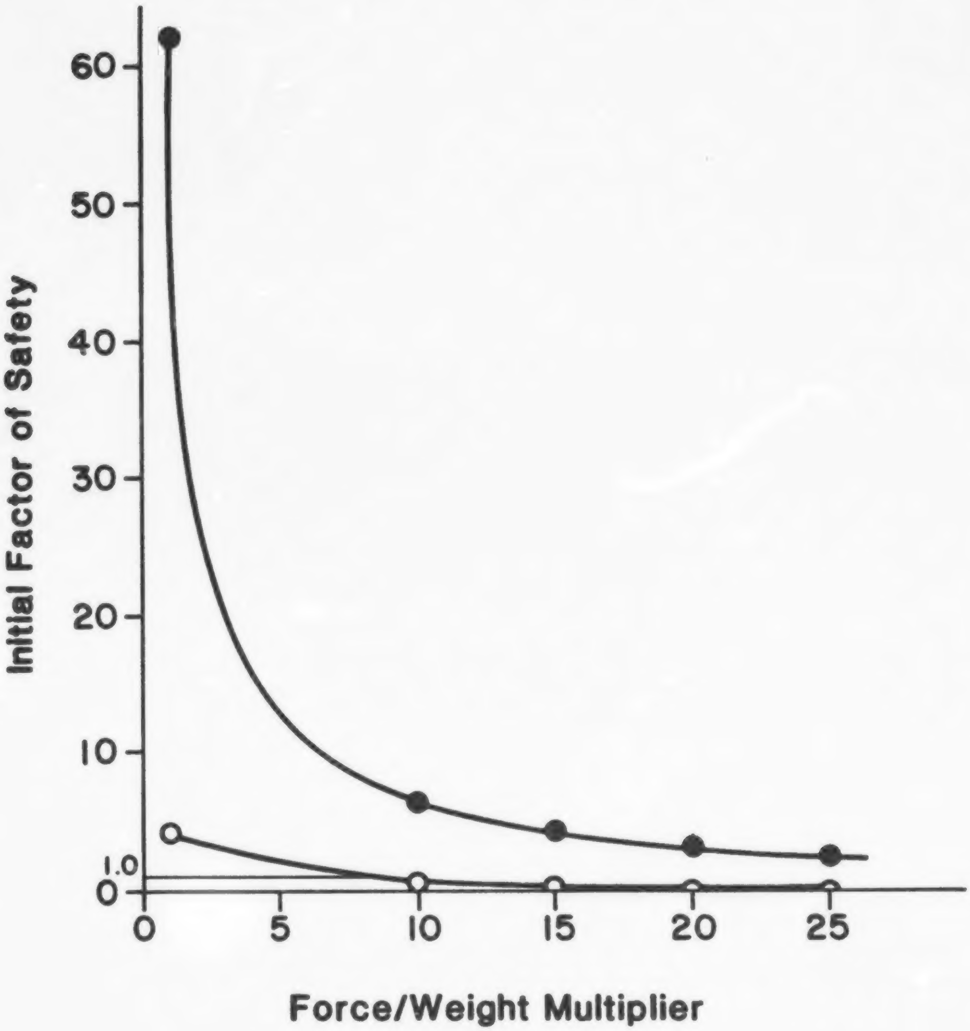

Figure 10.13 Relationship between initial Factor of Safety of roof beam and force/weight multiplier (for variables assumed see Section 10.4.1) (● max. Factor of Safety, 0 min. Factor of Safety)

Roof beam thickness and span are very significant (Figs. 10.11 and 10.12) with thin roof strata more likely to collapse by this mechanism. Relatively small changes in roof span precipitate large changes in the initial Factor of Safety.

Figure 10.13 illustrates the effect of roof loading increasing beyond self-weight conditions due, perhaps, to loading from higher beds in the roof. This is also seen to be very significant.

10.4.3 Implications for Support Design

Several important implications for support design can be derived from a study of the 2-hinge collapse mechanism. The central roof element (Fig. 10.8) is subjected only to vertical displacement. Therefore, in a series of stacked beams (there will be no differential slip between adjacent beds and the use of resin-grouted bolts which provide high resistance against differential slip are not warranted. Bolts installed in this region could be grouted with an inexpensive grout for corrosion protection only.

Differential slip does occur between adjacent beds in the hinge element zones (Fig. 10.8). For a bed of thickness, b, and a rotation of α degrees, the differential slip, δ, is given by (Fig. 10.14):

$$\delta = b \tan\alpha \qquad \ldots\ldots\ldots\ldots\ldots \quad (10.1)$$

Differential slip is constant throughout the hinge element and increases with increasing bed thickness and rotation (Fig. 10.15). In the sensitivity studies rotations at failure were less than 0.5 degrees.

Rock bolting support in the hinge element region should have high shear stiffness, i.e., resin-grouted bolts are appropriate.

Conceptually, the 2-hinge collapse mechanism could be controlled by installing short, high strength, high stiffness bolts in the hinge element regions. Recommendations for bolt layout design are discussed in more depth in Chapter 15.

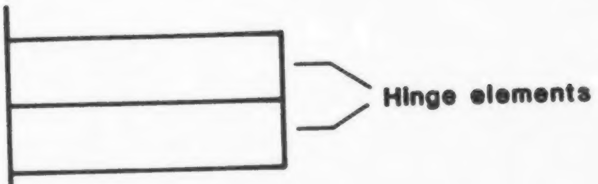
Hinge elements

(a) Before rotation

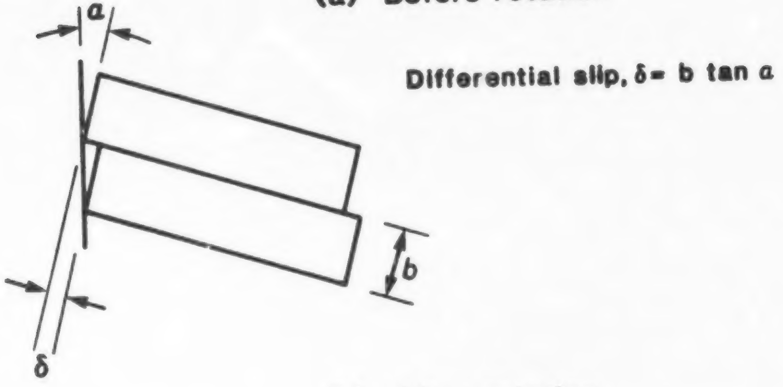
α
Differential slip, δ= b tan α
b
δ

(b) After rotation

Figure 10.14 Differential slip between beds in hinge element

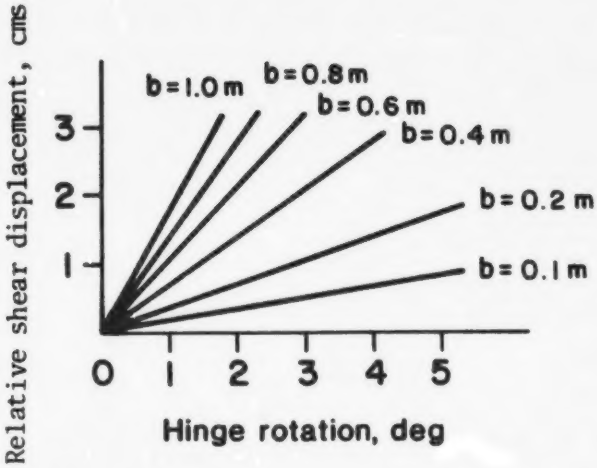

Figure 10.15 **Relative shear displacement vs. hinge rotation for beds of different thicknesses, b.**

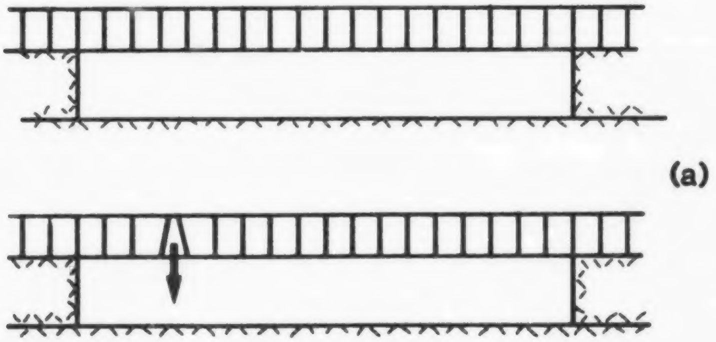

Figure 10.16 **(a) Stable roof from development of flat arch,**
(b) Unstable roof due to gravity collapse

10.5 ROOFS MOST SUBJECT TO 2-HINGE COLLAPSE MECHANISM

The sensitivity studies show that the types of roof most subject to development of the 2-hinge collapse mechanism have low intact rock strength, thin beds, wide spans, and are subjected to additional vertical loading, but low horizontal stresses. Where any of these conditions are missing, the roof is likely to sag and form a stable, flat arch.

10.6 STABLE FLAT ARCHES

10.6.1 Importance of Micro-Geology

Stability of flat arches in cross-jointing is very dependent upon micro-geology. For example, if the conditions of cross-jointing orthogonal to bedding is not met, other mechanisms of failure can develop. In Figure 10.16 a stable, flat arch becomes an unstable roof (by gravity fall of a single block followed by general roof collapse) by changing the orientation of only two cross-joints. Unfortunately, no broad description of geological conditions obtained from any sensibly economic program of drilling provides this type of detail.

Stable flat arches are predicted in the mathematical model when the initial Factor of Safety for all possible hinge elements is greater than 1.0. This calculation is predicted on the assumption that the hinge contact zones crush when the uniaxial compressive strength is exceeded. This assumption should be examined by conducting experiments on instrumented model beams in the laboratory. Failure may develop under lower stresses than the current assumption postulates.

A stable flat arch will sag and open joints may appear on the roof of the opening. Providing mining geometry and external loadings do not change, the hinge contact points are subject to constant, non-uniform stresses. To the writer's knowledge, there have been no studies of the long-term behaviour of flat arches under constant load.

10.6.2 Predicting the Vertical Displacement of a Flat, Stable Arch

Prior to the development of a 2-hinge collapse mechanism in the physical model tests, the roof beam was observed to sag or deflect with the vertical displacements distributed in a continuous manner from a maximum at the centre of the span to zero at the abutments. It is suggested that until the collapse mechanism starts to operate the jointed roof beams may be treated as solid beams, but with a reduced Young's modulus, since the roof deflections are larger than those for a truly solid beam. The increase in deflection is due to the low normal and shear stiffnesses of the joints, compared to intact rock. A method for estimating the reduced or effective Young's modulus is outlined in Appendix F and an approach for using this result to predict the behviour of layered roofs suggested.

10.7 MODEL STUDIES OF BEAMS WITH ROCK BOLTS

The initial model studies and the mathematical analysis described above provided important insights into failure mechanisms in this type of roof structure. The next step was to attempt the physical modelling of a number of rock bolt layouts in a two-layer roof using simulated rock bolts as described earlier. A relative measure of the strength of the bolting layouts was to be obtained by subjecting each model roof to a central load in the testing frame and determining the load required to deflect the roof "beam" by a standard, arbitrary amount at the centre (Fig. 10.17). The optimum roof bolt layout would be indicated by the test giving the highest load.

Before undertaking this task, a large number of exploratory tests were conducted over a period of three months to determine the response of a two-layer beam in the frame, and to establish a standardized testing procedure. Figure 10.18 illustrates the general experimental arrangement. Because of the sensitivity of the beam to small load changes and loading history, the set-up procedure had to be precise and repeated exactly for each test.

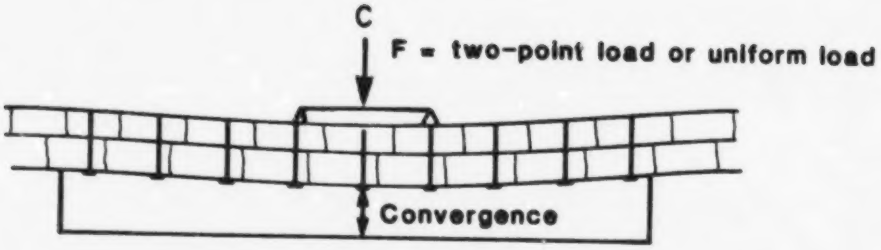
C
F = two-point load or uniform load
Convergence

Figure 10.17 Experimental principle for bolted, cross-jointed beam test

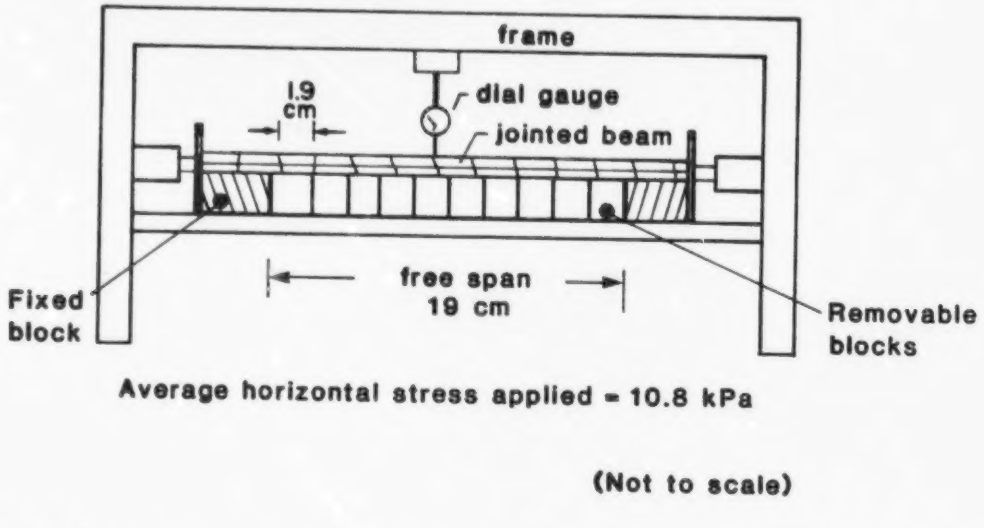
frame
1.9 cm
dial gauge
jointed beam
Fixed block
free span 19 cm
Removable blocks
Average horizontal stress applied = 10.8 kPa
(Not to scale)

Figure 10.18 General experimental arrangement of two-layer, cross-jointed beam configuration

rectangular pieces of lead weighing 122 gms each, was distributed over the upper surface in a fixed order. A free span was then created by carefully removing the supporting blocks and after five minutes the deflection was measured. This work was very tedious and demanding because of the sensitivity of beam response to the precise sequence of construction and loading. Despite the most careful experimental procedures, it was not possible to build two models ostensibly of the same geometry and obtain the same results. Even eight tests repeated on the same model did not give consistent results. After each test some damage to the joints was noted. On further detailed examination of results and the mode of displacement of the cross-jointed beams, it became apparent that the precise nature of the roughnesses in the cross-joints is important and that reproducibility between tests would require that cross-joints have identical roughness profiles. This phenomenom is examined in the next section.

After the experimental procedures had been refined and perfected as much as possible, a series of tests were carried out on beams in which two model rock bolts were inserted in the two joint blocks on either side of the centre line of the roof. Each bolt was vertical and of length equal to the total thickness of the two layers. The vertical displacement of the top of the beam after uniform loading, as described above, varied widely in eight tests: the following measurements are in millimetres - 2.46, 2.35, 2.24, 1.92, 2.11, 2.12, 1.83, 1.60 - arithmetic mean: 2.08: standard deviation: 0.28. The difference between the highest and lowest readings is 0.86 mm, thus indicating once again the difficulty of reproducibility.

10.8 SIGNIFICANCE OF CROSS-JOINT ROUGHNESS

10.8.1 Deflection of a Cross-Jointed Beam

Initial sagging of a cross-jointed beam prior to development of a 2-hinge collapse mechanism is accompanied by rotation of the individual joint blocks, as shown (much exaggerated) in Figure 10.19. This rotation involves interaction of the roughness

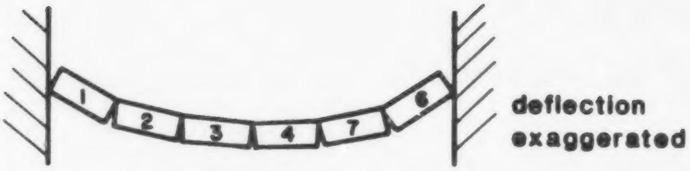
1
2
3
4
7
6
deflection
exaggerated

Figure 10.19 Individual block rotations of cross-jointed beam during "sagging" of roof

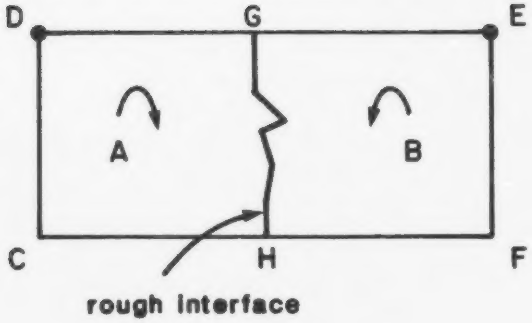
D
G
E
A
B
C
H
F
rough interface

Figure 10.20 Interaction of asperities along contact between two rotating blocks

asperities along each joint. For example, consider the very rough joint in Figure 10.20. Rotation of blocks DGHC and EGHF about D and E respectively, will result in interaction and shearing along certain segments of the joint. Under some circumstances, rotation may be prevented by the asperities.

10.8.2 Experiments to Investigate Influence of Joint Roughness

The influence of joint roughness was investigated in a further series of experiments as follows. A small Lucite frame was constructed to hold a model beam in plane strain. Model beams, 220 mm length x 65 mm depth, were cut from 9.5 mm thick "Gyproc" and a joint was created in the centre of each beam, thus forming the two-element structure shown in Figure 10.21. Three types of joint were prepared: (a) a rough tensile fracture produced by bending, (b) a smooth surface produced by a knife, and (c) a series of smooth interlocking semi-circles cut out on a band saw (Fig. 10.22).

The two extremities of the two-element beam were supported on metal pins and, in order to compare the strengths of the three different models, the structure was subjected to symmetrical, two point loading (Fig. 10.23). A loading rate of 2.5 mm/min was selected and a continuous record of applied load vs. time obtained for analysis.

A typical load vs. time curve for a beam with a rough joint is shown in Figure 10.24. From each plot, two different loads were selected for defining "strength" of the structure: (a) peak load (point A), i.e., maximum load before major crushing evident, and (b) load at which the load-time relationship began to depart from linearity (point B), i.e., a possible indication of the beginning of localized crushing. The load-time plots for the semi-circular joint profiles were non-linear throughout and therefore a point of departure from linearity could not be identified.

The various stages of a test are illustrated in Figure 10.25.

In total, twelve tests were performed with rough joints, twelve with smooth joints, and seven with semi-circular, interlocking, smooth joints. Results are tabulated in Table 10.1.

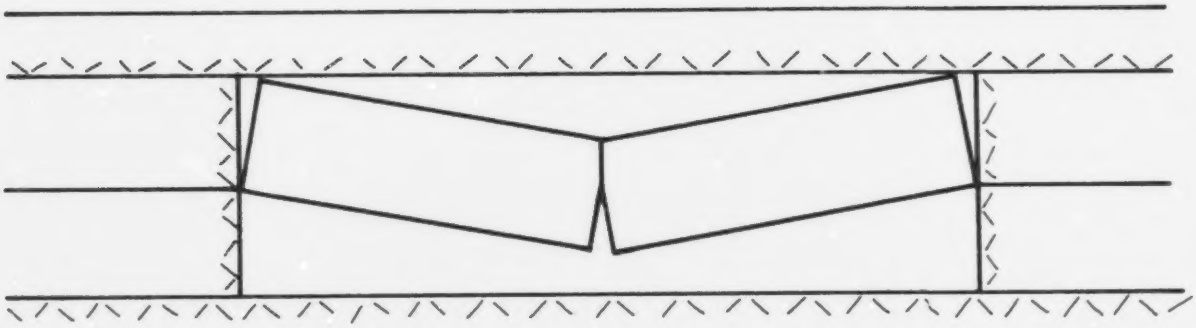

Figure 10.21 Two-element structure for investigating influence of joint roughness

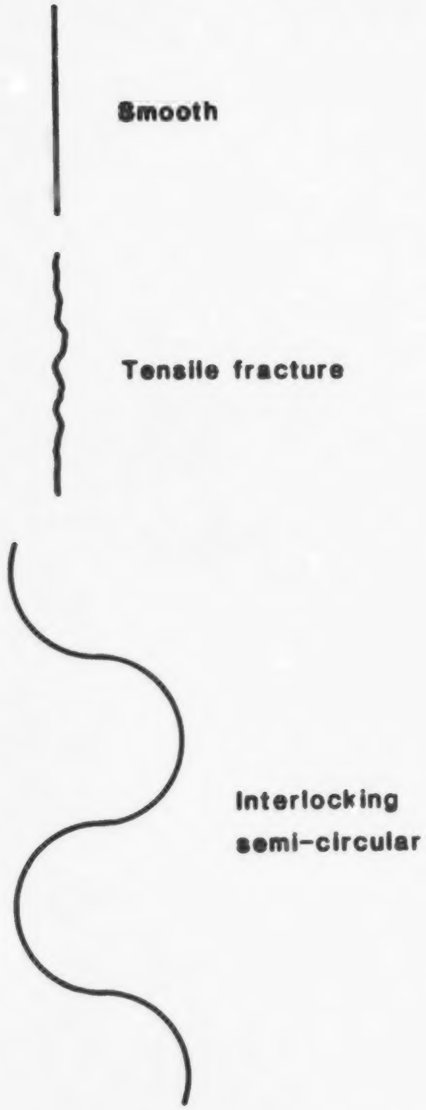
Smooth
Tensile fracture
Interlocking
semi-circular

Figure 10.22 Three types of joint roughness tested

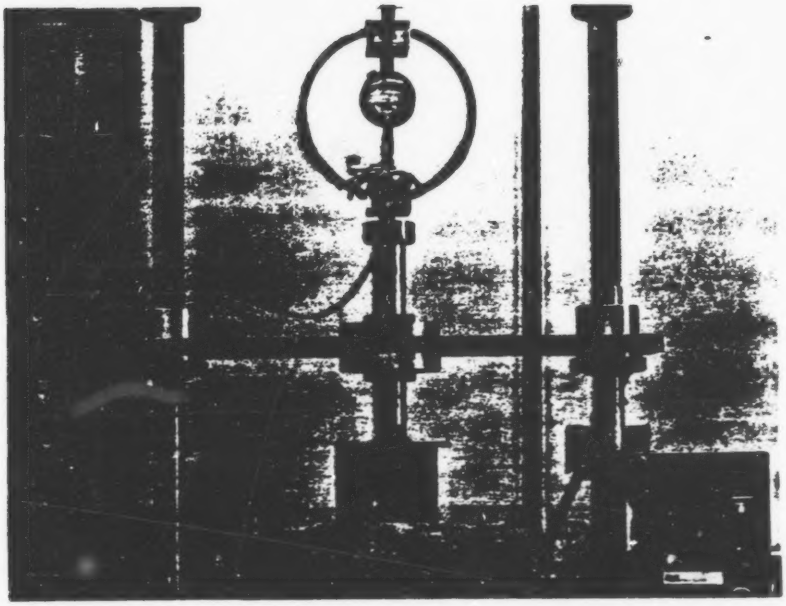

Figure 10.23 Testing frame for investigating influence of joint roughness

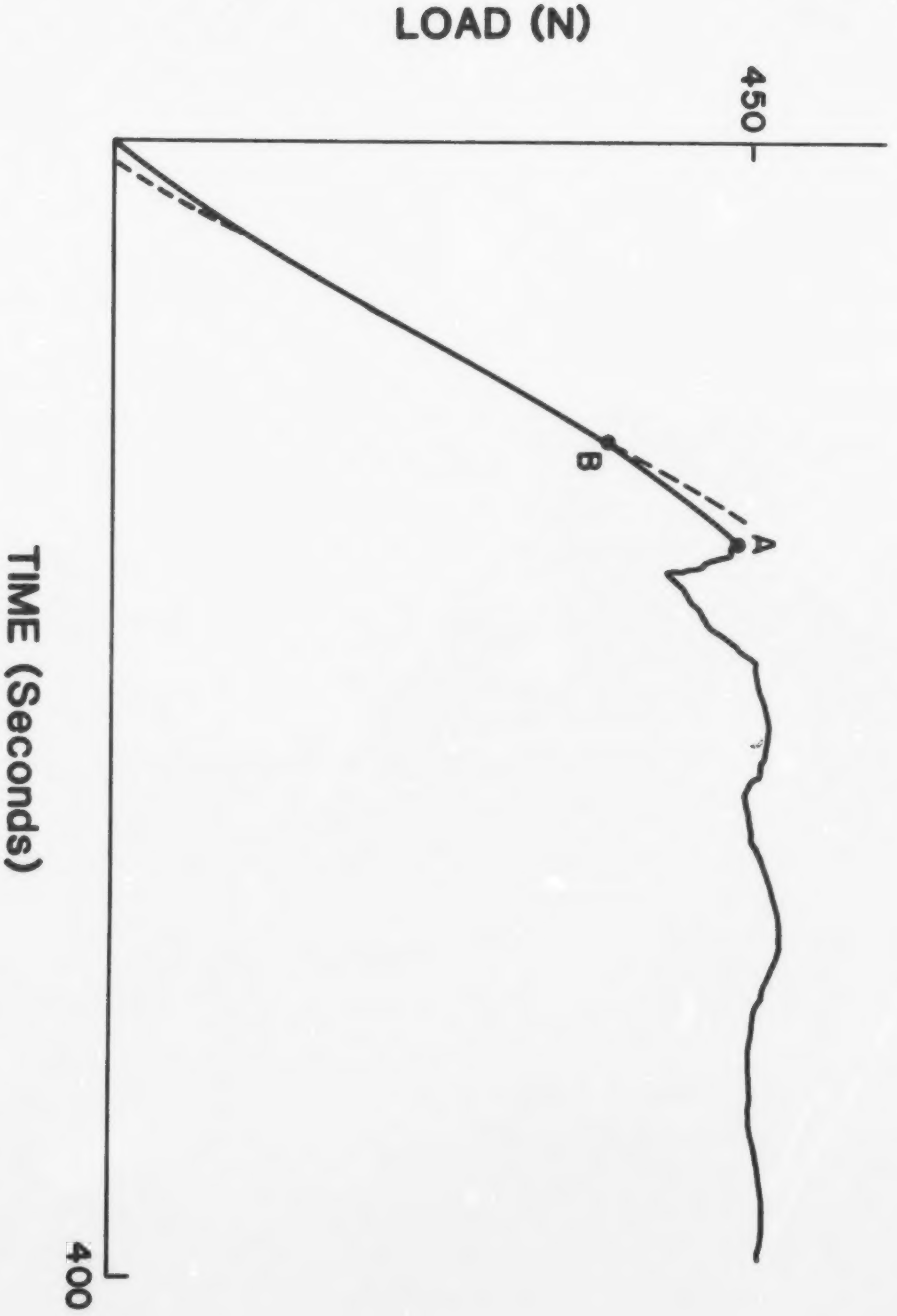

Figure 10.24 Typical load vs. time curve for beam with central joint

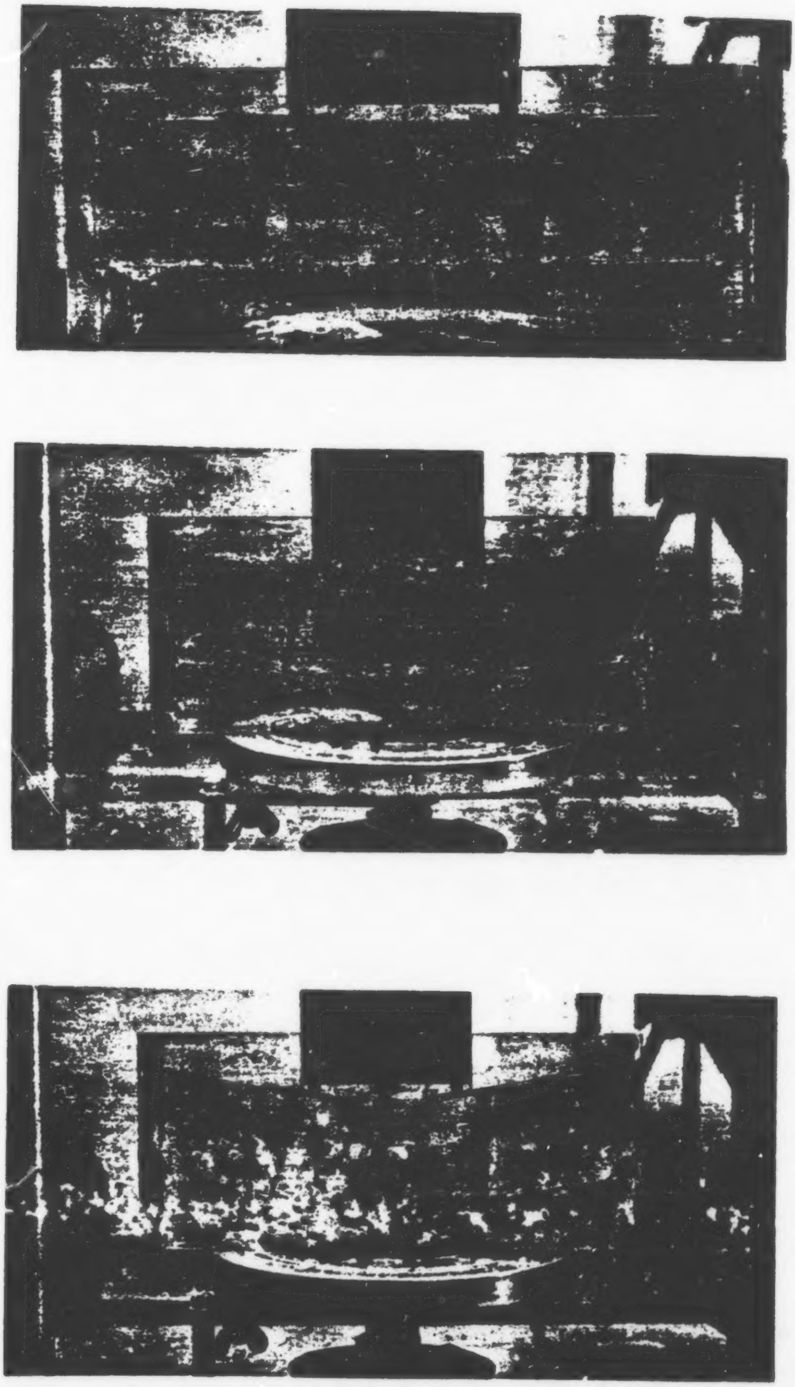

Figure 10.25 Sequence of photographs from a single test of beam with central joint

TABLE 10.1

SELECTED LOAD POINTS IN TWO ELEMENT BEAM TEST

Column 1 = Point A in Figure 10.24
Column 2 = Point B in Figure 10.24

Load in newtons (N)

	Smooth Joint		Rough Joint		Semi-circular Joint	
	Column 1	Column 2	Column 1	Column 2	Column 1	Column 2
	434	325	529	445	409	-
	398	178	712	534	278	-
	576	285	587	311	416	-
	487	294	532	316	456	-
	520	356	411	305	363	-
	503	407	620	391	347	-
	429	249	596	396	394	-
	578	338	552	480		
	423	180	587	423		
	536	356	578	329		
	547	431	543	445		
	500	156	417	358		
Mean:	494	296	555	394	390	-

Standard two-tailed tests for comparison of sample means were carried out to test the hypothesis that the sample means are identical. It is assumed that the samples are independent and have equal variances. Because of the small sample size t-Tables were used.

In the comparison of loads for smooth and rough joints the probability of the means being the same was 3 percent for peak load and 1 percent for loads at point of departure from non-linearity. It may therefore, be concluded from these model tests that the difference between the two selected loads for the rough and smooth joints is statistically highly significant.

By direct inspection of Table 10.1, it may be seen that the mean peak load for the beams with semi-circular joint profile is distinctly different from values obtained with smooth and rough joints; no statistical test is necessary to confirm this observation.

10.8.3 Conclusions

Cross-jointed roofs displace and fail by rotational mechanisms which are influenced by the scale and distribution of roughness of the cross-joints. Physical models of this type of roof are useful for understanding basic failure mechanisms, but have inherent difficulties when attempting to use them for comparative purposes. Unless the roughness of each cross-joint is identical between the different models, each model is dimensionially different. Local roughness differences, particularly when the model scale and loadings are small, are believed to account for the variation of results between different tests.

Most model studies of jointed rock have used smooth joints. Then this problem does not arise, but the model does not represent reaility and mechanical responses of the model can be considerably at variance with actual rock mass behaviour.

The significance of micro-geology is, once again, demonstrated by these results, in this case in the form of local differences in cross-joint roughness.

REFERENCES

1. Price, N.J. Fault and joint development in brittle and semi-brittle rock. Pergamon International Library (1966).

2. Stimpson, B. Modelling materials for engineering rock mechanics. Int. J. Rock Mech. Min. Sci., pp. 77-121 (1970)

CHAPTER 11

CONFINING STRESSES INDUCED BY BOLTING AND THE RESULTANT INCREASE IN ROOF STRENGTH

11.1 INTRODUCTION

In rock bolting practice a distinction is made between so-called "spot" bolting and pattern bolting. In the former case bolts are placed as and where required, usually on the basis of visual observations and estimates of the maximum rock load which the bolts will be required to support. This usually leads to a non-uniform distribution of bolts around the excavation. In pattern bolting the supports are installed according to some pre-selected uniform sequence; typically a fixed spacing of bolts is adopted.

Various mechanisms have been advanced to account for the support provided by pattern bolting. Krauland (1) considers that these can be reduced to four basic types (Fig. 11.1) comprising:

1. Suspension;
2. Beam formation of layered rock;
3. Strength increase arising from compressive stresses induced by bolting;
4. Arch formation.

In this paper a method is presented for estimating the strength increase in case 3 above. The technique also provides some quantitative guidance as to the range of rock bolt spacing over which pattern bolting is effective for a given type of rock mass.

11.2 METHOD

As a result of bolt pre-tensioning or of convergence of the opening, the bolt becomes axially tensioned. For simplicity, the common assumptions are made that the bolt load

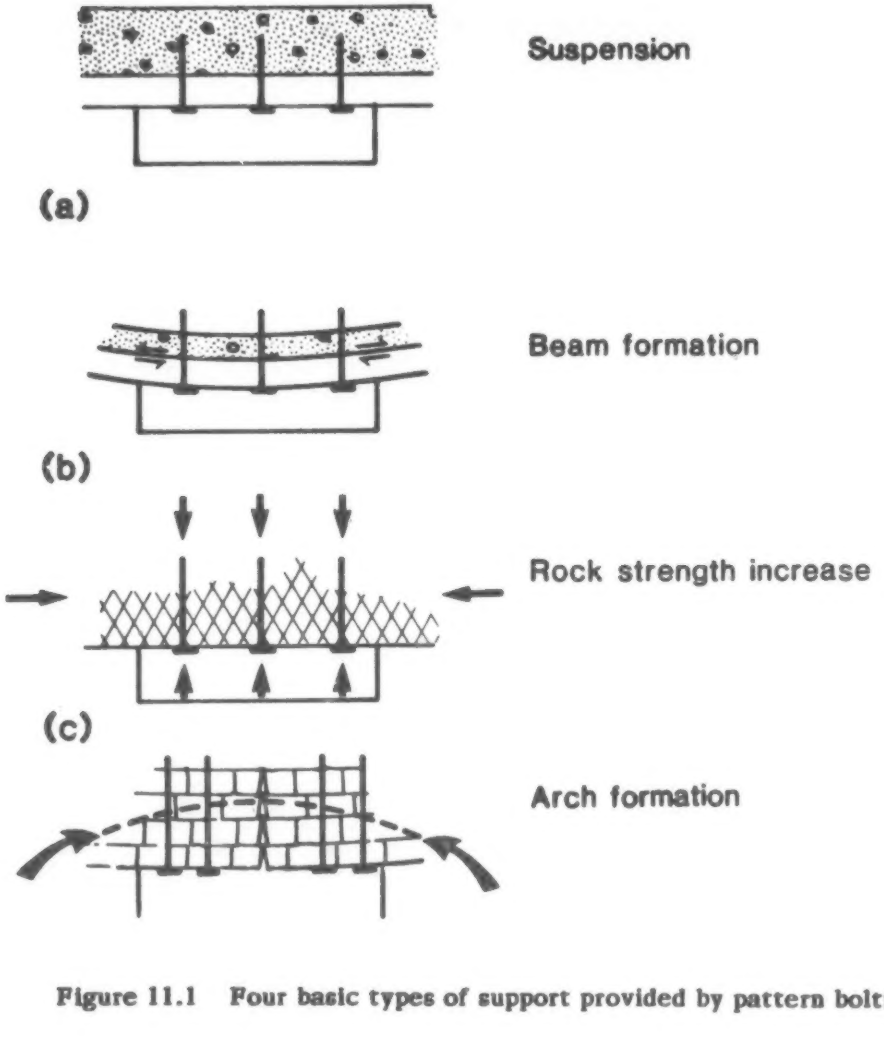
Suspension
(a)
Beam formation
(b)
Rock strength increase
(c)
Arch formation

Figure 11.1 Four basic types of support provided by pattern bolting

is distributed from points of action located at the two extremities of the bolt (Fig. 11.2), and that the stresses are distributed within a 45 degree cone from these end points. In pattern bolting the cones from each bolt overlap (Fig.11.2) and define a central zone of uniform compression, depth Z, in which the resistance to loading perpendicular to the bolting system is increased (see direction σ_1 in Fig. 11.2). For example, in a coal mine roof in horizontal strata resistance to lateral roof stresses would increase as a result of bolting perpendicular to the layers.

The depth of the compression zone, Z, is given by:

$$Z = L - D \qquad \ldots\ldots\ldots\ldots\ldots \qquad (11.1)$$

where L is the bolt length,

and D is the bolt spacing.

The maximum uniform confining stress, σ_{3bf}, that can be generated in this zone by bolting, is a function of the yield strength of the bolts, σ_y, their cross-sectional area, A, and bolt spacing, D, and is given by:

$$\sigma_{3bf} = \frac{\sigma_y A}{D^2} \qquad \ldots\ldots\ldots\ldots\ldots \qquad (11.2)$$

Geometrical considerations dictate that the 45 degree cones will only overlap and a zone of uniform compression, Z, form if bolt spacing, D, and bolt length, L, satisfy the inequality:

$$L - S > 0 \qquad \ldots\ldots\ldots\ldots\ldots \qquad (11.3)$$

The magnitude of strength increase is dependent upon the characteristics of the Mohr failure envelope of the rock mass and the increase in confining stress. In Figure 11.3 the two-dimensional Mohr circles of stress at failure are shown for the situations before and after bolting. From this diagram it may be seen that the increase in rock mass strength, $\Delta\sigma_{bf}$, is given by:

$$\Delta\sigma_{bf} = \sigma_{1bf} - \sigma_{1if} \qquad \ldots\ldots\ldots\ldots\ldots \qquad (11.4)$$

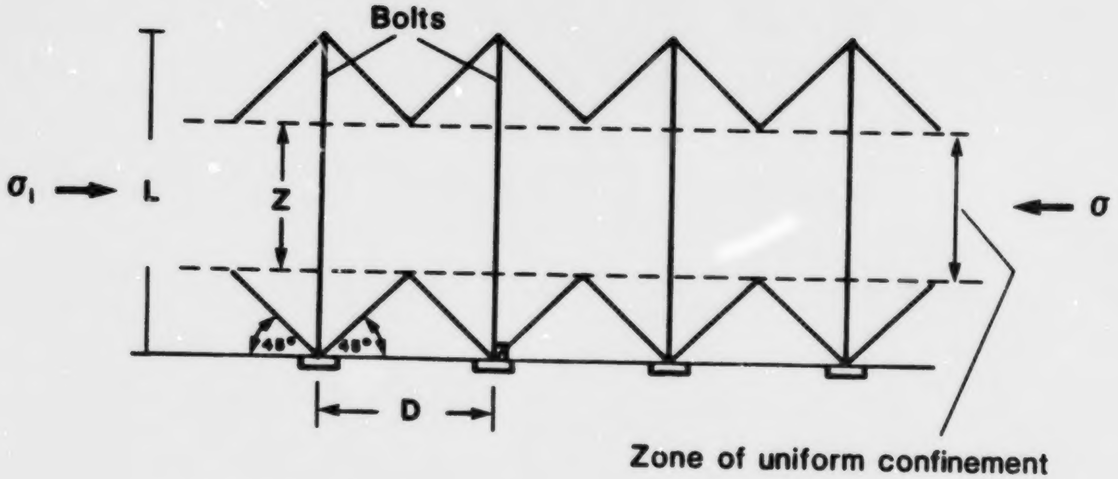
Bolts
σ_1
L
Z
45°
45°
D
σ
Zone of uniform confinement

Figure 11.2 Distribution of normal stresses beneath bolt plate

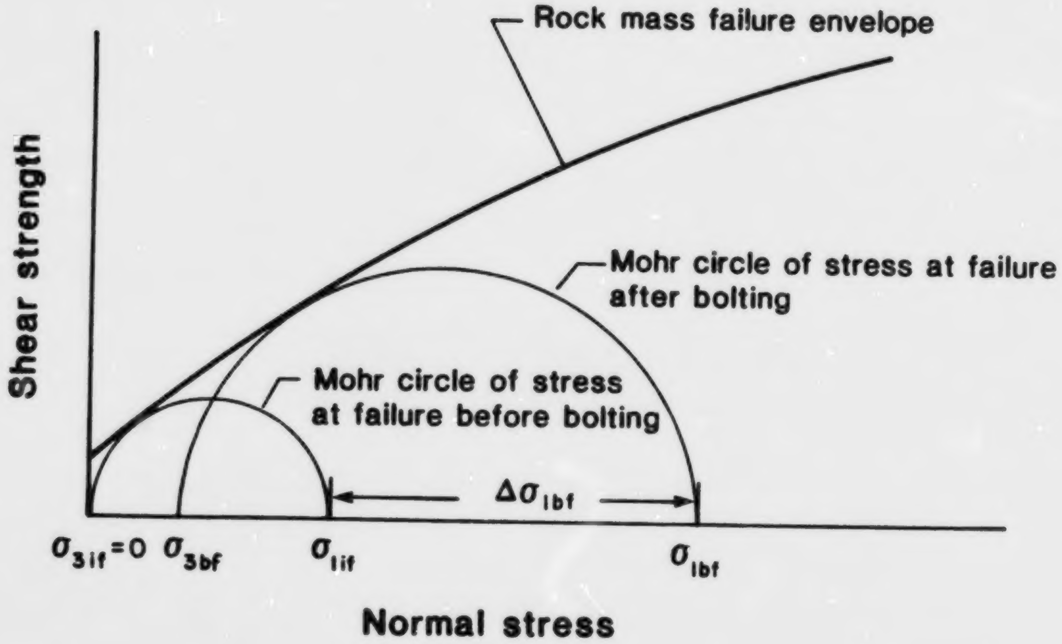
Rock mass failure envelope
Shear strength
Mohr circle of stress at failure after bolting
Mohr circle of stress at failure before bolting
$\Delta\sigma_{1bf}$
$\sigma_{3if}=0$
σ_{3bf}
σ_{1if}
σ_{1bf}
Normal stress

Figure 11.3 Mohr circles of stress for element of rock mass before and after bolting

11.3 ROCK MASS FAILURE ENVELOPE

The failure envelope for rock masses is, for practical reasons, rarely measured. Where the rock mass is very closely fractured, it is possible to obtain samples of sizes which are representative of the rock mass and can also be transported and tested in the laboratory. Such a procedure is described by Hoek and Brown (2) for the triaxial testing of closely jointed Panguna andesite. However, where joints are widely spaced, representative samples are of impractical dimensions for this procedure.

Considerable insight into the failure of rock masses has been obtained from laboratory investigations of simulated rock masses and from the study of the shear strength of joints (3 - 5). These all indicate a non-linear Mohr failure envelope for the so-called "triaxial" state of stress which is the most common testing arrangement ($\sigma_2 = \sigma_3 =$ confining pressure, $\sigma_1 =$ axial stress (taken to failure)). It is markedly non-linear at low confining pressures. This is significant for rock bolting because it means that relatively large increases in strength can be obtained from modest increases in confining pressure. It is the purpose of this article to examine the predictions as to the efficiency of pattern bolting resulting from the application of a suitable rock mass failure criterion to this support case.

In 1981 Hoek and Brown published a now well-known criterion in their text on underground excavations in rock (2). In two dimensional Mohr envelope form it is:

$$\tau_n = A(\sigma_n + B)^C \qquad \text{..............} \quad (11.5)$$

where τ_n = shear strength of rock mass,

σ_n = normal stress,

A,B,C = constants.

Suggested values of the constants A, B, and C, for rock masses of various lithologies and different qualities, as measured by their positions in the NGI (6) and CSIR (7) rock mass classifications, are provided in their Table 12, page 176. Figure 11.4 is a diagram of the predicted Mohr failure envelopes for lithified argillaceous rocks ranging from intact material (line A) to a very poor quality rock mass (line F). At normal stresses above about 2 MPa the failure envelope is, for practical purposes, linear. Of greater importance to rock bolting, however, is the non-linearity of the failure envelopes at normal stresses below 200 kPa and the cohesive resistance (shear strength at zero normal stress) of the various qualities of rock mass. Figure 11.5 illustrates the characteristics of these envelopes for lithified argillaceous rocks, once again, but over this narrower stress range, while Figure 11.6 examines the curves at very low normal stresses (10 kPa). The shapes of these envelopes are consistent with our present understanding of rock mass behaviour, though the precise values, particularly at low normal stresses must, of course, be treated with circumspection.

Rock masses described as of "Very Good" (line B) or "Good" (line C) quality have high effective friction angles at low normal stresses and significant cohesive resistances. With decreasing quality of rock mass (lines D,E, and F represent "Fair", "Poor", and "Very Poor" materials), the initially steep failure envelopes flatten more rapidly than the higher quality materials (lines B and C) and cohesions are small or zero (line F). From the viewpoint of strengthening by rock bolting, the higher quality rock masses will be strengthened more, in absolute terms, than lower quality materials for the same increase in confining pressure. Unfortunately, the better quality rock masses have high intrinsic strengths and do not generally need pattern bolting, except in very large excavations or where tangential stresses around the opening are high.

11.4 ESTIMATING ROCK MASS STRENGTH INCRERASE BY PATTERN BOLTING

The increase in rock mass strength, $\Delta\sigma_{bf}$, from pattern bolting (see equation (11.4)) requires Hoek and Brown's criterion expressed in terms of principal stresses:

$$\sigma_{1f} = \sigma_3 + \sqrt{m\sigma_c^2\,\sigma_3^3 + s\sigma_c^2} \quad \dots\dots\dots\dots\dots \quad (11.6)$$

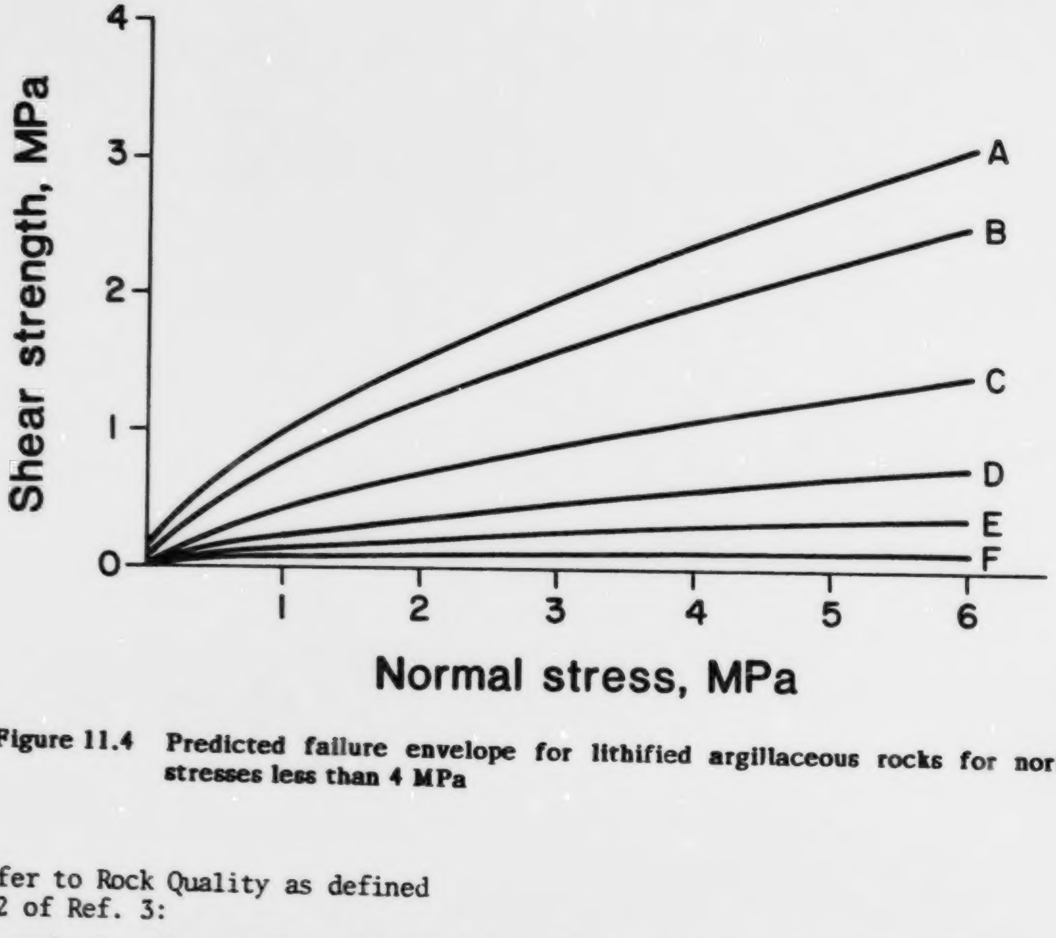

Figure 11.4 Predicted failure envelope for lithified argillaceous rocks for normal stresses less than 4 MPa

Letters refer to Rock Quality as defined
in Table 12 of Ref. 3:

A - Intact rock; B - Very good quality rock mass; C - Good quality rock mass;

D - Fair quality rock mass; E - Poor quality rock mass; F - Very poor quality rock mass

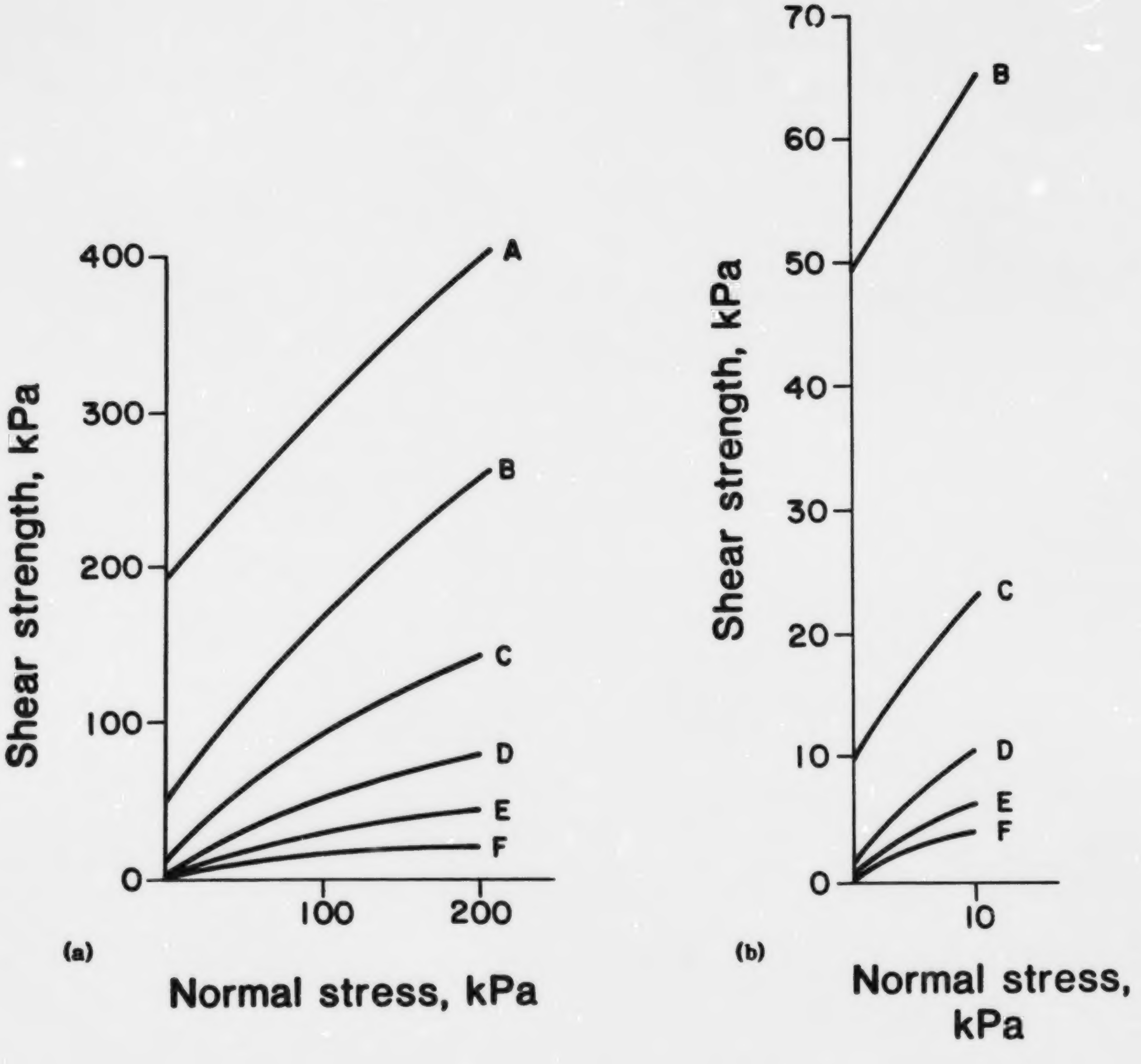

Figure 11.5 Predicted failure envelope for lithified argillaceous rocks for normal stresses less than (a) 200 kPa, (b) 10 kPa

For legend see Fig. 11.4

where σ_{1f} = rock mass strength,

σ_3 = minor principal stress (confining pressure),

σ_c = uniaxial compressive strength of intact rock,

m, s = constants.

The constant, m, is a measure of the rate at which the rock mass strength increases with confining pressure. The greater the magnitude of m the more rapid the increase.

The uniaxial compressive strength of the rock mass is equal to $\sqrt{s}\,\sigma_{ci}$, where σ_{ci} = uniaxial compressive strength of intact rock. For intact rock, s = 1 and for "very poor quality" rock, s = 0.

As was noted earlier, data on rock mass strength is sparse, yet this information is required in order to determine values of the constants, m and s, for rock masses. Hoek and Brown (2) suggest that a "very crude" estimate can be obtained from their Figure 84, which relates m and s values to the NGI (6) and CSIR (7) rock mass classifications (Fig. 11.6). The author has fitted equations to the lines in Figure 84 with the following results:

$$m/m_i = e^{0.637 \log_e Q - 3.818} \qquad \ldots\ldots\ldots\ldots\ldots \qquad (11.7)$$

$$m/m_i = e^{0.0743\ \mathrm{RMR} - 7.131} \qquad \ldots\ldots\ldots\ldots\ldots \qquad (11.8)$$

$$s = e^{1.3891 \log_e Q - 8.8049} \qquad \ldots\ldots\ldots\ldots\ldots \qquad (11.9)$$

$$s = e^{0.1561\ \mathrm{RMR} - 15.6115} \qquad \ldots\ldots\ldots\ldots\ldots \qquad (11.10)$$

where m_i = value of m for intact rock,

Q = rock quality number as estimated by the NGI classification (6) ($0 < Q \leq 400$, typically)

RMR = Rock mass rating as estimated by the CSIR classification (7) ($0 < \mathrm{RMR} \leq 100$, typically).

Fifty-nine pairs of values of m and the uniaxial compressive strength of intact

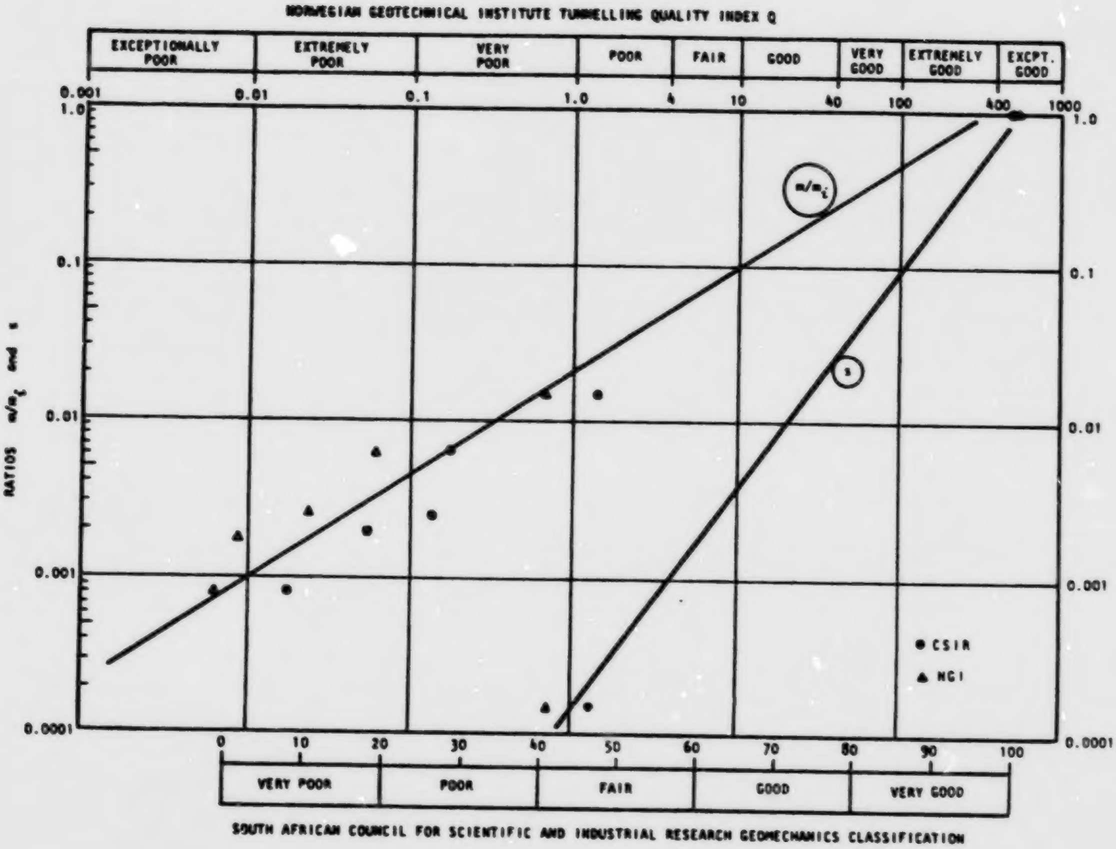

Figure 11.6 Failure envelope constants m and s and their relationship to RMR and NGI rock mass classifications (after Hoek and Brown (3))

rock obtained from analysis of triaxial test data on various rock types are tabulated by Hoek and Brown (2). The author has plotted these values in Figure 11.7 to determine if there is a useful, practical relationship but, as the Figure indicates, there is not. A high uniaxial compressive strength does not necessarily mean a high m value and vice versa.

In order to calculate the increase in rock mass strength due to bolting, it is assumed that the confining stress prior to bolting, σ_{3if}, is zero (Fig. 11.3). Therefore, the virgin rock mass strength, σ_{1if}, is found by substituting $\sigma_3 = 0$ in equation (11.6), so that:

$$\sigma_{1if} = \sqrt{s}\ \sigma_{ci} \qquad \text{..............} \qquad (11.11)$$

The rock mass strength after bolting is given by:

$$\sigma_{1bf} = \sigma_{3bf} + \sqrt{m\sigma_{ci}^2\ \sigma_{3bf} + s\ \sigma_{ci}^2} \qquad \text{..............} \qquad (11.12)$$

where the constants m and s are obtained from equations (11.7), (11.8), (11.9) or (11.10) and σ_{3bf} is obtained from equation (11.2).

Therefore, the increase in strength is, from equations (11.11) and (11.12):

$$\Delta\sigma_{bf} = \sigma_{3bf} + \sqrt{m\sigma_{ci}^2\ \sigma_{3bf} + s\sigma_{ci}^2} - s\sigma_{ci} \qquad \text{........} \qquad (11.13)$$

The units of (11.13) are force per unit area. The total resistance, R, of the rock mass over the zone of compression, depth Z, and for a unit length along the axis of the opening is:

$$R = (L - D)\sigma_{1bf} \qquad \text{..............} \qquad (11.14)$$

The percentage increase in strength due to bolting is:

$$\frac{100\,(\sigma_{1bf} - \sigma_{1if})}{\sigma_{1if}} \qquad \text{..............} \qquad (11.15)$$

From the standpoint of bolting efficiency, it is useful to compute the strength obtained per unit length of bolt, R_L. This value can be calculated from:

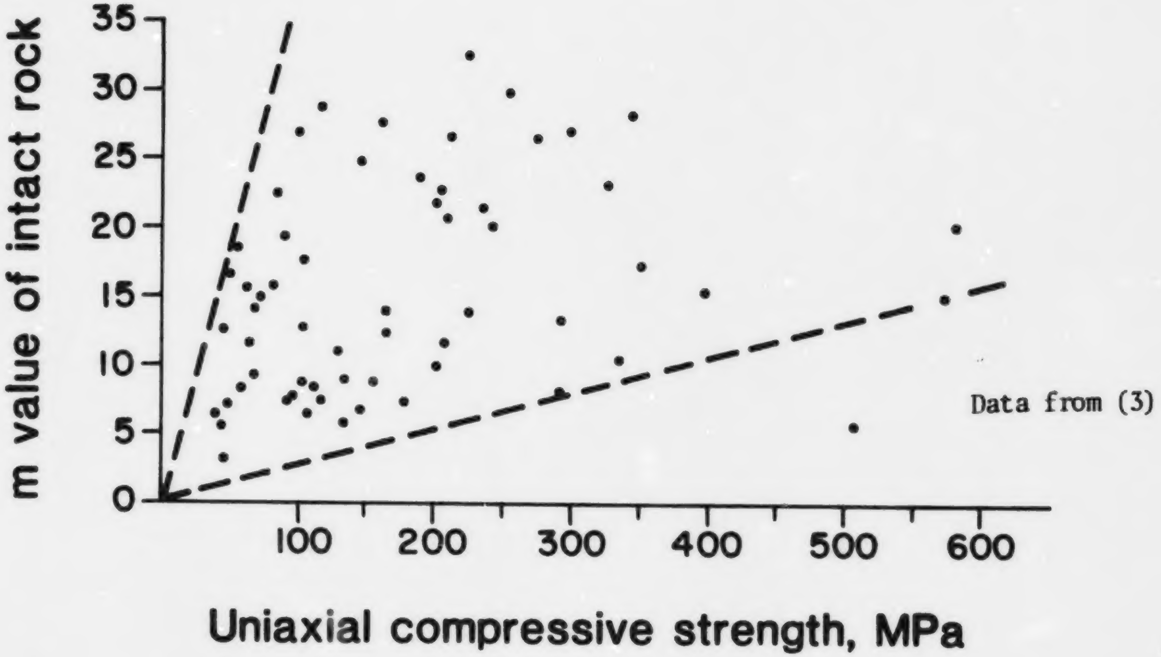

Data from (3)

Figure 11.7 Scatter diagram of failure envelope constants m and s

$$R_L = \frac{R}{L} \qquad \text{..............} \qquad (11.16)$$

11.5 RESULTS AND ANALYSIS

Graphs of the percentage increase in rock mass strength (equation (11.15)) vs. rock bolt spacing are plotted in Figures 11.8 - 11.12 to illustrate the sensitivity of this relationship to RMR, Ω, σ_c, m, and bolt diameter.

In all cases, the percentage increase in rock mass strength increases at an accelerating rate as rock bolt spacing decreases. The greatest rates of change are obtained for rock masses of low quality (Figs. 11.8 and 11.9), low intact uniaxial compressive strengths (Fig. 11.10), high m values (Fig. 11.11), and large bolt diameters (Fig. 11.12).

In order to use this methodology for design, it is necessary to know, or predict, the lateral stresses in the roof induced by excavation so that the percentage increase in rock mass strength required to resist these stresses, plus an appropriate Factor of Safety, can be estimated. Then a suitable rock bolt spacing can be estimated.

For demonstration purposes let us assume that, in general, the required percentage increase in rock mass strength is dependent on the rock mass quality which, in turn, determines the values of the constants m and s used to estimate strength. Since equations (11.7) - (11.10) indicate an exponential relationship between RMR or Q and m and s, it seems reasonable to assume that the required percentage increase in rock mass strength, P, will also be exponentially related to RMR or Q. Suppose that the relationship, then, is of the form:

$$P = e^{-K_1 \, RMR + K_2} \qquad \text{..............} \qquad (11.17)$$

where K_1 and K_2 are constants.

To determine these constants it is assumed that when RMR $\geq$ 90 no regular pattern of bolts is required, i.e., the required strength increase is 0 percent. No solution to

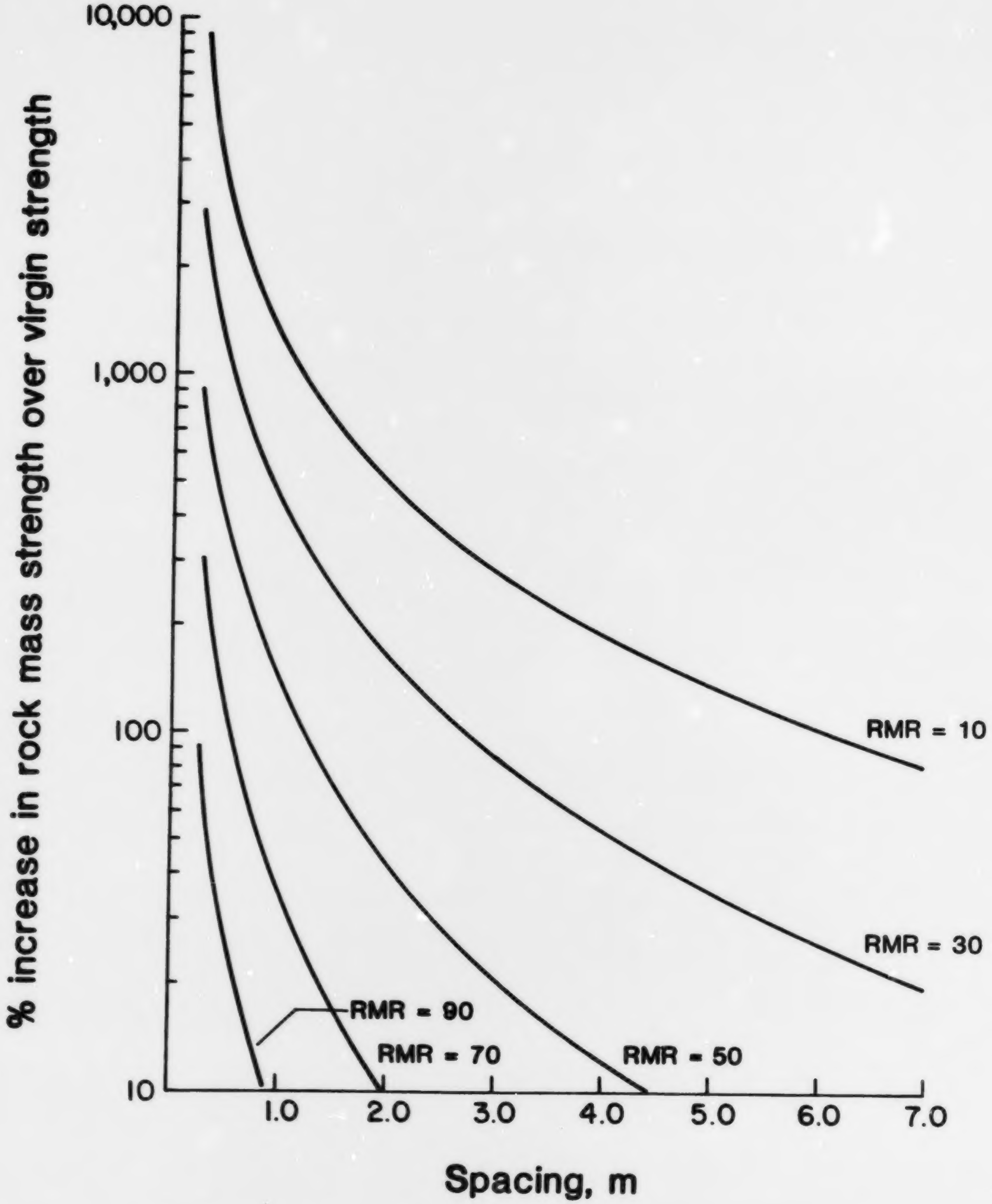

Figure 11.8 Percentage increase in rock mass strength vs. rock bolt spacing for various RMR values

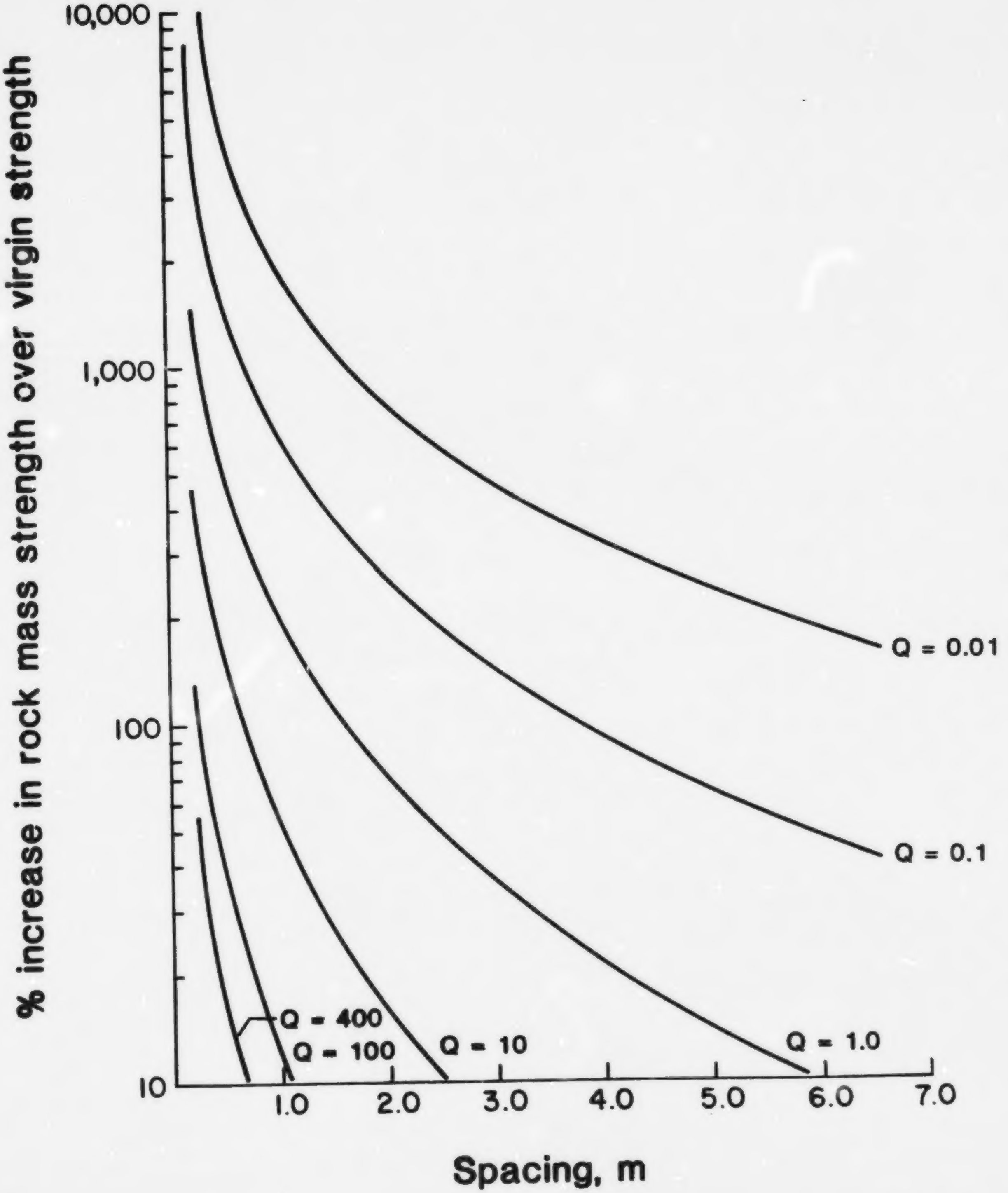

Figure 11.9 Percentage increase in rock mass strength vs. rock bolt spacing for various Q values

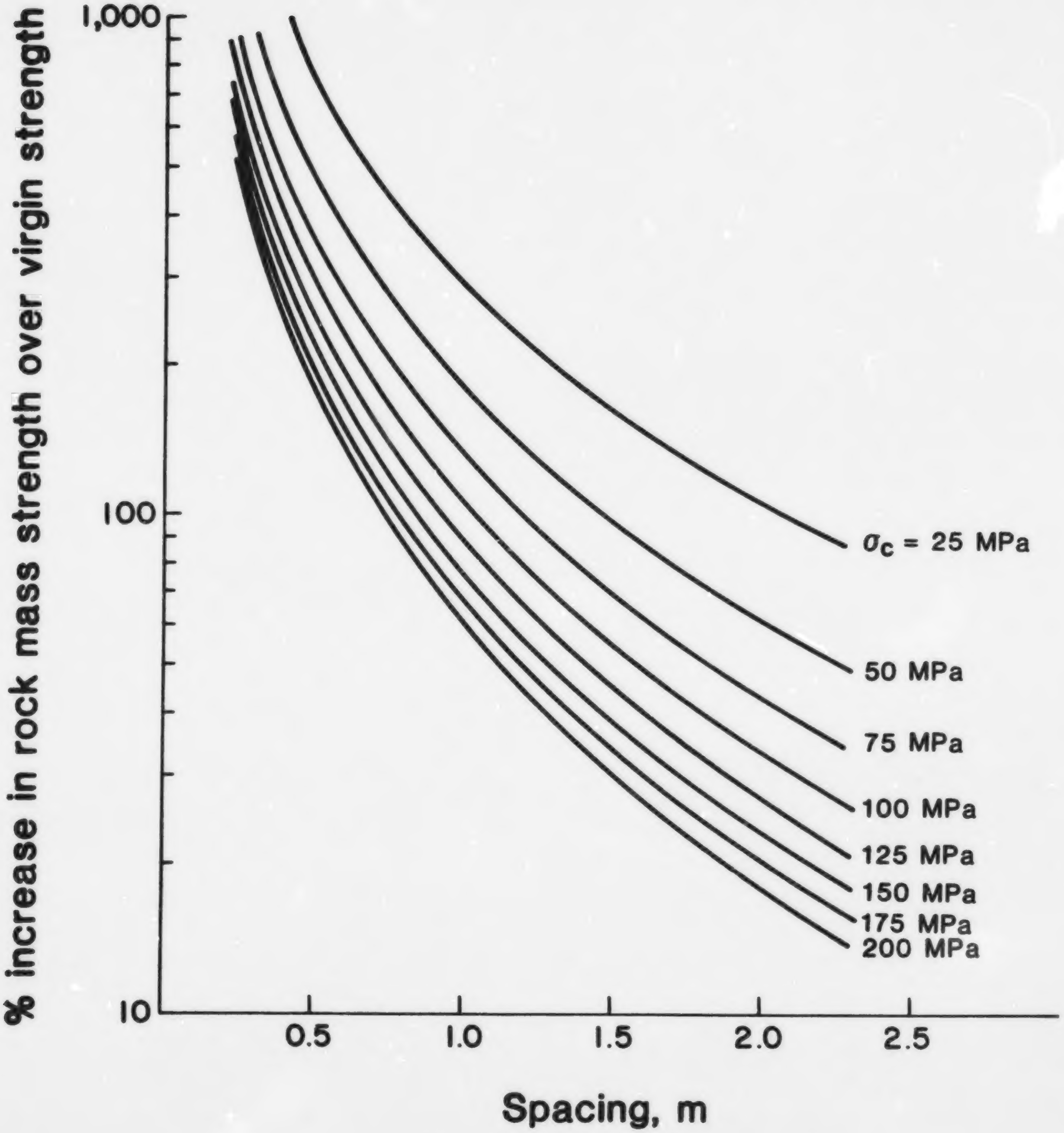

Figure 11.10 Percentage increase in rock mass strength vs. rock bolt spacing for various uniaxial compressive strength values

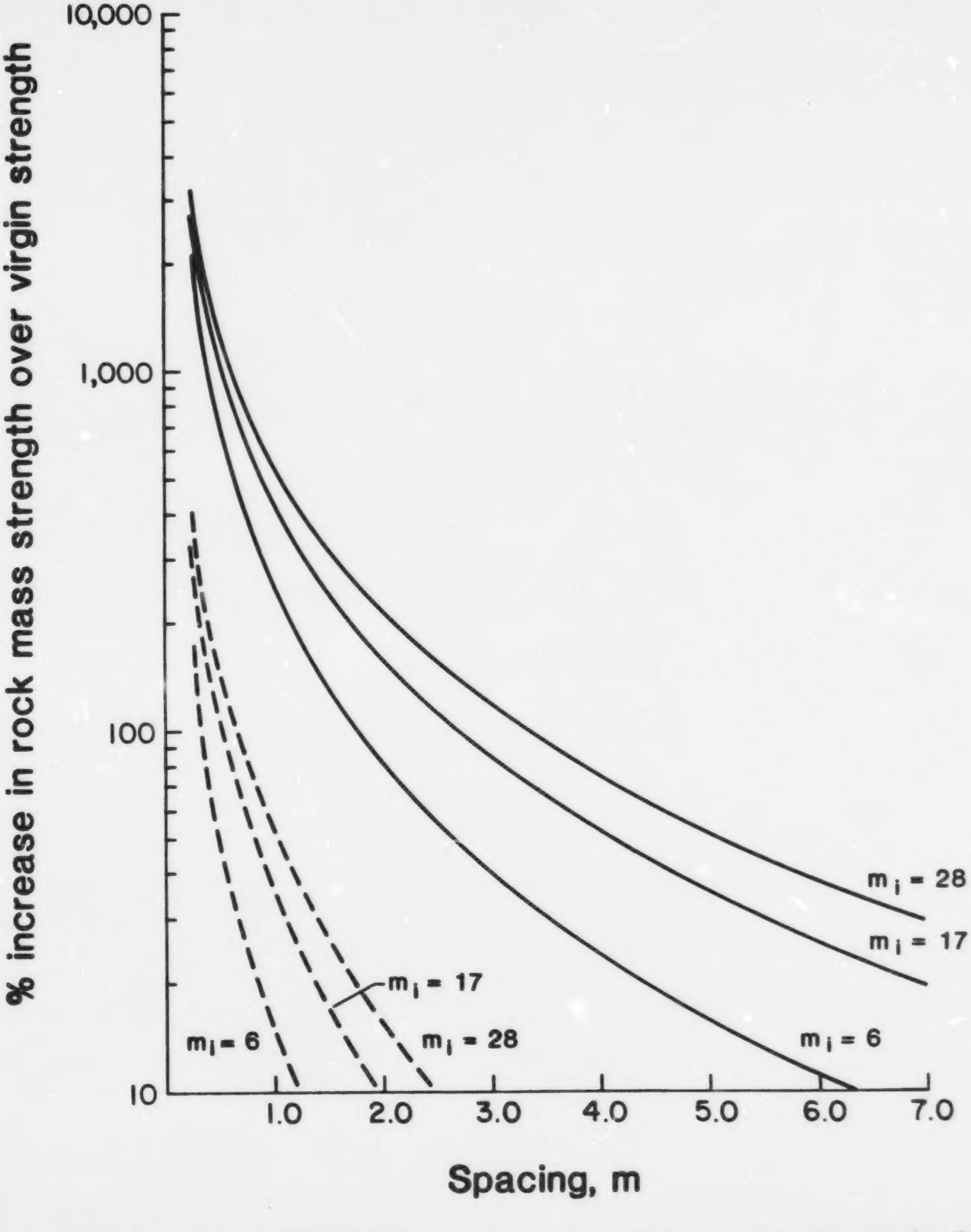

Figure 11.11 Percentage increase in rock mass strength vs. rock bolt spacing for various m values

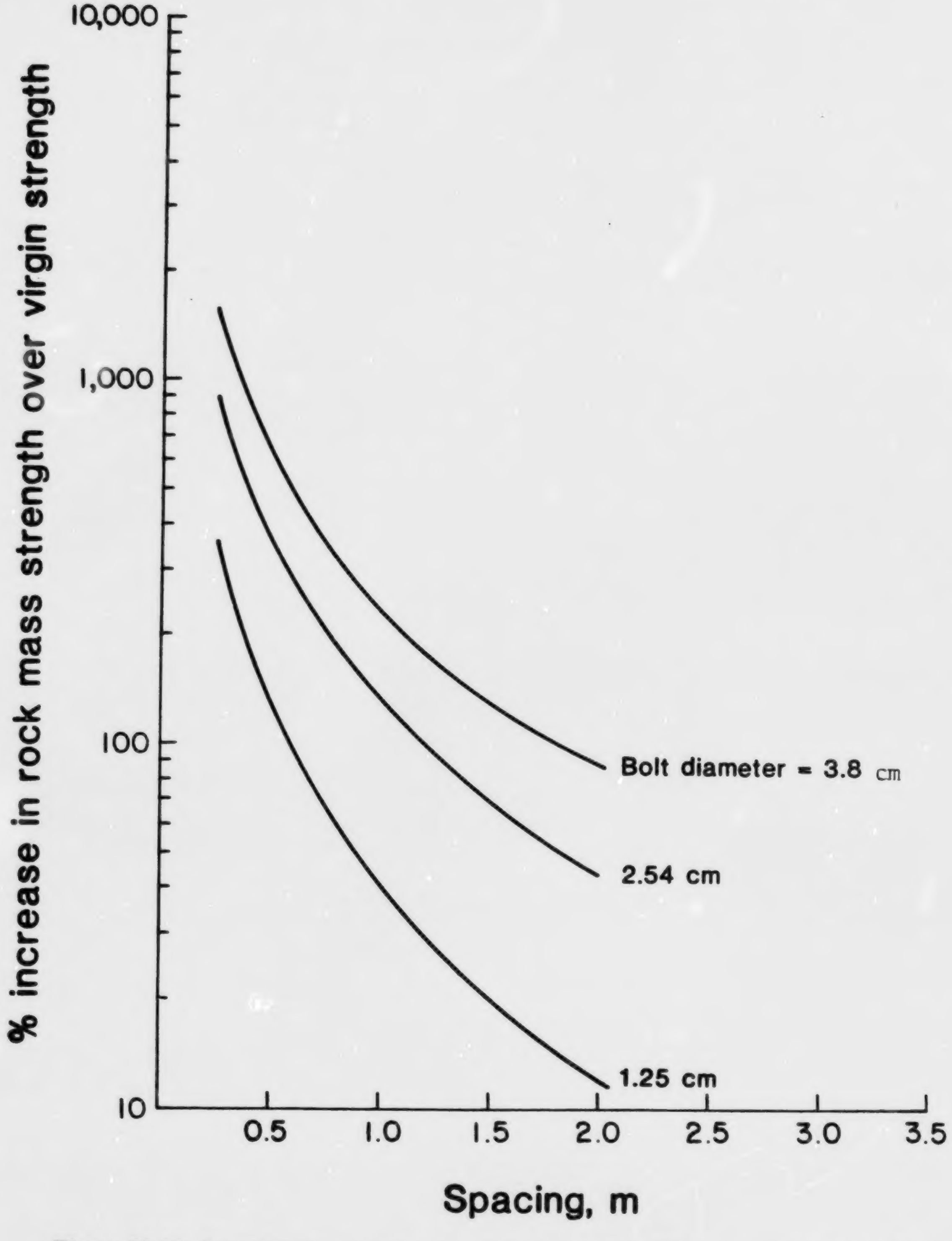

Figure 11.12 Percentage increase in rock mass strength vs. rock bolt spacing for various bolt diameters

(11.7) is possible with this boundary condition, so the value is made very small, say, 0.1%. At the other end of the range of rock quality, the extremely poor material with RMR = 10 would require very close bolt spacing to effect any significant improvement in strength. Figure 11.13 suggests spacings of 0.2 m or less are required to increase strength significantly. This estimated support density would indicate the need for spiling and heavy supports such as steel sets and lagging, rather than bolting. From Figure 11.8 it is seen that the percentage increase in strength approaches 20,000 percent for RMR = 10 and a spacing of 0.2 m. It is further assumed that this strength increase is sufficient to ensure a stable opening. With these two boundary conditions the constants in equation (11.17) can be determined:

$$P = e^{-0.153\ \mathrm{RMR} + 11.429} \qquad \ldots\ldots\ldots\ldots\ldots \qquad (11.18)$$

The spacings predicted by using equation (11.18) and then reading from Figure 11.8 are tabulated in the following Table:

TABLE 11.1 - PREDICTED PATTERN ROCK BOLT SPACING

RMR	Required Percentage Strength Increase	Bolt Spacing m
10	20,000	0.2
30	933	0.55
50	44	2.0
70	2	4.5

Rock bolt spacings of less than 1.2 m are seldom used for economic reasons. Therefore, this analysis suggests that this mode of rock bolt support (i.e. strength increase through confinement) cannot be made effective for economic reasons except for rock masses with RMR values of 45 or more. With higher quality rock masses (RMR > 45) the spacings are practicable, though the percentage change in strength is small because

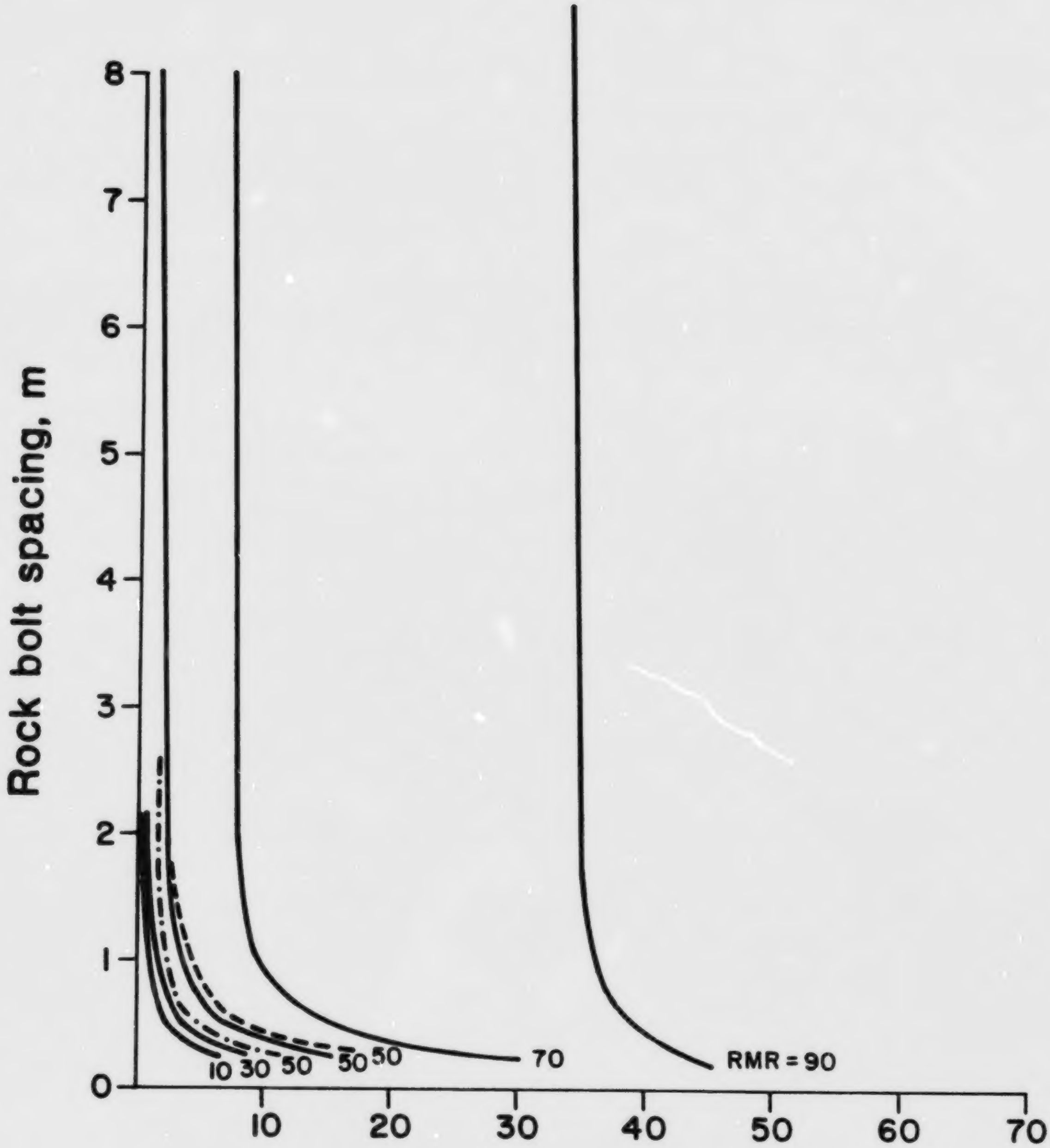

Figure 11.13 Tangential strength of rock in zone of uniform compression, MPa

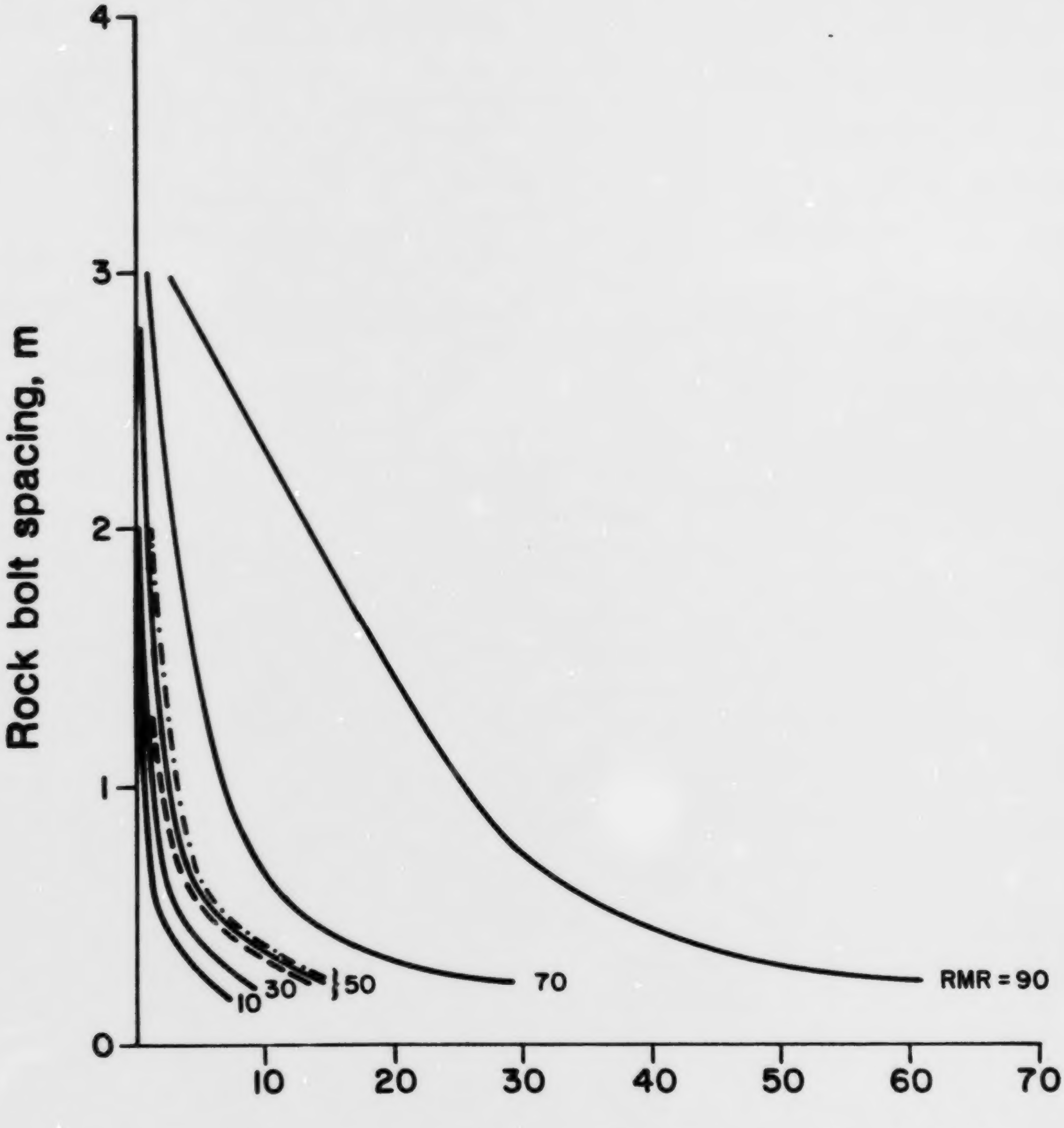

Figure 11.14 Strength of rock mass/m length of bolt

the rock mass already has considerable intrinsic strength (Fig.11.8). However, the specific strength, or strength of the rock mass per unit length of bolt, increases more rapidily with decreasing spacing for these higher quality materials than with lower quality rock masses (Fig. 11.14).

In order to produce overlapping zones (Fig. 11.2), the bolt length must be at least as long as the bolt spacing (equation (11.3)).

Krauland (1) has shown that longer bolts at wider spacings are more cost effective in Swedish conditions than many shorter bolts at smaller spacings.

Pattern bolting in very high quality rock masses (RMR > 80) is generally unnecessary and "spot" bolting is sufficient.

11.6 CONCLUSIONS

This analysis, which incorporates a realistic rock mass strength criterion, suggests that the "strength increase" mode of support does not produce significant changes to rock mass strength unless spacings are 0.5 m or less. It is concluded that the effectiveness of pattern bolting does not, therefore, reside in this mode of support.

New developments in equipment and materials leading to increased bolt installation rates and reduced unit costs are needed if rock bolt densities are to increase to levels at which this mode of support would be of significant effect.

REFERENCES

1. Krauland, N. Rock bolting and economy. Proceedings of the International Symposium on Rock Bolting, Abisko, Sweden, pp. 499-510 (1983).

2. Hoek, E. and Brown E.T. Underground Excavations in Rock. Institution of Mining and Metallurgy, London (1980).

3. Rosengren, K.J. and Jaeger, J.C. The mechanical properties of a low porosity interlocked aggregate. Geotechnique, Vol. 18, pp. 317-326 (1968).

4. Brown, E.T. Strength and models with intermittent joints. Journal of Soil Mechanics and Foundation Engineering Division, American Society of Civil Engineers, Vol. 96, No. SM6, pp. 1935-1949 (1970).

5. Barton, N.R. and Choubey, V. The shear strength of rock joints in theory and practice. Rock Mechanics and Engineering Geology, Vol. 10, Nos. 1,2, pp. 1-54 (1977).

6. Barton, N.R., Lien, R. and Lunde, J. Engineering classification of rock masses for the design of tunnel support. Rock Mechanics, Vol. 6, No. 4, pp. 189-236 (1974).

7. Bieniawski, Z.T. Rock mass classification in rock engineering. Proceedings of Symposium on Exploration for Rock Engineering, Johannesburg, Vol. 1, pp. 97-106 (1976).

CHAPTER 12

ROCK-BOLT SUPPORT INTERACTION ANALYSIS INCORPORATING TIMING OF INSTALLATION

12.1 GROUND CONVERGENCE AND SUPPORT REACTION

The loads developed on an untensioned rock bolt support system and therefore the support pressure applied to the rock, are dependent upon the response of the rock mass to excavation, the mechanical characteristics of the support unit, and the timing of installation.

Prior to excavation a point, B , (Fig. 12.1(a)) on the boundary of the proposed opening is subjected to the in-situ, or virgin stresses at that depth. As a result of excavation, the normal stress perpendicular to the opening at point B is reduced from p to zero with accompanying normal displacement, u, along line 00'. This is the ground convergence curve (Fig. 12.1(b)). Point 0' represents an equilibrium state; the opening is then stable without support. If rock failure occurs during the displacement along 00' and proceeds to ultimate collapse of the opening, the ground convergence curve would follow a line such as 00" (Fig. 12.1(b)). In such cases where failure would occur if the rock mass were unsupported, or where it is necessary to limit deformations of the opening, support must be provided.

If support is installed at some point during convergence it will provide an increasing support pressure as the opening continues to converge after installation. If the support unit has been adequately designed and installed, a point of equilibrium will be reached at E (Fig. 12.1(c)) and the opening will stabilize with an average support pressure, p_f, and a normal displacement, u_f. The line SS' is the support reaction curve of the support system.

Techniques for calculating the ground convergence reaction curve for circular

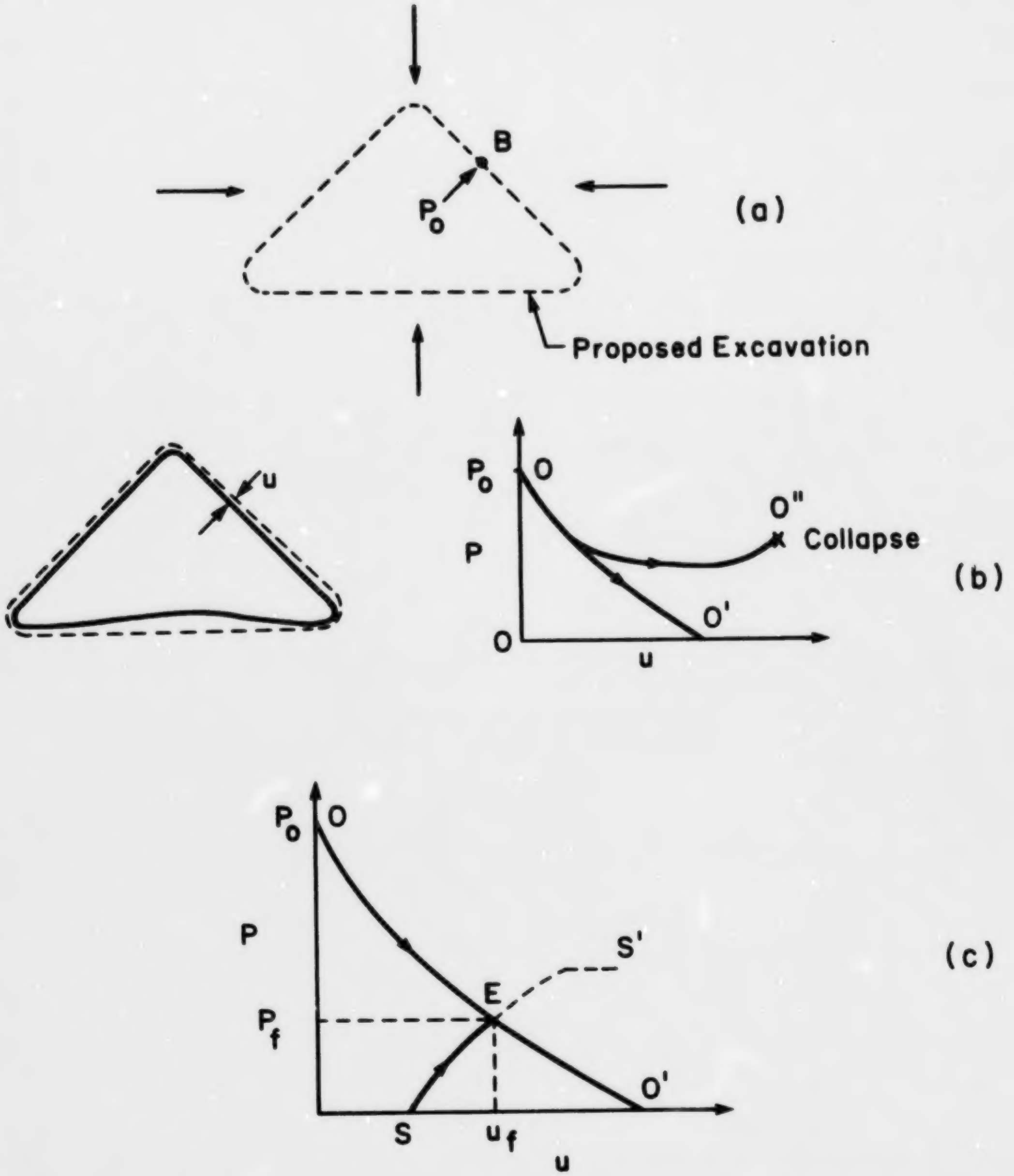
B
P_o
(a)
Proposed Excavation
u
P_o
O
O"
Collapse
P
(b)
O'
O
u
P_o
O
P
S'
(c)
E
P_f
O'
S
u_f
u

Figure 12.1 Ground convergence and support reaction curves (a) Normal stress, p_o, at B prior to excavation, (b) Ground convergence curves for stable and unstable cases, (c) Support reaction curve and point of equilibrium with ground convergence curve

openings in homogeneous, isotropic, rock under a hydrostatic state of stress are described by Hoek and Brown (1) and Brown, Bray, Ladanyi, and Hoek (2). The former publication also includes the formulae for determining the support reaction curves of the following types of support: shotcrete and concrete lining, blocked steel sets, and ungrouted anchors or point-anchor bolts. In this Chapter, methods are developed and illustrated for determining the ground convergence curve of bedded strata and the support reaction curve of grouted, untensioned bolts. These elements are then integrated into a general design procedure.

12.2 TIMING OF INSTALLATION

The total convergence does not take place instantaneously the moment the rock is excavated, even if the rock is elastic, because of the influence of the rock face. For an elastic rock mass convergence reaches a constant value at a distance, D , from the rock face (Fig. 12.2) and further excavation at the face will not result in any additional movement of this point.

If resin bolt supports are installed at or beyond the point at which elastic convergence ceases, no load can develop in the support, i.e., the support serves no useful purpose. The supports will be subjected to load if:

(a) The rock mass creeps, or its mechanical properties change with time due to such effects as weathering, fracturing, or opening of joints, etc.

(b) The external loads on the opening change due to excavation of adjacent openings.

(c) The rock swells as it interacts with groundwater flowing towards the excavation.

In all these cases loads on supports will generally increase with time and the supports will exert a stabilizing support pressure.

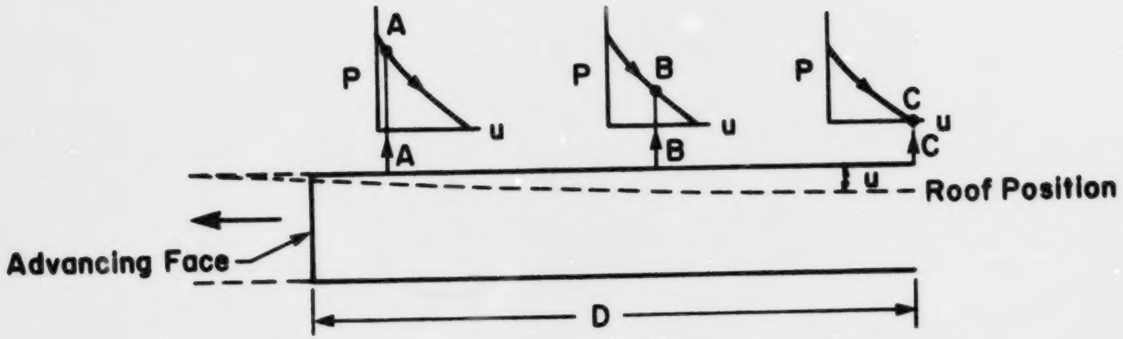
P
A
u
A
P
B
u
B
P
C
u
C
u
Roof Position
Advancing Face
D

Figure 12.2 Effect of face on roof convergence

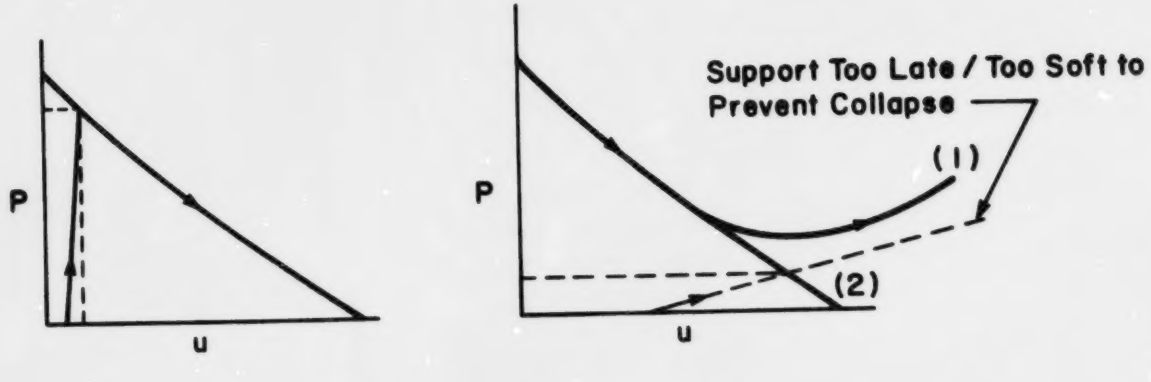

(a)

(b)

Figure 12.3 Effect of timing and support stiffness: (a) High stiffness support placed early, (b) Low stiffness support placed late (line 1 = unstable ground convergence curve, line 2 = stable ground convergence curve)

If stiff supports are placed close to the face they will develop high loads as excavation continues, but restrict displacements (providing they do not fail) (Fig. 12.3(a)). Alternatively, soft supports placed at some distance from the face will develop low support pressure with greater displacements (Fig. 12.3(b)), and if placed too late may be insufficient to support the roof (Fig. 12.3(c)). In mining, the latter case is of greatest significance since limiting the displacements around the opening is not generally of practical significance; the mine openings can fulfill their function as transportation corridors for ore, miners, air, and supplies, unless displacements become quite excessive.

12.3 GROUND CONVERGENCE CURVE FOR THE ROOF ABOVE A RECTANGULAR OPENING IN BEDDED STRATA

A detailed derivation of the ground convergence curve for a single roof layer above a rectangular opening is provided in Appendix I. For the purposes of this Chapter only the assumptions will be presented. Firstly, it is assumed that the single beam acts as an elastic, clamped beam that can be analysed by classical elastic beam theory. Thus, the maximum vertical displacement, u_{max}, is given by:

$$u_{max} = \frac{\gamma L^4}{32Et^2} \qquad \ldots\ldots\ldots\ldots\ldots \qquad (12.1)$$

where γ = density of roof beam

L = roof span

E = Young's modulus of roof beam

t = roof beam thickness.

The relationship betwen the two points, $p = p_o$, $u = 0$ and $p = 0$ and $u = u_{max}$, is linear (Fig. 12.4(a)). It is more convenient to plot this linear relationship in dimensionless terms (Fig. 12.4(b)):

$$\frac{u}{u_{max}} = 1 - \frac{p}{p_o} \qquad \ldots\ldots\ldots\ldots\ldots \qquad (12.2)$$

where $0 \leq p/p_o \leq 1$.

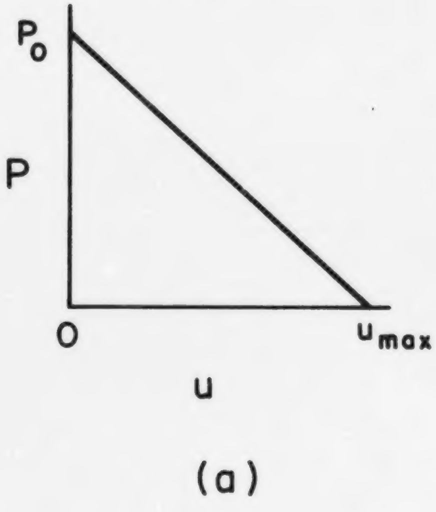

Figure 12.4 Ground convergence curve for a single, clamped, elastic beam, (a) p_o vs. u, (b) (p/p_o) vs. (u/u_{max})

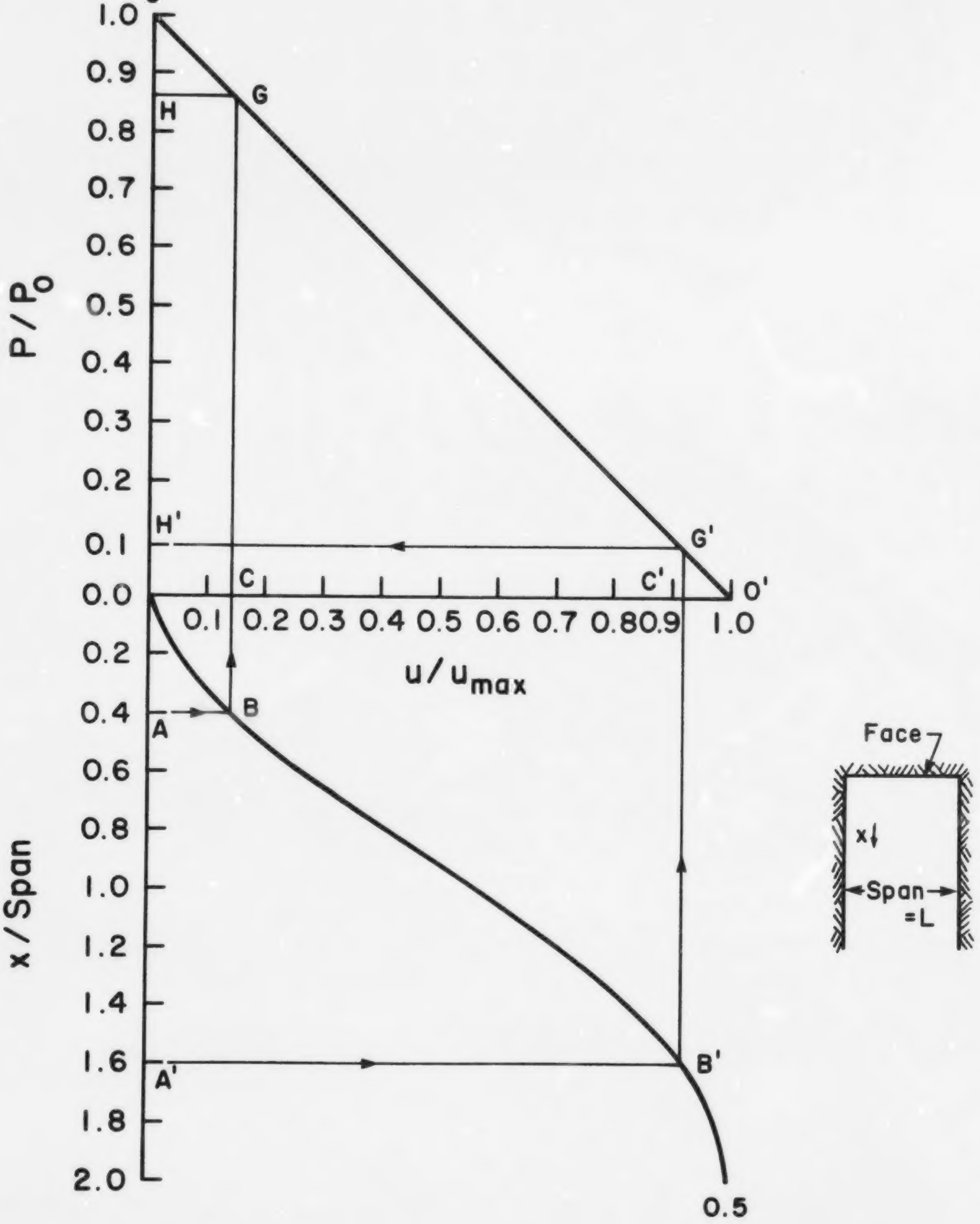

Figure 12.5 Relationship between ground convergence, required support pressure, and distance from face

Secondly, it is assumed that at a distance of 2 x span from the face, convergence is complete. This assumption is based on the solution for a rectangular clamped plate (Obert and Duvall (3)), which shows that once the ratio of the length of the plate to its width is greater than 2 the vertical displacement at the centre of the beam changes negligibly.

Thirdly, it is assumed that the shape of the convergence curve of the roof between the face and the point distant 2 x span from the face approximates the vertical deflection of a clamped beam between the abutment and the centre of the beam. This geometry leads to the following expression for the vertical displacement at distance, x , from the face ($0 \leq x \leq 2L$):

$$u = 16(x/4L)^2(1 - x/4L)^2 u_{max} \quad \ldots\ldots\ldots\ldots \quad (12.3)$$

where $0 \leq x \leq 2L$, and u_{max} is given by equation (12.1), or

$$\frac{u}{u_{max}} = 16(x/4L)^2(1-x/4L)^2 \quad \ldots\ldots\ldots\ldots\ldots \quad (12.4)$$

Equations (12.2) and 12.4) are plotted in a convenient form in Figure 12.5; the upper diagram is a graph of equation (12.2) and the lower diagram a graph of equation (12.4).

Suppose the span is 6 m. At a distance of 2.4 m from the face (point A) (Fig. 12.5) the convergence has reached 14% of maximum (point C) and the support pressure needed to prevent any further convergence equals 86% of the initial stress (point H). Similarly, at a distance of 9.6 m from the face (point A') the convergence has reached 92% of maximum (point C') and the support pressure needed to prevent any further convergence equals 8.6% of the initial stress (point H').

The initial stress, p_o , is given by:

$$p_o = \gamma t \quad \ldots\ldots\ldots\ldots\ldots \quad (12.5)$$

where γ = density of beam

t = beam thickness.

If the roof fails during convergence any supports installed prior to the failure will have to sustain an increased load if overall stability is to be maintained. This may be modelled by assuming that failure of the beam occurs where the horizontal tensile (fibre) stress first reaches the tensile strength of the material. For an elastic, clamped beam, this occurs over the abutments. After tensile failure, it is assumed the beam now acts as a simply supported beam. In this case the maximum vertical deflection is given by:

$$u = \frac{5\gamma L^4}{32Et^2} \qquad \ldots\ldots\ldots\ldots\ldots (12.6)$$

Note that the maximum deflection at the centre of the failed beam is five times larger than that for the unfailed beam (Eqn.(12.1)). The normal ground reaction curves for the failed and unfailed beams are shown in Figure 12.6 (the displacement axis has been normalized with respect to u_{max} for the unfailed beam).

Suppose an unsupported, newly excavated 8 m span fails in tension above the abutments when the face has advance 8 m (point A, Fig. 12.6). This corresponds to a convergence of 57% of the maximum (point C). Therefore, support should be installed such as to reach an equilibrium point with the ground convergence curve before 57% convergence is reached. If line CG' represents the support reaction curve of the bolts installed after the face has advanced 5.0 m equilibrium will not be established in time and the roof beam will fail. Stress on the support will then increase to almost 78% of the initial stress (point E). This increase may be sufficient to fail the bolts. If the same support were installed earlier so as to just come into equilibrium as the roof beam reaches the critical convergence limit, the support stresses would be reduced to 45% of the initial stress (point F).

Failure of the roof also considerably increases displacements. For the two cases just considered the failed beam undergoes twice the amount of convergence of the unfailed beam (compare points D and G in Figure 12.6).

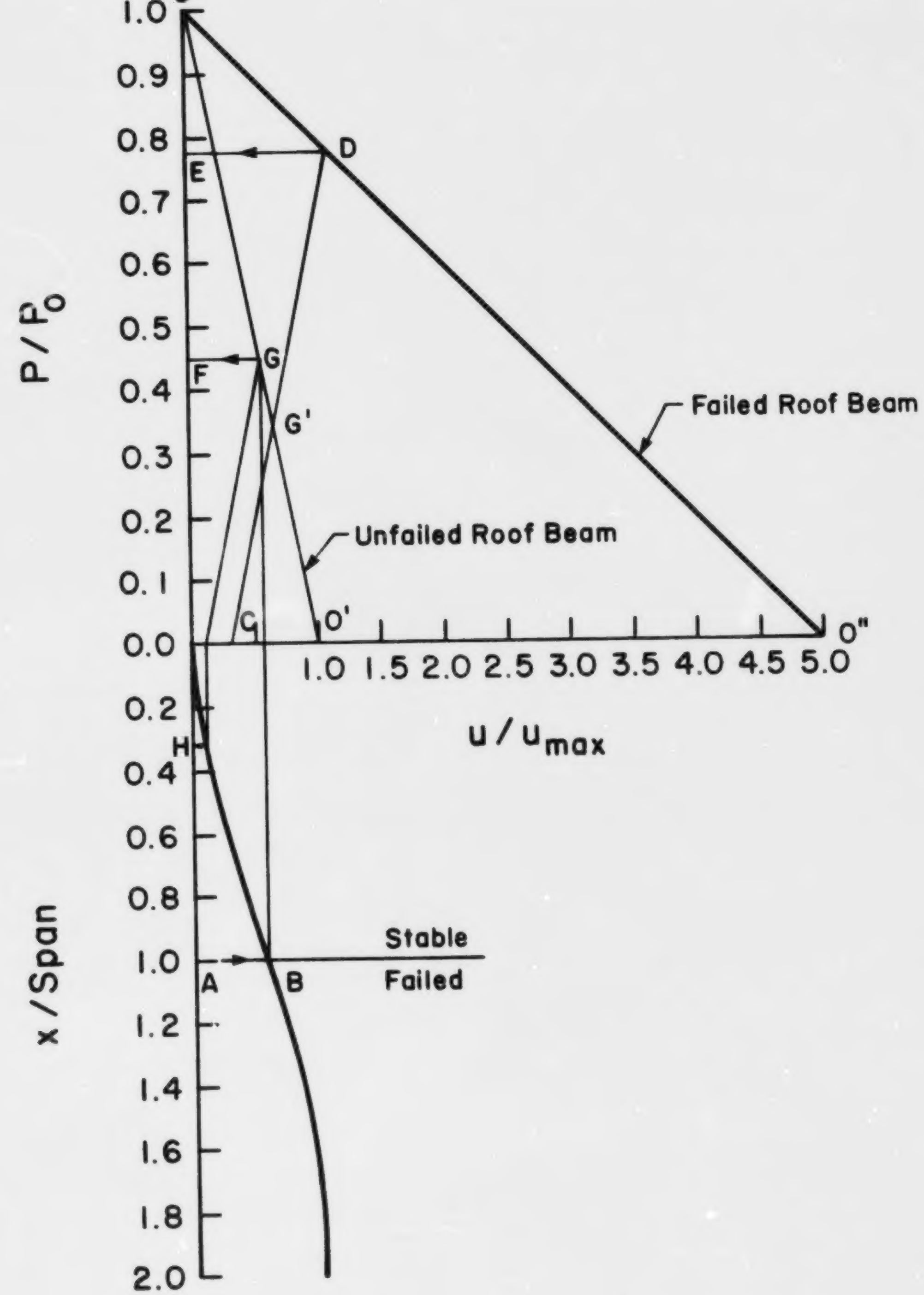

Figure 12.6 Relationship between ground convergence, required support pressure, and distance from face for failed and unfailed roof beams

12.4 SUPPORT REACTION CURVE OF A PATTERN OF GROUTED, UNTENSIONED BOLTS

12.4.1 Basic Formulae

A detailed derivation of the formula for the support reaction curve of a pattern of grouted, untensioned bolts is provided in Appendix J. For a single beam above a rectangular opening, span L, in which bolts are installed with a spacing of s_s across the span and s_a along the opening the support reaction curve is given by:

$$\frac{p}{p_o} = \frac{Ku}{u_{max}} \qquad \text{..............} \quad (12.7)$$

$$K = \frac{\pi d_1^2\ E_b(1+(E_g/E_b)\dfrac{(d_2^2-d_1^2))L^4}{d_1^2}}{128E_r\ t^3{}_a\ s_s\ l} \qquad \text{..............} \quad (12.8)$$

where d_1 = bolt diameter

d_2 = hole diameter

E_b = Young's modulus of bolt material

E_g = Young's modulus of grout

E_r = Young's modulus of rock, and

l = equivalent length of grouted bolt

t = beam thickness

The maximum support stress, p_{max}, a bolt can provide, or the maximum stress it can support, is given by:

$$p_{max} = \frac{T}{s_s\ s_a} \qquad \text{..............} \quad (12.9)$$

where T = pull-out strength of grouted bolt.

In terms of normalized stresses:

$$\frac{p}{p_o} = \frac{T}{\gamma\, t\, s_a\, s_s} \qquad \text{..............} \quad (12.10)$$

12.4.2 Sensitivity Study

The sensitivity of the normalized support reaction curve (Eqn.(12.8)) to the various parameters was examined by establishing a base case and changing each variable in turn while keeping all others constant. The base case was as follows:

Bolt diameter, d = 2.0 cms
Hole diameter, d = 2.8 cms
Young's modulus of bolt material, E_b = 207 GPa
Young's modulus of grout, E_g = 5.8 GPa
Young's modulus of rock, E_r = 4.8 GPa
Roof beam span, L = 6 m
Roof beam thickness, t = 0.3 m
Bolt spacing across span, s_s = 1 m
Bolt spacing along opening, s = 1 m
Equivalent length of grouted bolt (0.5 x thickness of layer requiring support + length of anchorage) = 2 m

Bolts installed 3.7 m from the face.

The sensitivity of the support reaction curve to each variable is represented by plotting each curve on a (p/p_o) vs. u/u_{max} diagram. As might be anticipated, the rock bolt spacing is an important variable. For example, in Figure 12.7 the support pressure is increased from 50% to 65% of the initial stress in decreasing bolt spacing from 2.5 m to 1.25 m while displacements are reduced from 54% to 41% of maximum.

Figures 12.8-12.10 illustrate sensitivity to Young's moduli of rock and bolt and to bolt diameter. The trends in Figure 12.10 appear contradictory until it is realized that the horizontal axis of the plot has been normalized with respect to u_{max} ; the latter increases with decreasing Young's modulus of the roof beam. Figure 12.10 is particularly instructive as it shows that bolts in weak roofs (low E_r) will develop high

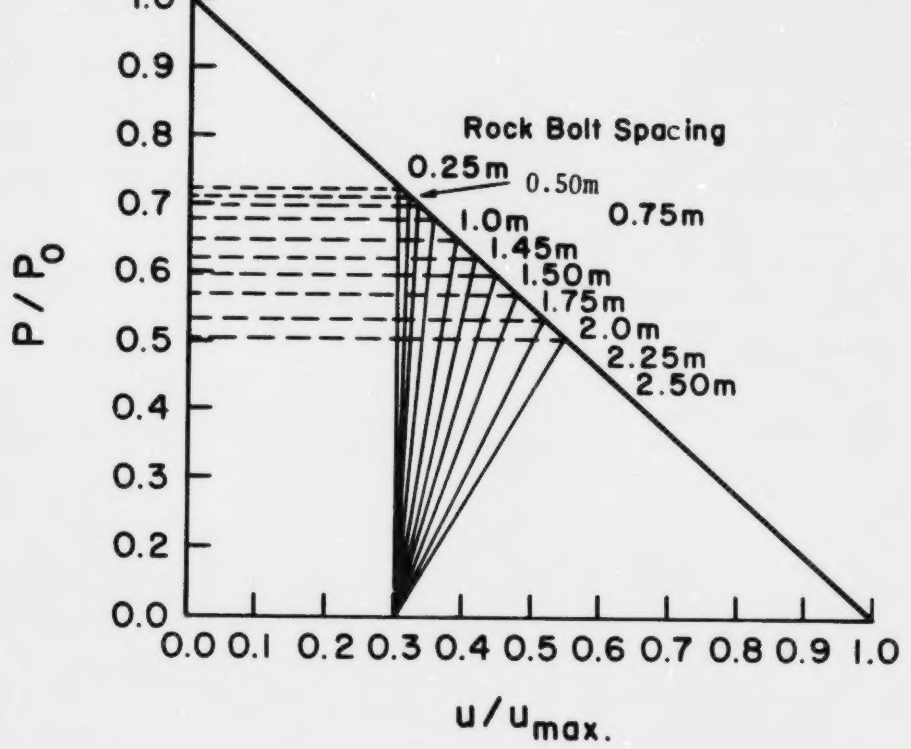

Figure 12.7 Effect of rock bolt spacing on normalized support reaction curve

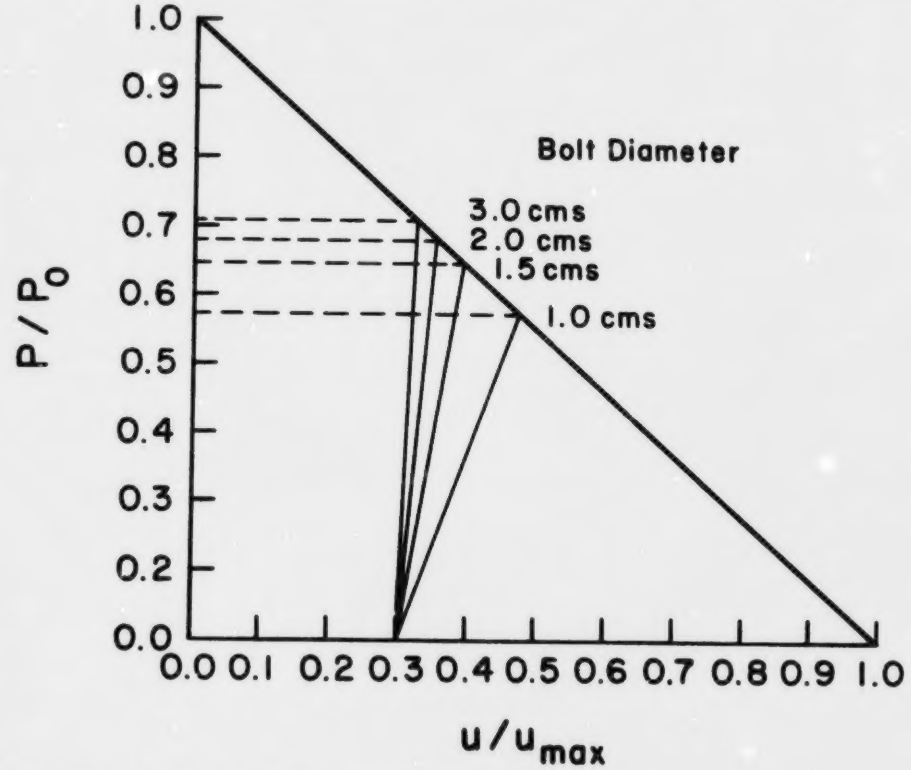

Figure 12.8 Effect of rock bolt diameter on normalized support reaction curve

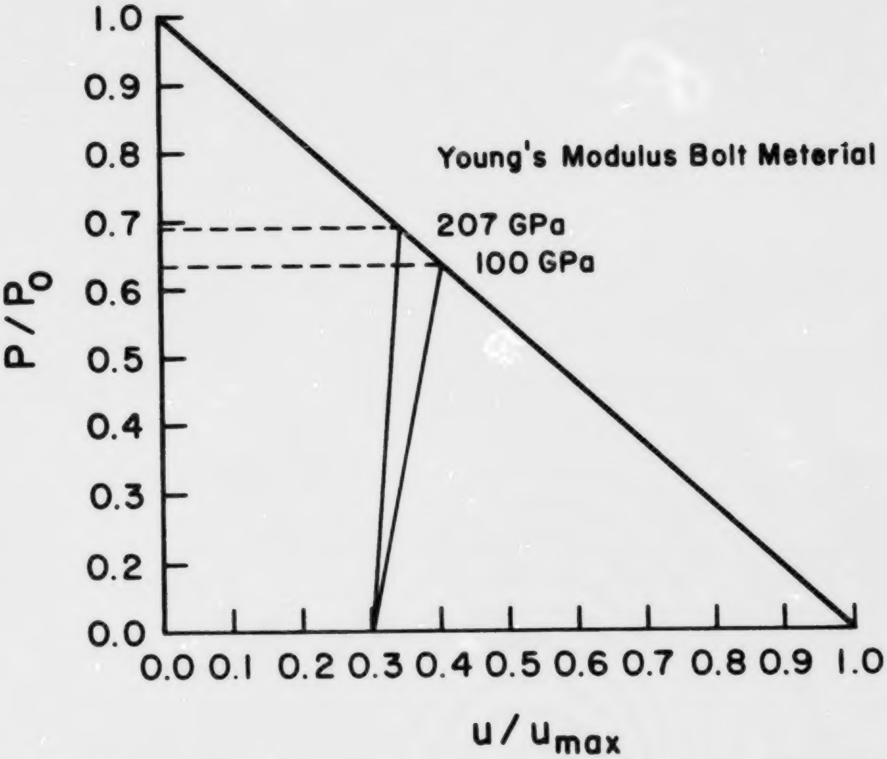

Figure 12.9 Effect of Young's modulus of bolt material on normalized support reaction curve

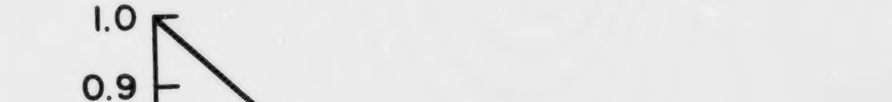

Figure 12.10 Effect of Young's modulus of rock on normalized support reaction curve

loads if installed too early. At the same time, if they are installed too late the roof may fail. The solution is to place bolts early and with a sufficiently close spacing that the high loads generated do not exceed the pull-out strength of the bolts.

The modulus of the grout and the thickness of the grout annulus around the bolt were both found to have a negligible effect on the normalized support curve, i.e., changes in grout properties and thickness cannot be used to effect changes in support pressures.

Figure 12.11 graphically demonstrates the importance of roof span. The same bolt pattern installed in a large span will develop significantly higher support pressures and bolt loads at equilibrium than for short spans.

A similar trend is shown with roof beam thickness (Fig. 12.12). For the same bolt pattern bolts will be subjected to a greater proportion of the initial stress, p_o, at equilibrium for a thin roof beam than for a thick roof beam. However, in this case, the initial stress is directly proportional to beam thickness so the absolute loads will show the reverse, e.g., for a 0.1 m thick beam the support pressure is $0.72 \times \gamma \times 0.1 = 0.072\gamma$ and for the 0.4 m thick beam is $0.62 \times \gamma \times 0.4 = 0.248\gamma$, i.e., approximately 3 times larger for the thicker beam.

Finally, (Fig. 12.13) a pattern with short bolts provides higher support pressures than one with long bolts because the axial stiffness of the short bolt is greater. On the other hand, the pull-out strength of a short bolt may be less than that of a longer bolt. The critical bolt length beyond which pull-out strength is constant should be determined by in-situ testing.

12.5 UNGROUTED, POINT-ANCHOR BOLTS VS. GROUTED BOLTS

The axial stiffness for a pattern of ungrouted, point-anchor bolt is given by Hoek and Brown (1) as:

$$K = \frac{1}{s_a\ s_s((4\ell/\pi d_1^2\ E_b) + Q)} \quad \ldots\ldots\ldots\ldots \qquad (12.11)$$

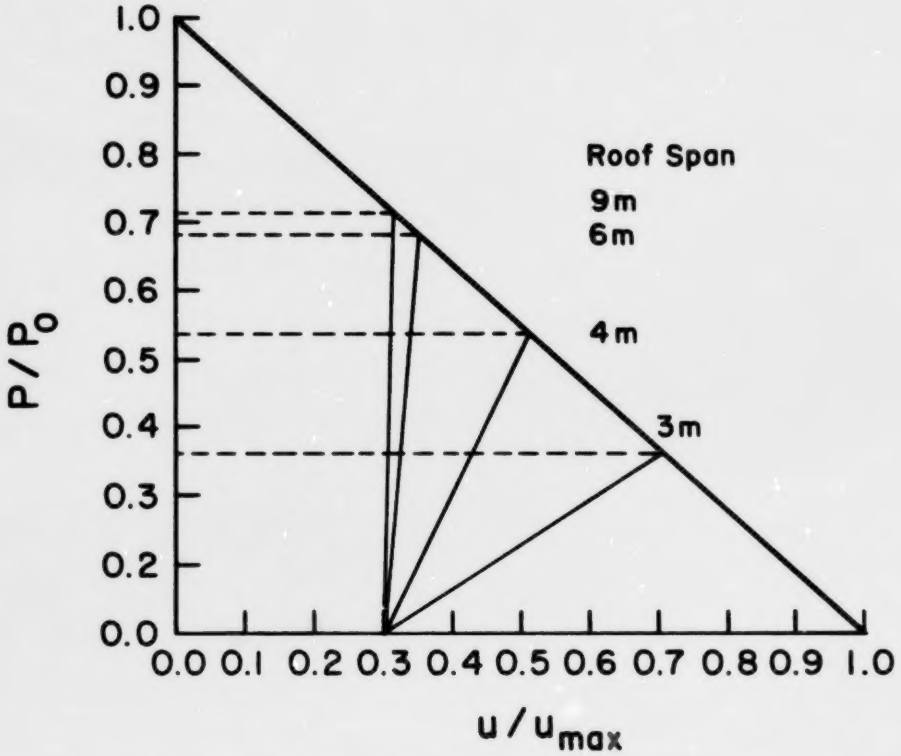

Figure 12.11 Effect of roof span on normalized support reaction curve

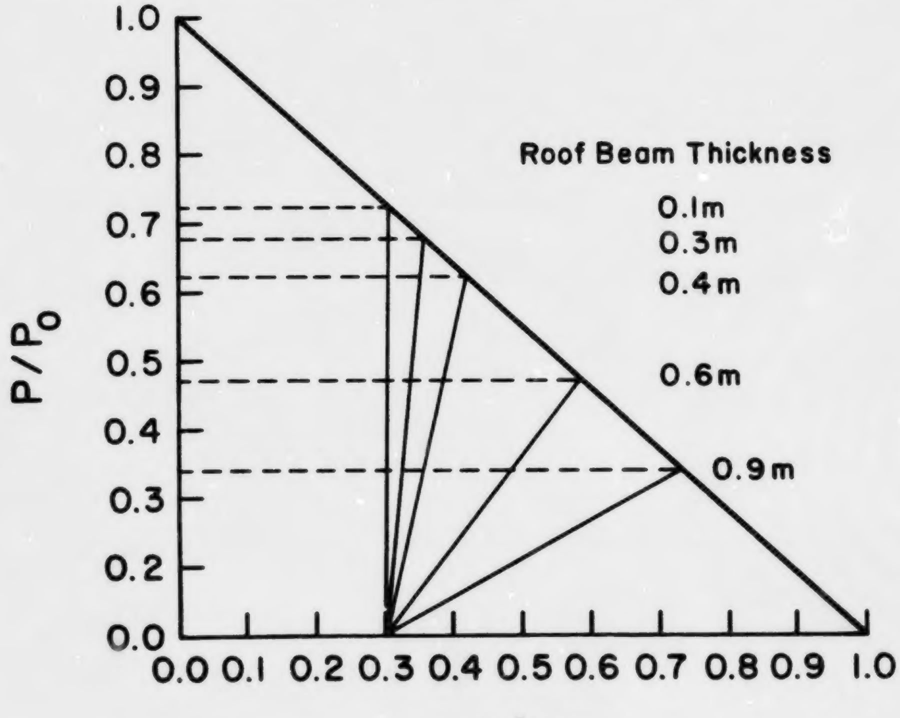

Figure 12.12 Effect of roof beam thickness on normalized support reaction curve

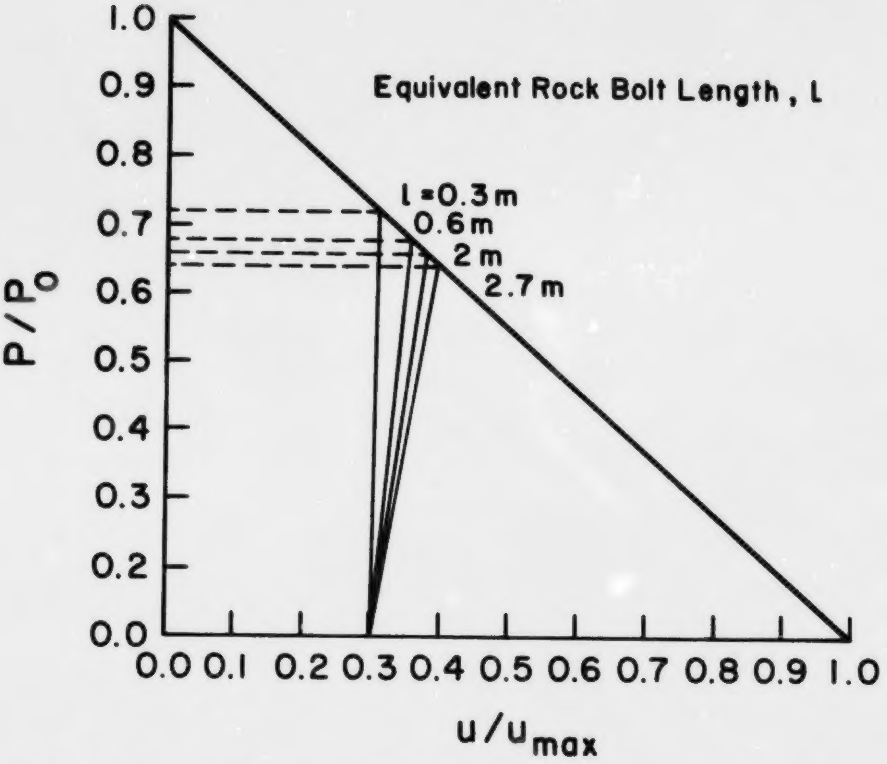

Figure 12.13 Effect of anchorage length on normalized support reaction curve

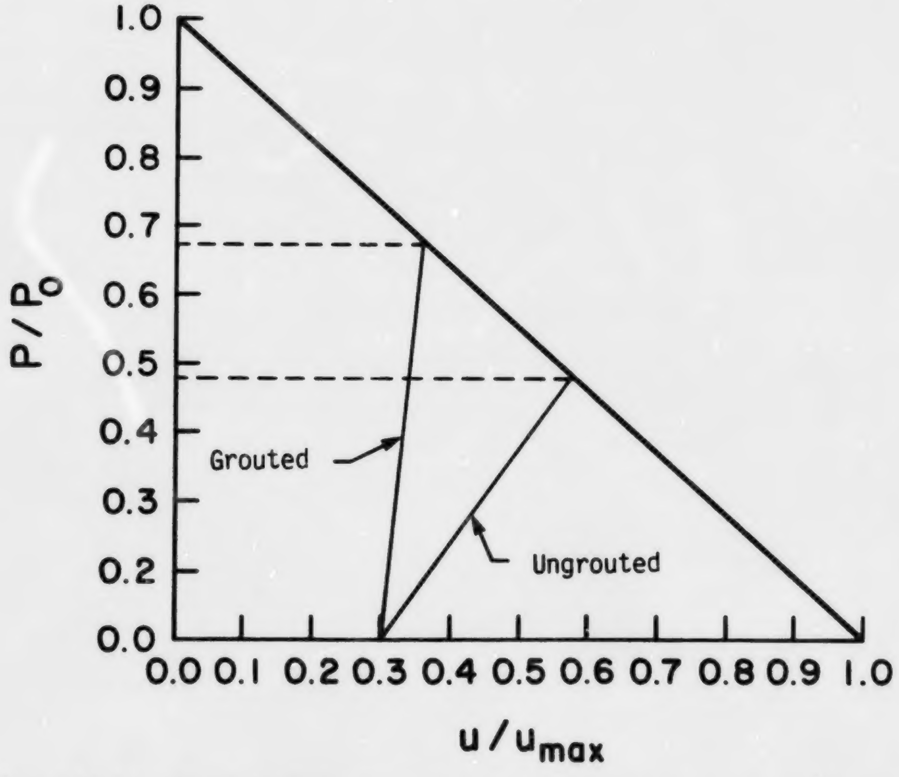

Figure 12.14 Comparison of normalized support reaction curve of an ungrouted, point anchor system and a grouted bolt system

where l = bolt length

Q = quantity related to the load-deformation characteristics of the anchor, washer plate and bolt head,

and the other variables are as in Equation (12.10).

In terms of normalized co-ordinates and the roof beam problem:

$$\frac{p}{p_o} = \frac{KL^4}{32\,E_b\,t}\;\frac{u}{u_{max}} \qquad \text{..............} \quad (12.12)$$

Figure 12.14 is a comparison between the support curve for the base case used above for the grouted bolt sensitivity study, and that for an ungrouted, point-anchor with the same rock and bolt properties and bolt pattern. In addition, a typical value for Q = 0.143 m/MN is assumed. Clearly, the ungrouted, point-anchor bolt is less effective in controlling displacements.

Another comparison can be made by finding the spacing of ungrouted, point-anchor bolts necessary to maintain the same support pressure and limit the convergence to the same magnitude as obtained with the following grouted bolt pattern:

Bolt diameter = 2 cms

Hole diameter = 2.8 cms

Young's modulus of bolt = 207 GPa

Young's modulus of grout = 5.8 GPa

Young's modulus of rock = 4.8 GPa

Roof beam span = 6 m

Roof beam thickness = 0.3 m

Bolt length = 2.5 m

Square bolt pattern = 1.5 m x 1.5 m

Assuming the same rock bolt length and a Q value of 0.143 m/MN, it may be shown that the ungrouted, point-anchor bolts would need to be spaced on a square pattern at 0.6 m x 0.6 m. For a 6 m span the total quantity of bolts required for the latter spacing would be approximately 5 times greater than for the wider spacing for a continuous length of opening.

12.6 APPLICATION TO DESIGN OF BEDDED MINE ROOFS

The theory developed above applies to a single layer, but its extension to multi-layer roofs is described by means of an example.

12.6.1 Design Problem

A roof bolting pattern is to be designed for a 6 m span rectangular opening in which the geometry and mechanical properties of the roof strata are as illustrated in Figure 12.15. A 0.2 m thick layer of coal is left to provide some support and protection to a 0.3 m thick layer of weak shale. The uppermost bed considered in the design is a 1.2 m thick sandstone layer.

12.6.2 Design Stages

The first step in design is to calculate the maximum deflection of each bed from equation (12.1) and determine which beds deflect sufficiently to rest upon, and therefore load lower beds. In such cases an estimate of the increased loading is made and the deflection of the loaded beam, due to the increased load, is calculated. In turn, the additional movement may cause this bed to contact the bed below. Obviously, the design must proceed in an iterative manner until a stable solution is attained.

Two design methods for this step are suggested; one provides a lower bound prediction of loads and the other an upper bound. In either case, the approach is to calculate an effective increased density for the lower beam resulting from the external loading.

Lower Bound:

Where one layer rests on the layer below its full weight is not transmitted to the

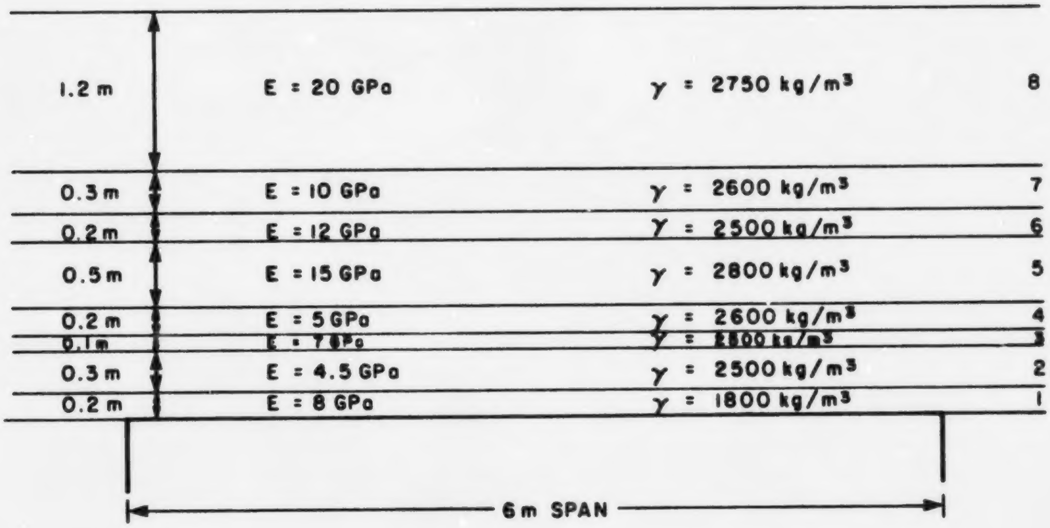
1.2 m
E = 20 GPa
γ = 2750 kg/m³
8
0.3 m
E = 10 GPa
γ = 2600 kg/m³
7
0.2 m
E = 12 GPa
γ = 2500 kg/m³
6
0.5 m
E = 15 GPa
γ = 2800 kg/m³
5
0.2 m
E = 5 GPa
γ = 2600 kg/m³
4
0.1 m
E = 7 GPa
γ = 2500 kg/m³
3
0.3 m
E = 4.5 GPa
γ = 2500 kg/m³
2
0.2 m
E = 8 GPa
γ = 1800 kg/m³
1
6 m SPAN

Figure 12.15 Roof strata conditions for design problem

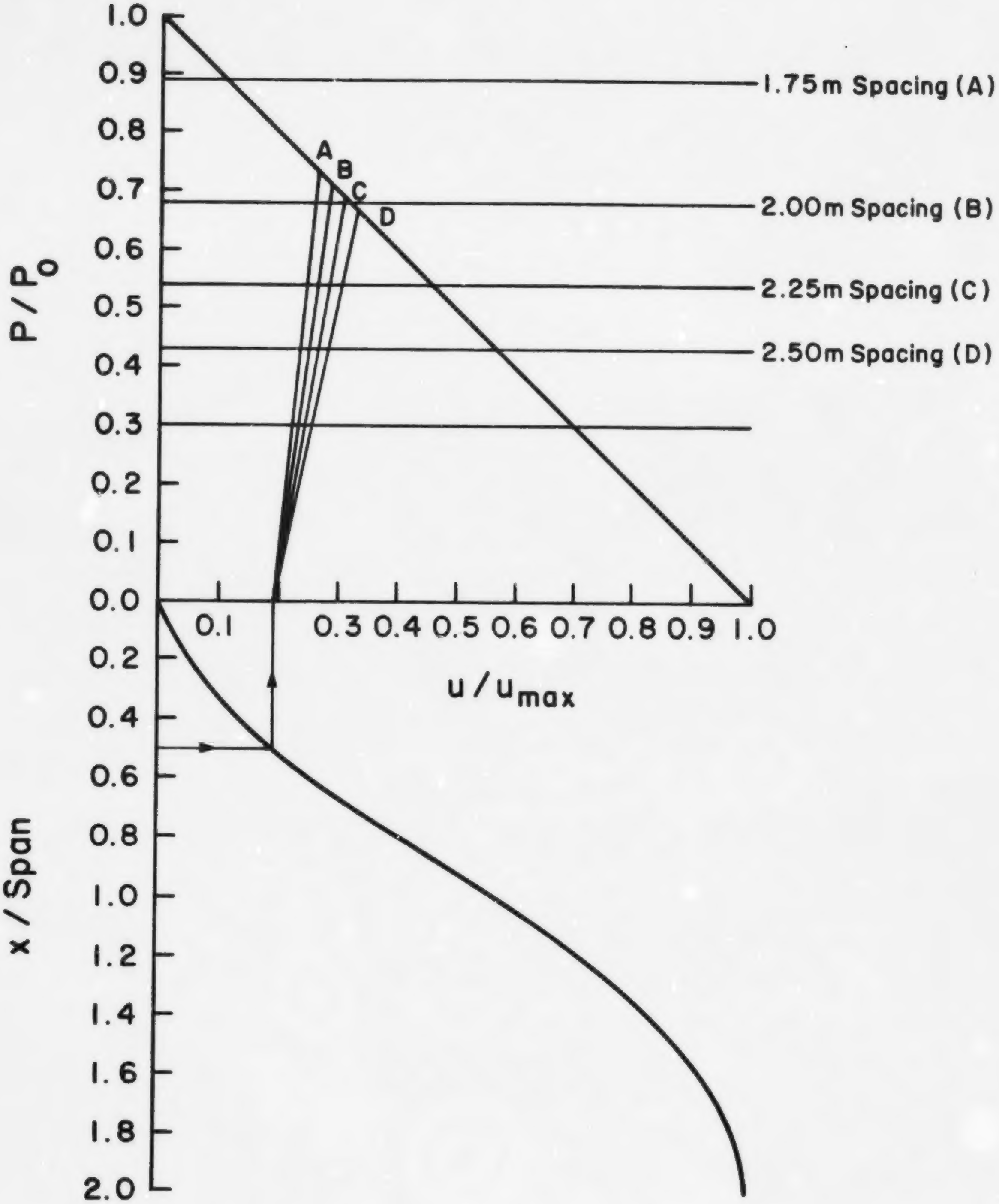

Figure 12.17 Ground convergence-support reaction analysis of layer #1, upper bound on equivalent density

lower layer because it has some capacity to support itself. From Peng (4), the effective density, γ_e, of the lower beam loaded from above by (n-1) layers, where n is the number of layers in contact with each other in the group, is:

$$\gamma_e = \frac{E_1\ t_1^2(\gamma_1\ t_1 + \gamma_2\ t_2 + \ldots\ldots\ldots + \gamma_n\ t_n)}{E_1\ t_1^3 + E_2\ t_2^3 + \ldots\ldots\ldots\ E_n\ t_n^3} \qquad \ldots\ldots\ldots \quad (12.13)$$

where E_n, t_n, and γ_n are the Young's modulus and thickness, and density of the n strata, with n = 1 for the lowest bed in the sequence.

Upper Bound:

If the stiffnesses of the beds, which are already loading the lower bed, decrease with time (e.g. weakening from exposure, water, creep), increasing loads will be experienced by the lower layer. Also, if there are other joint sets, in addition to orthogonal cross-joints, which would prevent the development of arching by creating conditions for individual blocks to separate from the rest of the layer (e.g. wedges free to fall out under gravity, if unsupported), greater loads will develop than those predicted by equation (12.13). In the limit, the full load of the upper beams will be exerted and the equivalent density of the lower bed is then given by:

$$= \frac{\gamma_1\ t_1 + \gamma_2\ t_2 + \ldots\ldots\ldots + \gamma_n\ t_n}{t_1 + t_2 + \ldots\ldots\ldots\ t_n} \qquad \ldots\ldots\ldots \quad (12.14)$$

Applying equation (12.13) iteratively to the strata sequence shown in Figure 12.15, it can be shown that the beds act in three groups as follows:

1) Bed 1 is loaded by beds 2, 3 and 4. Its effective density is between 2588 kg/cu.m. (lower bound) and 9400 kg/cu.m. (upper bound).

2) A bed separation occurs between bed 4 and bed 5.

3) Bed 5 is loaded by beds 6 and 7. Its effective density is between 4485 kg/cu.m. (lower bound) and 5360 kg/cu.m. (upper bound).

4) A bed separation occurs between bed 7 and bed 8.

5) Bed 8 is assumed to act on its own since data on higher beds are not given.

At this stage the stability of the layers #1, #5 and #8 is assessed using the two-hinge beam theory developed in Chapter 10. To allow for external loading of the beam the theory uses a force/weight multiplier term from which the magnitude of the external loading can be calculated. For example, if the beam is 0.2 m thick and the force/weight multiplier is 5.0, then the external loading is equivalent to 5 times the beam thickness, i.e., 5 x 0.2 m = 1 m thickness of rock.

The multiple beam analysis described above determines the equivalent density of the lower beam in each group of beams, e.g., layer #1 in group 1-4, layer #5 in group 5-7. The force/weight multiplier can be determined from this value as follows:

Let absolute density of bottom layer = γ_1
Let equivalent density of bottom layer = γ_{1e}
Let thickness of bottom layer = t_1
Let total thickness of group = T

Then weight, W_a , of beds above bottom layer in group

$$(\gamma_{1e} - \gamma_1)t. \qquad \text{..............} \quad (12.15)$$

Weight of bottom layer,

$$W_b = \gamma_1 t \qquad \text{................} \quad (12.16)$$

Therefore, force/weight multiplier

$$= W_a / W_b = \frac{(\gamma_{1e} - \gamma_1)}{\gamma_1} \qquad \text{..............} \quad (12.17)$$

The input data and results of a 2-hinge analysis of layers 1 and 5 are as follows:

Layer 1:

Uniaxial compressive strength of intact rock = 10 MPa

Uniaxial compressive strength of crushed rock = 0 MPa

Cross-joint spacing = 1 m

Friction angle of cross-joints = 40 deg.

For lower bound on effective density, force/weight multiplier = 0.44

Factor of Safety against 2-hinge collapse = 9.1

For upper bound on effective density, force/weight multiplier = 4.2

Factor of Safety against 2-hinge collapse = 0.95

Layer 5:

Uniaxial compressive strength of intact rock = 50 MPa

Uniaxial compressive strength of crushed rock = 20 MPa

Cross-joint spacing = 0.3 m

Friction angle of cross-joints = 45 deg.

For lower bound on effective density, force/weight multiplier = 0.6

Factor of Safety against 2-hinge collapse = 55.1

For upper bound on effective density, force/weight multiplier = 0.91

Factor of Safety against 2-hinge collapse = 36.4

Therefore, layer #1 is unstable only for the higher loading and layer #5 is stable for all loading conditions. (Note: the stability of layer #5 is dependent on the development of a flat arch (see Chapter 10). The presence of inclined joints could invalidate such an assumption).

On the basis of this analysis, it is decided to design a bolt pattern for 1.8 m long bolts, which extend to the top of layer #7.

The first step is to determine the normalized pull-out strength (Eqn.12.10) and the system axial stiffness (Eqn.12.8) for various possible rock bolt spacings. The values used in these two equations are as follows:

Bolt diameter = 2 cms

Hole diameter = 2.8 cms

Young's modulus of grout = 5.8 GPa

Young's modulus of layer #1 = 8.0 GPa

Pull-out strength after applying a Factor of Safety of 2.0 = 50 kN

Table 12.1 tabulates the values of normalized pull-out strength and system axial stiffness for various rock bolt spacings. Axial stiffness is listed as a slope in degrees, as this eases plotting.

TABLE 12.1
NORMALIZED PULL-OUT STRENGTHS AND SYSTEM AXIAL STIFFNESSES

	Normalized Pull-Out Strength (Eqn. 12.10)		System Axial Stiffness (Eqn. 12.8)
Bolt spacing, m	Lower Bound	Upper Bound	Deg.
1.0	9.85	2.71	88.1
1.25	6.30	1.74	87.0
1.50	4.38	1.20	85.7
1.75	3.22	0.89	84.2
2.00	2.46	0.68	82.5
2.25	1.95	0.54	80.5
2.50	1.58	0.43	78.3
3.00	1.09	0.30	73.4

From this Table, it may be seen that for the lower bound solution a single central bolt (spacing 3 m) would be sufficient to support the roof. This result is presented graphically in Figure 12.16 which illustrates the case of bolt installation at a distance of 3 m from the face. The slope of the line A'A is 73.4°, corresponding to the axial stiffness of the single bolt system. The normalized pull-out strength is shown by the horizontal line at the top of the diagram. The bolt load (0.62 p/p_o) at equilibrium (point A) is considerably less than the normalized pull-out strength (1.09 p/p_o).

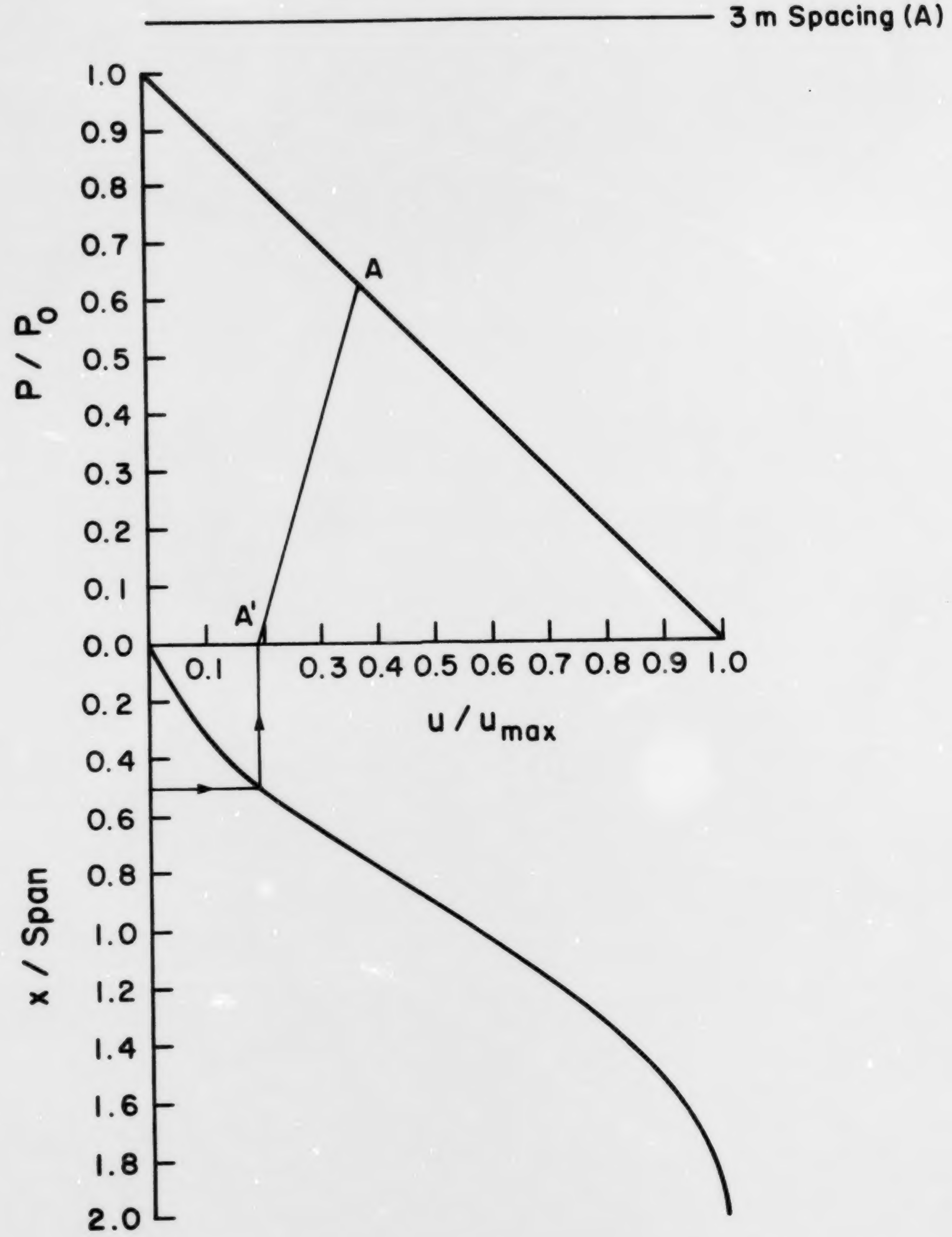

Figure 12.16 Ground convergence-support reaction analysis of layer #1, lower bound on equivalent density

For the upper bound solution the normalized pull-out strength is less than 1.0 for all rock bolt spacings less than 1.75 m. The associated system axial stiffnesses are plotted in Figure 12.17. The normalized bolt load at equilibrium is less than the normalized pull-out strength for rock bolt spacings of approximately 1.9 m or less. Given that the Factor of Safety on rock bolt strength was 2.0 an average spacing of 2.0 m could be tolerated.

The final step is to assess the effect of the loading of layers #1-4 on layers #5-7 in which the bolts are anchored. Load transfer to the latter group can be modelled as an increase in their effective density. Let the thickness of the lower layer of the anchor beds be T_1 and the thickness of the lowest layer of the supported beds be t_1 over a span L. The normalized bolt load at equilibrium, K, (e.g. point A in Fig. 12.16) is transferred to the upper beds and is given by:

$$K = p/p_o \qquad \ldots\ldots\ldots\ldots\ldots \quad (12.18)$$

Therefore,

$$p = Kp_o$$
$$= K\gamma_{1e}\,t_1 \qquad \ldots\ldots\ldots\ldots\ldots \quad (12.19)$$

where γ_{1e} is effective density of lowest bed in the lower group of beds.

Total load applied to upper beds

$$= LK\gamma_{1e}\,t_1 \qquad \ldots\ldots\ldots\ldots\ldots \quad (12.20)$$

Volume of lowest bed in upper group

$$= LT_1 \qquad \ldots\ldots\ldots\ldots\ldots \quad (12.21)$$

Therefore, increase in effective density of lower bed in upper group of beds is, from Equations (12.20) and (12.21)

$$= \frac{LK\gamma_{1e}\,t_1}{LT_1}$$

$$= K\gamma_{1e}\frac{t_1}{T_1} \qquad \ldots\ldots\ldots\ldots\ldots \quad (12.22)$$

In the example above, for the upper bound solution in which for a design bolt spacing of 2.00 m

$K = 0.71$

$T = 0.5$

$t = 0.2$

$\gamma_{1e} = 9400$ kg/cu.m.

Therefore, substituting these values in Equation (12.22):

$= 2670$ kg/cu.m.

The 2-hinge analysis is then reapplied to the upper group of beds to determine if the increased load will result in its instability.

There will be four loading cases to examine, leading to four different force/weight multipliers (Eqn.(12.17)). The four cases comprise:

	Lower Bed Equivalent Density	Upper Bed Equivalent Density
1.	Upper Bound	Upper Bound
2.	Upper Bound	Lower Bound
3.	Lower Bound	Upper Bound
4.	Lower Bound	Lower Bound

For design, cases 1 and 4 should be examined to provide the worst and best scenarios, respectively. For the design problem under study these two end cases provide equivalent densities for layer #5 of 8030 kg/cu.m. and 5188 kg/cu.m., respectively. A 2-hinge analysis of layer #5 under the conditions of increased loading leads to a reduction in the Factor of Safety against collapse to 13.8 in the worst case.

Suppose it had been necessary to consider bolting into layer #8. A second analysis would then have been necessary to consider the stability of the intermediate group anchored in layer #8. Once again the load transfer from the lowest group must be included as outlined above. The bolt length = half thickness of layers #5-7 + thickness of layer #8 = 1.7 m. The results of a complete ground convergence-support reaction analysis for layer #5 are shown in Figures 12.18 and 12.19; even for the worst case (Fig. 12.19) the bolt pull-out strength is not exceeded.

12.6.3 Design of Intersection

For a 4-way intersection the effective span across the diagonal is 8.5 m. A worst case analysis of this situation with the same geometric and mechanical rock properties as before is illustrated in Figure 12.20 and indicates that the bolt spacing should be reduced to about 1.75-1.85 m.

12.7 EFFECT OF ROOF FAILURE ON BOLT LOADINGS

The ground reaction curves used to this point model the reaction of layers which do not fracture following bolt installation, i.e., the bolt and ground come to a point of equilibrium before fracturing can develop. Should a roof fracture (but not collapse) with the bolt pattern in place it is to be expected that loads will increase on the bolts. For example, assume that prior to fracture a layer behaves as a clamped beam but after fracture as a simply supported beam (Fig. 12.21). Beam theory shows that vertical displacements of the latter are 5 times larger than for the clamped beam.

Suppose that this type of roof fracture develops when an unsupported roof is separated from the face by a distance equal to the span (point A in Fig. 12.22). At this stage the vertical displacement of the layer has reached 56% of ultimate. Now assume that bolts are installed at a distance of 0.8 x span from the face (point D in Fig. 12.22) and that the bolt system has an axial stiffness represented by line FG. At point G the roof will fracture. To continue with this analysis the same line, XY, in Figure 12.22, can be used to represent the ground reaction curves for the unfailed and failed layer by a change of scale. From point G the upper scale must be used to find the point of equilibrium between the bolting system and the now fractured roof layer. As can be seen, the support resistance required increases from 0.33 p if the roof had

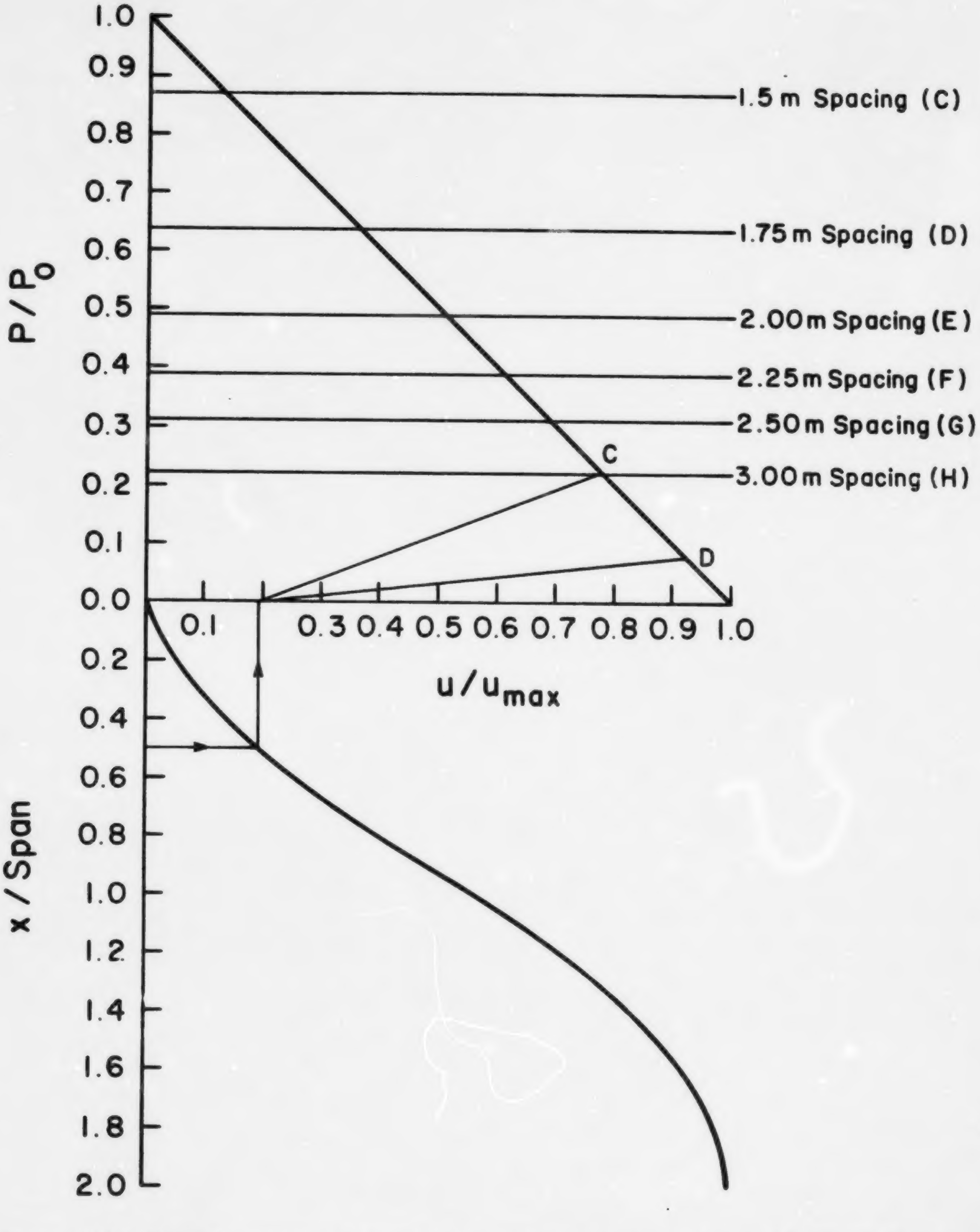

Figure 12.18 Ground convergence-support reaction analysis of layer #5, lower bound on equivalent density

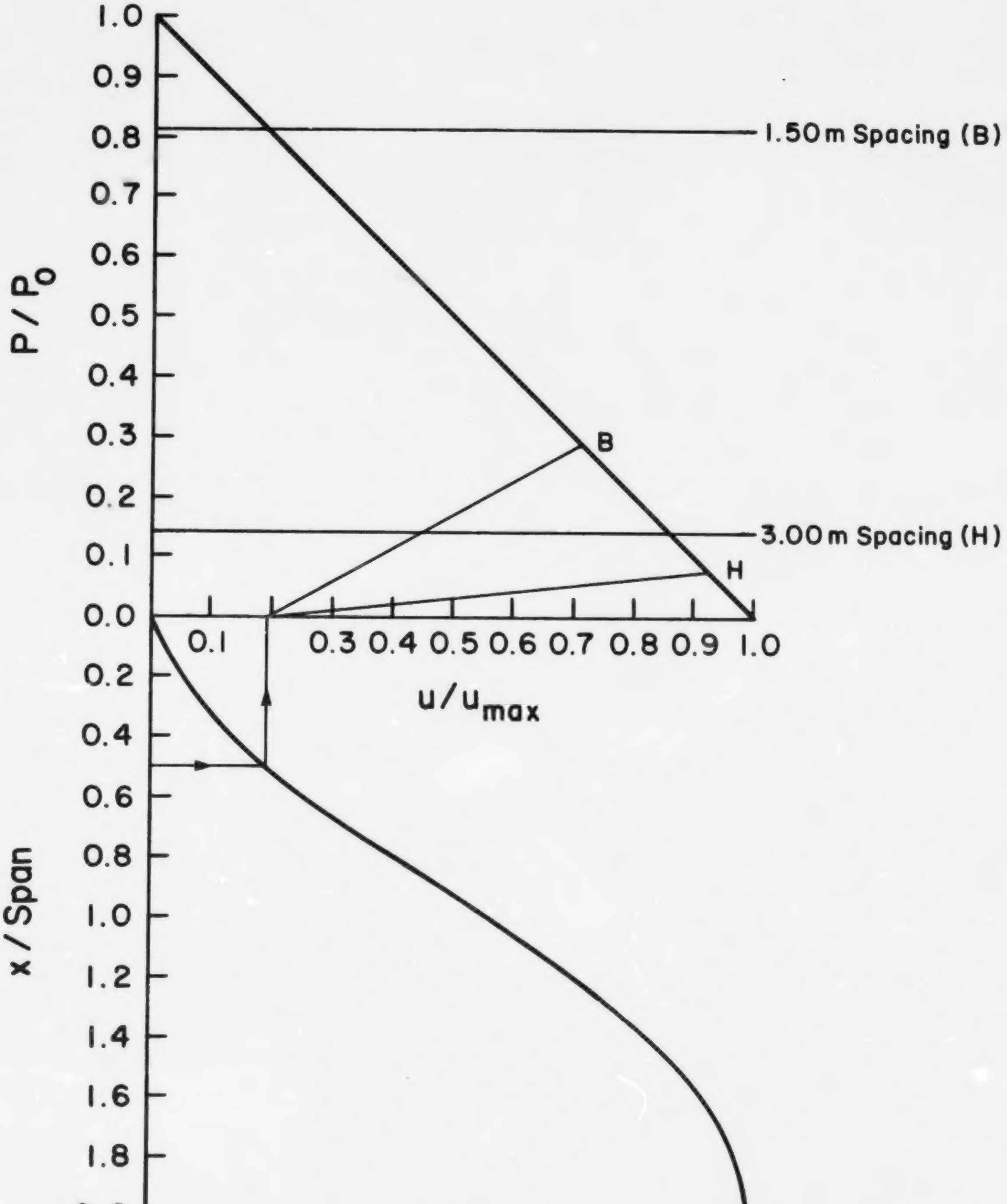

Figure 12.19 **Ground convergence-support reaction analysis of layer #5, upper bound on equivalent density**

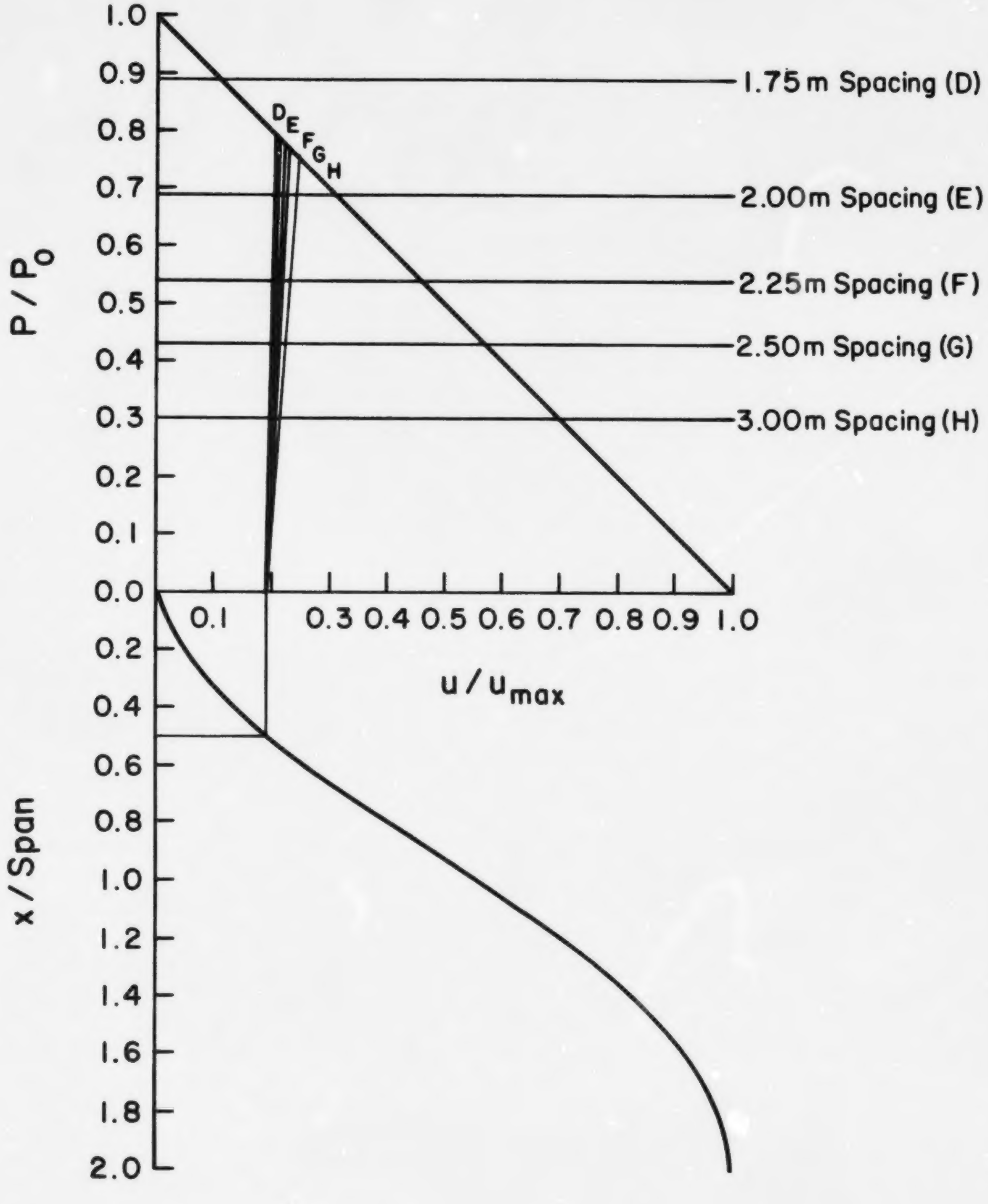

Figure 12.20 Ground convergence-support reaction analysis of layer #1 at intersection, upper bound on equivalent density

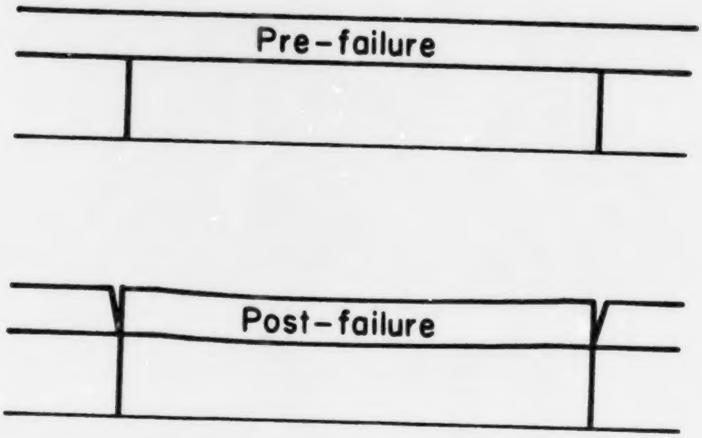
Pre-failure
Post-failure

Figure 12.21 Assumed pre-failure and post-failure state of roof layer

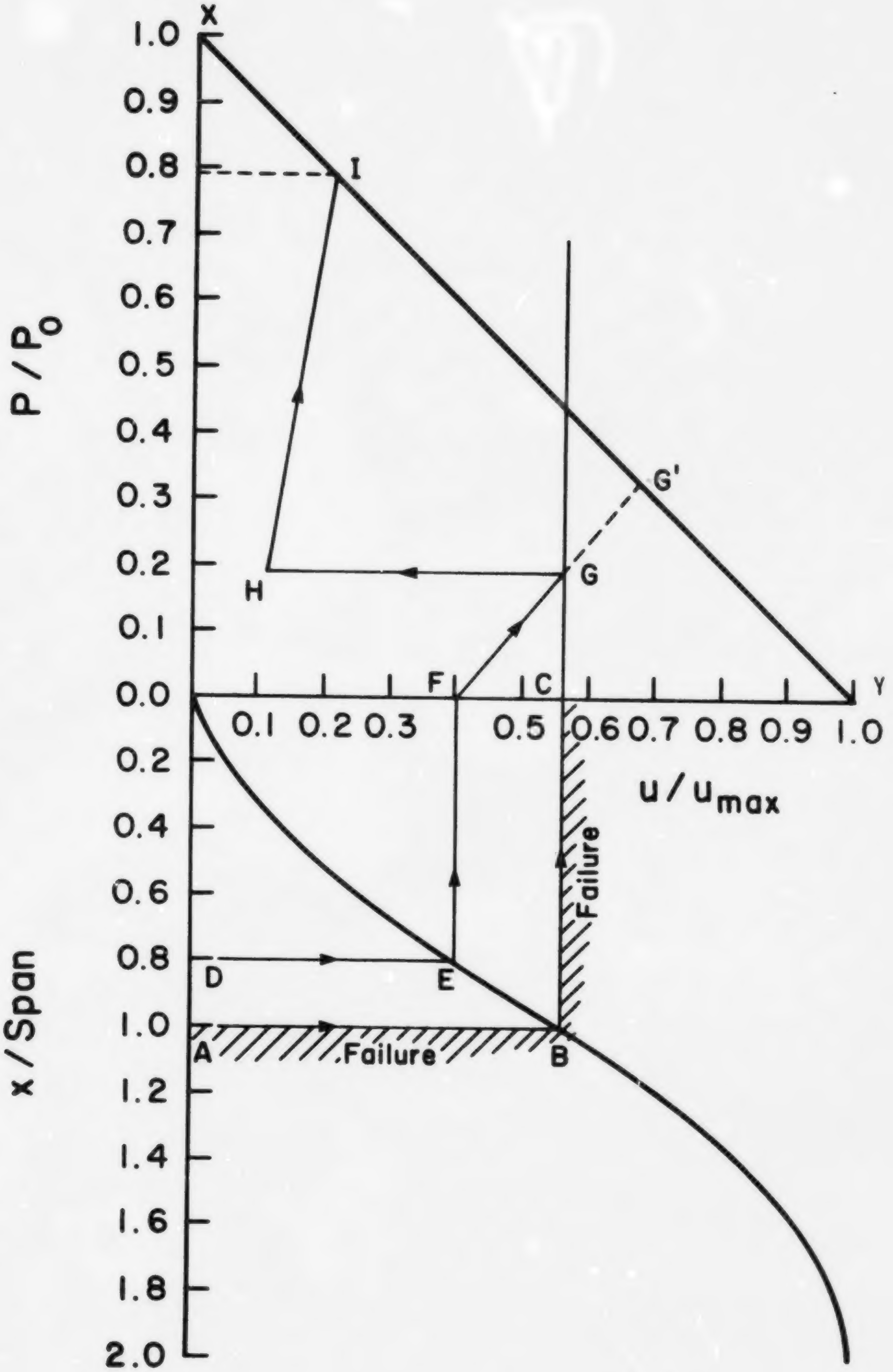

Figure 12.22 Ground convergence-support reaction analysis for a layer which fractures after bolt installation

not fractured (point G') to 0.79 p after fracture. This increase could lead to bolt pull-out. Four possible solutions for avoiding overstressing of bolts include (a) use of bolts at the same spacing, but with greater axial stiffness, (b) closer bolt spacing but retaining the same bolts, (c) earlier installation of bolt and retaining the same bolts, and (d) some combination of (a), (b) and (c).

12.8 CONCLUSIONS

A new design method for bolting of multiple layer roofs has been proposed based on the ground convergence-support reaction principle and 2-hinge collapse theory. Further work to define the technique and to translate it into a practical design tool is considered necessary. Details are given in the final Chapter of this report.

REFERENCES

1. Hoek, E. and Brown, E.T. Underground excavation in rock. Institution of Mining and Metallurgy, London (1980).
2. Brown, E.T., Bray, J.W., Ladanyi, B., and Hoek, E. Ground response curves for rock tunnels.
3. Obert, L. and Duvall, W.I. Rock mechanics and the design of structures in rock. Wiley & Sons, Inc. (1967).
4. Peng, S.S. Coal mine ground control. Wiley & Sons (Inc), (1978).

CHAPTER 13

INCLINED BOLTS

13.1 INTRODUCTION

Most modern rock bolting drilling equipment allows for the drilling of inclined holes. In this Chapter the effect of rock bolt inclination on support and reinforcement of mine roofs will be examined from the viewpoint of general pattern bolting of horizontally bedded strata.

13.2 EXPERIMENTAL DATA

The influence of bolt inclination has been determined experimentally by means of laboratory direct shear tests. Bjurstrom (1) conducted tests on 45 cm long, jointed rock blocks. His results are summarized in Figure 13.1 and clearly exhibit the existence of an optimum angle for bolting in the range of 45-60°. Haas (2) examined the direct shear strengths of joints bolted at 45° and 90° to the discontinuity surface (Fig. 13.2). A significant improvement in strength was found for the 45° angle. It is also of interest that failure of boits at this inclination occurred after shear displacements of about 2.5 cm, whereas for the 90° installation the equivalent figure was 6.5 to 7.5 cms. As Barton (3) has suggested, this indicates that there may be some advantage in using a low-alloy strain-hardening steel as a bolt material where large displacements need to be tolerated. Similar tests by Azur et al (4) showed greatest shear resistance when the bolt was installed at 30°.

13.3 THEORETICAL MODELS

It is useful to consider the behaviour of discontinuities bolted with inclined bolts and subjected to direct shear in two ways:

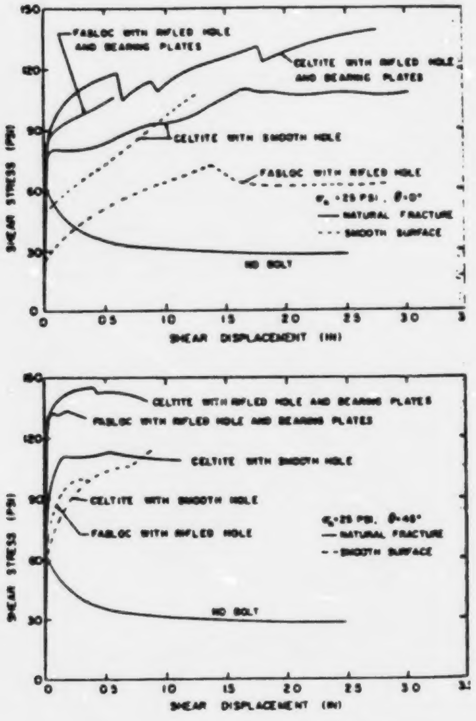

Figure 13.1 Results from laboratory direct shear box tests on bolted joints (after (2))

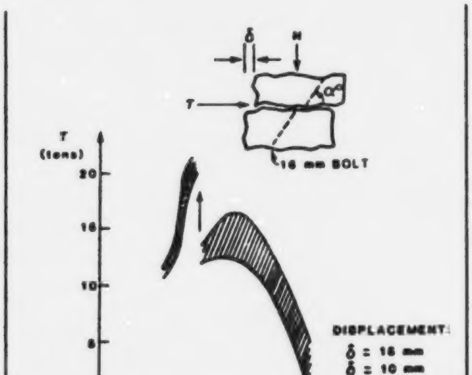

Figure 13.2 Results from laboratory direct shear box tests on bolted joints (after (1))

a) Ultimate resistance or strength

b) Shear stiffness or incremental resistance to shear displacement.

For each case, the role of bolt inclination is now examined from a theoretical basis.

13.3.1 Ultimate Shear Resistance or Strength

When an inclined bolt suffers relative movement across a discontinuity it provides resistance in two ways. First, the axial tensile loads developed in the bolt resist displacement. Clearly, this tensile effect is only mobilized when the bolt is inclined correctly with respect to the sense of relative motion across the discontinuity (Fig. 13.3).

Suppose the axial load in a bolt inclined at degrees to the discontinuity (Fig. 13.4) at some instant is P . Then, the total shear resistance, SR , mobilized by the force, P , is:

$$SR = P\cos\theta + P\sin\theta\tan\phi \qquad \ldots\ldots\ldots\ldots\ldots \qquad (13.1)$$

where ϕ is the effective angle of friction along the discontinuity.

Figure 13.5 is a graph of Equation (13.1) for a range of friction angles. It demonstrates there is a critical angle of installation at which the mobilized shear resistance, SR , reaches a maximum value. The critical installation angle, θ_{crit} , may be found by differentiating Equation (13.1) with respect to θ and equating to zero. This analysis shows that in order to optimize the tensile effect bolts should be installed at an angle equal to the effective angle of friction of the potential slip surface, i.e., $\theta = \phi$.

Figure 13.5 also indicates that although there is an optimum installation angle, the mobilized shear resistance is relatively insensitive to variations from this angle.

A component of force normal to the discontinuity is also developed as a result of dilation of the joint block during shearing when the surface is rough.

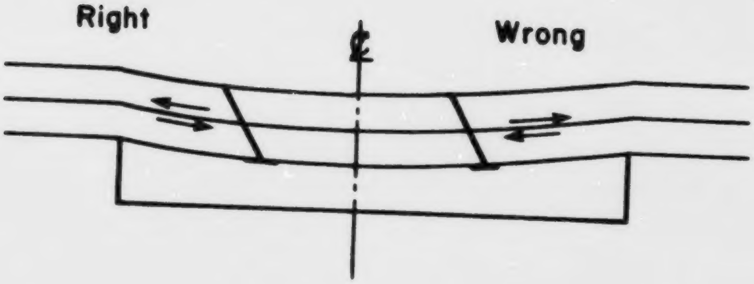
Right
℄
Wrong

Figure 13.3 Exploiting tensile behaviour of bolt by appropriate inclination of bolts in bedded mine roof

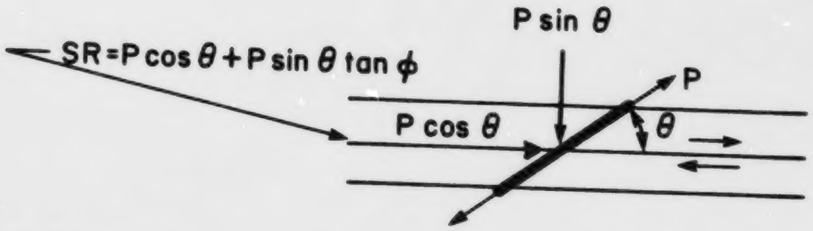
P sin θ
SR = P cos θ + P sin θ tan φ
P
P cos θ
θ

13.4 Development of tensile load in inclined bolt due to differential slip along bolted joint

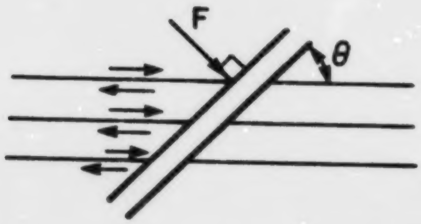

13.5 Shear strength developed by components of tensile load in bolt

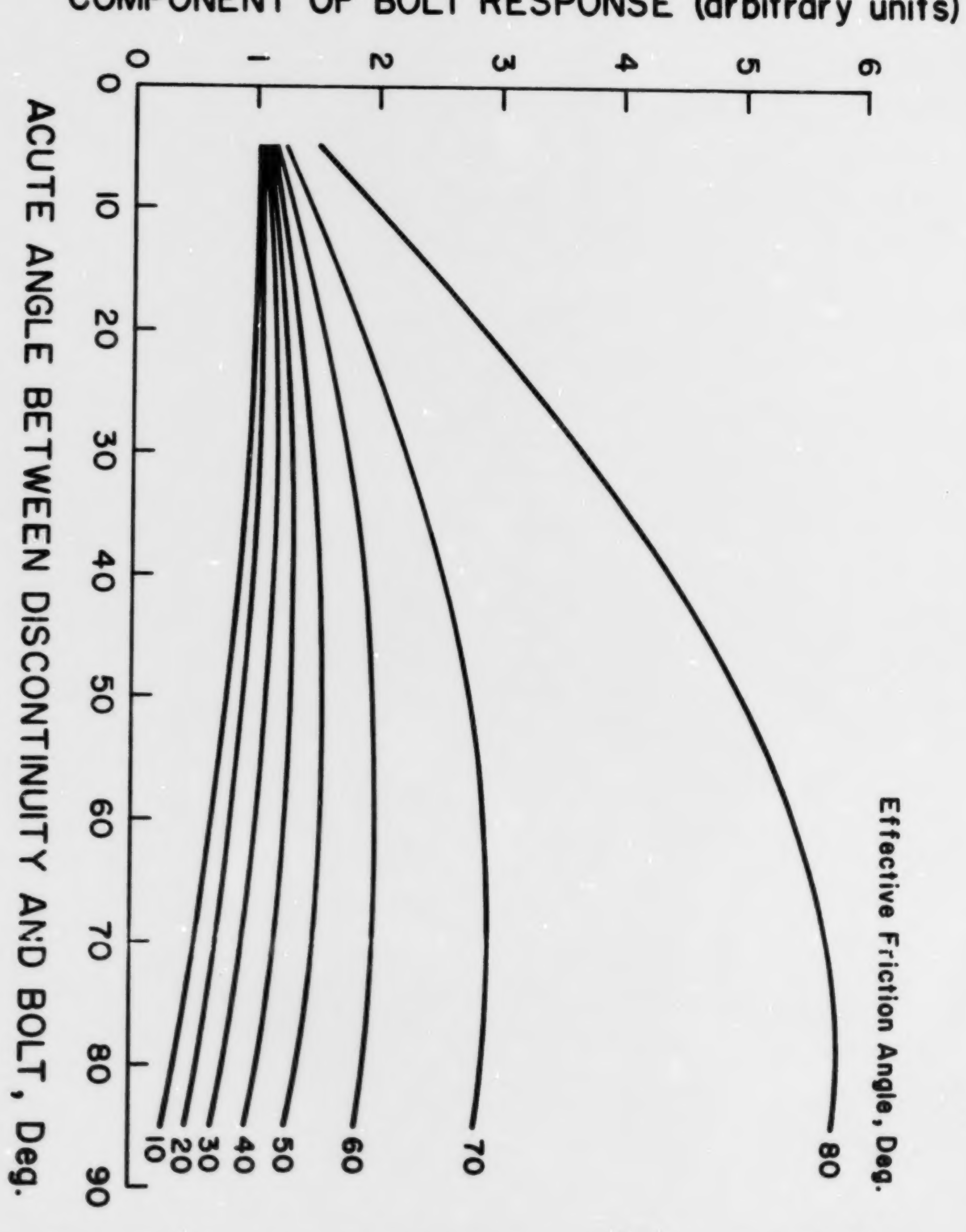

Figure 13.5 Shear strength developed by components of tensile load in bolt

In addition to the tensile effect, an inclined bolt also provides a dowel effect, i.e., bolt shear strength is mobilized. A theoretical model for this dowel effect has recently been proposed by Dight (5). The dowel may fail in three ways: (a) total yielding of the bolt when the tensile load in it reaches the yield strength, (b) crushing of the grout or resin around the bolt, and (c) crushing of the rock. For typical rebar bolts in medium strength sedimentary rock failure of the rock and/or grout occurs before bolt yielding. Whether grout or rock failure would constitute roof failure will depend on the mining situation. Certainly, with the onset of rock or grout crushing around the bolt, the roof may be expected to sag at an increased rate and may ultimately collapse if additional support is not provided.

Assuming the bolt behaves as a Tresca material, it may be shown that its shear strength is 0.5 T_y, where T_y is the yield strength.

For the purpose of this treatment of bolt inclination assume that the dowel force, F, generated by shearing of an inclined bolt along a discontinuity, acts normal to the bolt axis, as shown in Figure 13.6. Then the dowel force, SD, related to the direction of shear loading is:

$$SD = F/\sin\theta \qquad \ldots\ldots\ldots\ldots\ldots \qquad (13.2)$$

Equation (13.2) is plotted in Figure 13.7 and indicates that the dowel component of strength increases with decreasing angle between the discontinuity and the bolt. For angles less than 20° this dowel effect is particularly marked. However, as the angle decreases so the axial component of bolt loading increases, and hence the risk of failure of bolt pull-out increases. It is recommended that the angle of installation should be no less than 30° to the potential slip surface. At 30° the dowel effect increases ultimate shearing resistance by 100% over a 90° installation and this angle will also be close to optimizing the tensile component of bolt behaviour.

The addition of the tensile and dowel components of bolt resistance increases

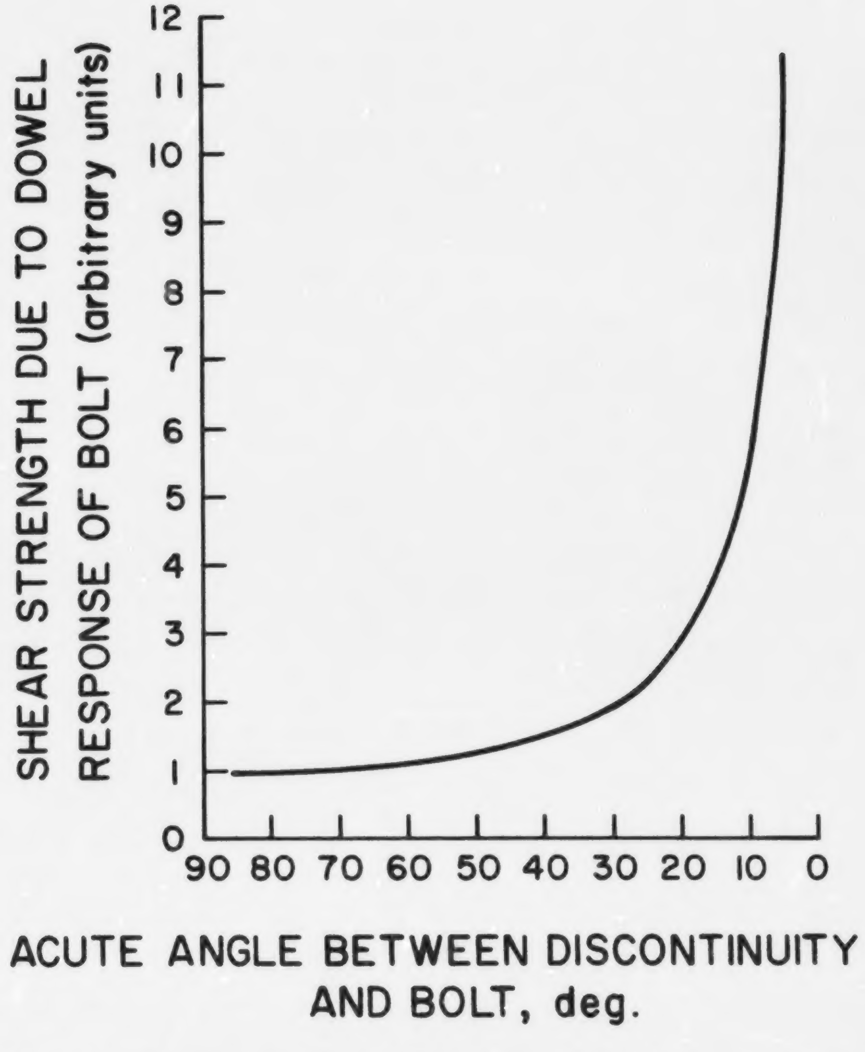

Figure 13.7 Component of dowel force along shear plane as a function of angle between joint and bolt

the natural shearing resistance of an unbolted joint, as illustrated in Figure 13.1.

At ultimate behaviour of a bolt (i.e., for large displacements) the tensile effect is likely more significant than the dowel effect (Fig. 13.1).

13.3.2 Shear Stiffness

It is self evident that the axial stiffness of a resin bolt is unaffected by bolt inclination. An examination of the influence of bolt inclination on shear stiffness was carried out both theoretically and experimentally.

In Appendix A2 a theoretical model is developed for determining the shear stiffness of a resin bolt which included bolt inclination as one of the variables. This model predicts that changes in shear stiffness resulting from changes in bolt inclination are negligibly small within the linear elastic range of behaviour. Thus, within the constraints of linear elastic response, it should not be anticipated that there will be less total sag in a roof supported with inclined bolts than in one with bolts installed normal to bedding.

The validity of this result was tested by a model study in which a "roof" comprised of two rectangular pieces of particle board (1.6 cm x 12.2 cm x 1.22 m) were clamped between two end abutments (Fig. 13.8). Simulated resin bolts were installed in a uniform pattern symmetrically about the centre of the beam. Each bolt consisted of a 4.8 mm diameter acrylic rod set in 8 mm diameter holes and grouted with sulfur set. A uniform and constant load from test to test was applied to the two-layer beam (Fig. 13.8) and the central deflection measured with a dial gauge. Models were tested with bolts installed at angles of 30, 45, 60, 75 and 90° to the "bedding" surface. No measurable difference was found in the central deflection for the different bolt inclinations, indicating all beams behaved identically and essentially "saw" the same shear stiffness along the central slip plane. It is suggested that only when inelastic deformations/failure of grout, rock, or bolt develop are the effects of bolt inclination significant.

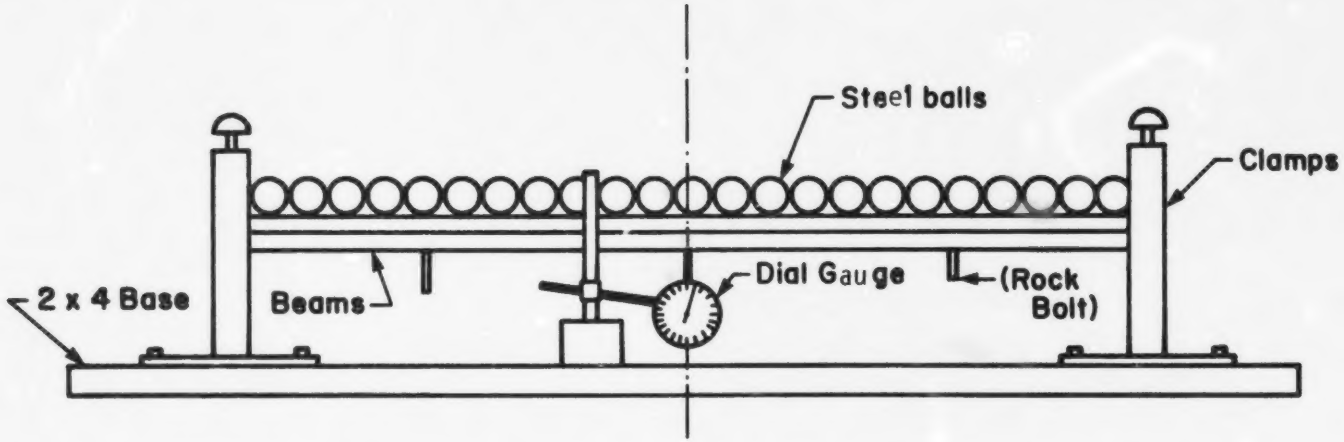
Steel balls
Clamps
2 x 4 Base
Beams
Dial Gauge
(Rock Bolt)

Figure 13.8 Laboratory testing arrangement used to examine influence of bolt inclination on roof beam reinforcement

13.4 CONCLUSIONS

Bolt inclination should be considered in the design of bolting patterns in bedded deposits. The integration of this concept with other design considerations is discussed in the final Chapter.

REFERENCES

1. Bjurstrom, S. Shear strength of hard rock joints reinforced grouted, untensioned bolts. Proc. 3rd. Cong. Int. Soc. Rock Mech., Denver, Vol. 11B, pp. 1194-1199. (1974).
2. Haas, C.J. Analysis of rock bolting to prevent shear movement in fractured ground. Mining Engineering, June, pp. 698-704. (1981).
3. Barton, N. and Bakhtar, K. Bolt design based on shear strength. Proc. Int. Symp. on Rock Bolting, Sweden, pp. 367-376. (1983).
4. Azur, A. et al. Rock mass reinforcement by passive rebars. Proc. 4th. Cong. Int. Soc. Rock Mech. Montreux, Vol. 1, pp. 23-30. (1979).
5. Dight, P.M. Improvements to the stability of rock slopes in open pit mines. Ph.D. Thesis, Monash University, Australia. (1983).

CHAPTER 14

ESTIMATING BOLT LOADINGS AND BOLT LENGTHS - A NEW TECHNIQUE

14.1 INTRODUCTION

Millions of rock bolts are used every year for temporary and permanent roof support in underground openings. The cost of installation varies widely depending on ground conditions, type and length of bolt, size and depth of mine, total number of bolts used, and geographical location, but whatever the specific cost figure at any site or operation, the goal in all cases is to provide safety against roof failure at minimum cost.

When the engineer is faced with choosing a rock bolt length, the decision is straightforward when a massive, rock formation close to the roof can be unequivocally relied upon to be stable and to provide permanent anchorage for the bolts (Fig. 14.1(a)), or when rock wedges defined by major joint sets can be identified (Fig. 14.1(b)). However, when the rock mass is closely jointed or bedded or has irregular, inconsistent, joint patterns and no dominant, massive rock member, a methodology for estimating bolt lengths and rock loadings is less clear.

One approach is to estimate the geometry of the arch which would form if the opening were left unsupported. The premise here is that the rock above the arch would provide a stable anchor zone, and therefore its position would determine bolt lengths and rock loads on bolts. This paper describes an approach for estimating the geometry of the arch above a horizontal, rectangular opening as a function of the span of the opening, the in-situ state of stress, and the rock quality as defined by the CSIR rock mass classification method.

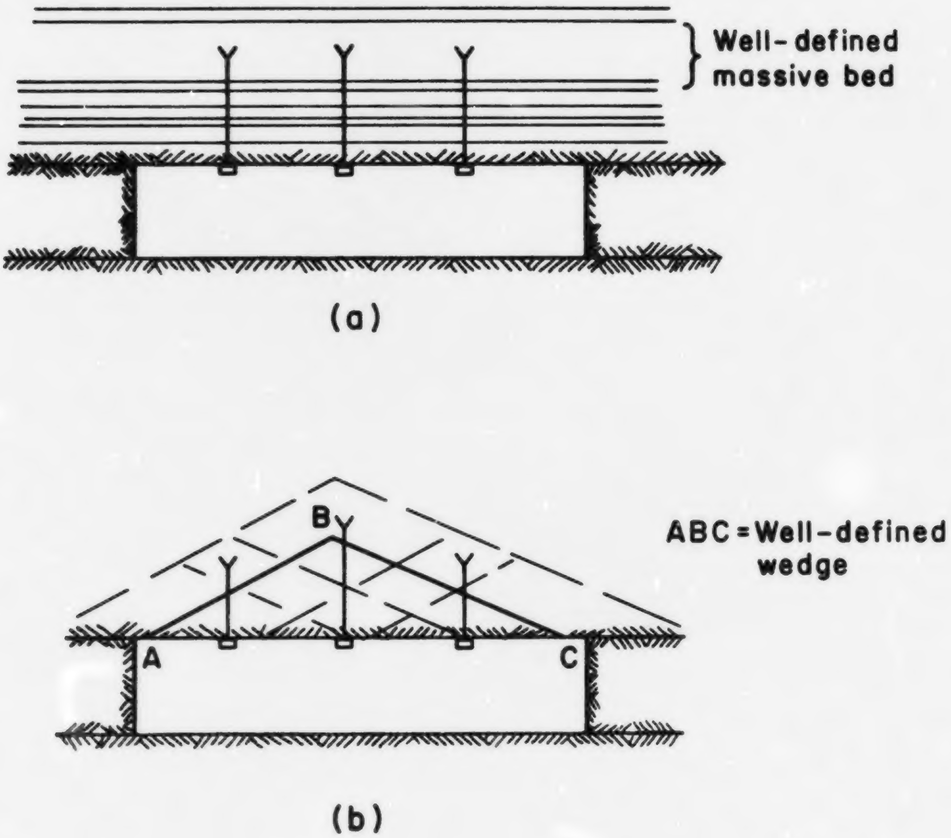
Well-defined
massive bed
(a)
B
A
C
ABC = Well-defined
wedge
(b)

Figure 14.1 (a) Bolts anchored into well-defined, massive bed
(b) Bolts anchoring well-defined wedge

14.2 FORMATION OF A STABLE ARCH ABOVE A HORIZONTAL RECTANGULAR OPENING

It is commonly found that where there is no massive bed in the roof, the geometry of a collapsed roof or back will ultimately reach a stable arch shape. The stable arch forms by collapse (sudden or progressive) of a zone of reduced stresses in the roof (Fig.14.2). In detail the geometry is not a smooth curve, but is stepped and irregular, reflecting local discontinuities and zones of weaker rock. However, the general form is arch-shaped.

A method for estimating the geometry of the arch is suggested by the study of stress distributions around openings in linear elastic, homogeneous, isotropic rock. Distant from the face so that a two-dimensional analysis is valid, it can be shown (1) that the optimum cross-sectional shape of an opening is elliptical such that the ratio of the lengths of the semi-major and semi-minor axes of the ellipse is equal to the ratio of the maximum to minimum principal field stresses acting on the excavation in the plane normal to the axis of the opening. Thus, in Figure 14.3:

$$a/b = \sigma_1/\sigma_3 \text{ (or } \sigma_2) = k \quad \ldots\ldots\ldots\ldots\ldots \quad (14.1)$$

where a = length of the semi-major axis

and b = length of the semi-minor axis.

For this optimum shape, the tangential stresses around the opening are compressive throughout. Therefore, unless these stresses exceed the uniaxial compressive strength of the rock mass, a stable arch has developed.

In Figure 14.4 a horizontal, rectangular opening is inscribed in an ellipse whose geometry is defined by Equation (14.1). Since the elliptical shape is more stable than the rectangular cross-section, the opening will tend with time and if unsupported to the elliptical form. The time required may be a few minutes or thousands of years, and the complete elliptical shape will not be observed because gravity in the floor and side walls acts to keep rock in place. The final geometry is, then, an arch-shaped opening. The zone labelled W_R (Fig. 14.4) represents the maximum weight of rock that may require

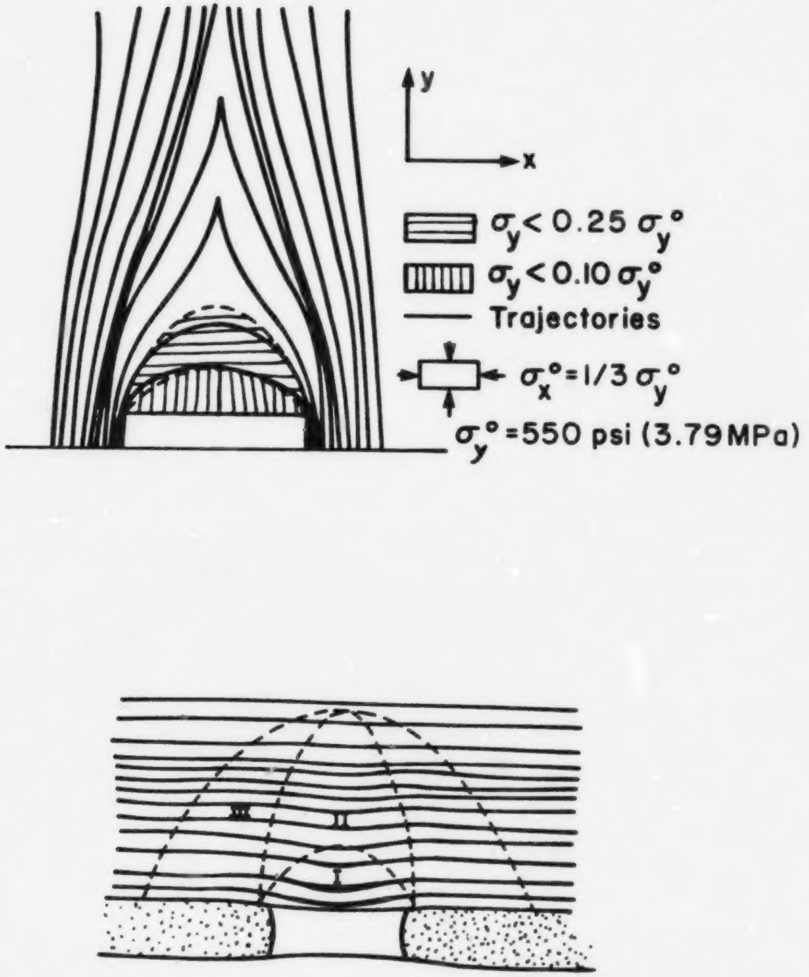
y
x
$\sigma_y < 0.25\ \sigma_y{}^\circ$
$\sigma_y < 0.10\ \sigma_y{}^\circ$
Trajectories
$\sigma_x{}^\circ = 1/3\ \sigma_y{}^\circ$
$\sigma_y{}^\circ = 550$ psi (3.79 MPa)
III
II
I

Figure 14.2 Stresses and displacements around a rectangular opening in horizontally bedded strata. Uper diagram - Trajectories of principal stress ($\sigma_y{}^\circ$ = initial vertical normal stress)
Lower diagram - zones of disturbance above roof: I = Differential sag leading to bed separation, II = Layer sag without bed separation and reduced horizontal stress, III = Horizontal and vertical pressures build-up to their undisturbed values. (Modified from Fairhurst and Singh (18)).

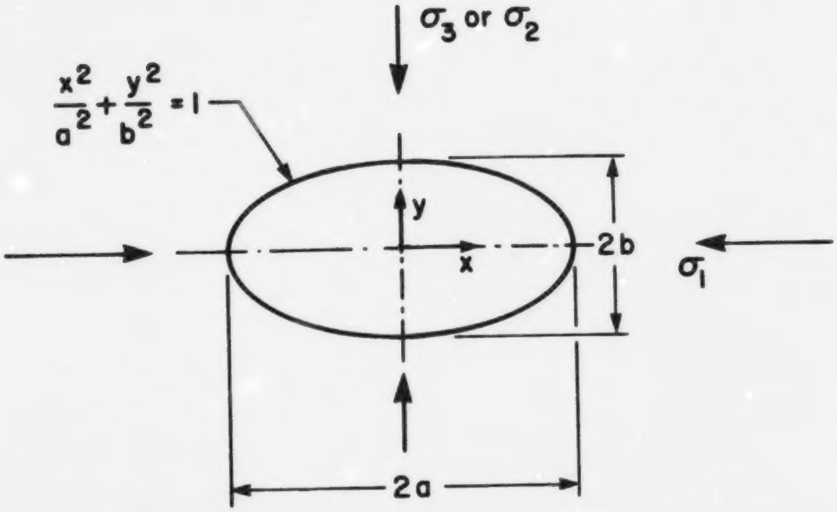

σ_3 or σ_2
$\frac{x^2}{a^2}+\frac{y^2}{b^2}=1$
y
x
2b
σ_1
2a

Figure 14.3 Relationship between elliptical geometry and applied principal stresses.

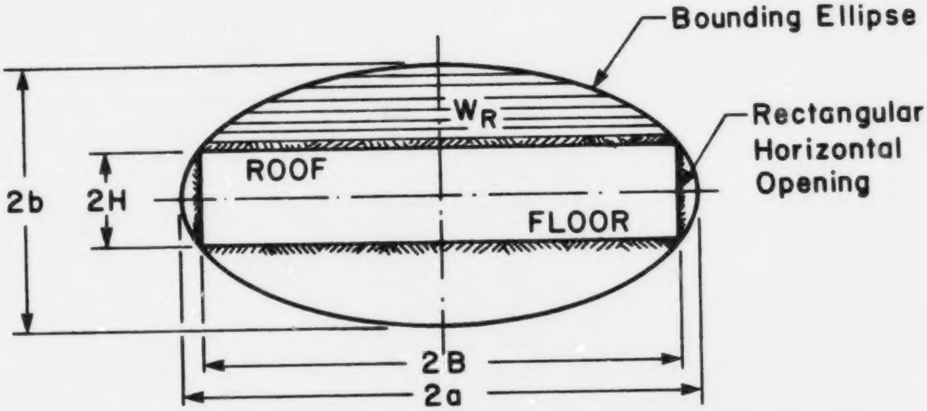

Bounding Ellipse
W_R
Rectangular
Horizontal
Opening
ROOF
2b
2H
FLOOR
2B
2a

Figure 14.4 Maximum roof volume requiring support.

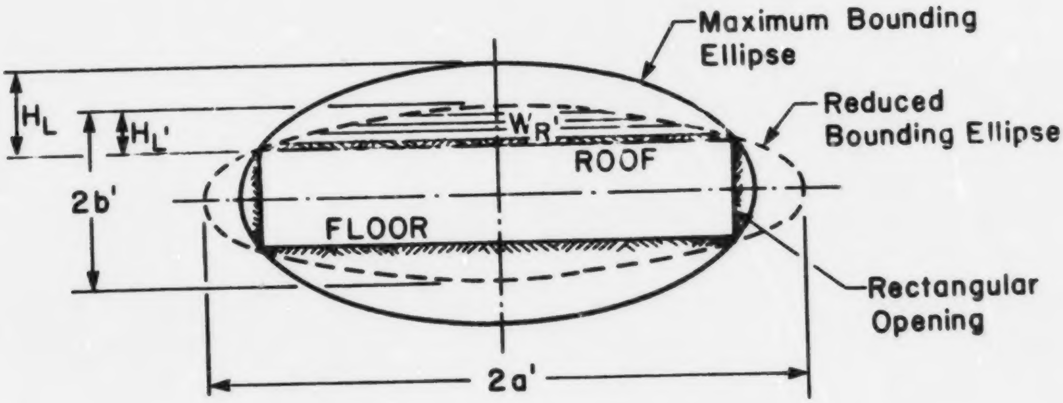

Maximum Bounding
Ellipse
H_L
H_L'
W_R'
Reduced
Bounding Ellipse
ROOF
2b'
FLOOR
Rectangular
Opening
2a'

Figure 14.5 Maximum and reduced roof volumes requiring support.

support by rock bolting.

The equations for the bounding ellipse, the maximum weight of roof rock requiring support, W_R, and the maximum height, H_L, in the roof, are derived in Appendix F. In summary:

Case I - Maximum principal stress horizontal:

Equation of bounding ellipse is:

$$(x^2 + k^2y^2) = B^2 + k^2H^2 \quad \ldots\ldots\ldots\ldots\ldots \quad (14.2)$$

where 2B = span of rectangular opening

2H = height of rectangular opening

k = ratio of maximum to minimum principal stresses in the plane of the opening cross-section.

Weight of a unit thickness, W_R, in the roof requiring support is:

$$W_R = \left[\frac{1}{k} \left\{ B(a^2 - B^2)^{\frac{1}{2}} + a^2 \sin^{-1}\left(\frac{B}{a} \right) \right\} - HB \right] \gamma_R\, g \quad \ldots \quad (14.3)$$

where $_R$ = mass density of roof material,

g = gravitational acceleration,

$$b = \frac{(B^2 + k^2H^2)^{\frac{1}{2}}}{k} \quad \ldots\ldots\ldots\ldots\ldots\ldots \quad (14.4)$$

and a = kb.

Maximum height of zone in the roof requiring support is:

$$H_L = b - H \quad \ldots\ldots\ldots\ldots\ldots\ldots \quad (14.5)$$

Case II - Maximum principal stress vertical:

Equation of bounding ellipse is:

$$(x^2 + k^2y^2) = H^2 + k^2B^2 \quad \ldots\ldots\ldots\ldots\ldots \quad (14.6)$$

Weight of a unit thickness, W_R, in the roof requiring support is:

$$W_R = [k\{H(b^2 - H^2)^{\frac{1}{2}} + b^2 \sin^{-1}(\frac{H}{b})\} - HB]\gamma_R g \quad \ldots\ldots\ldots\ldots \tag{14.7}$$

$$a = (H^2 + k^2B^2)^{\frac{1}{2}} \quad \ldots\ldots\ldots \tag{14.8}$$

and $b = a/k$

Maximum height of zone in roof requiring support is

$$H_L = a - H \quad \ldots\ldots\ldots\ldots\ldots \tag{14.9}$$

14.3 CORRECTIONS TO REDUCE SIZE OF ZONE REQUIRING SUPPORT

The size of the zone requiring support will only reach the maximum as expressed by the above equations for very weak rock masses. In all other cases use of these equations as design criteria for rock bolt length would be conservative since a portion of the zone of rock below the bounding ellipse will be self-supporting. In the best case the height of the rock zone requiring support, H_L' , will be zero, i.e. (self supporting). What value will H_L' take for intermediate cases?

Analysis of measurements made in U.S. coal mines by Unal (2) indicates that for these sedimentary rock masses the height, h_t, of the rock mass which should be considered to act as a dead load on a bolt is linearly related to rock quality:

$$h_t = \frac{100 - RMR}{50} \cdot B \quad \ldots\ldots\ldots\ldots\ldots \tag{14.10}$$

where RMR = CSIR's Rock Quality Rating (14), (see Appendix for description of the Rock Classification Method)

and 2B = span of opening.

Thus, for "very good rock" (RMR = 100), $h_t = 0$, and for "very poor rock" (RMR = 0), $h_t = 2B$ (maximum value).

In the absence of any further evidence, the author has chosen to adjust the height of the zone requiring support according to the following equation:

$$H_L' = CH_L \; (0 \le C \le 1) \quad \ldots\ldots\ldots\ldots\ldots \tag{14.11}$$

$$= (1 - 0.01\ RMR)H_L \qquad \text{..............} \qquad (14.12)$$

where $H_L^{'}$ = reduced height of rock requiring support,

and H_L = maximum height of rock requiring support as given by Equation (14.5) or (14.9).

The general shape of the reduced bounding ellipse is illustrated in Figure 14.5. The lengths of the semi-major and semi-minor axes are now a' and b', respectively. For calculation purposes it is assumed that the modified ellipse still passes through the corners of the opening. It should be noted, however, that this ellipse has no physical meaning, such as the maximum ellipse does. Its geometry is determined only in order to calculate the reduced weight of rock in the roof requiring support. The following equations for the reduced, bounding ellipse and the volume and height of rock requiring support are derived in Appendix A.

Case I - Maximum principal stress horizontal:

The equation of the reduced bounding ellipse is:

$$x^2(b'^2 - H^2) + y^2B^2 = B^2b'^2 \qquad \text{...........} \qquad (14.13)$$

$$b' = Cb - H(C-1) \qquad \text{.............} \qquad (14.14)$$

$$a' = \frac{Bb'}{(b'^2 - H^2)^{\frac{1}{2}}} \qquad \text{.............} \qquad (14.15)$$

The reduced weight of unit thickness, $W_R^{'}$, in the roof requiring support is obtained by substituting a = a' and b = b' in Equation (14.3), where a' and b' are given by Equations (14.15) and (14.14) respectively.

Reduced height of zone, $H_L^{'}$, in the roof requiring support is:

$$H_L^{'} = CH_L \qquad \text{..............} \qquad (14.16)$$

where H_L is given by Equation (14.5) and C = (1-0.01 RMR).

Case II - Maximum principal stress vertical:

The equation of the reduced bounding ellipse is:

$$B^2x^2 + y^2(a'^2 - H^2) = B^2a'^2 \quad \dots\dots\dots\dots\dots \quad (14.17)$$

$$a' = Ca - H(C-1) \quad \dots\dots\dots\dots\dots \quad (14.18)$$

$$b' = \frac{Ba'}{(a'^2 - H^2)^{\frac{1}{2}}} \quad \dots\dots\dots\dots\dots \quad (14.19)$$

The reduced weight of unit thickness, W_R', in the roof requiring support is obtained by substituting a = a' and b = b' in Equation (14.7), where a' and b' are given by Equations (14.18) and (14.19) respectively.

Reduced height of zone, H_L', in roof requiring support is given by

$$H_L' = CH_L \quad \dots\dots\dots\dots\dots \quad (14.20)$$

where H_L is given by Equation (14.9) and C = (1-0.01 RMR).

Results:

The sensitivity of the weight of the rock requiring support to height of opening, 2H, span of opening, 2B, in-situ stress ratio, k, and Rock Mass Rating, RMR, and the geometries of maximum and reduced, bounding ellipses for various cases are illustrated in Figures 14.6-14.13.

14.4 DISCUSSION OF RESULTS

The volume of roof requiring support reduces with increasing height of opening (Figs. 14.6 and 14.10). For example, for the 5 m span represented in Figure 14.10 the predicted height of the maximum zone needing support reduces from about 4.4 m for an opening height of 1 m to about 3.1 m for an opening height of 5 m. The rate of

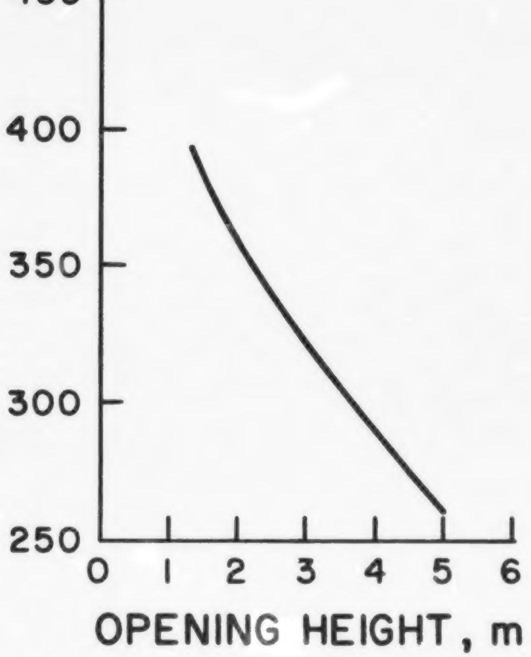

Figure 14.6 Relationship between maximum weight of roof requiring support and opening height (k = vertical/horizontal stress ratio = 2, span = 5 m, rock density = 2400 kg/cu.m.).

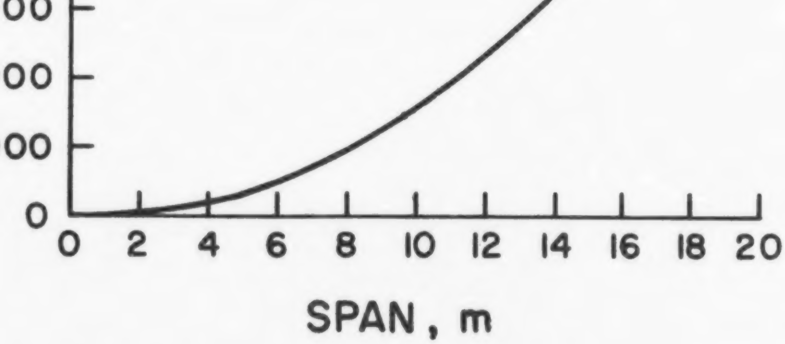

Figure 14.7 Relationship between maximum weight of roof requiring support and span (k = vertical/horizontal stress ratio = 2, opening height = 2.5 m, rock density = 2400 kg/cu.m.).

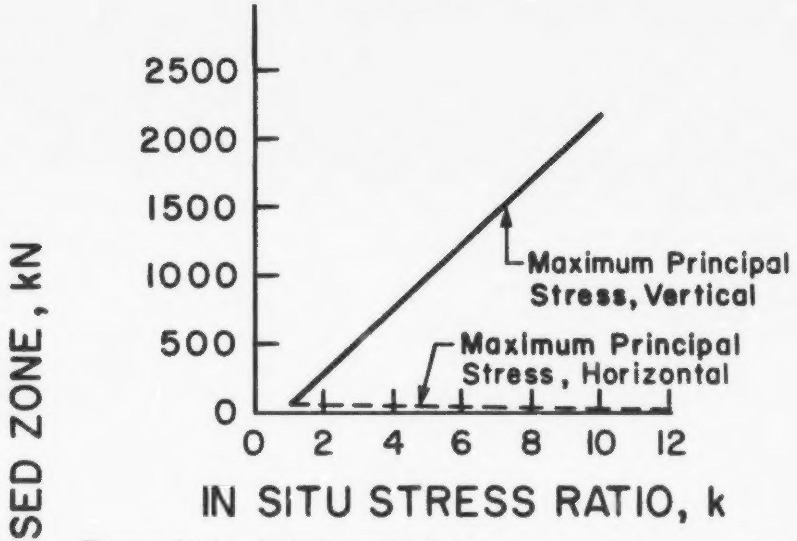

Figure 14.8 **Relationship between maximum weight of roof requiring support and in-situ stress ratio (opening height = 2.5 m, span = 5 m, rock density = 2400 kg/cu.m.).**

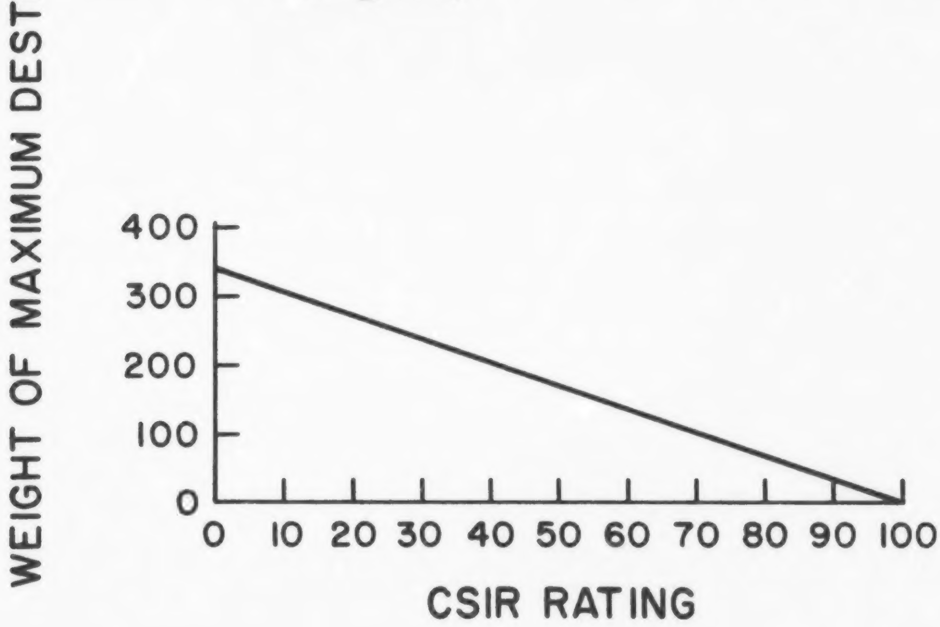

Figure 14.9 **Relationship between weight of roof requiring support and CSIR Rock Mass Rating (k = vertical/horizontal stress ratio = 2, opening height = 2.5 m, span = 5 m, rock density = 2400 kg/cu.m.).**

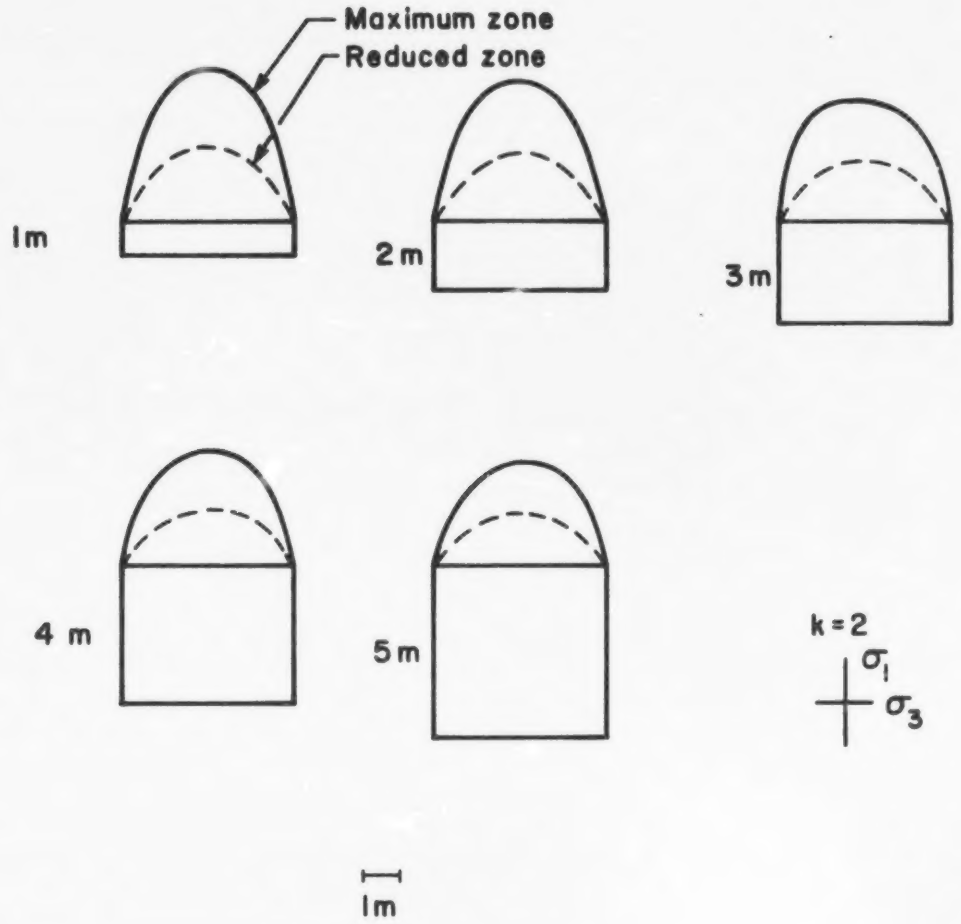
Maximum zone
Reduced zone
Im
2 m
3 m
4 m
5 m
k = 2
σ_1
σ_3
Im

Figure 14.10 Variation of roof support volumes with opening height. (CSIR Rock Mass Rating = 50, rock density = 2400 kg/cu.m.).

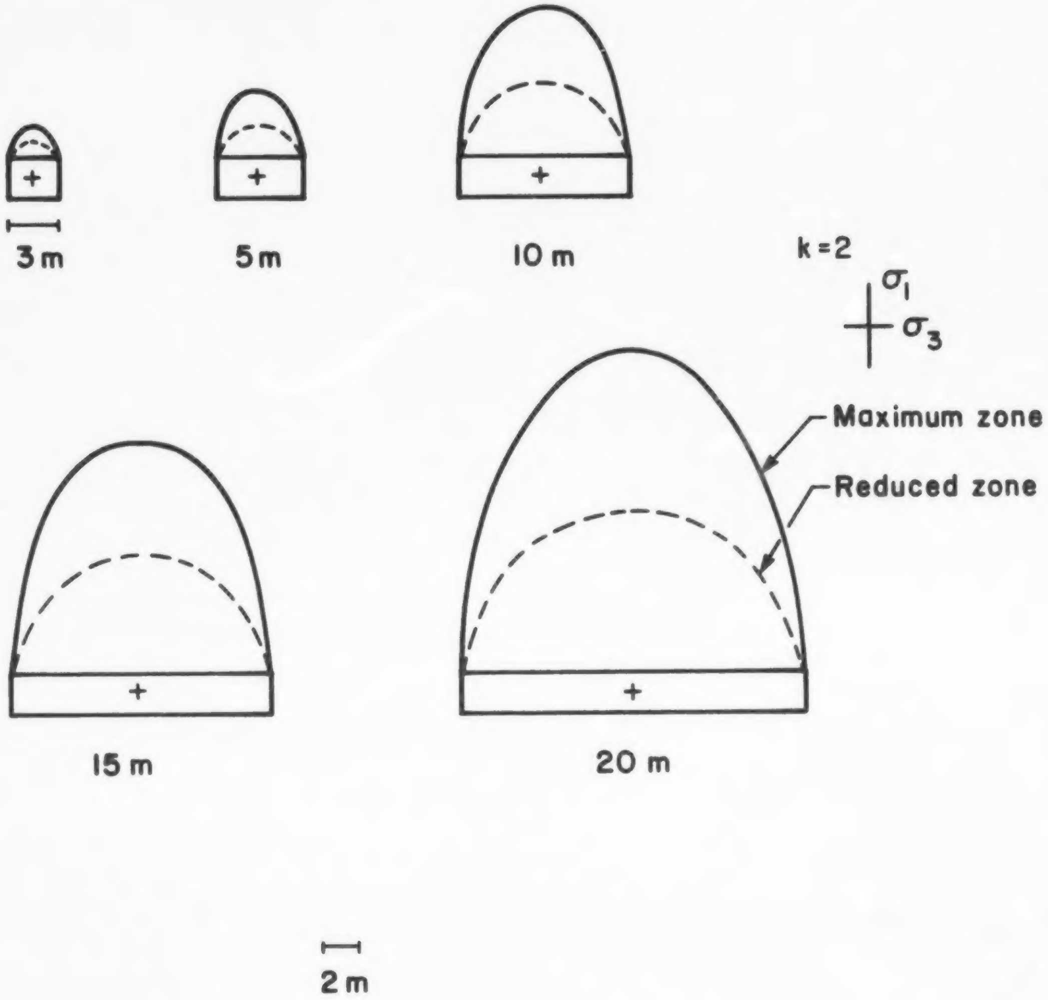
3 m
5 m
10 m
k = 2
σ_1
σ_3
Maximum zone
Reduced zone
15 m
20 m
2 m

Figure 14.11 Variation of roof support volumes with span (CSIR Rock Mass Rating = 50, rock density = 2400 kg/cu.m.).

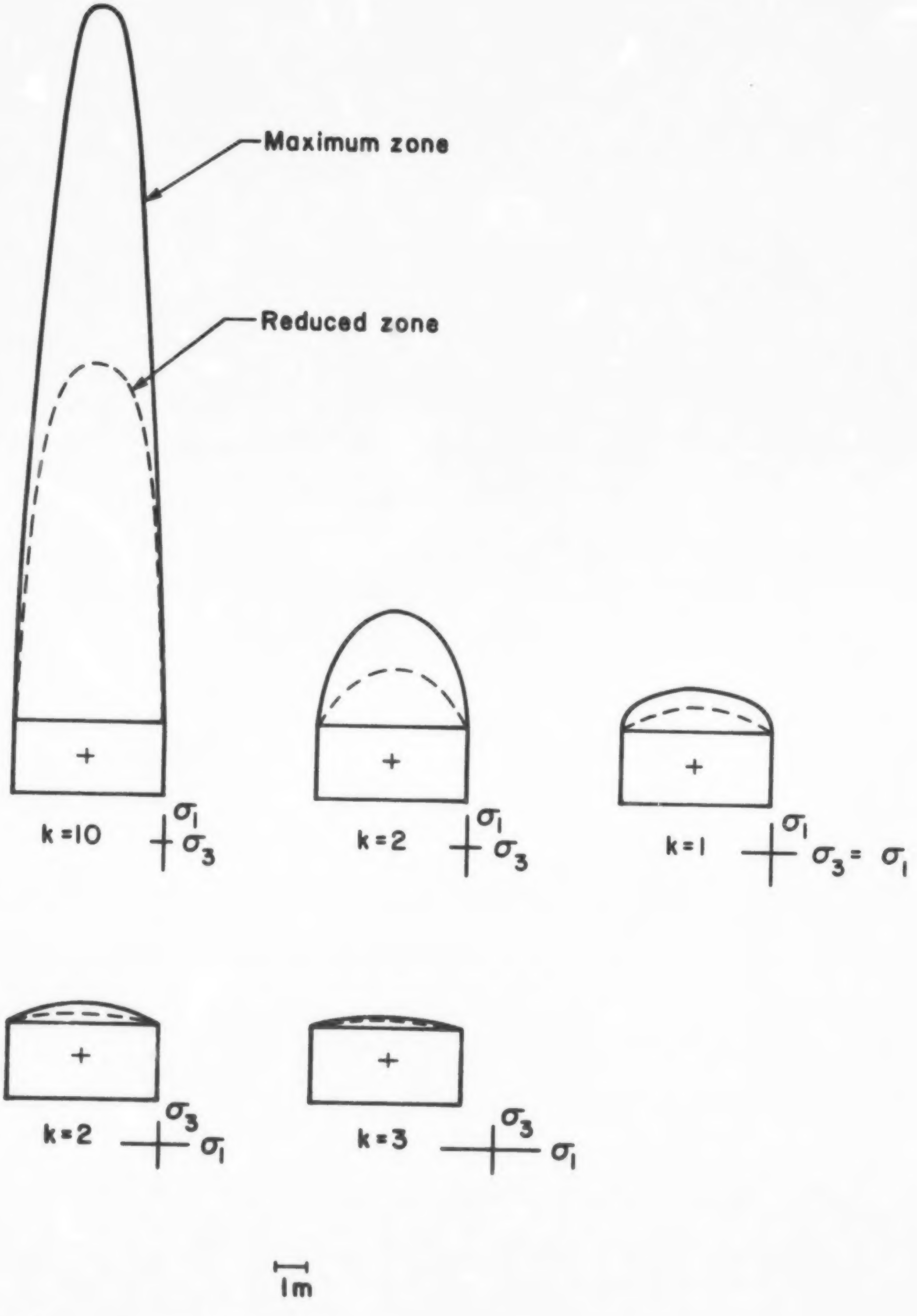
Maximum zone
Reduced zone
k = 10
σ_1
σ_3
k = 2
σ_1
σ_3
k = 1
σ_1
$\sigma_3 = \sigma_1$
k = 2
σ_3
σ_1
k = 3
σ_3
σ_1
1m

Figure 14.12 Variation of roof support volumes with in-situ stress ratio (CSIR Rock Mass Rating = 50, rock density = 2400 kg/cu.m.).

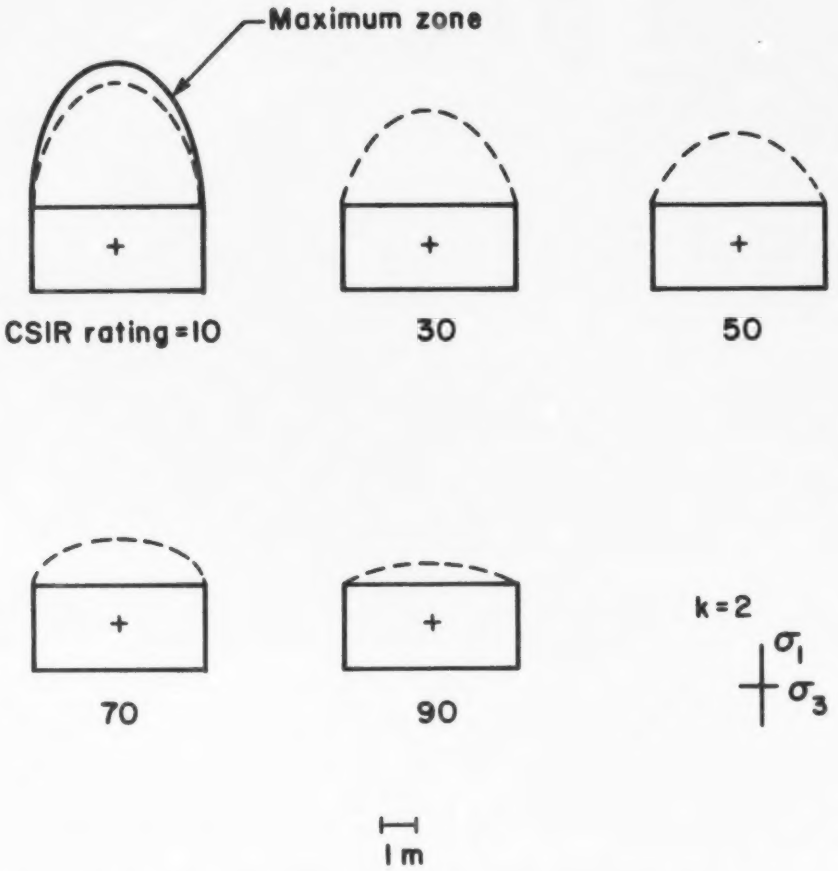
Maximum zone
CSIR rating=10
30
50
70
90
k=2
σ_1
σ_3
1 m

Figure 14.13 Variation of roof support volumes with CSIR Rock Mass Rating (rock density = 2400 kg/cu.m.).

reduction with increasing height is approximately linear (Fig. 14.6). It is interesting to note from the study of stress concentrations around ovaloidal openings (Coates (3), Fig. 14.3(f) that the tangential stress concentration at corners reduces as the opening height increases, while keeping the span constant. For example, for an in-situ horizontal to vertical stress ratio of 1/3 and a span of 5 m the corner tangential stress concentration is halved when the opening height is increased from 1 m to 5 m.

The support requirements are very sensitive to span (Figs. 14.7 and 14.11). For example, the weight of roof requiring support increases by a factor of approximately five in doubling the span from 4 m to 8 m (Fig. 14.7). Also, if the designer requires bolts of sufficient length to anchor beyond the boundaries of the elliptical zones, the total length of bolts required will increase rapidly with increasing span, i.e., longer bolts and at a closer spacing to resist increased total load.

The in-situ stress ratio has a profound influence on roof support requirements (Figs. 14.8 and 14.12). It is very favourable to have the horizontal in-situ stress greater than the vertical stress. Conversely, high, vertical to horizontal stress ratios are unfavourable. In the most extreme situation the elliptical zone in the roof will be much higher than any practical rock bolting scheme could support (see Fig. 14.12, k = 10). These cases correspond to "running ground" and to the ellipsoid of motion observed in drawdown of granular materials through a trap door (Fig. 14.14). Clearly, immediate, full-face support is required; bolting would not be appropriate.

The weights of the maximum height of roof zone for support from Unal's equation (see Eqn. 14.10), agree closely with those predicted by the elliptical theory proposed here. Span vs. rock load height relationships for these two approaches are compared for CSIR Rock Mass Ratings of 0 and 50 in Figure 14.15.

Some alternative graphical illustrations of the results of the elliptical theory are provided in Figures 14.16-14.19. The relationship between the maximum height of the ellipse and the span/height ratio of the opening is shown in Figures 14.16 and

14.17 for the vertical and horizontal major principal stress, respectively. A notable feature is the great sensitivity at low span/height ratios and attainment of an approximately constant maximum height at higher span/height ratios. The rapid increase in maximum height at low span/height ratios suggests that rock bolts, which are of adequate length at one span, may be inadequate if relatively small increases are made to the span.

Figures 14.16 and 14.17 also illustrate, once again, the significance of the in-situ stress ratio and the practical value from the viewpoint of roof stability of high horizontal stresses, providing these do not lead to other modes of failure, e.g., buckling in a thinly laminated roof.

Figure 14.18 illustrates the sensitivity of the height of the roof zone requiring support to the span/height ratio in a 2.5 m high opening for different Rock Mass Ratings and two spans - 5 m and 8 m. It is readily seen that changes to span are more significant for low Rock Mass Ratings, e.g., for RMR = 40, the height requiring support changes from 2.3 m to 4.1 m; while for RMR = 80, it changes from 0.75 m to 1.35 m.

The relationship between the height requiring support and the span/height ratio for a span of 5 m for a range of Rock Mass Ratings is demonstrated in Figure 14.19. The higher the quality of the rock, the lower the value of span/height ratio at which the height of the zone requiring support reaches a constant value for practical purposes, e.g., for RMR = 80, height of zone is approximately constant at an opening height of 2 x span, whereas for RMR = 60, the same condition is not reached until the opening height is about 4 x span.

It is interesting to examine the progressive change in support requirements as in-situ stress ratios and geometries alter during mining. For example, in Figure 14.20 the following situation is modelled: an entry, height 2.5 m, is driven with an initial span of 5 m in ground with a Rock Mass Rating of 50. Later, a cross cut is driven at

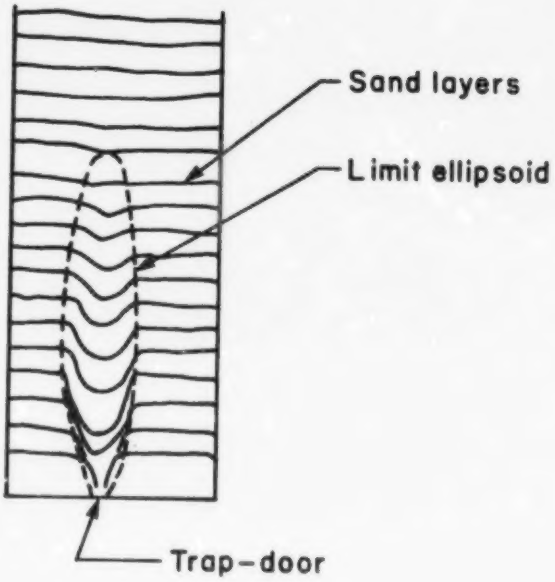
Sand layers
Limit ellipsoid
Trap-door

Figure 14.14 Ellipsoid of motion of granular particles above an open trap door (after Kvapil (17)).

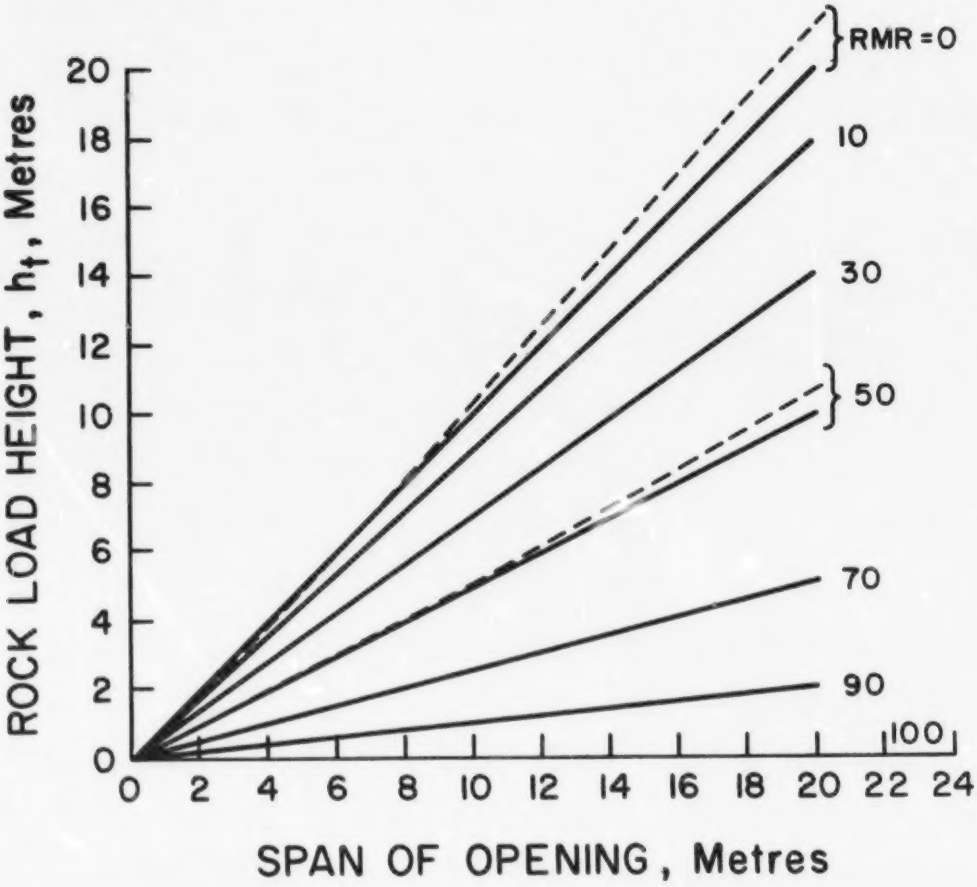

Figure 14.15 Relationship between rock load height and span (---- equation (10), after Unal (2); —— elliptical theory).

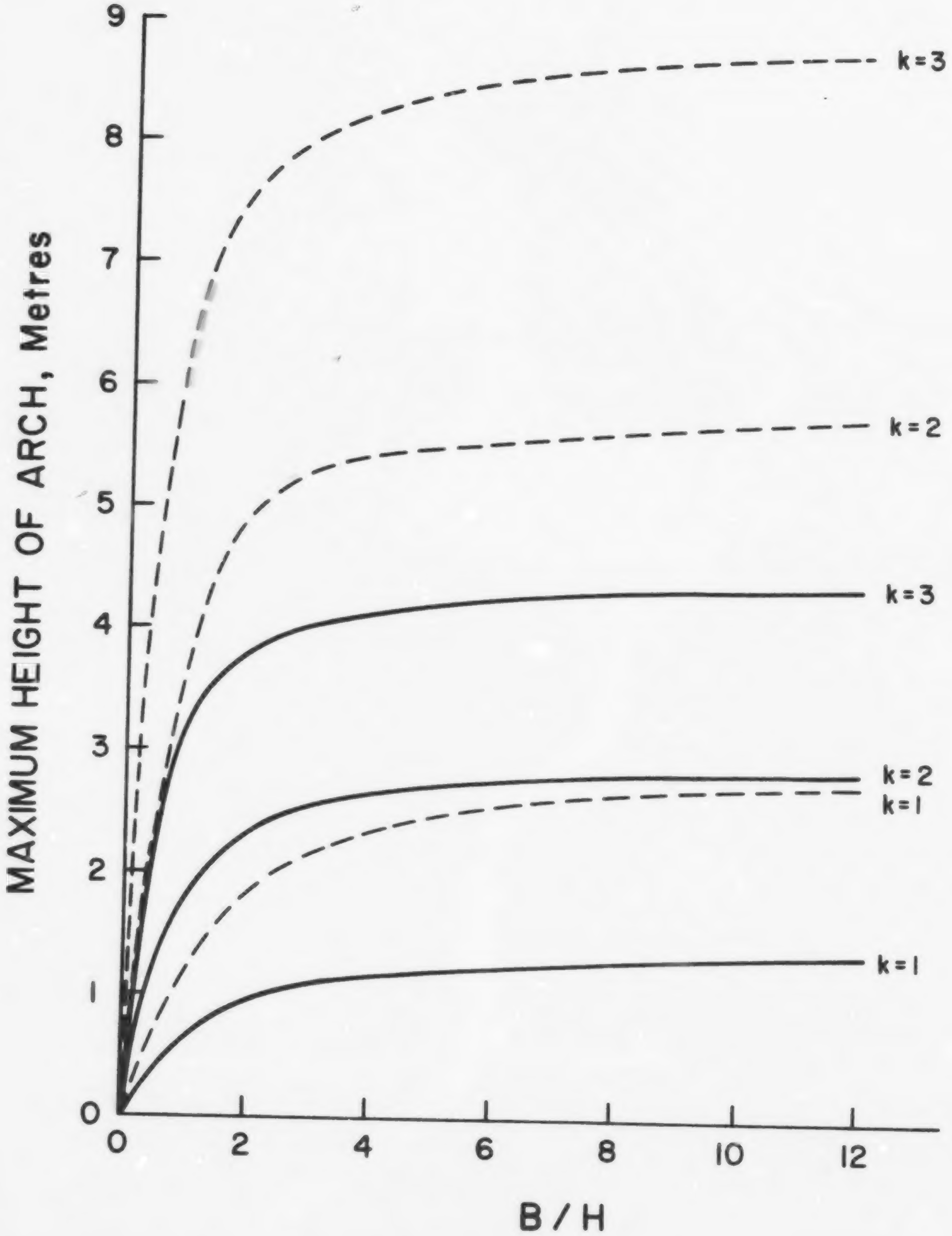

Figure 14.16 Relationship between maximum height of rock load arch and span/height ratio (—— span = 6 m; - - - span = 12 m; k = vertical/horizontal principal stress ratio, rock density = 2400 kg/cu.m., CSIR Rock Mass Rating = 50).

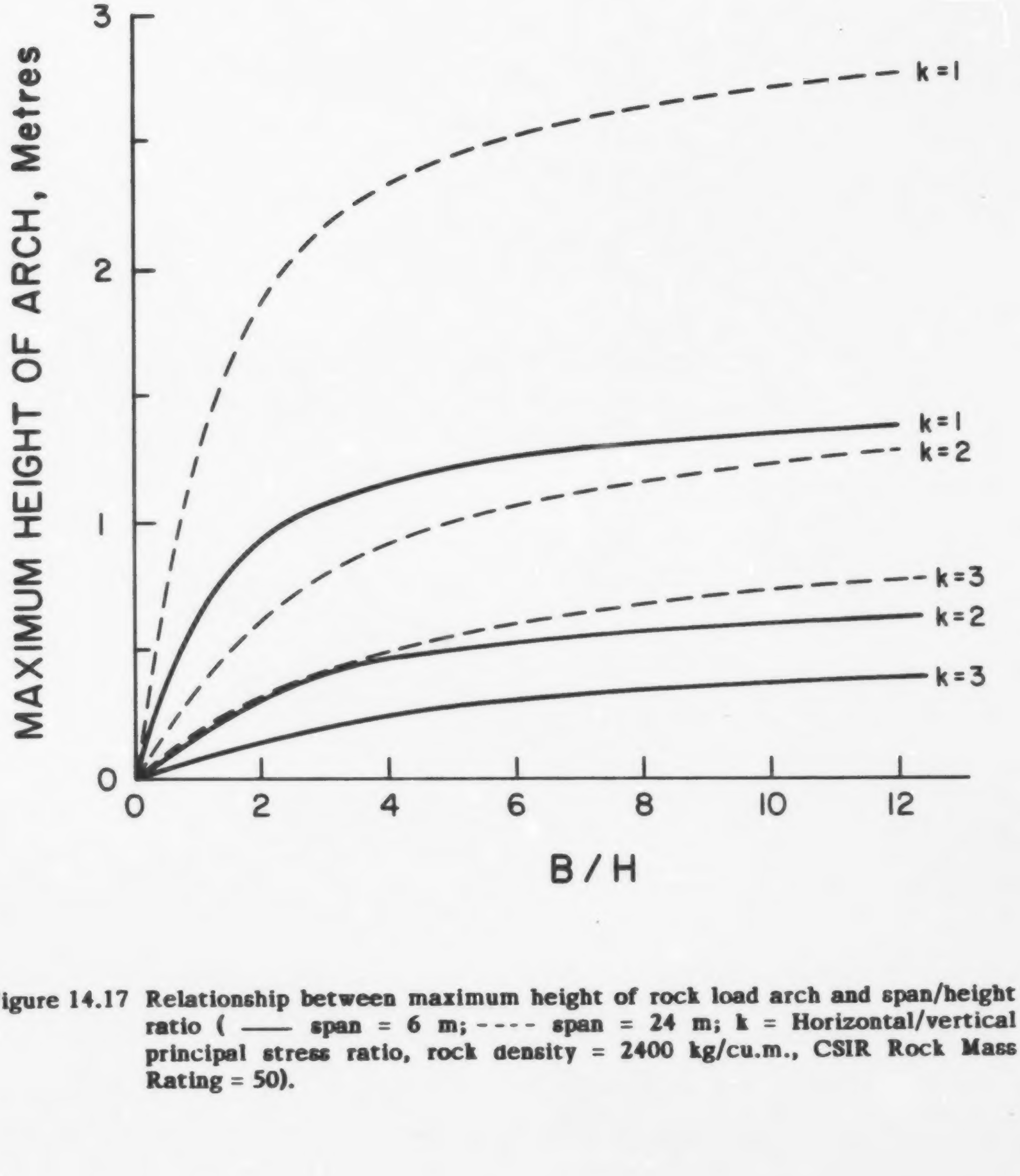

Figure 14.17 Relationship between maximum height of rock load arch and span/height ratio (—— span = 6 m; - - - - span = 24 m; k = Horizontal/vertical principal stress ratio, rock density = 2400 kg/cu.m., CSIR Rock Mass Rating = 50).

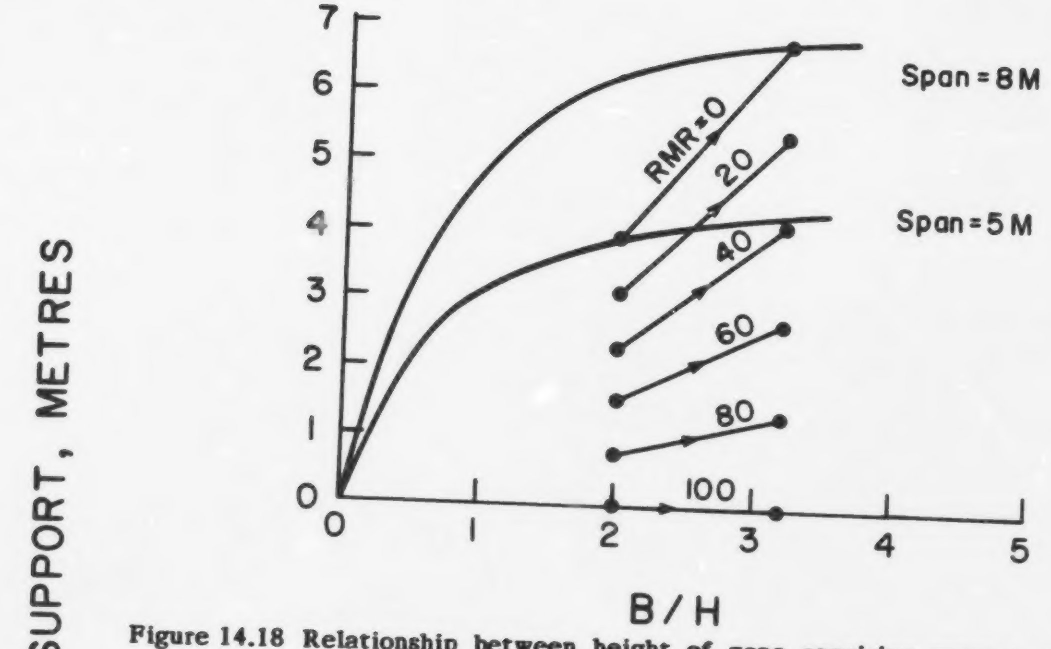

Figure 14.18 Relationship between height of zone requiring support and span/heigh ratio for different CSIR Rock Mass Rating and spans of 5 m and 8 m (k = vertical/horizontal principal stress ratio = 2, opening height = 2. m, rock density = 2400 kg/cu.m.).

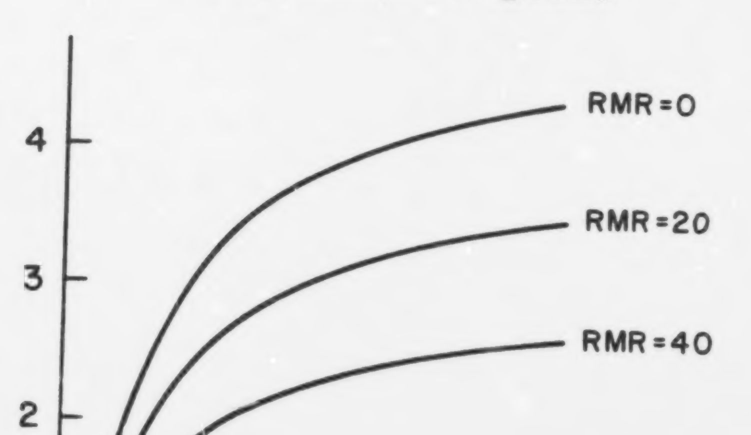

Figure 14.19 Relationship between height of zone requiring support and span/height ratio for different CSIR Rock Mass Rating (span = 5 m, k = vertical/horizontal principal stress ratio = 2, rock density = 2400 kg/cu.m.).

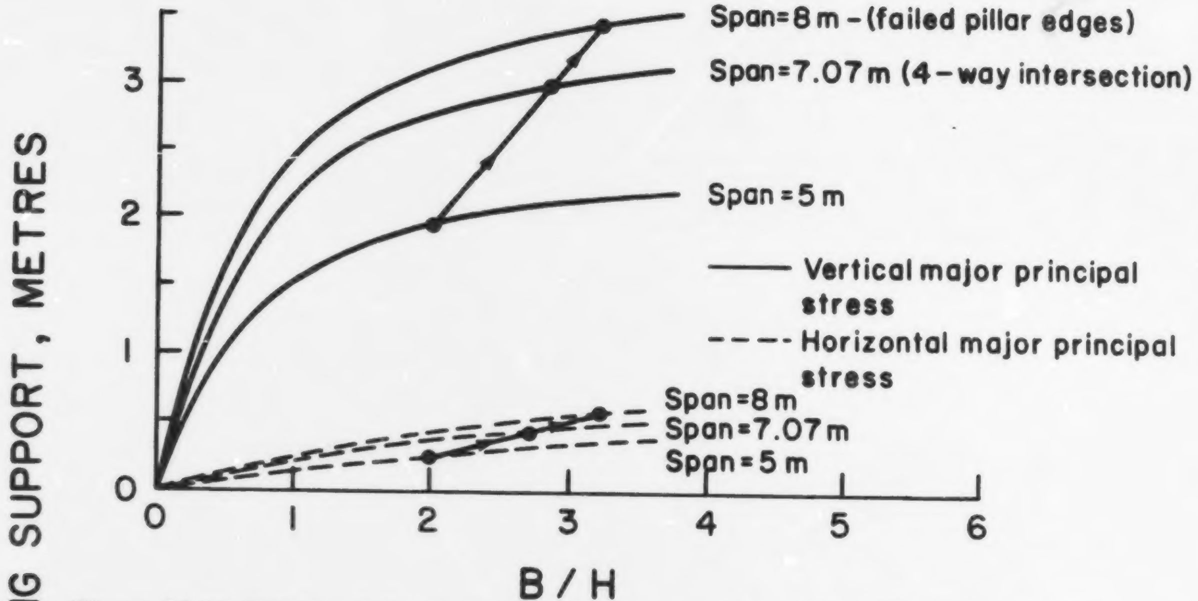

Figure 14.20 Effect of four-way intersection and rib failure on height of roof zone requiring support (k = vertical/horizontal principal stress ratio = 2, opening height = 2.5 m, CSIR Rock Mass Rating = 50, rock density = 2400 kg/cu.m.).

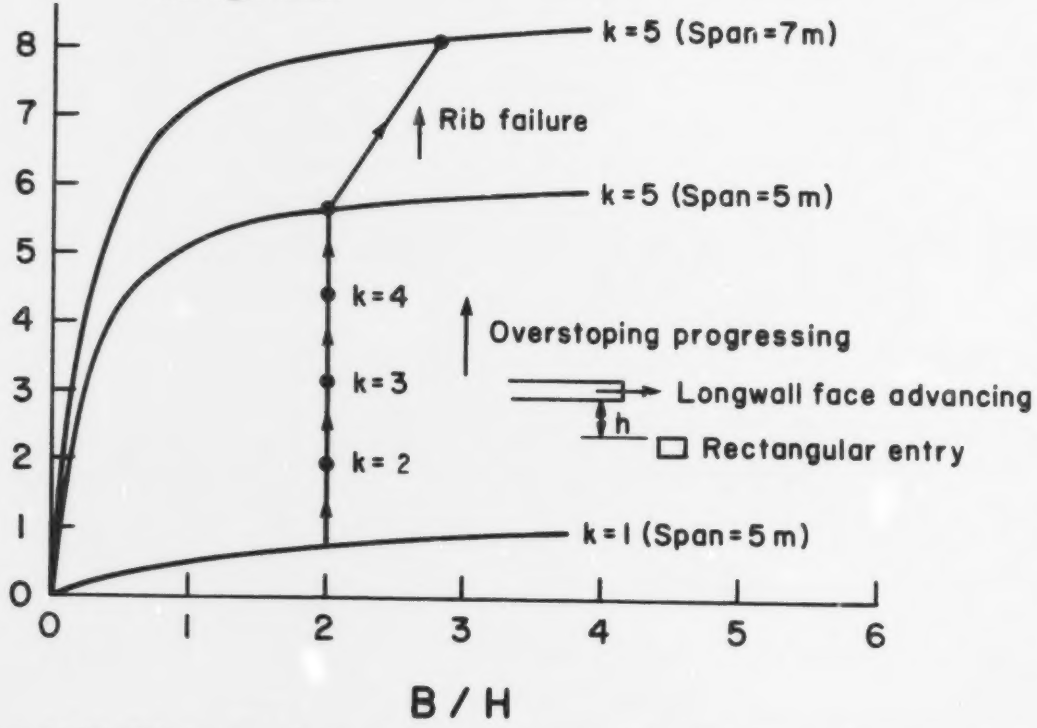

Figure 14.21 Effect of overstoping of rectangular opening on height of roof zone requiring support (k = vertical/horizontal principal stress ratio = 2, opening height = 2.5 m, span = 5 m, CSIR Rock Mass Rating = 50, rock density = 2400 kg/cu.m.).

right angles to the entry so that the diagonal span at the four-way intersection is 7.07 m. Subsequently, spalling and failure of the ribside increase the effective span of the single openings to 8 m. As these changes take place the span/height ratio increases and the effect this has on the predicted height requiring support is illustrated in Figure 14.20 for two in-situ stress cases: horizontal stress = 2 x vertical stress, and vertical stress = 2 x horizontal stress. The latter case is considerably more unfavourable than the former case. Support height requirements increase from 1.9 m to 3.85 m, whereas for the high horizontal stress state the increase is only from 0.25 m to 0.58 m. This is approximately the same percentage increase, but in absolute terms the increase in cost of bolting in the first case would be much greater.

The combined influence of in-situ stress changes and increases in span is seen in Figure 14.21, where overstoping and a rectangular opening of the same dimensions and in the same rock mass as in the previous example is postulated. As the longwall face approaches the opening the ratio of vertical to horizontal stress will increase before decreasing once again when the face has passed. Specific values of stress changes can be estimated by numerical methods. For example, Wagner (4) presents results of a 2-D simulation of overstoping a circular opening 40 m below for South African gold mine conditions. Maximum tangential stresses around the opening are shown to increase by a factor of approximately 3.5. In Figure 14.21 it is assumed that the ratio of in-situ vertical to horizontal stresses increases from 1 to 5 as the face approaches the entry. According to elliptical theory, the zone requiring support will increase from 0.75 m to 5.65 m. If it is further postulated that as a result of the increased vertical stresses the ribsides of the rectangular opening fail to a depth of 1 m then the effective roof span increases to 7 m. This increase will result in a further substantial increase in roof support requirements to 8.1 m.

The above examples indicate that the elliptical model qualitatively predicts the anticipated trends in roof support requirements with changes in span and in-situ stress state.

14.5 SHAPE OF VOLUME OF ROCK TO BE SUPPORTED:

The choice of an elliptical shape for the volume of rock to be supported was based on principles derived from stress distributions around 2-D openings in linear elastic material. Others have predicted different geometries. Denkhaus's model (5) gives a parabolic profile in cohesive materials. Peng (6) concluded that the arch shape formed by average roof fall dimensions at four-way intersections in selected coal mines in the eastern U.S.A. corresponds to the line in the roof along which $\sigma_o = 0.1\,\sigma_z$, as predicted by finite element stress analysis, where σ_o is the induced vertical normal stress in the roof and σ_z is the average vertical stress before mining. This geometry does not confirm to any of the conical sections. In practice, the precise shape will depend upon a number of physical and mechanical properties which are not included in simple mathematical models. Very limited number of measurements of void shapes above openings have been made. One recent study is of particular interest because it concerns the design of cable bolting systems in an underground stoping operation in South West Africa/Namibia (Stheeman (7)). Rock falls in newly bolted stopes prompted a detailed investigation of the mechanics of cable bolting and the volume of rock being supported. Measurements of the locations and attitudes of fracture planes in failed stope backs (Fig. 14.22) were used to determine whether the void shape best fitted a circular, parabolic or elliptical shape. In this case, the elliptical shape conformed most accurately. It is noteworthy that the stopes suffer high rock pressures and fractures are induced in the backs.

14.6 BACK ANALYSIS:

Case histories, such as Stheeman's above (7) for comparison with elliptical theory are limited in their usefulness because in-situ stress values and/or Rock Mass Ratings are not provided.

Walton and Taylor (8) collected information on void migration in shallow room and pillar mines exposed in opencast coal mines in the U.K. Figure 14.23 reproduces

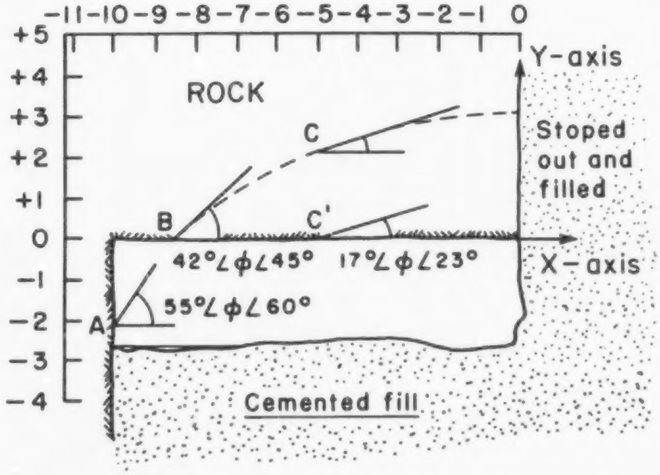
-11 -10 -9 -8 -7 -6 -5 -4 -3 -2 -1 0
+5
+4
+3
+2
+1
0
-1
-2
-3
-4
Y-axis
X-axis
ROCK
Stoped out and filled
C
B
C'
A
42°∠φ∠45°
17°∠φ∠23°
55°∠φ∠60°
Cemented fill

Figure 14.22 Observed fracture orientations in failed stope back at Tsumeb Mine (after Stheeman (7)).

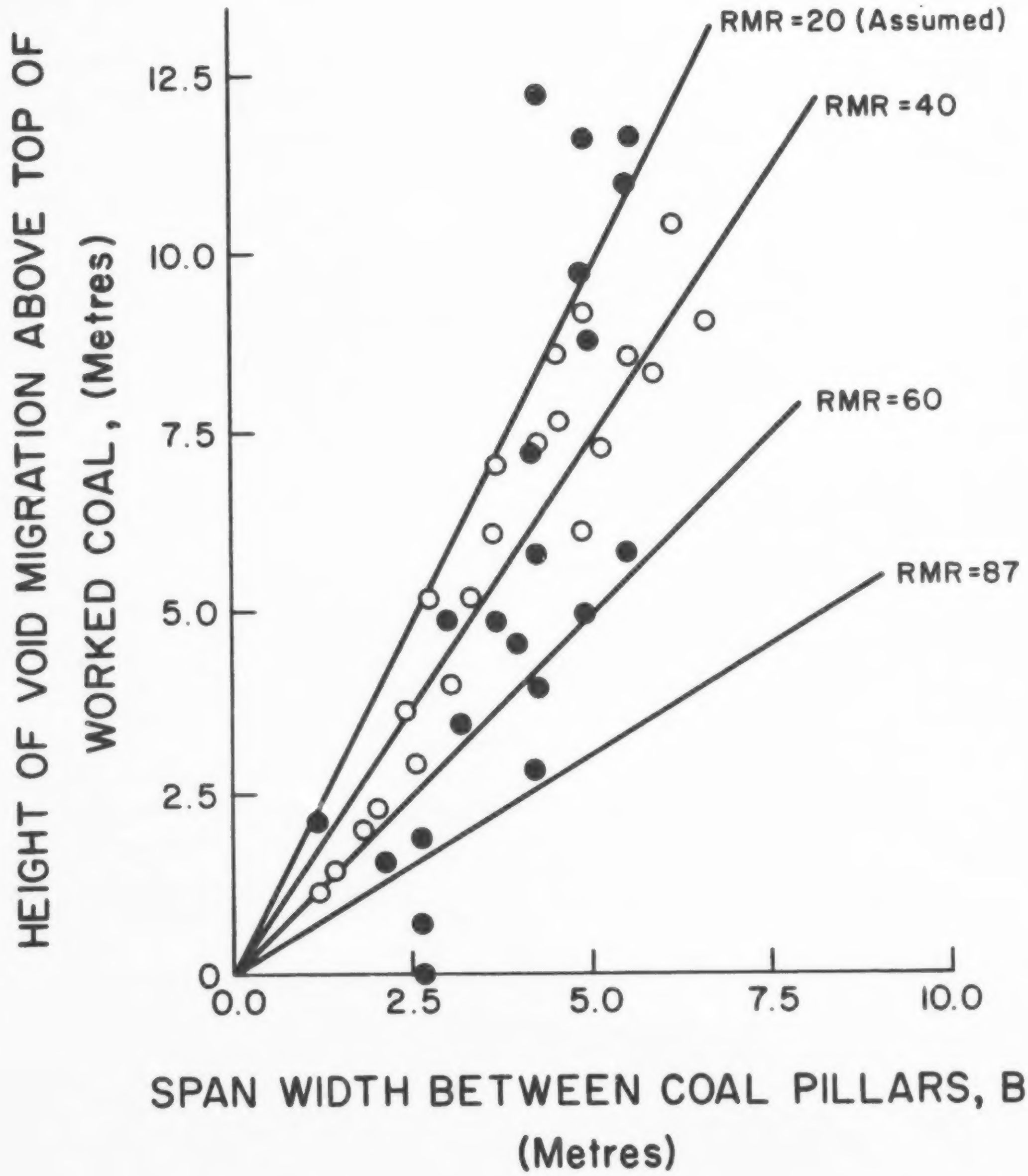

Figure 14.23 Relationship between height of void migration and span between coal pillars (o = arching in silty mudstones; ● = arching in sandstones) (after Walton and Taylor (8)).

the data points from Pethburn Opencast Site, Co. Durham, relating opening span to height of void migration. Naturally, given the variability of coal-bearing strata, there is considerable scatter.

To test elliptical theory it was assumed that the vertical in-situ stress is the major principal stress. Then, from Equations (14.8),(14.9) and (14.20), the height of void migration is given by:

$$H'_L = C\,[(H^2 + k^2B^2)^{\frac{1}{2}} - H] \quad \ldots\ldots\ldots\ldots \quad (14.21)$$

For the Pethburn Opencast Site neither the in-situ stress ratio, k, or the reduction factor, C, which is related to the Rock Mass Rating, RMR, via Equation (14.12), are known. One of these variables can be calculated from Equation (14.21) provided the value of the other is assumed. In this case, it was assumed on the basis of described rock conditions and the author's own familiarity with opencast properties in the U.K. (9) that the upper envelope to the data points in Figure 14.23 corresponds to materials with Rock Mass Ratings of 20%. The in-situ stress ratio, k, is then given by:

$$k = [\,\frac{H_L'^2 + 2H_L'^2CH}{CB^2}\,] \quad \ldots\ldots\ldots\ldots\ldots\ldots \quad (14.22)$$

Substituting appropriate values from Figure (14.23) in Equation (14.22) the in-situ stress ratio was estimated to be 2.5, i.e., vertical principal stress = 2.5 x horizontal principal stress. Given that these voids were observed in excavated slopes where lateral stress relief has occurred, the predicted in-situ stress ratio is not unreasonable. What is not known is whether the void migration is attributable completely, in part, or not at all to surface mining. In most cases, the voids predate surface mining but some additional migration may have occurred during the open cast operations.

The relationships between span and height of void migration for an in-situ stress ratio of 2.5 and various Rock Mass Ratings can be predicted from Equation (14.21), and are shown graphically in Figure 14.23. The lower envelope to the array of data points corresponds to a Rock Mass Rating of 87%, i.e., very good rock.

The four lines marked RMR = 20, 40, 60 and 87 in Figure 14.23 correspond to four lines in Walton and Taylor's original diagram (Fig. 14.1(8)) to which the following descriptions are given:

RMR Line	Description Associated with same line in Figure 14.1 (8)
20	Ultimate overbreak (arching) in rock (Szechy)*
40	Limit of primary arching in silty mudstone
60	Ultimate overbreak in hard stratified rock (Terzaghi)**
87	Arch height, silty mudstone, = 35° (Protodyakonov)***

* Ref. (10); ** Ref. (11); *** Ref. (12)

A similar approach using Stheeman's data (see Fig. (14.22)) leads to an estimate of k = 1.1, i.e., vertical principal stress = 1.1 x horizontal principal stress. However, the Rock Mass Rating of 60 was selected on the basis of photographs of stope conditions from his paper and is therefore subject to considerable uncertainty.

Peng's (6) data from selected eastern U.S.A. coal mines can also be interpreted on the basis of elliptical theory provided that Rock Mass Rating values are assigned. Assuming that for the highest falls Rock Mass Ratings lay between 10% and 30% (very poor to poor rock), it can be shown that for the particular intersection geometries the k value (vertical/horizontal in-situ stress ratio) lies between 1.0 and 1.1.

In Japan a number of large underground power stations in a variety of rock types have been instrumented to determine opening behaviour, including the deformation occurring in the cavern roofs (13). Results from five excavations are shown in Figure 14.24; associated data on rock type, cavern geometry, modulus of elasticity of rock, and in-situ stress are tabulated in Table 14.1.

TABLE 14.1 - CAVERN CONDITIONS (AFTER HIBINO, MOTOJIMA AND KANAGAWA (13))

PROJECT NUMBER AND ROCK	CAVERN SIZE HEIGHT, WIDTH, LENGTH			IN-SITU STRESS*		DEFORMABILITY**
				v	n	E
	m	m	m	MPa		GPa
7 - Shale, sandstone	42	20	160	6.6	6.9	13/6
10 - Conglomerate	49.4	26.6	116	4.5	7.0	16-20
12 - Black Schist	47.4	26.3	98	5.4	7.1	12/8
9 - Rhyolite	47.6	26	96.5	4.5	3.4	10
11 - Granite	20.8	14.6	30	1.3	1.9	4/2

* $_y$ = vertical normal stress, $_n$ = horizontal normal stress 13/6 Anisotropic

** Jack Tests

In all the cases shown in Figure 14.24 there is a zone of rapid relative movement over the first 5 m into the arched roof. In practical terms, this zone might be interpreted as equivalent to the height of the zone requiring support. Unfortunately, the measurements of roof subsidence were made in an arched roof so that direct comparisons with results predicted by elliptical theory, which assumes a flat roof, are questionable. However, it is still of some interest to make such a comparison.

Once again, estimates of Rock Mass Ratings (RMR) had to be made. In this case, these were derived from the Equation (14.14):

$$(EGPa) = 2(RMR) - 100 \qquad \ldots\ldots\ldots\ldots\ldots \qquad (14.23)$$

The predicted RMR values for the five caverns varied over a small range from 51% to 60% (fair rock).

During construction of these caverns the upper arched shape is first excavated and then the cavern is developed vertically. Therefore, the initial cavern has a slot

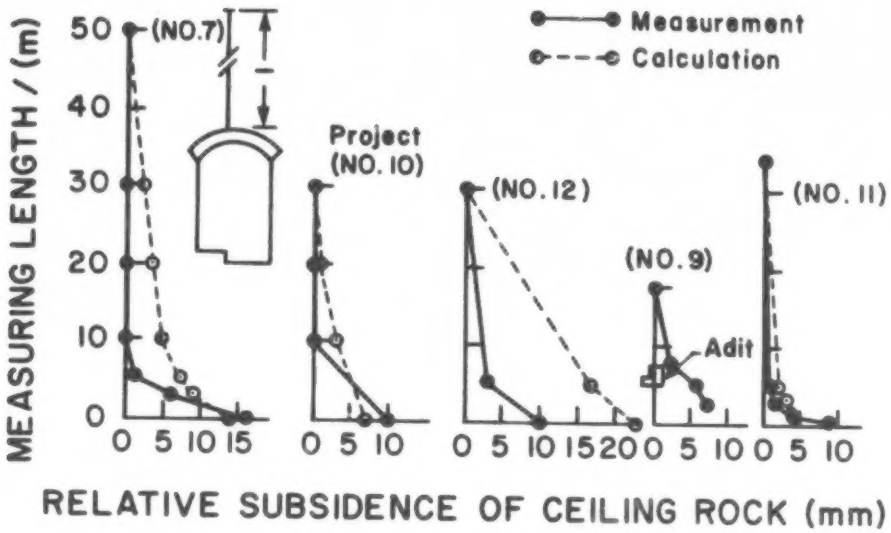

Figure 14.24 **Vertical movements in roofs above large caverns (after Hibino, Motojama, and Kanagawa (13)).**

shape with a high span/height ratio. From Figure 14.16 it can be seen that the height requiring support is approximately constant when the span/height ratio is 12 or greater. A geometry was selected to fit this condition and the appropriate in-situ stress ratios from Table 14.1 and the estimated RMR values were used to predict the depth of roof rock requiring support from the elliptical theory. Results are as follows:

Project Number	Predicted Height Requiring Support From Elliptical Theory
7	4.3
10	8.0
12	7.3
9	4.0
11	4.9

The reader is left to compare these results with Figure 14.24. Given the assumptions made and the lack of geometric equivalence of the caverns to the rectangular slot used in the theory, measured and predicted values are in reasonable agreement.

Earlier in this paper it was noted that as the height of the opening increases for a constant span, the predicted height requiring support decreases (see Figs. 14.6 and 14.10). Some confirmation of this behaviour is provided by data from the Japanese projects. Hibino et al (13) comment: "Almost all the total subsidence was generated at the stage of the arch part excavation, and the following excavation of the main part did not increase any subsidence; on the contrary, there was a tendency toward decreasing of the settlement." In other words, as the opening height increases for a constant span, roof deformations in the roof cease, or even reverse direction.

14.7 ROCK BOLT PATTERNS

The volume of rock requiring support, according to the design approach described in this paper, is elliptical in form. Bolts of constant length would be longer than necessary towards the walls of the openings (Fig. 14.25). The total length of bolts would be least

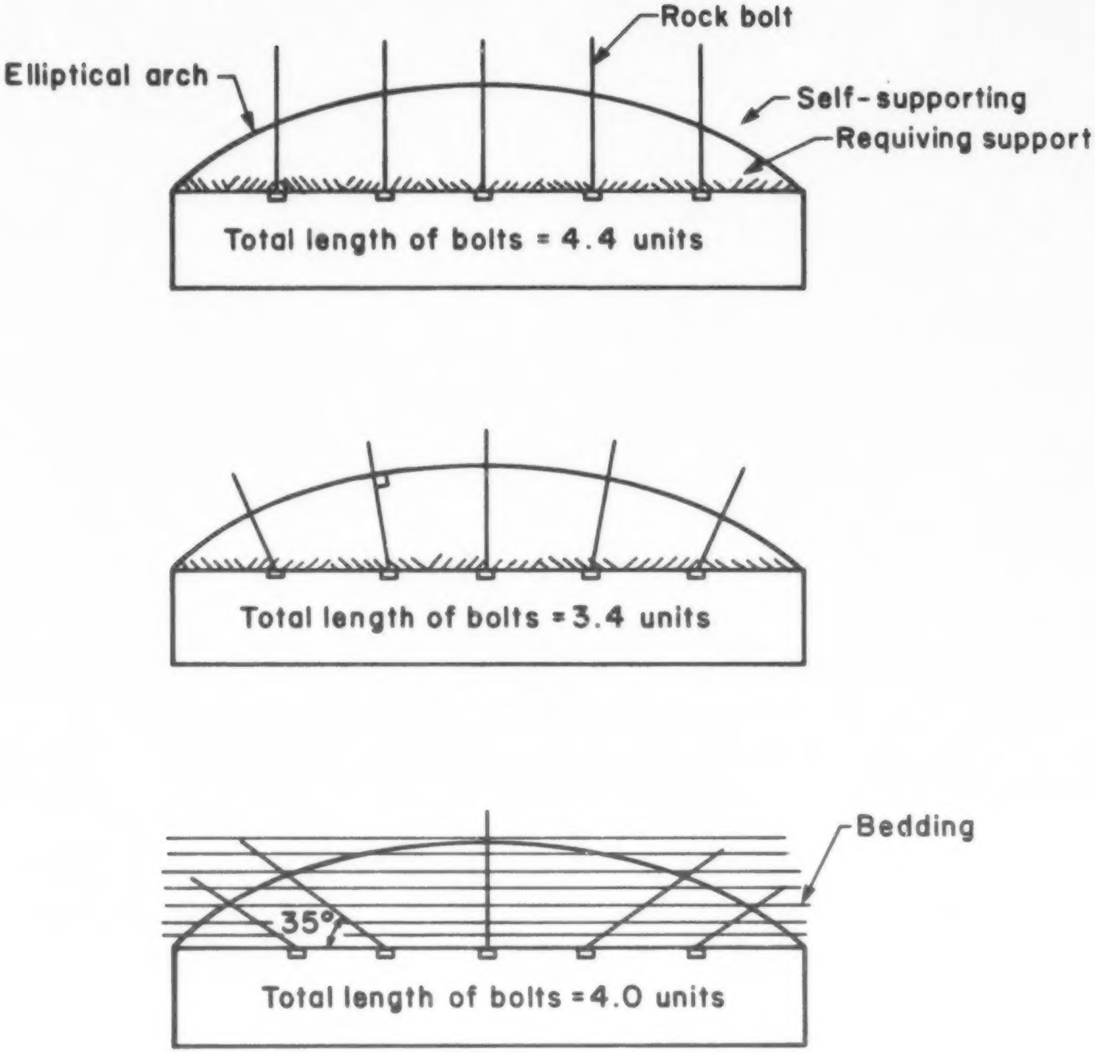
Rock bolt
Elliptical arch
Self-supporting
Requiving support
Total length of bolts = 4.4 units
Total length of bolts = 3.4 units
Bedding
35°
Total length of bolts = 4.0 units

Figure 14.25 Effect of rock bolt orientation on total length of bolts.

if bolt holes were oriented to intersect the boundary of the zone requiring support at right angles (Fig. 14.24). If the roof materials are bedded then the optimum angle of installation to the bedding is equivalent to the mobilized friction angle of the bedding planes, according to Barton and Bakhtar (15). In Figure 14.25 a mobilized friction angle of 35 degrees is assumed and this results in a total length of bolts intermediate between the two other cases.

In these three cases a uniform spacing of bolts was assumed. Stimpson (16) has demonstrated from mathematical and physical model studies that for horizontally bedded formations a non-uniform spacing is optimum for maximum reinforcement effect, with a denser bolting pattern towards the ribside of the opening.

14.8 CONCLUSIONS

The design method suggested in this paper requires data on in-situ stresses and Rock Mass Ratings before it can become used routinely. This information should be collected, along with internal roof deformation measurements, in order to optimize rock bolt patterns.

APPENDIX

CSIR ROCK MASS RATING (RMR)

This Appendix briefly outlines the rock mass classification method devised by the South African Council for Scientific and Industrial Research (CSIR). For more information the reader is referred to the paper by Z.T. Bieniawski: "**Rock Mass Classification in Rock Engineering**", which was presented to the Symposium on Exploration for Rock Engineering, Johannesburg, 1976 (Vol. 1, pp. 97-106).

The CSIR rock mass classification provides a means of describing rock quality on a scale of 0 to 100. For application the user must quantify the following variables: intact rock strength, drill core quality, spacing of discontinuities, roughness and infilling of discontinuities, groundwater conditions and orientation of discontinuities. A numerical rating is given to the rock mass for each of these characteristics according to the values listed in the following Tables.

TABLE 1 - INTACT ROCK STRENGTH

Point Load Index (MPa)	Unconfined Compressive Strength (MPa)	Rating
>8	>200	15
4 - 8	100 - 200	12
2 - 4	50 - 100	7
1 - 2	25 - 50	4
-	10 - 25	2
-	3 - 10	1
	>3	0

TABLE 2 - DRILL CORE QUALITY

Rock Quality Designation (RQD) (%)	Rating
91 - 100	20
76 - 90	17
51 - 75	13
25 - 50	8
<25	3

TABLE 3 - SPACING OF MOST INFLUENTIAL SET OF DISCONTINUITIES

Discontinuity Spacing (m)	Rating
>3	30
1 - 3	25
0.3 - 1	20
0.0005 - 0.3	10
<0.0005	5

TABLE 4 - ROUGHNESS AND INFILLING OF DISCONTINUITIES

Description	Rating
Very rough surface of limited extent; hard wall rock;	25
Slightly rough surfaces; aperture less than 1 mm; soft wall rock;	20
Slightly rough surfaces; aperture less than 1 mm; soft wall rock;	12
Smooth surfaces, or gouge filling 1 - 5 mm thick, or aperture of 1 - 5 mm; joints (discontinuities) extends more than several meters;	6
Open joints filled with more than 5 mm of gauge, or more open than 5 mm; joints (discontinuities) extend more than several meters.	0

TABLE 5 - GROUNDWATER CONDITIONS

Inflow per 10 m of Tunnel Length (1/min)	OR	Joint Water Pressure Divided by Major Principal Stress	General Conditions	Rating
0		0	Completely Dry	10
25		0.0 - 0.2	Moist	7
25 - 125		0.2 - 0.5	Water Under Moderate Pressure	4
125		0.5	Severe Water Problems	0

The ratings obtained from Tables 1 - 5 are summed to give the Rock Mass Rating (RMR) and then adjusted for the influence of joint (discontinuity) orientation according to Table 6:

TABLE 6 - ADJUSTMENTS TO RMR FOR ORIENTATION

Assessment of Influence of Joint (Discontinuity Orientation (see Table 7))	Rating Decrement (for tunneling only)
Very favourable	0
Favourable	-2
Fair	-5
Unfavourable	-10
Very Unfavourable	-12

TABLE 7 - EFFECT OF JOINT AND STRIKE DIP ORIENTATIONS ON TUNNELING

Strike Perpendicular to Tunnel Axis

Drive with Dip		Drive Against Dip	
Dip 45 - 90 Deg.	Dip 20 - 45 Deg.	Dip 45 - 90 Deg.	Dip 20 - 45 Deg.
Very Favourable	Favourable	Fair	Unfavourable

Strike Parallel to Tunnel Axis

Dip 45 - 90 Deg.	Dip 20 - 45 Deg.
Very Favourable	Fair

Dip 0 - 20 Deg. Irrespective of Strike

Unfavourable

REFERENCES

1. Morrison, R.G.K. A philosophy of ground control. Department of Mining and Metallurgical Engineering, McGill University, Montreal, Canada. (1970).

2. Unal, E. Design guidelines and roof control standards for coal mine roofs. Ph.D. Thesis, The Pennsylvania State University, U.S.A. (1983).

3. Coates, D.F. Rock mechanics principles. Energy, Mines and Resources Canada, Monograph 874 (Revised) (1981).

4. Wagner, H. In rock mechanics in mining practice. Edited by S. Budavari, Chapter 12: "Protection of Service Excavations." The South African Institute of Mining and Metallurgy, Johannesburg. (1983).

5. Denkhaus, H.G. Critical review of strata movement theories and their application to practical problems. Journal of the South African Institute of Mining and Metallurgy, 64, pp. 310-332. (1964).

6. Peng, S.S. Coal mine ground control. John Wiley & Sons, New York. (1978).

7. Stheeman, W.H. A practical solution to cable bolting problems at the Tsumeb Mine. The Canadian Mining and Metallurgical Bulletin, 75, No. 838, pp. 65-77. (1982).

8. Walton, G. and Taylor, R.K. Likely constraints on the stability of excavated slopes due to underground coal workings. Proceedings of Conference on Rock Engineering, Newcastle upon Tyne, England, pp. 329-349. (1977).

9. Stimpson, B. and Walton, R.K. Clay mylonites in English coal measures - their significance in opencast slope stability. Proceedings First International Congress of the International Association of Engineering Geology, Paris, Vol. 2, Sect. 9. (1970).

10. Szechy, K. The art of tunnelling. Akademiai Kiado, Budapest. (1966).

11. Terzaghi, K. Rock defects and loads on tunnel supports. In Rock Tunnelling with Steel Supports. Editors: R.V. Proctor and T.L. White. (1946).

12. Protodyakanov, M.M. Methods of studying the strength of rocks used in the U.S.S.R. Proceedings of International Symposium on Mining Research. Edited by G.B. Clark, Pergamon Press, London, pp. 649-668. (1962).

13. Hibino, S., Motojima, M. and Kanagawa, T. Behaviour of rocks around large caverns during excavation. Proceedings of the International Congress on Rock Mechanics, Melbourne, Australia, Vol. D, pp. 199-202. (1983).

14. Bieniawski, Z.T. Determining rock mass deformability - experience from case histories. International Journal of Rock Mechanics and Mining Sciences, 15, No. 5, pp. 237-248. (1978).

15. Barton, N. and Bakhtar, K. Bolt design based on shear strength. Proceedings of the International Symposium on Rock Bolting, Abisko, Sweden, pp. 367-376. (1983).

16. Stimpson, B. The influence of rock bolt location on the reinforcement of horizontally bedded roofs by full column grouted bolts. Ibid, pp. 195-204. (1983).

17. Kvapil, R. Gravity flow of granular materials in hoppers and bins: Parts I, II. International Journal of Rock Mechanics and Mining Sciences, 2, pp. 35-41 and 277-304. (1965).

18. Fairhurst, C. and Singh, B. Roofbolting in horizontally laminated rock. Engineering and Mining Journal, February, pp. 81-87, 89. (1974).

CHAPTER 15

RECOMMENDATIONS FOR DESIGN AND OPTIMIZATION OF ROOF BOLTING IN LAYERED STRATA

15.1 INTRODUCTION

The research results presented in this report represent an attempt to approach roof bolt design in layered strata by a rational, scientific approach which takes into account the modes of deformation and failure of two types of roof - layered, and layered with cross joints. These studies have emphasized the necessity for the designer of support systems to have a thorough understanding of rock mechanics, geology and ground/support interaction.

The types of roof encountered in underground mining are as varied as the geological conditions. Not every case will fall into the two categories examined here and will therefore need a different design approach. Chaper 14 presents one such method; others are described in a number of texts (1,2,3).

The mathematical modelling used in this report is important primarily in drawing attention to the factors which influence support loading and design. In no sense should it be expected that these, or any other design methods, will predict loads precisely; if they do, it is quite fortuitous. Indeed, owing to the influence of geology (joints, bedding, lateral and vertical variations in physical, mechanical and geometric properties), timing of installation, interaction between openings, and the quality of workmanship, it makes no sense to even talk of "the load" on a support.

Whatever statements have already been made in this report concerning design, or will be made subsequently, these must be viewed as concepts or suggested procedures whose veracity or otherwise can only be established by monitoring the performance of actual openings. Convergence is not only a mechanical process, but also a design process in which theory and observation allow the designer to converge, after a number of trials, upon the optimum solution for the support of a particular sequence of strata under a particular set of working conditions.

Finally, a single-minded attachment to production rates, or rates of advance with little attention paid to understanding support/rock interaction and roof behaviour, can ultimately lead to problems which result in a reduction or cessation of progress while the problem is solved or, in some cases, a change in mining method, layout or equipment.

15.2 DESIGN CONCEPTS

It is suggested that the following design concepts be tested:

1) Non-uniform spacing;
2) Bolting over abutments;
3) Non-uniform bolt lengths;
4) Replacement of resin grout with less expensive grouts;
5) Inclined bolts.

15.2.1 Non-uniform Spacing

Because differential slip between roof strata is greatest adjacent to the ribs or sides of the opening, bolt spacing should be closer over the 1/3 rd of the span adjacent to the walls than over the remaining 1/3 rd forming the centre of the span. For each row across the span two bolts should be installed about 0.2 x span from the ribside or tunnel wall. The average spacing should be equal to that determined on the basis of a uniform spacing (see, for example, the design method described in Chapter 13).

15.2.2 Bolting Over Abutments

Where the ribs supporting a roof, or an opening, are weak and deformable, consideration should be given to reinforcement of the roof strata over the abutment to prevent tensile and/or shear failures.

15.2.3 Non-Uniform Bolt Lengths

The patterns of displacement in bedded roofs following excavation suggest that bolt lengths close to the abutment can be reduced, compared to those in the central part of the span. A simple means of estimating bolt lengths is afforded by the elliptical theory developed in Chapter 14. For example, in Figure 15.1, which illustrates a vertical bolt installed from point A, the required total length is $(x_b + x_a)$, where x_a is the anchor length. x_a should be chosen to be of sufficient length to provide adequate pull-out strength, plus a Factor of Safety.

15.2.4 Replacement of Resin Grout

It has been shown in this research that horizontal slip is greatest towards the abutments. The high shear stiffness and shear strength of resin-grouted bolts is beneficial in these areas, but a less expensive grout could be substituted in most cases, especially in the central parts of the span where horizontal slip is negligible.

15.2.5 Inclined Bolts

Grouted, untensioned bolts should be placed at an angle to the anticipated direction of differential slip. Theoretically, the angle should be equal to the angle of effective friction of the slip surface, but some departure from this rule may be warranted on the basis of reducing overall bolt length. Excessive bolt length would otherwise be predicted for roofs with low effective friction angle along potential horizontal slip surfaces.

15.2.6 Conceptual Design

The various components discussed in 15.2.1 - 15.2.5 are combined conceptually in Figure 15.2. The upper diagram shows a conventional layout with bolts of uniform length and spacing. The lower diagram illustrates a layout with inclined bolts which are spaced non-uniformly and are of different lengths. The chosen lengths reflect a compromise between the minimum lengths to reach the elliptical boundary, plus an

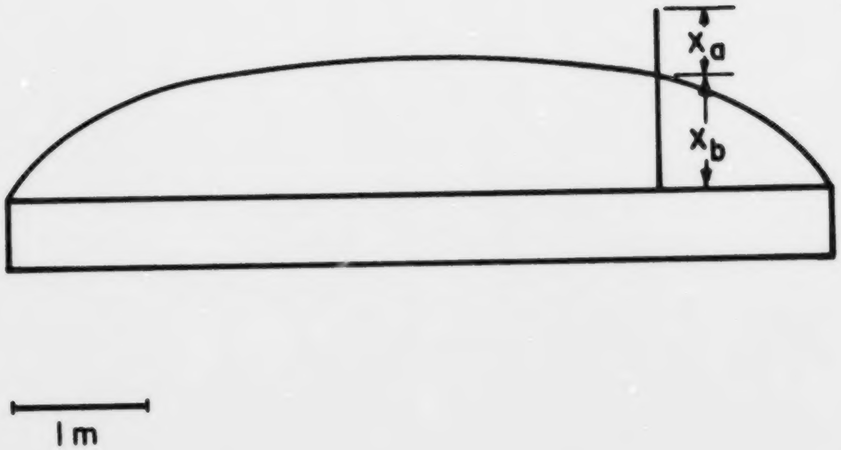

Figure 15.1 Example of non-uniform bolt lengths.

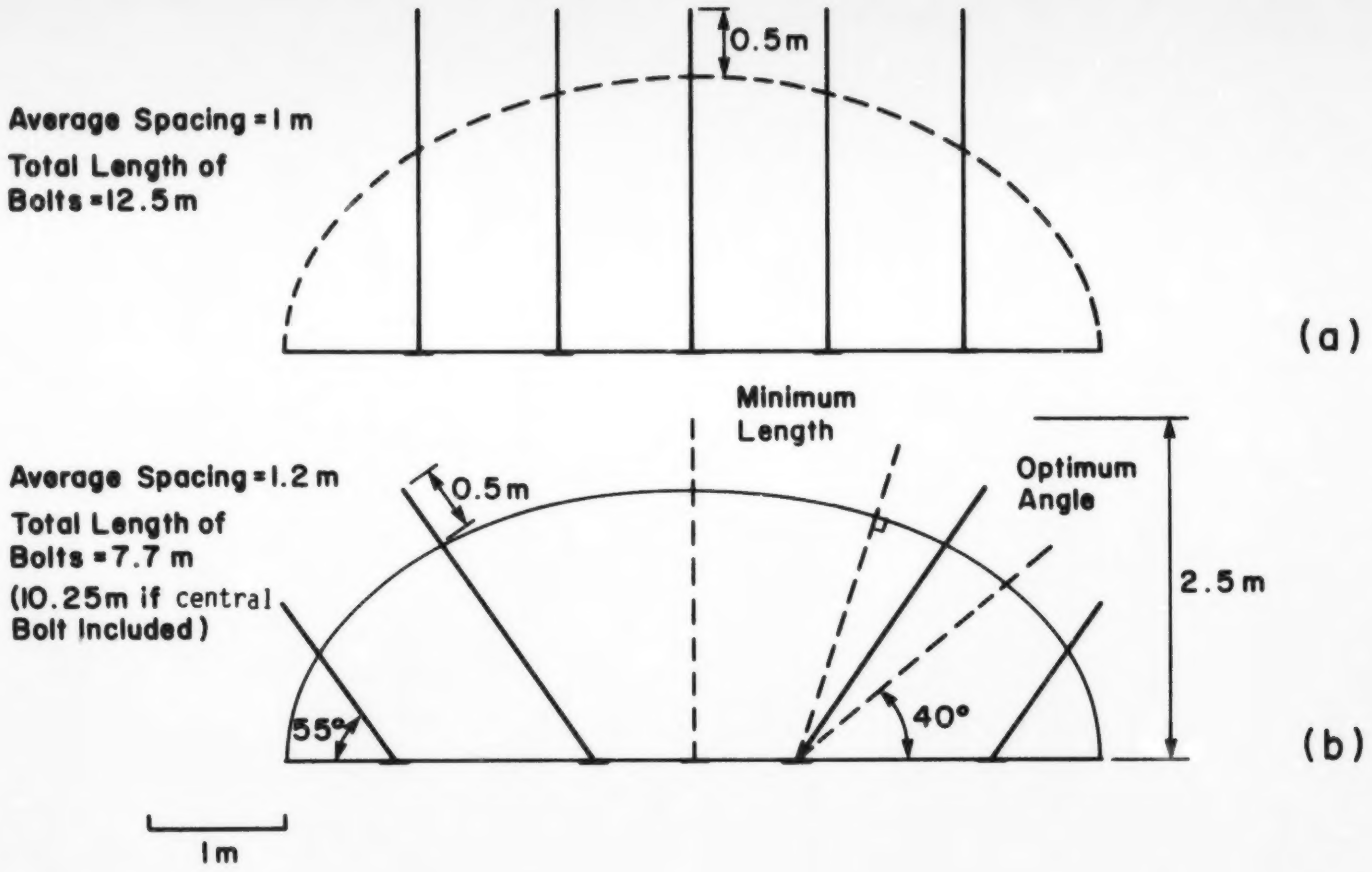
Average Spacing = 1 m
Total Length of Bolts = 12.5 m
0.5m
(a)
Minimum Length
Average Spacing = 1.2 m
Total Length of Bolts = 7.7 m
(10.25m if central Bolt included)
0.5m
Optimum Angle
2.5m
55°
40°
(b)
1m

Figure 15.2 Conceptual design using various principles - non-uniform spacing, different lengths, inclined.

anchor length and the requirement that the bolts be inclined at the effective friction angle of the potential slip surface (40 deg.). The bolt angle was allowed to vary by up to 15 deg. from this value to reduce bolt length. The pattern for minimum bolt length is also shown in Figure 15.2(b).

15.3 GRAPHICS SOFTWARE FOR MICROCOMPUTERS

It is recommended that consideration be given to producing an integrated graphics-supported program of the various design methods developed in this project. Such a package would have the following capabilities:

1) Representation on screen of the mine opening and strata in the roof, including mechanical properties, joint spacings, and rock mass ratings. These might be input by light pen or mouse, or by co-ordinates.
2) Determination of shear and axial stiffnesses of bolt given mechanical properties of bolt, rock and grout, hole and bolt diameter.
3) Determination of and representation on screen of the elliptical zone requiring support and the anticipated bolt loads for various bolt spacings.
4) Determination of bolt spacing for required Degree of Reinforcement and reproduction of bolting layout on screen.
5) Determination of Degree of Reinforcement for a given rock bolt spacing. Rock bolt positions may be entered on screen by light pen, mouse, or by co-ordinates.
6) Determination of bolt pattern by the ground convergence-support reaction design method, as described in Chapter 13. Graphs of p/p_o vs. u/u_{max} and normalized pull-out loads presented on screen.
7) Determination of modified bolt pattern to include bolt inclination and minimum bolt length to boundaries of elliptical zone.

8) Determination of the type of roof failure (if any) to be anticipated for an unsupported roof.

9) Deterministic or probabilistic solutions.

In order to reach these goals, some additional work is recommended to improve the design procedures: (a) finite element analysis of cross-jointed beams to develop an empirical relationship between effective Young's modulus, joint spacing and beam thickness, and (b) a modified analysis of multiple beam interaction to account for the fact that the effective span of beams decreases with their distance into the roof. This response is seen, for example, in the arch-shaped zone of loosening observed in the physical model studies described in Chapter 10.

15.4 IN-SITU DETERMINATION OF ROOF BOLT SPACING

It has already been noted that support design must take into account a complex series of factors, most of which cannot be quantitatively defined with any great precision. These include rock and water conditions, response to excavation, method of excavation, timing of support installation, type(s) and details of support, and quality of workmanship. Monitoring is therefore essential if a rational design of supports is to be achieved.

Essentially, what is required from a monitoring program is the location, extent and rates of rock movement, and support loading or strain. Ideally, this means the installation of extensometers anchored at various distances into roof **BEFORE** excavation and careful measurement of displacements as the face is advanced. Economics and safety only occasionally make this methodology practicable.

An alternative approach is to install a dense pattern of bolts in several test areas and, after establishing the long-term stability of the roof, successively remove bolts while measuring roof bolt strain and roof convergence. This method is only applicable where the test areas can be sacrificed (4).

In most situations, instrumentation can be installed close to the face, but only after the face has passed. Support is usually added, particularly if the ground conditions are poor. Detailed collection of data on convergence, roof separation and bolt loads as the face advances, face advance rates, and timing of installation, is essential. From these measurements, it is possible to determine whether bolt loads are stabilizing or steadily increasing.

It is essential that both bolt load and roof movements are collected. It is possible for bolt loads to remain constant while the roof is failing.

15.5 CLOSURE

The design of support systems on which human lives depend must of necessity lean towards conservatism. Thus, while the optimization of roof bolting patterns must always include a substantial safety factor, there is considerable opportunity for reducing costs while improving support through a combination of improved design methods and in-situ studies. It is the hope of the author that the results of this project have assisted in moving towards this goal.

REFERENCES

1. Hoek, E. and Brown, E. Underground excavations in rock. Inst. Min. Metall., London (1980).
2. Coates, D. Rock mechanics principles. Energy, Mines and Resources. (1981).
3. Peng, S.S. Coal mine ground control. John Wiley & Sons. (1978).
4. Merrill, R.H., Morgan, T.A., Stehlik, C.J. Determining the in-place support of mine roof with rock bolts, White Pine Copper Mine, Michigan. U.S.B.M., R.I. 5746.

APPENDIX A1

ESTIMATING AXIAL, BENDING AND SHEAR STIFFNESS OF A FULL COLUMN RESIN BOLT

Introduction:

A full column grouted bolt installed in a horizontally bedded roof is subjected to both axial and shear loads. In this appendix some approximate analyses are presented for determining equivalent stiffnesses of the rock fixture under axial and transverse loading (1). Only the bolt and resin properties are considered. Appendix A2 includes the effect of rock properties, bolt inclination and bed separation on shear stiffness of a bolted joint.

Axial Stiffness

The equivalent axial stiffness may be approximated by (Kamal (2)):

$$R = \frac{\pi}{4} d_1^2 E_b \left[1 + \frac{E_g}{E_b} \left(\frac{d_2^2 - d_1^2}{d_1^2} \right) \right] \text{ force/strain} \quad \ldots\ldots\ldots\ldots \quad (A1.1)$$

where d_1 = bolt diameter,
d_2 = hole diameter, $(d_2 - d_1)$ = grout annulus thickness,
E_b = modulus of steel bolt,
E_g = modulus of grout (resin).

The equivalent modulus may be defined as:

$$\overline{E} = \frac{R}{A_2}, \quad \ldots\ldots\ldots\ldots\ldots \quad (A1.2)$$

where $A_2 = \frac{\pi}{4} d_2^2$.

Therefore, from Equations (A1.1) and (A1.2):

$$\frac{\overline{E}}{E_b} = \frac{d_1^2}{d_2^2} \left[1 + \frac{E_g}{E_b} \left(\frac{d_2^2 - d_1^2}{d_1^2} \right) \right] \quad \ldots\ldots\ldots\ldots \quad (A1.3)$$

For a high stiffness grout, $E_g/E_b = 0.05$
For a low stiffness grout, $E_g/E_b = 0.005$
In both cases, $E_b = 207$ GPa

Then, for high stiffness grout (E_g = 10.35 GPa),

$$\overline{E}/E_b = \frac{1}{K^2}\,(1 + 0.05\,(K^2 - 1))\ . \qquad \ldots\ldots\ldots\ldots \qquad \text{(A1.4)}$$

And, for low stiffness grout (E_g = 1.04 GPA)

$$\overline{E}/E_b = \frac{1}{K^2}\,(1 + 0.005\,(K^2 - 1)) \qquad \ldots\ldots\ldots\ldots \qquad \text{(A1.5)}$$

where $K \equiv d_2/d_1$.

Values of $\overline{E}/E_b$ from Equations (A1.4) and (A1.5) are tabulated in Table A1.1.

TABLE A1.1

EQUIVALENT AXIAL STIFFNESS RATIOS FOR SOME TYPICAL BOLTING GEOMETRIES

d_1 mm	d_2 mm	$\overline{E}/E_b$ (Eqn. A1.4)	$\overline{E}/E_b$ (Eqn. A1.5)
19.1	25.4	0.59	0.57
22.2	28.6	0.62	0.60
25.4	34.9	0.55	0.53

From the values in this Table, it is apparent that the equivalent bolt axial stiffness is only slightly affected by the modulus of the grout.

Bending Stiffness

For bending analysis, the rock bolt, plus annulus of grout (resin) may be treated as a beam of circular cross-section containing a core of material (steel) of high flexural rigidity surrounded by a coaxial layer of material (grout) of low flexural rigidity. From classical, linear elastic beam theory it may be shown that the moment at any cross-section of this two-material beam is given by

$$M = \frac{1}{\rho}\left[\frac{E_b\,\pi\,d_1^4}{64} + \frac{E_g\,\pi}{64}\left(d_2^4 - d_1^4\right)\right] \qquad \ldots\ldots\ldots\ldots \qquad \text{(A1.6)}$$

where ρ = radius of curvature of beam.

A single-material beam of diameter, d_2 , will have the same flexural rigidity (bending stiffness), $\overline{EI}$, as the two-layer beam of the same diameter if:

$$\overline{EI} \equiv \rho M \qquad \ldots\ldots\ldots\ldots \qquad \text{(A1.7)}$$

where I is the second moment of area of the bolt about the central axis.

From Equations (A1.6) and (A1.7) and letting $I_2 = \frac{\pi d_2^4}{64}$:

$$\frac{\overline{EI}}{E_b\ I_2} = \left(\frac{d_1}{d^2}\right)^4 + \frac{E_g}{E_b}\left[1 - \left(\frac{d_1}{d_2}\right)^4\right] \quad \text{............} \quad (A1.8)$$

For a high stiffness grout, $E_g/E_b = 0.05$

For a low stiffness grout, $E_g/E_b = 0.005$

In both cases, E = 207 GPa.

Then, for high stiffness grout, (E_g = 10.35 GPa)

$$\frac{\overline{EI}}{E_b\ I_2} = 0.05 + \frac{0.95}{K^4} \quad \text{............} \quad (A1.9)$$

And, for low stiffness grout, (E_g = 1.04 GPa)

$$\frac{\overline{EI}}{E_b\ I_2} = 0.005 + \frac{0.995}{K^4} \quad \text{............} \quad (A1.10)$$

where $K \equiv d_2/d_1$.

Values of $\overline{EI}/E_b\ I_2$ from Equations (A1.9) and (A1.10) are tabulated in Table A1.2.

TABLE A1.2

EQUIVALENT FLEXURAL RIGIDITY RATIOS FOR SOME TYPICAL BOLTING GEOMETRIES

d_1 mm	d_2 mm	$\overline{EI}/E_b\ I_2$(Eqn. A1.9)	$\overline{EI}/E_b\ I_2$(Eqn. A1.10)
19.1	25.4	0.35	0.32
22.2	28.6	0.39	0.37
25.4	34.9	0.32	0.28

The ratios given in this Table indicate that flexural rigidity is only slightly influenced by the stiffness of the grout.

Shear Stiffness

A full column grouted bolt subjected to direct shear may be analysed by treating it as a transversely loaded beam (bolt) resting on an elastic foundation (grout) (Fig. A1.1).

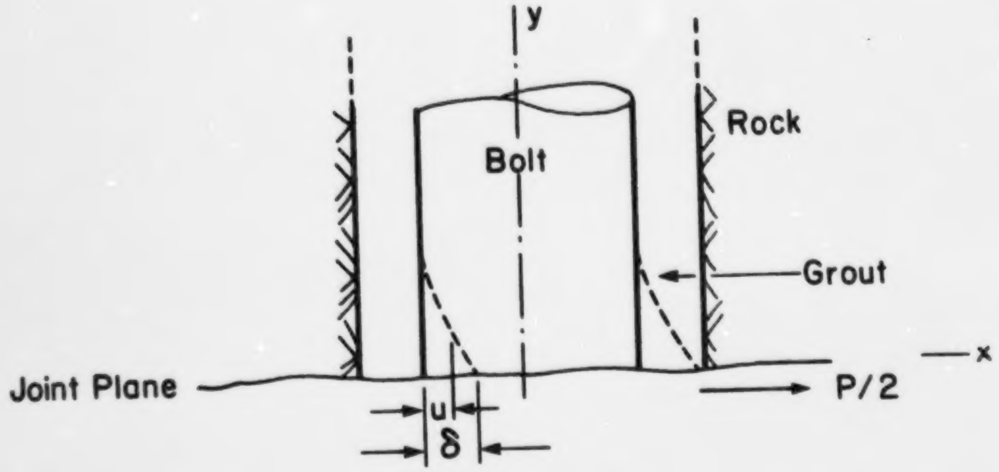
y
Rock
Bolt
Grout
x
Joint Plane
P/2
u
δ

----- Deflected Position of Bolt

Figure A1.1 Bolt subjected to direct shear

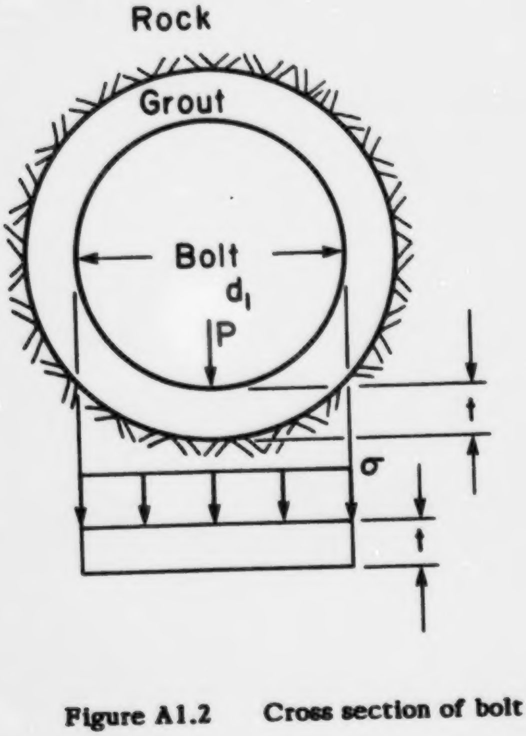
Rock
Grout
Bolt
d_1
P
t
σ
t

Figure A1.2 Cross section of bolt and assumed loading

Deflections are governed by the following differential equation:

$$E_b\, I \frac{d^4u}{dy^4} + Ku = 0 \qquad \text{............} \qquad (A1.11)$$

where E_b = Young's modulus of the bolt,
I = second moment of area of the bolt about its central axis,
u = deflection of the bolt in the x-direction (Fig. A1.1),
K = elastic foundation modulus of grout.

The solution of equation (A1.11) is:

$$u = e^{-\beta y}(C \cos\beta y + B \sin\beta y) \qquad \text{............} \qquad (A1.12)$$

where C, D, and β are constants whose values are determined from boundary conditions, leading to:

$$C = \frac{P}{2E_b\, I\beta^3}\ ,\ D = 0\ ,\ \text{and}\ \beta = \sqrt[4]{\frac{k}{4E_b\, I}}$$

where P is the shear force acting on the bolt.

An approximate value for K may be determined by assuming that the bolt bears on the grout with an average compressive stress, σ, over a distance equal to the bolt diameter, d_1, (Fig. A1.2). Thus,

$$P = Ku = \sigma d_1 = E_g\, \varepsilon_g\, d_1 = E_g \frac{u}{t} d_1$$

$$= \frac{2E_g\, d_1\, u}{d_2 - d_1}\ . \qquad \text{............} \qquad (A1.13)$$

Therefore, $$K \equiv 2E_g/((d_2/d_1) - 1)\ . \qquad \text{............} \qquad (A1.14)$$

The shear stiffness, K_s, of the bolted joint is given by:

$$K_s = \frac{P}{2\delta}\ , \qquad \text{............} \qquad (A1.15)$$

where δ = deflection of one half of the bolt at the plane of shear. 2 must be used in Equation (A1.15) since the bottom half of the joint block moves by the same amount in the opposite direction.

but δ = u(at y = 0) from Equation (A1.12).

Therefore, $\delta = u(y = 0) = C = \dfrac{P}{2EI\beta^3}$

From which,

$$\frac{P}{2u} = \frac{P}{2\delta} = EI\beta^3 \qquad \text{............} \quad \text{(A1.16)}$$

The effect of annulus thickness is tabulated in Table A1.3, using Equation (A1.16) for three typical bolthole diameters.

TABLE A1.3

BOLT SHEAR STIFFNESS FOR THREE BOLTHOLE DIAMETERS AND THREE BOLT DIAMETERS

d_1 mm	d_2 mm	$(d_2 - d_1)$	K_S(MN/m)
E = 10.35 GPa			
19.1	25.4	6.3	269
22.2	28.6	6.4	346
25.4	34.9	9.5	325
E = 1.04 GPa			
19.1	25.4	6.3	48
22.2	28.6	6.4	62
25.4	34.9	9.5	58

The rate at which the bolt deflection reduces along its axis in a direction away from the shear plane can be evaluated from Equation (A1.12). The deflection decays to 5% of its maximum value at the shear plane when (approximately):

$$e^{-\beta y} = 0.05 \qquad \text{............} \quad \text{(A1.16)}$$

Therefore,

$$y = 3/\beta \,. \qquad \text{............} \quad \text{(A1.17)}$$

Values of the distance y at which the deflection has declined to 5% of its value at the shear plane as predicted by Equation (A1.17) are in the range 2-10 cms. For example, For $d_1 = 19.1$ mm , $d_2 = 25.4$ mm , $E_b = 207$ GPa

i) $E_g = 10.35$ GPa , y(for 5% deflection) = 5.1 cms.

ii) $E_g = 1.04$ GPa , y(for 5% deflection) = 9.1 cms.

REFERENCES

1. Gerdeen J.C., Snyder, V.W., Viegelahn, G.L. and Parker, J. "Design criteria for roof bolting plans using fully resin-grouted nontensioned bolts to reinforce bedded mine roof." Vol. IV. Theoretical Analysis. Report prepared for USBM, Contract No. J036004 (1977).

2. Kamal, S.A. "Analysis of multi-axial anisotropic creep, roof resin bolts and bed separation in rock structures using the finite element method." Ph.D. Dissertation, Michigan Technological University, Houghton, Michigan (1976).

APPENDIX A2

NEW METHOD FOR ESTIMATING SHEAR STIFFNESS OF NON-TENSIONED, RESIN GROUTED BOLT WHICH INCLUDES RESIN, ROCK AND BOLT PROPERTIES, BED SEPARATION AND BOLT INCLINATION

When a non-tensioned resin bolt is installed in layered strata there may be bed separation, so that the bolt spans the gap developed between beds. Also, the bolt may not be perpendicular to the plane which has opened but be inclined at some other angle.

Figure A2.1 illustrates this general case. R is the shear force inducing differential movement and δ is the width of the gap. The shape of the bolt after some shear displacement is shown with dashed lines.

The total shear displacement of the bolt is made up of two components:

(a) Bending of bolt

(b) Compression of resin and rock.

Let M_o be the bending moment at end A of the bolt, as shown in Figure A2.1. Moment equilibrium at any point, x , along the bar requires:

$$M(x) = M_o - Rx \cos\alpha \ , \qquad \text{..............} \quad \text{(A2.1)}$$

where α = acute angle between bolt and shear plane.

But, from classical beam theory,

$$E_b \ I \frac{d^2y}{dx^2} = - M = - M_o + Rx \cos\alpha \ , \qquad \text{..............} \quad \text{(A2.2)}$$

where E_b = Young's modulus of bolt material,

I = moment of inertia of bolt about neutral axis.

Integrating (A2.2) ,

$$E_b \ I \frac{dy}{dx} = - M_o \ x + \frac{Rx^2 \cos\alpha}{2} + C_1 \ . \qquad \text{..............} \quad \text{(A2.3)}$$

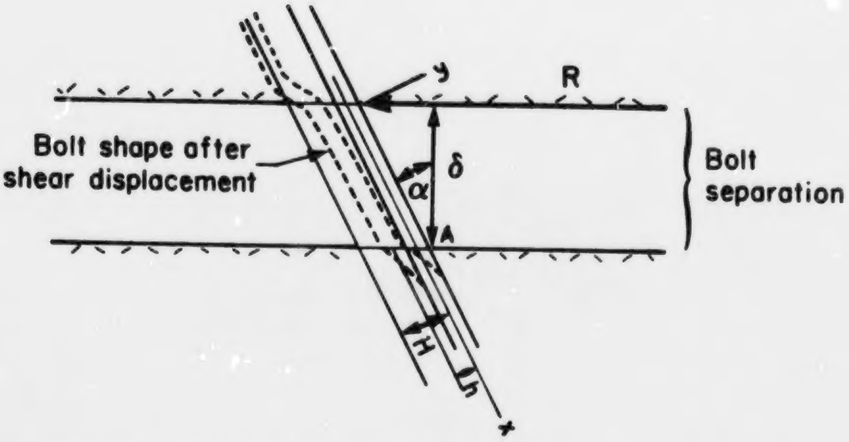
y
R
Bolt shape after shear displacement
δ
α
A
Bolt separation
H
h
x

Figure A2.1 Displacement of an inclined bolt subjected to direct shear along an open joint

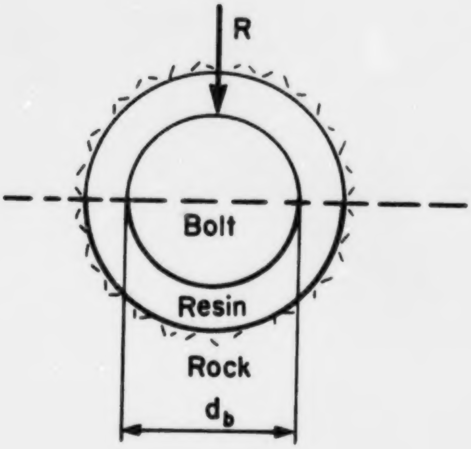
R
Bolt
Resin
Rock
d_b

Figure A2.2 Determination of foundation modulus of bolt

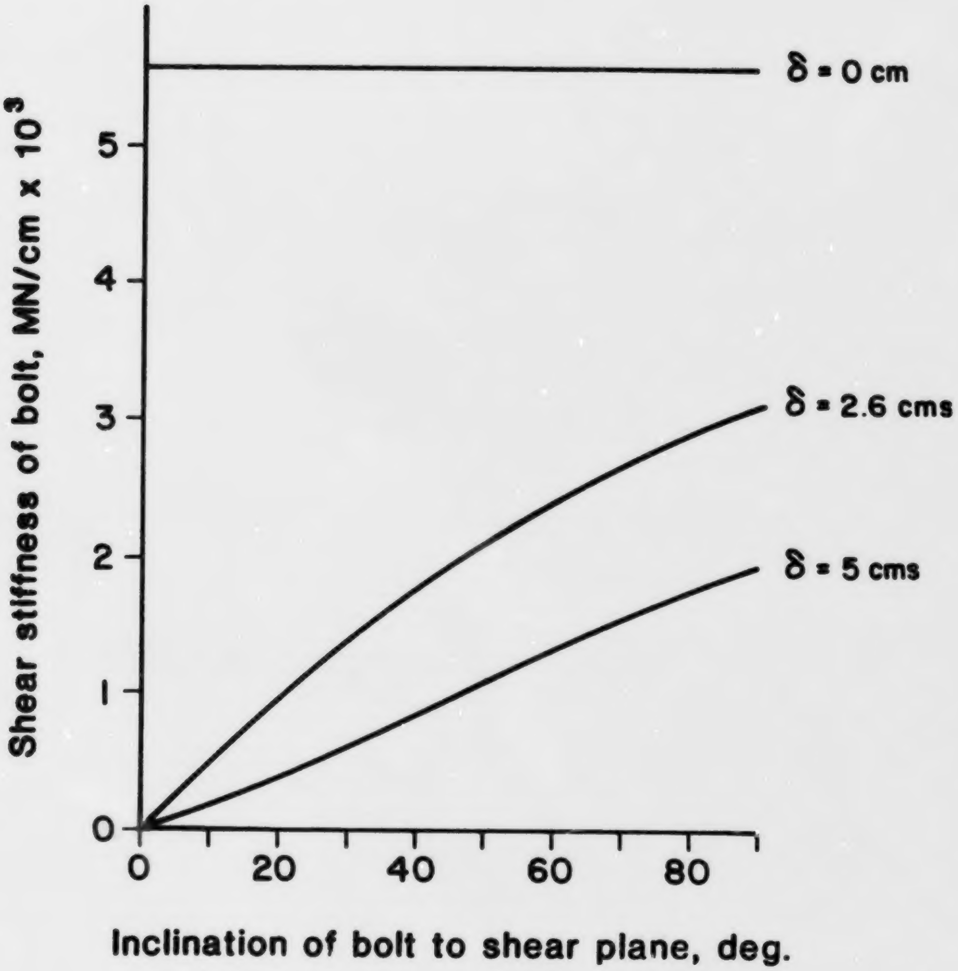

Figure A2.3 Effect of bolt inclination on shear stiffness for three joint openings (Young's modulus of rock = 20 GPa, Young's modulus of grout = 2 GPa,Young's modulus of bolt = 207 GPa, bolt diameter = 1.9 cm, hole diameter = 2.5 cm)

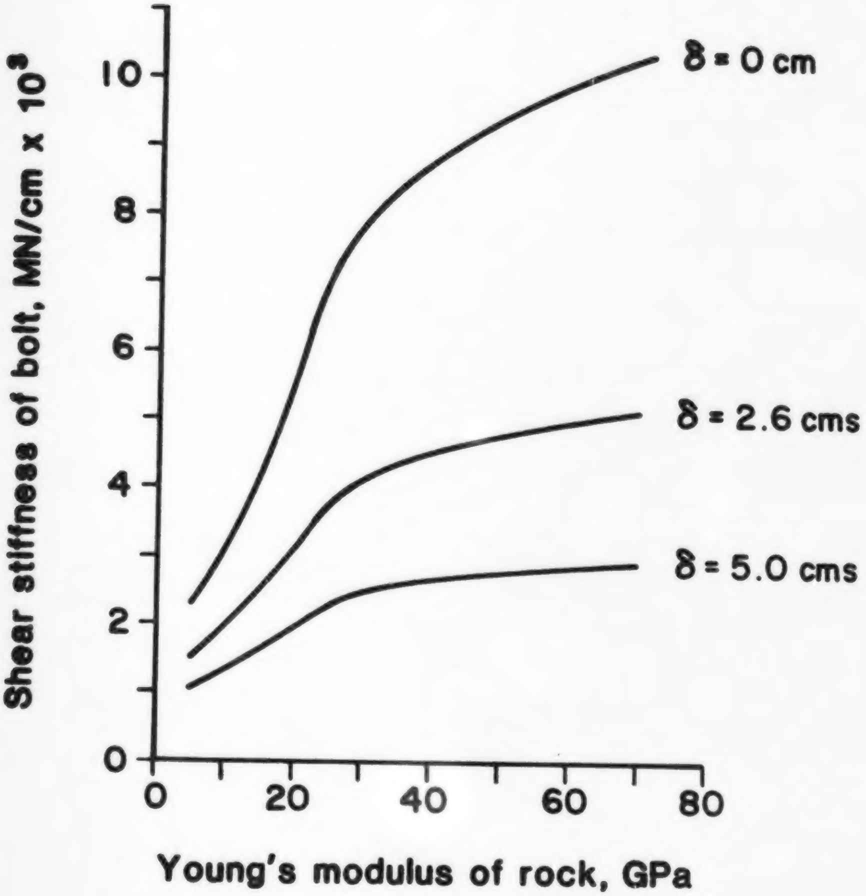

Figure A2.4 Effect of Young's modulus of rock on shear stiffness for three joint openings (Young's modulus of grout = 2 GPa, Young's modulus of bolt = 207 GPa, bolt diameter = 1.9 cm, hole diameter = 2.54 cm, bolt inclination = 90 deg.)

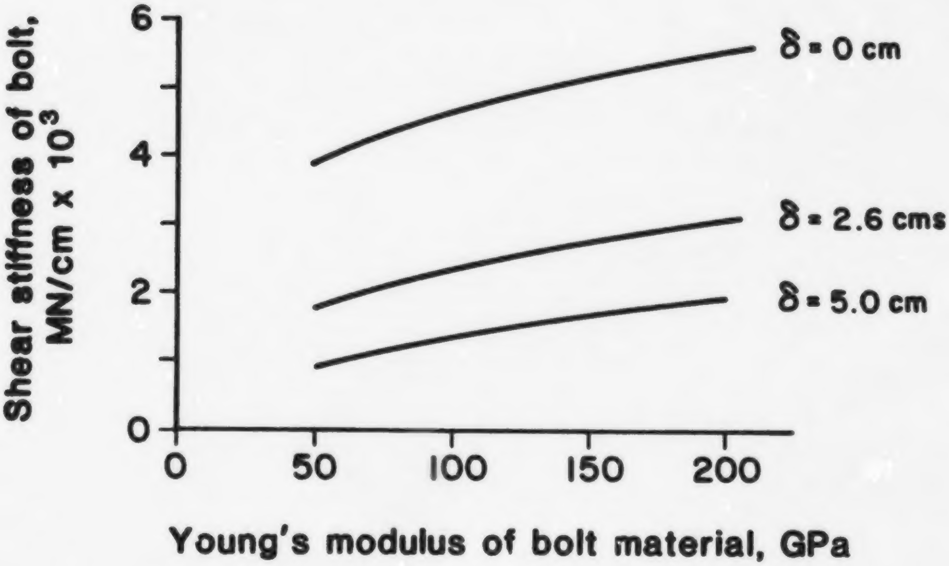

Figure A2.5 Effect of Young's modulus of bolt on shear stiffness for three joint openings (Young's modulus of rock = 20 GPa, Young's modulus of grout = 2 GPa, bolt diameter = 1.9 cm, hole diameter = 2.54 cm, bolt inclination = 90 deg.)

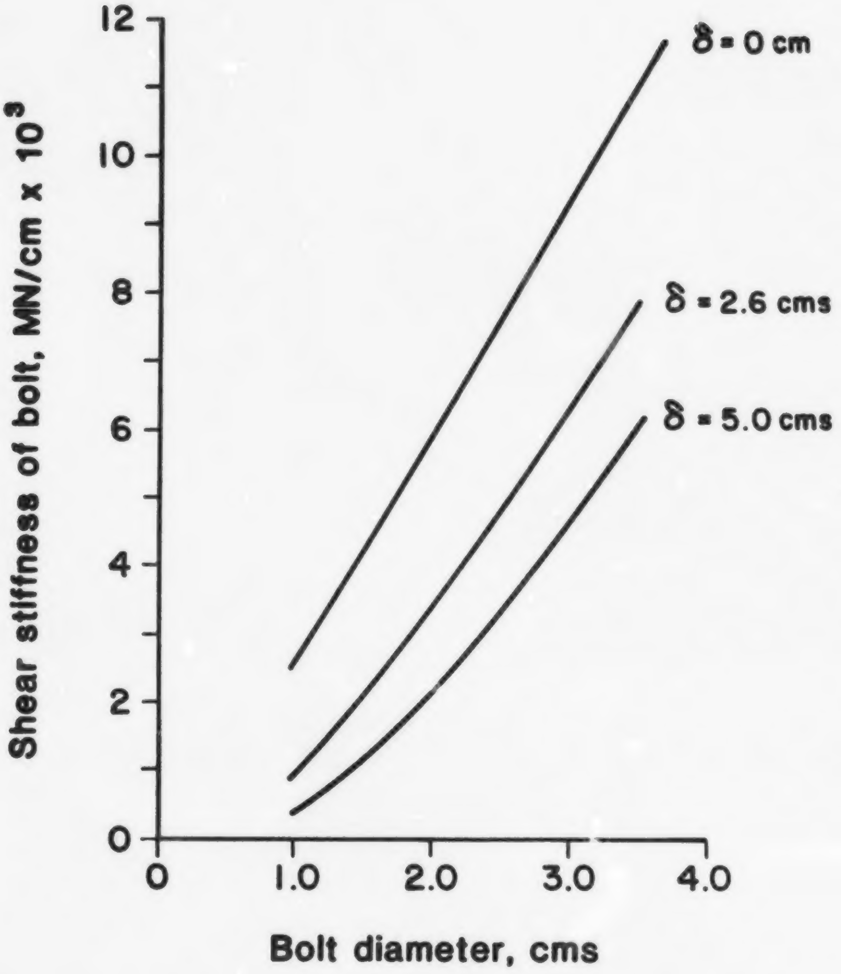

Figure A2.6 Effect of bolt diameter on shear stiffness for three joint openings (Young's modulus of rock = 20 GPa, Young's modulus of grout = 2 GPa, Young's modulus of bolt = 207 GPa, resin annulus thickness = 0.32 cm, bolt inclination = 90 deg.)

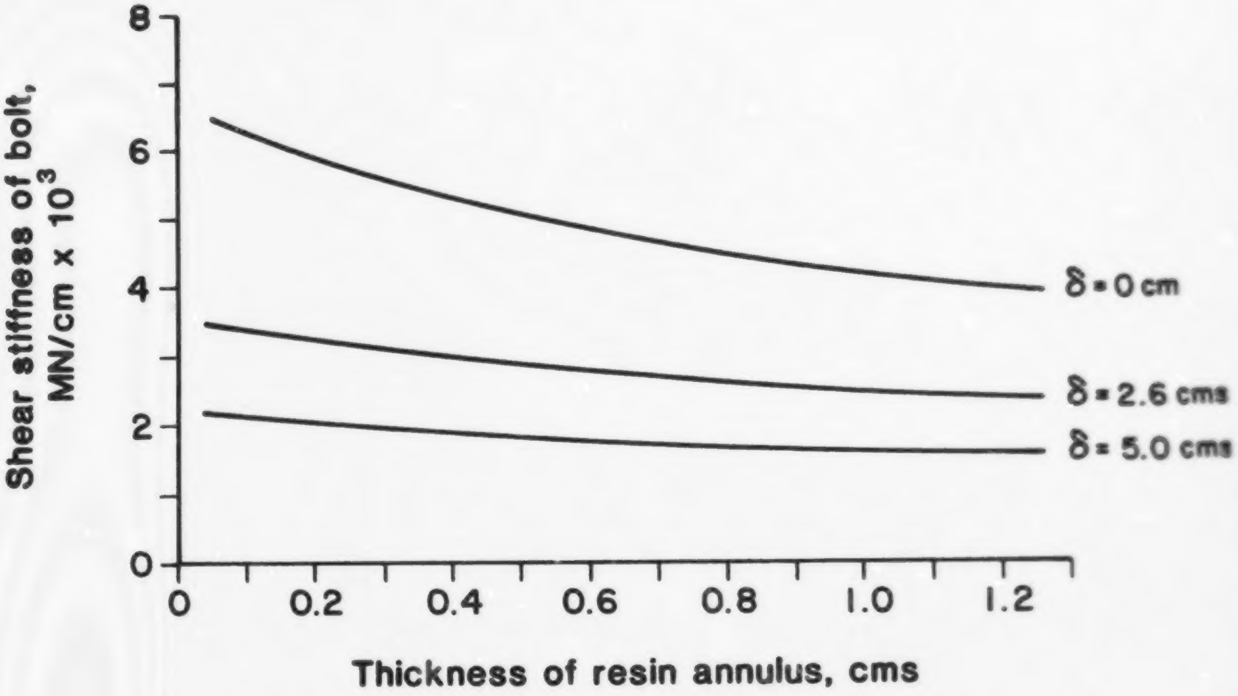

Figure A2.7 **Effect of thickness of grout annulus on shear stiffness for three joint openings (Young's modulus of rock = 20 GPa, Young's modulus of grout = 2 GPa, Young's modulus of bolt = 207 GPa, bolt diameter = 1.9 cm, bolt inclination = 90 deg.)**

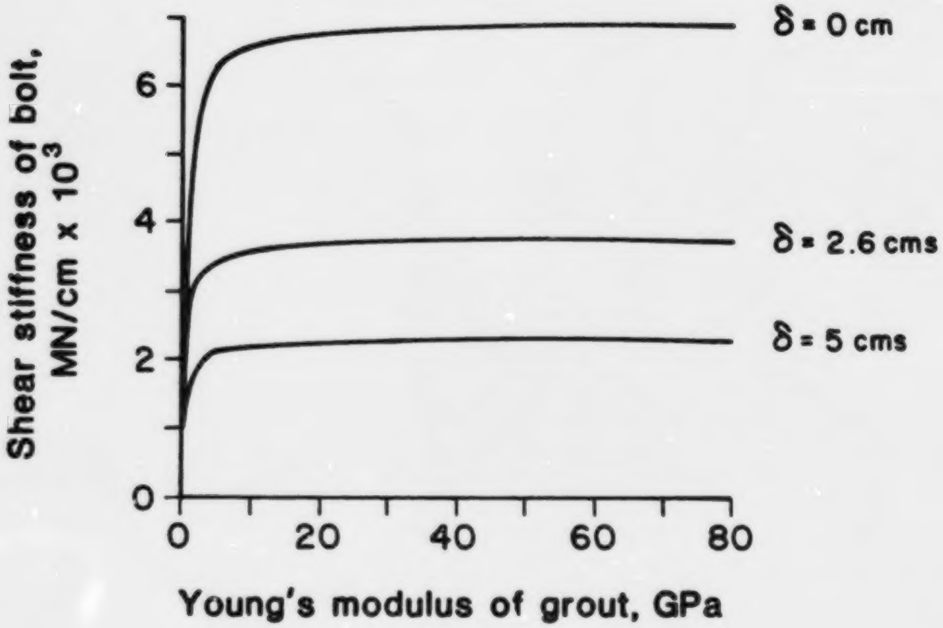

Figure A2.8 Effect of Young's modulus of grout on shear stiffness for three joint openings (Young's modulus of rock = 20 GPa, Young's modulus of bolt = 207 GPa, bolt diameter = 1.9 cm, hole diameter = 2.54 cm, bolt inclination = 90 deg.)

Integrating (A2.3),

$$E_b\,I\,y = -\frac{M_o\,x^2}{2} + \frac{Rx^3\cos\alpha}{6} + C_1\,x + C_2\,, \qquad \ldots\ldots\ldots\ldots\ldots \quad \text{(A2.4)}$$

where C_1 and C_2 are constants of integration.

From Appendix A1 it was shown that the vertical displacement of the bolt where it is embedded in the rock (points A and B, Fig. A2.1) is given by:

$$y = e^{-\beta x}\,C\cos\beta\,x \qquad \ldots\ldots\ldots\ldots\ldots \quad \text{(A2.5)}$$

where

$$\beta = \left(\frac{k}{4EI}\right)^{\frac{1}{4}}$$

$$C = \frac{R}{2E_b\,I\,\beta^3}\,,$$

$$k = \text{foundation modulus.} \qquad \ldots\ldots\ldots\ldots\ldots \quad \text{(A2.6)}$$

Differentiating (A2.5),

$$\frac{dy}{dx} = -\,C\beta e^{-\beta x}\,(\sin\beta x + \cos\beta x)\;. \qquad \ldots\ldots\ldots\ldots\ldots \quad \text{(A2.7)}$$

Now at $\quad x = 0;\ \frac{dy}{dx} = -\,C\beta \qquad \ldots\ldots\ldots\ldots\ldots \quad$ (A2.8)

now at $x = \delta\sec\alpha$, $\frac{dy}{dx}$ must also $= -\,C\beta$ by symmetry. .... (A2.9)

Similarly, at $x = 0$ and $x = \delta\sec\alpha$, $y = C = \frac{R}{2E_b\,I\,\beta^3}$ . ... (A.210)

Substituting $\frac{dy}{dx}$ from (A2.8) in (A2.3) ,

$$-\,C\beta E_b\,I = C_1\;. \qquad \ldots\ldots\ldots\ldots\ldots \quad \text{(A2.11)}$$

Substituting $\frac{dy}{dx}$ from (A2.9) in (A2.3) ,

$$\begin{aligned} -\,C\beta E_b\,I &= -\,M_o\,\delta\sec\alpha + \frac{R}{2}\,\delta^2\sec\alpha + C_1 \\ &= -\,M_o\,\delta\sec\alpha + \frac{R}{2}\,\delta^2\sec\alpha - C\beta E_b\,I \end{aligned}$$

$$\therefore \qquad M_o = \frac{R\delta}{2}\;. \qquad \ldots\ldots\ldots\ldots\ldots \quad \text{(A2.12)}$$

Now at $x = 0$, $y = H$. Substituting these values in (A2.4),

$$E_b \, IH = C_2 \qquad \text{.............} \quad \text{(A2.13)}$$

Also at $x = \delta\sec\alpha$, $y = h$. Substituting these values in (A2.4)

$$E_b \, Ih = -\frac{M_o}{2}\delta^2 \sec^2\alpha + \frac{R}{6}\delta^3 \sec^2\alpha + C_1\delta\sec\alpha + C_2 \qquad \text{.......} \quad \text{(A2.14)}$$

But from (A2.10) $h = \dfrac{R}{2E_b \, I\beta^3}$. Also, expressions for M_o, C_1, and C_2 are given by (A2.12), (A2.11) and (A2.13). Substituting for h, M_o, C_1 and C_2 in (A2.14):

$$E_b \, I \frac{R}{2\,I\beta^3} = -\frac{R}{4}\delta^3 \sec^2\alpha + \frac{R}{6}\delta^3 \sec^2\alpha - \frac{R\beta}{2\,I\beta^2} E_b \, I \; \delta\sec\alpha + E_b \, IH$$

$$\therefore \qquad R\left(\frac{E_b}{2\beta^3} + \frac{\delta^3 \sec^2\alpha}{12} + \frac{E_b \; \delta\sec\alpha}{2\beta^2}\right) = E_b \, IH$$

$$\text{Shear stiffness} = \frac{R}{H\sec\alpha}$$

$$= \frac{E_b \, I}{\left(\dfrac{1}{2\beta^3\sec\alpha} + \dfrac{\delta^3 \sec\alpha}{12} + \dfrac{\delta}{2\beta^2}\right)} \, . \qquad \text{.............} \quad \text{(A2.15)}$$

For a bolt with a circular cross-section

$$I = \frac{\pi d_b^4}{64}$$

where d_b = bolt diameter.

Foundation Modulus, k

The bolt reacts against a "foundation" of resin and rock (Fig. A2.2). Assume that the bolt loads this foundation with an average compressive stress, σ, over a width, d_b, and unit depth normal to plane of diagram.

$$R = ky_b \equiv \sigma d_b = E_f \, \varepsilon_f \, d_b$$

where y_b = vertical displacement of bolt

E_f = Young's modulus of foundation

ε_f = normal strain

ε_f = normal strain

$$= E_f \frac{y_b}{t} d_b \qquad \text{.............} \quad \text{(A2.16)}$$

where t = thickness of foundation.

$$k = \frac{E_f\ d_b}{t}$$

Foundation Thickness, t

The foundation thickness is actually infinite. However, at some distance below the bolt induced normal stresses will have fallen to negligible values. Examination of the bulbs of pressure beneath footings indicate that if the bearing width is B the induced normal stresses at depths greater than 5B are less than 10 percent of the applied stress.

$$t = 5d_b$$

$$k = \frac{E_f}{5} \qquad \text{.............} \quad \text{(A2.17)}$$

Young's Modulus of Foundation

The foundations consists of a layer of resin, thickness t_r, and a layer of rock, thickness $5d_b$.

The mean modulus of elasticity of this 2-layer system is given by

$$E_f = \frac{(t_r + 5d_b)E_r\ E_R}{t_r\ E_R + 5d_b\ E_r} \qquad \text{.............} \quad \text{(A2.18)}$$

where E_r = Young's modulus of resin

E_R = Young's modulus of rock

$$k = \frac{(t_r + 5d_b)E_r\ E_R}{5(t_r\ E_R + 5d_b\ E_r)} \ . \qquad \text{.............} \quad \text{(A2.19)}$$

FiguresA2.3 -A2.8 illustrate graphically the sensitivity of shear stiffness to the various parameters incorporated in this analytical model.

APPENDIX B

SHEAR STRENGTH DATA FROM DIRECT SHEAR TESTS OF RESIN BOLTED JOINTS

Introduction:

The testing of bolted rock joints in direct shear in the laboratory requires the services of a large shear rig. Few laboratories possess such equipment. One such device, located at the University of Lulea, Sweden, is illustrated in Figure B1. It comprises two steel boxes measuring 45 x 60 x 30 cm with 5 cm thick walls. The loading capacities are 3000 kN for the shear load cylinder and 500 kN for the normal load ram. Further details of this machine are described in (1).

Selected data from shear tests on resin grouted bolts on this and similar machines are presented below.

Testing Data:

Haas (2-5) has reported results of his work since the mid-1970's. Figures B2 and B3 are data for resin-grouted, untensioned and ungrouted, tensioned bolts installed in shale and limestone blocks, and clearly show the greater strength of the grouted system. The greatest relative effect occurs when the joint surface is under low normal stresses.

Later, Haas studied the influence of bolt orientation. Figure B4 shows that with bolts of 45 deg. the joint shear strength is considerably increased, but failure occurs at smaller shear displacements, as compared to perpendicular installation.

Bjurstrom (6) tested cement grouted bolts in granite blocks and found an optimum angle of installation of about 30 deg. (Fig. B5). Maximum shear resistance was reached after a shear displacement of about 1 cm (0.39 in.).

Several authors have conducted tests on bolted rock mass systems at a reduced scale. Horino, Duvall and Brady (7) experimented with models of mechanically bolted pillars, and Heuze and Goodman tested grouted bolts (0.48 cm diam. (3/16 in.)) installed in small sandstone blocks (12.07 cms square (4.75 in.)).

Closure:

From a practical viewpoint, direct shear tests of bolted joints have demonstrated the importance of bolt orientation and the added shear strength caused by the inherent resistance of the bolt to dilation.

More recently, direct shear box testing has been used to compare the shear strengths of the increasing variety of bolt types available to the support engineer (1).

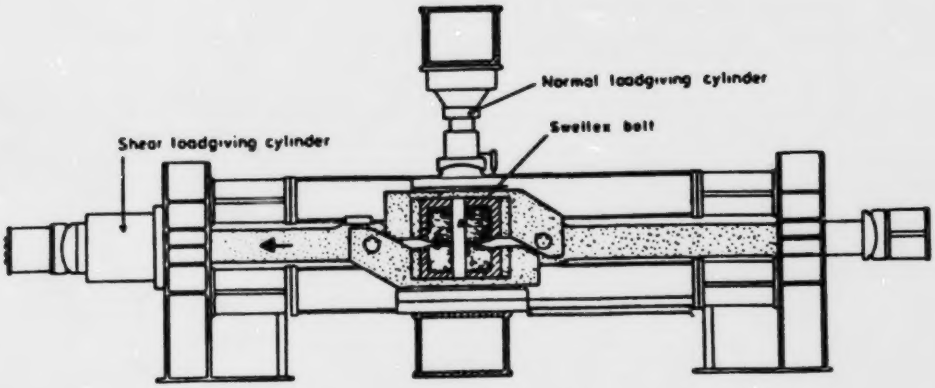
Normal loadgiving cylinder
Swellex bolt
Shear loadgiving cylinder

Figure B1 Large shear box for testing rock bolted joints (after (1))

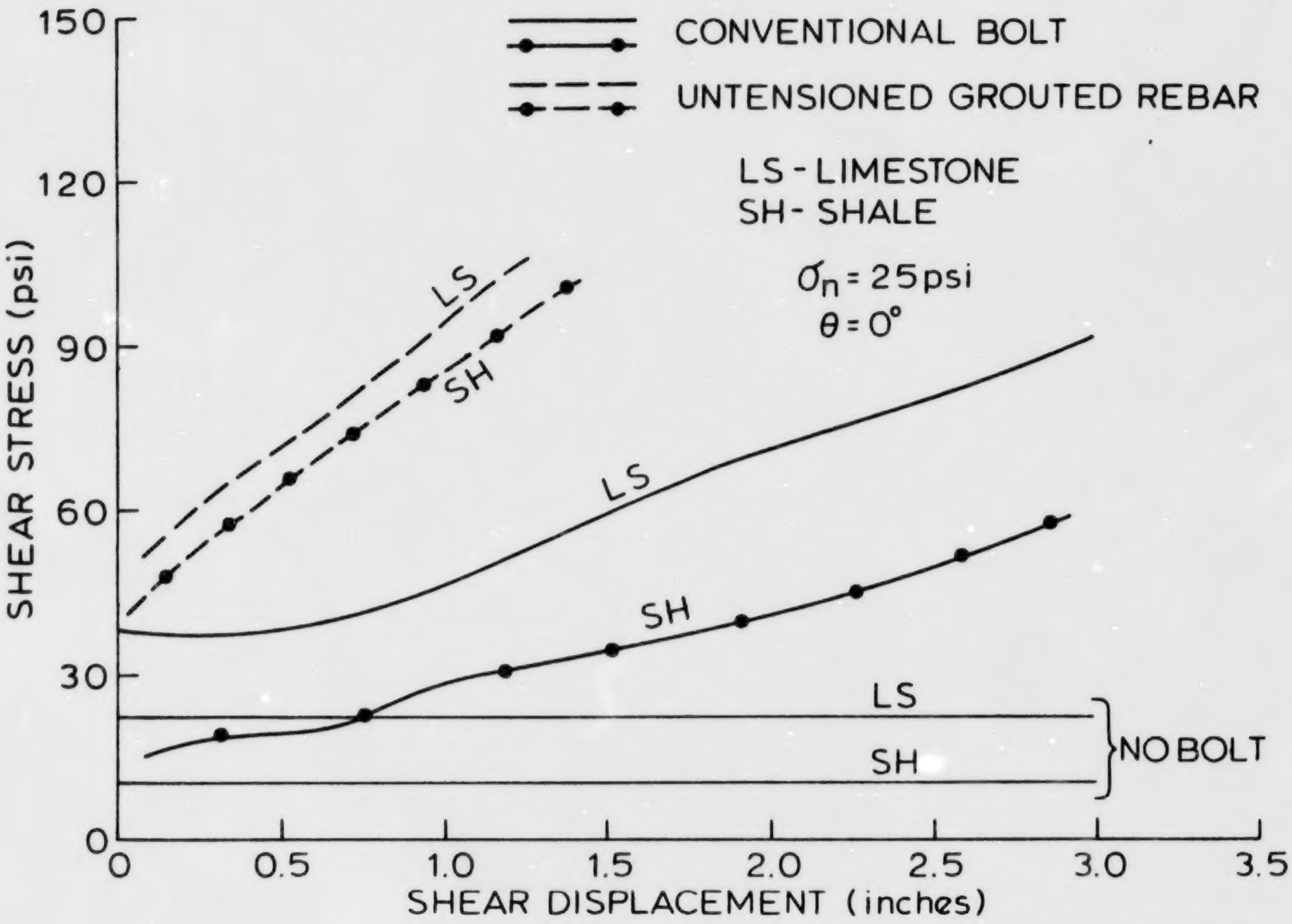

Figure B2 Shear behaviour of bolted joints in limestone and shale (5/8 in. conventional bolt, 7/8 in. grouted rebar in 1 and 3/8 in. holes) (after (2)).

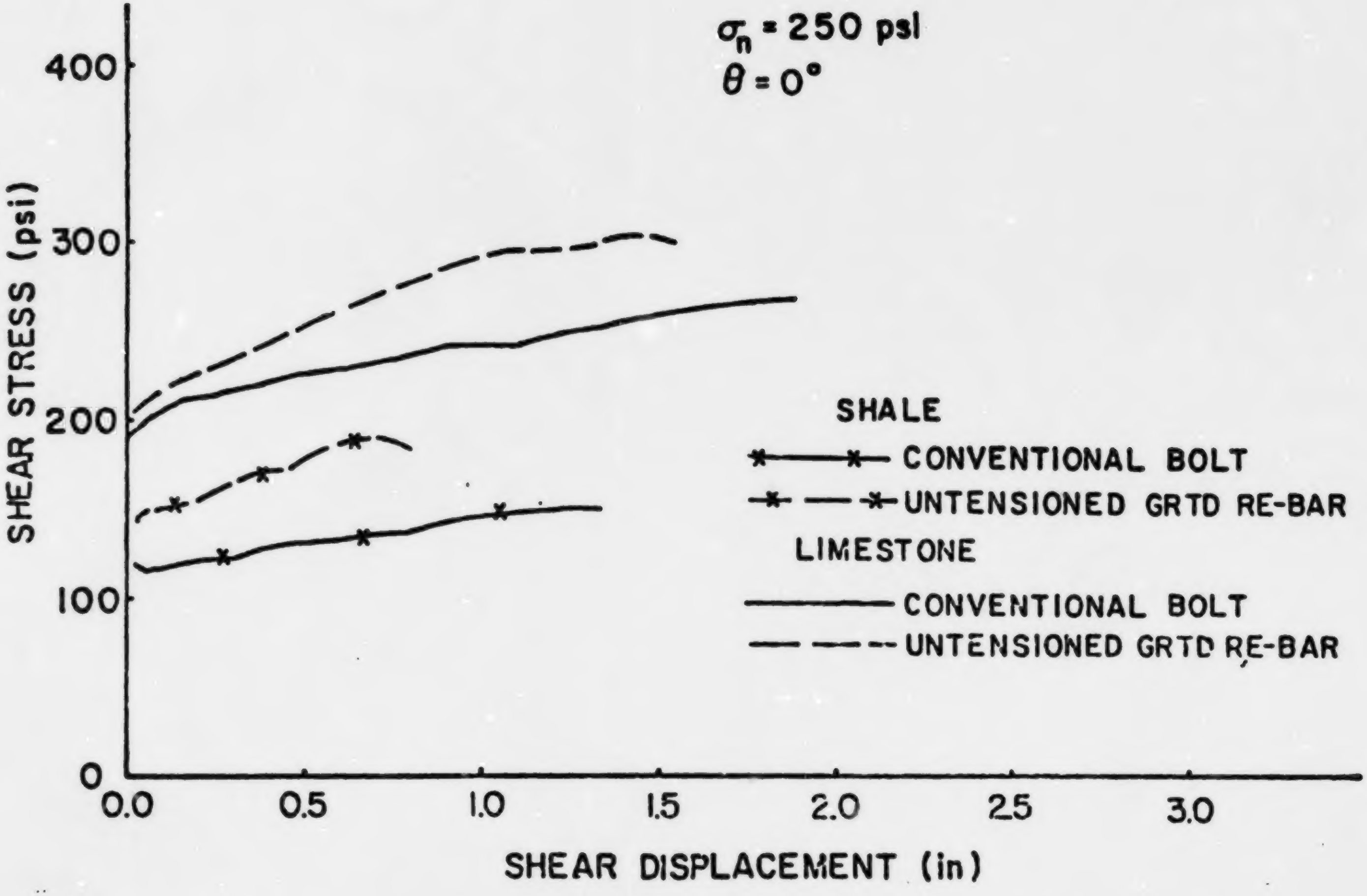

Figure B3 Shear behaviour of bolted joints in limestone and shale (5/8 in. conventional bolt, 7/8 in. grouted rebar in 1 and 3/8 in. holes) (after (2))

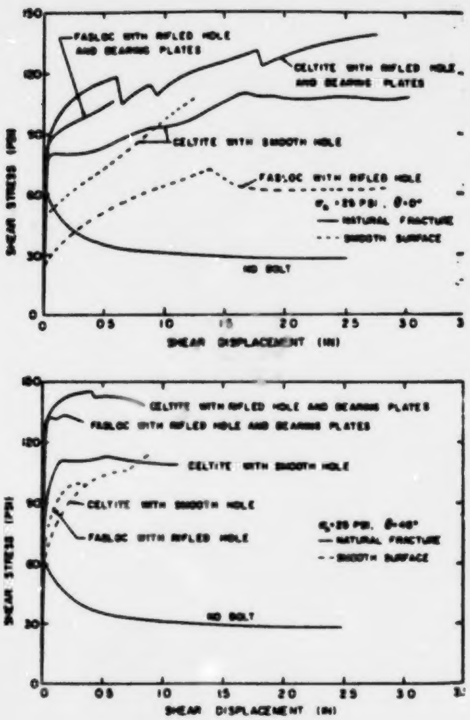

Figure B4 Shear behaviour of bolted joints installed at various angles (after (5)).

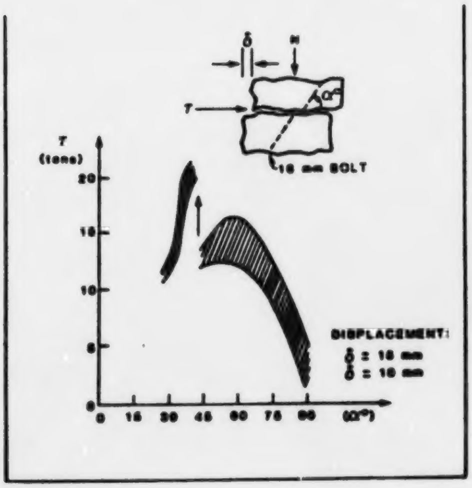

Figure B5 Effect of installation angle on shear strength of bolted joints (after (6))

REFERENCES

1. Ludvig, B. Shear tests on rock bolts. Proc. Int. Symp. on Rock Bolting, Sweden, pp. 113-123 (1983).

2. Haas, C.J., Keith, H.S., Nitzche, R.N., Dave, J., Hoffmann, R.L., and Patrick, W.C. An investigation of the interaction of rock and types of rock bolts for selected loading conditions. 2nd. Annual Report, Rock Mechanics and Explosives Research Centre, University of Missouri-Rolla, U.S. Bureau of Mines, Contract H0122110 (1975).

3. Haas, C.J., Dean, K.H., Nitzsche, R.N., Janakkumar, D., Hoffmann, R.L., and Patrick, W.C. An investigation of the interaction of rock and types of rock bolts for selected loading conditions. 1st. Annual Report, Rock Mechanics and Explosives Research Centre, University of Missouri-Rolla, U.S. Bureau of Mines, Contract H0122110 (1974).

4. Haas, C.J. Shear resistance of rock bolts. Presented at 104th. Annual Meeting of the American Society of Mining, Metallurgical and Petroleum Engineers, February (1975).

5. Haas, C.J. Analysis of rock bolting to prevent shear movement in fractured ground. Mining Engineering, pp. 698-704 (1981).

6. Bjurstrom, S. Shear strength of hard rock joints reinforced by grouted untensioned bolts. Proc. 3rd. Cong., ISRM Denver, Vol. II.B., pp. 1194-1199.

7. Heuze, F.E. and Goodman, R.D. Finite element and physical model studies of tunnel reinforcement in rock. Proc. 15th. Rock Mech. Symp., 1974.

APPENDIX C

BEAM EQUATIONS FOR BUILT-IN BEAM WITH PARABOLIC LOAD DISTRIBUTION

Differential sag of strata in a layered roof and the arch-shape of the zone of loosening above a rectangular opening may intensify loading over the central portions of a roof, (see Chapter 14). The exact form of this loading is difficult to estimate. For analytical purposes, a parabolic load distribution has been assumed.

The load, q , at any point, x , along the beam of unit width is described by:

$$q = q_o + \alpha x(L - x) \text{ ...... (Fig. C1)} \qquad \text{..............} \qquad \text{(C1)}$$

where q_o = load at $x = 0$ (abutment)

L = span

α = constant.

Let $q_o = \beta\gamma h$ and the load at the centre of the span, $q_c = \omega\gamma h$, where ω and β are load intensity factors, h is the roof beam thickness, and γ is the rock density, $(\omega \geq 1 , \beta \geq 1 , \omega \geq \beta)$. Therefore, from (C1),

At $x = 0 , q_o = \beta\gamma h$

$$\text{At } x = \frac{L}{2} , q_c = \omega\gamma h$$

$$= q_o + \frac{\alpha L^2}{4}$$

$$= \beta\gamma h + \frac{\alpha L^2}{4}$$

$$\alpha = \frac{4\gamma h(\omega-\beta)}{L^2} . \qquad \text{..............} \qquad \text{(C2)}$$

Now, from classical beam theory,

$$EI \frac{d^4y}{dx^4} = q$$

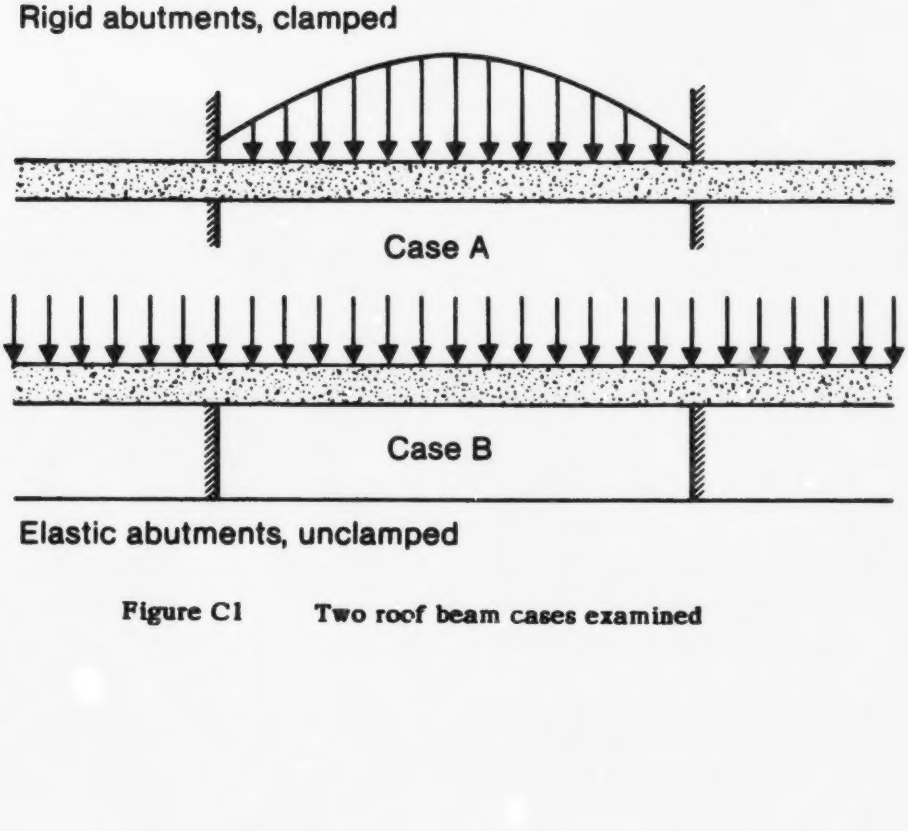
Rigid abutments, clamped
Case A
Case B
Elastic abutments, unclamped

Figure C1 Two roof beam cases examined

where E = modulus of elasticity

I = moment of inertia of the beam cross-section about the neutral axis

y = vertical deflection of the beam.

For the parabolic load distribution:

$$EI\,\frac{d^4y}{dx^4} = q_o + \alpha x(L - x)$$

$$= q_o + \alpha xL - \alpha x^2 \qquad \text{..............} \qquad (C3)$$

Integrating (C3) three times:

$$EI\,\frac{dy}{dx} = \frac{q_o\ x^3}{6} + \frac{\alpha x^4 L}{24} - \frac{\alpha x^5}{60} + \frac{Ax^2}{2} + Bx + C \qquad \text{..............} \qquad (C4)$$

where A, B, C are constants of integration. When x = 0, dy/dx = 0.

Substituting these values in (C4)

$$0 = \frac{q_o\ L^3}{6} + \frac{\alpha L^5}{24} - \frac{\alpha L^5}{60} + \frac{AL^2}{2} + BL$$

$$= \frac{q_o\ L^3}{6} + \frac{\alpha L^5}{40} + \frac{AL^2}{2} + BL\ . \qquad \text{..............} \qquad (C5)$$

Also when x = L/2, dy/dx = 0.

Substituting these values in (C4)

$$0 = \frac{q_o\ L^3}{48} + \frac{\alpha L^5}{384} - \frac{\alpha L^5}{1920} + \frac{AL^2}{8} + \frac{BL}{2}$$

$$= \frac{q_o\ L^3}{48} + \frac{\alpha L^5}{480} + \frac{AL^2}{8} + \frac{BL}{2}\ . \qquad \text{..............} \qquad (C6)$$

Solving the simultaneous equations (C5) and (C6)

$$A = -\left(\frac{q_o L}{2} + \frac{\alpha L^3}{12}\right) \qquad \text{..............} \qquad (C7)$$

$$B = \left(\frac{q_o\ L^2}{12} + \frac{\alpha L^4}{60}\right) \qquad \text{..............} \qquad (C8)$$

Integrating (C4) (C = 0)

$$EI = \frac{q_o\ x^4}{24} + \frac{\alpha x^5 L}{120} - \frac{\alpha x^6}{360} + \frac{Ax^3}{6} + \frac{Bx^2}{2} + D \quad \ldots\ldots\ldots\ldots\ldots \quad (C9)$$

where D = a new constant of integration. Now, when x = 0, y = 0.

Substituting these values in (C9), it is shown that D = 0, the vertical displacement, y , is

$$y = \left(\frac{q_o\ x^4}{24} + \frac{\alpha x^5 L}{120} - \frac{\alpha x^6}{360} + \frac{Ax^3}{6} + \frac{Bx^2}{2}\right)\frac{1}{EI} \quad \ldots\ldots\ldots\ldots\ldots \quad (C10)$$

where α, A, and B are given by (C1), (C7) and (C8).

From classical beam theory,

$$EI\ \frac{d^2y}{dx^2} = -\ M \quad \ldots\ldots\ldots\ldots\ldots \quad (C11)$$

where M = bending moment.

Differentiating (C10) twice

$$\frac{d^2y}{dx^2} = \left(\frac{q_o\ x^2}{2} + \frac{\alpha x^3 L}{6} - \frac{\alpha x^4}{12} + Ax + B\right)\frac{1}{EI} \quad \ldots\ldots\ldots\ldots\ldots \quad (C12)$$

Substituting $\frac{d^2y}{dx^2}$ from (C12) in (C11)

$$M = -\left(\frac{q_o\ x^2}{2} + \frac{\alpha x^3 L}{6} - \frac{\alpha x^4}{12} + Ax + B\right) \quad \ldots\ldots\ldots\ldots\ldots \quad (C13)$$

APPENDIX D

LIMITING EQUILIBRIUM ANALYSIS OF ROOF BEAMS REINFORCED WITH NON-TENSIONED, RESIN-GROUTED BOLTS

A short length δx of beam, width d, is illustrated in Figure D1 with the moment increasing from M for $(M + \delta M)$ over the length δx.

A slice, ABCD, of the beam is in equilibrium under the following forces:

(a) Force, F, along AC

(b) Force, $F + \delta F$, along BD

(c) Shearing force, S, along CD

For horizontal equilibrium,

$$(F + \delta F) - F - S = 0 \qquad \text{..............} \quad \text{(D1)}$$

or

$$(F + \delta F) - F - \tau_y \, d\delta x = 0 \qquad \text{..............} \quad \text{(D2)}$$

where τ_y = shear stress along CD.

From classical beam theory,

$$F = - \int_{+y}^{+y_1} \frac{My d \cdot dy}{I} \qquad \text{..............} \quad \text{(D3)}$$

and

$$F + \delta F = - \int_{+y}^{+y_1} \frac{(M + \delta M)}{I} \, yd \cdot dy \qquad \text{..............} \quad \text{(D4)}$$

where I = second moment of area about neutral axis.

Substituting (D3) and (D4) in (D2):

$$- \frac{\delta M}{I} \int_{+y}^{+y_1} d \cdot y \, dy - \tau_y \, d\delta x = 0 \qquad \text{..............} \quad \text{(D5)}$$

Therefore, as $\delta M \to 0$ and $\delta x \to 0$, from (D5):

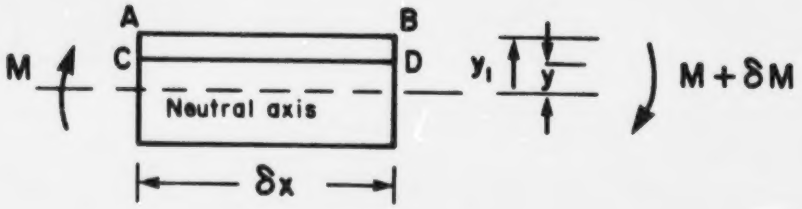
A
B
C
D
M
M + δM
Neutral axis
y_1
y
δx

Figure D1 Section of beam with moments acting

$$\tau_y = \frac{1}{I}\frac{dM}{dx}\int_{+y}^{+y_1} y\,.\,dy\;. \qquad \text{..............} \qquad \text{(D6)}$$

$\int_{+y}^{+y_1} d\,.\,y\,dy = Q$, the first moment of area of the cross-section above y about the neutral axis.When $y = y_1$, $Q = 0$ and the shear stress, τ_y, along AB is zero. Along the neutral axis $y = 0$, and τ_y reaches a maximum value, $\tau_{y\ max}$.

For a rectangular beam width d, depth h, the second moment of area I, is $\frac{1}{12}dh^3$ and $\int_{y=o}^{y_1=h/2} y\,.\,dy = \frac{1}{8}\ h^2$.

Substituting for I and Q in (D6)

$$\tau_{y\ max} = \frac{12}{dh^3}\frac{dM}{dx}\frac{h^2}{8}$$

$$= \frac{3}{2dh}\frac{dM}{dx}\;. \qquad \text{..............} \qquad \text{(D7)}$$

The total shear force along the neutral axis over a half span

$$T_{L/2} = \frac{3}{2dh}\int_{x=o}^{x=L/2} d\,\frac{dM}{dx}\,.\,dx = \frac{3}{2h}\int_{x=o}^{x=L/2}\frac{dM}{dx}\,dx\;. \qquad \text{...........} \qquad \text{(D8)}$$

Limiting Equilibrium Analysis of a Bolted Beam With Respect to Horizontal Shear Stresses

Figure D2 illustrates an assumed rock bolt pattern layout for non-tensioned resin-grouted bolts. For the purposes of this analysis no bolts are shown at the centre of the span, since no horizontal shear stresses develop here. Also, one bolt on each side is placed at 1/2 b from the ribside to locally increase shear resistance where shear forces are highest.

Let F = shear resistance of each bolt;

Let T = total shear force across span, L , along neutral axis;

Let b = average bolt spacing along a row;

Let d = bolt spacing along opening;

Let n = number of bolts in a row.

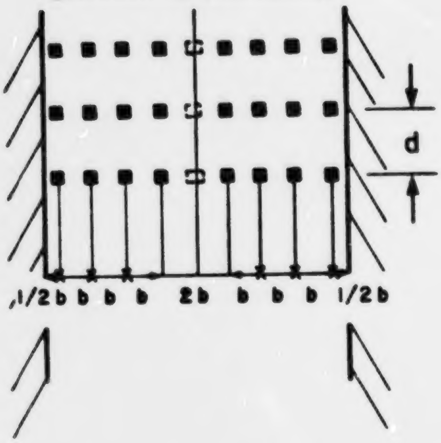
Span
d
1/2b b b b b 2b b b b 1/2b

■ Non-tensioned, resin-grout bolt

▭ Central bolt acting primarily in suspension (not included in reinforcement analysis)

Figure D2 Assumed rock bolt pattern for reinforcement analysis

For analysis it is assumed that a beam, width d , span L , is reinforced by n bolts (Fig. D2). For this beam, the total horizontal shear force along the neutral axis, T_L, is given by

$$T_L = 2T_{L/2}$$

$$= \frac{3}{h} \int_{x=o}^{x=L/2} \frac{dM}{dx} \cdot dx \; . \qquad \text{..............} \quad \text{(D9)}$$

The total resisting force mobilized by the bolts along one row, F_L, is given by:

$$F_L = nF \; , \qquad \text{..............} \quad \text{(D10)}$$

when $F_L = T_L$

$$nF = \frac{3}{h} \int_{x=o}^{x=L/2} \frac{dM}{dx} \quad dx \; . \qquad \text{..............} \quad \text{(D11)}$$

But, from Figure D2

$$n = \frac{L}{b} - 1 \; . \qquad \text{..............} \quad \text{(D12)}$$

Substituting (D12) in (D11)

$$\left(\frac{L}{b} - 1\right) F = \frac{3}{h} \int_{x=o}^{x=L/2} \frac{dM}{dx} \; . \, dx$$

$$b = \frac{LF}{\frac{3}{h} \int_{x=o}^{x=L/2} \frac{dM}{dx} \; dx + F} \; . \qquad \text{..............} \quad \text{(D13)}$$

Let ratio of resisting forces mobilized by bolts to horizontal shear force be defined as the Degree of Reinforcement, RF. Then,

$$RF = \frac{F_L}{T_L} \; . \qquad \text{..............} \quad \text{(D14)}$$

Application to Parabolically Loaded, Built-in, Elastic Beam

(a) Estimating spacing of bolts in a row:

The analysis of a parabolically loaded, built-in, elastic beam is developed in Appendix C. From it the special case of uniform loading is readily derived. The parabolic loading is assumed to have the distribution, for a beam of unit width,

$$q = q_o + \alpha x(L - x) \ , \qquad \text{..............} \quad \text{(D15)}$$

where q_o = load per unit length of beam at $x = 0$ (abutment)

α = constant

L = span.

From classical beam theory,

$$\frac{d^2M}{dx^2} = - q = - (q_o + \alpha xL - \alpha x^2)$$

$$\therefore \quad \frac{dM}{dx} = -\left(q_o\ x + \frac{\alpha x^2 L}{2} - \frac{\alpha x^3}{3} + A\right) ,$$

where, from Appendix C, $A = - L\left(\frac{q_o}{2} + \frac{\alpha L^2}{12}\right)$

$$\frac{dM}{dx} = - \left(q_o\ x + \frac{\alpha x^2 L}{2} - \frac{\alpha x^3}{3} - \frac{Lq_o}{2} - \frac{\alpha L^3}{12}\right) . \qquad \text{..............} \quad \text{(D16)}$$

$$\int_{x=o}^{x=L/2} \frac{dM}{dx}\, dx = - \int_{x=o}^{x=L/2} \left(q_o x + \frac{\alpha x^2 L}{2} - \frac{\alpha x^3}{3} - \frac{Lq_o}{2} - \frac{\alpha L^3}{12}\right) dx$$

$$= \underset{x=o}{\overset{x=L/2}{-}} \left[\frac{q_o\ x^2}{2} + \frac{\alpha x^3 L}{6} - \frac{\alpha x^4}{12} - \frac{Lq_o\ x}{2} - \frac{\alpha L^3}{12}\ x + B\right] ,$$

where B = constant of integration.

$$= - \left(\frac{q_o\ L^2}{8} + \frac{\alpha L^4}{48} - \frac{\alpha L^4}{192} - \frac{L^2\ q_o}{4} - \frac{\alpha L^4}{24}\right)$$

$$= -\left(- \frac{q_o\ L^2}{8} - \frac{5}{192}\alpha L^4\right) . \qquad \text{..............} \quad \text{(D17)}$$

$$= -\left(\frac{q_o\ L^2}{8} + \frac{5}{192}\ \alpha L^4\right)\ . \qquad \ldots\ldots\ldots\ldots\ldots \quad (D18)$$

Taking the absolute value of $\int_{x=o}^{x=L/2} \frac{dM}{dx} \cdot dx$ from (D18) and substituting in (D13):

$$b = \frac{LF}{\frac{3}{h}\left(\frac{q_o\ L^2}{8} + \frac{5}{192}\ \alpha L^4\right) + F}\ . \qquad \ldots\ldots\ldots\ldots\ldots \quad (D19)$$

But, from Appendix C,

$$q_o = \beta\gamma\ hd\ , \qquad \ldots\ldots\ldots\ldots\ldots \quad (D20)$$

where h = depth of beam

γ = rock density

and $$\alpha = \frac{4\gamma hd(\omega-\beta)}{L^2}\ , \qquad \ldots\ldots\ldots\ldots\ldots \quad (D21)$$

where ω = loading intensity at span centre

and β = loading intensity at abutment.

Substituting (D20) and (D21) in (D19):

$$b = \frac{LF}{\frac{3}{h}\left(\frac{\beta\gamma hdL^2}{8} + \frac{5}{192}\ \frac{4\gamma hd(\omega-\beta)}{}\ L^4\right) + F}$$

$$= \frac{LF}{\frac{3}{8}\ \gamma d(\beta L^2 + \frac{5}{6}\ (\omega-\beta)L^2)\ +\ F}$$

$$= \frac{LF}{0.375\ K\gamma d + F}\ . \qquad \ldots\ldots\ldots\ldots\ldots \quad (D22)$$

where $$K = (\beta L^2 + 0.833\ (\omega-\beta)L^2)\ . \qquad \ldots\ldots\ldots\ldots\ldots \quad (D23)$$

For a square bolting pattern ($b = d$), from (D22)

$$0.375\ K\ b^2 + Fb - LF = 0$$

$$\therefore \qquad b = \frac{-\ F+(F^2 + 1.5K\gamma LF)}{0.75\ K\gamma}\ . \qquad \ldots\ldots\ldots\ldots\ldots \quad (D24)$$

(Note: other root negative)

For uniform loading ($\omega = \beta$), from (D22) and (D24), for $b \neq d$,

$$b = \frac{LF}{0.375\ \beta\gamma\ dL^2 + F}\ . \qquad \text{..............} \qquad \text{(D25)}$$

For uniform loading ($\omega = \beta$), from (D23) and (D24), for $b = d$, (square pattern)

$$b = \frac{-\ F+(F^2+ 1.5\gamma\beta\ L^3F)^{\frac{1}{2}}}{0.75\beta\gamma\ L^2}\ . \qquad \text{..............} \qquad \text{(D26)}$$

(b) Estimating Degree of Reinforcement in a Bolted Roof

In this situation, it is required to estimate the Degree of Reinforcement given the bolt pattern, span, and bolt and rock/grout properties.

From (D14)

$$RF = \frac{F_L}{T_L}\ . \qquad \text{..............} \qquad \text{(D27)}$$

From equations (D9), (D12), (D20) and (D21):

$$\left|T_L\right| = \frac{3}{8}\ \gamma Kd\ , \qquad \text{..............} \qquad \text{(D28)}$$

where K is given by (D23).

Also, from (D10)

$$F_L = nF\ . \qquad \text{..............} \qquad \text{(D29)}$$

Substituting (D28) and (D29) in (D27)

$$RF = \frac{nF}{0.375\ \gamma Kd}\ . \qquad \text{..............} \qquad \text{(D30)}$$

(c) Estimating Average Spacing in Rows for a Given Degree of Reinforcement

Let required Degree of Reinforcement be RF_{des}.

Let spacing along opening = d

$$RF_{des} = \frac{nF}{0.375\ \gamma Kd} \text{ from (D30)} \qquad \text{..............} \qquad \text{(D31)}$$

But $n = \frac{L}{b} - 1$ (see Fig. 9.4)

$$RF_{des} = \frac{\left(\frac{L}{b} - 1\right)F}{0.375\ \gamma Kd}$$

$$b = \frac{FL}{0.375\ RF_{des}\ \gamma Kd + F}\ . \qquad \text{..............} \qquad (D32)$$

(d) Estimating Shear Resistance of a Non-Tensioned, Resin-Grouted Bolt

The shear resistance, F , of a single bolt, is required in this analysis. A method devised by Dight is described in Chapter 3 and used in this design method in Chapter 9.

APPENDIX E

DERIVATION OF STABILITY EQUATIONS DESCRIBING 2-HINGE COLLAPSE MECHANISM IN LAYERED, CROSS-JOINTED ROOF

E1.1 General Equilibrium

The appearance of a cross-jointed, horizontally layered roof before and after the development of a 2-hinge collapse mechanism is illustrated in Figure E1. Additional detail is provided in Figure E2, which shows that in order for rotation of the hinge element, ACGF, to continue there must be crushing at one or both rotation points. The zones of contact in Figure E2 are distributed along AB = X_1 and DE = Y_1.

Since there is a simple symmetry, it is sufficient to examine the kinematics and statics of one hinge (Fig. E3). Block PDTU moves vertically downwards while block ACGF rotates. The forces acting on ACGF are:

Horizontal thrusts T_1 and T_2;

Dead weight, W, of the rotating element;

A vertical force, N, applied to the hinge block, ACGF, by the roof and hinge blocks to the right;

Frictional forces, μT_2 and μT_1 at the abutment hinge point and roof hinge point respectively, where μ is the effective angle of friction of material at these points (assumed equal).

Horizontal Equilibrium

For block ACGF, resolving forces horizontally,

$$T_1 = T_2 = T \quad .... \quad \text{(E1)}$$

Vertical Equilibrium

Block ACGF could fall out under the action of gravity. This would result in instantaneous collapse of the roof block. For vertical equilibrium,

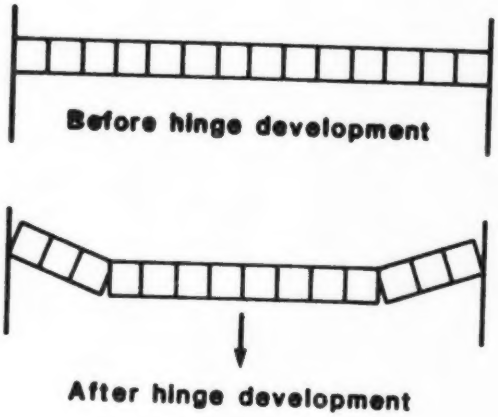
Before hinge development
After hinge development

Figure E1 Schematic illustration of 2-hinge failure mechanism

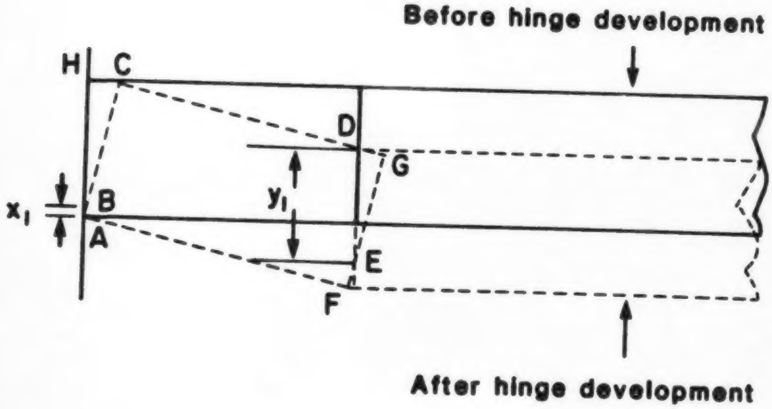
Before hinge development
H
C
D
G
x_1
B
A
y_1
E
F
After hinge development

Figure E2 Kinematics of one-hinge

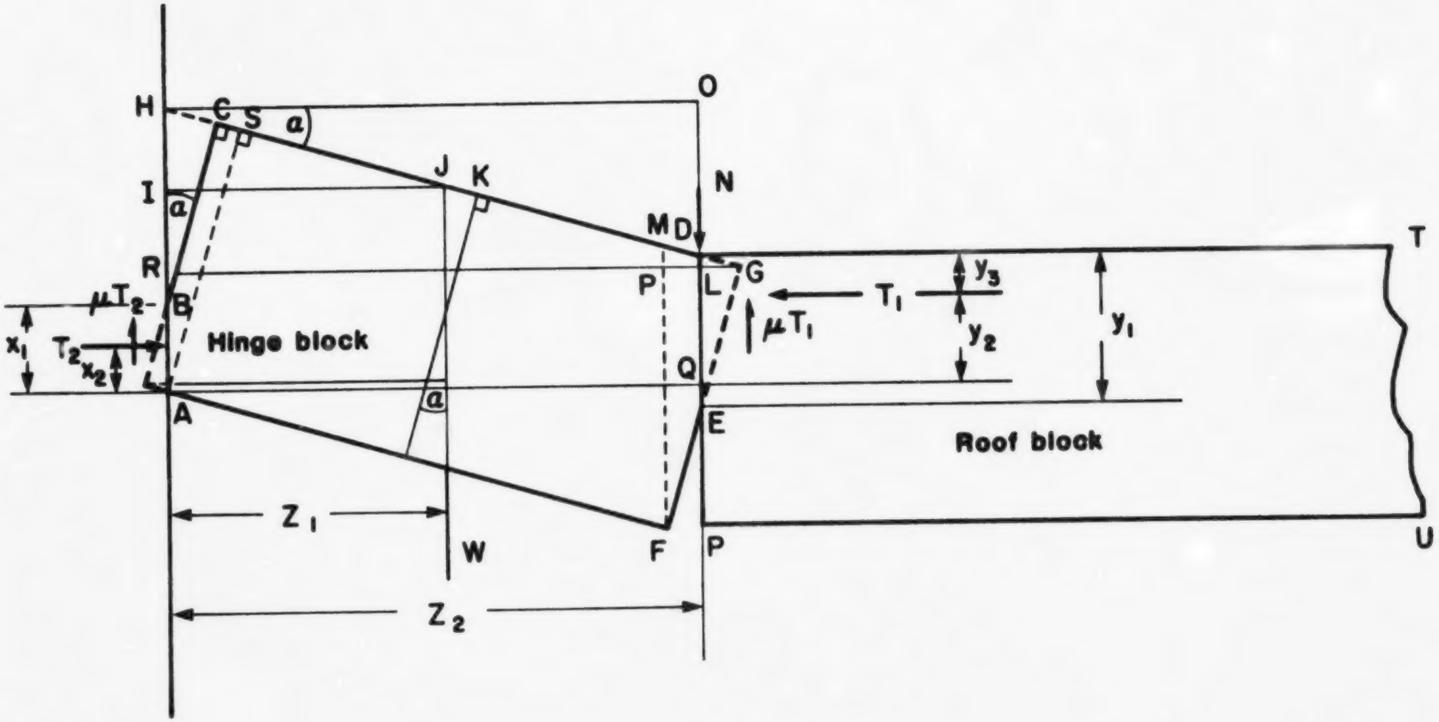
H
C
S
a
O
I
J
K
N
M
D
T
R
G
P
L
T₁
y₃
μT₂
B
μT₁
y₁
x₁
T₂
x₂
Hinge block
y₂
Q
A
a
E
Roof block
Z₁
W
F
P
U
Z₂

Figure E3 Geometry and forces acting on a single hinge

$$W \leq \mu T_1 + \mu T_2 = 2\,\mu T \quad . \qquad \ldots\ldots\ldots\ldots\ldots \qquad (E2)$$

Rotational Equilibrium

Let length, AF, of hinge block ACGF = a, and its thickness, GF = b. Providing the condition for vertical equilibrium is met (Eq. E2), there is no differential vertical movement along the contact between the hinge block, ACGF, and the roof block. Therefore, for rotational equilibrium, taking moments about A, (Fig. E3)

$$WZ_1 + NZ_2 + TX_2 = TY_2$$

$$T = \frac{WZ_1 + NZ_2}{Y_2 - X_2} \quad . \qquad \ldots\ldots\ldots\ldots\ldots \qquad (E3)$$

$\underline{Z_1}$ $Z_1 = IJ = HJ\cos\alpha$

(where α = instantaneous angle of rotation from vertical of hinge block, ACGF)

$= (HC + CK - JK)\cos\alpha$

$= (b\tan\alpha - X_1\sin\alpha + \frac{a}{2} - \frac{b}{2}\tan\alpha)\cos\alpha$

$$= \frac{1}{2}(b\sin\alpha + a\cos\alpha - X_1\sin 2\alpha) \quad . \qquad \ldots\ldots\ldots\ldots\ldots \qquad (E4)$$

$\underline{Z_2}$

$$Z_2 = a \quad . \qquad \ldots\ldots\ldots\ldots\ldots \qquad (E5)$$

$\underline{Y_2}$ $Y_2 = DQ - Y_3$

$= OQ - OD - Y_3$

$= HA - OD - Y_3$

$$= b\sec\alpha - a\tan\alpha - Y_3 \quad . \qquad \ldots\ldots\ldots\ldots\ldots \qquad (E6)$$

The magnitude of Y_3 and X_2 are dependent upon the distribution of horizontal stress along DE. For this analysis it is assumed that the horizontal thrust is largest at D and failure will initiate here when the local uniaxial compressive strength, σ_c, of the rock is exceeded. At an intermediate stage of rotation between initiation and ultimate failure a portion of DE (= x_{cc}) will have suffered compressive strength failure. It is assumed that the strength along this section x_{cc} has dropped from σ_c, the uniaxial compressive strength of intact rock, to σ_{cc}, the uniaxial compressive strength of crushed or fractured rock. The total horizontal thrust, T , is assumed to be distributed as shown in Figure E4.

For a further small increment in hinge rotation the horizontal thrust, and, therefore, x_{cc} increase.

E1.2 Modelling Progressive Failure

There will be some sagging of a cross-jointed roof after the opening has been excavated. Its magnitude will be a function of roof span, beam thickness, joint spacing, normal stiffness of intact rock, and normal and shear stiffness of joints. For the computer program written to simulate this 2-hinge failure mechanism an initial rotation of 0.1 deg. was given to the hinge block.

STEP 1 - Initialize rotation of hinge block by setting $\alpha = 0.1$ deg.

STEP 2 - Initialize contact conditions by setting $X_1 = 0$, $X_4 = 0$, $x_{cc} = 0$, i.e. no crushing at contacts initially.

STEP 3 - Calculate Y_1:

$$
\begin{aligned}
Y_1 &= DE = DL + LE \\
&= LG\tan\alpha + LG\cot\alpha \\
&= 2LG \operatorname{cosec} 2\alpha \quad . \qquad \text{..............} \qquad \text{(E7)}
\end{aligned}
$$

But

$$
\begin{aligned}
LG &= RG - Z_2 \\
&= (HG + CG)\cos\alpha - Z_2 \\
&= (b\tan\alpha - X_1 \sin\alpha + a)\cos\alpha - Z_2 \\
&= b\sin\alpha + a\cos\alpha - \frac{1}{2} X_1 \sin 2\alpha - a \ . \ \text{..........} \qquad \text{(E8)}
\end{aligned}
$$

Substituting for LG from (E8) in (E7)

$$Y_1 = 2(b\sin\alpha + a\cos\alpha - \frac{1}{2} X_1 \sin 2\alpha - a)\operatorname{cosec}2\alpha \ .. \qquad \text{(E9)}$$

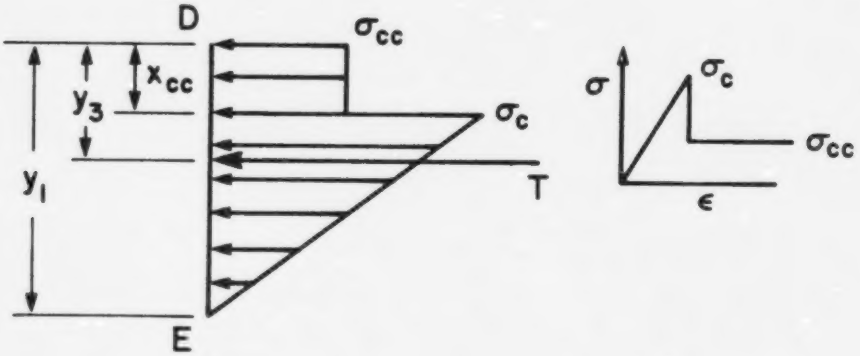
D
σ_{cc}
x_{cc}
y_3
y_1
σ_c
T
E
σ
σ_c
σ_{cc}
ϵ

Figure E4 Assumed distribution of horizontal thrust

STEP 4 - Determine Y_3 by assuming a linear distribution of horizontal thrust from a maximum at D to zero at E. Then,

$$Y_3 = \frac{Y_1}{3} \; . \qquad \ldots\ldots\ldots\ldots\ldots \qquad (E10)$$

STEP 5 - Calculate Y_2 from (E6).

STEP 6 - Calculate Z_1 from (E4).

STEP 7 - Calculate the horizontal thrust, T , from (E3).

STEP 8 - Calculate the maximum value of horizontal stress at D , σ_{max}, assuming a linear distribution as in Step 2 (Fig.5):

$$T = x_{cc}\,\sigma_{cc} + \frac{1}{2}\,\sigma_{max}(Y_1 - x_{cc})$$

$$\sigma_{max} = \frac{2(T - x_{cc}\,\sigma_{cc})}{Y_1 - x_{cc}} \; . \qquad \ldots\ldots\ldots\ldots\ldots \qquad (E11)$$

If σ_{max} is less than σ_c, the uniaxial compressive strength of the rock, the hinge is stable. Calculate the Factor of Safety, FS,

$$FS = \frac{\sigma_c}{\sigma_{max}} \; . \qquad \ldots\ldots\ldots\ldots\ldots \qquad (E12)$$

STEP 9 - Calculate the new length, x_{ccn}, along DE where the uniaxial compressive strength has been exceeded. From Figure E5:

$$x_{ccn} = Y_1 - \frac{\sigma_c(Y_1 - x_{cc})^2}{2(T \quad \sigma_{cc}\,x_{cc})} \; . \qquad \ldots\ldots\ldots\ldots\ldots \qquad (E13)$$

STEP 10 - Calculate a new value of horizontal thrust, T_n , from (Fig. E4).

$$T_n = x_{cc}\,\sigma_{cc} + \frac{1}{2}\,\sigma_c(Y_1 - x_{cc}) \; . \qquad \ldots\ldots\ldots\ldots\ldots \qquad (E14)$$

where σ_{cc} is the uniaxial compressive strength of crushed rock.

STEP 11 - Calculate X_1 by assuming intact rock failure along AB:

$$X_1 = \frac{T_n}{\sigma_c} \; . \qquad \ldots\ldots\ldots\ldots\ldots \qquad (E15)$$

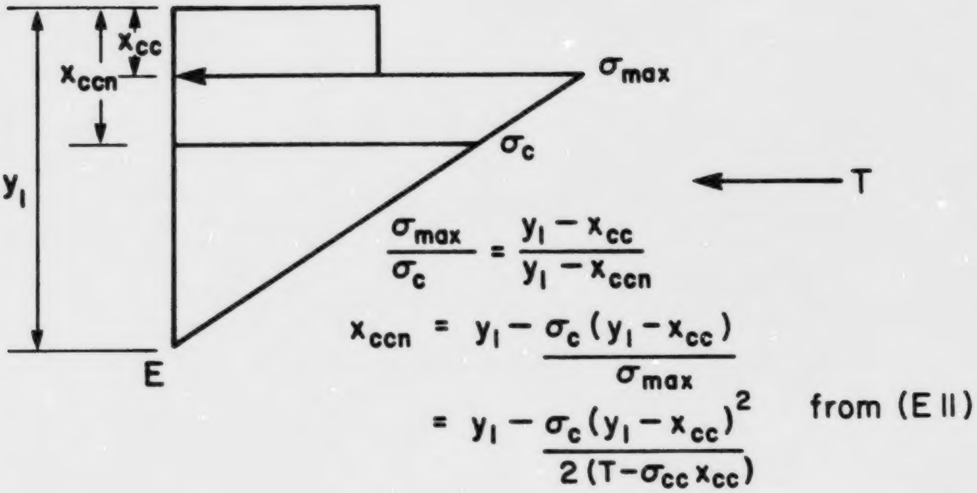
x_{cc}
x_{ccn}
y_1
σ_{max}
σ_c
T
E

$$\frac{\sigma_{max}}{\sigma_c} = \frac{y_1 - x_{cc}}{y_1 - x_{ccn}}$$

$$x_{ccn} = y_1 - \frac{\sigma_c (y_1 - x_{cc})}{\sigma_{max}}$$

$$= y_1 - \frac{\sigma_c (y_1 - x_{cc})^2}{2(T - \sigma_{cc} x_{cc})} \quad \text{from (E11)}$$

Figure E5 Method for estimating new value of x_{cc}

STEP 12 - Calculate X_2:

$$X_2 = \frac{X_1}{2} \quad . \qquad \ldots\ldots\ldots\ldots\ldots \qquad (E16)$$

STEP 13 - Calculate a new value of Z_1 from (E4).

STEP 14 - Increment rotation angle by 0.01 deg.

STEP 15 - Calculate the new position of the resultant horizontal thrust by determining Y_3 as follows. From Figure E4, taking moments about D

$$T_n \, Y_3 = \sigma_{cc} \, x_{cc} \cdot \frac{x_{cc}}{2} + \frac{1}{2} \, \sigma_c (Y_1 - x_{cc})(x_{cc} + \frac{1}{3} \, (Y_1 - x_{cc}))$$

$$Y_3 = \frac{\frac{1}{2} \, \sigma_{cc} \, x_{cc}^2 + \frac{1}{6} \, \sigma_c (Y_1 - x_{cc})^2 + \frac{1}{2} \, \sigma_c \, x_{cc} (Y_1 - x_{cc})}{T_n} \quad \ldots \qquad (E17)$$

STEP 16 - Calculate Y_2 from (E6).

STEP 17 - Go to step 7 and repeat 7-17 until stability or ultimate collapse is predicted.

E1.3 Failure Mechanisms

The computer program detects the following types of ultimate failure:

1) When $Y_2 < X_2$(Fig. E3) the horizontal thrust, T , contributes to the overturning moments. At this point collapse is catastrophic.

2) The uniaxial compressive strength of intact rocks is exceeded along the entire contact zone. It is assumed this indicates imminent collapse.

3) The horizontal deformations at the contact zones reach a magnitude at which the hinge block is free to fall out under gravity.

4) The frictional resistances μT_1 and μT_2 (Fig. E3) are insufficient to support weight of beam, plus superimposed loads.

APPENDIX F

DERIVATION OF EQUATIONS

Case I - Maximum Principal Stress Horizontal Volume of a Unit Thickness of Roof

Require area ABC (Figs. F1 and F2) = A_R

Let span of opening be 2B, and height of opening be 2H.

Area of slice, thickness, dx, is

$$\Delta A = Y\, dx$$

Total area, A_R, $2\int_{x=0}^{x=B} Y\, dx = 2\int_{x=0}^{x=B} (y - H)\,dx$ .... (F1)

But, for an ellipse,

$$y^2 = (1 - \frac{x^2}{a^2})b^2$$

Also, for this problem b = a/k

where a = semi-major axis of bounding ellipse

b = semi-minor axis of bounding ellipse

k = ratio of maximum to minimum principal stresses acting in cross-sectional plane.

$$y^2 = (1 - \frac{x^2}{a^2})\frac{a^2}{k^2}$$

$$= \frac{1}{k^2}(a^2 - x^2) \quad \text{..............} \quad (F2)$$

$$A_R = 2\int_{x=0}^{x=B} \{\frac{1}{k}(a^2 - x^2)^{\frac{1}{2}} - H\}\,dx$$

$$= \frac{2}{k}\int_{x=0}^{x=B} (a^2 - x^2)^{\frac{1}{2}}dx - H\int_{x=0}^{x=B} dx$$

$$= \frac{1}{k}\{B(a^2 - B^2)^{\frac{1}{2}} + a^2 \sin^{-1}(\frac{B}{a})\} - HB \quad \text{..............} \quad (F3)$$

Therefore, weight of maximum zone requiring support, W_R, for unit length, is:

$$W_R = A_R \gamma_R g \quad \text{..............} \quad (F4)$$

where γ_R = mass density of rock

g = gravitational acceleration

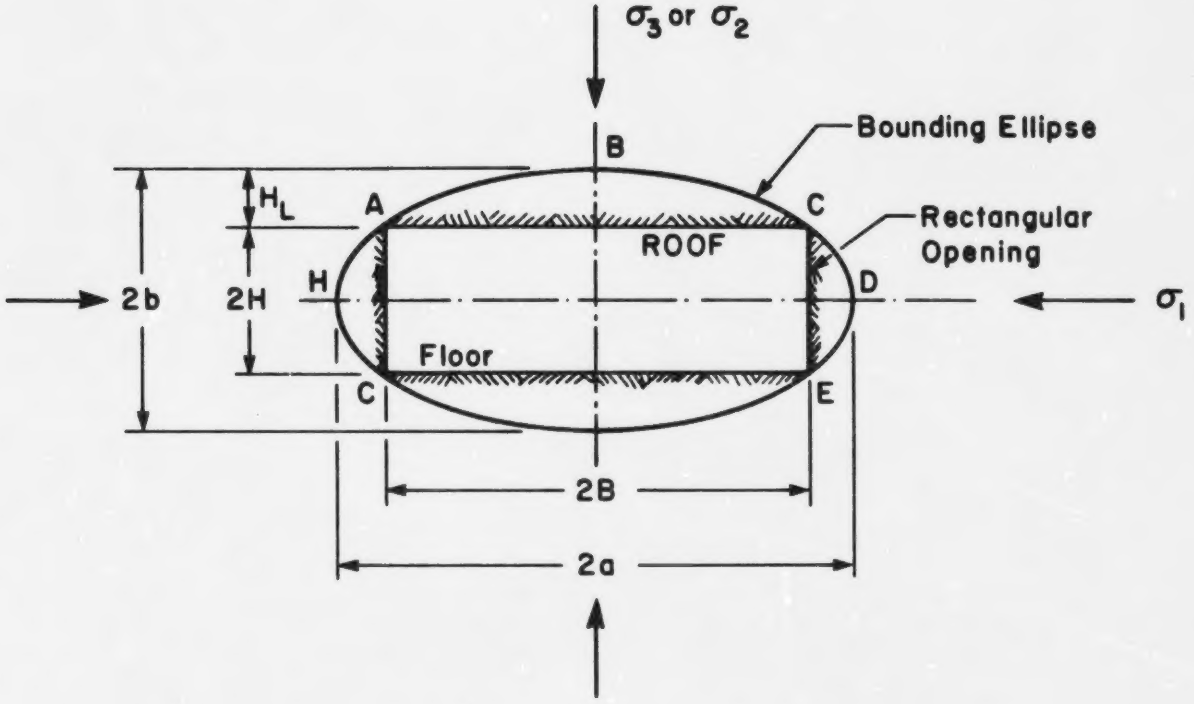
σ_3 or σ_2
Bounding Ellipse
Rectangular Opening
B
A
C
H_L
ROOF
H
D
2b
2H
σ_1
Floor
C
E
2B
2a

Figure F1 Bounding ellipse - geometry - major principal stress horizontal

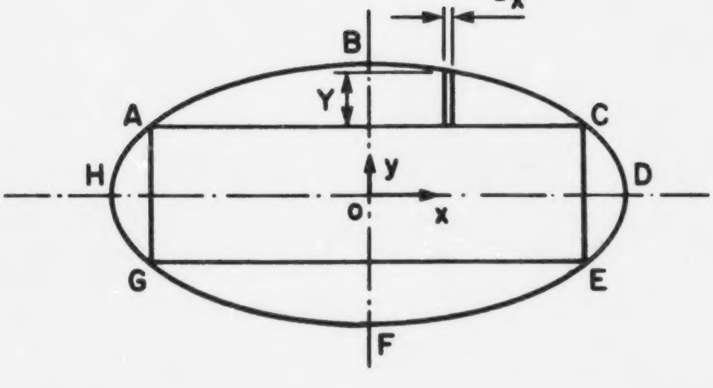
d_x
B
Y
A
C
H
D
y
o
x
G
E
F

Figure F2 Bounding ellipse - roof volume - major principal stress horizontal

To find a and b:

Equation of ellipse is:

$$\frac{x^2}{a^2} + \frac{y^2}{b^2} = 1 \qquad \text{...............} \quad \text{(F5)}$$

At C (Fig. F2), $y = H$, $x = b$, and, in general $a = kb$.

Substituting in (F4)

$$\frac{B^2}{k^2b^2} + \frac{H^2}{b^2} = 1$$

$$b^2 = \left(\frac{B^2 + k^2H^2}{k^2} \right)$$

$$b = \frac{1}{k} (B^2 + k^2H^2)^{\frac{1}{2}} \qquad \text{...............} \quad \text{(F6)}$$

and $a = kb$

To find maximum height of zone requiring support:

From Figure F1 , height requiring support is

$$H_L = b - H \qquad \text{...............} \quad \text{(F7)}$$

Equation of maximum bounding ellipse:

Since $a = kb$ and b is given by (6A), substituting for a and b in (F5)

$$(x^2 + k^2y^2) = B^2 + k^2H^2 \qquad \text{...............} \quad \text{(F8)}$$

Equation of reduced, bounding ellipse:

Let the reduced ellipse have a semi-major axis of length a', and a semi-minor axis of length b'.

The height of roof requiring support is reduced to H_L' such that

$$H_L' = CH_L \ (0 \le C \le 1) \qquad \text{...............} \quad \text{(F9)}$$

where H_L is given by equation (F7)

$C = (1-0.01 \ RMR)$

where RMR = Rock Mass Rating ($0 \le RMR \le 100$)

Substituting for H_L from (F7) in (F7),

$$H_L' = C(b - H) \qquad \text{...............} \quad \text{(F10)}$$

Also,

$$b' = H_L' + H \qquad \text{..............} \quad (F11)$$

Substituting for H_L' from (F10) in (F11)

$$b' = C(b - H) + H$$

$$= Cb - H(C - 1) \qquad \text{..............} \quad (F12)$$

Now, from general equation of ellipse (Eq. F5)

$$a'^2 = \frac{x^2 b'^2}{(b'^2 - y^2)} \qquad \text{..............} \quad (F13)$$

But from Fig. F2, at point C, x = B , y = H

∴ substituting in (F13)

$$a' = \frac{B\,b'}{(b'^2 - H^2)^{\frac{1}{2}}} \qquad \text{..............} \quad (F14)$$

∴ equation of reduced ellipse is

$$x^2(b'^2 - H^2) + y^2 B^2 = B^2 b'^2 \qquad \text{..............} \quad (F15)$$

Reduced value A_R':

To find reduced value A_R', of volume of unit thickness of roof requiring support, substitute a = a' and b = b' in equation (F3), where a' and b' are given by equations (F14) and (F12), respectively.

Therefore,

$$A_R' = \frac{1}{k'}\{B(a'^2 - B^2) + a'^2 \sin^{-1}(\frac{B}{a'})\} - HB \qquad \text{.............} \quad (F16)$$

where k' = a'/b'

Case II - Maximum principal stress vertical:

Volume of a unit length of roof

Require area ABC (Figs. F3 and F4)

Area of slice, thickness, dy, is:

$$\Delta A = X\ dy$$

$$\text{Total area, } A_R = 2\int_{y=o}^{y=B} X\,dy = 2\int_{y=o}^{y=B} (x - H)dy \qquad \text{..............} \quad (F17)$$

But for an ellipse,

$$x^2 = (1 - \frac{y^2}{b^2})a^2$$

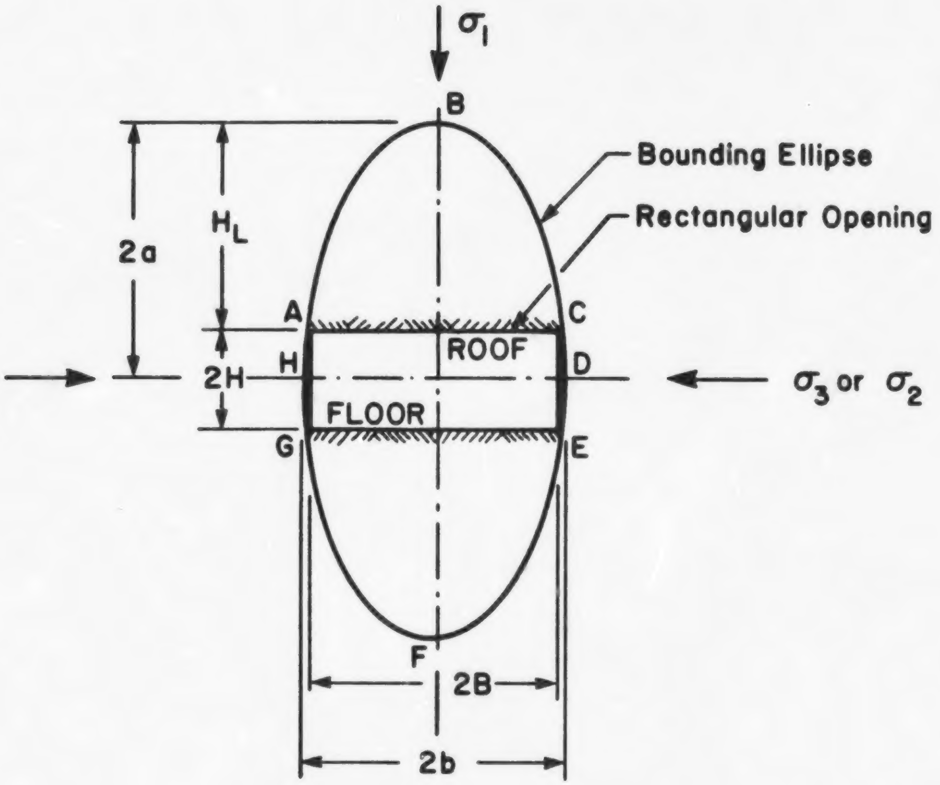

σ_1
B
Bounding Ellipse
Rectangular Opening
H_L
2a
A
C
ROOF
H
D
2H
σ_3 or σ_2
FLOOR
G
E
F
2B
2b

Figure F3 Bounding ellipse - geometry - major principal stress vertical

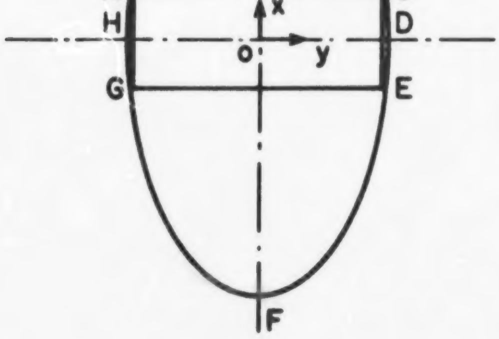

B
d_y
X
A
C
x
H
D
o
y
G
E
F

Figure F4 Bounding ellipse - roof volume - major principal stress vertical

Also, for this problem $a = kb$

$$x^2 = (1 - \frac{y^2}{b^2})k^2b^2$$

$$= k^2(b^2 - y^2) \qquad \text{..............} \quad \text{(F18)}$$

$$A_R = 2\int_{y=o}^{y=B} \{k(b^2 - y^2)^{\frac{1}{2}} - H\}\, dy$$

$$= 2k\int_{y=o}^{y=B} (b^2 - y^2)^{\frac{1}{2}}\, dy - H\int_{y=o}^{y=B} dy$$

$$= k\{H(b^2 - H^2)^{\frac{1}{2}} + b^2 \sin^{-1}(\frac{H}{b})\} - HB \qquad \text{..............} \quad \text{(F19)}$$

Therefore, weight of maximum zone requiring support, W_R' is for unit length.

$$W_R = A_R \gamma_R g \qquad \text{..............} \quad \text{(F20)}$$

To find a and b:

Equation of ellipse is:

$$\frac{x^2}{a^2} + \frac{y^2}{b^2} = 1 \qquad \text{..............} \quad \text{(F21)}$$

At C (Fig. F4), $y = B$, $x = H$, and, in general $a = kb$.
Substituting in (F21),

$$\frac{H^2}{a^2} + \frac{k^2B^2}{a^2} = 1$$

$$a^2 = (H^2 + b^2B^2)$$

$$a = (H^2 + k^2B^2)^{\frac{1}{2}} \qquad \text{..............} \quad \text{(F22)}$$

To find maximum height of zone requiring support:

From Figure F3, height requiring support is:

$$H_L = a - H \qquad \text{..............} \quad \text{(F23)}$$

Equation of maximum bounding ellipse:

Since $a = kb$ and b is given by (F22), substituting for a and b in (F21)

$$(x^2 + k^2y^2) = H^2 + k^2B^2 \qquad \text{..............} \quad \text{(F24)}$$

Equation of reduced bounding ellipse:

Let the reduced ellipse have a semi-major axis of length a' and a semi-a semi-minor axis of length b'.

The height of roof requiring support is reduced in H_L' such that:

$$H_L' = CH \quad (0 \le C \le 1) \qquad \text{..............} \quad (F25)$$

where H_L is given by equation (F23)

and $C = (1 - 0.01\,RMR)$,
where RMR = Rock Mass Rating ($0 \le RMR \le 100$).

Substituting for H_L frame (F23) in (F25)

$$H_L' = C(a - H) \qquad \text{..............} \quad (F26)$$

Also,

$$a' = H_L' + H \qquad \text{..............} \quad (F27)$$

Substituting for H_L' from (F26) in (F27)

$$\begin{aligned} a' &= C(a - H) + H \\ &= Ca - H(C-1) \end{aligned} \qquad \text{..............} \quad (F28)$$

Now, from general equation of ellipse (F21)

$$b'^2 = \frac{y^2 a'^2}{(a'^2 - H^2)} \qquad \text{..............} \quad (F29)$$

But, from Figure F4 at point C, $x = H$, $y = B$
Substituting in (F29)

$$b' = \frac{B\,a'}{(a'^2 - H^2)^{\frac{1}{2}}} \qquad \text{..............} \quad (F30)$$

equation of reduced ellipse is:

$$B^2x^2 + y^2(a'^2 - H^2) = B^2a'^2 \qquad \text{..............} \quad (F31)$$

Reduced value, A_R:

To find reduced value, A_R, of volume of unit thickness of roof requiring support, substitute $a = a'$ and $b = b'$ in equation (F19) where a and b are given by equations (F28) and (F30), respectively. Therefore,

$$A'_R = k'\{H(b'^2 - H^2)^{\frac{1}{2}} + b'^2 \sin^{-1}(\frac{H}{b'})\} - HB \text{ .... } (F32)$$

where $k' = \frac{a'}{b'}$.

NOTE: The adjustment from a maximum ellipse to a reduced ellipse for Case II may result in a reduced ellipse whose major semi-axis is no longer vertical, but horizontal. In this situation the equations for Case I should be used to find weights of the zone requiring support. To determine whether to use Case I or Case II equations for the Case II reduced ellipse, check that a' from equation (F28) is greater than, or equal to, a'_c, where

$$a'_c = (B^2 + H^2) \text{ .... } (F33)$$

If $a' \geq a'_c$, use equation (F32).

If $a' < a'_c$, use equation (F16). (a' (Eq. (F28)) is now b' and can be substituted in equation (F14) to find new a').

APPENDIX G

Copy of paper, **"A Simple Rock Bolt Pull-out Test Device for Teaching Purposes"**

Published in Int. J. Rock Mech. Min. Sci. & Geomech. Abstr. Vol. 21, No. 4, 1984.

Int J Rock Mech Min Sci & Geomech Abstr Vol 21, No 4, pp 217–218, 1984
Printed in Great Britain All rights reserved

0148-9062/84 $3.00 + 0.00
Copyright © 1984 Pergamon Press Ltd

428

Technical Note

A Simple Rock Bolt Pull-out Test Device for Teaching Purposes

B. STIMPSON*

INTRODUCTION

It is widely accepted practice to measure the short-term strength of rock bolts by an *in situ* pull-out test in which axial load is applied to the head of the bolt through a hollow-cylinder hydraulic ram and the head displacement recorded as a function of applied load up to failure [1].

The test is used for two primary purposes. It is commonly employed as a means of quality control to ensure that adequate standards are being maintained, but it is also widely used as a comparative measure of the strengths of different types of rock bolt when selecting or redesigning a support system. Short-term pull-out strength is seldom the only factor to be considered but it is an important and useful one. (Long-term strength, stiffness, ability to absorb large displacements, corrosion properties, blasting resistance, cost, ease of and time of emplacement, cost of maintenance of ancillary equipment, etc. are others.)

FAILURE OF BOLTS IN THE PULL-OUT TEST

If the strength of the component of the bolt that interacts with the rock (i.e. the anchor/rock interface or resin/rock contact) is adequate, then ultimate failure of the bolt will depend on the strength of the bolt material and details of its design. Failure may occur in the anchor, along the body or shank of the bolt, or at its head. However, if the weak link is the rock or the bolt/rock interface, then failure will occur by fracture of the rock or by shearing along the interface.

PULL-OUT TESTING IN THE LABORATORY

For laboratory testing of new types of bolt or for student laboratories in teaching institutions, it is common practice to insert the bolts in holes drilled in large blocks of concrete or plaster. This, of course, is a pragmatic solution to the problem of otherwise having to obtain and prepare large blocks of rock at considerable cost. The degree to which this affects the results of pull-out tests where the bolt itself fails is probably small, but the procedure obviously cannot provide data on the strength of bolts in specific rock types, more especially where the rock is of low strength and rock bolt pull-out strength is controlled by the rock and rock/bolt interface properties.

In the teaching as well as the research environment, a means of conducting pull-out tests in the laboratory in rock without having to procure large samples would clearly be most useful.

ROCK BOLT PULL-OUT TEST DEVICE

Figure 1 is a photograph of a laboratory rock bolt tester which permits the bolt to be inserted in small samples of rock. The rock sample in the form of a cylinder should be at least 10 cm in diameter and contains a pre-drilled central hole for the rock bolt. It is then grouted or cemented into a central hole prepared in a cylinder of concrete. The diameter of the latter should be a minimum of 25 cm. The rock sample does not have to be cylindrical in shape but could equally well be cut into blocks on a circular saw. Ideally, the rock sample should be continuous throughout the length of the concrete block but this would again involve securing very large blocks of rock. Therefore, the column of rock is formed by gluing together several rock samples with an epoxy resin.

An alternative to grouting the rock in a hole in a pre-cast concrete block may be to cast concrete around the rock sample. However, there is some question as to the strength of the bond between the rock and concrete and, therefore, the method has not been tried.

The loading system is standard and is comprised of a 200 kN (20-ton) hollow cylinder ram and a 69 MPa (10,000 psi) hand pump. In Fig. 1 a dial gauge is shown for measuring axial movement of the bolt head though other continuous methods of monitoring could readily be added.

CONCLUSIONS

The frame shown in Fig. 1 is a prototype for teaching purposes and large frames could be constructed to

---

* Department of Mineral Engineering, University of Alberta, Edmonton, Alberta, Canada T6G 2G6.

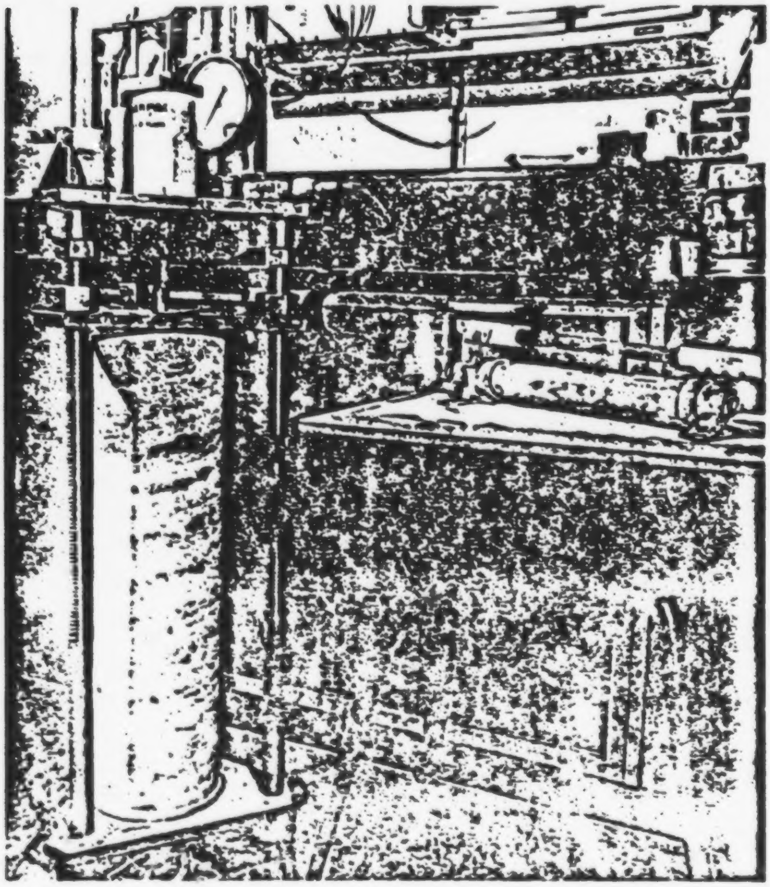

Fig. 1. Laboratory rock bolt pull-out tester showing concrete cylinder containing rock specimen, load frame, hydraulic cylinder and hand pump.

permit testing of longer bolts. The method offers some interesting possibilities for research into rock bolting under controlled conditions in the laboratory in actual mine rock.

Received 6 *February* 1984.

REFERENCE

1. International Society for Rock Mechanics. Commission on Standardization of Laboratory and Field Tests. Suggested methods for rock bolt testing. In *Rock Characterization, Testing and Monitoring. ISRM Suggested Methods* (Edited by E. T. Brown), pp. 161–168. Pergamon Press, Oxford (1981).

APPENDIX H

SUGGESTED METHOD FOR ESTIMATING THE REDUCED OR EFFECTIVE YOUNG'S MODULUS OF A CROSS-JOINTED ROOF AND ITS APPLICATION IN LAYERED ROOF STABILITY ANALYSIS

Introduction:

A component of the multi-layer roof analysis presented in Chapter 12 requires the estimation of beam deflections to determine where bed separations occur and where an upper bed loads the bed(s) beneath. The equations used for determining these deflections involve Young's modulus of the beam and assume an unjointed, isotropic medium. The presence of vertical cross-joints causes the beam deflections to increase, so that the development of bed separations and loadings will generally be different from that predicted for unjointed, isotropic materials. This appendix presents an approximate method for taking into account the effect of cross-joints on deflections.

Effective Young's Modulus of a Cross-Jointed Roof Beam

For an isotropic, unjointed clamped beam under uniform loading, the maximum deflection, δ_s, is given by:

$$\delta_s = \frac{\gamma L^4}{32 E_i\, D^2}$$

$$= \frac{C_b}{E_i} \qquad \text{...............} \qquad (H.1)$$

where C_b = constant for a given beam $= \gamma L/32D^2$,

γ = beam density,

L = beam span,

D = beam thickness, and

E_i = Young's modulus of beam.

Therefore,

$$E_i = \frac{C_b}{\delta_s} \qquad \text{..............} \qquad (H.2)$$

Let the maximum deflection of a jointed, clamped, uniformly loaded beam be δ_j. This deflection is equivalent to that of an isotropic, jointed beam of the same thickness, span, and loading, but with a reduced effective Young's modulus, E_j , such that:

$$E_j = \frac{C_b}{\delta_j} \qquad \text{..............} \qquad (H.3)$$

Therefore, from Equations (H.2) and (H.3),

$$\frac{E_j}{E_i} = \frac{\delta_s}{\delta_j} \qquad \text{..............} \qquad (H.4)$$

Or,

$$E_j = \frac{\delta_s}{\delta_j} E_i \ . \qquad \text{..............} \qquad (H.5)$$

Deflection of a Jointed Beam:

A continuum joint analysis of roof beams using a finite element code was used by Olson (1) to study the deflection behaviour of roof beams. The analytical model assumes that joint behaviour is approximately uniform over a region encompassing several parallel joints, and therefore the gross response of the rock mass can be approximated by a continuous displacement field. The total strain in a block of jointed rock is then the sum of the strains in the intact rock and strains resulting from dilation and shearing of the joints.

The joint properties required in the analysis are the normal stiffness, K_n, shear stiffness, K_s, joint spacing and joint inclination.

The deflections of a clamped beam, 4 ft. thick and 24 ft. span, were determined by this method for a range of joint angles and spacing, but for a fixed set of rock and joint properties as follows (Fig. H1):

Intact Rock	Joint Properties
$E_i = 2.8 \times 10^6$ psi	$K_n = 2.0 \times 10^5$ psi/in
$\nu = 0.15$	$K_s = 0.67 \times 10^5$ psi/in
$\rho = 0.091$ lb/in (density)	

Joint angles and spacings were varied as follows:

	α , deg.	β , deg.
Model 1	30	150
Model 2	45	135
Model 3	60	120

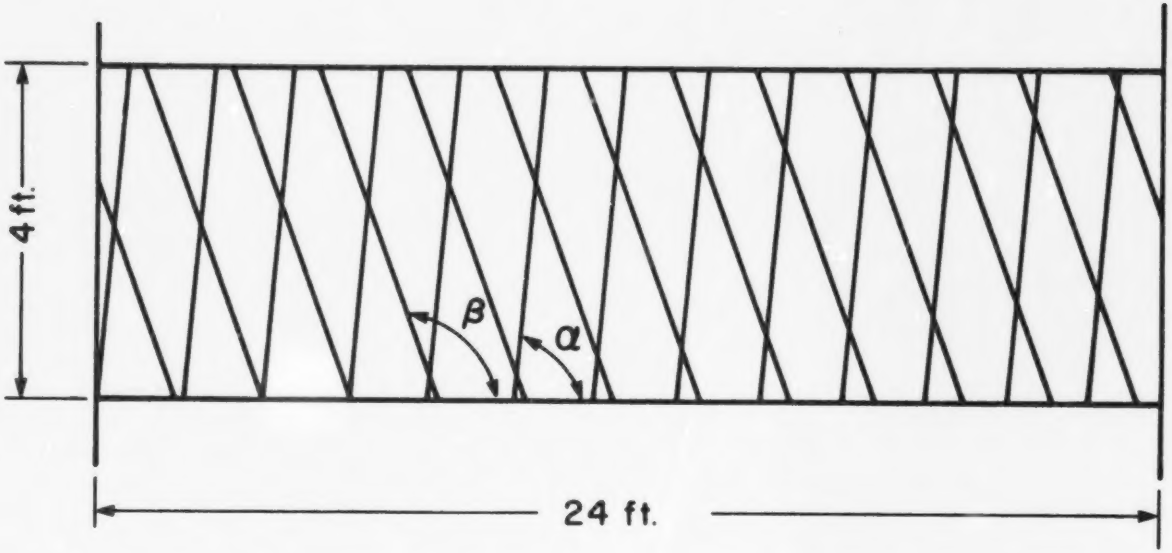

Figure H1 Jointed beam analysed by Olson (1)

Joint spacings of 4, 8, 16 and 32 inches were studied, bringing the total number of beam configurations to 12.

Results from Model 3 are shown in Figure H2, and were analysed in detail because the joint orientations are closest to those in a vertically, cross-jointed roof beam. A close relationship was found between the normalized maximum beam deflection and normalized joint spacing (Fig. H3):

$$\frac{\delta_j}{\delta_s} = 1.38 \left(\frac{d}{D}\right)^{-0.70} \qquad \text{..............} \qquad (H.6)$$

where d = joint spacing, and
D = roof beam thickness.

Because Equation (H.6) was developed for 60-120 deg. joint sets an ajustment must be made to correct to a 90 deg. joint angle (vertical cross-joints). Figure H4 shows the variation of beam deflection with angle of the joint sets for a beam with a joint spacing of 8 in. The relationship between maximum deflection and joint angle is plotted in Figure H5. The linear relationship between the two variables is given by:

$$\frac{\delta_j}{\delta_s} = 0.54\alpha + 2.03 \qquad \text{..............} \qquad (H.7)$$

where α = acute angle between beam axis and joint plane.

Therefore, to correct Equation (H.6) to a 90 deg. joint plane, it must be multiplied by:

$$\frac{\delta_j(\alpha=90°)}{\delta_j(\alpha=60°)} = \frac{0.054 \times 90 + 2.03}{0.054 \times 60 + 2.03} \qquad \text{.............} \qquad (H.8)$$

$$= 1.31 \; .$$

So that Equation (H.6) becomes:

$$\frac{\delta_j}{\delta_s} = 1.31 \times 1.38 \left(\frac{d}{D}\right)^{-0.70}$$

$$= 1.81 \left(\frac{d}{D}\right)^{-0.70} \qquad \text{..............} \qquad (H.9)$$

Therefore, substituting for $\frac{\delta_j}{\delta_s}$ from Equation (H.9) in Equation (H.5):

$$E_j = 0.552 \left(\frac{d}{D}\right)^{0.70} E_i \qquad \text{..............} \qquad (H.10)$$

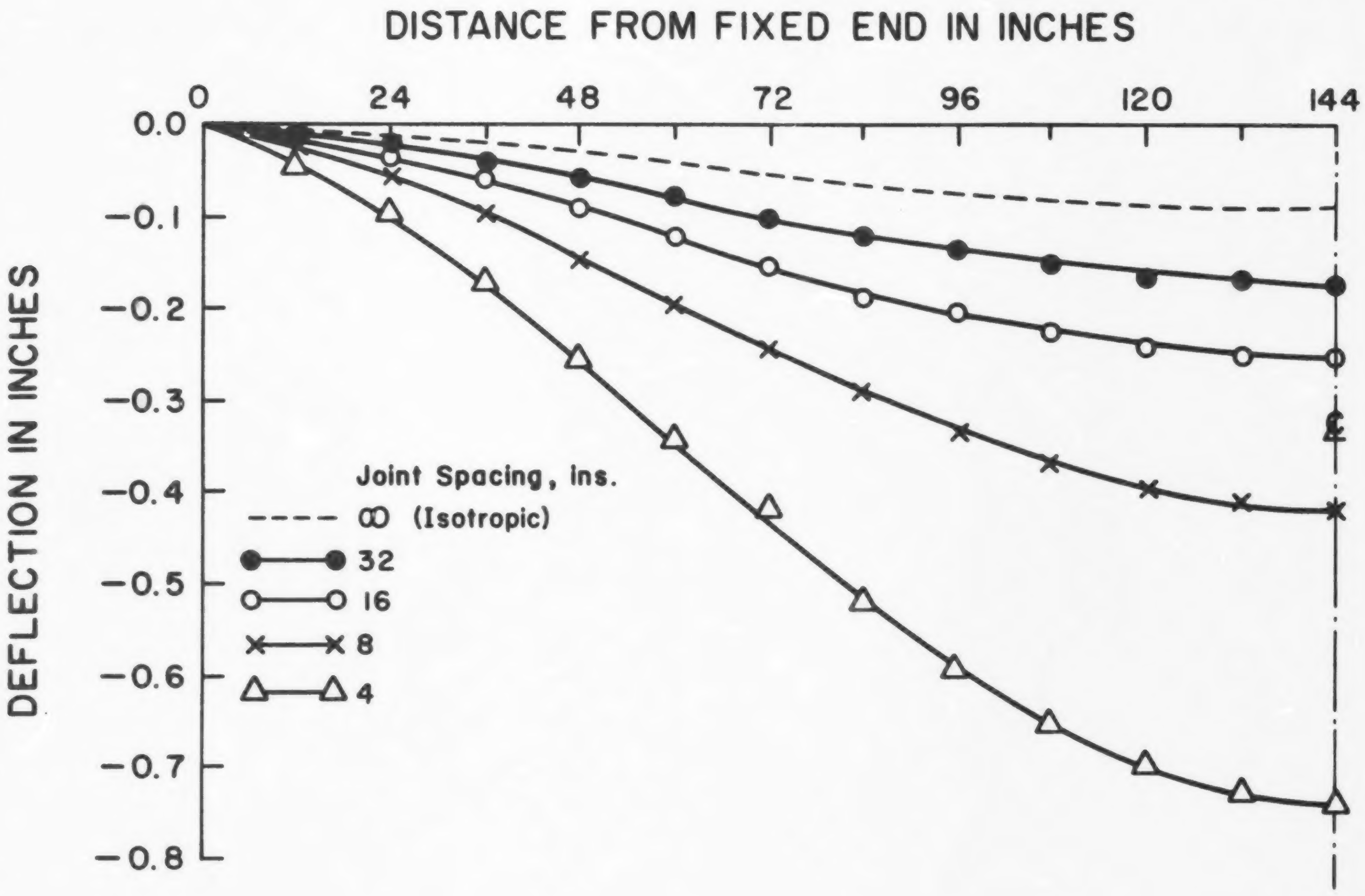

Figure H2 Deflections of a fixed end beam for various joint set spacings at 60-120 deg. joint set angles

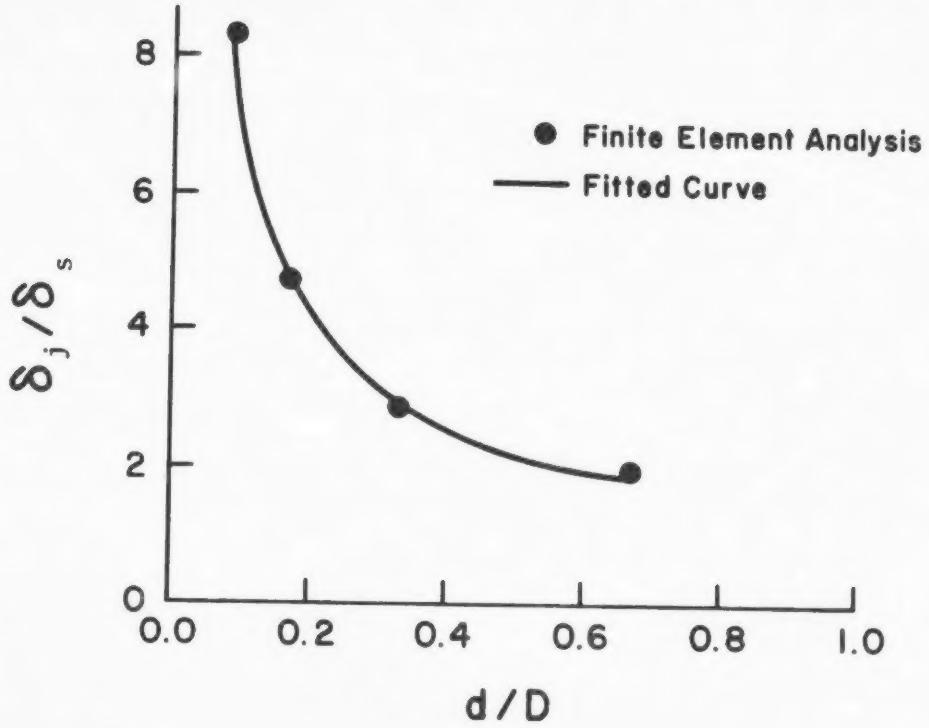

Figure H3 Relationship between δ_j / δ_s and (d/D)

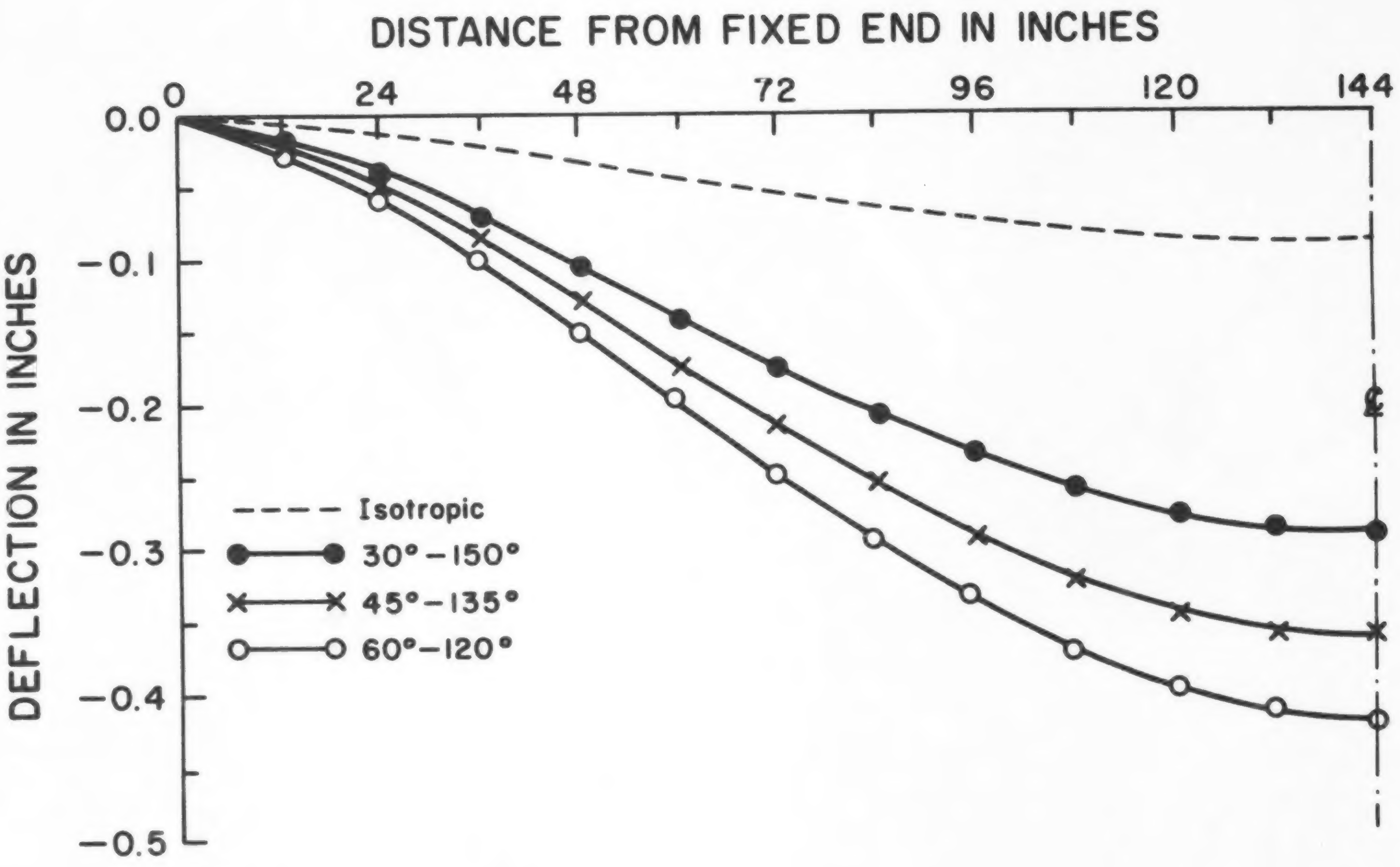

Figure H4 Deflections of a fixed end beam for various joint set angles at 8 inch joint set spacing

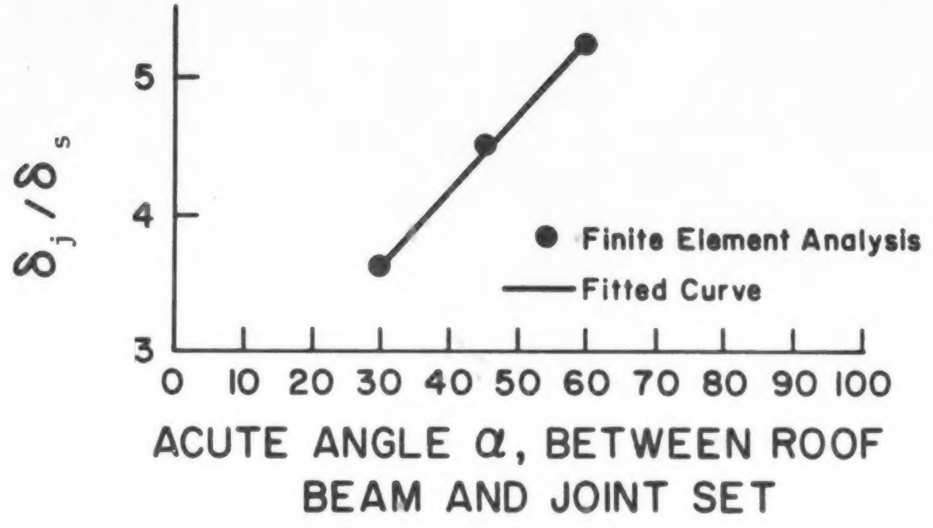

Figure H5 Relationship between joint angle and maximum deflection

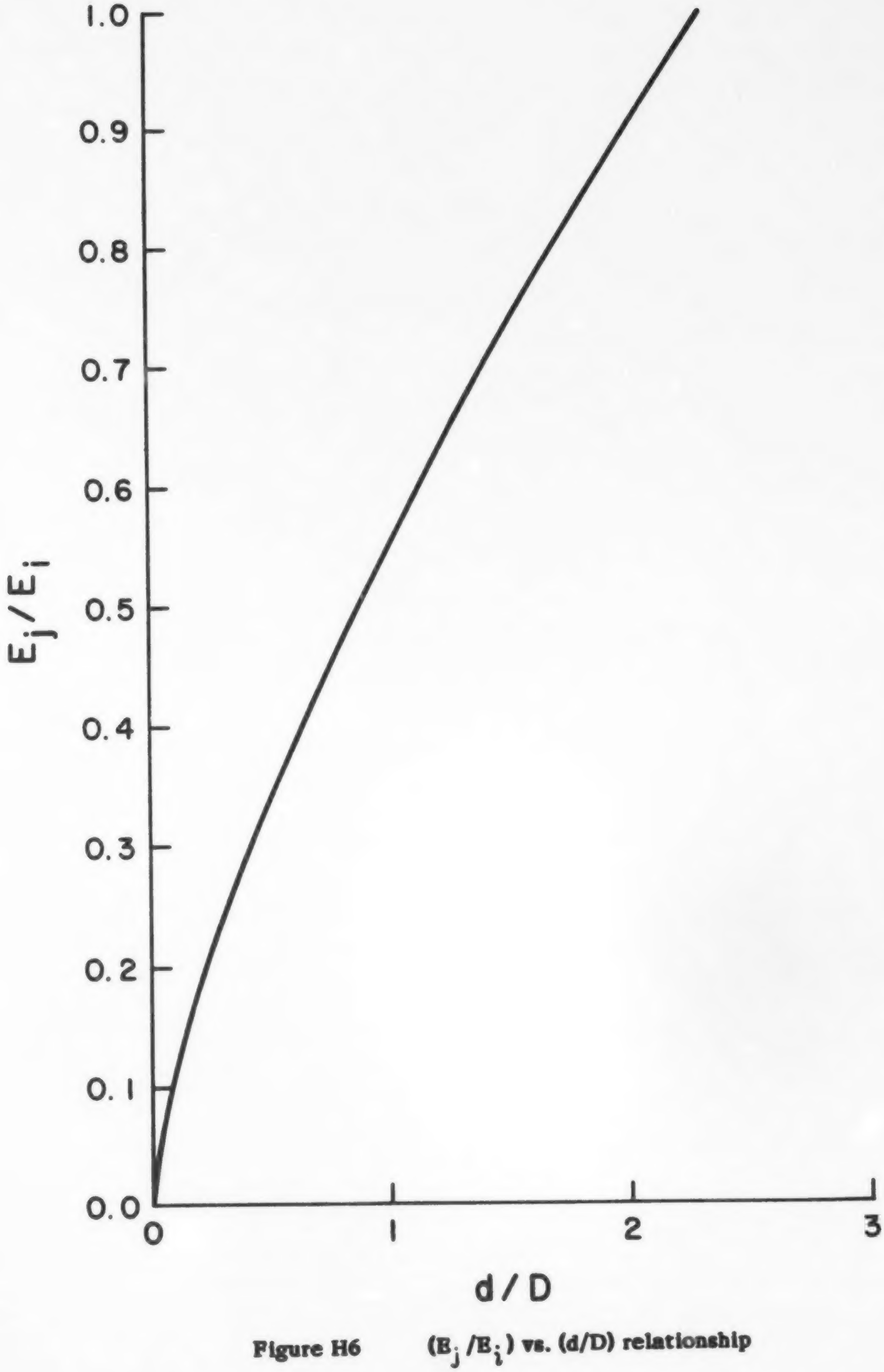

Figure H6 (E_j / E_i) vs. (d/D) relationship

The relationship between the ratios E_j/E_i and d/D is illustrated in Figure H6. If $E_i = 2.5$ GPa, d = 0.5 m, and D = 1.0 m, then, from Figure H6, $E_j/E_i = 0.355$ or $E_j = 0.84$ GPa.

Example of Multi-Layer Behaviour:

Suppose the beds in a three layer roof, span 6 m, have the following mechanical and geometric properties, in descending order:

Layer 3: E = 10.0 GPa, D = 1.5 m, d = 0.25 m
Layer 2: E = 12.0 GPa, D = 0.5 m, d = 0.5 m
Layer 1: E = 5.0 GPa, D = 0.25 m, d = 0.75 m

The density of the rock for all three layers is 2800 kg/cu.m.

Analyses to determine the deflections of each beam (see Chapter 12), first assuming intact rock Young's moduli and then reduced effective Young's moduli according to Figure H6, give the following results:

	E_i, GPa	E_j, GPa	δ_s, mm	δ_j, mm
Layer 1	10.0	2.6	1.6	6.1
Layer 2	12.0	6.7	11.9	21.3
Layer 3	5.0	5.0	113.9	113.9

Closure:

The analysis presented in this appendix is an initial attempt to account for the effect of joint spacing on roof beam deflections. It is suggested that further work be carried out to validate and refine the technique.

REFERENCES

1. Olson, R.J. A continuum approach to regularly jointed rock mass behaviour using existing finite element codes. M.Sc. Thesis, Michigan Technological University, Houghton, Michigan, 1977.

APPENDIX I

GROUND CONVERGENCE CURVE FOR A LAYER ABOVE A RECTANGULAR OPENING

Roof Displacement vs. Distance from Face:

The roof slab above a rectangular opening in horizontally bedded strata is supported on three sides and unsupported along the remaining side. At any point in the roof the vertical displacement will reach, for all practical purposes, a constant value, u_{max}, at some distance, D_{crit}, from the face (Fig. I1).

The theoretical prediction of vertical displacement vs. face distance is very complex even for the linear elastic case. For simplicity, it is assumed that the roof slab behaves as a linear elastic, uniformly loaded rectangular plate with built-in edges. The deflections of such a plate have been determined analytically by Timoshenko (1). His analysis shows that for ratios of plate length, b , to plate width, a , (Fig. I2) greater than 2, the maximum deflection approaches a constant value. In terms of face distance, this result suggests that negligible additional vertical displacement (roof convergence) occurs once the face has passed any point by a distance of 2 x roof span.

The maximum displacement, u_{max}, in the roof at a distance of 2 x span or greater from the face is given, without introducing any appreciable error, by the 2-D beam equation for a uniformly loaded, linear elastic beam of rectangular cross-section with built-in edges:

$$u_{max} = \frac{\gamma L^4}{32Et^2} \qquad \text{..............} \quad (AI.1)$$

where L = span,
E = modulus of elasticity,
t = beam thickness,
γ = density of beam.

It is now assumed that the vertical displacement varies from zero at the face to a maximum given by Equation (AI.1) at a distance 2 x span from the face. There will, in fact, be some vertical displacement at the face, whose magnitude will depend primarily upon the intensity of the abutment pressure over the face and the deformability of the face materials.

The vertical displacement at the centre of the roof, u , at a given dis-

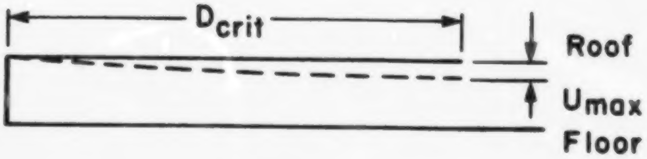
Dcrit
Roof
Umax
Floor

Figure 11 Roof deflection and distance from face

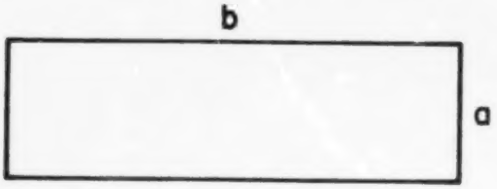

Figure 12 Rectangular plate

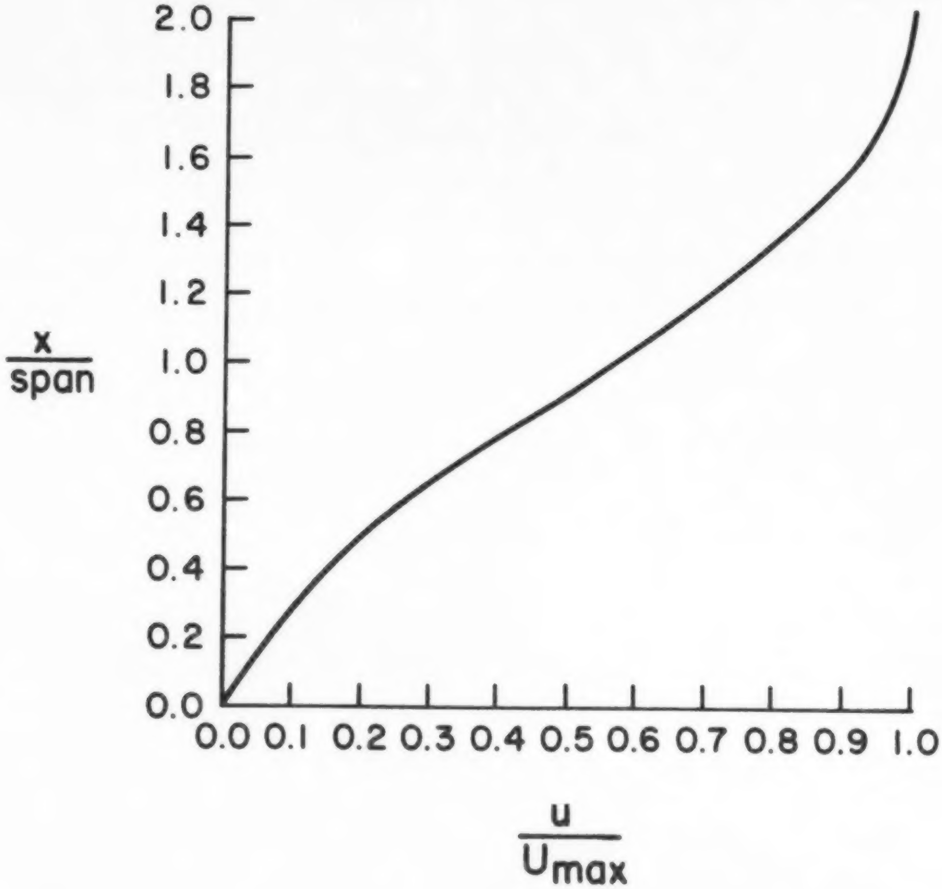

Figure 13 Roof displacement vs. distance from face

tance, x , from the face, where x ≤ 2 x span, may be determined from (Fig. I1):

$$u = Fu_{max} \qquad \text{...............} \quad (AI.2)$$

or

$$\frac{u}{u_{max}} = F \qquad \text{...............} \quad (AI.3)$$

where F is a weighting factor ($0 \le F \le 1$).

At the face F = 0, and at a distance, x = 2 x span, from the face (Fig. I1), F = 1. F is now assumed to vary in the same way as the vertical displacement of a built-in, uniformly loaded beam. Thus, from Equation (AI.2), at the centre:

$$F = \frac{\text{deflection at point } y \text{ along beam}}{\text{deflection at centre of beam}}$$

$$= \frac{x^2(L-x)^2}{2Et^2} \times \frac{32Et^2}{L^4}$$

$$= 16(x/L)^2\ (1-x/L)^2 \qquad \text{...............} \quad (AI.4)$$

Therefore, from (AI.3) and (AI.4), the roof convergence from the face to a point 2 x span from the face is given by:

$$\frac{u}{u_{max}} = 16(x/L)^2\ (1-x/L)^2 \qquad \text{...............} \quad (AI.5)$$

where $0 \le x \le \frac{1}{2} L$

Equation (AI.5) is plotted in Figure I3.

For points away from the centre of the span, u/u_{max} is also given by Equation (AI.5).

Ground Convergence Curve:

Let the normal stress, p , acting perpendicular to the roof plane at any point before excavation be $p = p_o$. After excavation p = 0. As p reduces to zero the vertical displacement, u , increases to a maximum value, u_{max}, such that:

$$\frac{p}{p_o} = 1 - \frac{u}{u_{max}} \qquad \text{...............} \quad (AI.6)$$

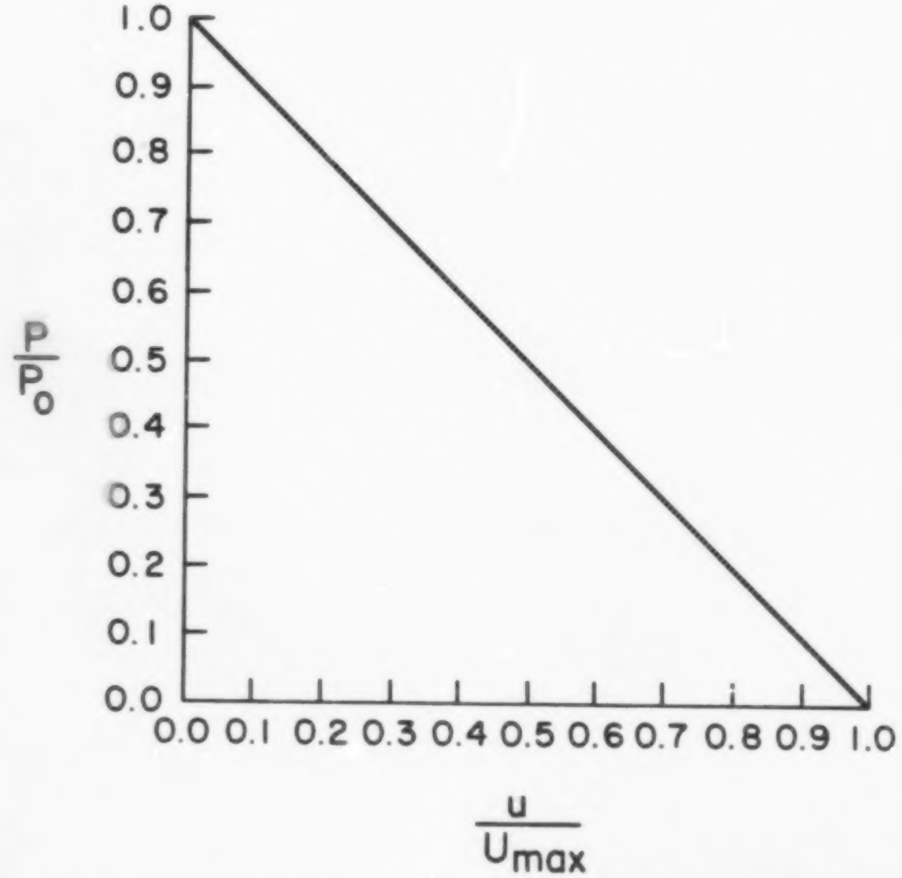

Figure 14 Ground reaction curve for a beam

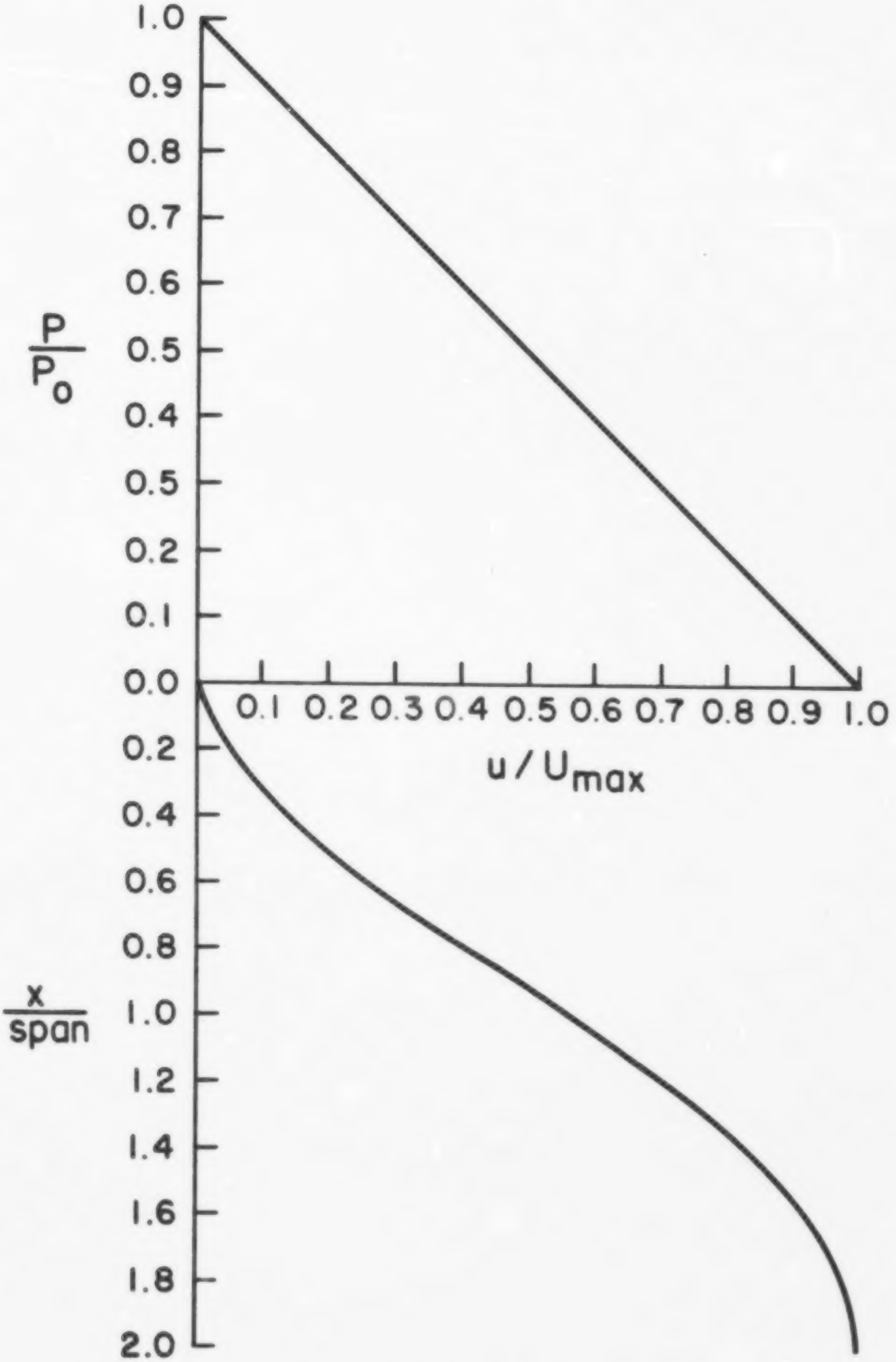

Figure 15 Ground reaction curve and timing of installation

For a single beam with no external loading:

$$p_o = \gamma t \qquad \text{..............} \qquad (AI.7)$$

Equation (AI.6) is plotted in Figure I4.

It is convenient to combine Figures I3 and I4 in one diagram as in Figure I5. The use of this diagram for bolting design is described in Chapter 12.

REFERENCES

1. Timoshenko, S. Theory of plates and shells. McGraw-Hill Book Co., New York (1940).

APPENDIX J

AXIAL STIFFNESS OF A GROUTED BOLTING PATTERN IN LAMINATED STRATA AXIAL STIFFNESS OF A GROUTED BOLT

Let the average support pressure provided by a uniformly spaced pattern of bolts be p_i. Bolt spacing along and between rows is s_a and s_s respectively (Fig. J1). Therefore, the support force, F , over an area $s_a \times s_s$ is:

$$F = s_a \, s_s \, p_i \qquad \text{............} \quad (J.1)$$

But for the bolt:

$$p_i = k \, \varepsilon_i \qquad \text{............} \quad (J.2)$$

where ε_i is the axial strain, and k is the axial stiffness expressed in stress-strain units.

Multiplying Equation (J.2) by $s_a \, s_s$:

$$\begin{aligned} p_i \, s_a \, s_s &= k \; s_a \, s_s \, \varepsilon_i \\ &= R \, \varepsilon_i \\ \text{where } R &= k \, s_a \, s_s \qquad \text{............} \quad (J.3) \end{aligned}$$

But from Equation (J.1) $p_i \, s_a \, s_s = F$.
Therefore, $F = R \, \varepsilon_i$ and R is the axial stiffness of the bolt in units of axial load/axial strain.

Kamal (1) has shown that the equivalent axial stiffness, R , of a grouted bolt can be approximated by:

$$R = \frac{\pi}{4} d_1^2 \, E_b \left(1 + \frac{E_g}{E_b} \; \frac{(d_2^2 - d_1^2)}{d_1^2} \right) \qquad \text{............} \quad (J.4)$$

where d_1 = bolt diameter
d_2 = hole diameter
E_b = Young's modulus of bolt
E_g = Young's modulus of grout.

From Equations (J.3) and (J.4)

$$k = \frac{\pi \; d_1^2}{4 \; s_a \; s_s} \; E_b\left(1 + \frac{E_g}{E_b}\,\frac{(d_2^2 - d_1^2)}{d_1^2}\right) \qquad \ldots\ldots\ldots\ldots \qquad (J.5)$$

Support Reaction Curve

The roof displacement, u , at a point in a bolted roof is given by (Fig. J2):

$$u = u_{i0} + \frac{p_i l}{k} \qquad \ldots\ldots\ldots\ldots \qquad (J.6)$$

where u = roof displacement before support is installed, and
and $p_i l/k$ = roof displacement after support is installed up to point of equilibrium at A (Fig. J3),
and l = effective bolt length.

Depending on the type of loading to which the bolt is subjected, all, or only a section of the bolt will experience axial loading. For example, in a pull-out test of a grouted bolt load transfer to the rock on either side of the bolt limits the transfer of pull-out load along the bolt. However, the actual loading of a grouted bolt in-situ is not reproduced by a pull-out test. In the absence of other well-proven alternatives, l is assumed to be equal to the bolt length.

It is more useful to plot the support reaction curve in dimensionless terms (p/p_o vs. u/u_{max} - see Appendix 1):

$$\frac{u}{u_{max}} = \frac{u_{i0}}{u_{max}} + \frac{p}{p_o}\left(\frac{l \; p_o}{k \; u_{max}}\right) \qquad \ldots\ldots\ldots\ldots \qquad (J.7)$$

The support component of displacement in Equation (J.7) is:

$$\frac{u}{u_{max}} = \frac{p}{p_o}\left(\frac{l \; p_o}{k u_{max}}\right)$$

$$\text{or} \quad \frac{p}{p_o} = \left(\frac{k u_{max}}{l \; p_o}\right)\frac{u}{u_{max}} \qquad \ldots\ldots\ldots\ldots \qquad (J.8)$$

$$= K \, \frac{u}{u_{max}} \, . \qquad \ldots\ldots\ldots\ldots \qquad (J.9)$$

But, for a built-in roof beam of rectangular cross-section with uniform loading:

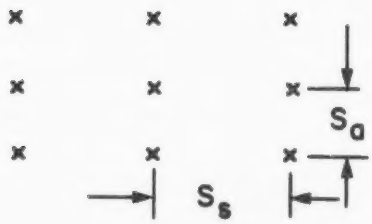

Figure J1 Bolt spacing

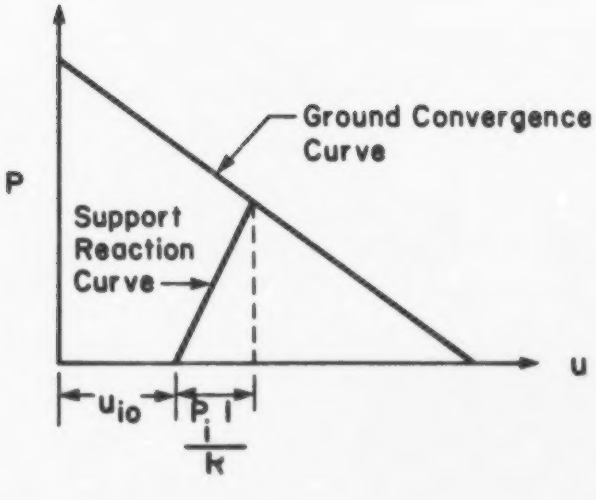

Figure J2 Support reaction curve

$$p_o = \gamma t \qquad \text{(J.10)}$$

and

$$u_{max} = \frac{\gamma L^4}{32Et^2} \qquad \text{(J.11)}$$

where L = roof span

t = roof beam thickness

E = Young's modulus of roof beam

γ = density of roof beam

Substituting for p_o, u_{max} and k from Equations (J.10), (J.11) and (J.5) in Equation (J.8), it is found that the slope, K of the ground reaction curve is given by

$$K = \frac{\pi d_1^2 E_b (1 + (E_g/E_b)\dfrac{(d_2^2 - d_1^2))L^4}{d_1^2}}{128 E_r \, t^3 \, s_a \, s_s \, l} \qquad \text{(J.12)}$$

REFERENCES

1. Kamal, S.A. Analysis of multi-axial anisotropic creep, roof resin bolts and bed separation in rock structures using the finite element method. Ph.D. Dissertation, Michigan Technological University (1974).